

**Stilbene-Conjugated Terpyridine Complexes of Ru(II) and
Os(II): Experimental and Theoretical Investigations on
Photophysics, Trans-Cis Photoisomerization, Ion Sensing,
and Aggregation-Induced Emission Characteristics**

A Thesis

Submitted for the Degree of

Doctor of Philosophy (Science)

of

Jadavpur University

by

Tanusree Ganguly



DEPARTMENT OF CHEMISTRY

JADAVPUR UNIVERSITY

JADAVPUR, KOLKATA 700032

INDIA

2025

Dr. Sujoy Baitalik
Professor
Department of Chemistry
Inorganic Chemistry
Section



JADAVPUR UNIVERSITY
KOLKATA – 700032, INDIA
Telephone: 91-033-2414-6666
Facsimile : 91-033-2414-6584
E-mail: sbaitalik@hotmail.com,
Sujoy.baitalik@jadavpuruniversity.in

CERTIFICATE FROM THE SUPERVISOR

This is to certify that the thesis entitled “Stilbene-Conjugated Terpyridine Complexes of Ru(II) and Os(II): Experimental and Theoretical Investigations on Photophysics, Trans-Cis Photoisomerization, Ion Sensing, and Aggregation-Induced Emission Characteristics” submitted by **Smt. Tanusree Ganguly** who got her name registered on 10.10.2018 for the award of Ph. D. (Science) Degree of Jadavpur University, is absolutely based upon her own work under the supervision of Prof. Sujoy Baitalik and that neither this thesis nor any part of it has been submitted for either any degree / diploma or any other academic award anywhere before.

Sujoy Baitalik

*Professor Sujoy Baitalik
Department of Chemistry
Jadavpur University
Kolkata- 700 032, India*

(SUJOY BAITALIK)

Signature of the Supervisor

& Date with official seal

Dedicated
to
My Family

"यदि मन्यसे सुवेदेति नूनं त्वं वेत्थ दहमेवापि।"

"If you think you have fully understood, you have understood little"

- Upanishad

PREFACE

The research documented in the thesis titled “Stilbene-Conjugated Terpyridine Complexes of Ru(II) and Os(II): Experimental and Theoretical Investigations on Photophysics, Trans-Cis Photoisomerization, Ion Sensing, and Aggregation-Induced Emission” was conducted at the Department of Chemistry of Jadavpur University from 2018 to 2025. The thesis comprises of seven chapters.

Chapter 1 provides a comprehensive review of the photophysical and electrochemical properties of Ru(II) and Os(II) polypyridine complexes, along with the photoisomerization behavior of stilbene- and azo-functionalized metal complexes. The discussion also examines aggregation-induced emission modulation and the role of non-covalent interactions in anion and cation sensing. The chapter concludes by outlining the key objectives and scope of this dissertation.

Chapter 2 deals with the synthesis, structural characterization, photophysical properties, aggregation-induced emission and light induced reversible photoisomerization behaviors of a series of stilbene-appended terpyridine systems of the type tpy-pvp-X , where $\text{X} =$ naphthalene, anthracene and pyrene. Presence of the stilbene unit facilitates reversible trans/cis isomerization upon visible light exposure, with the reverse process occurring in the dark, facilitating "on-off" and "off-on" emission switching in both free and aggregated form. Computational investigations involving density functional theory (DFT) of the compounds were performed to gain insights on their electronic structures and for appropriate assignment of the spectral bands.

Chapter 3 reports synthesis, characterization, photophysical nature, redox properties, aggregation-induced emission, and light induced reversible photoisomerization behaviors of homoleptic Ru(II) bis-terpyridine complexes of the type $[\text{Ru}(\text{tpy-pvp-X})_2](\text{ClO}_4)_2$, where $\text{X} =$ naphthalene, anthracene and pyrene. Aggregated forms can also undergo isomerization under visible light but at a slower rate. In conjunction with experiment, DFT calculations were also performed for understanding their electronic structures and nature of transition associated with the spectral bands.

Chapter 4 deals with the synthesis, characterization of a new series of heteroleptic Ru(II)-terpyridine complexes of the type $[(\text{tpy-PhCH}_3)\text{Ru}(\text{tpy-pvp-X})](\text{ClO}_4)_2$ and thorough investigation of their photo-redox behaviors. The complexes selectively recognize fluoride (F^-) among various anions through a combination of various non-classical interactions such as $\text{CH}\cdots\text{F}$ hydrogen bonding, $\text{CH}-\pi$, anion- π , to name a few. DFT calculations further elucidate the receptor-anion interactions. The complexes also undergo reversible trans-cis isomerization under visible and UV light, with the cis-form exhibiting reduced anion interaction compared to the trans-form.

Chapter 5 explores the aggregation-induced modulation of room temperature luminescence of $[(\text{tpy-PhCH}_3)\text{Ru}(\text{tpy-pvp-X})](\text{ClO}_4)_2$ using various solvent mixtures. The complexes exhibit both aggregation-induced emission enhancement (AIEE) and aggregation-caused quenching (ACQ), depending on the solvent combination. Trans \rightarrow cis photoisomerization of the aggregated complexes occurs under visible light but at a slower rate compared to the non-aggregated forms.

Chapter 6 explores the synthesis, characterization and investigation of the photophysical properties of a series of homoleptic Os(II) complexes of the type $[\text{Os}(\text{tpy-pvp-X})_2](\text{ClO}_4)_2$. They exhibit reversible trans-trans to cis-cis photoisomerization under alternative treatment with visible and UV light. Substantial enhancement of the rate of photo-isomerization has been achieved upon oxidation with ceric ammonium nitrate (CAN) as well as reduction with metallic sodium.

Chapter 7 deals with selective cation and anion sensing properties of $[\text{Os}(\text{tpy-pvp-X})_2](\text{ClO}_4)_2$ complexes. They can act as dual molecular sensors for fluoride (F^-) and mercury (Hg^{2+}) ions. The complexes selectively detect these ions through various non-classical interactions such as $\text{CH}\cdots\text{F}$ hydrogen bonding, $\text{CH}-\pi$, cation- π and anion- π . Light-induced trans-trans \rightarrow cis-cis photoisomerization of the stilbene unit alters sensing efficacy, with notable differences among the isomeric forms. Computational studies are also conducted to support experimental findings on ion-receptor interactions.

ACKNOWLEDGEMENTS

As I pen down these words, I find myself reflecting on the incredible journey that brought me here—a journey filled with moments of discovery, challenge, perseverance, and growth. This thesis is not just the culmination of years of research, but a testament to the unwavering support, encouragement, and kindness of so many who have shaped this path.

First and foremost, I owe my deepest gratitude to my supervisor, Professor Sujoy Baitalik, whose wisdom, patience, and indomitable support has been the foundation of this research. More than just an advisor, he has been a mentor who has instilled in me the values of perseverance, curiosity, and academic integrity. His encouragement in moments of doubt and rigorous attention to detail has shaped not just this work, but also the scientist I have become. Every discussion, every suggestion, and every challenge he presented became a stepping stone toward growth. I am truly fortunate to have had his mentorship, and this thesis stands as a testament to his invaluable influence on my journey.

I sincerely appreciate the Department of Chemistry, Jadavpur University, for providing an enriching environment that enabled me to carry out my research. I am also deeply grateful to the present Dean, Faculty Council of Science, Prof. Chittaranjan Sinha, the Head of the Department, Prof. Kajal Krishna Rajak and the Section-in-Charge, Prof. Partha Roy, whose support and guidance have played a crucial role in shaping this academic journey. To my research advisory committee member, Prof. Amit Majumder, I extend my sincere appreciation for his invaluable feedback, thought-provoking discussions, and his ability to challenge me in ways that have strengthened my research. Their expertise and encouragement have played a vital role in shaping this work. I wish to express my profound gratitude to Prof. Samarendra Bhattacharya, Prof. Nitin Chattopadhyay, Prof. Chittaranjan Sinha, Prof. Subrata Mukhopadhyay, Prof. Soumen Ghosh, Prof. Jnan Prakash Naskar, Prof. Mahammad Ali, Prof. Saurabh Das, Dr. Tapan Kumar Mondal, Dr. Bibhuti Bhusan Shaw, Dr. Partha Mahata and Dr. Ananya Bakshi for their kind cooperation and constant encouragement throughout my journey of research.

I am thankful to the State Government for providing the SVMCM fellowship to carry out my research work smoothly. I would also like to acknowledge DST for providing single crystal X-ray diffractometer in FIST and Time-Resolved Nanosecond Spectrofluorimeter in PURSE programme to the Department of Chemistry, Jadavpur University.

A special thanks to my former lab-mates Dr. Amit Chakraborty, Dr. Papri Mondal, Dr. Dinesh Maity, Dr. Manoranjan Bar, Dr. Poulami Pal, Dr. Animesh Paul, Dr. Shruti Mukherjee Dr. Sourav Deb and Dr. Anik Sahoo who have already completed their doctoral degree from our lab. I am also fortunate to have wonderful junior lab-mates Touseque Ahmed, Soumi Das, Sohini Bhattacharya, Raju Biswas, Tuhin Abedin and Sucheta Gorain who turned long days in the lab into a journey of shared successes, laughter, and growth. Science is never a solitary pursuit, and I am grateful for the brainstorming sessions, the troubleshooting marathons, and the countless cups of coffee that sustained us through late nights. This journey would not have been the same without them, and for that, I am truly thankful.

No words can truly express the depth of my gratitude to my family and my friends, whose love and unwavering support have been my greatest pillar of strength. To my incredible parents, Dr. Pranab Kumar Ganguly and Kakali Ganguly, your sacrifices, boundless encouragement, and steadfast belief in me have shaped every step of this journey. To my dearest sister, Moon, your constant support, patience, and warmth have been a source of comfort and motivation. Whether through heartfelt encouragement or playful teasing, you have filled my life with strength and joy.

To my beloved husband, Subhopriya, your endless love, constant support, and unshakable faith in me have been my greatest blessing. Through every challenge and triumph, you have stood by my side, lifting me with your encouragement and belief. I am truly fortunate to have you. With all my heart, I am also profoundly grateful for my loving in-laws, whose warmth, support, and heartfelt encouragement have enriched my journey with love, strength, and gratitude.

Lastly, to every person who has, in one way or another, contributed to this journey—whether through advice, encouragement, or simply by being there when I needed it most—thank you. This achievement is not mine alone; it is a reflection of all

the support, inspiration, and kindness I have been blessed to receive. I carry this gratitude with me, always.

Finally, with deepest reverence, I surrender in gratitude to the Almighty, whose divine benevolence, sagacity, and boundless grace have unwaveringly sustained my odyssey.

A handwritten signature in dark blue ink, reading "Tanusree Ganguly". The signature is written in a cursive, flowing style. A thin vertical line is positioned to the right of the signature.

(Tanusree Ganguly)

Department of Chemistry,
Inorganic Chemistry Section,
Jadavpur University,
Kolkata-700032, India

CONTENTS

	Page No.
Chapter 1: General Introduction and Brief Review on Photoisomerization and Stimuli-Responsive Behaviors of Luminescent Ru(II) and Os(II)-Polypyridine Complexes and Objective and Scope of the Present Work	1-82
1.1 General Introduction	1
1.2 An Overview of Photophysical Properties of Ru(II) and Os(II) Polypyridine Complexes	3
1.3 Electrochemical Behavior of Ru(II) and Os(II) Polypyridine Complexes	5
1.4 Comprehensive Review of Ruthenium (II) and Osmium (II) Complexes Derived from Poly-Pyridine Ligands	6
1.4.1 Common Pathway for Synthesis of Monometallic Complexes	6
1.4.2. A Brief Literature Analysis on Photophysical and Electrochemical Aspects.	6
1.5 Brief Survey on Photoisomerization Behaviors of Metal Complexes	19
1.6 Brief Review on the Aggregation Induced Emission Properties of Ligands and Metal complexes	31
1.7 Brief Review on the Non-Covalent (Anion- π and Cation- π) Interactions of Ligands and Metal complexes	40
1.8 Objective and Scope of the Present Work	47
1.9 References	55
Chapter 2: Synthesis and Manifold but Controllable Emission Switching of Stilbene-Appended Polyaromatic Terpyridine Derivatives via Aggregation and Trans-Cis Isomerization	83-121
2.1 Introduction	83
2.2 Experimental Section	85
2.2.1 Materials	85

2.2.2 Synthesis of the Compounds	85
2.2.3 Physical Measurements	86
2.2.4 Determination of Photoisomerization Rate Constants and Quantum Yields	87
2.2.5 Computational Studies	88
2.3 Results and Discussion	88
2.3.1 Synthesis and Characterization	88
2.3.2 Absorption and Emission Spectra	90
2.3.3 Aggregation-Induced Modulation of the Photophysical Properties	96
2.3.3.1 Concentration Dependent Studies	96
2.3.3.2 Aggregation Studies in Different Solvent Mixtures	98
2.3.4 Photo-isomerization of the Compounds in Their Non-Aggregated Forms	100
2.3.5 Photo-isomerization in the Aggregated Forms of the Compounds	107
2.4 Conclusions	112
2.5 References	113

Chapter 3: Synthesis, Characterization and Emission Switching Behaviors of Styrylphenyl-Conjugated Ru (II)-Terpyridine Complexes via Aggregation and Trans-Cis Photoisomerization 122-155

3.1 Introduction	122
3.2 Experimental Section	124
3.2.1 Materials	124
3.2.2 Synthesis of Metal Complexes	124
3.2.3 Instruments and Physical Methods	125
3.3 Results and Discussion	126
3.3.1 Synthesis and Characterization	126
3.3.2 Computational Investigations	127
3.3.3 Absorption Spectra	130
3.3.4 Luminescence Spectra	130
3.3.5 Electrochemistry	132
3.3.6 Aggregation-induced Modulation of the Emission Spectral Characteristics	134
3.3.7 Photoisomerization Behaviors	138
3.3.8 Photoisomerization in the aggregated forms	141

3.3.9 Accomplishment of the Metal Complexes Over their Ligand Precursors	144
3.4 Conclusions	145
3.5 References	146
Chapter 4: Luminescent Ruthenium-Terpyridine Complexes Coupled with Stilbene-Appended Naphthalene, Anthracene and Pyrene Motifs Demonstrate Fluoride Ion Sensing and Reversible Trans-Cis Photoisomerization	156-195
4.1 Introduction	156
4.2 Experimental Section	159
4.2.1 Materials	159
4.2.2 Synthesis of Metal Complexes	159
4.2.2 Instruments and Physical Methods	160
4.3 Results and Discussion	160
4.3.1 Synthesis and Characterization	160
4.3.2 Mass Spectra	160
4.3.3 NMR Spectroscopy	160
4.3.4 Absorption Spectra	162
4.3.5 Emission Spectra	163
4.3.6 Redox Properties	167
4.3.7 Anion Sensing Characteristics	168
4.3.8 Photo-Isomerization	181
4.3.9 Anion Sensing Characteristics of the Cis-form of the Complexes	185
4.4 Conclusions	187
4.5 References	188
Chapter 5: Modulation of Room Temperature Emission Characteristics of Heteroleptic Ruthenium-Terpyridine Complexes via Aggregation	196-220
5.1 Introduction	196
5.2 Experimental Section	198
5.2.1 Materials	198
5.2.2 Instruments and Physical Methods	199

5.3 Results and Discussions	199
5.3.1 Synthesis and Characterization	199
5.3.2 Computational Investigation	199
5.3.3 Aggregation-induced Modulation of the Emission	
Characteristics of the Complexes	199
5.3.4 Photoisomerization in the Aggregated Forms of the Complexes	207
5.4 Conclusions	209
5.5 References	211

**Chapter 6: Remarkable Increase in the Rate of Trans-Cis
Photoisomerization of Os(II)-Terpyridine
Complexes via Oxidation and Reduction** **221-264**

6.1 Introduction	221
6.2 Experimental Section	223
6.2.1 Materials	223
6.2.2 Synthesis of the ligands	223
6.2.3 Synthesis of the Metal Complexes	223
6.2.4 Instruments and Physical Methods	224
6.3 Results and Discussion	224
6.3.1 Synthesis and Characterization	224
6.3.2 Mass Spectra	225
6.3.3 NMR Spectra	226
6.3.4 Geometry Optimization of the Complexes via DFT	228
6.3.5 Absorption and Emission Spectral Characteristics	230
6.3.6 Electrochemical Behaviors	236
6.3.7 Photoisomerization Behaviors	238
6.3.8 Enhancement of Photoisomerization Rate via	
Chemical Oxidation and Reduction	245
6.4 Conclusions	252
6.5 References	253

**Chapter 7: Osmium-Terpyridine Complexes Linked with
Stilbene-Coupled Naphthalene, Anthracene,
and Pyrene Moieties Act as Multichannel Sensors
for F⁻ and Hg²⁺ via Non-Classical Interactions** **265-293**

7.1	Introduction	265
7.2	Experimental Section	268
7.2.1	Materials	268
7.2.2	Synthesis of the Metal Complexes	268
7.2.3	Instruments and Physical Methods	268
7.3	Results and Discussion	268
7.3.1	Anion Sensing Behaviors of the Complexes	268
7.3.2	Cation Sensing Behaviors of the Complexes	279
7.4	Conclusions	284
7.5	References	286

List of Publications

Chapter 1

**General Introduction and Brief Review on
Photoisomerization and Stimuli-Responsive
Behaviors of Luminescent Ru(II) and Os(II)-
Polypyridine Complexes**

and

Objective and Scope of the Present Work

1.1 General Introduction

Over the past few decades, there has been a significant surge in research endeavors focused on various critical domains such as solar energy conversion, artificial photosynthesis, photo-catalysis, photoactive DNA cleavage, and photo-switching.¹⁻¹¹ Design of molecular ensembles that are capable of responding to specific functions upon interaction with external stimuli (light, pH, other chemicals etc.) are widely utilized for fabricating the molecular devices.¹²⁻²¹ Given that light stands as one of the most environmental benign energy sources, the impulsion to harness its power has grown significantly. This drive has, in turn, spurred the development of light-responsive building materials.¹⁸⁻²¹ Polypyridine complexes featuring low spin d^6 metals, notably Ru(II) and Os(II), are quite desirable due to their thermal and photochemical stabilities along with remarkable photoredox behaviors which in turn can be precisely tuned via synthetic modification or using external stimuli.²²⁻²⁸ As a matter of fact, designing building blocks with tailored ligand architecture enables research in various applications like molecular sensors, switches, solar cells, and drugs.³¹⁻⁴⁴ Ru(II) and Os(II) complexes are often designed using bidentate {such as 2,2'-bipyridine (bpy) and 1,10-phenanthroline (phen)} and terpyridine-type {2,2':6',2''-terpyridine (tpy)} polypyridine ligands.^{22-30,45-50} While tpy complexes exhibit superior enantiomeric purity, their photophysical properties are often suboptimal to bpy complexes due to unfavorable energy level arrangements. Therefore, strategic design of tpy complexes is crucial to optimize the excited state energies and enhance their luminescence properties.⁴⁵⁻⁵⁰

The development of light-emitting metal complexes has become a prominent focus in scientific research due to their potential applications in diverse fields, including molecular sensors, bioimaging probes, optoelectronic devices, and photocatalysis.^{18-21,31-44} Pure organic moieties are highly luminescent in dilute solutions, but their luminescence weakens in concentrated solutions due to detrimental π - π stacking interaction which is termed as aggregation caused quenching (ACQ).⁵¹⁻⁵⁴ Additionally, they exhibit relatively narrow spectral and electrochemical window. To eliminate this issue, Tang and coworkers introduced a new phenomenon called Aggregation Induced Emission (AIE),⁵⁵ wherein addition of a non-solvent to dilute solutions causes them to aggregate thereby making them emissive at RT. To date, a plethora of research work has been dedicated to study the AIE effect on the organic moieties⁵⁵⁻⁷⁶ but very little work is done on their inorganic coordination complexes.⁷⁵⁻⁸⁴ Introduction of metal greatly improves the emission intensity and lifetime, resulting in improved sensitivity for sensors and bio-imaging.⁷⁷⁻⁸⁶ Thus, inclusion of an inorganic moiety

such as a metal greatly enhances the physicochemical properties of the complexes. Transition metal complexes using Cu(I), Zn(II), Ir(III), Pt(II), Ru(II) and Au(I) are mostly found to be AIE-active.⁸⁷⁻⁹³ Amongst these, the superior chemical and redox properties of Ru(II)-tpy based derivatives makes it a good candidate for the construction of light emitting diodes.

Another important aspect of material construction greatly relies on the ability to switch between their ground and excited state properties using external stimuli.⁹⁴⁻¹⁰⁵ Inclusion of a photoresponsive component to the complex backbone greatly improve their light-responsive behavior, leading to the formation of artificial photochemical molecular devices such as photo switches, optical materials and memory devices.⁹⁴⁻¹⁰⁵ Tailored design of ligands incorporating double bonds, like azo- and stilbene units, enhance both the electron delocalization and light responsive behavior of the resulting metal complexes.¹⁰⁶⁻¹¹³ These metal complexes are expected to exhibit light-induced trans-cis isomerization which significantly alters their photo-redox behaviors. Although the photo-isomerization behaviors of pure organic compounds are widely studied,¹⁰⁶⁻¹¹⁸ similar studies with metal complexes are relatively less.¹¹⁹⁻¹²⁶ It is to be noted that the isomerizable appended group(s) in the metal complexes are usually more constrained with involvement of numerous metal-centered excited states.

Ru(II) and Os(II) polypyridyl complexes consisting of aromatic and heteroaromatic moieties often offer various non-covalent interactions with suitable incoming species. These interactions comprise of hydrogen bonding, π - π stacking, CH- π , cation- π and anion- π interactions and have orchestrated immense attention in diverse fields of supramolecular chemistry and structural biology.¹²⁷⁻¹³⁷ Recognition of specific cations and anions through the intermediacy of various non-covalent interactions would significantly fuel the rapid development of the field.¹³³⁻¹³⁶ Customarily, the anion- π interactions are comparatively weaker than the cation- π interactions because of the larger van der Waals radii of anions.¹³⁸ In light of the omnipresence of ions in various chemical and biochemical systems, the current focus is also to exploit the vast potential of the cation- π and anion- π interactions to fabricate highly selective ion sensors for their utilization in fields of sensors, catalysts, switches and many more.

In the present dissertation, we have targeted to design homo- and heteroleptic terpyridine complexes of Ru(II) and Os(II) having photo-responsive styrylbenzene units. Incorporation of styrylbenzene unit is expected to amplify the emission behaviors due to enhanced conjugation at the 4'-position of the terpyridine ligand. Efforts will also be given to

fine-tune the photophysics of the complexes upon inducing aggregation by the use of various binary solvent mixtures. These sort of metal complexes containing styrylbenzene units are expected to display reversible trans-cis isomerization with significant alteration of photo-redox properties which in turn could be useful for the fabrication of photoswitches. Another important aspect of the present work includes the selective recognition of both cations and anions through the intermediacy of various non-covalent interactions. The ultimate goal of the work is construct stimuli-responsive multi-channel molecular sensors and switches.

1.2 An Overview of Photophysical Properties of Ru(II) and Os(II) Polypyridine Complexes

Polypyridine-based Ru(II) and Os(II) complexes have attracted widespread interest for their diverse applications in advanced materials and molecular technologies.¹⁶⁻²¹ Polypyridine ligands commonly feature bidentate chelating units such as 2,2'-bipyridine (bpy) and 1,10-phenanthroline (phen) or tridentate frameworks like 2,2':6',2''-terpyridine (tpy). These coordinating moieties are often integrated with diverse aromatic or heteroaromatic spacers to fine-tune the structural topology and electronic properties of metal-ligand assemblies.^{19,22-30,139-148} The field of bipyridine and oligopyridine coordination chemistry has seen remarkable advancements, largely initiated by the discovery of the exceptional photosensitizing ability of $[\text{Ru}(\text{bpy})_3]^{2+}$, which subsequently led to the development of a wide range of tris-bidentate Ru(II) complexes with tailored photophysical and electronic properties.^{22-30,139-148} The characteristic features of the complexes usually consist of strong absorption throughout the entire UV-vis region which can be modulated by proper ligand design. They exhibit spin-allowed metal ($d\pi$) to ligand (π^*) charge transfer ($^1\text{MLCT}$) bands in the visible region. Furthermore, Os(II) complexes display a weak and broad band at longer wavelength region attributed to spin forbidden ^1GS to $^3\text{MLCT}$ transition.^{140-145,149} The next higher energy intense bands are intraligand (ILCT) as well as π - π^* bands mainly due to the coordinated polypyridine units.^{22-30,40-50,139-148}

Excitation of the complexes at their lowest energy absorption band promotes them to their $^1\text{MLCT}$ excited state which then undergoes very fast intersystem crossing to either ^3MC or $^3\text{MLCT}$ state(s) or both. Thereafter, they deactivate to the ground state either through radiative ($^3\text{MLCT}$) or non-radiative (^3MC) decay process. Each of the intramolecular decay processes has its own respective rate constant (k_r), excited state lifetime (τ) and quantum yield (Φ) values. The energy difference between the triplet MLCT and MC states is crucial in

determining the luminescence properties of the resulting metal complexes. Smaller energy gap between the two above-mentioned states, usually caused by weak ligand field strength, leads to an increase in population of the ^3MC state and poor emission characteristics.

Ru(II) complexes with bidentate ligands exhibit superior luminescence due to suitable disposition of $^3\text{MLCT}$ state, resulting in an excited state lifetime of 860 ns and a quantum yield of 0.062 for $[\text{Ru}(\text{bpy})_3](\text{PF}_6)_2$ in MeCN.^{22,150} However, tris(bpy) complexes inherently leads to a mixture of Δ and Λ diastereomers, making their separation challenging. In contrast, bis-terpyridine complexes, when substituted at the 4'-position, adopt achiral rod-like structures. However, their inherently weak luminescence and extremely short excited-state lifetimes, attributed to the unfavorable bite angle of terpyridine, hinder their efficiency as photosensitizers. These observations motivates us to design Ru(II) complexes with bis-tridentate skeletons having long-lived excited states.^{48,151} Several synthetic approaches have been adopted to enlarge the energy barrier between the luminescent $^3\text{MLCT}$ and non-luminescent ^3MC states. The energy of $^3\text{MLCT}$ state could be lowered upon incorporation of electron-withdrawing group-,¹⁵³⁻¹⁵⁸ coplanar heteroaromatic motif,¹⁵⁹⁻¹⁶² organic chromophores,¹⁶³ or by the destabilization of ^3MC level so as to enhance the donating capacity of the ligand through the use of carbanionic aromatic units (cyclometalating ligands).¹⁶⁴⁻¹⁶⁸ Another method is the introduction of auxiliary chromophores onto the tpy unit that are isoenergetic to the $^3\text{MLCT}$ state. Polyaromatic moieties such as anthracene, naphthalene and pyrene consists of a $^3(\pi-\pi^*)$ state that is quasi-isoelectronic to the $^3\text{MLCT}$ state of the Ru-terpyridine complex.^{47,169-170} Upon excitation, reversible intercomponent energy transfer between $^3\text{MLCT}$ and $^3(\pi-\pi^*)$ enables adjacent polyaromatic chromophores to function as energy reservoirs. This facilitates the repopulation of the emissive $^3\text{MLCT}$ state, effectively delaying emission and prolonging the excited-state lifetime. Addition of a spacer group such as phenyl or styrylbenzene unit to the Ru-tpy complex further aids to make the $^3\text{MLCT}$ - $^3\pi-\pi^*$ equilibrium more facile.

Os(II) polypyridyl complexes have almost similar photophysical properties except that the larger 5d orbitals of the metal induces a red shift in absorption and emission spectra due to comparatively stronger spin-orbit coupling (SOC) effects.^{25-28,41-42,143-145} Despite that, Os(II) diimine complexes have shorter luminescence lifetimes than Ru(II) counterparts because of the energy gap law. On the contrary, Os-terpyridine derivatives have quite longer (~50-500 ns) lifetime than their Ru-terpyridine analogues despite low-lying emissive $^3\text{MLCT}$ state. Both Ru(II) and Os(II) polypyridine complexes emit above 600 nm from the $^3\text{MLCT}$

state and may stretch upto NIR region, with lifetimes in the nanosecond to microsecond range. A generalized state diagram (Figure 1.1) exhibits the photophysical behavior of Ru^{II} and Os^{II} diimine and triimine complexes and the photophysical data of representative Ru(II) and Os(II) complexes are summarized in Table 1.1.

1.3 Electrochemical Behavior of Ru(II) and Os(II) Polypyridine Complexes

The Ru(II) and Os(II) polypyridine complexes exhibit rich electrochemical behaviors that are both reversible and tunable in nature. Mononuclear complexes usually show one reversible oxidation peak in the positive potential region and multiple reversible reduction peaks in the negative potential region. The highest occupied molecular orbitals (HOMO) is localized mainly on the metal centre indicating oxidation from Ru(II)/Os(II) to Ru(III)/Os(III), while the lowest unoccupied molecular orbitals (LUMO) are mostly pyridine based, indicating reduction.¹²³ The Os(II) complexes usually display oxidation peak at lower potential relative to their Ru(II) analogues, mostly due to higher stability of third row transition metal ions over the second row in higher oxidation states.

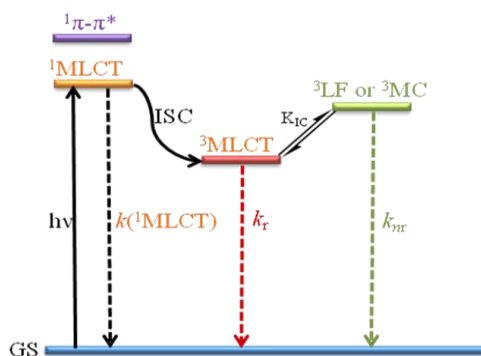


Figure 1.1

Table 1.1. Photophysical properties of bpy- and tpy based Ru(II) and Os(II) complexes in CH₃CN at 298 K.

Complex	$\lambda_{\max}^{\text{abs}}/\text{nm}$ (¹ MLCT)	$\lambda_{\max}^{\text{em}}/\text{nm}$ (³ MLCT)	τ/ns	Ref
[Ru(bpy) ₃] ²⁺	454	620	800	22, 28
[Ru(tpy) ₂] ²⁺	475	628	< 5	22, 28
[Os(bpy) ₃] ²⁺	480	715	19	22, 28
[Os(tpy) ₂] ²⁺	477,657	718	269	22, 28

1.4 Comprehensive Review of Ruthenium (II) and Osmium (II) Complexes Derived from Poly-Pyridine Ligands

A diverse array of mono- and multimetallic ruthenium and osmium complexes with tridentate ligands, detailing their synthesis, structural attributes, and physicochemical properties, have been reported globally. This dissertation focuses on the synthesis and physicochemical properties of monometallic ruthenium and osmium complexes coordinated to tridentate ligands.

1.4.1 Common Pathway for Synthesis of Monometallic Complexes: Synthetic strategies of homo- and heteroleptic monometallic complexes of ruthenium and osmium with tridentate polypyridine ligands are well documented in literature.^{30,48,171-173} Metal complexes of the type $[M(tpy)_2]^{2+}$ ($M = Ru$, and Os) typically exhibit a distorted octahedral geometry as confirmed by single crystal X-ray diffraction studies.¹⁷² The synthesis strategy for homo- and heteroleptic complexes is illustrated in the Figure 1.2. The purification of the complexes is usually done by column chromatography and recrystallization techniques.

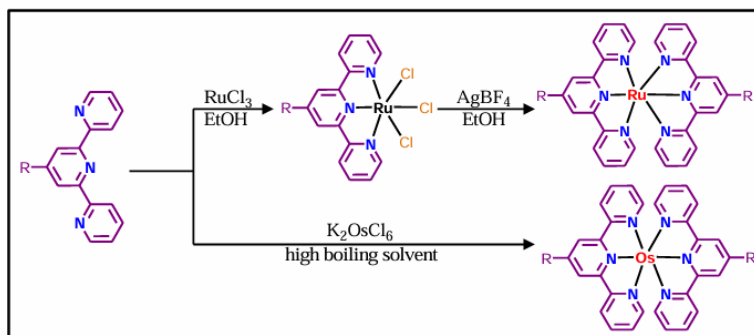


Figure 1.2

1.4.2. A Brief Literature Analysis on Photophysical and Electrochemical Aspects.

Terpyridine complexes of Ru(II) and Os(II) are of interest due to their achiral linear structures, despite their inferior excited state properties.^{19-21,28,30,33,159-162} Researchers have sought to enhance their photophysical and electrochemical characteristics by introducing substituents that facilitate electron delocalization in the complex backbone.^{153-156,160-168,174-179} Complexes with enhanced photo-redox capabilities can serve as building blocks for light-harvesting assemblies and supramolecular structures.¹⁴¹⁻¹⁴⁴ These terpyridine-based complexes have been studied for use in molecular machines, dye-sensitized solar cells, optical sensors, and biological applications.^{9-21,145,149,180-183} This dissertation reviews the physicochemical properties of various monometallic complexes of ruthenium and osmium.

In their recent reports, Wang and coworkers reveal how the luminescence lifetime significantly affects the reactivity of triplet state in both energy and electron transfer reactions.¹⁸⁴ By incorporating two phenyl anthracene moieties into the $[\text{Ru}(\text{dqp})_2]^{2+}$ ($\text{dqp} = 2,6\text{-di(quinolin-8-yl)pyridine}$) complex, the Ru^{II} triad was developed with a luminescence lifetime of up to 115 μs (Figure 1.3). This Ru^{II} triad shows greater efficiency in triplet-triplet energy transfer (TTET) than the archetypical reference Ru^{II} complex. It enables red-to-blue photon upconversion with a large pseudo anti-Stokes shift of 0.94 eV and an upconversion efficiency of about 0.8% in aerated conditions, increasing to 2% with a more efficient annihilator (An-TIPS). This triad is the first Ru^{II} complex known for red-to-blue upconversion, comparable to Os^{II} and Pt^{II} -based sensitizers. In photoredox catalysis, the Ru^{II} triad demonstrates higher oxidative quenching efficiency than the reference complex due to its longer luminescence lifetime, making it highly reactive in excited-state electron transfer. This reactivity leads to significantly faster photopolymerization of acrylate and acrylamide monomers under red light and aerobic conditions, suggesting its potential for applications like 3D printing.

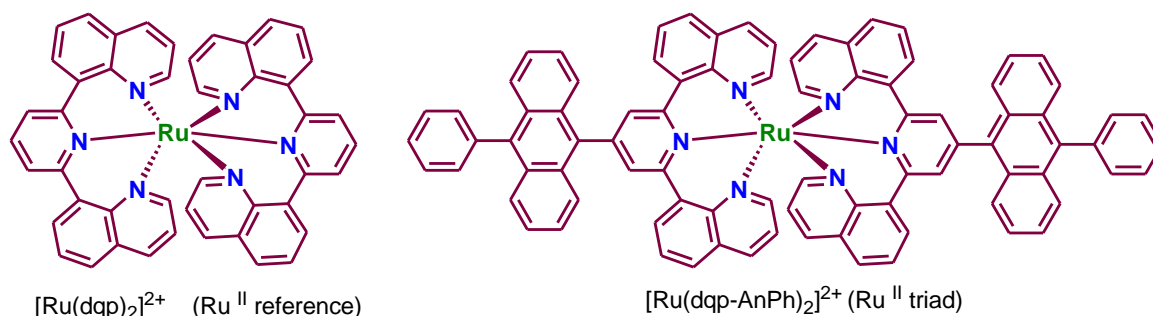


Figure 1.3

Berlinguette et al. presented the synthesis and characterization of a series of heteroleptic ruthenium(II) complexes with a substituted 2,2':6',2''-terpyridine (terpy) ligand, (Figure 1.4) which show long excited-state lifetimes in the microsecond range at room temperature.¹⁷⁹ This is due to a strongly σ -donating, weakly π -accepting tridentate carbene ligand ($\text{C}^{\wedge}\text{N}^{\wedge}\text{C}$) adjacent to terpy, which maintains significant separation between the ligand field and metal-to-ligand charge transfer (MLCT) states while preserving high $^3\text{MLCT}$ energy. These lifetimes surpass those of $[\text{Ru}(\text{terpy})_2]^{2+}$ by four orders of magnitude. Electrochemical analysis shows shifts in HOMO and LUMO energies, while time-dependent DFT calculations reveal good agreement with experimental data, indicating potential applications in energy transfer processes in biological systems and materials science.

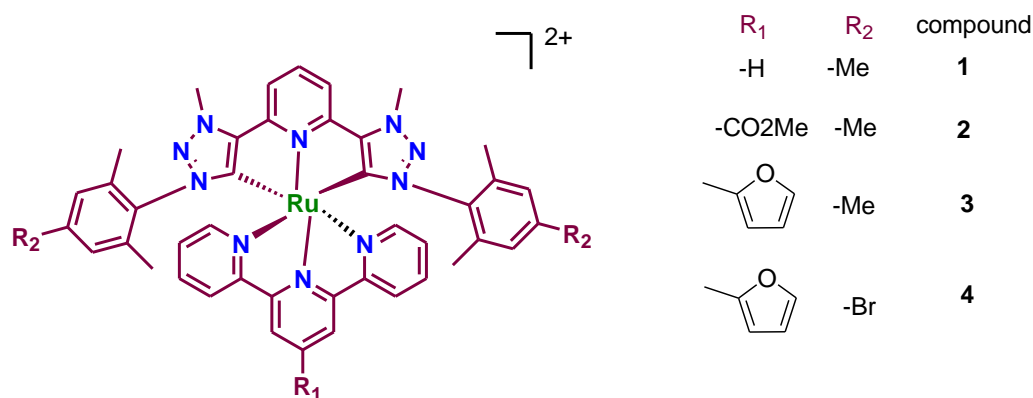


Figure 1.4

Hanan and Kurth explored the effects of N-methylation on the electronic and photophysical properties of both heteroleptic (**1** and **3**) and homoleptic (**2** and **4**) Ru(II) bis-terpyridine complexes,^{7,185} specifically focusing on the ligand 4'-(4-bromophenyl)-4,4'':4'',4'''-dipyridinyl-2,2':6',2''-terpyridine (Bipytpy). The first reduction of the methylated complexes occurs at the pyridinium site, identified as a multi-electron process (Figure 1.5). After N-methylation, these complexes show increased luminescence quantum yields and extended excited-state lifetimes; however, they are ineffective as photosensitizers (except for the parent complex **1**) for hydrogen evolution due to decomposition likely caused by the loss of methyl groups. The photophysical properties of both heteroleptic and homoleptic complexes are similar, as confirmed by TD-DFT calculations. Additionally, the study finds that homoleptic complexes are harder to oxidize yet easier to reduce compared to their heteroleptic counterparts, highlighting their distinct electrochemical behavior.

Additionally, Kurth and Hanan presented a series of non-symmetric 2,6-di(pyridin-2-yl)pyrimidine ligands with different pyridine substituents (Figure 1.6) and their corresponding Ru(II) complexes.¹⁸⁶ These complexes exhibit improved photophysical and electrochemical properties due to the pyrimidine ring, which stabilizes the lowest unoccupied molecular orbital (LUMO), leading to red-shifted emission and longer excited-state lifetimes. This makes them more effective for photocatalytic hydrogen production under blue and red light compared to traditional bis(terpyridine) Ru complexes. However, while these new complexes show higher activity, they are less stable, likely due to an additional decomposition pathway in the reduced state. A small shift in reduction potential significantly affects hydrogen evolution performance. They also examined the effect of pyridine substituents at different positions, with time-dependent density functional theory, revealing that those at the 4-pyrimidine position have the most significant influence on the photophysical and electrochemical properties of the complexes.

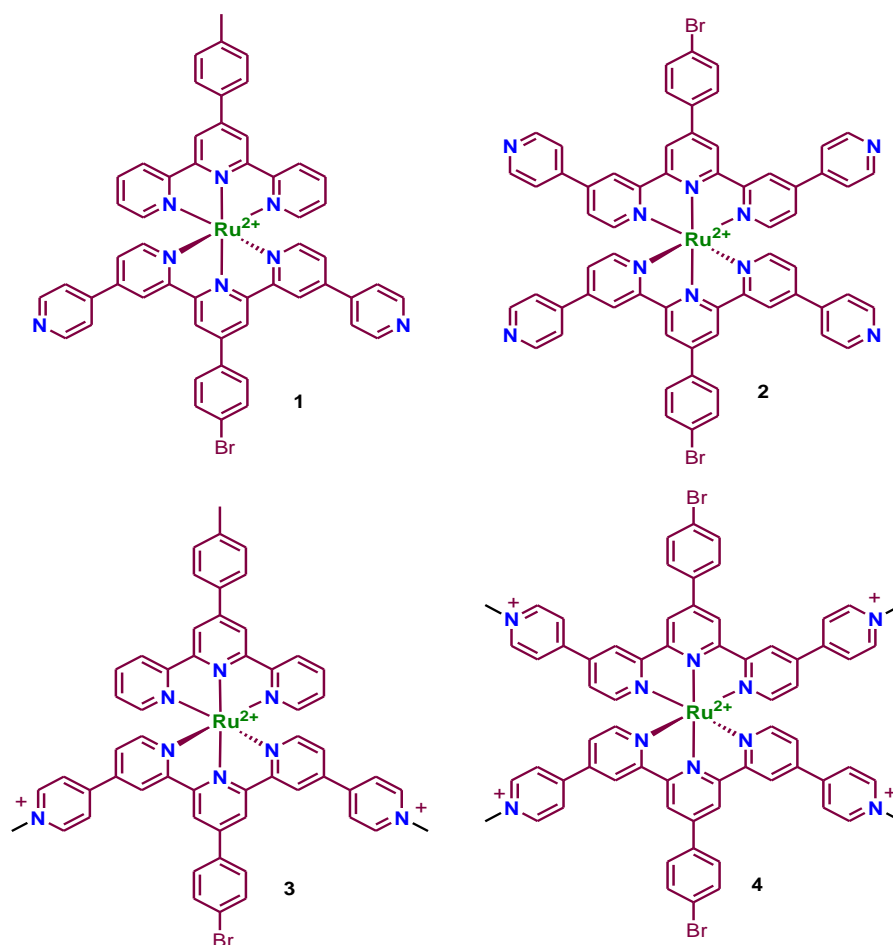
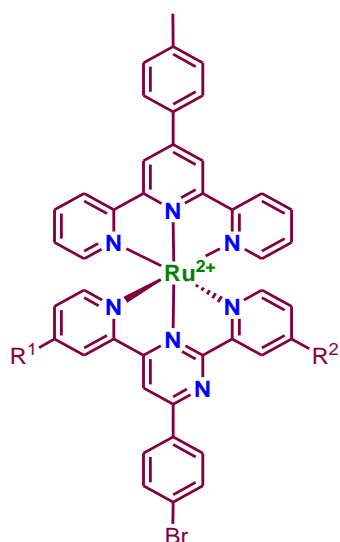


Figure 1.5



- Ru1:** $R^1=H$, $R^2=H$; 86%
Ru2: $R^1=4\text{-pyridine}$, $R^2=H$; 32%
Ru3: $R^1=H$, $R^2=4\text{-pyridine}$; 49%
Ru4: $R^1=4\text{-pyridine}$, $R^2=4\text{-pyridine}$; 18%

Figure 1.6

They also explored the spectroelectrochemical properties of iron and ruthenium bis-terpyridine complexes featuring pyridinium units, serving as models for supramolecular polymers (Figure 1.7).¹⁸⁷ They synthesized monotopic and ditopic terpyridine ligands,

creating both mononuclear complexes and metallo-supramolecular polyelectrolytes (MEPEs). UV-vis spectroscopy revealed that the mononuclear complexes exhibited similar absorption characteristics to the MEPEs. Additionally, all the complexes and MEPEs demonstrated electrochromic properties. However, only the MEPEs could be deposited to different substrates using a layer-by-layer method, making them suitable for electrochromic device applications. Due to poor solubility of Ru-L2-MEPE, characterization in solution state was challenging, thus mononuclear complexes were used to model MEPE properties, providing a simpler way to study these systems and aiding in the development of advanced metallo-supramolecular materials for future applications.

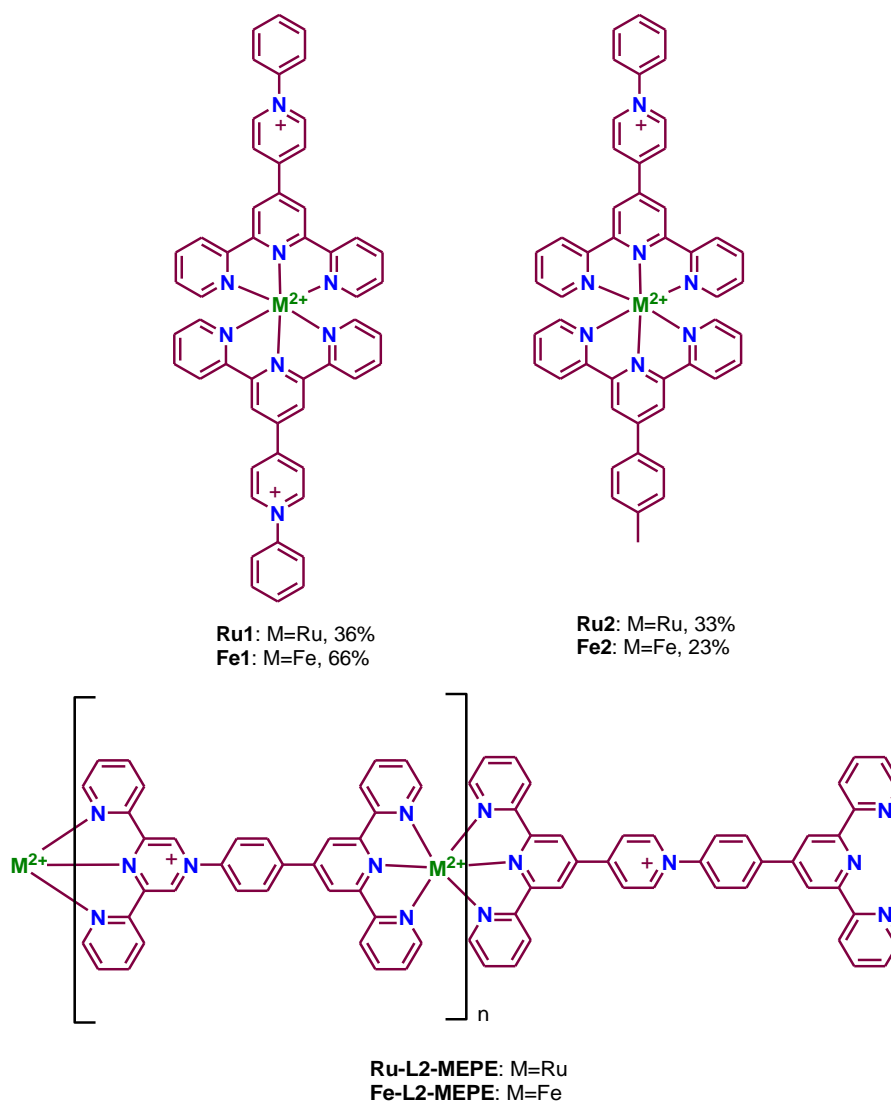
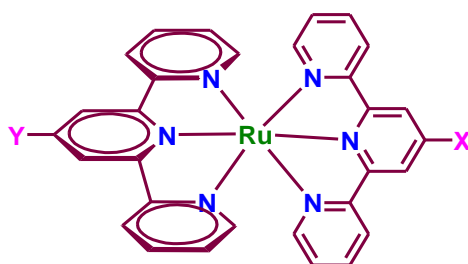


Figure 1.7

Balzani and Constable's research explored the luminescent properties of $[Ru(tpy-X)(tpy-Y)]^{2+}$ metal complexes, focusing on the effects of electron-withdrawing and electron-donating groups (X and Y) attached to the 4' position of the terpyridine (tpy) ligand (Figure

1.8).^{156,188} Their findings revealed that both the absorption and emission maxima of these complexes were red-shifted compared to the parent $[\text{Ru}(\text{tpy})_2]^{2+}$ complex, regardless of the substituents. Complexes with electron-withdrawing groups exhibited higher emission quantum yields and longer luminescence lifetimes, while those with electron-donating groups showed the opposite. Luminescence lifetimes ranged from 0.2 to 50 ns at room temperature and 1 to 10 μs at 77 K, depending on the solvent and substituents. A strong correlation was found between emission energies, redox potentials, and Hammett σ parameters, with electron-withdrawing groups stabilizing ligand-based LUMOs while electron donors destabilizing HOMOs. Further studies by Hanan demonstrated that substituting strong electron-withdrawing groups such as CN and MeSO_2 significantly increased the lifetimes of Ru-tpy complexes ($\tau = 25\text{--}50$ ns).



X	Y	τ/ns (298 K)
MeSO_2	MeSO_2	25.0
OH	MeSO_2	50.5
CN	CN	50.0
CN	H	75.0
H	MeSO_2	36.0
Ph	Ph	1.0
Cl	EtO	0.2
OH	Ph	0.4
H	H	0.25
Cl	H	0.7
Cl	Cl	0.2

Figure 1.8

Baley et al. investigated the addition of furyl, pyrrolyl, thienyl, and bithienyl groups to the 4'-position of terpyridine,¹⁷⁴ and found out the enhanced excited state behaviors of their Ru(II) complexes (Figure 1.9). These five-membered heterocycles stabilize the $^3\text{MLCT}$ state by extending electron delocalization, thereby increasing the energy gap between the emissive $^3\text{MLCT}$ and non-emissive ^3MC states. This leads to improved luminescence, with the bithienyl-substituted complex showing a 100-fold increase in emission quantum yield compared to the parent $[\text{Ru}(\text{tpy})]^{2+}$ complex.

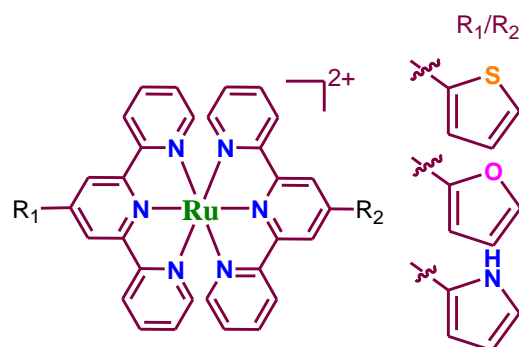
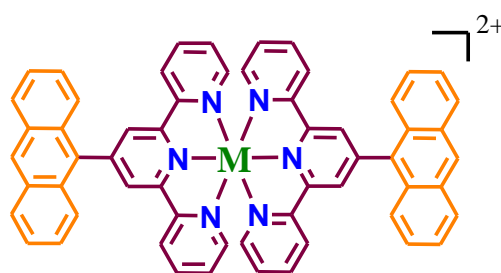


Figure 1.9

Maestri and Balzani synthesized homoleptic Ru(II) and Os(II) complexes featuring an anthracene unit at the 4'-position of the terpyridine framework¹⁸⁹ (Figure 1.10). Unfortunately, these complexes are non-emissive at room temperature, attributed to energy transfer from the Ru-tpy-derived ³MLCT state to the non-emissive triplet state of anthracene (³An) moiety. Similarly, Os(An-tpy)₂²⁺ demonstrated excited-state behavior very much akin to Os(tpy)₂²⁺, since the ³MLCT state in Os-terpyridine complexes remains the lowest emissive state, owing to the expanded energy gap between the MC and MLCT states.



M = Ru(II), Os(II)

Figure 1.10

Campagna and Hanan designed Ru-terpyridine complexes with anthracene units to improve excited-state properties by linking Ru(II) complexes with chromophores whose excited states are isoenergetic with the ³MLCT of Ru(II). They developed both homo- and heteroleptic Ru(II) complexes using pyrimidyl-terpyridine ligands attached to anthracene¹⁷⁵ (Figure 1.11a-b). Additionally, Ru(II) complexes with a pyrimidyl-tpy unit for electron delocalization and an anthryl-terpyridine unit as an energy reservoir (Figure 1.11c)¹⁷⁶ were created. These highly emissive complexes show long-lived bi-exponential decay, with the longer component (402-1806 ns) due to equilibration between ³MLCT and ³An states.

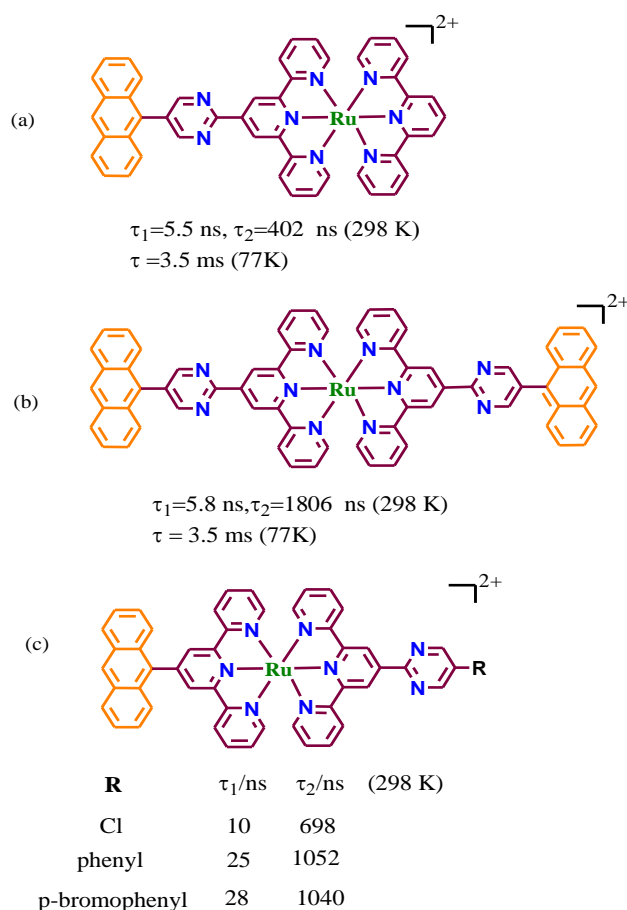


Figure 1.11

In a systematic investigation of luminescent bis(terdentate) osmium(II) complexes, Elliott and coworkers identified a crucial reversal in photophysical tuning linked to the stabilization of the ligand-based lowest unoccupied molecular orbital (LUMO).¹⁹⁰ This stabilization caused blue shifts in optical absorption and emission bands. The complexes, including variants $[\text{Os}(\text{N}^{\wedge}\text{N}'^{\wedge}\text{N}'')_2]^{2+}$ (**Os1** to **Os6**), exhibited phosphorescence from orange to near-IR regions (Figure 1.12). Notably, replacing pyridine with the stronger π -accepting pyrazine in **Os2** resulted in a 55 nm red-shift, while **Os3** experienced an additional 107 nm red-shift. **Os4**, however, showed no further red-shift. The donor arrangement in **Os5** yielded an expected red-shift, whereas **Os6** experienced a blue-shift due to the incorporation of a second pyrazine donor. Electrochemical studies confirmed that pyrazine incorporation stabilizes both the ligand's LUMO and the metal's highest occupied molecular orbital (HOMO), resulting in coincident emission maxima for **Os3** and **Os4**, while **Os6** displayed a blue-shift. This study highlights the complicated interplay in photophysical tuning, providing insights into emission adjustments in simple ligand structures.

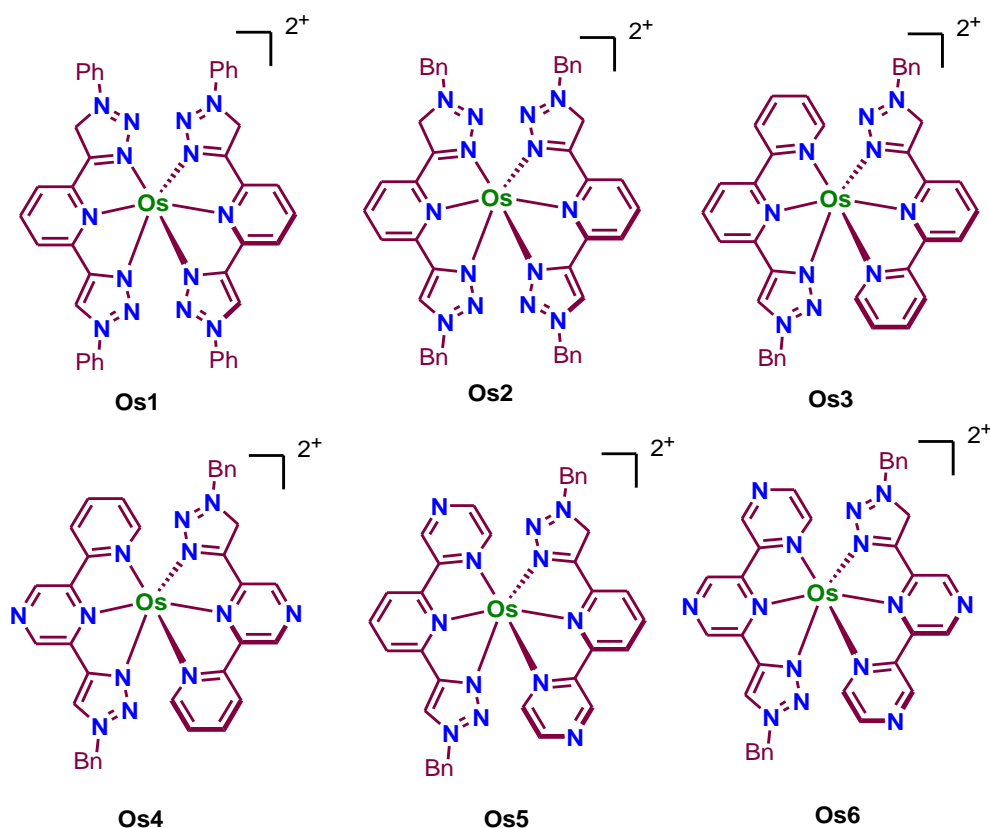


Figure 1.12

Kimizuka and team explored the relationship between the structure of Os(II)/ Ru(II) bis(terpyridine) complexes combined with perylenyl groups and their excited-state lifetimes to elucidate the heavy-atom effect on attached perylene chromophores (Figure 1.13).¹⁹¹ A comparison of phosphorescence lifetimes reveals that incorporating a twisted phenylene bridge into the perylene-Os complex ($[\text{Os}(\text{petpy})_2]^{2+}$) increases the excited-state lifetime by an order of magnitude with respect to its parent $[\text{Os}(\text{tpy})_2]^{2+}$ complex. Furthermore, $[\text{Os}(\text{peptpy})_2]^{2+}$ and meta-phenylene bridged ($[\text{Os}(m\text{-peptpy})_2]^{2+}$) complexes significantly extended their triplet lifetime to 24 and 81 μs , respectively, the later being over 400 times longer than that of $[\text{Os}(\text{tpy})_2]^{2+}$. This extended lifetime is due to the reduced electronic interaction between the Os complex and the perylene moiety, effectively suppressing the heavy-atom effect on perylene and retaining its intrinsic long excited-state lifetime. Additionally, this design protocol minimizes the energy loss by optimizing the energy gap between excited states and suppressing thermal deactivation to short-lived states. The findings suggest that careful manipulation of the triplet energy levels and bridge structure can yield highly efficient, long-lived triplet sensitizers. Replacing Os(II) with Ru(II) further

lengthens the excited-state lifetime, confirming the significant role of the metal center in influencing the triplet excited state.

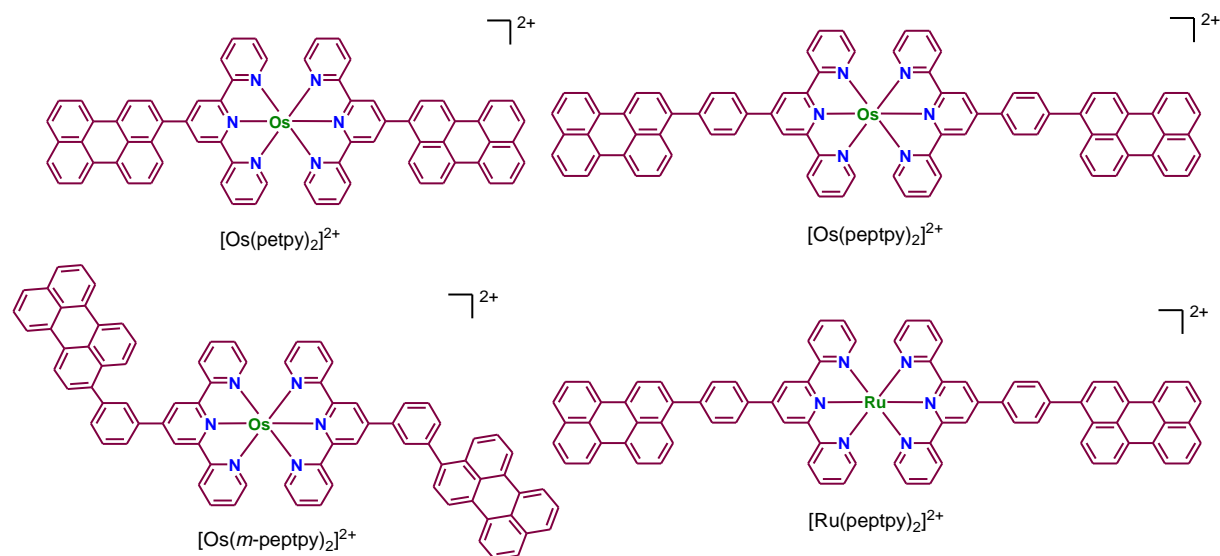


Figure 1.13

Harriman and colleagues examined the photophysical properties of Ru(II)-terpyridine complexes featuring an ethynylene substituent and focused on their temperature-sensitive emission spectral behaviors. The complexes exhibit a pronounced MLCT absorption near 490 nm and emit at around 680 nm in butyronitrile at room temperature (Figure 1.14a).⁹⁵ Notably, as temperature decreases, both luminescence intensity and quantum yield significantly increases. In a related study, they incorporated a hydroquinone unit into the Ru(II)-tpy-phenylethynyl moiety to modulate its luminescence properties (Figure 1.14b,c).¹⁹² Excitation at the MLCT band in these complexes generates a triplet state, which becomes delocalized onto the tpy-phenylethynyl moiety. The excited-state lifetime of the complex is approximately 46 ns, significantly increasing with a decrease in temperature. However, upon the oxidation of hydroquinone to benzoquinone, an electron is promoted from the ³MLCT state to the quinone moiety, resulting in a reduction of the excited-state lifetime to 190 ps, accompanied by emission quenching.

Baitalik and group reports three Ru(II)-terpyridine complexes (**1-3**) featuring a terpyridyl-imidazole ligand (tpy-HImzPh₃Me₂) that exhibit room-temperature luminescence with lifetimes ranging from 2.3 to 43.7 ns (Figure 1.15).¹⁹³ Protonation of the imidazole nitrogen(s) with perchloric acid significantly enhances emission intensity, quantum yield, and emission lifetime, with lifetimes increasing by up to 80 times compared to their free forms.

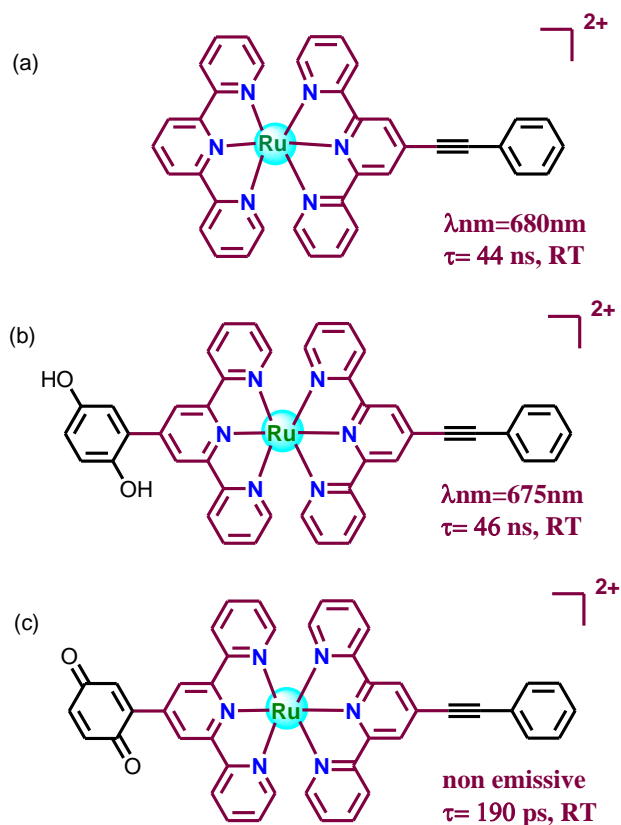


Figure 1.14

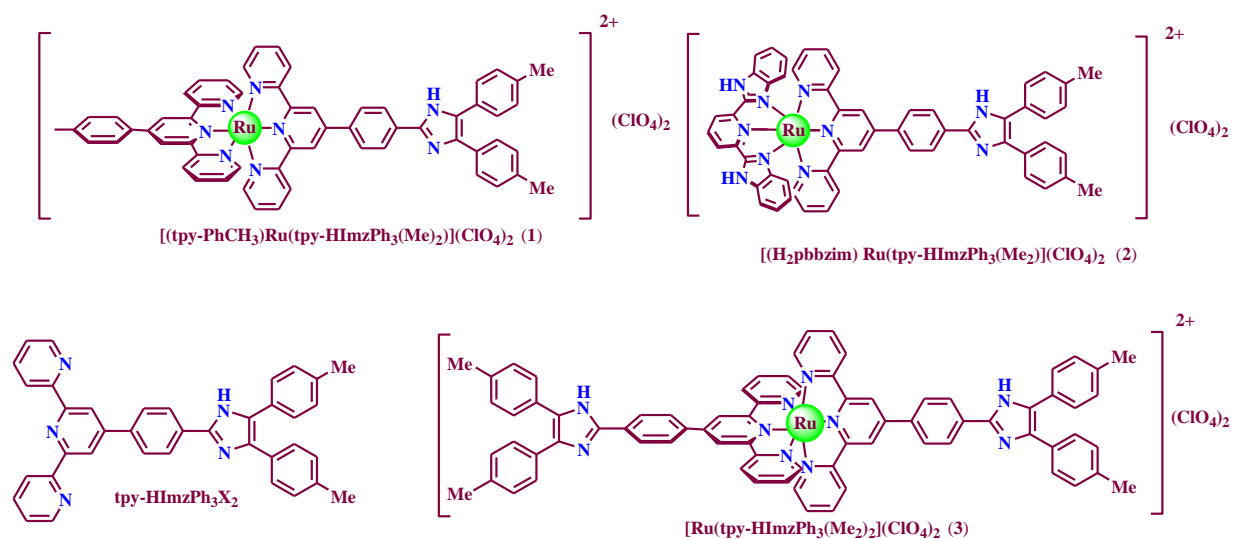


Figure 1.15

This enhancement is attributed to a higher thermal barrier for relaxation and increased energy separation between the emitting $^3\text{MLCT}$ and non-emitting ^3MC states. Additionally, the complexes demonstrate selective recognition of cyanide ions (CN^-) in water with a detection

limit as low as 10^{-8} M, achieving notable modulation of optical and photophysical properties through ligand perturbation.

Baitalik *et al.* also examined a series of trimetallic complexes of Fe(II), Ru(II), and Os(II) linked by a conjugated heteroditopic bipyridine-terpyridine type bridge, designed as light-harvesting antennae.¹⁹⁴ These complexes feature two Ru(II) peripheral units transferring energy to a central Fe(II) or Os(II) energy sink, with strong UV-visible absorption and luminescence at room temperature (Figure 1.16). Ultrafast energy transfer ($>10^{-12}$ s⁻¹) occurs in RuOsRu with near-unity quantum yield, while RuFeRu and RuRuRu exhibit slower but effective energy transfer ($\sim 10^{-8}$ s⁻¹). Notably, the RuFeRu complexes produce long-lived Fe(II)-based excited states due to careful ligand design, and the Fe(II) center does not fully quench the Ru(II)-centered emission. Additionally, these complexes show reversible redox processes, positioning them as efficient light-harvesting systems and multilevel molecular electronic materials.

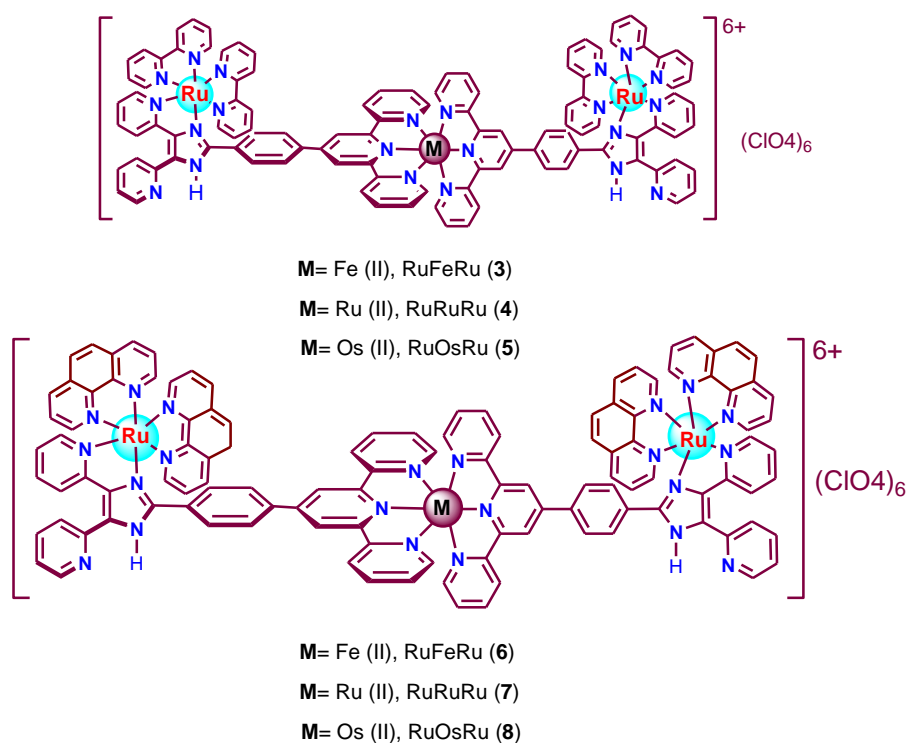


Figure 1.16

Baitalik and group reported a series of Ru(II)-terpyridine complexes functionalized with an anthraquinone moiety (Figure 1.17).¹⁹⁵ These complexes demonstrated exceptional luminescent properties at RT, with lifetimes ranging from 1.5 to 52.8 ns, depending on the solvent and ligand structure. The incorporation of the electron-withdrawing anthraquinone unit increased the acidity of the NH protons. Exploiting this feature, the complexes were

subjected to anion-induced modulation of their photophysical properties in both organic and aqueous media. Notably, the complexes exhibited remarkable selectivity for cyanide (CN^-) in aqueous solutions, with detection limits in the order of 10^{-8} M.

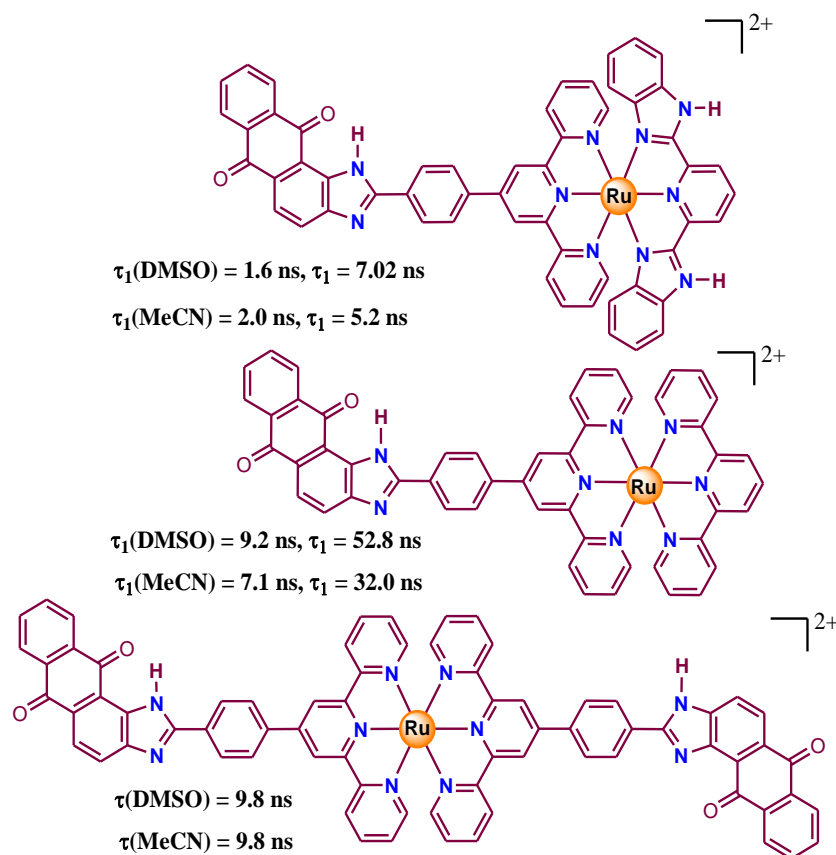


Figure 1.17

Baitalik and group also synthesized a series of bimetallic Ru(II)-Ru(II) and Ru(II)-Rh(III) complexes featuring a heteroditopic phenanthroline-terpyridine bridge (phen-Hbzim-tpy) linked via a phenyl-imidazole spacer (Figure 1.18) and consequently investigated their photo-redox behavior.¹⁹⁶ In Ru(II)-Ru(II) homodimeric complexes, red-shifted emission and ~99% quenching indicated efficient energy transfer from the excited $[(\text{bpy})_2\text{Ru(II)}(\text{phen-Hbzim-tpy})]$ to the $^3\text{MLCT}$ state of the tpy chromophore. The ΔG_{ET} lies in the range of -0.18 to -0.27 eV, while the rate constant (k_{en}) of the energy transfer vary between 6.4×10^6 and $5.7 \times 10^7 \text{ s}^{-1}$. The heterometallic Ru(II)-Rh(III) complexes, on the other hand, exhibit photoinduced electron transfer from the excited Ru^{II} moiety to the Rh^{III} -based unit. The ΔG_{ET} lies in the range of -0.23 to -0.32 eV and the rate constant of electron transfer (k_{et}) vary between $1.56 \times 10^5 \text{ s}^{-1}$ and $7.75 \times 10^6 \text{ s}^{-1}$.

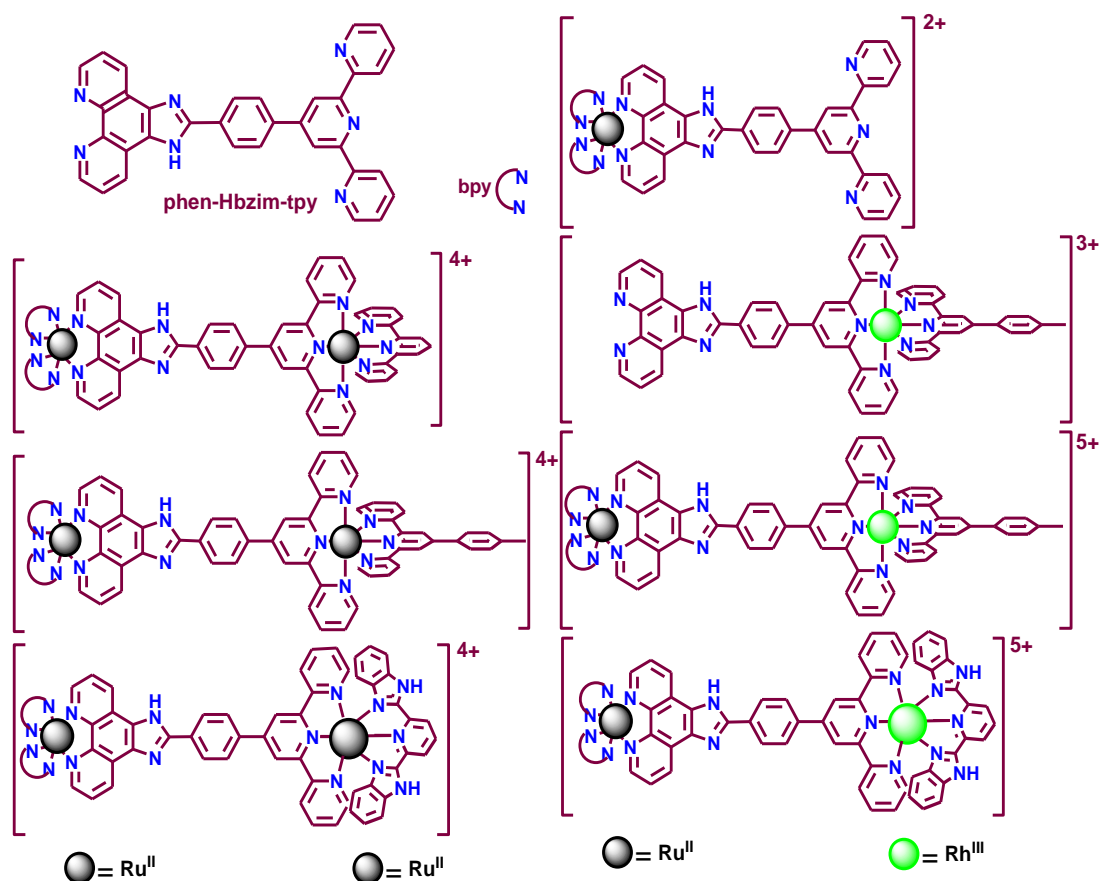


Figure 1.18

1.5 Brief Survey on Photoisomerization Behaviors of Metal Complexes

Molecular species that can reversibly change their physicochemical properties in response to external stimuli are highly valuable for potential applications in photoswitches and molecular memory.¹⁹⁷⁻²⁰¹ Recent investigations into high-density molecular data storage systems focus on devices that include simple on-off switches as well as those capable of performing logic operations.^{31-44,197-201} Since light is one of the most environment benign source of energy, molecular units that enable reversible changes in specific electronic properties in response to light are particularly promising for optical data storage materials.¹⁻²¹ Among photoswitchable materials, photochromic compounds that undergo light-induced reversible changes between two forms with distinct change in their spectral profiles are garnering significant interest for applications in optical data storage, optoelectronics, and display devices.^{7-11,20-22,34-38}

Double-bond compounds can isomerize between *trans* and *cis* forms under light,¹¹³⁻¹¹⁸ mechanical stress,²⁰² or electrostatic stimulation.²⁰³⁻²⁰⁴ This reversible process is notable for its impact on configurational change leading to switching in excited-state and photo-redox properties.²⁰⁵⁻²⁰⁸ Azobenzenes, stilbenes, spiropyrans, and diarylethenes are key photoactive and photochromic compounds that exhibit reversible photoreactions between two stable states in dilute solutions, making them valuable components for memory device applications.^{119-126,205-208} Photoisomerization is an important process that confers the photo-responsive functionality to the families of azobenzenes and stilbenes. The photoisomerization of various organic molecules, including azobenzene, stilbene, and spiropyrans, is well-documented in the literature.^{106-118,205-214} However, studies on the photoisomerization of metal complexes are relatively less explored compared to those of pure organic compounds. Various research groups such as Iha, Yam, Lees, Nishihara, Daniel and others have extensively investigated the photo-isomerization behavior of various transition metal complexes (Re, Co, Rh, Ir, Fe, Zn etc.) that are coupled to stilbene-, azo-, spirooxazine-, and diarylethylene units.^{119-126, 215-226} Although a good deal of work has already been carried out on the azo-appended bipyridine and terpyridine-based metal complexes, photoisomerization studies on stilbene appended metal complexes has been sporadically focused and barely well-documented.^{119-126, 215-226} This dissertation aims to explore the photoisomerization behaviors of terpyridine-based Ru(II) and Os(II) complexes possessing stilbene-type units in the complex architectures. To the best of our knowledge, no other group addresses the isomerization behavior of stilbene-conjugated terpyridine systems. Herein, we present a brief survey on the photophysical and photo-isomerization behaviors of some specific metal complexes that incorporate azo- or stilbene moiety in the complex architecture.

Nishihara and coworkers extensively investigated the *trans-cis* photoisomerization behaviors of a diverse spectrum of azobenzene-appended complexes with various transition metal ions.^{225,227-228} They investigated the photophysical, photochemical and *trans* to *cis* photoisomerization behaviors of mono-(tpy-AB) and di-nuclear (tpy-AB-tpy) Ru(II) and Rh(III) complexes derived from azobenzene-bridged terpyridine ligands (Figure 1.19). Both tpy-AB and tpy-AB-tpy ligands exhibited reversible *trans-cis* photoisomerization under UV (366 nm) and visible (450 nm) light. However, the dinuclear Ru(II) complex (di-Rutpy.PF₆) did not isomerize under 366 nm light, while the mononuclear Ru(II) complex (mono-Rutpy.2PF₆) showed a 20% conversion efficiency upon UV irradiation. The backward isomerization of the mononuclear Ru(II) complex was accelerated by 440 nm light. The poor

photoisomerization efficiency in Ru(II) complexes was attributed to complex energy levels and energy transfer from the azo chromophores to the metal centers. Rh(III) complexes, although non-emissive, exhibited slow thermal cis-to-trans conversion while photoinduced isomerization was not observed. They also noted an approximately 80 mV negative shift in the Rh(III)/Rh(I) potential upon trans to cis conversion. The study also explored the effects of counter ions and solvents on photoisomerization rates and quantum yields, noting that larger counter ions prevent ion pairing, reducing the effective rotor volume and making trans-cis rotation feasible. The Rh(III) complexes showed enhanced photoisomerization efficiency with photosensitizers like benzophenone or anthraquinone, achieving rates comparable to organic azobenzenes. By contrast, increased energy transfer from the azo π - π^* to Ru MLCT in the presence of sensitizers renders Ru(II) complexes inactive for trans-to-cis conversion.

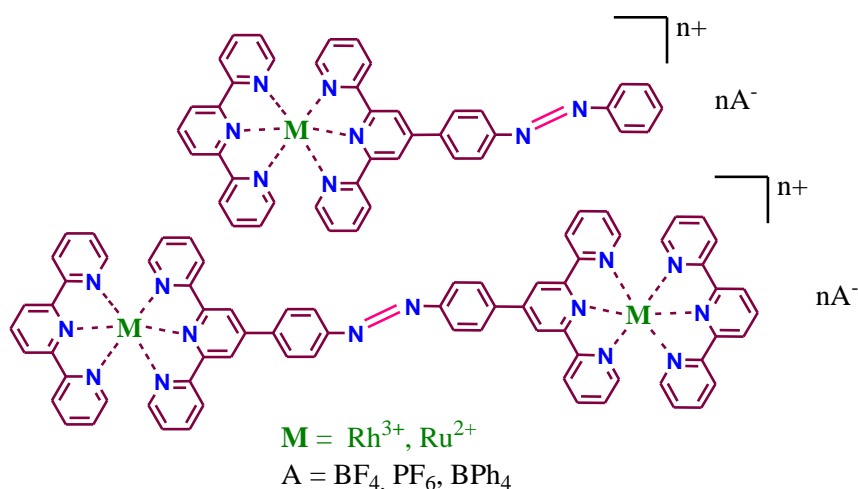


Figure 1.19

Nishihara and colleagues also focused on azo-based Pt-terpyridine complexes, which display better emissive properties compared to Ru and Rh complexes.¹²¹ They monitored the reversible trans-cis photoisomerization and emission switching behaviors of the complexes using IR, UV-vis absorption, emission spectroscopy, and 1H NMR spectrometry (Figure 1.20). Time-resolved emission and transient absorption spectroscopy were employed to understand the excited state deactivation dynamics. Solvent studies revealed that the quantum yield for photoisomerization (Φ_{t-c}) decreased with increasing solvent polarity (MeCN > DMF > DMSO > PC). The Pt complexes underwent reversible cis-to-trans isomerization under visible light ($\lambda > 430$ nm) or heating. While the trans forms were nearly non-emissive at room temperature and 77K, the cis forms emitted at ~480 nm and ~600 nm, attributed to ligand $^3\pi$ - π^* and 3MLCT states, respectively. Emission enhancement in the cis form occurs due to

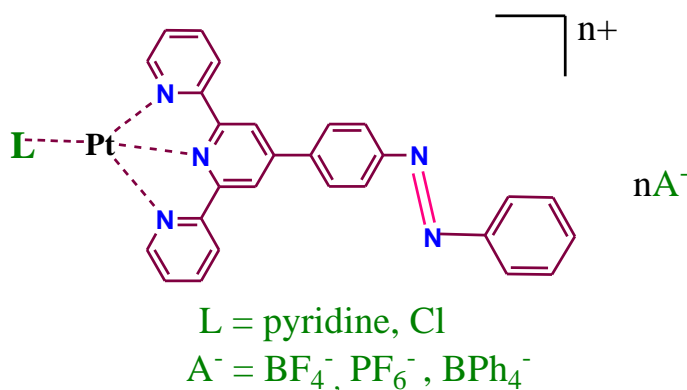


Figure 1.20

decreased π -conjugation, which inhibits photo-induced electron transfer from the nitrogen lone pair to the emissive unit. Additionally, the energy of $^3\pi\text{-}\pi^*$ being higher in case of *cis* form due to which non-radiative deactivation decreases leading to increase in emission characteristics. Emission lifetimes ranged from 2 ns to 40 μs . The lack of emission of the *trans* form at 600 nm allows effective off-on emission switching through reversible photoisomerization.

The Nishihara group explored the behavior of azo-conjugated metalladithiolene complexes (Ni, Pd, Pt) with diphenylphosphinoethane coligands under proton-coupled and photo-responsive conditions (Figure 1.21).²²⁹ They discovered that photoisomerization relies on the complexes' chemical and electronic structures, substituents, and metal-centered redox potentials. Notably, *trans*-to-*cis* isomerization in metalladithiolene systems occurs at a lower energy (405 nm) and their *cis* forms are more stable compared to organic azobenzenes. The reverse *cis*-to-*trans* process requires higher energy UV light. Upon adding a small amount of acid ($\text{CF}_3\text{SO}_3\text{H}$), the *cis* form of the complexes promptly converted to the *trans* form. The proton-catalyzed isomerization rate, which varies with the metal center, was found to be up to 150 times faster than the thermal isomerization rate, which does not depend on the metal center. This rate was exponentially related to the redox potential of the metalladithiolene complexes, increasing as the reduction potential shifted negatively. Thus, appropriate integration of proton and photo responses provides an innovative approach for reversible *trans*-*cis* isomerization in these systems.

Lees *et al.* explored the photochemistry of an array of self-assembled macrocyclic transition metal complexes linked by either isomerizable 4,4'-azopyridine (AZP) or 1,2-bis(4-pyridyl)ethylene (BPE) (Figure 1.22).¹²⁴ They found that tetranuclear squares composed of Pd(II)-Re(I) complexes, underwent a *trans*-to-*cis* photoisomerization when exposed to light at

313 or 366 nm, leading to their conversion into dinuclear forms (Figure 1.22). This process could be reversed through heating, allowing for sequential disassembly and reassembly upon alternating light exposure and heating. However, Pt(II)-Re(I)-based squares did not demonstrate this reversible disassembly and reassembly behavior.

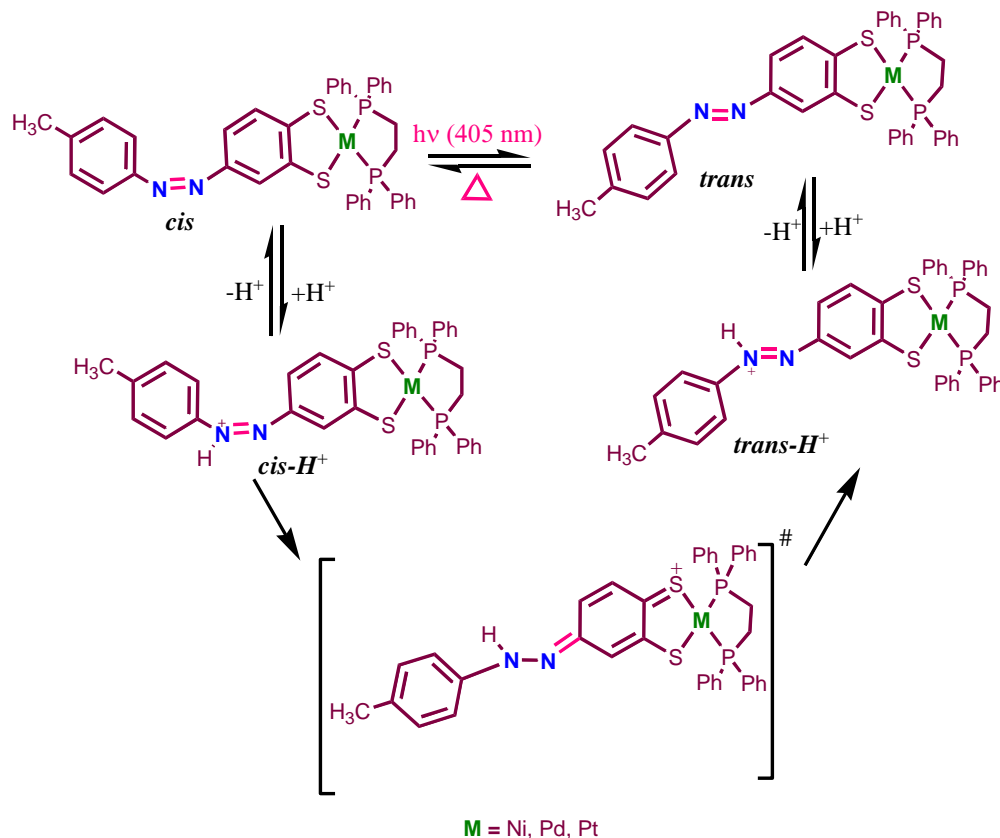


Figure 1.21

Frexia and colleagues developed tris-cyclometalated Ir(III) compounds incorporating up to three azobenzene units into their complex architecture, using 2-phenylpyridyl-type ligands (Figure 1.23).²³⁰ They studied the photochromic properties and photoisomerization behaviors of these compounds, examining the effects of substitution patterns, coordination modes, metal-azobenzene distances, and the number of azobenzene units in the complex structure.

The photoisomerization of stilbene-appended metal complexes, particularly Re(I) polypyridyl complexes, has been a subject of interest for several decades. Wrington et al. first reported the photoisomerization of stilbene-based Re(I) complexes²²⁰ in 1975 (Figure 1.24). They synthesized complexes with the formula $\text{XRe}(\text{CO})_3\text{L}_2$, where $\text{X} = \text{Cl, Br}$ and $\text{L} = \text{trans-3-styrylpyridine}$ or $\text{trans-4-styrylpyridine}$. These complexes exhibited trans-to-cis

photoisomerization with substantial quantum efficiency (0.49-0.64) when irradiated at their lowest absorption band (313 or 366 nm).

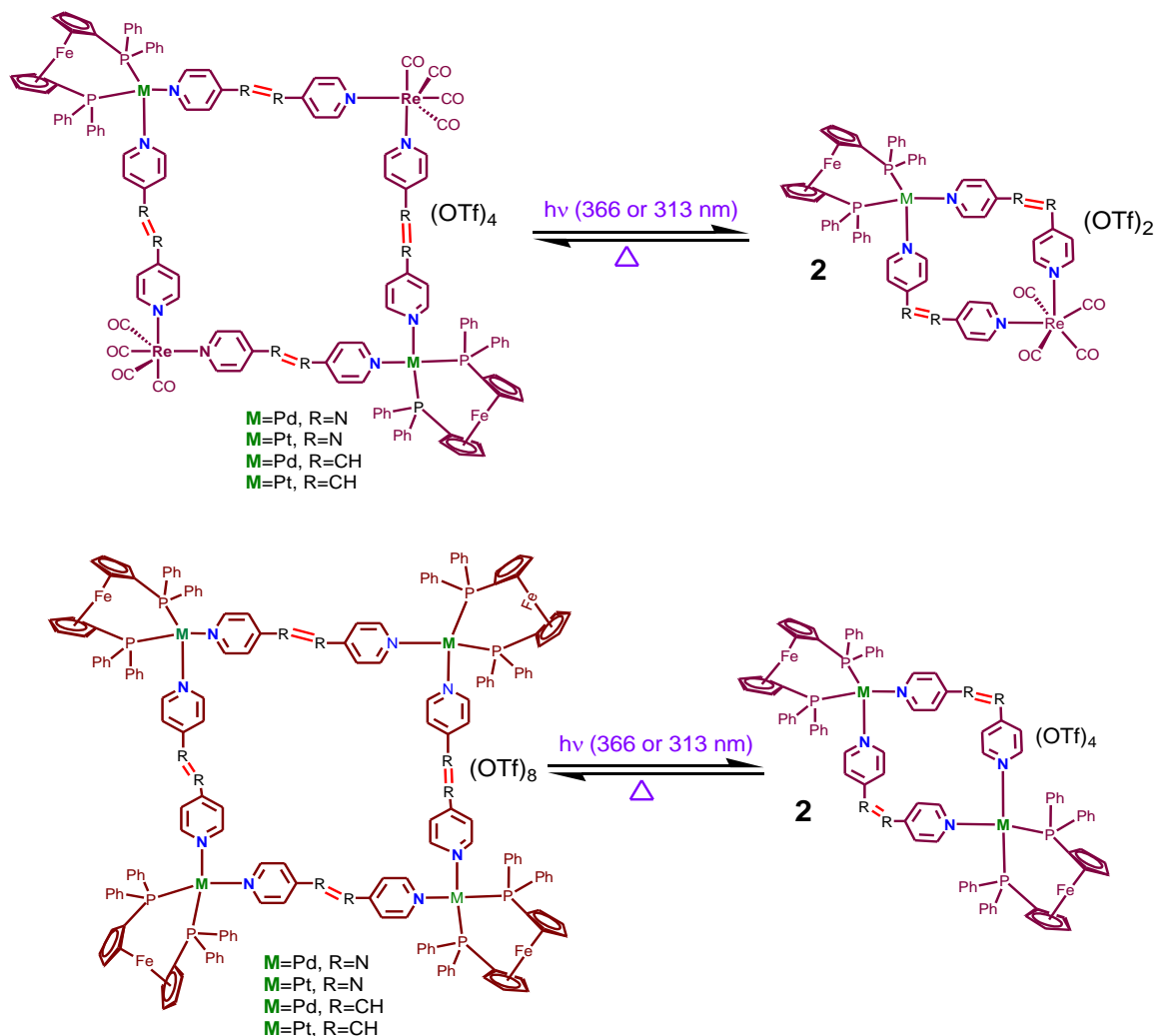


Figure 1.22

Hary Gray and coworkers investigated the trans-cis photoisomerization behaviors of $[\text{Re}(\text{diimine})(\text{CO})_3(\text{dpe})](\text{PF}_6)$ complexes where $\text{dpe}=1,2\text{-di}(4\text{-pyridyl})\text{-ethylene}$.²²¹ Photoisomerization occurred in CH_2Cl_2 with a quantum yield of 0.2 upon irradiation with 350 nm light (Figure 1.25). The photostationary state consisted of 70% cis and 30% trans forms. The reverse process occurred upon irradiation with 250 nm light. The trans forms of the complexes were non-luminescent, while the cis forms exhibited yellow luminescence, which could be used for luminescence switching.

Iha and coworkers investigated the photoisomerization of stilbene-based Re complexes. They developed a diverse range of organometallic $\text{Re}(\text{I})$ -carbonyl complexes such as $\{\text{fac-}[\text{Re}(\text{CO})_3(\text{dmcb})(\text{trans-stpyR})]^+\}$, where $\text{dmcb}=4,4'\text{-dimethoxycarbonyl-}$

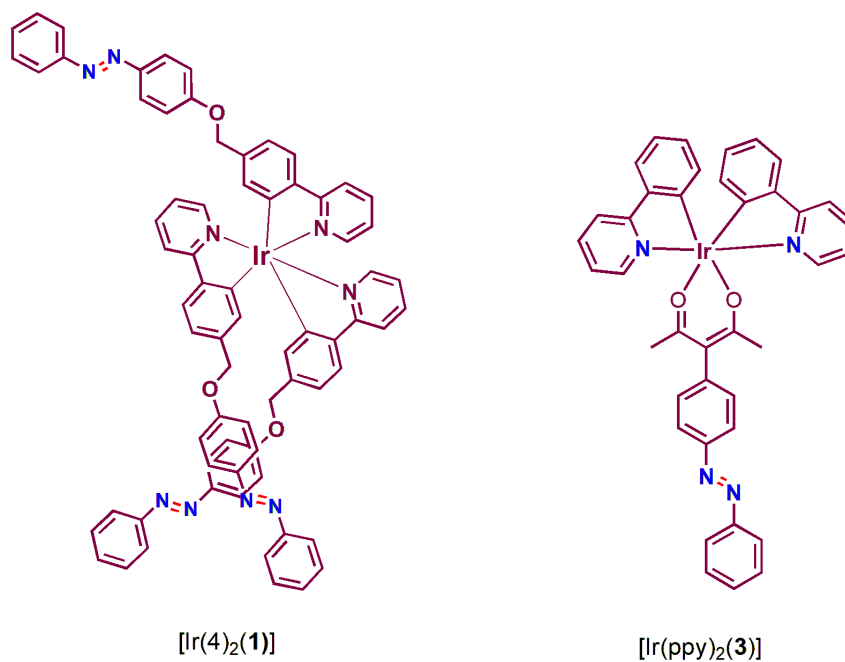


Figure 1.23

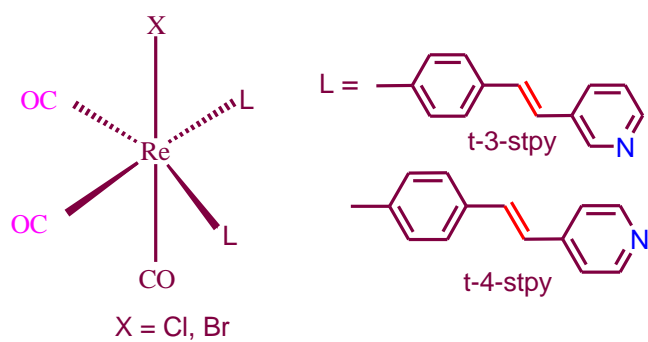


Figure 1.24

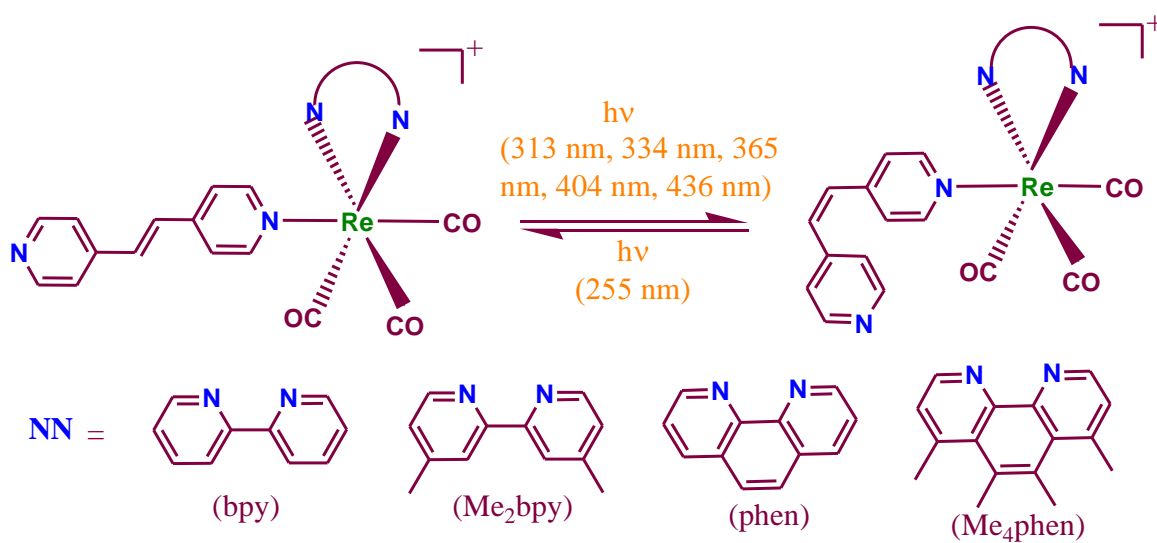


Figure 1.25

2,2'-bipyridine, *trans*-stpyR=*trans*-4-styrylpyridine (*trans*-stpy) or *trans*-4-(4-cyano)styrylpyridine (*trans*-stpyCN)}²²² and {*fac*-[Re(CO)₃(NN)(*trans*-stpyCN)]⁺, where NN = 2,2'-bipyridine (bpy) or 4,4'-dimethyl-2,2'-bipyridine (dmb), and stpyCN=4-(4-cyano)styrylpyridine} (Figure 1.26).²²³ They extensively examined the photophysical, photochemical, and photoisomerization behaviors of the complexes using various spectroscopic techniques, including absorption, emission, and ¹H NMR spectroscopy. The complexes exhibit high *trans*-to-*cis* isomerization quantum yield values (0.37-0.64) when exposed to a broad range of UV and visible light sources, specifically at wavelengths of 313 nm, 334 nm, 365 nm, 404 nm, and 436 nm (Figure 1.26). The reverse *cis*-to-*trans* photoisomerization also occurs efficiently at 255 nm. Furthermore, they also explored the role of the ³ILstpyCN state in their photophysical and photochemical behavior, providing new insights into their potential applications.

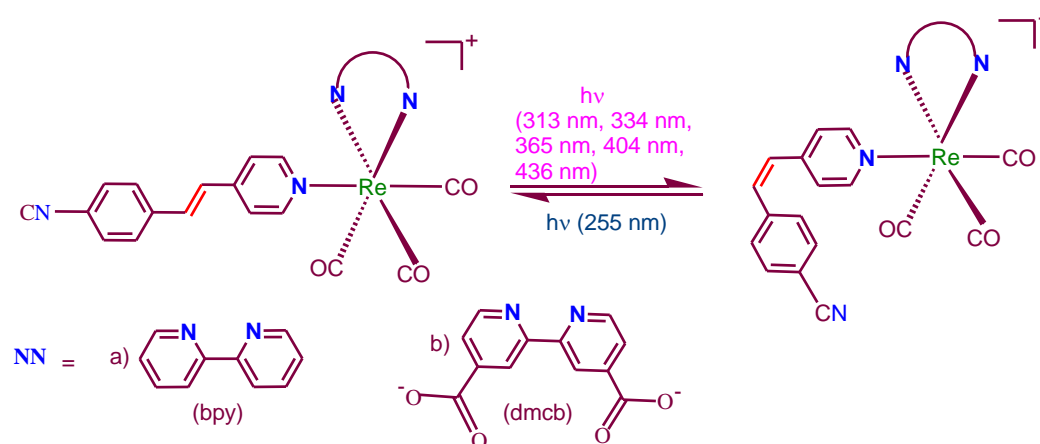


Figure 1.26

Lees' group explored the photophysical and photoisomerization properties of various trinuclear diimine Re(I)-tricarbonyl complexes connected by stilbene-like ligands (Figure 1.27).²²⁶ The trinuclear complexes exhibited low emission quantum yields and short excited state lifetimes in MeCN. Upon irradiation with 366 nm light, these complexes transitioned from a *trans-trans-trans* configuration to a *cis-cis-cis* configuration (achieving 75-95% conversion after 36 hours), with a notable increase in lifetime. This process could be reversed by heating at 60 °C for 5 hours.

Daniel and coworkers investigated the photoisomerization of the *fac*-[Re(CO)₃(bpy)(*t*-stpy)]⁺ complex under visible-light irradiation, highlighting the role of MLCT states in driving isomerization, unlike conventional organic systems.²³¹ They emphasized the role of spin-orbit and vibronic couplings in enabling singlet-triplet transitions. Analysis of potential energy

curves revealed that the torsional and angular deformations in the C=C bond play a key role in the trans→cis isomerization process. Combining theoretical ab initio calculations with experimental UV-Vis, Resonance Raman, and IR spectroscopy, they provided a detailed understanding of the multi-step trans→cis isomerization process in rhenium complexes.

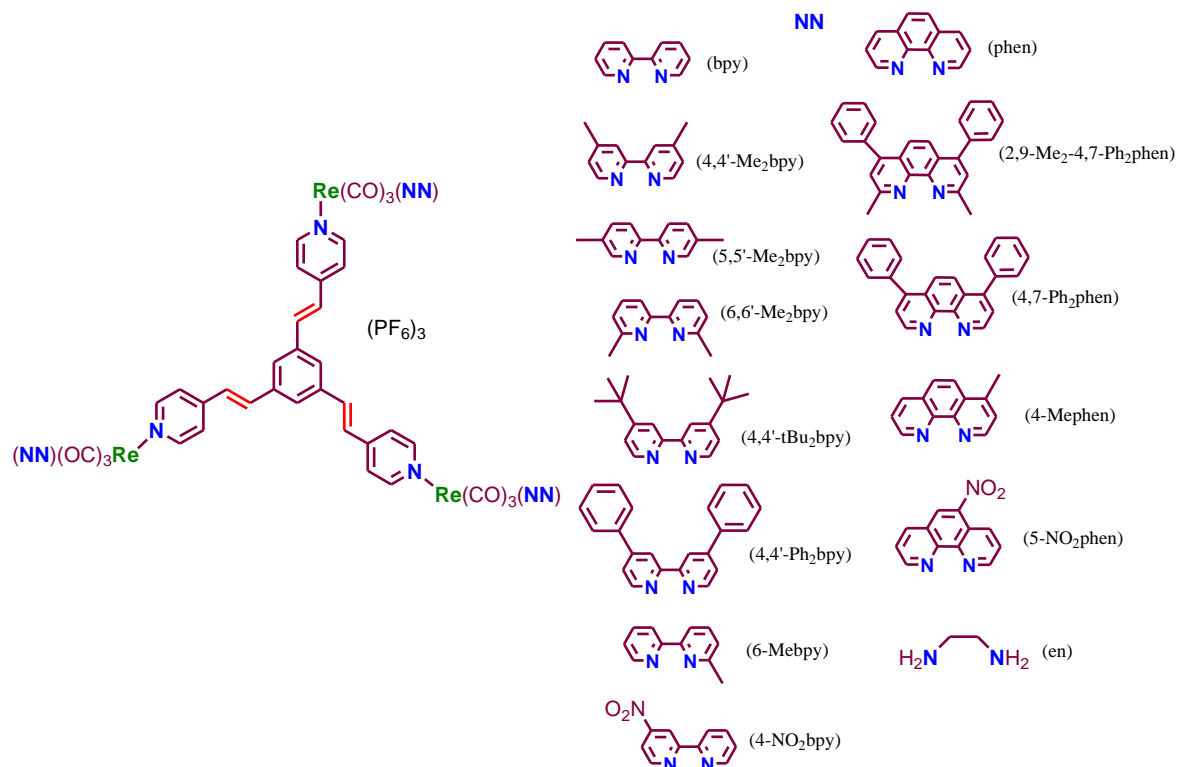


Figure 1.27

In another work, they carried out detailed mechanism of photo-induced trans-cis isomerization in stilbene-coordinated rhenium(I) complexes.²³² Through computational methods such as DFT and MS-CASPT2 and using the B3LYP functional with solvent corrections, the study deciphers how the antenna ligand influences the mixing of intra-ligand (IL) and metal-to-ligand charge transfer (MLCT) states (Figure 1.28). The isomerization is triggered by irradiation, with MLCT states playing a crucial role in sensitizing the stilbene-like pathway, especially through triplet states (³ILL). The dynamics of the process are influenced by several factors, including the energy gap between ³MLCT and ³ILL states, which is modulated by the antenna ligand. The presence of conical intersections between MLCT and IL states introduces complexity, leading to ultra-fast concurrent deactivation processes. The study shows that stpy-containing complexes are more sensitive to irradiation wavelengths than bpe-containing ones. Additionally, time-dependent DFT (TD-DFT) was used to calculate absorption spectra, highlighting how spin-orbit coupling shifts the lowest MLCT bands and affects the isomerization process.

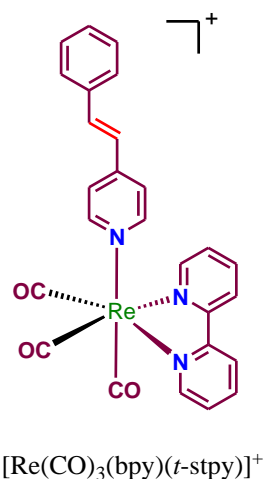


Figure 1.28

Yam and coworkers synthesized and characterized a series of azo- and stilbene-containing Re(I) surfactant complexes and reported their applications along with photoisomerization. Rhenium(I) tricarbonyl diimine complexes with low-lying MLCT states were used as photoisomerization sensitizers (Figure 1.29).²¹⁶ Azo-containing complexes exhibited reversible trans-cis isomerization upon alternately shining with 365 nm and 450 nm

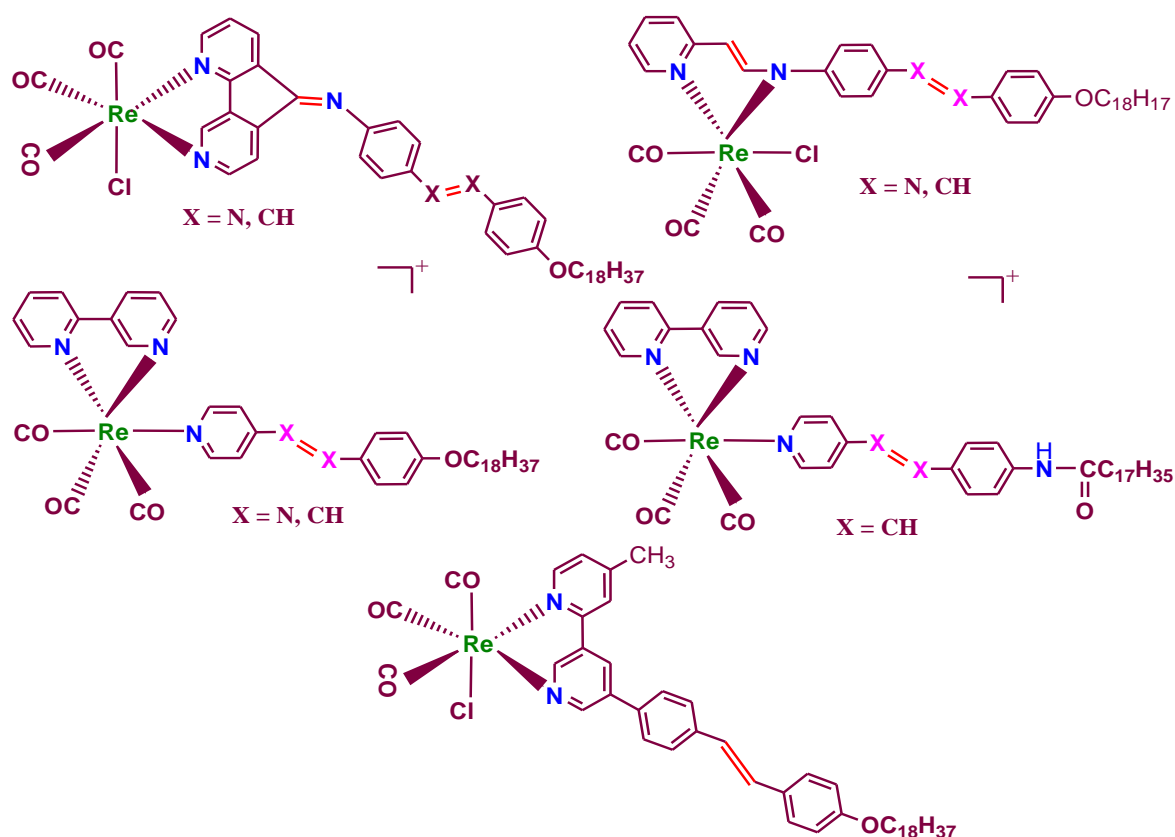


Figure 1.29

lights. However, the complex with an alkoxy substituent on the phenylazopyridine did not undergo isomerization, probably because of the steric constraint. Stilbene-based complexes showed reversible isomerization at different wavelengths (365 nm and 254 or 480 nm), with lower quantum yields compared to their free ligands.

Lin and co-workers synthesized a series of lanthanide complexes (La, Nd, Eu, Gd, Yb) using the stilbene derivative, N',N'-bis(pyridin-2-ylmethyl)-4-styrylbenzoyl hydrazide (HL) and benzoyltrifluoroacetate ligands (tfd), and characterized using various techniques like MS, ^1H NMR, FT-IR, and X-ray diffraction (Figure 1.30).²³³ The cis-trans photoisomerization of free ligand (HL) and its complexes was studied in acetonitrile, revealing that gadolinium complex (**4**) exhibited a five-fold increase in isomerization rate and

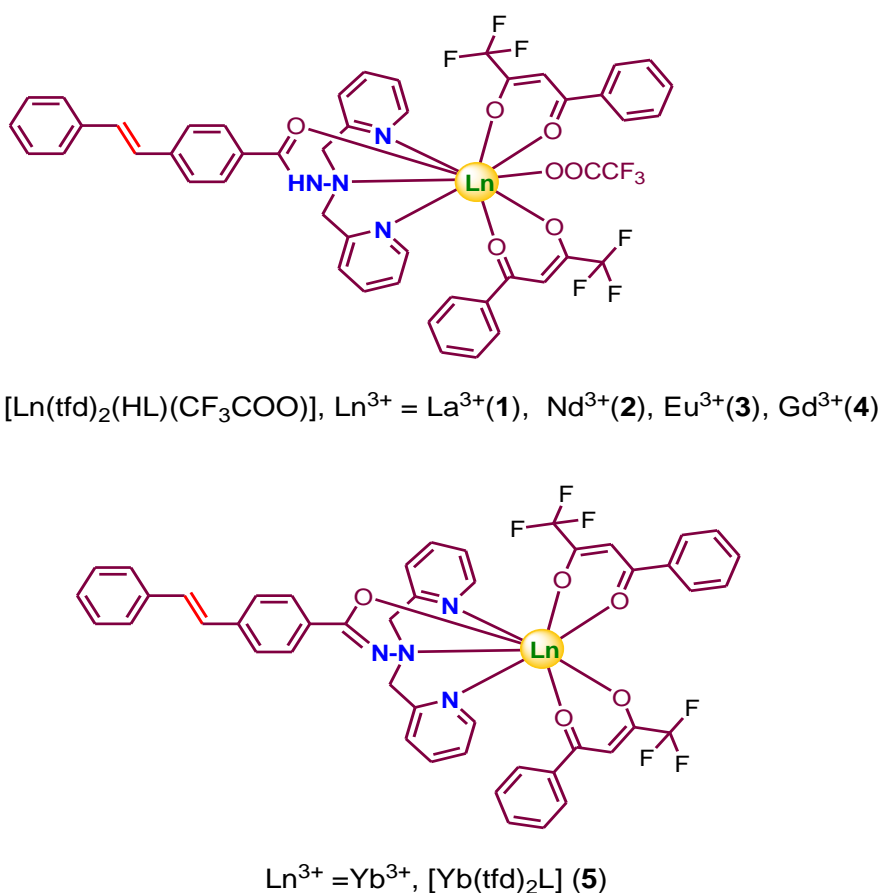


Figure 1.30

quantum yield compared to HL. This enhancement is attributed to the coordination of the ligand with the metal centres, which stabilizes the excited state and improves photostability. On one hand, the europium complex (**3**) showed efficient energy transfer from the ligand (HL) to the Eu³⁺ ion, resulting in a high luminescence quantum yield and efficient sensitization, while on the other hand it suppressed the photoisomerization of the stilbene

group. The luminescence lifetimes of complexes, specifically complexes **2** (Nd^{3+}) and **5** (Yb^{3+}), were measured in the solid state which exhibited near-infrared (NIR) luminescence, with observed lifetimes exceeding 10 microseconds (μs). This performance is notable because these complexes contain only two diketonate ligands, which typically result in shorter lifetimes compared to systems with three ligands. The longer lifetimes suggest that the N',N' -bis(pyridin-2-ylmethyl)-4-styrylbenzoyl hydrazide (HL) ligand contributes to enhancing the luminescence properties, making these complexes promising for applications in luminescent materials. TD-DFT calculations provided insight into the electronic transitions, explaining the enhanced photostability and optical properties of the complexes, which were attributed to various charge transfer mechanisms and energy transfers between ligands and metal ions. Thus, the study provides a new approach for designing lanthanide-based molecular switching materials.

Baitalik and group described the photoisomerization behavior of a series of stilbene appended terpyridine derivatives that are covalently attached to various aliphatic electron donating/withdrawing groups (Figure 1.31). They also performed detailed investigation of

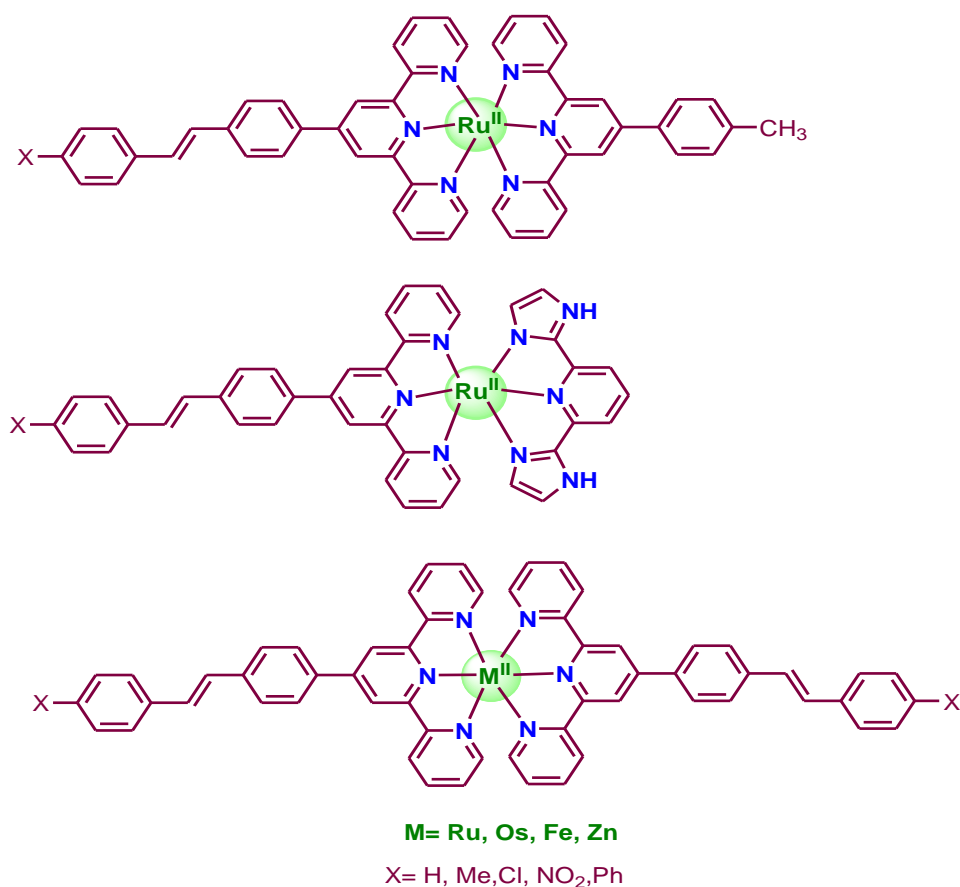


Figure 1.31

photoisomerization behavior of various metal complexes such as Ru, Os, Fe and Zn.^{157-158,162, 234-236} The ligand moiety, along with heteroleptic or homoleptic metal complexes, can undergo reversible isomerization between their trans and cis forms when alternately exposed to visible and UV light. In certain cases, the reversal from cis to trans form also occurs through thermal treatment. In addition to light-induced isomerization, heteroleptic complexes with benzimidazole units can be deprotonated in basic conditions or at high pH which can modulate their ground and excited state properties. The complexes exhibit faster photoisomerization in their deprotonated forms together with proton-coupled oxidative electrochemical behavior.

1.6 Brief Review on the Aggregation Induced Emission Properties of Ligands and Metal complexes

Luminescent materials have become essential to scientific and technological progress, enabling significant advancements in fields ranging from optoelectronics to biological imaging.^{12-21,57-65} These luminescent materials can be used in different physical states, viz. gaseous, liquid, and solid. However, in most practical applications, they are employed as thin films or in aggregate form.^{56,59-60,69} For instance, in organic light-emitting diodes (OLEDs) and organic field-effect transistors (OFETs), luminescent materials are utilized in the solid state. Similarly, in biomedical imaging, luminescent probes are frequently handled in aqueous or physiological environments. Despite their versatility, luminescent materials face aggregation-caused quenching (ACQ), where light emission diminishes as molecules aggregate.⁵¹⁻⁵⁴ First documented by Förster⁵¹ in 1954, ACQ is common in aromatic luminophores, where strong π - π stacking interactions of planar aromatic rings lead to non-radiative decay.

In contrast to ACQ, a phenomenon known as aggregation-induced emission (AIE) has been discovered, where non-emissive molecules in their dispersed form become highly emissive upon aggregation.⁵⁶⁻⁷⁶ The term "AIE" was coined in 2001 by a research group of Ben Zhong Tang upon studying hexaphenylsilole (HPS)⁵⁵, a molecule that is non-luminescent in its isolated state but emits intensely when aggregated. In 2002 Park *et al* documented the aggregation induced emission enhancement (AIEE)⁶⁶ wherein moderately emissive molecules exhibit emission enhancement upon aggregation. Unlike traditional luminophores, AIE materials, or AIEgens, overcome the detrimental effects of aggregation. This is achieved

through mechanisms such as restricted intramolecular rotations (RIR),²³⁸⁻²³⁹ which prevent non-radiative energy dissipation. In the aggregated state, these molecules avoid the π - π stacking interactions that lead to ACQ, allowing them to emit bright light. Another well-studied AIEgen is tetraphenylethene (TPE),^{60,81} which has a central olefinic core surrounded by four phenyl rings. In solution, TPE exhibits little to no luminescence due to the free rotation of its phenyl rings, which dissipates energy non-radiatively. However, upon aggregation, the intramolecular rotations are restricted, and the emission is activated. This restriction, combined with a highly twisted molecular structure, prevents the π - π stacking that typically leads to ACQ, making TPE a prototypical AIE material.

Three key mechanisms are highlighted to explain the phenomenon of aggregation-induced emission (AIE):

1. **Restriction of Intramolecular Rotations (RIR):** This mechanism focuses on the free rotation of molecular units, such as phenyl rings, in AIE-active molecules.²³⁸⁻²³⁹ In solution, these rotational motions lead to non-radiative dissipation of energy, which causes weak or no light emission. However, upon aggregation, these rotations are restricted, thereby preventing energy loss and activating radiative transitions that result in enhanced light emission.
2. **Restriction of Intramolecular Vibrations (RIV):** Vibrational motions within molecules, such as bond stretching or bending, also consume exciton energy and reduce the efficiency of light emission.²⁴⁰⁻²⁴² The RIV mechanism suggests that by restricting these vibrational motions when the molecules aggregate, AIEgens can more efficiently emit light.
3. **Restriction of Intramolecular Motions (RIM):** RIM is a broader mechanism that encompasses both RIR and RIV. It posits that any form of restricted molecular motion, whether rotational or vibrational, contributes to enhanced emission by activating radiative pathways that are otherwise deactivated in solution.²⁴³⁻²⁴⁶ This mechanism provides a more comprehensive explanation of the AIE phenomenon.

The transition from ACQ to AIE is achieved by integrating AIE properties into ACQ systems, preserving beneficial characteristics while eliminating quenching effects. Strategies include modifying ACQphores with AIEgen moieties, replacing ACQ units with AIEgens, or designing new AIEgens from ACQphores.^{55-60,77-82} AIE materials have significant applications in bioimaging, optoelectronics, and environmental monitoring.^{70-76,78} They serve

as fluorescence biosensors, organelle imaging tools, hazardous substance detectors, and components in OLEDs and optical devices, enabling the development of advanced luminescent materials.^{55-60,77-82,87-93} Although a great deal of work has been carried out on various organic molecules (e.g., TPE, DSA, and silole), comparatively less work is explored for the metal complexes.⁷⁷⁻⁹⁰ Herein, we present a brief survey on the aggregation induced emission of both the organic molecules as well as metal complexes.

BZ Tang and group synthesized a series of Rhodamine B-based compounds (BISX, ISX, MISX and MTSX) with cross-shaped structures using a simple cyclization reaction, exhibiting AIE behavior (Figure 1.32).²⁴⁷ Unlike conventional AIEgens, their emission was not influenced by viscosity or temperature, suggesting a mechanism beyond RIM. Structural analysis and theoretical calculations revealed that molecular conformation changes in aggregates facilitated intramolecular charge transfer (CT) transitions, leading to the observed AIE behavior in solid states. Additionally, these compounds demonstrated potential applications in detecting seafood spoilage due to their sensitive "turn-on/off" emission responses to acid-base treatments.

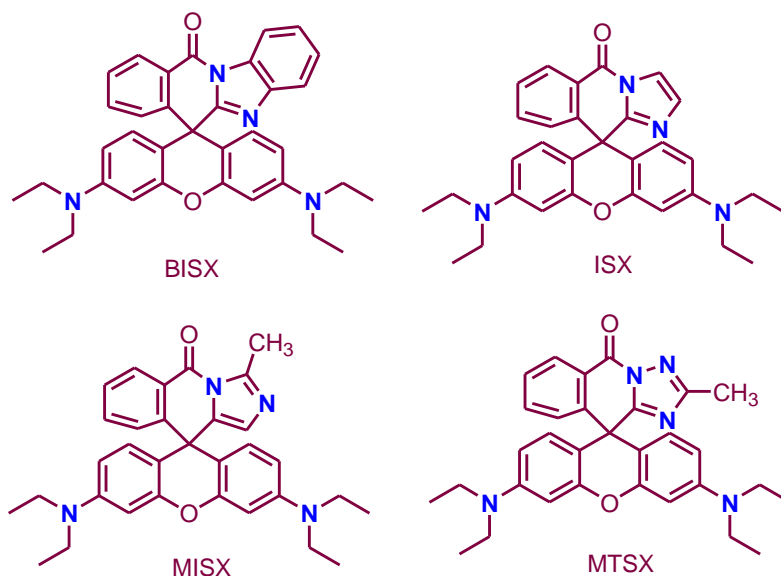


Figure 1.32

Tang *et al.* has developed a pH-responsive fluorogen, TPE-Cy, composed of tetraphenylethene (TPE) and cyanine (Cy) units (Figure 1.33).²⁴⁸ This organic fluorogen demonstrates AIE characteristics and intracellular pH sensing in living cells. TPE-Cy exhibits pH sensitivity with its emission color shifting from red to blue as pH increases. It is cell-permeable, highly biocompatible, and interacts with cellular lipid components to adjust its color transition point from extracellular pH 10 to intracellular physiological pH range of the

cell. This allows TPE-Cy to cover the entire intracellular pH (pH_i) range from 4.7 to 8.0, a range that most conventional pH indicators cannot achieve. Additionally, TPE-Cy employs a ratiometric sensing method, measuring the ratio of fluorescence intensity between two peaks, which helps dodging issues related to uneven dye distribution and other technical artifacts. TPE-Cy has been effectively used for pH_i imaging and monitoring through confocal microscopy, ratiometric analysis, and flow cytometry, showcasing its potential for high-resolution and high-throughput intracellular analysis, with promising applications in cancer diagnosis and drug screening.

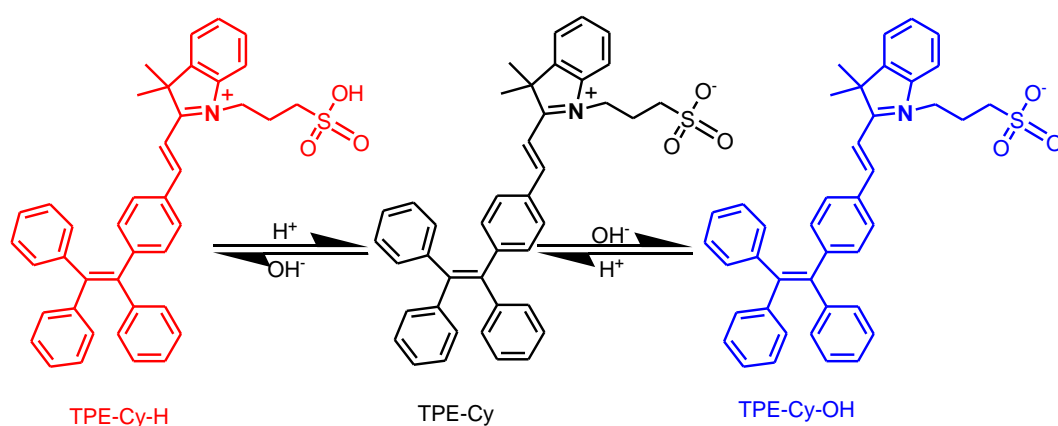


Figure 1.33

In another study, Tang and coworkers introduced a cyanostilbene-based luminophore exhibiting AIE characteristics. Upon adjusting the aggregate morphology or changing the irradiation wavelength, the molecule demonstrated a range of efficient, controllable photoreactions. These include: (1) remarkable Z/E isomerization under ambient light and thermal treatment in organic solvents, 2) UV light-induced photocyclization resulting in a pronounced fluorescence increase, and 3) Highly selective regio- and stereospecific photodimerization in aqueous media, accompanied by microcrystal formation. Experimental analyses provided clear insights into these photoreaction processes, while DFT calculations offered a detailed mechanism for photodimerization in the microcrystalline state (Figure 1.34).²⁴⁹ A fluorescent 2D photopattern was generated from Z-MPPMNAN, displaying an improved signal-to-background ratio before and after photo irradiation, as well as tunable fluorescence switching in different states. These findings highlight the integration of multiple photoreactions within a single system while enabling precise control over their functionalities. Additionally, incorporating this fluorophore into a polymer matrix could lead

to formation of materials with photo-triggered macroscopic behaviors, a prospect to explore in future research.

Li and coworkers synthesized four 4,4'-bis(1,2,2-triphenylvinyl)biphenyl (BTPE) derivatives, viz. methyl-BTPE, isopropyl-BTPE, Ph-BTPE, and Cz-BTPE, by modifying the linkage modes and dihedral angles of the biphenyl cores to explore new approaches for blue

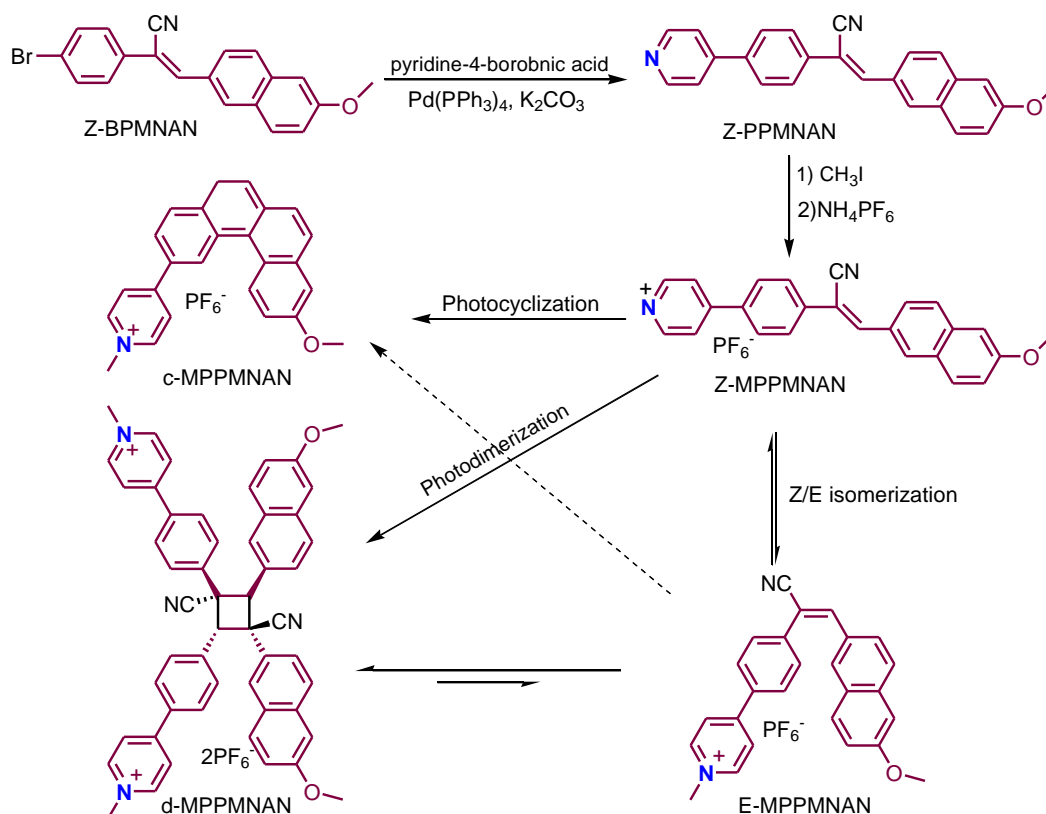


Figure 1.34

and deep-blue AIE emitters.²⁵⁰ The modifications resulted in high thermal stability and varied emission properties. The thermal properties, including thermal decomposition temperatures and glass transition temperatures, were investigated (Figure 1.35). The maximum absorption wavelengths of the derivatives were blue-shifted compared to BTPE, reflecting shorter π -conjugation lengths due to the introduction of different substituents. The AIE properties were confirmed by fluorescence measurements in THF-water mixtures, showing significant emission enhancements in the aggregate state. Density Functional Theory (DFT) calculations revealed shorter π -conjugation length of the complexes in comparison to BTPE. Additionally, Cz-BTPE shows enhanced hole-transport due to its carbazole units. The compounds demonstrated efficient blue emissions with enhanced performance in OLED devices, especially the aromatic-substituted BTPE compounds like phenyl and carbazole-substituted

derivatives (L_{\max} , $\eta_{C,\max}$, and $\eta_{P,\max}$ of 6497 and 9911 cd m^{-2} , 3.10 and 3.74 cd A^{-1} , as well as 2.13 and 2.55 lm W^{-1} , respectively), which exhibited superior electroluminescence performance compared to the alkyl-substituted ones. Thus the research presents an effective strategy to develop efficient blue and deep-blue AIE luminogens, thereby advancing OLED technology.

Yam and coworkers have designed, synthesized, and characterized a series of alkynylplatinum(II) terpyridine complexes incorporating tetraphenylethylene (TPE) moieties. When water is added, the alkynylplatinum(II) complexes with unsubstituted terpyridine,



Figure 1.35

exhibit intriguing spectroscopic changes which are attributed to the presence of $\text{Pt}\cdots\text{Pt}$ and/or π - π stacking interactions, along with the AIE effect imparted by the TPE unit. (Figure 1.36).²⁵¹ The distinctive colorimetric and luminescence changes arising from the interactions between the two different chromophores offer potential for designing functional materials sensitive to micro environmental changes. Molecular engineering can hinder the AIE effect from the TPE moiety by adding bulky tert-butyl groups to the terpyridine ligand, and restore it by extending the separation between the tri-tert-butylterpyridine platinum(II) unit and the TPE motif. The lengthening of spacers between the alkynylplatinum(II) terpyridine unit and the TPE moiety leads to the formation of various superstructures, including long wire-like nanostructures and nanoleaf structures at high water content. Additionally, different superstructures are achieved from self-assembly processes by regulating $\text{Pt}\cdots\text{Pt}$ and π - π stacking interactions through molecular alteration of the ligands and tailoring the hydrophilicity of complexes. Through meticulous molecular engineering, they have successfully controlled various intermolecular interactions, resulting in the formation of diverse, distinctive structures. This highlights the crucial role of directional $\text{Pt}\cdots\text{Pt}$ and/or π - π interactions in the self-assembly process. Thus, the work has introduced a novel class of

platinum(II)-AIE hybrids, providing valuable advancements in the design of metal complexes with AIE characteristics for advanced functional materials.

De Cola and group explored the phenomenon of aggregation-induced electrochemiluminescence (AIECL) in platinum(II) complexes, a process where electrochemiluminescence (ECL) is enhanced through the self-assembly of these complexes into nanostructures.²⁵² The study examines two specific Pt(II) complexes consisting of a tridentate ligand, 2,6-bis(3-(trifluoromethyl)-1*H*-1,2,4-triazol-5-yl)pyridine (pyC₅-CF₃-tzH₂)

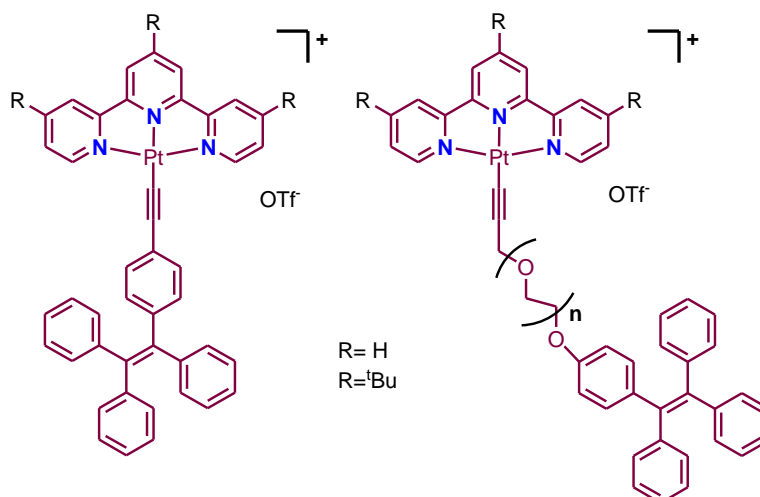


Figure 1.36

and a 4-amino pyridine substitute with one (Pt-PEG) or two (Pt-PEG₂) triethylene glycols, both of which form different types of supramolecular assemblies depending on their chemical structures and environmental conditions (Figure 1.37). In aqueous solution, the complex formed aggregates with short Pt...Pt distances (<3.5 Å), leading to highly intense red-shifted emission and destabilized *dz*² orbitals. This formed a new metal-based HOMO thereby facilitating MMLCT transitions. TEM analysis confirmed the formation of spherical particles with a diameter of approximately 22 nm. For ECL measurements, in aqueous media and solid-state experiments, Pt-PEG₂ demonstrated strong ECL, particularly when paired with specific co-reactants like TPrA and oxalate, which stabilize the platinum oxidation state (Pt⁺⁴) and enhance light emission, surpassing the efficiency of the widely used Ru(bpy)₃²⁺ complex in some cases. However, Pt-PEG showed significant ECL only in the solid state when subjected to mechanical stress thus showing that mechanical stress can enhance their ECL by converting them into more aggregated forms. This research opens new possibilities for using platinum(II) complexes as highly efficient ECL labels in bioanalytical applications, especially in environments where traditional emitters like Ru(bpy)₃²⁺ are less effective.

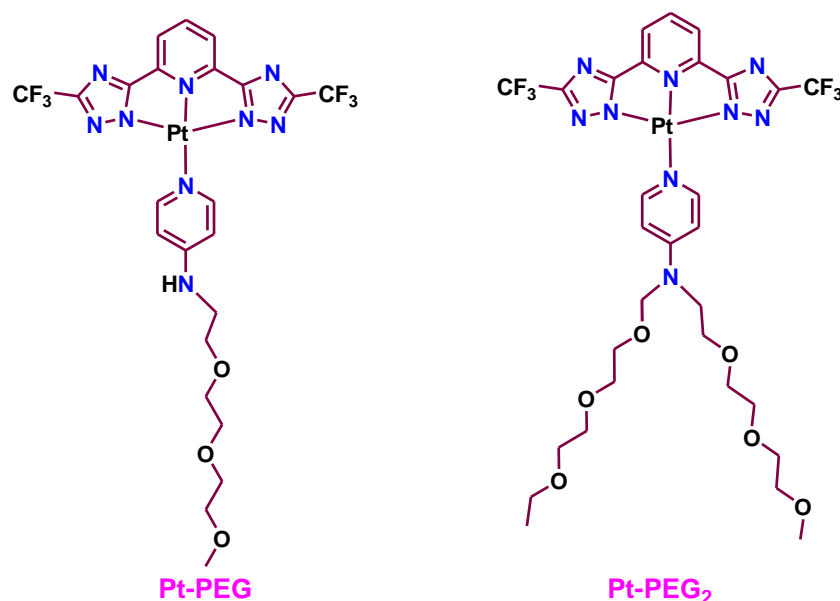


Figure 1.37

Khatua *et al.* have developed a new bis-heteroleptic ruthenium(II) complex, **Ru-1**, featuring a 2-aminoethylamino-substituted 1,10-phenanthroline ligand, which exhibits aggregation-induced emission (AIE) properties.²⁵³ The AIE effect in **Ru-1** is achieved through restricted intramolecular motion and intermolecular hydrogen bonding, leading to the formation of a unique vesicular structure in a polar aprotic [CHCl₃/CH₃CN (95:5,v/v)] solvent mixture, as confirmed by transmission electron microscopy (TEM), field emission scanning electron microscopy (FESEM), and atomic force microscopy (AFM) imaging (Figure 1.38). This complex serves as a highly selective luminescent probe for real-time detection of phosgene, distinguishing it from other analytes and chemical warfare agents with a low detection limit (13.9 nM in CH₃CN) and also differentiating between phosgene and triphosgene in CH₃CN. The 2-aminoethylamino groups in **Ru-1** react with the carbonyl group of phosgene, undergoing intramolecular cyclization to form **Ru-1-Phos**, which contains 2-imidazolidinone groups. This was verified by electrospray ionization mass spectrometry and ¹H NMR spectroscopy, with ¹H NMR titration supporting the reaction mechanism and indicating simultaneous reactions at two aminoethylamino sites. The crystal structure of **Ru-1-Phos**, determined through single-crystal X-ray diffraction, provides structural confirmation supporting the proposed reaction mechanism. Time-dependent density functional theory (TD-DFT) calculations indicate that the weak luminescence of **Ru-1** is primarily due to the population of the non-emissive ³MC state. Upon cyclization with phosgene, the formation of the corresponding 2-imidazolidinone product facilitates the population of the emissive

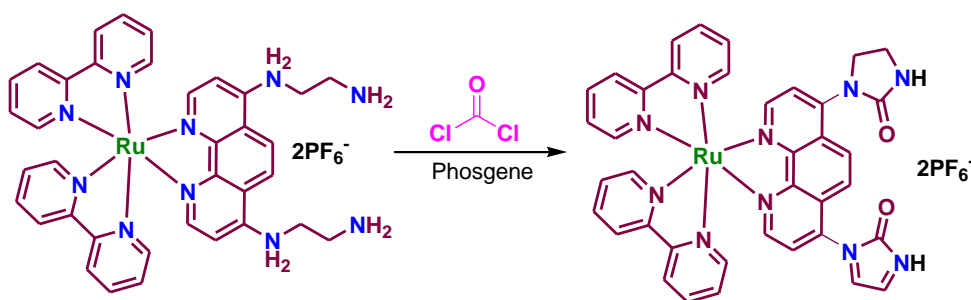


Figure 1.38

$^3\text{MLCT}$ state in **Ru-1-Phos**, resulting in enhanced luminescence. Additionally, a practical application involves a solid-state paper strip coated with **Ru-1**, capable of selectively detecting phosgene vapor at various concentrations without interference from other analytes.

Xu and coworkers designed and synthesized a series of multifunctional ruthenium-based AIE probes, **Ru1-3**, to explore the selective identification and efficient elimination of Gram-positive bacteria (G+) bacteria (Figure 1.39).²⁵⁴ Infections caused by G+ pose a significant threat to public health due to their high rates of morbidity and mortality. Aggregation-induced emission (AIE) materials have shown considerable potential for microbial detection and antimicrobial treatment. The selective recognition of G+ by **Ru2** is attributed to the interaction between lipoteichoic acids (LTA) and **Ru2**. The accumulation of **Ru2** on the G+ membrane activates its AIE luminescence, enabling specific staining of G+ bacteria, and distinguishes them from Gram-negative bacteria using a wash-free staining method. Additionally, **Ru2** demonstrates robust antibacterial activity against G+ both in vitro and in vivo when exposed to light. Hence, **Ru2** plays dual roles of detecting and treating G+ bacteria, setting a precedent for future advancements in antibacterial agents.

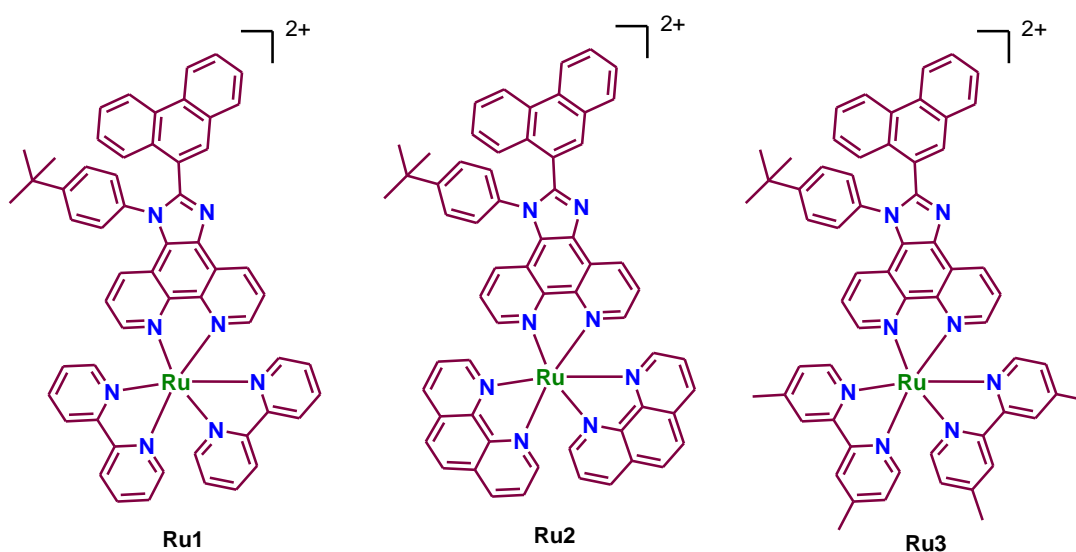


Figure 1.39

1.7 Brief Review on the Non-Covalent (Anion- π and Cation- π) Interactions of Ligands and Metal complexes

Well-organized non-covalent interactions are essential in various chemical processes, with aromatic interactions playing a key role in drug recognition, protein folding, and crystal engineering.¹²⁷⁻¹³⁷ π - π stacking in amino acid side chains, as well as in DNA and RNA, exemplifies these interactions.^{130-131,137,255-258} In addition to π - π stacking, other non-covalent interactions such as CH- π , lone-pair- π , cation- π and anion- π bonding are vital for biochemical recognition and the stabilization of biological macromolecules.²⁵⁸⁻²⁶⁵ These interactions also have significant relevance in organic synthesis and reaction control.^{127-129, 131-136,259-262}

The cation- π interaction is a significant non-covalent force in molecular recognition, influencing macromolecular structures and drug-receptor interactions. Cation- π interactions arise from the electrostatic attraction between a positively charged cation and the electron-rich π system of an aromatic ring, with electrostatic forces as the dominant factor supplemented by dispersion forces.^{128,134,137-138} In this interaction, the cation binds to the face of the π system. Experimental evidence from gas-phase and aqueous studies highlights their strength, comparable to hydrogen bonds.^{128,134,266} Early studies demonstrated that cations could preferentially bind to hydrophobic cavities lined with π systems, even in aqueous environments. In 1981, Kabarle highlighted the existence of an attractive non-covalent interaction between alkali metal cations and aromatic compounds.²⁶⁶ Experiments on the formation of a benzene- K^+ complex in the gas phase revealed the interaction energy to be 19 kcal/mol. In 1985, Meot-Ner reported that the binding energies between quaternary ammonium ions and π systems ranged from 10 to 22 kcal/mol.²⁶⁷⁻²⁶⁸ The term "cation- π interaction" was finally coined by Dougherty in 1990 to describe the attractive interactions between cations and π systems.²⁶⁹⁻²⁷⁰ Theoretical models and quantum calculations have advanced predictions of cation- π binding.²⁷¹⁻²⁷⁴ Applications include synthetic receptors like cyclophanes, demonstrating selective cation binding in supramolecular systems. This interaction is prevalent in biological systems, notably in stabilizing protein structures, molecular recognition, and neurotransmitter-receptor interactions; with acetylcholine as a key example.²⁷⁵⁻²⁷⁶ It is now clear that cation- π interactions are widespread and fundamental in various systems.

Anion- π interactions, unlike their cation- π counterparts, remained largely overlooked for years due to their seemingly counterintuitive nature. The first experimental validation of

this interaction was reported by Schneider *et al.*²⁷⁷ Computational investigations by Mascal, Alkorta, Deya, and collaborators later confirmed the attractive nature of interactions between anions and electron-deficient aromatic systems.^{138,278-282} Deya's team coined the term "anion- π interaction" revealing the energetically favorable interaction between hexafluorobenzene and anions, driven mainly by electrostatic and polarization effects.²⁸¹ Fundamental studies published in 2002 help shift attention to the anion- π interaction, prompting further computational and experimental investigations. Anion- π interactions, as distinct non-covalent forces, play a crucial role in driving various supramolecular processes.²⁷⁸⁻²⁸³ These include anion recognition, selective sensing, anion-directed self-assembly of complex structures, the formation of stimulus-responsive aggregates, and catalysis.²⁷⁸⁻²⁸⁵ The unique nature of these interactions enables them to influence diverse applications across both chemical and biological systems.²⁸⁶ A literature survey demonstrating both cation- π and anion- π interactions in various molecules are provided here.

Some preliminary work done by Pere M. Deyá *et al.* provides computational evidence confirming the existence of anion- π interactions. These interactions occur between anions and electron-deficient π -systems, driven by electrostatic forces and polarization effects (Figure 1.40).²⁷⁸ The study explores various anions and π -systems, showing that interaction strength depend on the π -system's electron density and the anion's polarizability. These findings highlight the significance of anion- π interactions in molecular recognition, supramolecular chemistry, and catalysis, positioning them as a versatile tool for designing functional materials and systems.

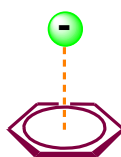


Figure 1.40

Saha and colleagues designed and synthesized a series of naphthalene diimide (NDI) receptors to investigate their supramolecular interactions with fluoride ions (F^-).¹³⁶ These receptors include a short receptor (SR) with a bisamide linker connecting two NDI units, a long receptor (LR) containing a tetraamide linker between two NDI units, and a control tetraamide receptor (CR) lacking any NDI units (Figure 1.41). Their study revealed a unique interaction between F^- and the π -electron-deficient, colorless NDI receptors. This interaction is driven by strong electronic coupling between the lone-pair electrons of the fluoride ion and the π^* -orbitals of the NDI unit, initiating an unprecedented electron transfer event. This

process produces an orange-colored NDI \cdot^- radical anion, which, upon further reduction by an additional fluoride ion, forms a pink-colored NDI $^{2-}$ dianion. This redox-driven color change establishes NDI as an effective colorimetric sensor for fluoride ions. Additionally, the strategic preorganization of two NDI units in an overlapping configuration using folded linkers enhances their selectivity and sensitivity for F $^-$, enabling detection at nanomolar concentrations in 85:15 DMSO/H $_2$ O solutions.

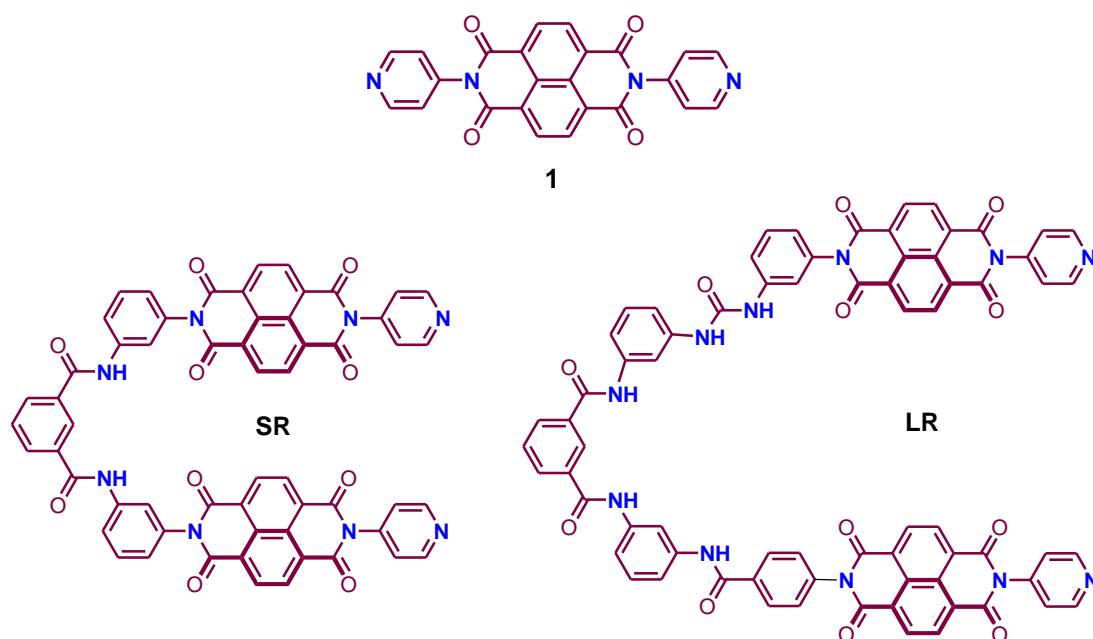


Figure 1.41

Dunbar *et al.* investigated the reactions of 3,6-bis(2'-pyridyl)-1,2,4,5-tetrazine (bptz) and 3,6-bis(2'-pyridyl)-1,2-pyridazine (bppn) with AgX salts ([PF $_6$] $^-$, [AsF $_6$] $^-$, [SbF $_6$] $^-$, and [BF $_4$] $^-$) which yields complexes with distinct structural motifs dictated by the π -acidity of the ligand's central ring and the outer-sphere anion (Figure 1.42).²⁸⁴ Bptz forms polymeric, dinuclear and propeller-type structures, characterized by strong anion- π interactions with the electron-deficient tetrazine ring. In contrast, bppn forms grid-type complexes, driven by maximized π - π stacking interactions due to the electron-rich pyridazine ring, with weaker anion- π interactions. These differences, supported by density functional theory (DFT) and electrostatic potential maps, highlight the greater π -acidity of bptz. The findings underscore the significant role of anion- π interactions in determining the self-assembly outcomes of these complexes.

The group also investigated the pivotal role of anion- π interactions in driving the self-assembly of Fe(II)-templated metallacycles with 3,6-bis(2-pyridyl)-1,2,4,5-tetrazine (bptz). Comprehensive analyses using X-ray crystallography, NMR spectroscopy (^1H , solution ^{19}F , and MAS ^{19}F), cyclic voltammetry, and mass spectrometry demonstrate that smaller anions ($[\text{BF}_4]^-$, $[\text{ClO}_4]^-$) template molecular squares, while larger anions ($[\text{SbF}_6]^-$, $[\text{AsF}_6]^-$, $[\text{PF}_6]^-$) form pentagonal metallacycles.²⁸⁵ Encapsulation within π -acidic cavities establishes strong, short $\text{F}\cdots\text{C}$ contacts, confirmed by X-ray structures and DFT calculations. Solid-state ^{19}F MAS NMR showed downfield shifts for the templated anions, corroborating their involvement in non-covalent interactions. Solution studies reveal that anions not only template polygon formation but also influence stability and nuclearity, with pentagons exhibiting remarkable robustness despite angle strain (Figure 1.42). Anions like $[\text{CF}_3\text{SO}_3]^-$ fail to induce self-assembly, underscoring the essential templating role of specific anions. These metallacycles exhibit high stability in solution, driven by strong anion- π interactions with low activation energies ($\Delta G^\ddagger \approx 50$ kJ/mol). The findings underscore the critical role of templating anions in dictating polygon geometry and stability.

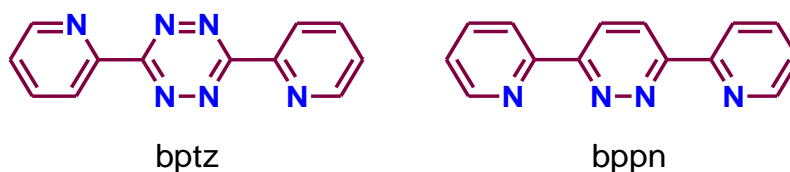


Figure 1.42

Zhong-Min Su and group reported a series of four cationic iridium(III) complexes featuring pyridine-azole ancillary ligands and 1-(2,4-difluorophenyl)-1H-pyrazole as a cyclometalated ligand (Figure 1.43).²⁸⁶ These complexes exhibit weak photoluminescence in dilute solutions (quantum yields $\sim 1\%$) but enhanced phosphorescence in the aggregated state. The weak emission in isolated states arises from significant structural relaxation between the ground and triplet excited states. Aggregation suppresses detrimental π - π stacking and structure relaxation, facilitated by anion- π interactions between the counter anion and π -systems, as supported by single-crystal analysis and theoretical calculations. These interactions reduce non-radiative decay pathways, leading to strong emission in the aggregated state. The robust emission properties of these complexes demonstrate potential application in information security and storage. This study introduces a novel design approach for AIE-active cationic complexes, utilizing weak anion- π interaction engineering to modulate molecular packing and optimize photophysical behavior.

The 1993 *Science* article by Kumpf and Dougherty explores how cation- π interactions contribute to ion selectivity in potassium channels.²⁷¹ Through computational studies, the authors evaluated the binding affinities of monovalent cations (Li^+ , Na^+ , K^+ , Rb^+) to the π -face of benzene. In the gas phase, binding affinities followed the expected electrostatic trend, with Li^+ showing the strongest affinity. However, in aqueous environments, a reordering occurred, with K^+ being preferred in 2:1 benzene:ion complexes (Figure 1.44). This selectivity sequence parallels to that observed in voltage-gated potassium channels. Given the presence of conserved aromatic residues in the pore region of these channels, the study suggests that cation- π interactions may play a significant role in their ion selectivity.

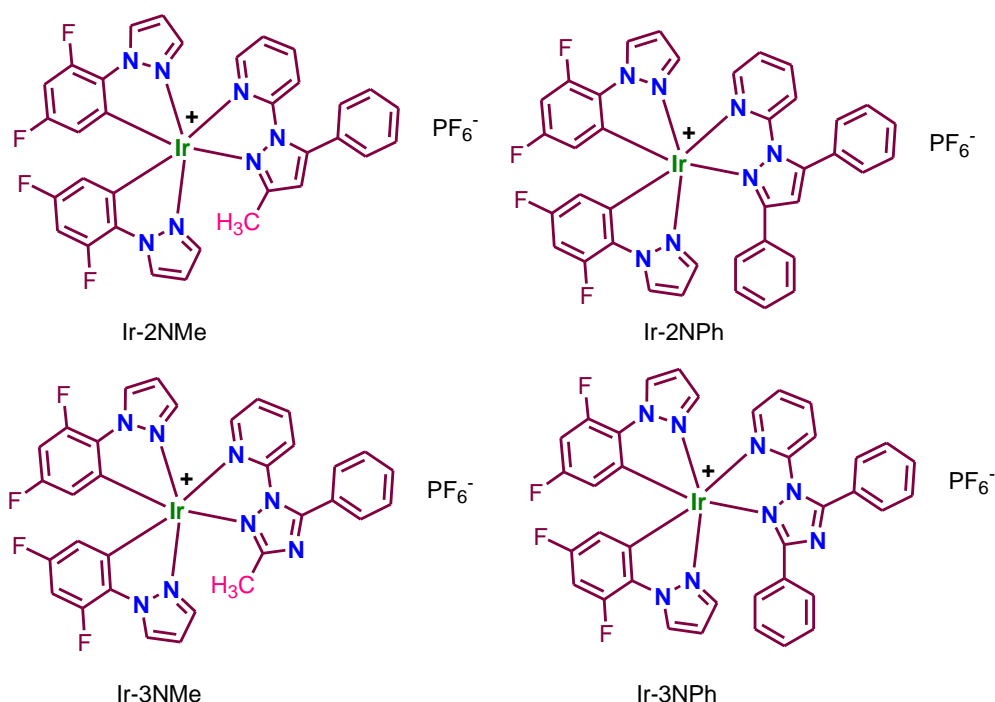


Figure 1.43

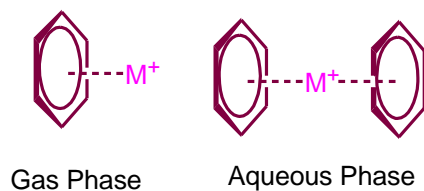


Figure 1.44

Zaric and coworkers propose a novel type of cation- π interaction in metalloproteins, involving aromatic amino acid side chains (phenylalanine, tyrosine, and tryptophan) and positively charged ligands coordinated to a metal cation.²⁷² They termed it the metal-ligand aromatic cation- π (MLAC π) interaction, where a ligand coordinated to a metal cation engages

with an aromatic component (Figure 1.45). Coordinated ligands include amino acids like asparagine, aspartate, glutamate, histidine, threonine, as well as water and small molecules like ethanol. These interactions contribute to the stability and conformation of metalloproteins and may play a direct role in enzymatic mechanisms at the metal centre. For instance, quantum chemical calculations for superoxide dismutase show that Trp163 interacts with iron-coordinated ligands with energy of 10.09 kcal/mol.

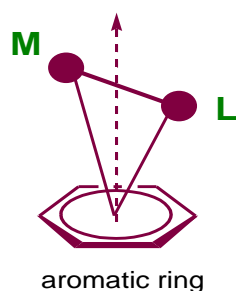


Figure 1.45

CW Tsang and group investigate how alkali metal cations (Li^+ , Na^+ , K^+) interact with phenylalanine. Using advanced density functional theory, the study reveals that these cations preferentially bind to phenylalanine through a tridentate interaction involving the carbonyl oxygen ($\text{O}=\text{C}$), amino nitrogen (NH_2), and aromatic π -ring.²⁷³ The optimized geometries of the most stable M^+ -phenylalanine (Phe) isomer, at the B3LYP/6-31G(d) level of theory is depicted in Figure 1.46. All the bond lengths [\AA] are given in the order (from top to bottom) $\text{M}^+=\text{Li}^+$, Na^+ , K^+ . The binding affinities follow the order $\text{Li}^+ > \text{Na}^+ > \text{K}^+$, with estimated energies of 275, 201, and 141 kJ/mol, respectively. Key factors influencing the stability of different binding modes and conformers were identified, with ion-dipole interactions playing a significant role. The trends in cation- π and non- π bonding distances (e.g., $\text{Na}^+-\pi > \text{Na}^+-\text{N} > \text{Na}^+-\text{O}$ and $\text{K}^+-\pi > \text{K}^+-\text{N} > \text{K}^+-\text{O}$) align with X-ray crystal structures of synthetic receptors, such as sodium and potassium-bound lariat ether complexes. However, the cation- π distances in the crystal structures are longer, likely due to the higher coordination numbers of the cations in these complexes.

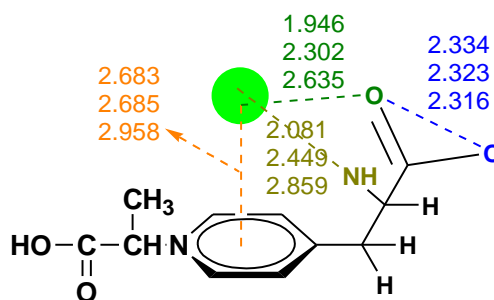


Figure 1.46

Dennis A. Dougherty *et al.* compares cation- π interactions and salt bridges in aqueous and various organic solvents using a consistent theoretical approach. It finds that cation- π interactions are stronger, with an energy of 5.5 kcal/mol compared to 2.2 kcal/mol for salt bridges in water. Notably, cation- π interactions maintain their strength across different solvents, whereas the strength of salt bridges diminishes significantly when moving from the gas phase to water.²⁷⁴ Analyzing protein structures, the authors observe that significant cation- π interactions are typically solvent-exposed rather than buried. This insight suggests potential for engineering surface-exposed cation- π interactions to enhance protein stability, offering valuable implications for protein design and engineering.

Yakiyama and group reported four homo- and heteroleptic luminescent Ru(II) complexes (**C1-C4**) incorporating sumanene-functionalized terpyridine ligands which exhibits enhanced emission compared to conventional $[\text{Ru}(\text{terpy})_2]^{2+}$ complexes (Figure 1.47).²⁸⁷ Phenylene-containing complexes exhibited dual emission via TICT due to rapid rotation between sumanene and terpyridine. Additionally, the cation sensing abilities of **C1-C4** were examined, revealing that all complexes function as Li^+ detectors, most likely through cation- π interactions.

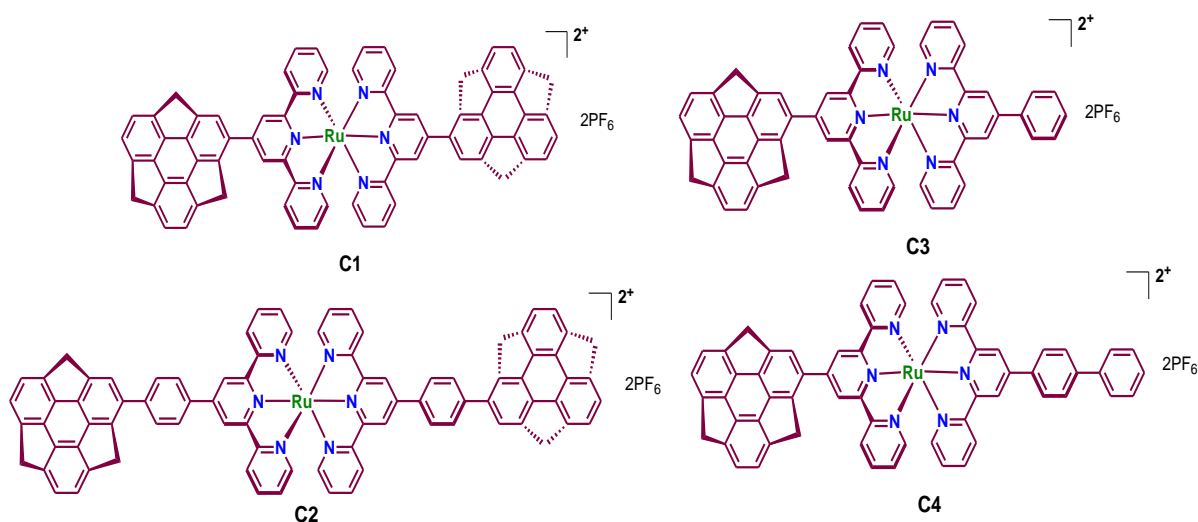


Figure 1.47

Bozkaya and colleagues conducted a computational study on the structures and interaction energies of complexes formed by Fe^{2+} , Co^{2+} , Ni^{2+} , Cu^{2+} , and Zn^{2+} upon binding with benzene (Bz) molecules using high-level quantum chemical methods, such as MP2, CCSD, and CCSD (T). The study also investigated relativistic effects using Douglas-Kroll-Hess computations. This work is the first to examine both the structures and energetics of Bz-M^{2+} and $\text{Bz-M}^{2+}\text{-Bz}$ complexes (Figure 1.48).²⁸⁸ The results show strong binding between

transition metal cations and benzene, with interaction energies for the Bz-M²⁺ type of complexes ranging between -131.9 and -189.8 kcal/mol, while between -206.4 and -258.6 kcal/mol for the Bz-M²⁺-Bz type complexes. The later is 1.2-1.5 times larger than for Bz-M²⁺ complexes, further emphasizing the strength of these interactions. Relativistic effects proved significant, with energy corrections between -1.9 and -7.7 kcal/mol. The study demonstrates that the binding energies from transition metal cation- π interactions were significantly larger than those of π - π and main group cation- π interactions, suggesting new possibilities for exploring cation- π interactions.

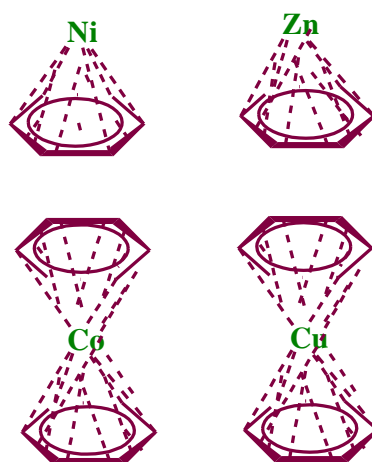


Figure 1.48

1.8 Objective and Scope of the Present Work

The literature on Ru(II) and Os(II) complexes reveals a preponderance of complexes derived from bidentate chelating units, such as bipyridine and phenanthroline, due to their favorable ground and excited state properties. However, bidentate ligands often result in isomeric impurities within the resulting octahedral complexes, which can be challenging to separate. To address this issue, the use of tridentate terpyridine-type ligands can be advantageous, as they can yield achiral linear complexes. Nonetheless, a significant drawback of Ru(II) terpyridine complexes is their often inferior room temperature excited state properties, frequently resulting in non-luminescence or weak luminescence with exceedingly short excited state lifetimes. Consequently, designing Ru(II) terpyridine complexes with enhanced excited state behaviors presents a formidable challenge for researchers.

With this in mind, the primary objective of this dissertation is to develop Ru(II) terpyridine complexes with improved ground and excited state properties, thereby rendering them suitable as potential building blocks for the design of photochemical molecular devices.

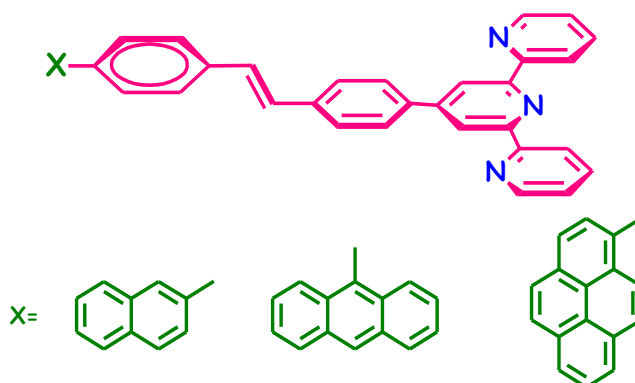
Additionally, we sought to explore the synthesis of Os(II) analogues of the terpyridine ligands, aiming to extend the range of their absorption and emission spectral domain into the infrared region, thereby enhancing their applicability for biological systems.

Another method to improve the RT emission characteristics is via aggregation. Aggregation-Induced Emission (AIE) significantly enhances the excited state properties of ruthenium terpyridine complexes, in contrast to the typical quenching as seen in many chromophores. In solution, terpyridine ligands and metal complexes exhibit free rotation and non-radiative decay, resulting in weak emission, but upon aggregation, the restricted motion reduces non-radiative decays, enhancing luminescence. Thus, AIE behavior makes ruthenium terpyridine complexes valuable for applications in sensing, bioimaging, and optoelectronics.

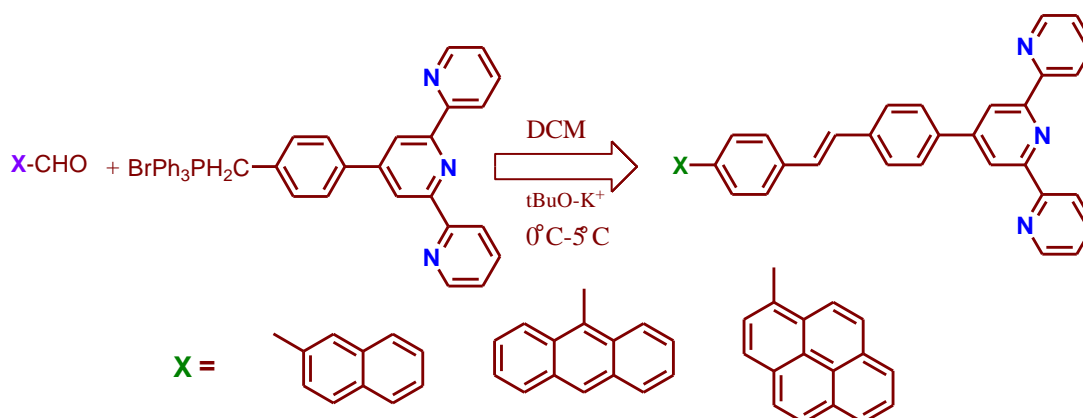
The second goal of this research is to create molecular systems capable of reversibly modifying their physicochemical properties in response to external stimuli, thereby improving their functionality and potential applications in designing functional molecules. Stimuli-responsive molecules have wide-ranging uses, including in information processing, sensors, and molecular switches. Coordination complex-based materials hold an advantage over organic alternatives due to their greater tunability in structural, photophysical, and electrochemical properties. Among various stimuli, light is especially valuable for developing molecular devices, as it can trigger structural changes in molecular systems, leading to substantial alteration in their physicochemical behavior. Although the photoisomerization of stilbene-appended metal complexes-such as those incorporating Re, Co, Rh, and Ir has been extensively researched, there is limited literature on light-induced trans/cis isomerization in stilbene-appended Ru- and Os-terpyridine complexes. Apart from this, chemical stimuli including anions and cations can also exert a significant influence on the photophysical properties of metal complexes. Ions such as F^- and Hg^{+2} pose a serious threat to both the environment and human health, necessitating their detection. Given their environmental and health concerns, the development of chemosensors capable of selectively detecting anions and cations has become a critical research area. Metal-based chemosensors, when designed with specific ligands and functional groups, can detect ions via non-covalent interactions like hydrogen bonding, $CH\cdots\pi$, cation- π and anion- π interactions through changes in their photophysical properties, enabling qualitative and quantitative analysis in various samples, including environmental water, biological fluids, and industrial effluents. Non-covalent interactions are the fundamental forces that hold molecules together without forming chemical bonds, driving processes such as molecular recognition and sensing. Thus, study of

non-covalent interactions is crucial for understanding a wide range of fundamental biological and chemical processes.

To fulfill our objective, we have synthesized an array of terpyridine ligands, tpy-pvp-X (X = naphthalene, anthracene, pyrene), incorporating polyaromatic-substituted styrylbenzene moiety at the 4'-position of the terpyridine motif to tune the photophysical properties as well as to modulate the HOMO-LUMO energy gap. (Scheme 1.1). The desired ligands are synthesized by stoichiometric reaction between tpyPhCH₂PPh₃Br and the corresponding aldehyde in 1:1 molar ratio in dichloromethane at the temperature range of 0-5°C under argon protection (Scheme 1.2).



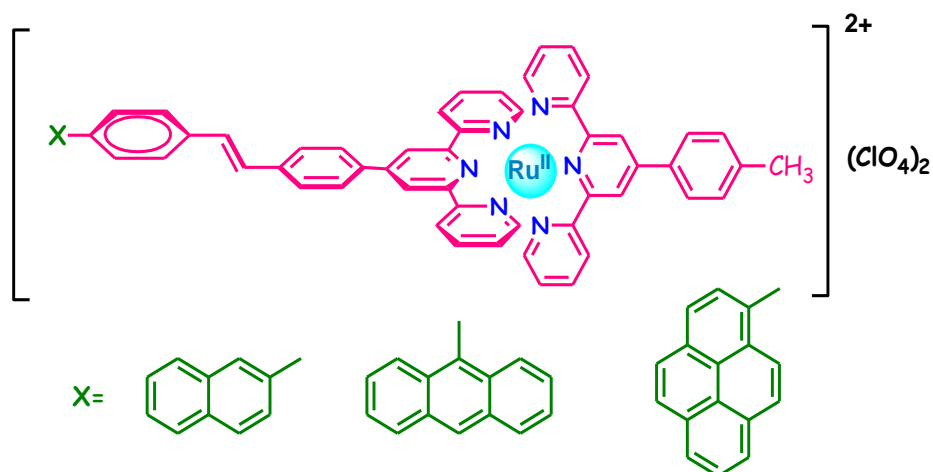
Scheme 1.1



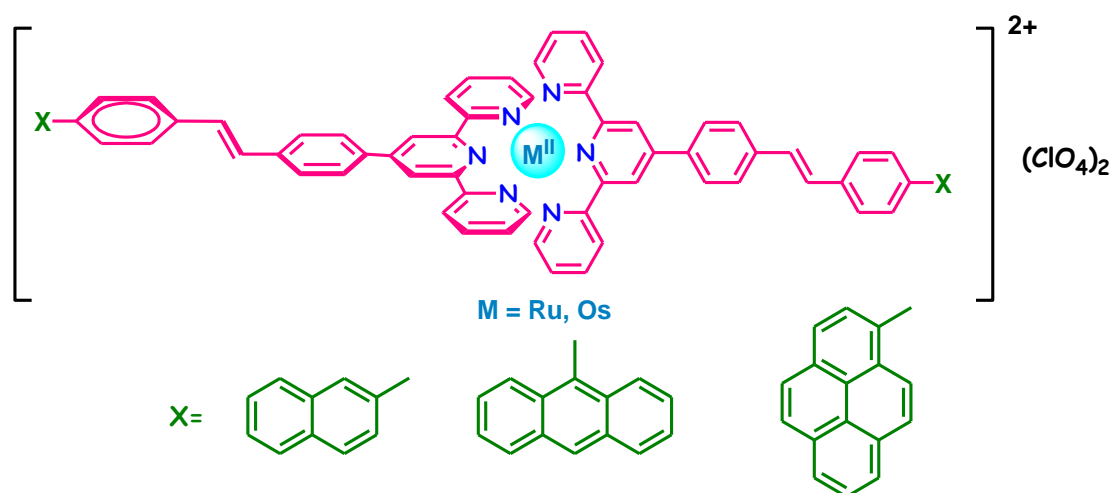
Scheme 1.2

The scope of formation of various homo- and heteroleptic complexes of Ru(II) and Os(II) with the proposed styrylbenzene appended terpyridine ligand (tpy-pvp-X) are summed up in Scheme 1.3-1.4. Variation in the electronic nature of the polyaromatic moiety could induce π -electron delocalization in the excited state, leading to enhanced RT emission characteristics in the resulting complexes.

After synthesizing the ligands and their metal complexes, they will be characterized using standard analytical techniques, including elemental analysis, ESI mass spectrometry, and NMR spectroscopy. Their absorption and emission properties will be systematically studied, and excited-state lifetimes will also be measured using time-correlated single photon counting. Electrochemical properties will be examined via cyclic voltammetry. Additionally,



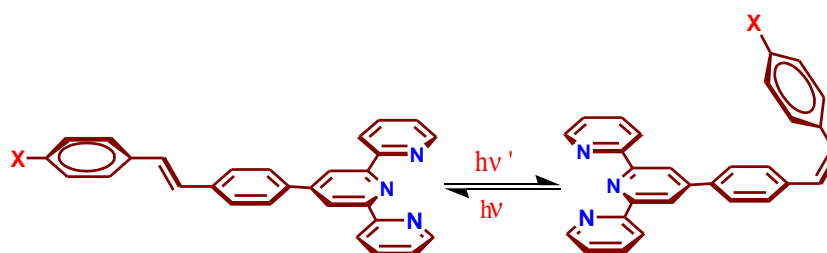
Scheme 1.3



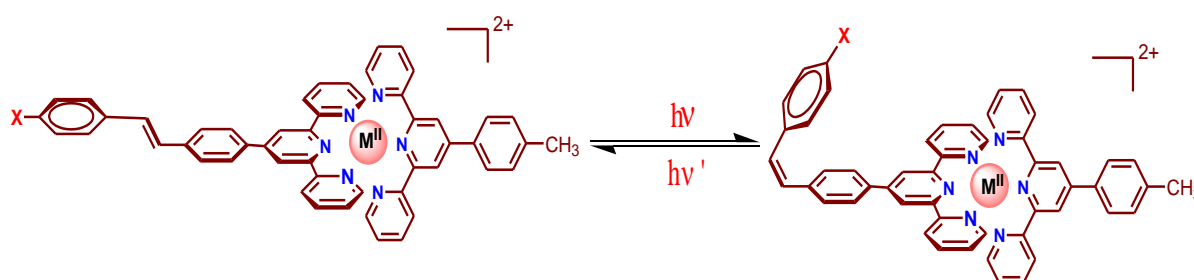
Scheme 1.4

density functional theory (DFT) and time-dependent DFT calculations will be performed to understand their electronic structures and assign the respective absorption and emission spectral bands. The stimuli-responsive behavior, including light-induced rotation around the C=C bond, will also be explored (Scheme 1.5-1.6). While the heteroleptic complexes can

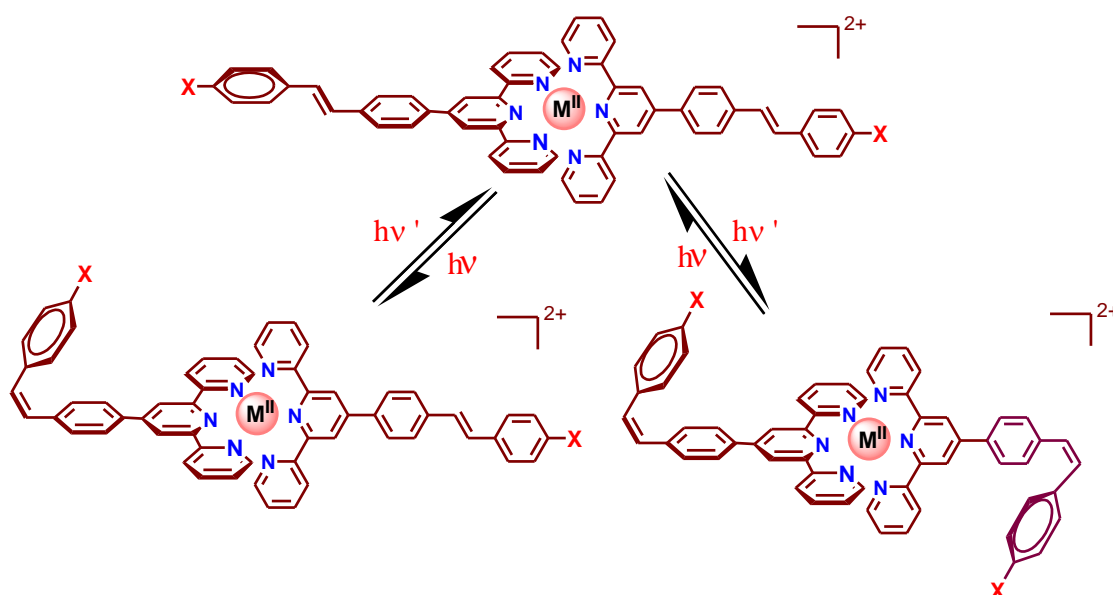
undergo reversible trans to cis isomerization, homoleptic complexes can either go from trans-trans to trans-cis or cis-cis forms upon shining visible light (Scheme 1.7). The reverse process is explored using light of different wavelength. The rate of photoisomerization can be modulated through the use of various solvents, oxidants, reductants and light of appropriate wavelengths, thereby aiding in the construction of efficient multi-state photoswitches.



Scheme 1.5

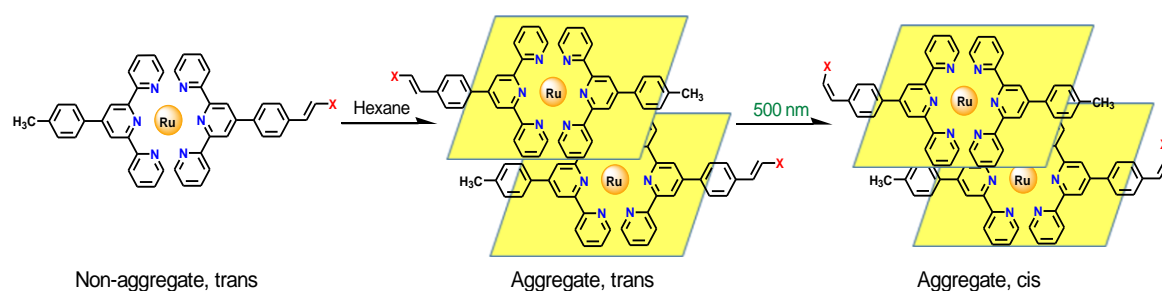


Scheme 1.6



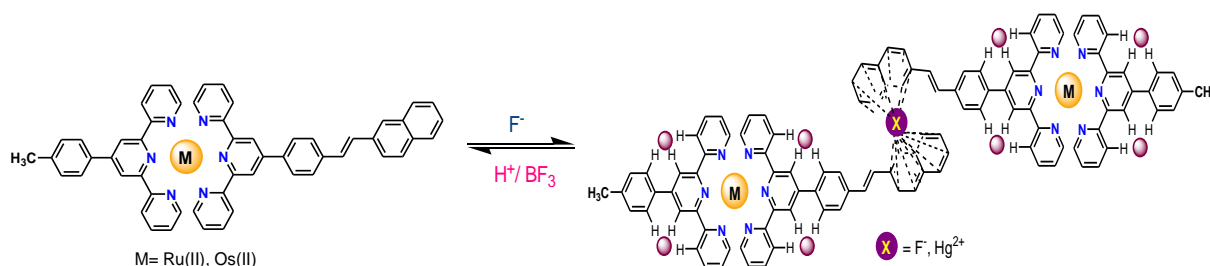
Scheme 1.7

Due to the presence of different polyaromatic and heteroaromatic moieties, the complexes can undergo aggregation upon using various solvent mixtures. Different binary solvents induce distinct modes of self-assembly, leading to either aggregation-induced emission enhancement or aggregation-induced emission quenching, accompanied by red or blue shifts, in the emission maxima. Since the aggregated form of the complexes also consist of the C=C bond, hence we will also be interested to investigate the effect of aggregation on the rate of photoisomerization (Scheme 1.8).



Scheme 1.8

Another key objective of this dissertation is to modulate the photoredox properties of the complexes by strategically manipulating their secondary coordination sphere through the application of various external stimuli, such as anion or cation, with the aim of developing potential molecular sensors and switches. This can be done by taking advantage of various non-covalent interactions since the molecular backbone consist of a large delocalized π -cloud due to the presence of various polyaromatic and heteroaromatic moieties (Scheme 1.9). The interaction between the complexes and ions will be assessed through absorption, emission and NMR titration experiments, whereas the extent of interaction is evaluated through their binding constants. Additionally, changes in the excited-state lifetime of the complexes in the presence of different ions will be explored to evaluate their potential as lifetime-based ion sensors.



Scheme 1.9

The execution of different scopes along with relevant investigations has been reported in chapter 2-7.

Chapter 2 introduces a series of stilbene-appended terpyridine systems coupled with anthracene, naphthalene, and pyrene moiety, which exhibit efficient and versatile photo-responsive behaviors. The compounds show either aggregation-induced blue-shifted emission (AIBSE) or emission quenching accompanied with a red shift, dependent on the type of solvent mixtures, attributed to H- and J-aggregate formation. Additionally, both the free and aggregated forms of the compounds undergo trans/cis isomerization upon visible light exposure, with the reverse process occurring in the dark, facilitating "on-off" and "off-on" emission switching. The rate constants and quantum yields of the photoisomerization processes decrease with increased aggregation, thereby offering a strategy to design smart molecular switches.

Chapter 3 presents synthesis and characterization of a new series of Ru(II) bis-terpyridine complexes incorporating a styrylphenyl unit linked to anthracene, naphthalene, and pyrene unit. Comprehensive experimental and theoretical analyses were conducted to investigate their photophysical, electrochemical, aggregation-induced emission, and photoisomerization properties. Visible light triggers trans-trans to trans-cis isomerization, as evidenced by changes in their absorption, emission spectra, and NMR data, with the reverse cis-to-trans isomerization triggered by UV light, facilitating reversible "on-off" emission switching. In dilute solutions, the complexes show weak emission at room temperature, but aggregation significantly enhances emission intensity, quantum yield, and lifetime. Aggregated forms also undergo slower isomerization under visible light. These systems can act as potential smart molecular switches, with controllable emission behavior through solvent-induced aggregation and light irradiation.

Chapter 4 deals with a new series of heteroleptic Ru(II)-terpyridine complexes featuring stilbene-appended naphthalene, anthracene, and pyrene motifs, designed as potential molecular sensors and switches. Notably, they selectively recognize fluoride (F⁻) among various anions through a combination of CH...F hydrogen bonding, CH- π , anion- π , and electrostatic interactions, confirmed by spectroscopic and DLS experiments. DFT calculations further elucidate the mode of receptor-anion interactions. The complexes also display reversible trans-cis isomerization under alternate treatment with visible and UV light, functioning as photo-molecular switches. The cis-form shows reduced complex-anion interaction efficacy compared to the respective trans-form. Additionally, the fluoride-induced

changes are reversible, allowing repeated "on/off" emission switching with alternative treatment with F^- and $BF_3/HClO_4$.

Chapter 5 explores the aggregation-induced modulation of the room temperature luminescence characteristics in heteroleptic Ru(II)-terpyridine complexes using varied solvent mixtures. The complexes exhibit both aggregation-induced emission enhancement (AIEE) and aggregation-caused quenching (ACQ), depending on the solvent combination. Notably, their lifetime also increase quite significantly upon aggregation. Trans→cis photoisomerization of the aggregated complexes occurs under visible light but at a slower rate compared to the non-aggregated forms. The emission switching is efficiently controlled by varying solvent mixtures and wavelength of irradiation light, making these complexes promising candidates for smart molecular switches.

Chapter 6 copes with synthesis and thorough characterization of a new family of homoleptic luminescent Os(II) bis-terpyridine complexes featuring stilbene-coupled naphthalene, anthracene, and pyrene motifs. These complexes are moderately emissive in the near-infrared (NIR) region with enhanced lifetimes at room temperature. They exhibit reversible trans-trans to cis-cis photoisomerization under alternative treatment with visible and UV light, functioning as a photo-molecular switch in the NIR domain. Remarkably, the photoisomerization rate increases by nearly two orders of magnitude when oxidized with ceric ammonium nitrate (CAN) or reduced using metallic sodium, enabling rapid and efficient three-state "on-off" photo-switching in the NIR domain.

Chapter 7 deals with multi-channel anion and cation sensing efficacies of the said homoleptic Os(II) bis-terpyridine complexes. The complexes are very much selective towards fluoride and mercuric ion, among the studied anions and cations, respectively and thus act as dual sensors of the said ions in near-infrared (NIR) domain. The complexes selectively detect these ions through the intermediary of different non-classical interactions such as $CH\cdots F$ hydrogen bonding, $CH\cdots\pi$, cation- π and anion- π . Light-induced trans-trans→cis-cis photoisomerization of the stilbene unit alters sensing efficacy, with notable differences among the isomeric forms. Computational results also support the experimental findings in elucidating the mode of ion-receptor interactions. Thus the present complexes are promising candidates for NIR-emitting molecular switches.

1.9 References

- (1) Meyer, T. J. Chemical Approaches to Artificial Photosynthesis. *Acc. Chem. Res.* **1989**, 22, 163-170.
- (2) Natali, M.; Campagna, S.; Scandola, F. Photoinduced Electron Transfer Across Molecular Bridges: Electron- and Hole-Transfer Superexchange Pathways. *Chem. Soc. Rev.* **2014**, 43, 4005- 4018.
- (3) Beaujuge, P.; Fréchet, J. Molecular Design and Ordering Effects in π -Functional Materials for Transistor and Solar Cell Applications. *J. Am. Chem. Soc.* **2011**, 133, 20009-20029.
- (4) Scandola, F.; Chiorboli, C.; Indelli, M. T.; Rampi, M. A. In *Electron Transfer in Chemistry*; Balzani, V., Ed.; VCH-Wiley: 2001; Vol. 3, p 337.
- (5) Glaser, F.; Wenger, O. S. Recent Progress in the Development of Transition-Metal Based Photoredox Catalysts. *Coord. Chem. Rev.* **2020**, 213139.
- (6) Zhang, T.; Lin, W. Metal-Organic Frameworks for Artificial Photosynthesis and Photocatalysis. *Chem. Soc. Rev.* **2014**, 43, 5982-5993.
- (7) Rupp, M.; Auvray, T.; Rousset, E.; Mercier, G.M.; Marvaud, V.; Kurth, D.G.; Hanan, G.S. Photocatalytic Hydrogen Evolution Driven by a Heteroleptic Ruthenium (II) Bis (Terpyridine) Complex. *Inorg. Chem.* **2019**, 58, 9127-9134.
- (8) Ray, D.; Liang, C. K.; McClenaghan, N.; Bassani, D. Organic and Supramolecular Materials for LED and Photovoltaic Applications. *Curr. Phys. Chem.* **2011**, 1, 169-180.
- (9) Sun, Y.; Joyce, L. E.; Dickson, N. M.; Turro, C. Efficient DNA Photocleavage by $[\text{Ru}(\text{bpy})_2(\text{dppn})]^{2+}$ with Visible Light. *Chem. Commun.* **2010**, 46, 2426-2428.
- (10) Zhao, W.-W.; Xu, J.-J.; Chen, H.-H. Photoelectrochemical DNA Biosensors. *Chem. Rev.* **2014**, 114, 7421-7441.
- (11) Rice, A. M.; Martin, C. R.; Galitskiy, V. A.; Berseneva, A. A.; Leith, G. A.; Shustova, N. B. Photophysics Modulation in Photoswitchable Metal-Organic Frameworks. *Chem. Rev.* **2020**, 120, 8790-8813.
- (12) Balzani, V.; Credi, A.; Venturi, M. *Molecular Devices and Machines*; Wiley-VCH: Weinheim, 2003.
- (13) *Intelligent Stimuli-Responsive Materials*; Li, Q., Ed.; John Wiley & Sons, Inc.: Hoboken, Nj, 2013.

- (14) McConnel, A.J.; Wood, C. S.; Neelakandan P. P.; Nitschke, J. R. Stimuli-responsive Metal-ligand Assemblies, *Chem. Rev.* **2015**, *115*, 7729-7793.
- (15) Martinez-Manez, R.; Sancenon, F. Fluorogenic and Chromogenic Chemosensors and Reagents for Anions. *Chem. Rev.* **2003**, *103*, 4419-4476.
- (16) Grusenmeyer, T. A.; Chen, J.; Jin, Y.; Nguyen, J.; Rack, J. J.; Schmehl, R. H. pH Control of Intramolecular Energy Transfer and Oxygen Quenching in Ru(II) Complexes Having Coupled Electronic Excited States. *J. Am. Chem. Soc.* **2012**, *134*, 7497-7506.
- (17) Amendola, V.; Fabbrizzi, L.; Licchelli, M.; Mangano, C.; Pallavicini, P.; Parodi, L. Poggi, A. Molecular Events Switched by Transition Metals. *Coord. Chem. Rev.* **1999**, *190-192*, 649-669.
- (18) McConnell, A. J.; Wood, C. S.; Neelakandan, P. P.; Nitschke, J. R. Stimuli-Responsive Metal-Ligand Assemblies. *Chem. Rev.* **2015**, *115*, 7729-7793.
- (19) Haga, M.; Takasugi, T.; Tomie, A.; Ishizuya, M.; Yamada, T.; Hossain, M. D.; Inoue, M. Molecular Design of a Proton-Induced Molecular Switch Based on Rod-Shaped Ru Dinuclear Complexes with Bis-Tridentate 2,6-Bis(Benzimidazol-2-Yl)Pyridine Derivatives. *Dalton Trans.* **2003**, 2069-2079.
- (20) Kume, S.; Nishihara, H. Photochrome-Coupled Metal Complexes: Molecular Processing Of Photon Stimuli. *Dalton Trans.* **2008**, 3260-3271.
- (21) Balzani, V.; Credi, A.; Venturi, M. Light Powered Molecular Machines. *Chem. Soc. Rev.* **2009**, *38*, 1542-1550.
- (22) Juris, A.; Balzani, V.; Barigelletti, F.; Campagna, S.; Belser, P.; von Zelewsky, A. Ru(II) Polypyridine Complexes: Photophysics, Photochemistry, Eletrochemistry, and Chemiluminescence. *Coord. Chem. Rev.* **1988**, *84*, 85-277.
- (23) Caspar, J. V.; Meyer, T. J. Photochemistry of Tris(2,2'-bipyridine)Ruthenium(2+) Ion ($\text{Ru}(\text{bpy})_3^{2+}$): Solvent Effects. *J. Am. Chem. Soc.* **1983**, *105*, 5583-5590.
- (24) Van Houten, J.; Watts, R. J. Temperature Dependence of The Photophysical and Photochemical Properties of the Tris(2,2'-Bipyridyl)Ruthenium(II) Ion in Aqueous Solution. *J. Am. Chem. Soc.* **1976**, *98*, 4853-4858.
- (25) Balzani, V.; Juris, A.; Venturi, M.; Campagna, S.; Serroni, S. Luminescent and Redox-Active Polynuclear Transition Metal Complexes. *Chem. Rev.* **1996**, *96*, 759-834.

- (26) Creutz, C.; Chou, M.; Netzel, T.; L. Okumura, M.; Sutin, N. Lifetimes, Apectra, and Quenching of The Excited States of Polypyridine Complexes of Iron (II), Ruthenium (II), and Osmium (II). *J. Am. Chem. Soc.* **1980**, *102*, 1309-1319.
- (27) Meyer, T. J. Photochemistry of Metal Coordination Complexes: Metal to Ligand Charge Transfer Excited States. *Pure Appl. Chem.* **1986**, *58*, 1193.
- (28) Wang, X.; Guerzo, A.; Baitalik, S.; Simon, G.; Shaw, G. B.; Chen, L.; Schmechl, R. H. The Influence of Bridging Ligand Electronic Structure on the Photophysical Properties of Noble Metal Diimine and Triimine Light Harvesting Systems. *Photosynth. Res.* **2006**, *87*, 83-103.
- (29) Ali, C.; Banaszak, M.; Astumian, R. D.; Stoddart, J. F.; Grzybowski, B. A. Great Expectations: Can Artificial Molecular Machines Deliver on Their Promise? *Chem. Soc. Rev.* **2012**, *41*, 19-30.
- (30) Sauvage, J.-P.; Collin, J. P.; Chambron, J. C.; Guillerez, S.; Coudret, C.; Balzani, V.; Barigelletti, F.; De Cola, L.; Flamigni, L. Ruthenium(II) and Osmium(II) Bis(terpyridine) Complexes in Covalently-Linked Multicomponent Systems: Synthesis, Electrochemical Behavior, Absorption Spectra, and Photochemical and Photophysical Properties. *Chem. Rev.* **1994**, *94*, 993-1019.
- (31) Kalyanasundaram, K.; Gratzel M.; Applications of Functionalized Transition Metal Complexes in Photonic and Optoelectronic Devices. *Coord. Chem. Rev.* **1998**, *177*, 347-414.
- (32) Khaled, R.M.; Abo-Elfadl, M.T.; Radacki, K.; Zeid, M.A.A.; Shehab, O.R.; Abdel-Kader, N.S.; Mostafa, G.A.; Ali, E.A.; Al Neyadi, S.S.; Mansour, A.M. Visible-Light-Induced CO-Releasing Properties and Cytotoxicity of a Ru (II) Carbonyl Complex Containing 2-(pyridin-2-yl)-quinoxaline. *Dalton Trans.* **2025**.
- (33) Momeni, B.Z.; Davarzani, N.; Janczak, J.; Ma, N.; Abd-El-Aziz, A.S. Progress in Design and Applications of Supramolecular Assembly of 2,2':6',2''-Terpyridine-Based First Row d-Block Elements. *Coord. Chem. Rev.* **2024**, *506*, 215619.
- (34) Bera, M.K.; Sarmah, S.; Santra, D.C.; Higuchi, M., Heterometallic Supramolecular Polymers: From Synthesis to Properties and Applications. *Coord. Chem. Rev.* **2024**, *501*, 215573.
- (35) Mandal, A.A.; Upadhyay, A.; Mandal, A.; Nayak, M.; Mohammad S, K.; Mukherjee, S.; Banerjee, S.; Visible-Light-Responsive Novel Ru (II)-Metallo-Antibiotics with

- Potential Antibiofilm and Antibacterial Activity. *ACS Appl. Mater. Interfaces* **2024**, *16*, 28118-28133.
- (36) Juwita, R.; Liao, J. M.; Chen, C. Y.; Tsai, H. H. G. Enhancing Near-Infrared Absorption in Terpyridyl Ru/Os Complexes with Ancillary Ligands to Activate Spin-Forbidden Transitions in Dye-Sensitized Solar Cells: A TDDFT Investigation. *J. Phys. Chem. A* **2024**, *128*, 880-894.
- (37) Balzani, V.; Bergamini, G.; Marchioni, F.; Ceroni, P. Ru(II)-bipyridine Complexes in Supramolecular Systems, Devices and Machines. *Coord. Chem. Rev.* **2006**, *250*, 1254-1266.
- (38) Yersin, H.; Rausch, A. F.; Czerwieniec, R.; Hofbeck, T.; Fischer, T. The Triplet State of Organo-Transition Metal Compounds. Triplet Harvesting and Singlet Harvesting for Efficient OLEDs. *Coord. Chem. Rev.* **2011**, *255*, 2622-2652.
- (39) Liu, P.; Wu, B. Y.; Liu, J.; Dai, Y. C.; Wang, Y. J.; Wang, K. Z. DNA Binding and Photocleavage Properties, Cellular Uptake and Localization, and In-Vitro Cytotoxicity of Dinuclear Ruthenium(II) Complexes with Varying Lengths in Bridging Alkyl Linkers. *Inorg. Chem.* **2016**, *55*, 1412-1422.
- (40) Mardanya, S.; Karmakar, S.; Mondal, D.; Baitalik, S. Homo- and Heterobimetallic Ruthenium(II) and Osmium(II) Complexes Based on a Pyrene-Biimidazolate Spacer as Efficient DNA-Binding Probes in the Near-Infrared Domain. *Inorg. Chem.* **2016**, *55*, 3475-3489.
- (41) Maity, D.; Bhaumik, C.; Mardanya, S.; Karmakar, S.; Baitalik, S. Light Harvesting and Directional Energy Transfer in Long-Lived Homo- and Heterotrimetallic Complexes of Fe^{II}, Ru^{II}, and Os^{II}. *Chem. -Eur. J.* **2014**, *20*, 13242-13252.
- (42) Arrigo, A.; Santoro, A.; Puntoriero, F.; Lainé, P. P. Campagna, S. Photoinduced Electron Transfer in Donor-Bridge-Acceptor Assemblies: The Case Of Os(II)-Bis(Terpyridine)-(Bi)Pyridinium Dyads. *Coord. Chem. Rev.* **2015**, *304-305*, 109-116.
- (43) Manner, V. W.; Mayer, J. M.; Concerted Proton-Electron Transfer in a Ruthenium Terpyridyl-Benzooate System with a Large Separation between the Redox and Basic Sites. *J. Am. Chem. Soc.* **2009**, *131*, 9874-9875.
- (44) Chang, K. C.; Sun, S. S.; Odago, M. O.; Lees, A. J. Anion Recognition and Sensing by Transition-Metal Complexes with Polarized N-H Recognition Motifs. *Coord. Chem. Rev.* **2015**, *284*, 111-123.

- (45) Constable, E. C. 2,2':6',2''-Terpyridines: From Chemical Obscurity to Common Supramolecular Motifs. *Chem. Soc. Rev.* **2007**, *33*, 246-253.
- (46) Harriman, A.; Ziessel, R. Making Photoactive, Molecular-Scale Wires. *Chem. Commun.* **1996**, 1707-1716.
- (47) Pal, A. K.; Hanan, G. S. Design, Synthesis and Excited-State Properties of Mononuclear Ru(II) Complexes of Tridentate Heterocyclic Ligands. *Chem. Soc. Rev.* **2014**, *43*, 6184-6197.
- (48) Hofmeier, H.; Schubert, U. S. Recent Developments in the Supramolecular Chemistry of Terpyridine-Metal Complexes. *Chem. Soc. Rev.* **2004**, *33*, 373-399.
- (49) Winkler, J. R.; Netzel, T.; Creutz, C.; Sutin, N. Direct Observation of Metal-To-Ligand Charge-Transfer (MLCT) Excited States of Pentaammineruthenium(II) Complex. *J. Am. Chem. Soc.* **1987**, *109*, 2381-2392.
- (50) Medlycott, E. A.; Hanan, G. S. Synthesis and Properties of Mono- and Oligo-Nuclear Ru(II) Complexes of Tridentate Ligands: The Quest for Long-Lived Excited States at Room Temperature. *Coord. Chem. Rev.* **2006**, *250*, 1763-1782.
- (51) Forster, T.; Kasper, K. Ein Konzentrationsumschlag der Fluoreszenz. *Z. Phys. Chem.* (Muenchen, Ger.) **1954**, *1*, 275-277.
- (52) Photophysics of Aromatic Molecules; Birks, J. B., Ed.; Wiley: London, 1970.
- (53) Zhelev, Z.; Ohba, H.; Bakalova, R. Single Quantum Dot-Micelles Coated with Silica Shell as Potentially Non-Cytotoxic Fluorescent Cell Tracers. *J. Am. Chem. Soc.* **2006**, *128*, 6324-6325.
- (54) Bakalova, R.; Zhelev, Z.; Aoki, I.; Ohba, H.; Imai, Y.; Kanno, I. Silica-Shelled Single Quantum Dot Micelles as Imaging Probes with Dual or Multimodality. *Anal. Chem.* **2006**, *78*, 5925-5932.
- (55) Luo, J.; Xie, Z.; Lam, J. W. Y.; Cheng, L.; Tang, B. Z.; Chen, H.; Qiu, C.; Kwok, H. S.; Zhan, X.; Liu, Y. Aggregation-Induced Emission of 1-Methyl-1,2,3,4,5-Pentaphenylsilole. *Chem. Commun.* **2001**, 1740-1741.
- (56) Mei, J.; Leung, L. C. N.; Kwok, T. K. R.; Lam, W. Y. J.; Tang, B. Z. Aggregation-Induced Emission: Together We Shine, United We Soar! *Chem. Rev.* **2015**, *115*, 11718-11940.
- (57) Chen, Z.; Qin, H.; Yin, Y.; Deng, D.; Qin, S. -Y.; Li, N.; Wang, K.; Sun, Y.; Full-Color Emissive D-D-A Carbazole Luminophores: Red-to-NIR Mechano-

- fluorochromism, Aggregation-Induced Near-Infrared Emission, and Application in Photodynamic Therapy. *Chem. Eur. J.* **2023**, 29, e202203797.
- (58) Yin, Y.; Chen, Z.; Li, R. H.; Yi, F.; Liang, X.C.; Cheng, S.Q.; Wang, K.; Sun, Y.; Liu, Y. Highly Emissive Multipurpose Organoplatinum (II) Metallacycles with Contrasting Mechanoresponsive Features. *Inorg. Chem.* **2022**, 61, 2883-2891.
- (59) Xie, H.; Wang, J.; Lou, Z.; Hu, L.; Segawa, S.; Kang, X.; Wu, W.; Luo, Z.; Kwok, R.T.; Lam, J.W.; Zhang, J. Mechanochemical Fabrication Of Full-Color Luminescent Materials from Aggregation-Induced Emission Prefluorophores for Information Storage and Encryption. *J. Am. Chem. Soc.* **2024**, 146, 18350-18359.
- (60) Zhao, Z.; Lam, J. W. Y.; Tang, B. Z. Tetraphenylethene: A Versatile AIE Building Block for the Construction of Efficient Luminescent Materials for Organic Light-Emitting Diodes. *J. Mater. Chem.* **2012**, 22, 23726-23740.
- (61) Wei, P.; Zhang, J-X.; Zhao, Z.; Chen, Y.; He, X.; Chen, M.; Gong, J.; Sung, H. Y. H.; Williams, I. D.; Lam, W. Y. J.; Tang, B. Z. Multiple yet Controllable Photoswitching in a Single AIEgen System. *J. Am. Chem. Soc.* **2018**, 140, 1966-1975.
- (62) Li, K.; Cui, J.; Yang, Z.; Huo, Y.; Duan, W.; Gong, S.; Liu, Z. Solvatochromism, Acidochromism and Aggregation-Induced Emission of Propeller-Shaped Spiroborates. *Dalton Trans.* **2018**, 47, 15002-15008.
- (63) Islam, M. M.; Hu, Z.; Wang, Q.; Feng, C. R. X. Pyrene-Based Aggregation-Induced Emission Luminogens and their Applications. *Mater. Chem. Front.* **2019**, 3, 762-781.
- (64) Zhao, Z.; Shen, S. C.; Mahtab, X. F.; Yu, Y.; Lu, P.; Lam, J.W.; Kwok, H. S.; Tang, B. Z. Aggregation-Induced Emission Self-Assembly, and Electroluminescence of 4, 4'-Bis (1, 2, 2-triphenylvinyl) Biphenyl. *Chem. Commun.* **2010**, 46, 686-688.
- (65) Kaur, M.; Kaur, H.; Kumar, M.; Bhalla, V.; Light-Up AIE-Active Materials: Self Assembly, Molecular Recognition and Catalytic Applications. *Chem. Rev.* **2021**, 21, 240-256.
- (66) An, B.-K.; Kwon, S.-K.; Jung, S.-D.; Park, S. Y. Enhanced Emission and its Switching in Fluorescent Organic Nanoparticles. *J. Am. Chem. Soc.* **2002**, 124, 14410-14415.
- (67) Zhang, W.; Kong, J.; Miao, R.; Song, H.; Ma, Y.; Zhou, M.; Fang, Y. Integrating Aggregation Induced Emission and Twisted Intramolecular Charge Transfer Via Molecular Engineering. *Adv. Funct. Mater.* **2024**, 34, 2311404.

- (68) Gao, B. R.; Wang, H.Y.; Hao, Y.W.; Fu, L.M.; Fang, H. H.; Jiang, Y.; Wang, L.; Chen, Q. D.; Xia, H.; Pan, L.Y.; Ma, Y. G. Time-Resolved Fluorescence Study of Aggregation-Induced Emission Enhancement by Restriction of Intramolecular Charge Transfer State, *J. Phys. Chem. B* **2009**, *114*, 128-134.
- (69) Cai, M.; Gao, Z.; Zhou, X.; Wang, X.; Chen, S.; Zhao, Y.; Qian, Y.; Shi, N.; Mi, B.; Xie, L.; Huang, W. A Small Change in Molecular Structure, a Big Difference in the AIEE Mechanism. *Phys. Chem. Chem. Phys.* **2012**, *14*, 5289-5296.
- (70) Zhu, F. Y.; Mei, L. J.; Tian, R.; Li, C.; Wang, Y. L.; Xiang, S. L.; Zhu, M. Q.; Tang, B. Z., Recent Advances in Super-Resolution Optical Imaging Based on Aggregation-Induced Emission. *Chem. Soc. Rev.* **2024**, *53*, 3350-3383.
- (71) Mazumdar, P.; Das, D.; Sahoo, G. P.; Salgado-Mora'n, G.; Misra, A. Aggregation Induced Emission Enhancement of 4,40-bis(Diethylamino)Benzophenone with an Exceptionally Large Blue Shift and its Potential use as Glucose Sensor. *Phys. Chem. Chem. Phys.* **2015**, *17*, 3343-3354.
- (72) Ye, S.; Bao, Y. Recent Advances in Fluorescent Polymers with Color-Tunable Aggregate Emission. *Chem. Mater.* **2024**, *36*, 5878-5896.
- (73) Liu, Y.; Zhang, Y.; Wu, X.; Lan, Q.; Chen, C.; Liu, S.; Chi, Z.; Jiang, L.; Chen, X.; Xu, J.; Deep-blue Luminescent Compound that Emits Efficiently Both in Solution and Solid State with Considerable Blue-Shift Upon Aggregation. *J. Mater. Chem. C*, **2014**, *2*, 1068-1075.
- (74) Wu, Q.; Zhang, T.; Peng, Q.; Wang, D.; Shuai, Z. Aggregation Induced Blue-Shifted Emission -The Molecular Picture from a QM/MM Study. *Phys. Chem. Chem. Phys.* **2014**, *16*, 5545-5552.
- (75) Banerjee, S.; Both, A. K.; Sarkar, M. Probing the Aggregation and Signaling Behavior of Some Twisted 9,9'-Bianthryl Derivatives: Observation of Aggregation-Induced Blue-Shifted Emission. *ACS Omega* **2018**, *3*, 15709-15724.
- (76) Zhao, Z.; Zhang, H.; Lam, J.W.Y. Tang, B. Z. Aggregation-Induced Emission: New Vistas at the Aggregate Level. *Angew. Chem. Int. Ed.* **2020**, *59*, 9888-9907.
- (77) Fan, W.-J.; Sun, B.; Ma, J.; Li, X.; Tan, H.; Xu, L. Coordination-Driven Self-Assembly of Carbazole-Based Metallodendrimers with Generation-Dependent Aggregation Induced Emission Behavior. *Chem. Eur. J.* **2015**, *21*, 12947-12959.

- (78) Prasad, P.; Gupta A.; Sasmal, P. K. Aggregation-Induced Emission Active Metal Complexes: A Promising Strategy to Tackle Bacterial Infections. *Chem. Commun.* **2021**, 57, 174-186.
- (79) Goswami, N.; Yao, Q.; Luo, Z.; Li, J.; Chen, T.; Xie, J. Luminescent Metal Nanoclusters with Aggregation-Induced Emission. *J. Phys. Chem. Lett.* **2016**, 7, 962-975.
- (80) Alama, P.; Climent, C.; Alemany, P.; Laskar, I. R. "Aggregation-Induced Emission" of Transition Metal Compounds: Design, Mechanistic Insights, and Applications. *Jour. of Photochem. and Photobiol. C: Photochem. Rev.* **2019**, 41, 100317.
- (81) Yan, X.; Wang, H.; Hauke, C. E.; Cook, T. R.; Wang, M.; Saha, M. L.; Zhou, Z.; Zhang, M.; Li, X.; Huang, F.; Stang, P.J. A Suite of Tetraphenylethylene-Based Discrete Organoplatinum(II) Metallacycles: Controllable Structure and Stoichiometry, Aggregation-Induced Emission, and Nitroaromatics Sensing. *J. Am. Chem. Soc.* **2015**, 137, 15276-15286.
- (82) Ravotto, L.; Ceroni, P. Aggregation Induced Phosphorescence of Metal Complexes: From Principles to Applications. *Coord. Chem. Rev.* **2017**, 346, 62-76.
- (83) Yan, X.; Cook, T. R.; Wang, P.; Huang, F.; Stang, P. J. Highly Emissive Platinum(II) Metallacages. *Nat. Chem.* **2015**, 7, 342-348.
- (84) Cheng, H.-K.; Yeung, M. C.-L.; Yam, V. W.-W. Molecular Engineering of Platinum (II) Terpyridine Complexes with Tetraphenylethylene-Modified Alkynyl Ligands: Supramolecular Assembly via Pt...Pt and/or π - π Stacking Interactions and the Formation of Various Superstructures. *ACS Appl. Mater. Interfaces* **2017**, 9, 36220-36228.
- (85) Law, A. S.Y.; Lee, L. C.-C.; Lo, K. K.-W.; Yam, V. W.W. Aggregation and Supramolecular Self-Assembly of Low-Energy Red Luminescent Alkynylplatinum(II) Complexes for RNA Detection, Nucleolus Imaging, and RNA Synthesis Inhibitor Screening. *J. Am. Chem. Soc.* **2021**, 143, 5396-5405.
- (86) Yam, V. W.-W. Chan, K. H. Y.; Wong, K. M.C.; Zhu, N. Luminescent Platinum(II) Terpyridyl Complexes: Effect of Counter Ions on Solvent-Induced Aggregation and Color Changes. *Chem. Eur. J.* **2005**, 11, 4535-4543.
- (87) Maji, S.; Alam, P.; Kumar, G.S.; Biswas, S.; Sarkar, P.K.; Das, B.; Rehman, I.; Das, B.B.; Jana, N.R.; Laskar, I.R.; Acharya, S. Induced Aggregation of AIE-Active

- Mono-Cyclometalated Ir(III) Complex into Supramolecular Branched Wires for Light-Emitting Diodes, *Small* **2017**, *13*, 1603780.
- (88) Ma, J.; Zeng, Y.; Liu, Y.; Wu, D. Thermostable Polymeric Nanomicelles of Iridium(III) Complexes with Aggregation-Induced Phosphorescence Emission Characteristics and their Recyclable Double-Strand DNA Monitoring, *J. Mater. Chem. B* **2017**, *5*, 123-133.
- (89) Honda, H.; Ogawa, Y.; Kuwabara, J.; Kanbara, T. Emission Behavior of Secondary Thioamide-Based Cationic Pincer Platinum (II) Complexes in the Aggregate State, *Eur. J. Inorg. Chem.* **2014**, *2014*, 1865-1869.
- (90) Wang, D.; Li, S.-M.; Zheng, J. Q.; Kong, D. Y.; Zheng, X. J.; Fang, D. C.; Jin, L. P.; Coordination-Directed Stacking and Aggregation-Induced Emission Enhancement of the Zn(II) Schiff Base Complex, *Inorg. Chem.* **2017**, *56*, 984-990.
- (91) Kang, X.; Wang, S.; Song, Y.; Jin, S.; Sun, G.; Yu, H.; Zhu, M. Bimetallic Au₂Cu₆ Nanoclusters: Strong Luminescence Induced by the Aggregation of Copper(I) Complexes with Gold(0) Species. *Angew. Chem. Int. Ed.* **2016**, *55*, 3611-3614.
- (92) Procopio, E.Q.; Mauro, M.; Panigati, M.; Donghi, D.; Mercandelli, P.; Sironi, A.; D'Alfonso, G.; De Cola, L. Highly Emitting Concomitant Polymorphic Crystals of a Dinuclear Rhenium Complex, *J. Am. Chem. Soc.* **2010**, *132*, 14397-14399.
- (93) Alam, P.; Climent, C.; Alemany, P.; Laskar, I. R. "Aggregation-Induced Emission" Of Transition Metal Compounds: Design, Mechanistic Insights, and Applications. *J Photochem. Photobiol. C: Photochem. Rev.* **2019**, *41*, 100317.
- (94) Bar, M.; Deb, S.; Paul, A.; Baitalik, S.; Stimuli-Responsive Luminescent Bis-Tridentate Ru(II) Complexes Toward the Design of Functional Materials. *Inorg. Chem.*, **2018**, *57*, 12010-12024.
- (95) Benniston, A. C.; Chapman, G. M.; Harriman, A.; Rostron, S. A.; Reversible Luminescence Switching in a Ruthenium(II)Bis(2,2':6',2''-Terpyridine)-Benzoquinone Dyad. *Inorg. Chem.* **2005**, *44*, 4029-4036.
- (96) Mardanya, S.; Karmakar, S.; Das, S.; Baitalik, S. Anion And Cation Triggered Modulation of Optical Properties of a Pyridyl-Imidazole Receptor Rigidly Linked to Pyrene and Construction of INHIBIT, OR and XOR Molecular Logic Gates: A Combined Experimental and DFT/TD-DFT Investigation. *Sens. Actuators B* **2015**, *206*, 701-713.

- (97) Meng, T.-T.; Wang, H. Zheng, Z. Wang, K.-Z. pH-Switchable “Off-On-Off” Near-Infrared Luminescence Based on a Dinuclear Ruthenium(II) Complex. *Inorg. Chem.* **2017**, *56*, 4775-4779.
- (98) Akasaka, T.; Otsuki, J.; Araki, K. Redox-Responsive Molecular Switches Based on Azoterpyridine-Bridged Ru/Os Complexes. *Chem. Eur. J.* **2001**, *8*, 130-136.
- (99) Ko, C. C.; Yam, V. W.W. Transition Metal Complexes with Photochromic Ligands Photosensitization and Photoswitchable Properties. *J. Mater. Chem.* **2010**, *20*, 2063-2070.
- (100) Harvey, E. C.; Feringa, B. L.; Vos, J. G.; Browne, W. R.; Pryce, M. T. Transition Metal Functionalized Photo- and Redox-Switchable Diarylethene Based Molecular Switches. *Coord. Chem. Rev.* **2015**, 282-283, 77-86.
- (101) Unjaroen, D.; Kasper, J. B.; Browne, W. R. Reversible Photochromic Switching in Ru(II) Polypyridyl Complex. *Dalton Trans.* **2014**, *43*, 16974-16976.
- (102) Jacquet, M.; Lafalet, F.; Cobo, S.; Loiseau, F.; Bakkar, A.; Boggio-Pasqua, M.; Saint-Aman, E.; Royal, G. Efficient Photoswitch System Combining a Dimethyldihydropyrene Pyridinium Core and Ruthenium(II) Bis-Terpyridine Entities. *Inorg. Chem.* **2017**, *56*, 4357-4368.
- (103) Bianchi, A.; Delgado-Pinar, E.; García-España, E.; Giorgi, C.; Pina, F. Highlights of Metal Ion-Based Photochemical Switches. *Coord. Chem. Rev.* **2014**, *260*, 156-215.
- (104) Guerchais, V.; Ordonneau, L.; Bozec, H. Recent Developments in the Field of Metal Complexes Containing Photochromic Ligands: Modulation of Linear and Nonlinear Optical Properties. *Coord. Chem. Rev.* **2010**, *254*, 2533-2545.
- (105) Colasson, B.; Credi, A.; Ragazzon, G. Light-Driven Molecular Machines Based on Ruthenium(II) Polypyridine Complexes: Strategies and Recent Advances. *Coord. Chem. Rev.* **2016**, *325*, 125-134.
- (106) Rau, H.; Photoisomerization of Azobenzenes. *Photoreact. Org. Thin Films*, **2002**, *3*, 47.
- (107) Feringa, B. L.; van Delden, R. A.; Koumura, N.; Geertsema, E. M. Chiroptical Molecular Switches. *Chem. Rev.* **2000**, *100*, 1789-1816.
- (108) Ikeda, T.; Tsutsumi, O. Optical Switching and Image Storage by Means of Azobenzene Liquid-Crystal Films. *Science* **1995**, *268*, 1873-1875.

- (109) Anggia, I.S.; Hayati, D.; Hong, J. Synthesis and Photophysical Characterization of Push-Pull Azobenzene Derivatives Featuring Different π -Bridges for Photoresponsive Applications. *Dyes Pigm.* **2025**, *234*, 112550.
- (110) Ichimura, K.; Oh, S. K.; Nakagawa, M. Light-Driven Motion of Liquids on a Photoresponsive Surface. *Science* **2000**, *288*, 1624-1626.
- (111) Staniak, N. T.; Staniak, M.; Dudek, M.; Grzelczak, M.; Matczyszyn, K. Thermoplasmonic Effect Enables Indirect ON-OFF Control over the *Z-E* Isomerization of Azobenzene-Based Photoswitch. *Small* **2024**, *20*, 2404755.
- (112) Waldeck, D. H. Photoisomerization Dynamics of Stilbenes. *Chem. Rev.* **1991**, *91*, 415-436.
- (113) Tian, H.; Zhang, J. *Photochromic Materials: Preparation, Properties and Applications*; Wiley-VCH: Weinheim, Germany, 2016.
- (114) Dürr, H.; Bouas-Laurent, T. H. In *Photochromism: Molecules and Systems*; Elsevier, Amsterdam, 1990.
- (115) Oelgemöller, M.; Frank, R.; Lemmen, P.; Lenoir, D.; Lex, J.; Inoue, Y. Synthesis, Structural Characterization and Photoisomerization of Cyclic Stilbenes. *Tetrahedron*, **2012**, *68*, 4048-4056.
- (116) Saltiel, J.; Papadimitriou, D.; Krishna, T.S.R.; Huang, Z.-N.; Krishnamoorthy, G.; Laohhasurayotin, S.; Clark, R.J. Photoisomerization of All-cis-1,6-diphenyl-1,3,5 Hexatriene in the Solid State and in Solution: A Simultaneous Three-Bond Twist Process. *Angew. Chem. Int. Ed.* **2009**, *48*, 8082-8085.
- (117) Fan, Y.; Chen, J.; Yu, L.; Li, A.; Zhai, G.; Lei, Y.; Zhu, C. Methyl Substitution Enhanced Photoisomerization of Trans,Trans-1,4-Diphenyl-1,3-Butadiene: Direct ab Initio Trajectory Surface Hopping Dynamic Simulations. *Phys. Chem. Chem. Phys.* **2018**, *20*, 2260-2273.
- (118) Jędrzejewska, B.; Ośmiałowska, B.; Zaleśny, R. Application of Spectroscopic and Theoretical Methods in the Studies of Photoisomerization and Photophysical Properties of the Push-Pull Styryl-Benzimidazole Dyes. *Photochem. Photobiol. Sci.* **2016**, *15*, 117-128.
- (119) Matos, L. S.; Amaral, R. C.; Iha, N. Y. M. Visible Photosensitization of *Trans*-Styrylpyridine Coordinated to fac-[Re(CO)₃(dcbH₂)]⁺: New insights. *Inorg. Chem.* **2018**, *57*, 9316-9326.

- (120) Polo, A. S.; Itokazu, M. K.; Frin, K. M.; Patrocínio, A. O. T.; Iha, N. Y. M. Light Driven *Trans*-To-*Cis* Isomerization of Stilbene-Like Ligands in *fac*-[Re(CO)₃(NN)(*trans*-L)]⁺ and Luminescence of their Photoproducts. *Coord. Chem. Rev.* **2006**, *250*, 1669-1680.
- (121) Yutaka, T.; Mori, I.; Kurihara, M.; Mizutani, J.; Tamai, N.; Kawai, Tsuyoshi.; Irie, M, Nishihara, H. Photoluminescence Switching of Azobenzene-Conjugated Pt(II) Terpyridine Complexes by Trans-Cis Photoisomerization. *Inorg. Chem.* **2002**, *41*, 7143-7150.
- (122) Bardaj, M.; Barrio, M.; Espinet, P. Photosensitive Azobispyridine Gold(I) and Silver(I) Complexes. *Dalton Trans.* **2011**, *40*, 2570-2577.
- (123) Vlcek A. J.; Busby, M. Ultrafast Ligand-to-ligand Electron and Energy Transfer in The Complexes *fac*-[ReI(L)(CO)₃(bpy)]ⁿ⁺. *Coord. Chem. Rev.* **2006**, *250*, 1755-1762.
- (124) Sun, S. S.; J. A.; Lees, A. J. Self-assembly of Transition-Metal-Based Macrocycles Linked by Photoisomerizable Ligands: Examples of Photoinduced Conversion of Tetranuclear-Dinuclear Squares. *Inorg. Chem.* **2002**, *41*, 1862-1869.
- (125) Kayanuma, M.; Daniel, C.; Koppel, H.; Gindensperger, E. Photophysics of Isomerizable Re (I) Complexes: A Theoretical Analysis. *Coord. Chem. Rev.* **2011**, *255*, 2693-2703.
- (126) Irie, M. Diarylethenes for Memories and Switches. *Chem. Rev.* **2000**, *100*, 1685-1716.
- (127) Neel, A. J.; Hilton, M. J.; Sigman, M. S.; Toste, F. D. Exploiting Non-Covalent π Interactions for Catalyst Design. *Nature* **2017**, *543*, 637.
- (128) Dougherty, D. A. The Cation- π Interaction. *Acc. Chem. Res.* **2013**, *46*, 4, 885-893.
- (129) Chifotides, H. T.; Dunbar, K. R. Anion- π Interactions in Supramolecular Architectures. *Acc. Chem. Res.* **2013**, *46*, 4, 894-906.
- (130) Platzer, G.; Mayer, M.; Beier, A.; Brgschweiler, S.; Fuchs, J. E.; Engelhardt, H.; Geist, L.; Bader, G.; Schörghuber, J.; Lichtenecker, R. *et al.* PI by NMR: Probing CH- π Interactions in Protein-Ligand Complexes by NMR Spectroscopy. *Angew. Chem. Int. Ed.* **2020**, *59*, 14861-14868.
- (131) Salonen, L. M.; Ellermann, M.; Diederich, F. Aromatic Rings in Chemical and Biological Recognition: Energetics and Structures. *Angew. Chem. Int. Ed.* **2011**, *50*, 4808-4842.
- (132) Tam, A. Y. Y.; Wong, K. M. C.; Wang, G.; Yam, V. W. W. Luminescent Metallogels of Platinum (II) Terpyridyl Complexes: Interplay of Metal...Metal, π - π and

- Hydrophobic-Hydrophobic Interactions on Gel Formation. *Chem. Commun.* **2007**, 2028-2030.
- (133) Biedermann, F.; Schneider, H.-J. Experimental Binding Energies in Supramolecular Complexes. *Chem. Rev.* **2016**, *116*, 5216.
- (134) Zacharias, N.; Dougherty, D. A. Cation- π Interactions in Ligand Recognition and Catalysis. *Trends Pharmacol. Sci.* **2002**, *23*, 281-287.
- (135) Wang, D.-X.; Wang, M.-X. Exploring Anion- π Interactions and their Applications in Supramolecular Chemistry. *Acc. Chem. Res.* **2020**, *53*, 7, 1364-1380.
- (136) Guha, S.; Saha, S.; Fluoride Ion Sensing by an Anion- π Interaction. *J. Am. Chem. Soc.* **2010**, *132*, 17674-17677.
- (137) Zhao, H.; Tang, L.; Fang, Y.; Liu, C.; Ding, W.; Zang, S.; Chen, Y.; Xu, W.; Yuan, Y.; Fang, D. *et al.* Manipulating Cation- π Interactions of Reader Proteins in Living Cells with Genetic Code Expansion. *J. Am. Chem. Soc.* **2023**, *145*, 30, 16406-16416.
- (138) Garau, C.; Frontera, A.; Quinonero, D.; Ballester, P.; Costa, A.; Deya, P. M. Cation- π versus Anion- π Interactions: Energetic, Charge Transfer, and Aromatic Aspects. *J. Phys. Chem. A* **2004**, *108*, 9423-9427.
- (139) Schanze, K. S.; Neyhart, G. A. *et al.* Excited-State Electron Transfer in Ligand-Bridged Dimeric Complexes of Osmium. *J. Phys. Chem.* **1986**, *90*, 2182-2193.
- (140) Kober, E. M.; Caspar, J. V.; Lumpkin, R. S.; Meyer, T. J. Application of the Energy Gap Law to Excited-State Decay of Osmium(II)-Polypyridine Complexes: Calculation of Relative Nonradiative Decay Rates From Emission Spectral Profiles. *J. Phys. Chem.* **1986**, *90*, 3722-3734.
- (141) Belser, P.; Dux, R.; Baak, M.; Decola, L.; Balzani, V. Electronic Energy Transfer in a Supramolecular Species Containing the $[\text{Ru}(\text{Bpy})_3]^{2+}$, $[\text{Os}(\text{Bpy})_3]^{2+}$, and Anthracene Chromophoric Units. *Angew. Chem. Int. Ed. Engl.* **1995**, *34*, 595-598.
- (142) Kober, E. M.; Sullivan, B. P.; Meyer, T.J. Solvent Dependence of Metal-To-Ligand Charge-Transfer Transitions. Evidence for Initial Electron Localization in MLCT Excited States of 2,2'-Bipyridine Complexes of Ruthenium(II) and Osmium(II). *Inorg. Chem.* **1984**, *23*, 2098-2104.
- (143) Wang, X.-Y.; Guerzo, A. D.; Tunuguntla, H.; Schmehl, R. H. Photophysical Behavior of Ru(II) and Os(II) Terpyridyl Phenylene Vinylene Complexes: Perturbation of MLCT State by Intra-Ligand Charge-Transfer State. *Res. Chem. Intermed.* **2007**, *33*, 63-77.

- (144) Bhaumik, C.; Das, S.; Maity, D.; Baitalik, S. Luminescent Bis-Tridentate Ruthenium(II) and Osmium(II) Complexes Based on Terpyridyl-Imidazole Ligand: Synthesis, Structural Characterization, Photophysical, Electrochemical, and Solvent Dependence Studies. *Dalton Trans.* **2012**, *41*, 2427-2438.
- (145) Paul, A.; Sahoo, A.; Bhattacharya, S.; Baitalik, S. Anion and Temperature Responsive Molecular Switches Based on Trimetallic Complexes of Ru(II) and Os(II) That Demonstrate Advanced Boolean and Fuzzy Logic Functions. *Inorg. Chem.* **2022**, *61*, 3186-3201.
- (146) Friedman, A. E.; Chambron, J. C.; Sauvage, J. P.; Turro, N. J.; Barton, J. K. Molecular "Light Switch" for DNA: Ru(bpy)₂(dppz)²⁺. *J. Am. Chem. Soc.* **1990**, *112*, 4960-4962.
- (147) Bera, M. K.; Ninomiya, Y.; Higuchi, M. Stepwise Introduction of Three Different Transition Metals in Metallo-Supramolecular Polymer for Quad-Color Electrochromism. *Commun Chem* **2021**, *4*, 1-12.
- (148) Zanzi, J.; Pastorel, Z.; Duhayon, C.; Lognon, E.; Coudret, C.; Monari, A.; Dixon, I.M.; Canac, Y.; Smietana, M.; Baslé, O. Counterion Effects in [Ru(bpy)₃](X)₂-Photocatalyzed Energy Transfer Reactions. *JACS Au*, **2024**, *4*, 3049-3057.
- (149) Bhattacharya, S.; Pal, P.; Gorain, S.; Baitalik, S. Enhancing Near-Infrared Absorption in Osmium (II) Complexes Under the Cumulative Influence of Terpyridine Ligand and Anions: Combined Experimental and DFT/TD-DFT Investigation. *Eur. J. Inorg. Chem.* **2024**, e202400758.
- (150) Campagna, S.; Puntoriero, F.; Nastasi, F.; Bergamini, G.; Balzani, V. Photochemistry and Photophysics of Coordination Compounds: Ruthenium. *Top. Curr. Chem.* **2007**, *280*, 117.
- (151) Brown, D. G.; Sanguantrakun, N.; Schulze, B.; Schubert, U. S.; Berlinguette, C. P. Bis(tridentate) Ruthenium-Terpyridine Complexes Featuring Microsecond Excited-State Lifetimes. *J. Am. Chem. Soc.* **2012**, *134*, 12354-12357.
- (152) Rupp, M.T.; Shevchenko, N.; Hanan, G.S.; Kurth, D.G. Enhancing The Photophysical Properties of Ru(II) Complexes by Specific Design of Tridentate Ligands. *Coord. Chem. Rev.* **2021**, *446*, 214127.
- (153) Wang, J.; Fang, Y. Q.; Hanan, G. S.; Loiseau, F.; Campagna, S. Synthesis and Properties of the Elusive Ruthenium(II) Complexes of 4'-cyano-2,2':6',2''-terpyridine. *Inorg. Chem.* **2005**, *44*, 5-7.

- (154) Indelli, M. T.; Bignozzi, C. A.; Scandola, F.; Collin, J.-P. Design of Long-Lived Ru(II) Terpyridine MLCT States. Tricyano Terpyridine Complexes. *Inorg. Chem.* **1998**, *37*, 6084-6089.
- (155) Kübel, J.; Schroot, R.; Wachtler, M.; Schubert, U. S.; Dietzek, B.; Jager, M. Photoredox-Active Dyads Based on a Ru (II) Photosensitizer Equipped with Electron Donor or Acceptor Polymer Chains: A Spectroscopic Study of Light-Induced Processes Toward Efficient Charge Separation. *J. Phys. Chem. C* **2015**, *119*, 4742-4751.
- (156) Maestri, M.; Armaroli, N.; Balzani, V.; Constable, E. C.; Thompson, A. M. W. C. Complexes of the Ruthenium (II)-2,2':6',2''- Terpyridine Family. Effect of Electron-Accepting and -Donating Substituents on the Photophysical and Electrochemical Properties. *Inorg. Chem.* **1995**, *34*, 2759-2767.
- (157) Pal, P.; Mukherjee, S.; Maity, D.; Baitalik, S.; Synthesis, Structural Characterization, and Luminescence Switching of Diarylethene-Conjugated Ru(II)-Terpyridine Complexes by Trans-Cis Photoisomerization: Experimental and DFT/TD-DFT Investigation. *Inorg. Chem.* **2018**, *57*, 5743-5753.
- (158) Pal, P.; Ganguly, T.; Maity, D.; Baitalik, S. Experimental and Theoretical Exploration of Photophysics and Trans-Cis Photoisomerization of Styrylbenzene Conjugated Terpyridine Complexes of Ru(II): Strong Effect of Deprotonation from Second Coordination Sphere. *J. Photochem. Photobiol. A* **2020**, *392*, 112409.
- (159) Maity, D.; Das, S.; Mardanya, S.; Baitalik, S. Synthesis, Structural Characterization, and Photophysical, Spectroelectrochemical, and Anion-Sensing Studies of Heteroleptic Ruthenium(II) Complexes Derived from 4'-Polyaromatic-Substituted Terpyridine Derivatives and 2,6-Bis(benzimidazol-2-yl)pyridine. *Inorg. Chem.* **2013**, *52*, 6820-6838.
- (160) Encinas, S.; Flamigni, L.; Barigelletti, F.; Constable, E. C.; Housecroft, C. E.; Schofield, E. R.; Figgemeier, E.; Fenske, D.; Neuburger, M., *et al.* Electronic Energy Transfer and Collection in Luminescent Molecular Rods Containing Ruthenium(II) and Osmium(II) 2,2':6',2''-Terpyridine Complexes Linked by Thiophene-2,5- diyl Spacers. *Chem. Eur. J.* **2002**, *8*, 137-150.
- (161) Dietrich, J.; Thorenz, U.; Förster, C.; Heinze, K. Effects of Sequence, Connectivity, and Counter Ions in New Amide-Linked Ru(tpy)₂-Re(bpy) Chromophores on Redox Chemistry and Photophysics. *Inorg. Chem.* **2013**, *52*, 1248-1264.

- (162) Pal, P.; Ganguly, T.; Sahoo, A.; Baitalik, S. Emission Switching in the Near-Infrared by Reversible Trans-Cis Photoisomerization of Styrylbenzene-Conjugated Osmium Terpyridine Complexes. *Inorg. Chem.* **2021**, *60*, 4869-4882.
- (163) Duati, M.; Tasca, S.; Lynch, F. C.; Bohlen, H.; Vos, J. G.; Stagni, S.; Ward, M. D. Enhancement of Luminescence Lifetimes of Mononuclear Ruthenium(II)-Terpyridine Complexes by Manipulation of the Sigma-Donor Strength of Ligands. *Inorg. Chem.* **2003**, *42*, 8377-8384.
- (164) Wadman, S. H.; Lutz, M.; Tooke, D. M.; Spek, A. L.; Hartl, F.; Havenith, R. W. A.; van Klink, G. P. M.; van Koten, G. Consequences of N,C,N- and C,N,N-Coordination Modes on Electronic and Photophysical Properties of Cyclometalated Aryl Ruthenium(II) Complexes. *Inorg. Chem.* **2009**, *48*, 1887-1900.
- (165) Kreitner, C.; Erdmann, E.; Seidel, W. W.; Heinze, K. Understanding the Excited State Behavior of Cyclometalated Bis(tridentate)ruthenium(II) Complexes: A Combined Experimental and Theoretical Study. *Inorg. Chem.* **2015**, *54*, 11088-11104.
- (166) Beley, M.; Collin, J.-P.; Louis, R.; Metz, B.; Sauvage, J.-P. 3,3',5,5'-Tetrapyridylbiphenyl: A Biscyclometalating Bridging Ligand with a High Coupling Ability in Ru^{III}, Ru^{II} Mixed Valence Systems. *J. Am. Chem. Soc.* **1991**, *113*, 8522-8524.
- (167) Duati, M.; Fanni, S.; Vos, J. G. A New Luminescent Ru(terpy) Complex Incorporating a 1,2,4-Triazole Based σ -Donor Ligand. *Inorg. Chem. Commun.* **2000**, *3*, 68-70.
- (168) Constable, E. C.; Dunne, S. J.; Rees, D. G. F.; Schmitt, C. X. Reversible Cyclometallation at a Ruthenium(II) Centre. *Chem. Commun.* **1996**, 1169.
- (169) Goze, C.; Sabatini, C.; Barbieri, A.; Barigelletti, F.; Ziessel, R. Ruthenium-Terpyridine Complexes with Multiple Ethynylpyrenyl or Ethynyltoluyl Subunits: X-ray Structure, Redox, and Spectroscopic Properties. *Inorg. Chem.* **2007**, *46*, 7341-7350.
- (170) Prieto, J. P.; Pe'rez, L. P.; Gonza'lez-Be'jar, M.; Miranda, M. A. Stiriba, S.-E. Pyrene-Benzoylthiophene Bichromophores as Selective Triplet Photosensitizers. *Chem. Commun.* **2005**, 5569.
- (171) Constable, E. C.; Thompson, M. W. C. Multinucleating 2,2':6',2''-Terpyridine Ligands as Building Blocks for the Assembly of Co-ordination Polymers and Oligomers. *J. Chem. Soc. Dalton Trans.* **1992**, 3467-3475.

- (172) Lashgari, K.; Kritikos, M.; Norrestam, R.; Norrby, T. *Acta Crystallogr., Sect. C: Cryst. Struct. Commun.* **1999**, *55*, 64-67.
- (173) Maestri, M.; Armaroli, N.; Balzani, V.; Constable, E. C.; Thompson, A. M. W. C. Complexes of the Ruthenium (II)-2,2':6',2''-Terpyridine Family. Effect of Electron Accepting and -Donating Substituents on the Photophysical and Electrochemical Properties. *Inorg. Chem.* **1995**, *34*, 2759-2767.
- (174) Beley M.; Delabouglise D.; Houppy, G.; Husson, J.; Petit, J.-P. Preparation and Properties of Ruthenium (II) Complexes of 2,2':6',2''-Terpyridines Substituted at the 4'-Position with Heterocyclic Groups. *Inorg. Chim. Acta* **2005**, *358*, 3075-3083.
- (175) Passalacqua, R.; Loiseau, F.; Campagna, S.; Fang, Y.-Q.; Hanan, G. S. In Search of Ruthenium (II) Complexes Based on Tridentate Polypyridine Ligands that Feature Long-Lived Room-Temperature Luminescence: The Multichromophore Approach. *Angew. Chem. Int. Ed.* **2003**, *42*, 1608-1611.
- (176) Wang, J.; Hanan, G. S.; Loiseau, F.; Campagna, S. Prolonged Luminescence Lifetimes of Ru(II) Complexes via the Multichromophore Approach: The Excited-State Storage Element can be on a Ligand not Involved in the MLCT Emitting State. *Chem. Commun.* **2004**, 2068-2069.
- (177) Siebert, R.; Winter, A.; Dietzek, B.; Schubert, U. S.; Popp, J. Dual Emission From Highly Conjugated 2,2':6':2''-Terpyridine Complexes-a Potential Route to White Emitters. *Macromol. Rapid Commun.* **2010**, *31*, 883-888.
- (178) Schulze, B.; Escudero, D.; Friebe, C.; Siebert, R.; Görls, H.; Köhn, U.; Altuntas, E.; Baumgaertel, A.; Hager, M. D.; Winter, A.; Dietzek, B.; Popp, J.; González, L.; Schubert, U.S.A Heteroleptic Bis(Tridentate) Ruthenium(II) Complex of a Click-Derived Abnormal Carbene Pincer Ligand with Potential for Photosensitizer Application. *Chem. Eur. J.* **2011**, *17*, 5494-5498.
- (179) Brown, D. G.; Sanguantrakun, N.; Schulze, B.; Schubert, U. S.; Berlinguette, C. P. Bis(tridentate) Ruthenium-Terpyridine Complexes Featuring Microsecond Excited-State Lifetimes. *J. Am. Chem. Soc.* **2012**, *134*, 12354-12357.
- (180) Ge, C.; Zhu, J.; Ouyang, A.; Lu, N.; Wang, Y.; Zhang, Q.; Zhang, P. Near-Infrared Phosphorescent Terpyridine Osmium(II) Photosensitizer Complexes for Photodynamic and Photooxidation Therapy. *Inorg. Chem. Front.* **2020**, *7*, 4020-4027.

- (181) Liu, B.; Gao, Y.; Javed, M. A. Kilina, S.; Liu, G.; Sun, W. Lysosome Targeting Bis-Terpyridine Ruthenium(II) Complexes: Photophysical Properties and In Vitro Photodynamic Therapy. *ACS Appl. Bio Mater.* **2020**, *3*, 6025-6038.
- (182) Yoshikawa, Kai.; Motoyama, Daisuke.; Hiruma, Yusuke.; Ozawa, Hiroaki.; Nagano, Shusaku.; Haga, M. Proton-Rocking-Chair-Type Redox Capacitors Based on Indium Tin Oxide Electrodes With Multilayer Films Containing Ru Complexes. *ACS Appl. Mater. Interfaces.* **2018**, *10*, 26990-27000.
- (183) Zheng, Z. B.; Kang, S. Y.; Yi, X.; Zhang, Na.; Wang, K.-Z. Off-on-off pH Luminescence Switching and DNA Binding Properties of a Free Terpyridine-Appended Ruthenium Complex. *J. Inorg. Biochem.* **2014**, *141* 70-78.
- (184) Hammecke, H.; Fritzler, D.; Vashistha, N.; Jin, P.; Dietzek-Ivanšić, B.; Wang, C. 100 μ s Luminescence Lifetime Boosts the Excited State Reactivity of a Ruthenium (II)-Anthracene Complex in Photon Upconversion and Photocatalytic Polymerizations with Red Light. *Chem. Eur. J.* **2024**, e202402679.
- (185) Rupp, M.T.; Auvray, T.; Hanan, G.S.; Kurth, D.G.; Electrochemical and Photophysical Study of Homoleptic and Heteroleptic Methylated Ru(II) Bis-terpyridine Complexes. *Eur. J. Inorg. Chem.* **2021**, 2822-2829.
- (186) Rupp, M.T.; Auvray, T.; Shevchenko, N.; Swoboda, L.; Hanan, G.S.; Kurth, D.G. Substituted 2,4-Di(pyridin-2-yl)pyrimidine-Based Ruthenium Photosensitizers for Hydrogen Photoevolution Under Red Light. *Inorg. Chem.* **2021**, *60*, 292-302.
- (187) Gamache, M.T.; Gehring, B.; Hanan, G.S.; Kurth, D.G. Spectro-Electrochemical Study of Iron and Ruthenium Bis-Terpyridine Complexes with Methyl Viologen-Like Subunits as Models for Supramolecular Polymers. *Dalton Trans.* **2024**, *53*, 13151-13159.
- (188) Medlycott, E. A.; Hanan, G. S. Designing Tridentate Ligands for Ruthenium (II) Complexes with Prolonged Room Temperature Luminescence Lifetimes. *Chem. Soc. Rev.* **2005**, *34*, 133-142.
- (189) Albano, G.; Balzani, V.; Constable, E.C.; Maestri, M.; Smith, D.R. Photoinduced Processes in 4'-(9-anthryl)-2,2':6',2''-Terpyridine, its Forms and Zn (II), Ru (II) and Os (II) Complexes *Inorg. Chim. Acta* **1998**, *277*, 225-231.
- (190) Scattergood, P.A.; Roberts, J.; Omar, S.A.; Elliott, P.I. Observation of an Inversion in Photophysical Tuning in a Systematic Study of Luminescent Triazole-Based Osmium (II) Complexes. *Inorg. Chem.* **2019**, *58*, 8607-8621.

- (191) Sasaki, Y.; Yanai, N.; Kimizuka, N. Osmium Complex-Chromophore Conjugates with Both Singlet-to-Triplet Absorption and Long Triplet Lifetime Through Tuning of the Heavy-Atom Effect. *Inorg. Chem.* **2022**, *61*, 5982-5990.
- (192) Benniston, A. C.; Chapman, G.; Harriman, A.; Mehrabi, M.; Sams, C. A. Electron Delocalization in a Ruthenium (II) Bis(2,2':6',2''-terpyridyl) Complex. *Inorg. Chem.* **2004**, *43*, 4227-4233.
- (193) Deb, S.; Sahoo, A.; Pal, P.; Baitalik, S. Exploitation of the Second Coordination Sphere to Promote Significant Increase of Room-Temperature Luminescence Lifetime and Anion Sensing in Ruthenium-Terpyridine Complexes. *Inorg. Chem.* **2021**, *60*, 6836-6851.
- (194) Paul, A.; Bar, M.; Deb, S.; Baitalik, S. Long-Lived Trimetallic Complexes of Fe(II), Ru(II), and Os(II) Based on a Heteroditopic Bipyridine-Terpyridine Bridge: Synthesis, Photophysics, and Electronic Energy Transfer. *Inorg. Chem.* **2019**, *58*, 10065-10077.
- (195) Mondal, D.; Bar, M.; Mukherjee, S.; Baitalik, S. Design of Ru(II) Complexes Based On Anthraimidazoledione-Functionalized Terpyridine Ligand for Improvement of Room-Temperature Luminescence Characteristics and Recognition of Selective Anions: Experimental and DFT/TD-DFT Study. *Inorg. Chem.* **2016**, *55*, 9707-9724.
- (196) Maity, D.; Bhaumik, C.; Karmakar, S.; Baitalik, S. Photoinduced Electron and Energy Transfer and Ph-Induced Modulation of the Photophysical Properties in Homo- and Heterobimetallic Complexes of Ruthenium (II) and Rhodium (III) Based on a Heteroditopic Phenanthroline-Terpyridine Bridge. *Inorg. Chem.* **2013**, *52*, 7933-7946.
- (197) Bissell, R. A.; Córdova, E.; Kaifer, A. E.; Stoddart, J. F. A Chemically and Electrochemically Switchable Molecular Shuttle. *Nature* **1994**, *369*, 133-137.
- (198) Crowley, J. D.; Leigh, D. A.; Lusby, P. J.; McBurney, R. T.; Perret-Aebi, L. E.; Petzold, C.; Slawin, A. M. Z.; Symes, M. D. A Switchable Palladium-Complexed Molecular Shuttle and its Metastable Positional Isomers. *J. Am. Chem. Soc.* **2007**, *129*, 15085-15090.
- (199) MacDonald, T. S. C.; Schmidt, T. W.; Beves, J. E. An All-Photonic Molecular Amplifier and Binary Flip-Flop. *J. Phys. Chem. Lett.* **2021**, *12*, 1236-1243.
- (200) Ishizuka, T.; Tobita, K.; Yano, Y.; Shiota, Y.; Yoshizawa, K.; Fukuzumi, S.; Kojima, T. Proton-Coupled Electron Shuttling in a Covalently Linked Ruthenium-Copper Heterodinuclear Complex. *J. Am. Chem. Soc.* **2011**, *133*, 18570-18573.

- (201) Gan, Q.; Ferrand, Y.; Bao, C.; Kauffmann, B.; Grélard, A.; Jiang, H.; Huc, I. Helix-Rod Host-Guest Complexes With Shuttling Rates Much Faster Than Disassembly. *Science* **2011**, *331*, 1172-1175.
- (202) Turansky, R.; Konopka, M.; Doltsinis, N. L.; Stich, I.; Marx, D. Switching of Functionalized Azobenzene Suspended Between Gold Tips by Mechanochemical, Photochemical, and Opto-Mechanical Means. *Phys. Chem. Chem. Phys.* **2010**, *12*, 13922-13932.
- (203) Henzl, J.; Mehlhorn, M.; Gawronski, H.; Rieder K.-H.; Morgenstern, K. Reversible *Cis-Trans* Isomerization of a Single Azobenzene Molecule. *Angew. Chem. Int. Ed.* **2006**, *45*, 603-606.
- (204) Tong, X.; Pelletier, M.; Lasia A.; Zhao, Y. Fast *Cis-Trans* Isomerization of an Azobenzene Derivative in Liquids and Liquid Crystals under a Low Electric Field. *Angew. Chem., Int. Ed.* **2008**, *47*, 3596-3599.
- (205) Feringa, B. L.; van Delden, R.A.; ter Wiel, M.K.J. Chiroptical Molecular Switches. Ed.; Wiley-VCH, **2001**, pp 123-163.
- (206) Norikane, Y.; Tamaoki, N. Light-Driven Molecular Hinge: A New Molecular Machine Showing a Light-Intensity-Dependent Photoresponse that Utilizes the *Trans-Cis* Isomerization of Azobenzene. *Org. Lett.* **2004**, *6*, 2595-2598.
- (207) Sakamoto, R.; Kume, S.; Nishihara, H. Visible-light Photochromism of Triarylamine- or Ferrocene-Bound Diethynylethenes that Switches Electronic Communication Between Redox Sites and Luminescence. *Chem. -Eur. J.*, **2008**, *14*, 6978-6986.
- (208) Li, Y.; Fei, Y.; Sun, H.; Yu, S.; Liu, J. Regulation of the Switchable Luminescence of Tridentate Platinum(II) Complexes by Photoisomerization. *Front. Chem.* **2020**, *8*, 622256.
- (209) Troe, J. Quantitative Analysis Of Photoisomerization Rates in *Trans-Stilbene* and 4-Methyl-*Trans-Stilbene*. *Chem. Phys. Lett.* **1985**, *114*, 241-247.
- (210) Bandara, H.M.D.; Burdette, S.C. Photoisomerization in Different Classes of Azobenzene. *Chem. Soc. Rev.* **2012**, *41*, 1809-1825.
- (211)(a) Dugave, C.; Demange, L. *Cis-Trans* Isomerization of Organic Molecules and Biomolecules: Implications and Applications. *Chem. Rev.* **2003**, *103*, 2475-2532.
(b) Otolowski, C. J.; Raj, A.; Sharma, M. G.; Prabhakar, R.; Ramamurthy, V.; Elles, C. G. Ultrafast *Trans*→*Cis* Photoisomerization Dynamics Of Alkyl-Substituted Stilbenes In A Supramolecular Capsule. *J. Phys. Chem. A* **2019**, *123*, 5061-5071.

- (212) Zhou, W.; Chen, D.; Li, J.; Xu, J.; Lv, J.; Liu, H.; Li, Y. Photoisomerization of Spiropyran for Driving a Molecular Shuttle. *Org. Lett.* **2007**, 9, 3929-3932.
- (213) Dennis, J.M.; Patterson, B.A.; Dolinski, N.D.; Fawcett, S.A.; Lenart, W.R.; Sirk, T.W.; Mrozek, R.A.; Rowan, S.J.; Lenhart, J.L. Photoinduced Plasticization of Azobenzene-Containing Epoxy Glasses for Impact Mitigation. *Macromolecules* **2025**.
- (214) Anggia, I.S.; Hayati, D.; Hong, J. Synthesis and Photophysical Characterization of Push-Pull Azobenzene Derivatives Featuring Different π -Bridges for Photoresponsive Applications. *Dyes Pigm.* **2025**, 234, 112550.
- (215) Yam V. W. W.; Lau, V. C. Y.; Wu, L. X. Synthesis, Photophysical, Photochemical and Electrochemical Properties of Rhenium(I) Diimine Complexes with Photoisomerizable Pyridyl-Azo, -Ethenyl Or -Ethyl Ligands. *J. Chem. Soc. Dalton Trans.* **1998**, 1461-1468.
- (216) Yam, V. W. W.; Yang, Y.; Zhang, J.; Chu, B. W.-K., Zhu, N. Synthesis, Characterization, and Photoisomerization Studies of Azo- and Stilbene-Containing Surfactant Rhenium(I) Complexes. *Organometallics* **2001**, 20, 4911-4918.
- (217) Muraoka, T.; Kinbara, K.; Kobayashi, Y.; Aida, T. Light-driven Open-Close Motion of Chiral Molecular Scissors. *J. Am. Chem. Soc.* **2003**, 125, 5612-5613.
- (218) Muraoka, T.; Kinbara, K.; Aida, T. Mechanical Twisting of a Guest by a Photoresponsive Host. *Nature* **2006**, 440, 512-515.
- (219) Marchi, E.; Baroncini, M.; Bergamini, G.; Van Heyst, J.; Vögtle, F.; Ceroni, P. Photoswitchable Metal Coordinating Tweezers Operated by Light Harvesting Dendrimers. *J. Am. Chem. Soc.* **2012**, 134, 15277-15280.
- (220) Wrighton, M. S.; Morse, D. L.; Pdungsap, L. Intraligand Lowest Excited States in Tricarbonylhalobis(Styrylpyridine)Rhenium(I) Complexes. *J. Am. Chem. Soc.* **1975**, 97, 125, 2073-2079.
- (221) Wenger, O. S.; Henling, L. M.; Day, M. W.; Winkler, J. R.; Gray, H. B. Photoswitchable Luminescence of Rhenium(I) Tricarbonyl Diimines. *Inorg. Chem.* **2004**, 43, 2043-2048.
- (222) Amaral, R. C.; Iha, N. Y. M. Molecular Engineered Rhenium(I) Carbonyl Complexes to Promote Photoisomerization of Coordinated Stilbene-Like Ligands in the Visible Region. *Dalton Trans.* **2018**, 47, 13081-13087.

- (223) Amaral, R. C.; Matos, L. S.; Zanoni, K. P. S.; Iha, N. Y. M. Photoreversible Molecular Motion of Stpycn Coordinated to $\text{Fac}[\text{Re}(\text{CO})_3(\text{NN})]^+$ Complexes. *J. Phys. Chem. A* **2018**, 122, 6071-6080.
- (224) Faustino, L. A.; Machado A. E. H.; Patrocínio, A. O. T. Photochemistry of $\text{fac}[\text{Re}(\text{CO})_3(\text{dcbH}_2)(\text{trans-stpy})]^+$: New insights on the isomerization mechanism of coordinated stilbene-like ligands. *Inorg. Chem.* **2018**, 57, 2933-2941.
- (225) Yutaka, T.; Mori, I.; Kurihara, M.; Mizutani, J.; Kubo, K.; Furusho, S.; Matsumura, K.; Tamai, N.; Nishihara, H. Synthesis, Characterization, and Photochemical Properties of Azobenzene-Conjugated Ru(II) and Rh(III) Bis(Terpyridine) Complexes. *Inorg. Chem.* **2001**, 40, 4986-4995.
- (226) Sun, S. S.; Lees, A. J. Synthesis, Photophysical Properties, and Photoinduced Luminescence Switching of Trinuclear Diimine Rhenium(I) Tricarbonyl Complexes Linked by an Isomerizable Stilbene-Like Ligand. *Organometallics* **2002**, 21, 39-49.
- (227) Yutaka, T.; Kurihara, M.; Kubo, K.; Nishihara, H. Novel Photoisomerization Behavior of Rh Binuclear Complexes Involving an Azobenzene-Bridged Bis(Terpyridine) Ligand. Strong Effects of Counterion and Solvent and the Induction of Redox Potential Shift. *Inorg. Chem.* **2000**, 39, 3438-3439.
- (228) Yutaka, T.; Kurihara, M. Nishihara, H. Synthesis and Physical Properties of a π -Conjugated Ruthenium(II) Dinuclear Complex Involving an Azobenzene-Bridged Bis(Terpyridine) Ligand. *Mol. Cryst. Liq. Cryst.* **2000**, 343, 193-198.
- (229) Nihei, M.; Kurihara, M.; Mizutani, J.; Nishihara, H. Synthesis of Azo-Conjugated Metalladithiolenes and their Photo- and Proton-Responsive Isomerization Reactions. *J. Am. Chem. Soc.* **2003**, 125, 2964-2973.
- (230) Pérez-Miqueo, J.; Telleria, A.; Muñoz-Olasagasti, M.; Altube, A.; García-Lecina, E.; de Cózar, A.; Freixa, Z. Azobenzene-functionalized Iridium(III) Triscyclometalated Complexes. *Dalton Trans.* **2015**, 44, 2075-2091.
- (231) Gindensperger, E.; Köppel, H.; Daniel, C. Mechanism of Visible-Light Photoisomerization of a Rhenium (I) Carbonyl-Diimine Complex. *Chem. Commun.* **2010**, 46, 8225-8227.
- (232) Kayanuma, M.; Gindensperger, E.; Daniel, C. Inorganic Photoisomerization: The Case Study of Rhenium (I) Complexes. *Dalton Trans.* **2012**, 41, 13191-13203.
- (233) Chen, L.; Tan, Y.; Xu, H.; Wang, K.; Chen, Z.H.; Zheng, N.; Li, Y.Q.; Lin, L.R. Enhanced E/Z-Photoisomerization and Luminescence of Stilbene Derivative Co-

- coordinated in Di- β -Diketonate Lanthanide Complexes. *Dalton Trans.* **2020**, 49, 16745-16761.
- (234) Mukherjee, S.; Pal, P.; Maity, D.; Baitalik, S. Photophysics and Luminescence Switching Properties of a Series of Photochromic Styrylbenzene-Terpyridine Conjugate: Experimental and DFT/TD-DFT Investigation. *J Photochem. Photobiol. A* **2019**, 378, 94-104.
- (235) Mukherjee, S.; Pal, P.; Sahoo, A.; Baitalik, S. Photo-switchable Iron-Terpyridine Complexes Functionalized with Styrylbenzene Unit. *J Photochem. Photobiol. A* **2021**, 407, 113059.
- (236) Mukherjee, S.; Pal, P.; Sahoo, A.; Baitalik, S. Low-Cost Photo-Switches Based on Stilbene-Appended Zn (II)-Terpyridine Complexes. *Photochem. Photobiol. Sci.* **2021**, 20, 1125-1145.
- (237) Zhang, Y.; Hao, J. Metal-ion Doped Luminescent Thin Films for Optoelectronic Applications. *J. Mater. Chem. C*, **2013**, 1, 5607-5618.
- (238) Chen, J.; Law, C. C. W.; Lam, J. W. Y.; Dong, Y.; Lo, S. M. F.; Williams, I. D.; Zhu, D.; Tang, B. Z. Synthesis, Light Emission, Nanoaggregation, and Restricted Intramolecular Rotation of 1,1 Substituted 2,3,4,5-Tetraphenylsiloles. *Chem. Mater.* **2003**, 15, 1535-1546.
- (239) Ren, Y.; Lam, J. W. Y.; Dong, Y.; Tang, B. Z.; Wong, K. S. Enhanced Emission Efficiency and Excited State Lifetime Due to Restricted Intramolecular Motion in Silole Aggregates. *J. Phys. Chem. B* **2005**, 109, 1135-1140.
- (240) Kumar, S.; Singh, P.; Mahajan, A.; Kumar, S. Aggregation Induced Emission Enhancement in Ionic Self-Assembled Aggregates of Benzimidazolium Based Cyclophane and Sodium Dodecylbenzenesulfonate. *Org. Lett.* **2013**, 15, 3400-3403.
- (241) Nishiuchi, T.; Tanaka, K.; Kuwatani, Y.; Sung, J.; Nishinaga, T.; Kim, D.; Iyoda, M. Solvent-Induced Crystalline-State Emission and Multichromism of a Bent π -Surface System Composed of Dibenzocyclooctatetraene Units. *Chem. Eur. J.* **2013**, 19, 4110-4116.
- (242) Yuan, C.; Saito, S.; Camacho, C.; Kowalczyk, T.; Irle, S.; Yamaguchi, S. Hybridization of a Flexible Cyclooctatetraene Core and Rigid Aceneimide Wings for Multiluminescent Flapping π Systems. *Chem. Eur. J.* **2014**, 20, 2193-2200.
- (243) Yao, L.; Zhang, S.; Wang, R.; Li, W.; Shen, F.; Yang, B.; Ma, Y. Highly Efficient Near-Infrared Organic Light-Emitting Diode Based on a Butterfly-Shaped Donor-

- Acceptor Chromophore with Strong Solid State Fluorescence and a Large Proportion of Radiative Excitons. *Angew. Chem., Int. Ed.* **2014**, 53, 2119-2123.
- (244) Liu, J.; Meng, Q.; Zhang, X.; Lu, X.; He, P.; Jiang, L.; Dong, H.; Hu, W. Aggregation-Induced Emission Enhancement Based on 11,11,12,12,-Tetracyano-9,10-anthraquinodimethane. *Chem. Commun.* **2013**, 49, 1199-1201.
- (245) nee Kamaldeep, K.S.; Kaur, S.; Bhalla, V.; Kumar, M.; Gupta, A. Pentacenequinone Derivatives for Preparation of Gold Nanoparticles: Facile Synthesis and Catalytic Application. *J. Mater. Chem. A* **2014**, 2, 8369-8375.
- (246) Banal, J. L.; White, J. M.; Ghiggino, K. P.; Wong, W. W. H. Concentrating Aggregation-Induced Fluorescence in Planar Wave guides: A Proof-of-Principle. *Sci. Rep.* **2014**, 4, 4635.
- (247) Yang, L. L.; Wang, H.; Zhang, J.; Wu, B.; Li, Q.; Chen, J. Y.; Tang, A. L.; Lam, J.W.; Zhao, Z.; Yang, S.; Tang, B.Z. Understanding the AIE Phenomenon of Nonconjugated Rhodamine Derivatives Via Aggregation-Induced Molecular Conformation Change. *Nat. Commun.* **2024**, 15,999.
- (248) Chen, S.; Hong, Y.; Liu, Y.; Liu, J.; Leung, C.W.; Li, M.; Kwok, R.T.; Zhao, E.; Lam, J.W.; Yu, Y.; Tang, B.Z. Full-range Intracellular pH Sensing by an Aggregation-Induced Emission-Active Two-channel Ratiometric Fluorogen. *J. Am. Chem. Soc.* **2013**, 135, 4926-4929.
- (249) Wei, P.; Zhang, J. X.; Zhao, Z.; Chen, Y.; He, X.; Chen, M.; Gong, J.; Sung, H. H. Y.; Williams, I. D.; Lam, J. W.; Tang, B. Z. Multiple Yet Controllable Photoswitching in a Single AIEgen System. *J. Am. Chem. Soc.* **2018**, 140, 1966-1975.
- (250) Huang, J.; Sun, N.; Chen, P.; Tang, R.; Li, Q.; Ma, D.; Li, Z. Largely Blue-Shifted Emission Through Minor Structural Modifications: Molecular Design, Synthesis, Aggregation-Induced Emission and Deep-Blue OLED Application. *Chem. Commun.* **2014**, 50, 2136-2138.
- (251) Cheng, H. K.; Yeung, M. C. L.; Yam, V. W. W. Molecular Engineering of Platinum (II) Terpyridine Complexes with Tetraphenylethylene-Modified Alkynyl Ligands: Supramolecular Assembly via Pt···Pt And/Or π - π Stacking Interactions and the Formation of Various Superstructures. *ACS Appl. Mater. Interfaces* **2017**, 9, 36220-36228.

- (252) Carrara, S.; Aliprandi, A.; Hogan, C.F.; De Cola, L., Aggregation-induced Electrochemiluminescence of Platinum (II) Complexes. *J. Am. Chem. Soc.* **2017**, *139*, 14605-14610.
- (253) Sen, B.; Patra, S.K.; Khatua, S. Ruthenium (II) Polypyridine Complex-Based Aggregation-Induced Emission Luminogen for Rapid and Selective Detection of Phosgene in Solution and in the Gas Phase. *Inorg. Chem.* **2021**, *60*, 19175-19188.
- (254) Liu, M.; Song, W.; Deng, P.; Nong, S.; Zhang, X.; Yu, Y.; Li, G.; Xu, L. Specific Discrimination and Efficient Elimination of Gram-Positive Bacteria by an Aggregation-Induced Emission-Active Ruthenium (II) Photosensitizer. *Eur. J. Med. Chem.* **2023**, *251*, 115249.
- (255) Xiu, X.; Puskar, N. L.; Shanata, J. A. P.; Lester, H. A.; Dougherty, D. A. Nicotine Binding to Brain Receptors Requires a Strong Cation- π Interaction. *Nature* **2009**, *458*, 534.
- (256) Burley, S.; Petsko, G. Aromatic-Aromatic Interaction: A Mechanism of Protein Structure Stabilization. *Science* **1985**, *229*, 23-28.
- (257) Li, S.; Cooper, V. R.; Thonhauser, T.; Lundqvist, B. I.; Langreth, D. C. Stacking Interactions and DNA Intercalation. *J. Phys. Chem. B* **2009**, *113*, 11166-11172.
- (258) Steiner, T.; Koellner, G. Hydrogen Bonds with π -Acceptors in Proteins: Frequencies and Role in Stabilizing Local 3D Structures. *J. Mol. Biol.* **2001**, *305*, 535-557.
- (259) Tuo, D. H.; Liu, W.; Wang, X. Y.; Wang, X. D.; Ao, Y. F.; Wang, Q. Q.; Li, Z. Y.; Wang, D. X. Toward Anion- π Interactions Directed Self-Assembly with Predesigned Dual Macrocyclic Receptors and Dianions. *J. Am. Chem. Soc.* **2019**, *141*, 1118-1125.
- (260) Amendola, V.; Bergamaschi, G.; Boiocchi, M.; Fabbrizzi, L.; Mosca, L. The Interaction of Fluoride with Fluorogenic Ureas: An ON¹-OFF-ON² Response. *J. Am. Chem. Soc.* **2013**, *135*, 6345-6355.
- (261) Amendola, V.; Gómez, D. E.; Fabbrizzi, L.; Licchelli, M. What Anions Do to N-H-Containing Receptors. *Acc. Chem. Res.* **2006**, *39*, 343-353.
- (262) Amendola, V.; Fabbrizzi, L.; Mosca, L. Anion Recognition by Hydrogen Bonding: Urea-Based Receptors. *Chem. Soc. Rev.* **2010**, *39*, 3889-3915.
- (263) Schneider, H.J. Binding Mechanisms in Supramolecular Complexes. *Angew. Chem. Int. Ed.* **2009**, *48*, 3924-3977.
- (264) Meyer, E.A.; Castellano, R.K.; Diederich, F. Interactions with Aromatic Rings in Chemical and Biological Recognition. *Angew. Chem. Int. Ed.* **2003**, *42*, 1210-1250.

- (265) Sutton, C.; Risko, C.; Brédas, J.-L. Non-covalent Intermolecular Interactions in Organic Electronic Materials: Implications for the Molecular Packing *vs* Electronic Properties of Acenes. *Chem. Mater.* **2016**, *28*, 3-16.
- (266) Sunner, J.; Nishizawa, K.; Kebarle, P. Ion-Solvent Molecule Interactions in the Gas Phase. The Potassium Ion and Benzene. *J. Phys. Chem.* **1981**, *85*, 1814-1820.
- (267) Meot-Ner, M.; Deakyne, C. A. Unconventional Ionic Hydrogen Bonds. 1. $\text{CH}^{\delta+}-\text{X}$. Complexes of Quaternary Ions with n - and π Donors. *J. Am. Chem. Soc.* **1985**, *107*, 469-474.
- (268) Meot-Ner, M.; Deakyne, C. A. Meot-Ner (Mautner), M. Unconventional Ionic Hydrogen Bonds. 2. $\text{NH}^+\cdots\pi$. Complexes of Onium Ions with Olefins and Benzene Derivatives. *J. Am. Chem. Soc.* **1985**, *107*, 474-479.
- (269) Stauffer, D.A.; Barrans, R.E. Jr.; Dougherty, D.A. Biomimetic Catalysis of an $\text{S}_{\text{N}}2$ Reaction Resulting from a Novel Form of Transition-State Stabilization. *Angew. Chem., Int. Ed. Engl.* **1990**, *29*, 915-918.
- (270) Ma, J.C.; Dougherty, D.A. The Cation- π Interaction. *Chem. Rev.* **1997**, *97*, 1303-1324.
- (271) Kumpf, R. A.; Dougherty, D. A. A Mechanism for Ion Selectivity in Potassium Channels: Computational Studies of Cation- π Interactions. *Science*, **1993**, *261*, 1708-1710.
- (272) Zarić, S.D.; Popović, D.M.; Knapp, E.W. Metal Ligand Aromatic Cation- π Interactions in Metalloproteins: Ligands Coordinated to Metal Interact With Aromatic Residues. *Chem. Euro. J.* **2000**, *6*, 3935-3942.
- (273) Siu, F. M.; Ma, N. L.; Tsang, C. W. Competition Between π and Non- π Cation-Binding Sites in Aromatic Amino Acids: A Theoretical Study of Alkali Metal Cation (Li^+ , Na^+ , K^+)-Phenylalanine Complexes. *Chem. Euro. J.* **2004**, *10*, 1966-1976.
- (274) Gallivan, J. P.; Dougherty, D. A. A Computational Study of Cation- π Interactions *vs* Salt Bridges in Aqueous Media: Implications for Protein Engineering. *J. Am. Chem. Soc.* **2000**, *122*, 870-874.
- (275) Yamato, T.; Tokuhisa, K.; Tsuzuki, H. Medium-Sized Cyclophanes-Part 51. Acylation of [2.2] Metaparacyclophanes: Through-Space Electronic Interactions between Two Benzene Rings. *Can. J. Chem.* **2000**, *78*, 238-247.

- (276) Shimizu, T.; Tanaka, K.; Paudel, A.; Yamato, T. Medium Sized Cyclophanes-Part 85: Benzylolation by 8-(Bromomethyl) [2.2]metacyclophanes. Through-Space Electronic Interactions of [2.2]Metacyclophane Benzyl Cations. *Can. J. Chem.* **2010**, *88*, 458-462.
- (277) Schneider, H.J.; Werner, F.; Blatter, T., Attractive Interactions Between Negative Charges and Polarizable Aryl Parts of Host-Guest Systems. *J. Phys. Org. Chem.* **1993**, *6*, 590-594.
- (278) Quinonero, D.; Garau, C.; Rotger, C.; Frontera, A.; Ballester, P.; Costa, A.; Deya, P. M. Anion- π Interactions: Do They Exist? *Angew. Chem., Int. Ed.* **2002**, *41*, 3389-3392.
- (279) Mascals, M.; Armstrong, A.; Bartberger, M. D. Anion-Aromatic Bonding: A Case for Anion Recognition by π -Acidic Rings. *J. Am. Chem. Soc.* **2002**, *124*, 6274-6276.
- (280) Alkorta, I.; Rozas, I.; Elguero, J. Interactions of Anions with Perfluoro Aromatic Compounds. *J. Am. Chem. Soc.* **2002**, *124*, 8593-8598.
- (281) Dawson, R. E.; Hennig, A.; Weimann, D. P.; Emery, D.; Ravikumar, V.; Montenegro, J.; Takeuchi, T.; Gabutti, S.; Mayor, M.; Mareda, J. *et al.* Experimental Evidence for the Functional Relevance of Anion- π Interactions. *Nat. Chem.* **2010**, *2*, 533-538.
- (282) Gorteau, V.; Bollot, G.; Mareda, J.; Perez-Velasco, A.; Matile, S. Rigid Oligonaphthalenediimide Rods as Transmembrane Anion- π Slides. *J. Am. Chem. Soc.* **2006**, *128*, 14788-14789.
- (283) Wang, D.X.; Wang, M.X., Exploring Anion- π Interactions and their Applications in Supramolecular Chemistry. *Acc.Chem.Res.* **2020**, *53*, 1364-1380.
- (284) Schottel, B.L.; Chifotides, H.T.; Shatruk, M.; Chouai, A.; Pérez, L.M.; Bacsa, J.; Dunbar, K.R. Anion- π Interactions as Controlling Elements in Self-Assembly Reactions of Ag (I) Complexes with π -acidic Aromatic Rings. *J. Am. Chem. Soc.* **2006**, *128*, 5895-5912.
- (285) Chifotides, H.T.; Giles, I.D.; Dunbar, K.R. Supramolecular Architectures with π -acidic 3, 6-bis (2-pyridyl)-1, 2, 4, 5-tetrazine Cavities: Role of Anion- π Interactions in the Remarkable Stability of Fe (II) Metallacycles in Solution. *J.Am.Chem.Soc.* **2013**, *135*, 3039-3055.
- (286) Song, W.; Gao, J.; Gao, Y.; Shan, G.G.; Geng, Y.; Shao, K.; Su, Z.M. Constructing Anion- π Interactions in Cationic Iridium (III) Complexes to Achieve Aggregation-Induced Emission Properties. *Inorg. Chem. Front.*, **2024**, *11*, 1198-1206.

- (287) Han, J.; Yakiyama, Y.; Takeda, Y.; Sakurai, H. Sumanene-Functionalised Bis (terpyridine)-Ruthenium (II) Complexes Showing Photoinduced Structural Change and Cation Sensing. *Inorg. Chem. Front.* **2023**, *10*, 211-217.
- (288) Demircan, C.A.; Bozkaya, U. Transition Metal Cation– π Interactions: Complexes Formed By Fe^{2+} , Co^{2+} , Ni^{2+} , Cu^{2+} , and Zn^{2+} Binding with Benzene Molecules. *J. Phys. Chem. A* **2017**, *121*, 6500-6509.



Chapter 2

**Synthesis and Manifold but Controllable
Emission Switching of Stilbene-Appended
Polyaromatic Terpyridine Derivatives via
Aggregation and Trans-Cis Isomerization**

2.1 Introduction

Molecular switching processes are becoming an increasingly important technological objective for the construction of devices that can operate at both molecular and supramolecular levels.¹⁻⁶ The interest arises because of their useful roles in multiple optoelectronic devices, viz. optical memory, photo-optical switching and display.⁷⁻⁹ The high density molecular data storage systems that are actively investigated in recent times include simple on-off switches and capable of performing logic operations.¹⁰⁻¹⁵ The molecular units that permit reversible alteration of a specific electronic property upon the action of external stimuli such as light are of particular interest as materials for optical data storage.^{7-9, 16-20} Among the photoswitchable materials, the photochromic compounds capable of undergoing light-induced reversible alteration between two forms possessing distinguishable absorption spectral features are attracting special attention with regard to the exploration of optical data storage, optoelectronics, and display devices.

Azobenzenes, stilbenes, spiropyrans and diarylethenes are the important class of photoactive and photo-chromic organic moieties that undergo a reversible photoreaction in dilute solutions between two states, with fairly high stability, which led to their practical utility in aforementioned field of memory devices.²¹⁻²⁷ Among the said photo-responsive systems, azobenzenes and stilbenes often undergo reversible *trans-cis* isomerization upon the action of light of appropriate wavelength giving rise to significant alteration in their spectral profiles.²⁸⁻³² Difference in the spectral properties of the *trans* and *cis* isomer can be attributed to their difference in planarity and extent of π - conjugation.³³⁻³⁹

In connection with our sustained curiosity of tailored design of photo-switchable and photochromic molecules, we synthesize here a series of terpyridine-stilbene conjugate (tpy-styr-X) covalently coupled with various polyaromatic motifs such as naphthalene, anthracene and pyrene (Chart 2.1). Prior to this work, the anthracene- and pyrene-terpyridine derivatives were utilized by other groups for the detection of metal ions as well as of nitroaromatics.⁴⁰⁻⁴¹ Since its inception in the early 1930s, the chemistry associated with 2,2':6',2''-terpyridine (tpy) and its derivatives, have been extensively investigated due to their huge prospects in the diverse fields of organic and inorganic supramolecular photochemistry.⁴²⁻⁴⁴ The design protocol offers a stilbene motif at the 4'-position of the terpyridine unit, which undergoes reversible *trans-cis* isomerization upon irradiation with UV and/or visible light. In a previous report, we designed

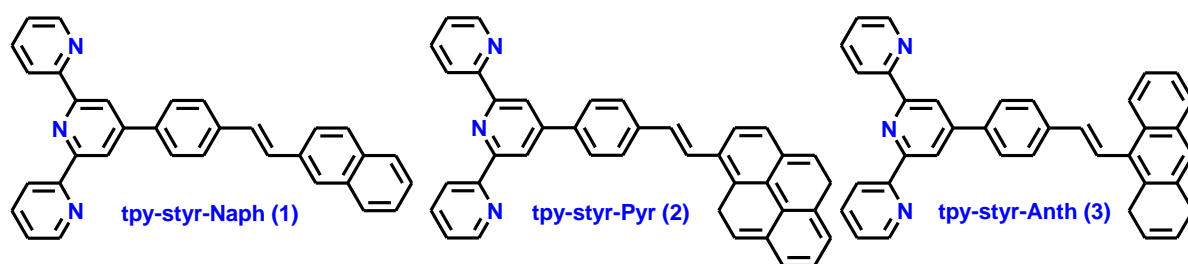


Chart 2.1. Chemical structure of the compounds in this work.

a similar terpyridine-stilbene assembly (tpy-pvp-X) wherein the tpy motif was covalently coupled with stilbene moiety incorporating electron-pushing and electron-withdrawing substituent ($X = \text{H, Me, Cl, NO}_2, \text{ and Ph}$) to tune their photophysical and photoisomerization behaviors.⁴⁵⁻⁴⁹ In the present study, we inserted rigid polyaromatic moieties (naphthalene, anthracene and pyrene) onto the tpy system to further improve the photophysical and in particular the emission characteristics of the resulting assembly. In addition, these polyaromatic moieties are very prone to undergo aggregation under suitable condition. Conjoining of a stilbene moiety and terpyridine acceptor unit through π -linker also instigates the ligand-to-ligand charge transfer (LLCT) character in the resultant assembly.

The tpy derivatives are usually good emitters in their solution state but in most cases the emissive properties fade away abruptly in aggregated form due to inevitable intermolecular π - π stacking. This phenomenon, which is commonly known as Aggregation Caused Quenching (ACQ), has become a thorny obstacle in synthesizing solid state optoelectronic devices.⁵⁰⁻⁵³ Numerous strategies were developed to alienate this ubiquitous ACQ effect but none succeeded until Tang and co-workers pioneered the concept of restriction of intermolecular rotation⁵⁴⁻⁵⁵ (RIM) in 2001.⁵⁶ They designed silole-based organic fluorphores and explicated the phenomenon of aggregation-induced emission (AIE), wherein the molecule showed higher emission in aggregated or solid state rather than in its solution state.⁵⁷⁻⁶¹ Later, in 2002, Park and coworkers elucidated the aggregation induced emission enhancement effect (AIEE) in which the molecules which show significant emission in solution, enhances upon aggregation.⁶² It is expected that the inclusion of naphthalene, anthracene and pyrene motifs into the present styryl-terpyridine system will give rise to AIEE.⁶³⁻⁶⁵ To this end, we thoroughly investigated the photophysical and aggregation-induced emission characteristics of the present compounds in various solvent mixtures having different polarity and viscosity. Contrary to most of the reported systems which exhibit red-shift of emission maxima upon aggregation, the present systems display emission

enhancement together with blue-shift upon aggregation. This blue-shift along with enhancement of emission is termed as Aggregation-Induced Blue-Shifted Emission (AIBSE) and extensive research is now being carried out to develop such quantum efficient systems.⁶⁶⁻

⁶⁹ In addition to the aggregation behaviors, the photoisomerization properties of the compounds will also be thoroughly studied in both of their free and aggregated forms in different solvents. The kinetic and thermodynamic aspects of the isomerization behavior of the compounds are discussed quite elaborately. Lastly, DFT-TDDFT calculations are also performed which show a moderate correlation with the experimentally obtained results and gives us a proper insight about their electronic structures as well as proper assignment of the experimentally observed absorption and emission spectral bands.

2.2 Experimental Section

2.2.1 Materials. Analytical grade solvents and reagents, viz. 2-napthaldehyde, 9-anthracenealdehyde and 1-pyrenecarboxaldehyde were purchased from Merck. The other precursor, 4'-(2,2':6',2''-terpyridyl-4)benzyl triphenyl phosphonium bromide (tpy-PhCH₂PPh₃Br) was synthesized following reported literature procedure.^{45,46}

2.2.2 Synthesis of the Compounds. The general procedure followed for the synthesis of the desired compounds is described below.

2-(4-(4-((*E*)-2-(naphthalen-2-yl)vinyl)-6-(pyridin-2-yl)pyridine [tpy-styr-Naph].
A mixture of tpy-PhCH₂PPh₃Br (332 mg, 0.5 mmol) and 2-napthaldehyde (78 mg, 0.5 mmol) was continuously stirred in dry DCM and was placed in an ice-bath maintaining the temperature within 0-5° C under nitrogen atmosphere. To this mixture, t-BuOK (130 mg, 1.0 mmol) was added bit by bit and magnetically stirred for ~12 h. The resulting solution was filtered and dried in a rota-evaporator. This crude compound was thoroughly washed in water, dried in air and then purified by silica gel column chromatography using 10:1 (v/v) CHCl₃-MeOH mixture. Finally, purification and recrystallization from CHCl₃-MeOH (1:2, v/v) mixture yielded a white color amorphous product. Yield: 164 mg (71%). Elemental Anal. Calcd. for C₃₃H₂₃N₃: C, 85.87; H, 5.02; N, 9.10. Found: C, 85.75; H, 5.07; N, 9.05. ¹H NMR (400 MHz, CDCl₃, δ/ppm) : 8.79 (s, 2H, 2H_{3'}), 8.75 (d, 2H, *J*=4.0 Hz, 2H₆), 8.71 (d, 2H, *J*=7.2 Hz, 2H₃), 7.96 (d, 2H, *J*=8.0 Hz, 2H₈), 7.90 (d, 2H, *J*=7.6 Hz, 2H₇), 7.88-7.82 (m, 4H, 2H₄+H₁₁+H₁₆), 7.78 (d, 1H, *J*=8.8 Hz, H₉), 7.71 (d, 1H, *J*=8.0 Hz, H₁₂), 7.51-7.44 (m, 2H, H₁₀+H₁₃), 7.41-7.34 (m, 4H, 2H₅+H₁₄+H₁₅), 7.30 (s, 1H, H₁₇). ¹³C NMR (100 MHz, CDCl₃, δ/ppm) : 156.37, 156.05, 149.73, 149.22, 138.26, 137.52, 136.96, 134.76, 133.79,

133.23, 129.70, 128.46, 128.39, 128.15, 127.80, 127.72, 127.15, 127.00, 126.46, 126.10, 123.92, 123.58, 121.47, 118.61. ESI-MS (positive, MeOH): m/z =462.04 (100%) [(tpy-styr-Naph+H⁺)].

2-(4-(4-((*E*)-2-(pyren-4-yl)vinyl)phenyl)-6-(pyridin-2-yl)(pyridin-2-yl)pyridine [tpy-styr-Pyr]. The compound is synthesized by following the similar method as above except by using 1-pyrenecarboxaldehyde (116 mg, 0.5 mmol). Yield: 180 mg (67%). Elemental anal. Calcd. for C₃₉H₂₅N₃: C, 87.45; H, 4.70; N, 7.84. Found: C, 87.39; H, 4.75; N, 7.80. ¹H NMR (400 MHz, CDCl₃, δ/ppm) : 8.80 (s, 2H, 2H_{3'}), 8.75 (d, 2H, *J*=5.2 Hz, 2H₆), 8.69 (d, 2H, *J*=8.0 Hz, 2H₃), 8.57 (d, 1H, *J*=9.2 Hz, H₁₄), 8.39 (d, 1H, *J*=8.0 Hz, H₁₅), 8.32 (t, 1H, *J*=8.0 Hz, H₁₆), 8.22-8.17 (m, 4H, H₁₁+H₁₃+H₁₇+H₁₈), 8.04-7.99 (m, 3H, 2H₈+H₁₂), 7.93 (t, 2H, *J*=6.8 Hz, 2H₄), 7.86 (d, 2H, *J*=7.6 Hz, 2H₇), 7.61 (d, 1H, *J*=8.0 Hz, H₉), 7.47-7.39 (m, 4H, 2H₅+H₁₀+H₁₉). ¹³C NMR (100 MHz, CDCl₃, δ/ppm) : 156.04, 155.25, 150.72, 149.17, 139.35, 137.52, 136.98, 133.28, 132.23, 131.74, 131.16, 130.45, 129.75, 128.99, 128.46, 127.64, 127.32, 126.88, 126.49, 126.12, 125.50, 125.18, 124.72, 124.43, 123.95, 123.04, 122.34, 121.90, 121.43, 118.53. ESI-MS (positive, MeOH): m/z =536.11 (100%) [(tpy-styr-Pyr+H⁺)].

2-(4-(4-((*1E*)-2-(5,8-dihydroanthracen-10-yl)vinyl)phenyl)-6-pyridin-2-ylpyridine -2-yl)pyridine [tpy-styr-Anth]. The compound is synthesized by adopting the same procedure as above except by using 9-anthracenealdehyde (104 mg, 0.5 mmol) in place of 2-napthaldehyde. Yield: 166 mg (65%). Elemental Anal. Calcd. for C₃₇H₂₅N₃: C, 86.86; H, 4.93; N, 8.21. Found: C, 86.78; H, 4.96; N, 8.18. ¹H NMR (400 MHz, CDCl₃, δ/ppm) : 8.81 (s, 2H, 2H_{3'}), 8.76 (d, 2H, *J*=4.4 Hz, 2H₆), 8.70 (d, 2H, *J*=8.0 Hz, 2H₃), 8.43 (s, 1H, H₁₅), 8.39 (t, 2H, *J*=5.0 Hz, 2H₄), 8.06-8.02 (m, 4H, *J*=2.2 Hz, 2H₈+2H₁₃), 7.90 (t, 2H, *J*=7.8 Hz, 2H₁₂), 7.82 (d, 2H, *J*=8.4 Hz, 2H₇), 7.51-7.48 (m, 4H, 2H₁₁+2H₁₄), 7.39-7.36 (m, 3H, 2H₅+H₉), 7.05 (d, 1H, *J*=16 Hz, H₁₀). ¹³C NMR (100 MHz, CDCl₃, δ/ppm) : 156.09, 155.07, 151.29, 149.15, 138.38, 137.10, 133.16, 132.16, 131.02, 130.33, 129.63, 128.62, 127.73, 127.17, 126.64, 125.92, 125.66, 125.26, 124.56, 123.95, 121.39, 118.51. ESI-MS (positive, MeOH): m/z =512.11 (100%) [(tpy-styr-Anth+H⁺)].

2.2.3 Physical Measurements. Elemental analyses of the compounds were performed with a Vario-Micro V2.0.11 elemental (CHNSO) analyzer. NMR spectra were collected on a Bruker 400 MHz spectrometer in CDCl₃. High resolution mass spectroscopy was performed on a Waters Xevo G2 QTOF mass spectrometer. The UV-vis absorption spectra were

recorded with a Shimadzu UV 1800 spectrometer. Steady state luminescence spectra were obtained by a Horiba Fluoromax-4 spectrometer. Luminescence quantum yields were determined by using literature method taking quinine sulphate as the standard. Luminescence lifetime measurements were carried out by using time-correlated single photon counting set up from Horiba Jobin-Yvon. The luminescence decay data were collected on a Hamamatsu MCP photomultiplier (R3809) and were analyzed by using IBH DAS6 software.

Experimental uncertainties are as follows: absorption maxima, ± 2 nm; molar absorption coefficients, 10%; emission maxima, ± 5 nm; excited-state lifetimes, 10%; luminescence quantum yields, 20%.

2.2.4 Determination of Photoisomerization Rate Constants and Quantum Yields.

A 1-cm light path length quartz cell was used for the photoisomerization measurements. The concentration of the complexes was maintained in the range of $\sim 1.0 \times 10^{-5}$ - 2.0×10^{-5} M, and the solution was thoroughly degassed with N_2 before photoirradiation and stirred magnetically during photoirradiation. Isomerization studies were carried out in a photocatalytic reactor designed by Lelesil Innovative Systems by using 250 W Xenon lamp and light of specific wavelengths were isolated using band pass filters (405 nm). The apparent rate constant of the isomerization process were evaluated from the absorbance titration data using equation 2.1.⁷⁰ We used the term "apparent rate constant" as it depends on the intensity of light. The intensity of the light source at the cell position is ~ 0.11 W.

$$\ln \{(A_0 - A_\infty)/(A_t - A_\infty)\} = k_{iso} t \quad (2.1)$$

where A_0 , A_t , and A_∞ is the absorbance of the complexes at time $t = 0$, t , and ∞ respectively. k_{iso} is the rate constant of photoisomerization process. Both k_{iso} and A_∞ were evaluated by a nonlinear least squares method. Quantum yields (ϕ) of the photoisomerization process were obtained by using the equation 2.2.⁷¹

$$v = (\phi I_0/V) (1 - 10^{-Abs}) \quad (2.2)$$

where v is the rate of the photoisomerization, I_0 is the photon flux at the front of the cell, V is the volume of the solution, and Abs is the initial absorbance at the irradiation wavelength. We have estimated the photon flux by a relative method using azobenzene which was extensively studied in literature.⁷²⁻⁷³ Then we have calculated the quantum yield of photoisomerization of the present complexes by using equation 2.2.

2.2.5 Computational Studies. All calculations were performed with the Gaussian 09 program⁷⁴ employing the DFT method with Becke's three-parameter hybrid functional and

Lee-Yang-Parr's gradient corrected correlation functional B3LYP level of theory using 6-31G(d) basis.⁷⁵⁻⁷⁶ Geometries were fully optimized using the criteria of the respective programs. To compute the UV-vis transitions of the compounds, the time-dependent DFT (TD-DFT)⁷⁷⁻⁷⁹ scheme was adopted considering the ground state geometries optimized in solution phase. The excitation energies, computed in DCM were simulated by PCM model.⁸⁰⁻⁸² The geometries of the lowest energy singlet states of the compounds were also optimized in DCM by using TD-DFT method and employing the PCM model to calculate the emission energies. Orbital and fractional contribution analysis was done with Gauss View⁸³ and Gauss Sum 2.1.⁸⁴

2.3 Results and Discussion

2.3.1 Synthesis and Characterization. The compounds are synthesized by stoichiometric reaction between $\text{tpyPhCH}_2\text{PPh}_3\text{Br}$ and corresponding aldehyde in dichloromethane at the temperature range of 0-5°C under argon protection and thoroughly characterized by NMR and ESI mass spectrometric techniques as well as by elemental analysis. The ESI mass spectra of **1-3** in methanol are presented in Figure 2.1. All the compounds showed a single strong peak at their corresponding $m/z = [\text{MH}]^+$ value. $^1\text{H-NMR}$ and $^{13}\text{C-NMR}$

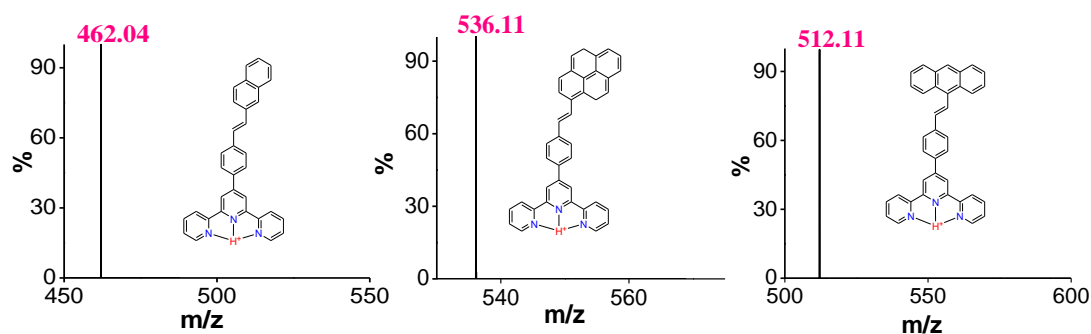


Figure 2.1 ESI mass spectra of compounds **1-3** in MeOH.

spectroscopy are employed to confirm the structure of the compounds in their solution state (Figure 2.2 and Figure 2.3). The singlet appearing in the most downfield region within 8.81-8.79 ppm is assignable to the H_3 of the tpy-styr-X moiety, whereas the next two doublets in the region of 8.76-8.69 ppm are assignable as H_6 and H_3 protons since they lie closer to the electronegative nitrogen atom which forces them to move to the downfield region. The

olefinic protons appeared within 7.78-7.05 ppm with the value of the coupling constants (J) being ~16Hz indicating the *trans* conformation of the compounds.

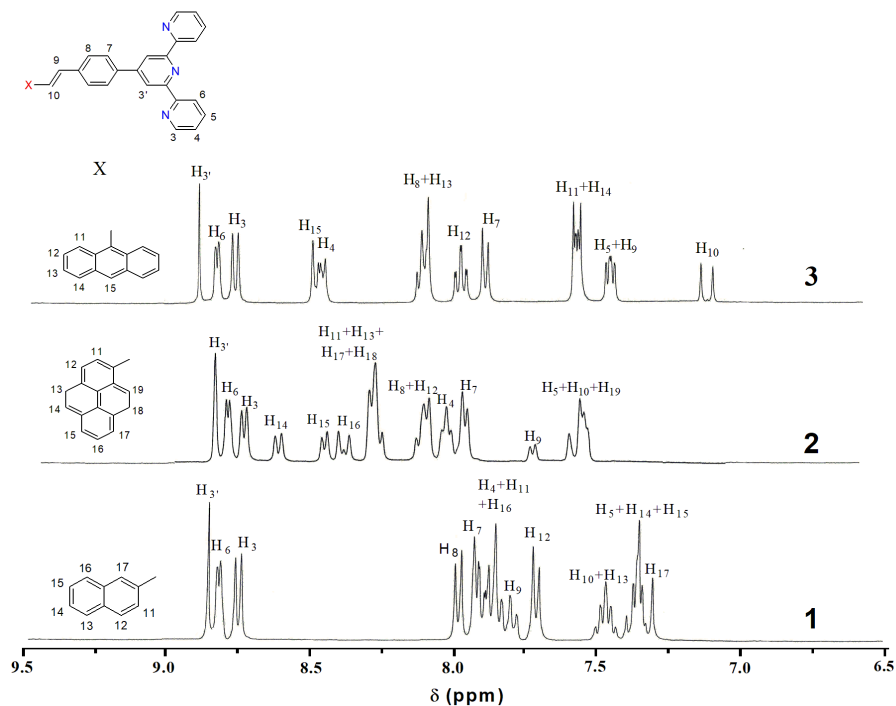


Figure 2.2 NMR spectra of **1-3** in CDCl_3 .

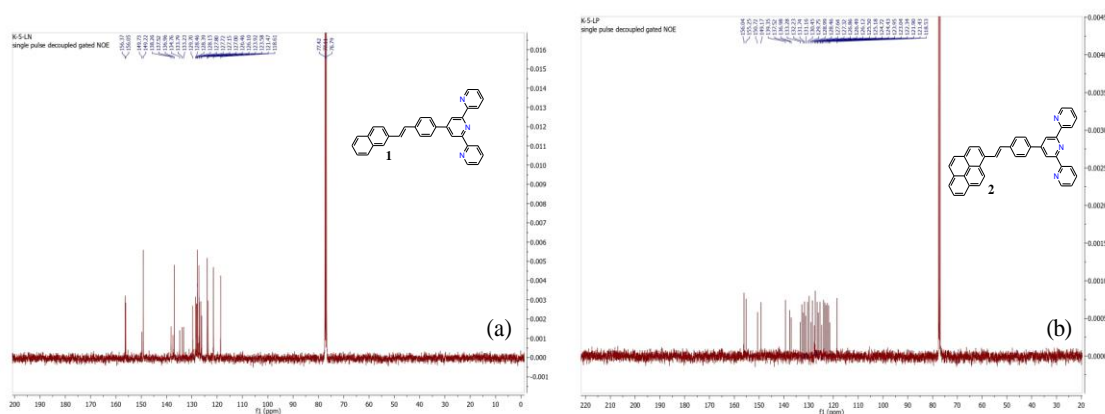


Figure 2.3 ^{13}C -NMR spectra of **1** (a) and **2** (b) in CDCl_3 .

2.3.2 Absorption and Emission Spectra. Absorption spectra of the compounds are recorded in some selected solvents, viz. DCM, DMSO and THF (Figure 2.4 and Figure 2.5) and the relevant photophysical parameters are summarized in Table 2.1. The compounds are

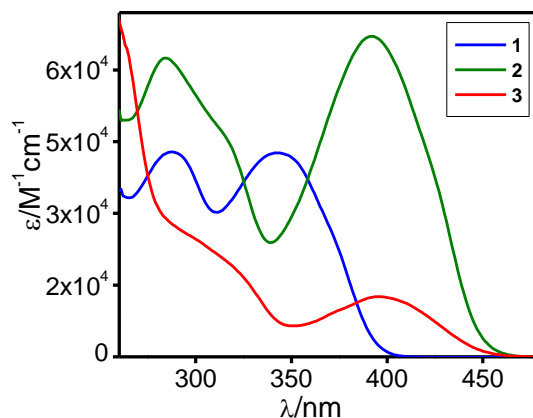


Figure 2.4 UV-vis absorption (a) and emission ($\lambda_{ex}=360$ nm) (b) spectra of isomolar solutions of **1-3** in DMSO. Emission decay profiles ($\lambda_{ex}=370$ nm NanoLED) together with the values of lifetime are shown in figure (c).

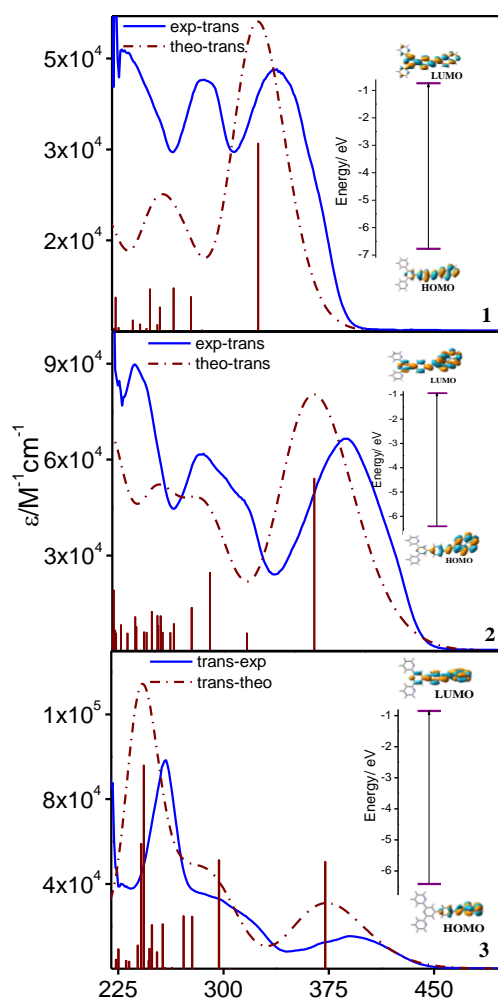


Figure. 2.5 Overlay of the experimental (blue) and calculated (employing 6-31G(d)/CAM-B3LYP) (wine) absorption spectra of **1-3** in DCM. The MOs associated with lowest energy band are shown in the inset.

Table 2.1 Photophysical data for the compounds **1-3** in different solvents.

Compsds		Absorption λ_{\max}/nm ($\epsilon/M^{-1}\text{cm}^{-1}$)	Luminescence				
			λ_{\max}/nm	τ/ns	Φ	$k_r(\times 10^8)/\text{s}^{-1}$	$k_{nr}(\times 10^8)/\text{s}^{-1}$
1	THF (298K)	342(br)(63100), 286(br)(55100), 243(br)(54500)	412	1.19	0.46	3.87	4.54
2		389(86400), 300(br)(61800), 236(104000)	460	1.68	0.72	4.29	1.67
3		390(21500), 319(sh)(35200), 258(15500)	487	2.64	0.36	1.36	2.42
1	DCM (298 K)	335(39500), 286(br)(38000), 245(26500)	416	1.13	0.44	3.89	4.95
2		386 (52400), 300(br)(44000), 240(sh) (70000)	467	1.73	0.66	3.81	1.96
3		395(15600), 323(54800), 306(br)(27800), 259(101000)	492	2.59	0.34	1.31	2.55
1	DMSO (298 K)	344(br) (42900), 288(br)(43000)	434	1.34	0.38	2.83	4.62
2		392(67500), 318(45000), 283(63000)	488	1.88	0.54	2.87	2.44
3		398(br)(13000), 317(sh)(19700), 262(70000)	504	2.40	0.18	0.75	3.41
1	THF (77K)	-	410	-	0.48	-	-
2		-	443 469	-	0.78	-	-
3		-	483	-	0.51	-	-

embroidered with electron donating polyaromatic moiety and electron accepting terpyridine motif connected by a styrylbenzene linker. The optimized structures of the compounds are provided in Figure 2.6. DFT calculations propose that the HOMOs are mostly localized on the polyaromatic moiety and to some extent on the styrylbenzene unit, while the LUMOs are primarily located on the terpyridine as well as polyaromatic moiety (Table 2.2). The lowest energy band lies between 335 and 398 nm while the next higher band is situated within the range of 236-323 nm, depending upon the nature of the solvent as well as on the type of the

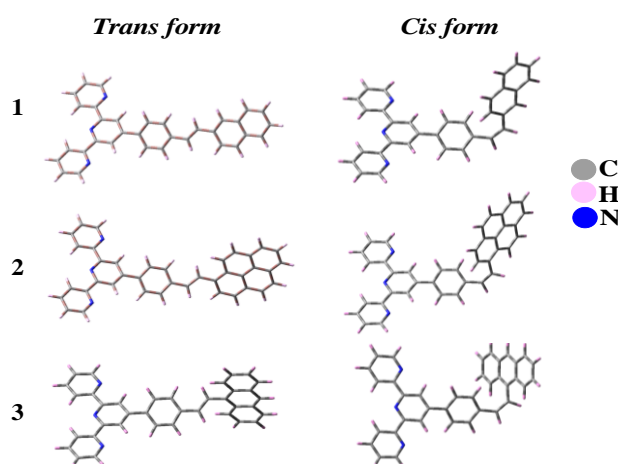


Figure 2.6 Ground state optimized structure of *trans* and *cis* forms of **1-3** in DCM by employing 6-31G(d)/B3LYP.

Table 2.2 Selected MOs along with their energies and compositions for **1** at the TD-DFT/B3LYP level in dichloromethane.

MO	[(tpy-pvp-Naph)] (1)							
	Energy/eV		% Compositions					
	<i>trans</i>	<i>cis</i>	<i>trans</i>			<i>cis</i>		
			Terpy	Vinyl-phenyl	napthal	Terpy	Vinyl-phenyl	napthal
LUMO+4	-0.67	-0.67	91.32	2.37	6.31	87.16	3.66	9.18
LUMO+3	-0.92	-0.92	11.56	10.47	77.97	19.42	18.73	61.85
LUMO+2	-1.33	-1.31	58.02	12.75	29.22	41.95	14.01	44.04
LUMO+1	-1.56	-1.56	99.17	0.83	0.00	99.15	0.84	0.01
LUMO	-1.93	-1.83	34.56	44.09	21.34	45.83	39.14	15.03
HOMO	-5.50	-5.64	4.57	48.36	47.07	3.84	42.33	53.83
HOMO-1	-6.19	-6.13	2.82	15.05	82.13	3.90	23.03	73.07
HOMO-2	-6.31	-6.31	99.77	0.23	0.00	99.75	0.25	0.00
HOMO-3	-6.84	-6.77	38.62	21.22	40.16	26.24	28.99	44.77
HOMO-4	-6.91	-6.91	87.25	12.75	0.00	86.56	12.06	1.37

polyaromatic unit (Table 2.1). The higher energy band is mainly due to local excitation (LE) whereas the lower energy band is assigned as dual contributions from intra-ligand charge transfer (CT) and LE transitions (Table 2.3). These conclusions can be corroborated from TD-DFT calculations which show moderate correlation with the experimentally obtained spectra (in

Table 2.3 Selected UV-vis energy transitions at the TD-DFT/B3LYP level for **3** in dichloromethane along with experimental results.

$\lambda_{\text{expt}}/\text{nm}$	$\lambda_{\text{cal}}/\text{nm}$	Oscillator strength(f)	Excited state	Key transitions	Character
<i>Trans (3)</i>					
395	450	0.65	S ₁	H→L (94%)	CT _{phvn→tpy} , LE _{phvn→phvn}
307	338	0.27	S ₄	H-1→L (81%), H→L+3 (11%)	CT _{tpy→anth, phvn} , LE _{tpy→tpy}
259	259	0.45	S ₂₅	H-5→L+2 (52%), H-2→L+3 (20%), H-2→L+4 (14%)	LE _{tpy→tpy}
	257	0.66	S ₂₆	H-3→L+1 (32%), H-1→L+3 (36%), H→L+6(19%)	CT _{tpy→anth, anth→tpy}
	256	0.57	S ₂₈	H-1→L+3 (53%), H-3→L+1 (21%), H→L+6(13%)	CT _{tpy→anth}
<i>Cis (3)</i>					
403	417	0.18	S ₁	H→L (95%)	CT _{phvn→anth, tpy} , LE _{phvn→phvn}
332	336	0.12	S ₄	H-1→L (81%), H-1→L+1 (12%)	CT _{tpy→anth} , LE _{tpy→tpy}
292	311	0.63	S ₈	H-1→L+1 (83%), H-1→L (13%)	LE _{tpy→tpy}
257	257	0.41	S ₂₈	H-7→L+2 (43%), H-2→L+3 (29%), H-2→L+4 (13%)	LE _{tpy→tpy}
	250	1.17	S ₃₄	H-3→L (10%), H→L+6 (27%), H-3→L+1 (23%), H-1→L+6 (11%)	LE _{anth→anth}

DCM) and the low-energy band arises mainly due to HOMO-LUMO transition (inset to Figure 2.5). For proper characterization of TD-DFT electronic excitations, we also calculated the natural transition orbital analysis (NTO) and electron density difference maps (EDDM) (Figure 2.7-2.8). EDDM and NTO plots also support the above band assignment. A small bathochromic-shift of the lowest energy band is noticed upon increase in the polarity of the solvents. Irrespective of the solvents, the lowest energy band displays a small but gradual red-shift upon increase of π -

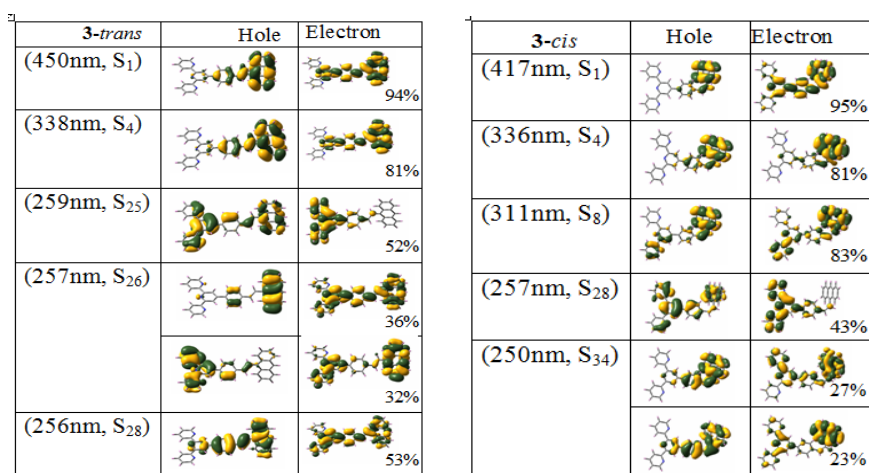


Figure 2.7 NTOs demonstrating the nature of optically active singlet excited states in the absorption bands for **3** in both their *trans* and *cis* form. The occupied (holes) and unoccupied (electrons) NTO pairs that have major contribution to each excited state are only represented.

conjugation in the polyaromatic hydrocarbon. The compounds exhibit broad and intense emission band at RT within the spectral domain of 412-504 nm (Figure 2.9). Among the three compounds, **2** is highly emissive while **3** has the lowest emission intensity which is also supported by their observed quantum yield (Φ) values. In order to understand the nature of the emitting excited state, TD-DFT calculations is also performed by using B3LYP functional. The results indicate that the emitting excited state is primarily ¹LE in nature together with the involvement of some CT character (Table 2.4). The emission spectra of the compounds are found to be more solvent-sensitive compared to their absorption counterpart (Table 2.1). It has been noticed that with increase in polarity as well as hydrogen bonding ability of the solvent, the position of emission maximum gets red-shifted (~10-30 nm) along with a decrease in emission intensity.

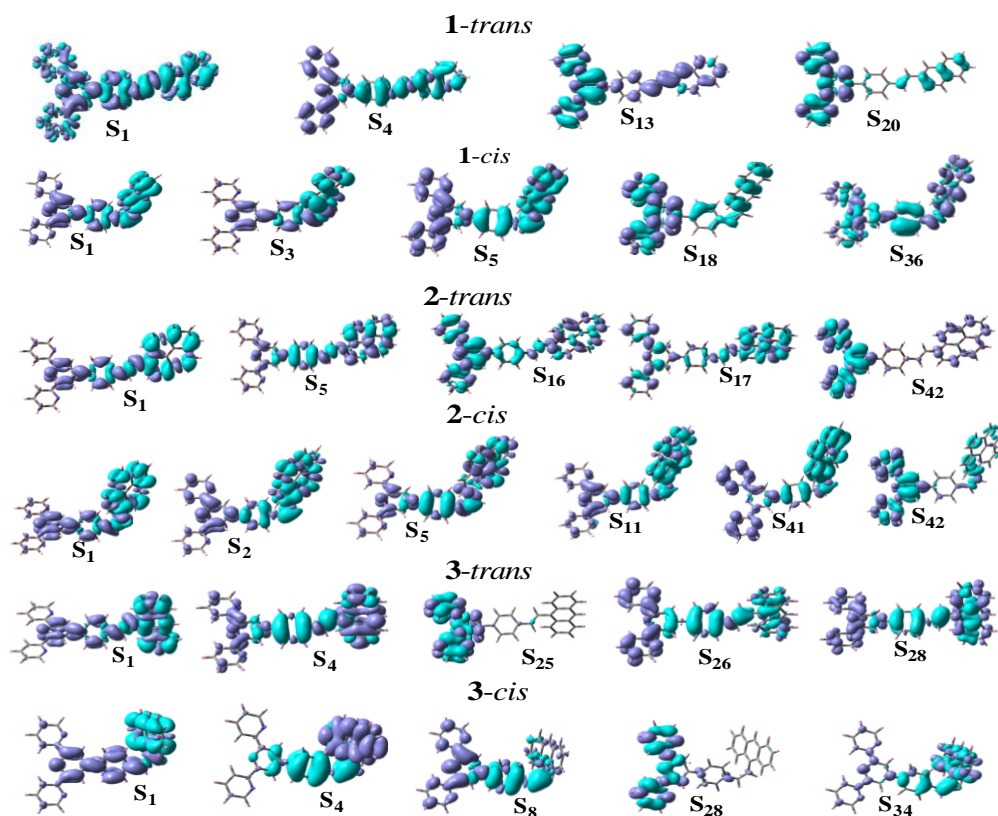


Figure 2.8 Difference in electron density upon excitation from the ground S_0 state to the excited state in *trans* and *cis* forms of **1-3**. Violet and cyan color shows regions of increasing and decreasing electron density, respectively.

A large Stokes' shift ($4500\text{--}5800\text{ cm}^{-1}$ in DCM) is observed for all the three compounds (Table 2.5). In addition, enhanced polarity of the solvent induces further increase in their Stokes' shift values ($5000\text{--}6200\text{ cm}^{-1}$ in DMSO). The emission lifetime is also acquired at RT using different exciting light sources (370, 330 and 280 nm). All the three compounds display mono-exponential decay having lifetime between 1.13 (**1**) and 2.64 (**3**) ns, depending upon the nature of solvent (Figure 2.10 and Table 2.1). The lifetime of the compounds is independent of the exciting light source. The emission spectra are also acquired at 77K in THF as well as in their powdered form. The compounds except **3** display structured emission spectra in both the media with significant enhancement of their emission intensity. The normalized emission spectra are shown in Figure 2.9. Thus, the rigidity constraint imposed by different polyaromatic moiety play important role in their spectral pattern.

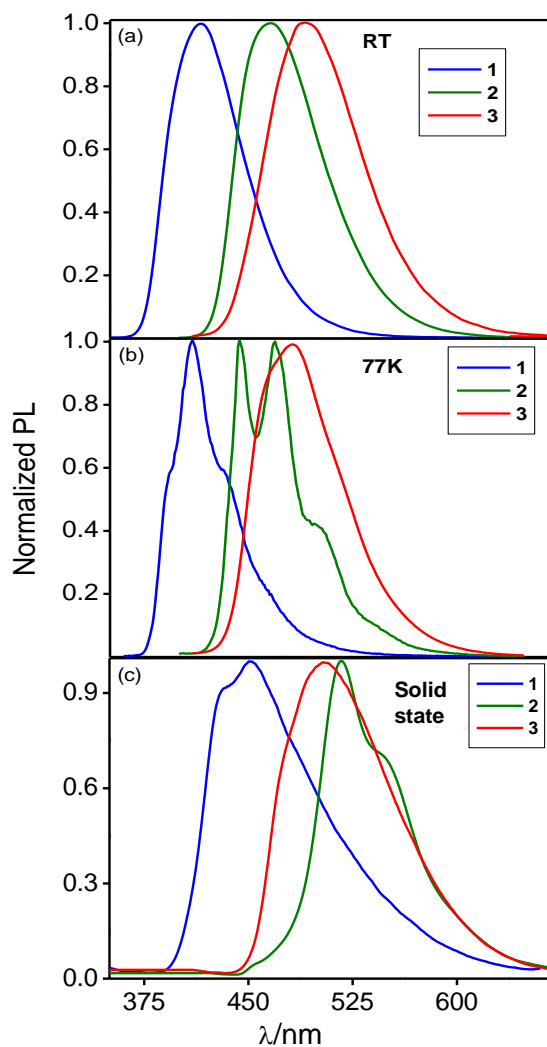


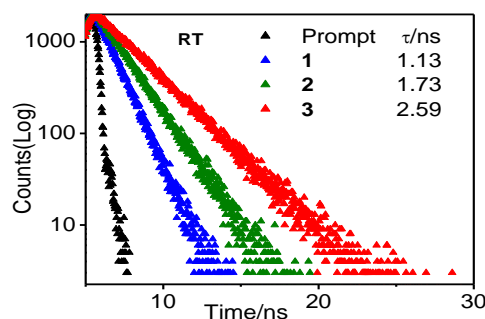
Figure 2.9 Normalized photoluminescence ($\lambda_{\text{ex}}=350$ nm) spectra of **1-3** in DCM at RT (a), THF glass at 77 K (b) and in the solid powder state (c).

Table 2.4 Calculated and experimental emission bands of tpy-pvp-X (**1-3**) in DCM by B3LYP method in their *trans* and *cis* form.

Compds	forms	Experimental (nm)	Theoretical (nm)
1	<i>trans</i>	415	433
2		467	505
3		493	583
1	<i>cis</i>	426	513
2		468	546
3		500	512

Table 2.5 Table for comparison of Stoke's shift in different solvents.

	Stoke's shift/cm ⁻¹		
	1	2	3
DCM	5800	4500	5000
DMSO	6000	5000	5500

**Figure 2.10** Emission decay profiles (λ_{ex} =370 nm NanoLED) together with the values of lifetime of **1-3** in DCM.

2.3.3 Aggregation-Induced Modulation of the Photophysical Properties

2.3.3.1 Concentration Dependent Studies. To study the effect of aggregation, we first demonstrate the effect of concentration on the photoluminescence properties of the compounds at RT. Two solvents are initially used for this purpose, viz. DCM and DMSO. The broad and structureless emission of the compounds gradually quench with increasing concentration. While DMSO shows a continuous decrease in emission intensity, some variations are observed for DCM (Figure 2.11). Interestingly, when the concentration is increased (5 μM \rightarrow \sim 50 μM) in DCM, a sharp increase in emission intensity is seen, while further increase in concentration (up to 1000 μM) leads to continuous drop in the emission intensity. This phenomenon is observed for compounds **2** and **3** only. By contrast, **1** shows no such variation. Dipole- π type interaction probably occurs between the solvents (DCM and DMSO) and the polyaromatic compounds. When toluene is used, where the mode of interaction is expected to be of π - π type, the compounds display structured emission which gradually quenches upon increasing the concentration (Figure 2.12a). We also performed the concentration effect in toluene at low temperature. We initially performed the measurement upon slightly reducing the temperature at 263K (Figure 2.12b). But the emission quenching profile is very similar to that of the RT.

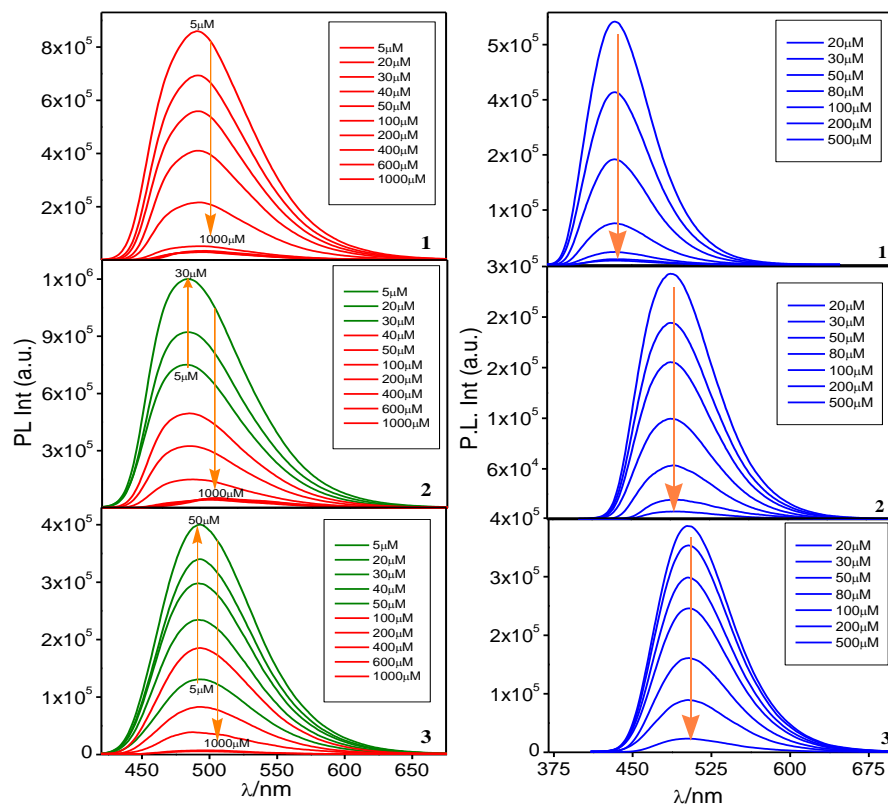


Figure 2.11 The concentration dependent emission ($\lambda_{\text{ex}}=350$ nm) spectra of **1-3** in DCM (left panel) and DMSO (right panel).

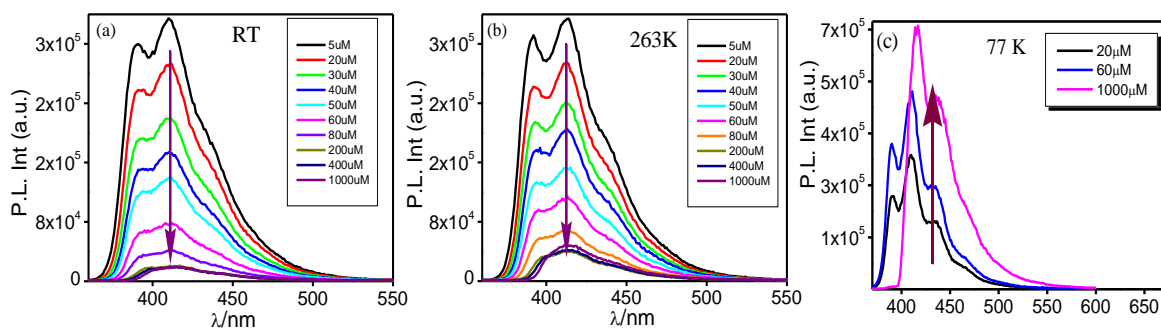


Figure 2.12 The concentration dependent emission ($\lambda_{\text{ex}}=350$ nm) spectra of **1** in toluene at RT (a) 263K (b) and at 77K (c).

Subsequently, we carried out the experiment at three different concentrations (20 μ M-1000 μ M) at 77K (Figure 2.12c). To our surprise, we observed exactly opposite behavior and the emission intensity is substantially enhanced for all the compounds upon increasing concentration at 77K. Thus, the concentration-induced quenching phenomenon is overpowered by temperature-induced enhancement.

2.3.3.2 Aggregation Studies in Different Solvent Mixtures. The aggregation behavior of the compounds is also studied in the mixed environment of solvents. Two combinations of solvent and non-solvent mixtures (DMSO/H₂O and DCM/hexane) are employed. In the case of DMSO/H₂O mixture where DMSO is the solvent and water is the non-solvent, it is observed that the fluorescence intensity gradually decreases with the increase in volume of the water fraction (f_w) (Figure 2.13). The variation of fluorescence intensity as well as the emission maximum as a function of f_w is also displayed in the insets of Figure 2.13. A large red-shift of emission maximum is observed for both **1** (67 nm) and **2** (56 nm), while a very small red-shift of 5 nm is noticed for **3**. The observation indicates the formation of J-aggregates in DMSO-H₂O mixture.⁸⁵

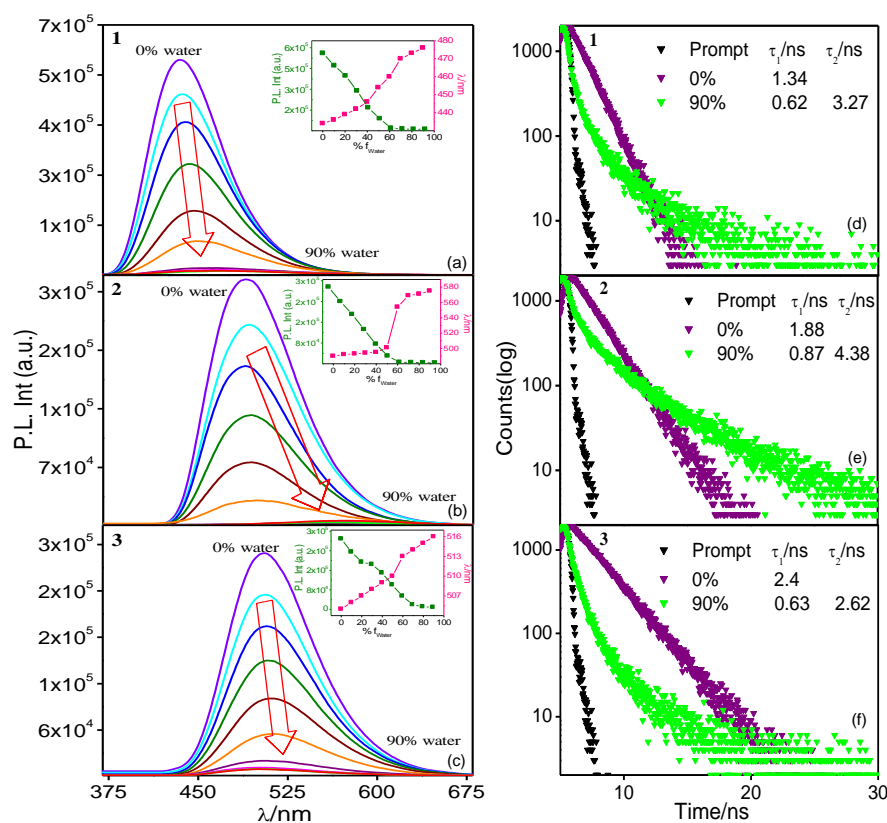


Figure 2.13 The emission (left panel, $\lambda_{ex}=360$ nm) spectral changes of **1-3** upon varying the relative ratio of DMSO and water. The insets to figure a-c show the variation of emission intensity and maximum (λ_{max}) upon increasing the water fraction. Right panel shows the corresponding change in emission decay ($\lambda_{ex}=370$ nm NanoLED) along with the lifetime values of the initial and final form of **1-3**.

The emission lifetime values, on the other hand, shows an enhancement upon gradual addition of water. The initial and the final (aggregated form) solution are clearly distinguished upon illumination with UV light. The aggregated form shows practically no

emission, whereas the initial solution displays a bright green emission. The emission spectral behaviors of the compounds follow a totally reverse trend in DCM/hexane mixture (where DCM is the solvent and hexane is the non-solvent) as compared with DMSO-H₂O mixture. In DCM/hexane, a remarkable emission enhancement accompanied with substantial blue-shift of emission maximum takes place in all the three compounds upon gradual increase of the hexane fraction (f_H) (Figure 2.14). This process is known as Aggregation Induced Blue-Shifted Emission

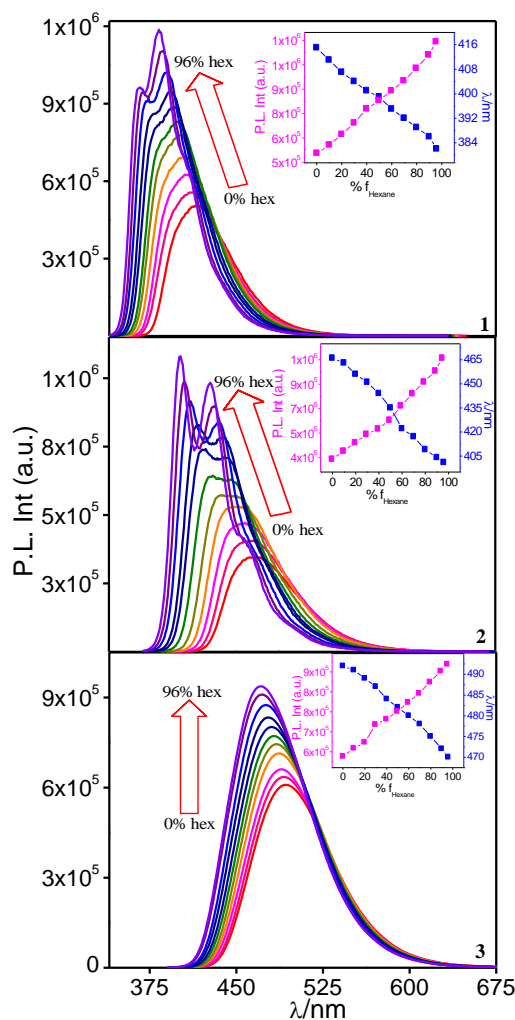


Figure 2.14 The emission ($\lambda_{ex}=350$ nm) spectral changes of **1-3** upon varying the relative ratio of DCM and hexane. The insets show the variation of emission intensity as well as emission maximum upon increasing the hexane fraction.

(AIBSE) and is quite uncommon and is in contrast to widely studied aggregation process that occurs via red-shift of emission maximum.⁶⁶⁻⁶⁹ The extent of emission enhancement for the present compounds varies between 35 and 70%, depending on the nature of the polyaromatic ring. The variation in photoluminescence intensity as well as emission maximum as a

function of f_H is also displayed in the inset of Figure 2.14. Gradual enhancement of emission intensity upon increasing the hexane fraction within a wide domain (10-96%) suggests the aggregation of molecules in the solution mixture with an f_H -activated restricted intermolecular motion (RIM). Apart from emission enhancement, as hexane volume is gradually increased, a structured emission profile is also observed for both **1** and **2**. To our surprise, the emission lifetime of the compounds remains almost unaltered upon aggregation in DCM-hexane mixture. This change in emission spectral profile clearly corroborates the formation of aggregates in the solution mixture.⁸⁶⁻⁸⁹ No structured emission is seen in case of **2** but there is a blue-shift of emission maximum along with increase in intensity. The structured emission clearly indicates that the molecular rotations that are taking place in the solution state are frozen due to aggregation and hence vibronic transitions became visible. It can be said in this context that the aggregation occurring is mostly due to the formation of H-aggregates.⁸⁵ Thus, we are able to reverse the mode of emission switching of the compounds via the formation of two different types of aggregates (J- and H) upon judicious choice of two types of solvent mixtures.

2.3.4 Photo-Isomerization of the Compounds in Their Non-Aggregated Forms.

Due to the presence of C=C unit, it is anticipated that each of the compounds may undergo *trans/cis* isomerization under photo-irradiation. To this end, we have thoroughly studied the isomerization behavior of the compounds in two selected solvents of varying polarity upon irradiation with visible light ($\lambda=405$ nm) (Figure 2.15 and Figure 2.16). The progress of isomerization is monitored through absorption and both steady state and time-resolved emission spectroscopic techniques.

Upon exposure of the DCM solution of the compound, the lowest energy absorption band in the range of ~335-395 nm shifted progressively to the shorter wavelength region together with decrease in band intensity. While **1** and **2** shows a blue-shift of the band maximum to the extent of 7-10 nm, **3** displays only a gradual decrease in absorbance without any spectral shift (Figure 2.15a-c). Additionally, new absorption bands within the range of 376-526 nm appeared and gradually intensified upon exposure to light. Two isosbestic points are clearly visible which

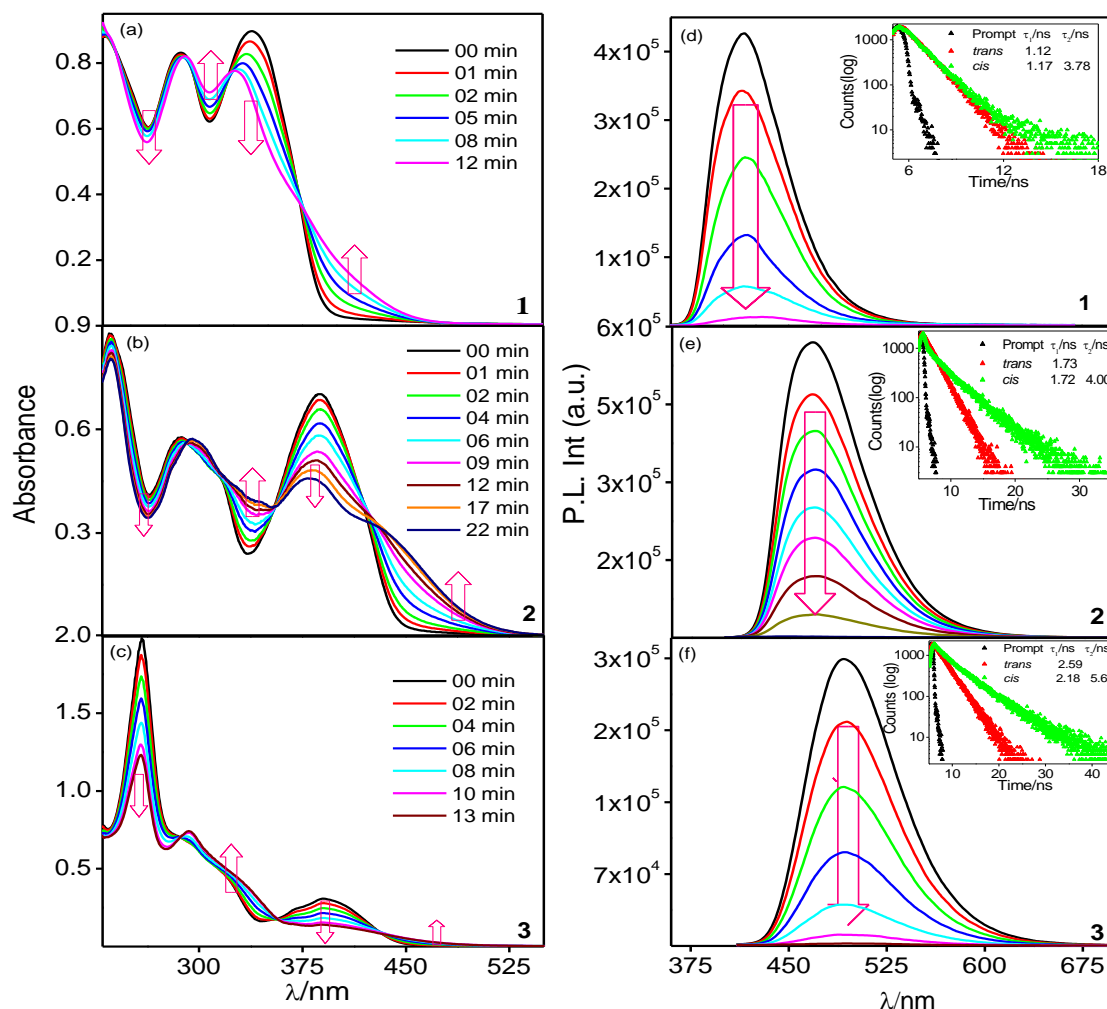


Figure 2.15 Absorption and emission ($\lambda_{\text{ex}}=350$ nm) spectral changes of **1** (a and d, respectively), **2** (b and e, respectively) and **3** (c and f, respectively) upon irradiation with visible light in DCM. Inset to the figure d, e, and f shows the corresponding change in emission decay ($\lambda_{\text{ex}}=370$ nm NanoLED) along with lifetime upon photo-irradiation.

indicate that two species are at equilibrium during the entire process of photo-irradiation. The observed spectral change may be attributed to the *trans*→*cis* photoisomerization process. During irradiation of the DMSO solutions of the compounds, a decrease in the CT band is observed, but unlike in previous case, no evolution of band is observed in the visible domain (Figure 2.16a-c). On the contrary, a simultaneous increase in the LE band intensity is observed. A single isosbestic point is noticed in all cases indicating the presence of two equilibrating species.

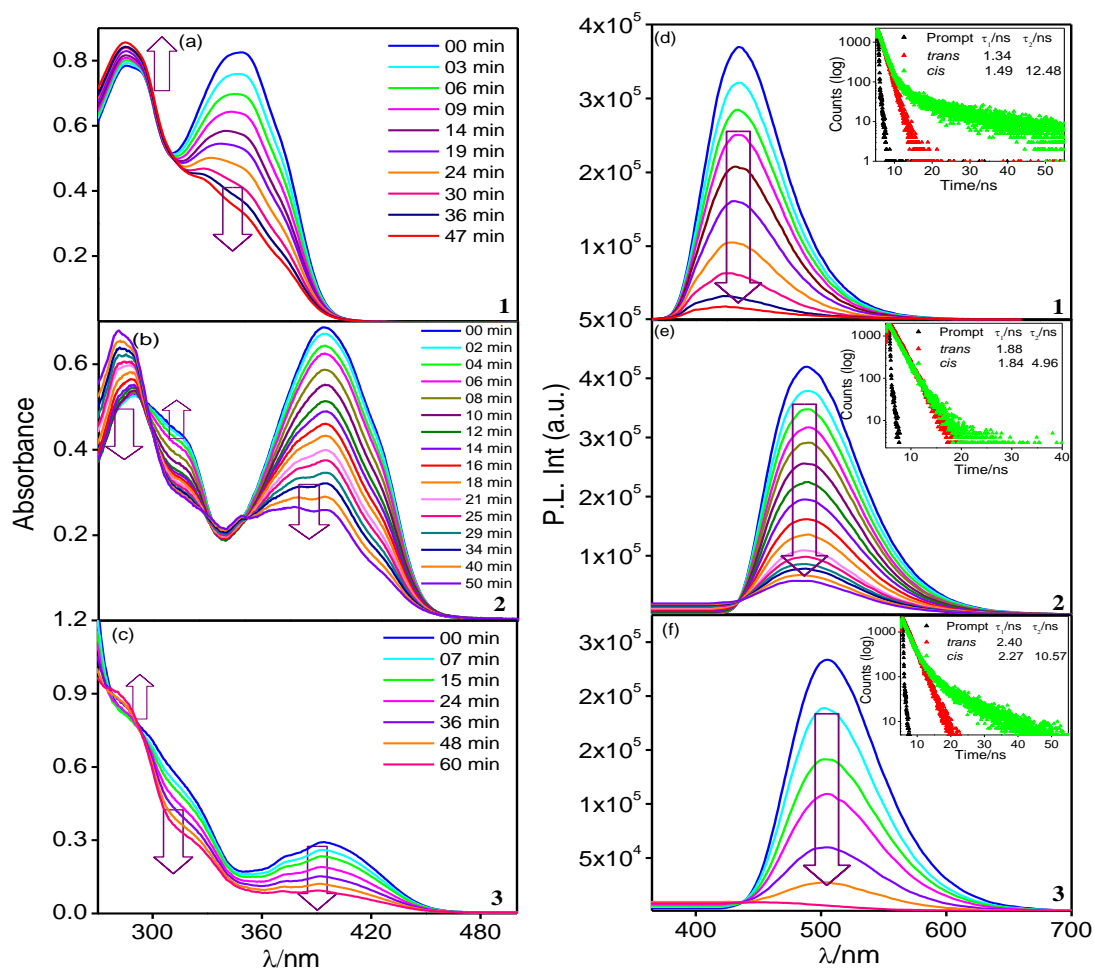


Figure 2.16 Absorption and emission ($\lambda_{\text{ex}}=360$ nm) spectral changes of **1** (a and d, respectively), **2** (b and e, respectively) and **3** (c and f, respectively) upon irradiation with visible light in DMSO. Inset to the figure d, e, and f shows the corresponding change in emission decay ($\lambda_{\text{ex}}=370$ nm NanoLED) along with lifetime upon photo-irradiation.

In the emission side, a complete quenching in the fluorescence intensity is observed in the DCM solution of the compounds during photo-irradiation process (Figure 2.15d-f), thereby converting from the emissive *trans*-isomer ($\phi \sim 0.34\text{--}0.66$) to the practically non-emissive *cis*-isomer ($\phi \sim 0.001\text{--}0.002$). A red-shift of the emission maximum to the extent of 5–15 nm is noticed for **1** and **3**. In line with DCM, the DMSO solution of the compounds also exhibit emission quenching but in contrast to DCM, blue-shift of emission maximum to the extent of 6–10 nm takes place for **1** and **3** (Figure 2.16d-f). Although the photoluminescence intensity quench substantially, the lifetime of the compounds increases to some extent in both solvents upon photo-irradiation indicating that the *cis*-isomers are longer lived than that of their *trans* forms (inset to Figure 2.15d-f and Figure 2.16d-f). We also carried out

isomerization experiments upon irradiating at shorter wavelength. The extent of change is found to be almost similar but it takes longer time to reach the photo-stationary state.

The backward *cis*→*trans* isomerization proceeds smoothly upon keeping the photolyzed solution of the compounds in the dark. Both the absorption and emission spectra of the compounds revert back to almost their initial position in the dark. Interestingly, non-emissive *cis* form can be switched back to the highly emissive *trans* form when kept in dark for some time. Thus, the present compounds can act as ‘on-off-on’ emission switches upon successive exposure to light and keeping in the dark.

Interestingly, the visual color change is clearly observed on going from their original *trans* to the corresponding *cis*-forms upon treating with visible light. Thus, the compounds display photochromic behavior (Figure 2.17). The initial *trans* form of the compounds are strongly fluorescent, while their final *cis* forms are very weakly emissive. Consequently, a sharp emission color change is clearly viewed under UV illumination (Figure 2.17).

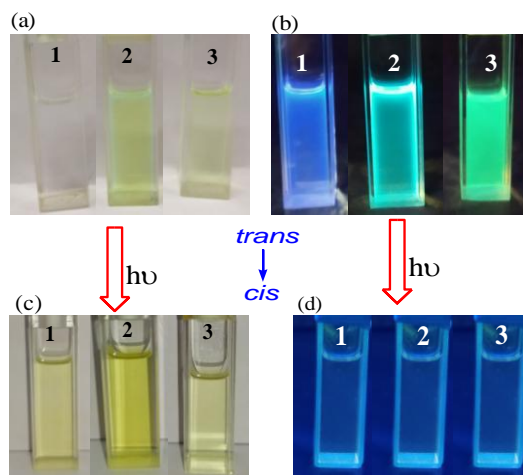


Figure 2.17 The color changes of the DCM solutions of **1-3** that are observed in the naked eye (a→c) and under UV illumination (b→d) on going from their *trans* to the *cis* forms.

In order to gather some direct proof of *trans*→*cis* isomerization, we acquire the ^1H NMR spectra of **3** in CDCl_3 before and after photo-irradiation. The spectrum of **3** is displayed in Figure 2.18. The H_9 and H_{10} protons in stilbene unit in both cases undergo a remarkable up-field shift (from 7.05-7.78 ppm to 6.60-6.82 ppm) together with substantial lowering of their coupling constants ($J \approx 16 \text{ Hz} \rightarrow J \approx 12 \text{ Hz}$). H_7 and H_8 also shift to the up-field region as they are adjacent to the double bond. Along with this, the protons associated with the polyaromatic moiety (H_{11} , H_{12} , H_{13} and H_{17} for **1** and H_{11} , H_{12} , H_{15} for **3**) that are close by the double bonds,

undergo a considerable shift towards the up- field region. The observed changes clearly indicate the transformation of *trans* to the *cis* form in presence of light.

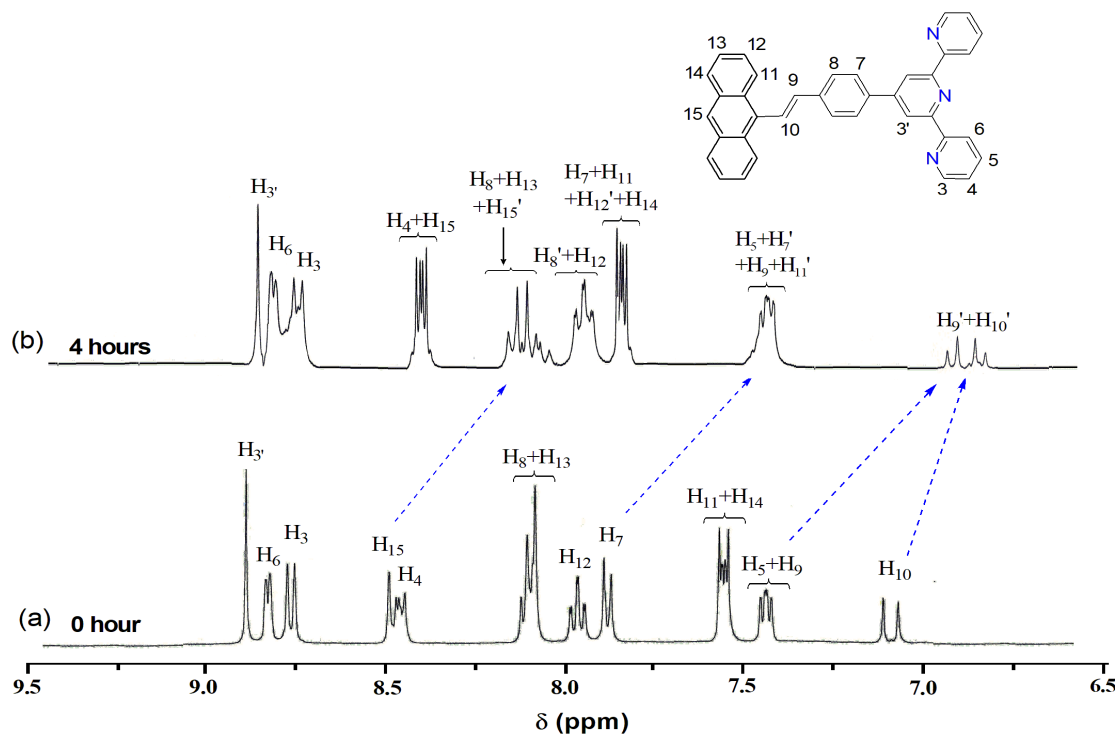


Figure 2.18. ^1H NMR spectrum of **3** before (a) and after (b) photo-irradiation with visible light in CDCl_3 .

DFT and TDDFT calculations are also carried out in the *cis* forms of the compounds and the overlaid absorption spectra of both forms of the compounds are displayed in Figure 2.19. Good correlation between the experimental results and theoretical calculations also suggest that isomerization is taking place from *trans* to the corresponding *cis* form upon irradiation with light for all the compounds. A small blue-shift (7-10 nm) of the lowest energy absorption maximum, whereas a small red-shift of emission maximum (5-15 nm) takes place on going from *trans* to the *cis* form upon photo-irradiation. The experimentally observed trend in spectral shift is mostly reproduced by calculation, although the extent of shift is critically dependent on the use of basis set and functional.

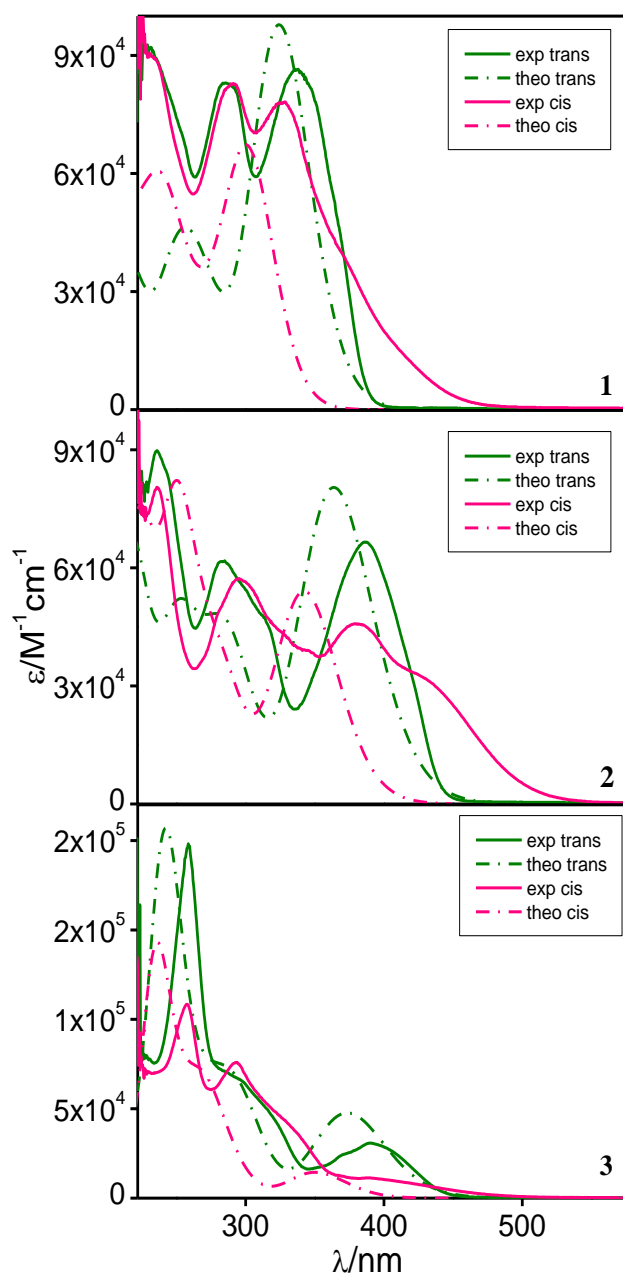


Figure 2.19. Overlay of the calculated (dotted line) and experimental (solid lines) absorption spectra of both *trans* (green) and *cis* (pink) form of **1-3**.

We are interested to find out the kinetic and thermodynamic aspects of the photoisomerization process. To this end, the rate constant (k_{iso}) and quantum yields ($\Phi_{\text{t} \rightarrow \text{c}}$) of isomerization is estimated from the absorption spectral profiles of the compounds (Figure 2.20, Table 2.6). The k_{iso} is found to be dependent on the solvent polarity ($k_{\text{iso}}^{\text{DCM}} > k_{\text{iso}}^{\text{DMSO}}$). k_{iso} of the backward *cis* \rightarrow *trans* process has also been calculated and provided in Table 2.7.

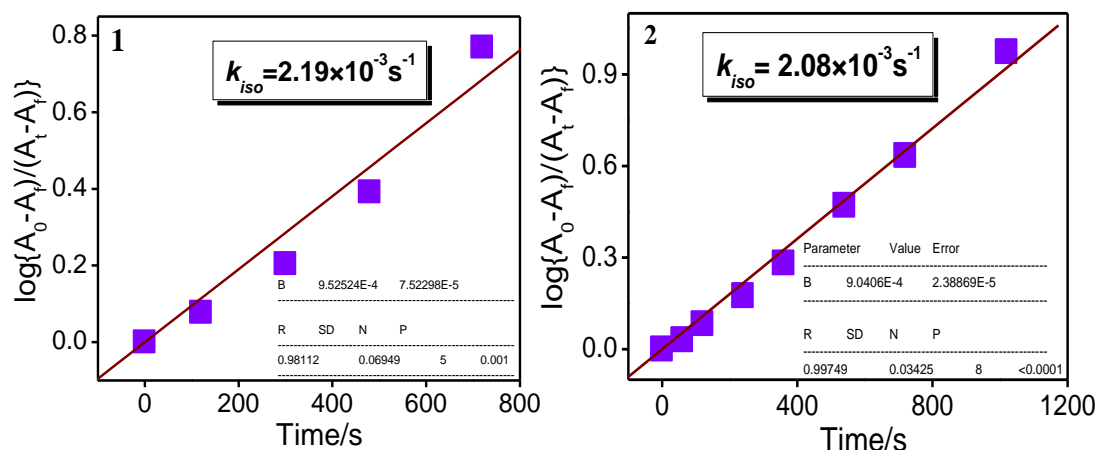


Figure 2.20 Linear plot of $\log (A_0-A_f)/(A_t-A_f)$ vs. time (t) for the absorption spectral change due to *trans*→*cis* process of **1-2** upon irradiation with visible light in DCM. Inset to these plots give the values of rate constant for forward photo-isomerization for the compounds.

Table 2.6 Table for comparison of the values of rate constant (k_{iso}) and photoisomerization quantum yields ($\Phi_{t\rightarrow c}$) for *trans*→*cis* process in both of their free and aggregated forms.

Forms		1		2		3	
	solvents	$k_{iso}\times 10^4$	$\Phi_{t\rightarrow c}$	$k_{iso}\times 10^4$	$\Phi_{t\rightarrow c}$	$k_{iso}\times 10^4$	$\Phi_{t\rightarrow c}$
Free	DCM	31.9	0.12	21.0	0.019	16.5	0.025
	DMSO	2.82	0.11	7.45	0.006	9.54	0.014
Aggregated							
30%	DCM-Hexane	8.48	0.55	5.76	0.005	5.69	0.02
60%	DCM-Hexane	5.04	0.33	3.71	0.003	3.79	0.01
90%	DCM-Hexane	3.44	0.22	2.50	0.002	2.67	0.007

Table 2.7 Table showing the value of rate constant (k_{iso}) for the reverse *cis*→*trans* process.

Compds	DCM	DMSO
	$k_r/s^{-1}\times 10^{-4}$	$k_r/s^{-1}\times 10^{-4}$
1	4.48	2.67
2	4.80	4.50
3	3.22	2.50

2.3.5 Photo-Isomerization in the Aggregated Forms of the Compounds. We are now interested to see the effect of aggregation phenomenon on the photo-isomerization behavior of the compounds. Like their free forms, we used visible light source for irradiation and the progress of the reaction is monitored through absorption and emission spectroscopy. Three different DCM/hexane mixtures are taken, viz. 30%, 60% and 90% f_H .

The absorption and emission spectral profiles of the three fractions of **1** are shown in Figure 2.22. The lowest energy CT band gradually decreases while the higher energy LE bands

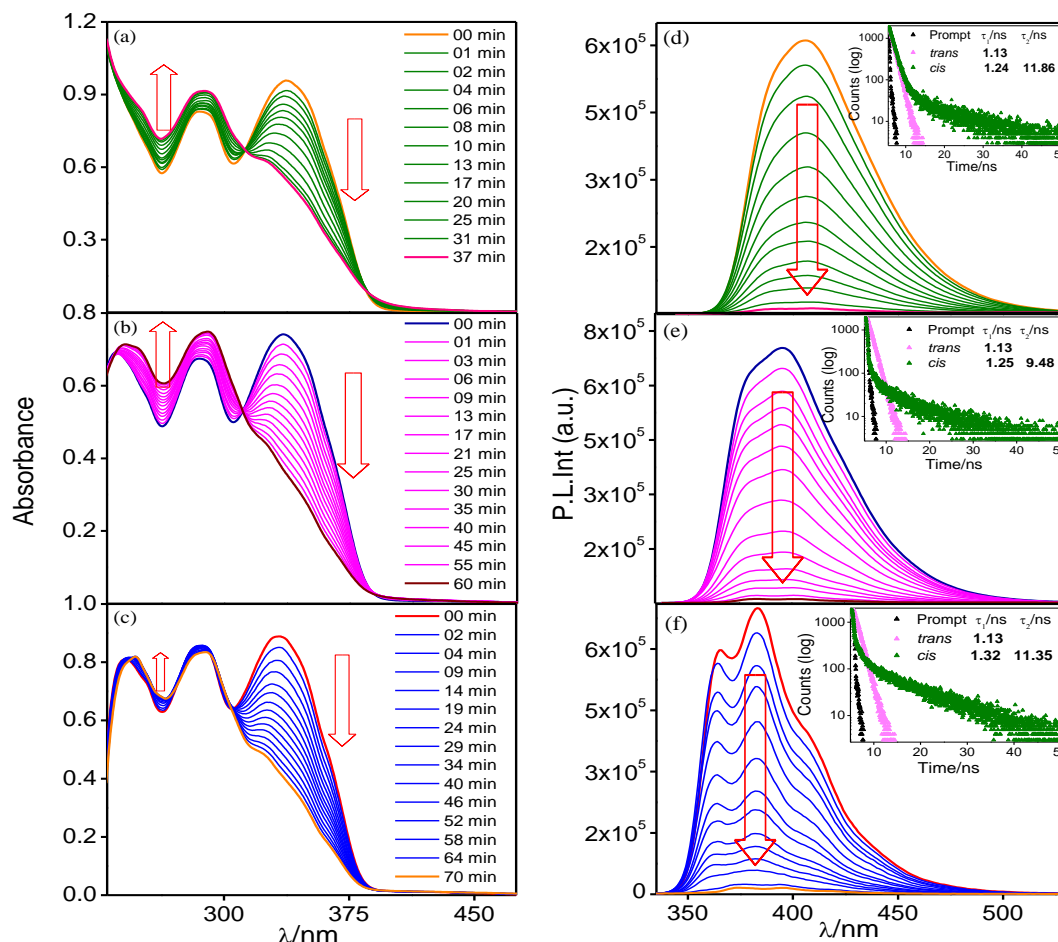


Figure 2.22 Absorption and emission ($\lambda_{\text{ex}}=350$ nm) spectral changes of 30% (a and d, respectively), 60% (b and e, respectively) and 90% (c and f, respectively) hexane fraction in DCM-hexane mixture of **1** upon irradiation with visible light. Inset to the figure d, e, and f shows the corresponding change in emission decay ($\lambda_{\text{ex}}=370$ nm NanoLED) along with lifetime upon photo-irradiation.

increase in intensity, although the extent of decrease is more marked (Figure 2.22a-c). Presence of an isosbestic point clearly indicates the occurrence of two equilibrating species. A complete quenching of emission is seen in all three cases upon photo-irradiation. In case of 30% and 60% f_{H} , the initially broad emission spectrum transforms to the structured form. In case of 90% f_{H} , the initial spectrum is structured and it retains its structured form up to the end of irradiation. We have also measured the lifetime of the aggregated form of the

compounds after photo- irradiation (inset of Figure 2.22d-f). The values obtained after reaching the photo stationary state are found to be more or less same for all the three fractions with considerable increase in lifetime. It is of interest to note that the extent of increase is more marked here compared with neat DCM medium. The spectral profile for the photoisomerization of the three aggregated forms of **2** is shown in Figure 2.23. Unlike in previous case, the decrease in absorbance of both the CT and LE bands are accompanied by a concomitant increase of a new broad band in the visible domain (420-525 nm), the intensity of which varies with extent of hexane fractions (Figure 2.23a-c). Clean isosbestic points corroborate the presence of two species at equilibrium. Substantial quenching of emission takes place in all the three fractions upon photo-irradiation keeping the shape of the spectrum unaltered. The lifetime, on the other hand, shows an increase on going from the *trans* aggregated form to the corresponding *cis* form and the values of lifetime are found to be approximately same in all hexane fractions and the values are comparable to that of the *cis* form in neat DCM medium (inset to Figure 2.23d-f). On viewing the solution under UV light, it is seen that the blue fluorescence of the solution completely vanishes upon isomerization. For **3**, a similar decrease of optical density in the CT and LE band is seen for all the three hexane fractions. Clean isosbestic point once again marks the presence of two species at equilibrium. In the emission side, quenching of emission intensity along with broadening is seen in all cases. Unlike the previous two compounds, no structured spectrum is observed in the present case. For 30 and 60% hexane fractions, we see a red-shift of ~20 nm, while a small blue-shift of ~5 nm is seen for the 90% fraction. Here too the greenish yellow fluorescence under UV illumination turns colourless upon isomerization. The lifetimes of 30% and 60% f_H obtained upon reaching the photo-stationary state is found to be comparable to their free *cis* form, while the lifetime of 90% f_H is nearly double. This behaviour is some way different from **1** and **2** where the lifetime values obtained are very close among the three different fractions.

Thus, the distinct change in the absorption and emission spectra clearly indicates that all the three compounds in their varying extent of aggregated form undergo *trans*→*cis* isomerization upon irradiation with visible light. The presence of isosbestic points clearly indicates the

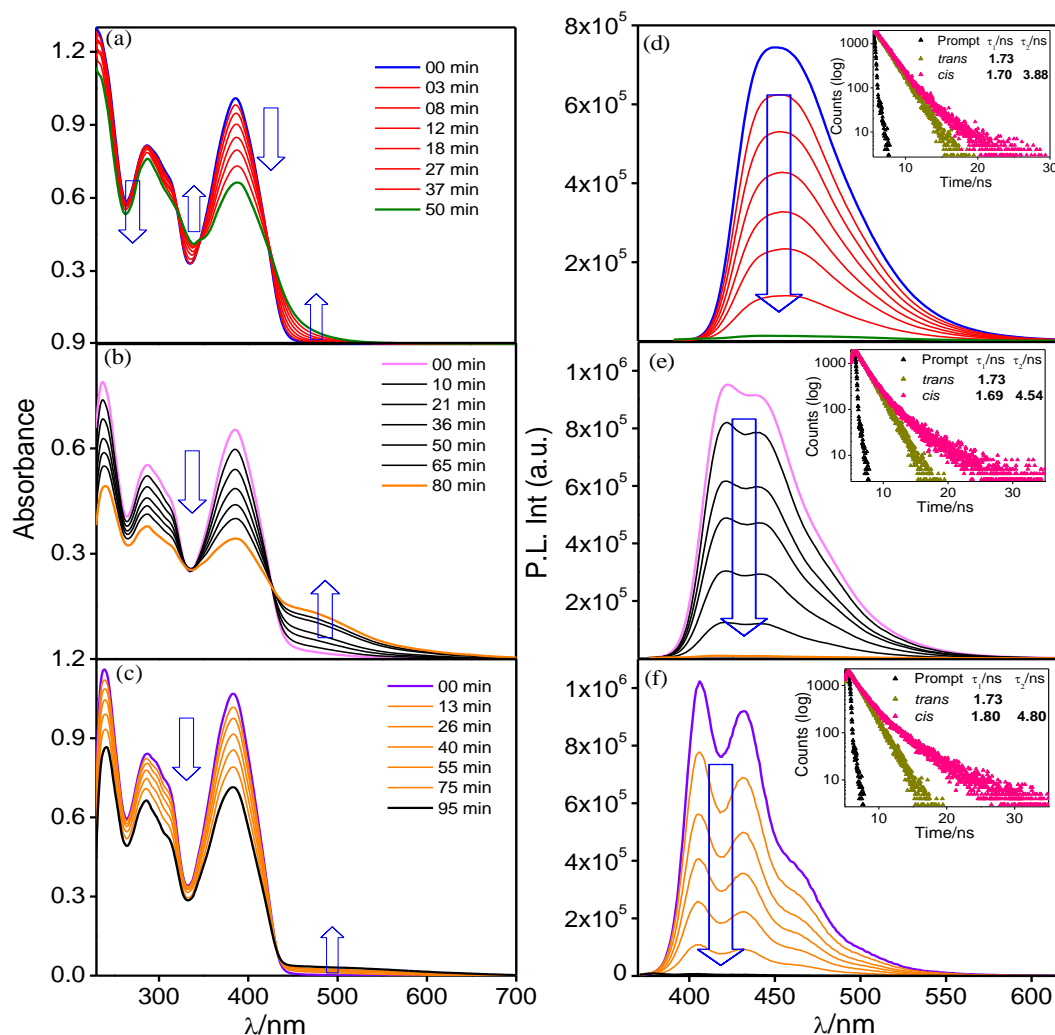


Figure 2.23 Absorption and emission ($\lambda_{\text{ex}}=350$ nm) spectral changes of 30% (a and d, respectively), 60% (b and e, respectively) and 90% (c and f, respectively) hexane fraction in DCM-hexane mixture of **2** upon irradiation with visible light. Inset to the figure d, e, and f shows the corresponding change in emission decay ($\lambda_{\text{ex}}=370$ nm NanoLED) along with lifetime upon photo-irradiation.

presence of *trans* and *cis* form at equilibrium. We have estimated the rate constant as well as the quantum yield of the photoisomerization in the different aggregated forms of the compounds and

the values are summarized in Table 2.6 and Figure 2.24. The results indicate that there is gradual decrease in the rate constant and the quantum yield of photo-isomerization as the extent of aggregation increases. The observed results are quite expected because the increase

of hexane fraction induces the extent of aggregation and therefore gradually becomes difficult for the aggregate to transform from the *trans* to the *cis* form.

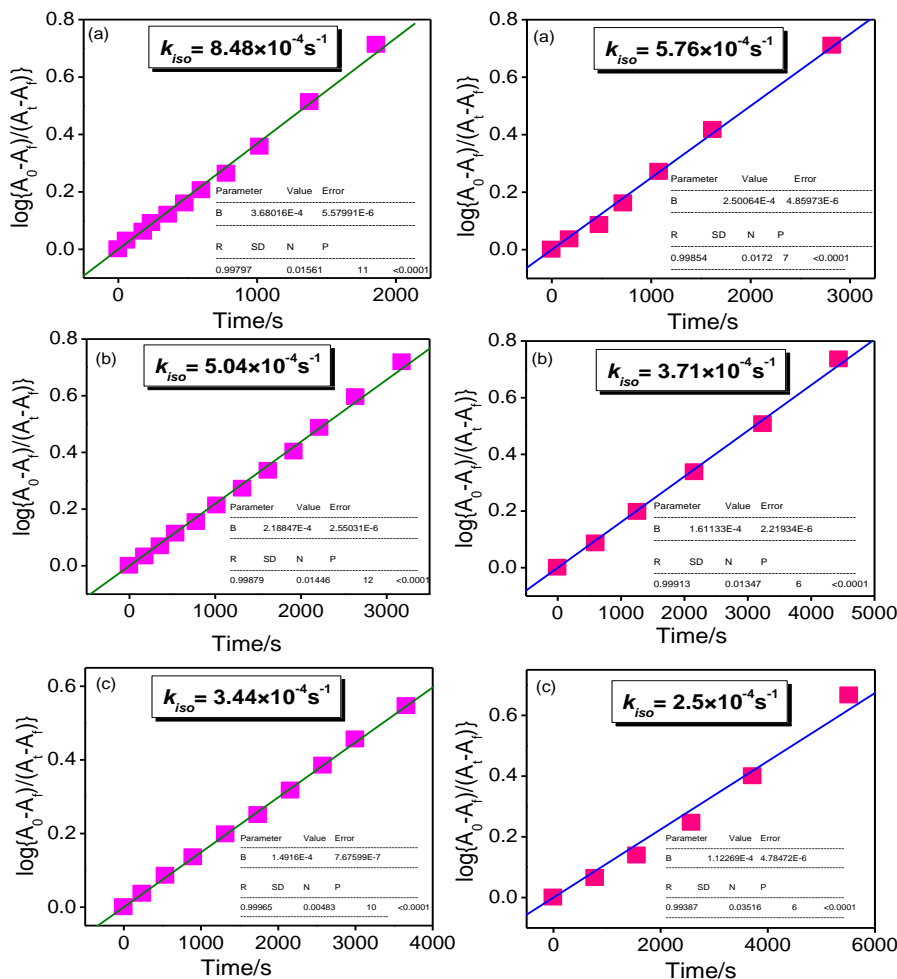


Figure 2.24 Linear plot of $\log(A_0 - A_f)/(A_t - A_f)$ vs. time (t) for the absorption spectral change due to *trans*→*cis* process of **1**(left) and **2**(right) upon irradiation with visible light at different DCM-hexane mixtures [30% (a), 60% (b) and 90% (c)]. These plots give the values of rate constant of forward photo-isomerization of the compound.

On keeping the photo-irradiated aggregated solutions of the compounds in dark, the reverse isomerization (*cis* to *trans*) takes place and requires ~6-8 h, depending upon the extent of aggregation, to revert back to ~80-90% of the initial *trans* form. It is to be noted that the reverse isomerization process is much slower in DCM-hexane mixture than that of neat DCM where the reversal of the *cis* to *trans* form is completed within couple of hours. Thus, we can effectively control the photo-isomerization behaviors of the compounds by inducing aggregation with appropriate solvents. Hence, such kind of systems can be used for preparation of selective molecular switches.

We are interested to model *trans-cis* isomerization computationally and tried to understand how the excited states evolve during the C=C rotation. We calculated the energies of both the *trans* and *cis* forms of the compounds in their ground state (Table 2.8). The calculated energy of the *trans* form is comparatively lower than that of the *cis* form and the energy barrier on going from *trans* to *cis* form lies between 0.12 and 0.25 eV, depending upon the nature of the compounds. This energy barrier could not be overcome thermally while it is easily accessible upon light irradiation (the energy of 405 nm light is 3.06 eV). Thus, it is evident that the *trans*-to-*cis* thermal isomerization does not take place and requires light irradiation, while the *cis*-to-*trans* reversion proceeds in a thermal way. A schematic representation for the *trans-cis* isomerization is presented in Figure 2.25.

Table 2.8 Table showing the calculated energies of both the *trans* (E_T) and *cis* (E_C) forms of the compounds in their ground state along with their energy difference (ΔE).

Compds	E_T/eV	E_C/eV	$\Delta E/\text{eV}$
1	-39065.86	-39065.61	0.25
2	-45321.05	-45320.86	0.19
3	-43246.26	-43246.15	0.12

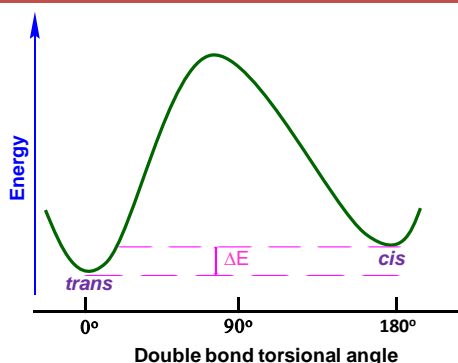


Figure 2.25. A schematic representation indicating the thermodynamic feasibility for the *trans-cis* photo-isomerization of the compounds.

2.4 Conclusions

Exploring new strategy to achieve synthetic as-required photo-switching systems possessing different functionalities remains challenging. Majority of the reported systems own one particular function and their non-emissive behavior in the aggregated state automatically restrict their practical applications. In this report, we designed a new array of stilbene-appended terpyridine systems covalently coupled with anthracene, naphthalene and pyrene moieties and is found to display efficient, manifold and manageable photo-responsive

behaviors under divergent conditions. The compounds display broad and structureless emission spectra at RT in different solvents but in the aggregated state both remarkable emission enhancement together with blue-shifted structured emission band (in DCM-hexane mixture) as well as substantial quenching of emission together with red-shift of emission maximum (DMSO/H₂O mixture) occurs depending upon the nature of the solvent mixture. The former process is known as Aggregation Induced Blue-Shifted Emission (AIBSE) and is quite uncommon and relatively sparse in literature. The extent of emission enhancement has also been altered upon changing the nature of the polyaromatic ring in the compounds. The spectral behavior of the compounds suggests the formation of J-aggregates in DMSO/H₂O, while H-aggregates in DCM/hexane mixture. Thus, one of the most interesting aspects of the present study is that we are able to reverse the mode of emission switching of the compounds via the formation of two different types of aggregates (J- and H) upon judicious choice of solvent mixtures.

Another interesting aspect of the present work is that both the free- as well as the aggregated forms of the compounds undergo *trans/cis* isomerization upon treating with visible light accompanied with significant alteration of their absorption and emission spectral profiles. The backward *cis*→*trans* process is also achieved on keeping the photolyzed solution of the compounds in the dark. Thus, the present compounds can act as ‘on-off’ and ‘off-on’ emission switches in both of their free- and aggregated forms upon successive exposure to light and keeping in the dark. The rate constants as well as the quantum yield of the photoisomerization process of the free- as well as different aggregated forms of the compounds are also calculated and the results indicate that there is gradual decrease of both the parameters as the extent of aggregation is increased. Thus, we can effectively control the photo-isomerization behaviors of the compounds by inducing aggregation with appropriate solvent mixtures. Hence, such kind of systems pave an easy yet efficient way to construct smart molecular switches.

2.5 References

- (1) Zhan, X.; Sun, N.; Wu, Z.; Tu, J.; Yuan, L.; Tang, X.; Xie, Y.; Peng, Q.; Dong, Y.; Li, Q.; Ma, D.; Li, Z. Polyphenylbenzene as a Platform for Deep-Blue Oleds: Aggregation Enhanced Emission and High External Quantum Efficiency Of 3.98%, *Chem. Mater.* **2015**, 27, 1847-1854.
- (2) Hagfeldt, A.; Grätzel, M. Molecular Photovoltaics, *Acc. Chem. Res.* **2000**, 33, 269-277.
- (3) Liang, J.; Li, C.; Zhuang, X.; Ye, Liu, K. Y.; Wang, Y. Novel Blue Bipolar Thermally Activated Delayed Fluorescence Material as Host Emitter for High-Efficiency Hybrid Warm-White Oleds with Stable High Color-Rendering Index. *Adv. Funct. Mater.* **2018**, 28, 1707002-1707010.
- (4) Hua, J.; Nie, H.; Zeng, J.; Zhuang, Z.; Gan, S.; Cai, Y.; Guo, J.; Su, S. J.; Zhao, Z.; Tang, B. Z. Highly Efficient Nondoped Oleds with Negligible Efficiency Roll Off Fabricated From Aggregation-Induced Delayed Fluorescence Luminogens. *Angew Chem. Intd. Ed.* **2017**, 56, 12971-12976.
- (5) Shyamal, M.; Mazumdar, P.; Maity, S.; Sahoo, G. P.; Moran, G. S.; Misra, A. Pyrene Scaffold as Real-Time Fluorescent Turn-On Chemosensor For Selective Detection of Trace-Level Al(III) and its Aggregation-Induced Emission Enhancement, *J. Phys. Chem. A* **2016**, 120, 210-220.
- (6) Dey, S.; Maity, A.; Shyamal, M.; Das, D.; Maity, S.; Giri, P. K.; Mudi, N.; Samanta, S. S.; Hazra, P.; Misra, A. Antipyrine Based Fluorescence “Turn-On” Dual Sensor for Zn^{2+} and Al^{3+} and its’ Selective “Turn-Off” Fluorescence Sensing Towards 2,4,6-Trinitrophenol (TNP) in Aggregated State. *Photochem. Photobiol. Sci.* **2019**, 18, 2717-2729.
- (7) Ma, C.; Xu, B.; Xie, G.; He, J.; Zhou, X.; Peng, B.; Jiang, L.; Xu, B.; Tian, W.; Chi, Z.; An AIE-Active Luminophore with Lunable and Remarkable Fluorescence Switching Based on the Piezo and Protonation-Deprotonation Control. *Chem. Commun.* **2014**, 50, 7374-7377.
- (8) Tian, H.; Yang, S.; Recent Progresses on Diarylethene Based Photochromic Switches, *Chem. Soc. Rev.* **2004**, 33, 85-97.
- (9) Han, P.; Lin, C.; Ma, D.; Qin, A.; Tang, B. Z. Violet-blue Emitters Featuring Aggregation-Enhanced Emission Characteristics for Nondoped OLEDs with CIEy Smaller Than 0.046. *ACS Appl. Mater. Interfaces.* **2020**, 12, 46366-46372.

- (10) Andreasson, J.; Pischel, U. Molecules with a Sense of Logic: A Progress Report. *Chem. Soc. Rev.* **2015**, *44*, 1053-1069.
- (11) Daly, B.; Ling, J.; de Silva, A. P. Current Developments In Fluorescent PET (Photoinduced Electron Transfer) Sensors and Switches. *Chem. Soc. Rev.* **2015**, *44*, 4203-4211.
- (12) Karmakar, S.; Mardanya, S.; Pal, P.; Baitalik, S. Design of Multichannel Osmium-Based Metalloreceptor for Anions and Cations by Taking Profit From Metal-Ligand Interaction and Construction of Molecular Keypad Lock and Memory Device, *Inorg. Chem.* **2015**, *54*, 11813-11825.
- (13) Mondal, D.; Pal, P.; Baitalik, S. Anthraquinone-biimidazole Based Ruthenium(II) Complexes as Selective Multichannel Anion Sensors and Multi-Readout Molecular Logic Gates and Memory Devices: Combined Experimental and DFT/TD-DFT Study, *Sens. Actuators B:Chem.* **2017**, *242*, 746-75.
- (14) Deb, S.; Sahoo, A.; Ahmed, T.; Baitalik, S. Stimuli-Responsive Molecular Switches and Logic Devices Based on Ru(II)-Terpyridyl-Imidazole Coordination Motif, *J. Phys. Chem. B*, **2021**, *125*, 8919-8931.
- (15) Karmakar, S.; Mardanya, S.; Maity, D.; Baitalik, S. Polypyridyl-Imidazole Based Os(II) Complex as Optical Chemosensor for Anions and Cations and Multi-Readout Molecular Logic Gates and Memory Devices: Experimental and DFT/TDDFT Study, *Sens. Actuators B:Chem.* **2016**, *226*, 388-402.
- (16) Tian, H.; Zhang, J. Photochromic Materials: Preparation, Properties and Applications, (Eds.). Wiley-VCH, Weinheim, Germany, **2016**.
- (17) Wu, N. M. W.; Ng, M.; Lam, W. H.; Wong, H.-L.; Yam, V. W. W. Photochromic Heterocycle-Fused Thieno[3,2-B]Phosphole Oxides as Visible Light Switches Without Sacrificing Photoswitching Efficiency, *J. Am. Chem. Soc.* **2017**, *139*, 15142-15150.
- (18) Nishihara, H.; Kodansha, Y. F.; Inorganic Photochromism. (Ed.), Springer (**2007**) 239-257.
- (19) Mazumdar, P.; Maity, S.; Shyamal, M.; Das, D.; Sahoo, G. P.; Misra, A. Proton Triggered Emission and Selective Sensing of Picric Acid by the Fluorescent Aggregates of 6,7-Dimethyl-2,3-Bis-(2-Pyridyl)-Quinoxaline, *Phys. Chem. Chem. Phys.* **2016**, *18*, 7055-7067.
- (20) Shyamal, M.; Mazumdar, P.; Maity, S.; Samanta, S.; Sahoo, G. P.; Misra, A. Highly Selective Turn-On Fluorogenic Chemosensor for Robust Quantification of Zn(II) Based

- on Aggregation Induced Emission Enhancement Feature, *ACS Sensors*. **2016**, *1*, 739-747.
- (21) Irie, M; Diarylethenes for Memories and Switches, *Chem. Rev.* **2000**, *100*, 1685-1716.
- (22) Feringa, B. L.; van Delden, R. A.; Koumura, N. Chiroptical Molecular Switches, *Chem. Rev.* **2000**, *100*, 1789-1816.
- (23) Ikeda, T.; Tsutsumi, O. Optical Switching and Image Storage by Means of Azobenzene Liquid-Crystal Films, *Science* **1995**, *268*, 1873-1875.
- (24) Ichimura, K.; Oh, S. K.; Nakagawa, M. Light-driven Motion of Liquids on a Photoresponsive Surface. *Science* **2000**, *288*, 1624-1626.
- (25) Yutaka, T.; Mori, I.; Kurihara, M.; Mizutani, J.; Tamai, N.; Kawai, T.; Irie, M.; Nishihara, H. Photoluminescence Switching of Azobenzene-Conjugated Pt(II) Terpyridine Complexes by Trans-Cis Photoisomerization. *Inorg. Chem.* **2002**, *41*, 7143-7150.
- (26) Kobatake, S.; Takami, S.; Muto, H.; Ishikawa, T.; Irie, M. Rapid and Reversible Shape Changes of Molecular Crystals on Photoirradiation, *Nature* **2007**, *446*, 778-781.
- (27) Matsuda, K.; Irie, M. Diarylethene as a Photoswitching Unit. *J. Photochem. Photobiol. C* **2004**, *5*, 169-182.
- (28) Kayanuma, M.; Daniel, C.; Koppel, H.; Gindensperger, E. Photophysics of Isomerizable Re(I) Complexes: A theoretical Analysis. *Coord. Chem. Rev.* **2011**, *255*, 2693-2703.
- (29) Polo, A. S.; Itokazu, M. K.; Frin, K. M.; Patrocínio, A. O. T.; Iha, N. Y. M. Light Driven *Trans*-To-*Cis* Isomerization of Stilbene-Like Ligands in *Fac*-[Re(CO)₃(NN)(*Trans*-L)]⁺ and Luminescence of their Photoproducts. *Coord. Chem. Rev.* **2006**, *250*, 1669-1680.
- (30) Bossert, J.; Daniel, C. Trans-cis Photoisomerization of the Styrylpyridine Ligand in [Re(CO)₃(2,2'-Bipyridine)(T-4-Styrylpyridine)]⁺: Role of the Metal-To-Ligand Charge-Transfer Excited States. *Chem. Eur. J.* **2006**, *12*, 4835- 4843.
- (31) Zanoni, K. P. S.; Iha, N. Y. M. Reversible *Trans* ⇌ *Cis* Photoisomerizations of [Re(CO)₃(Ph₂phen)(Stpycn)]⁺ Towards Molecular Machines. *Dalton Trans.* **2017**, *46*, 9951-9958.
- (32) Matos, L. S.; Amaral, R. C.; Iha, N. Y. M. Visible Photosensitization Of *Trans*-Styrylpyridine Coordinated To *Fac*-[Re(CO)₃(Dcbh₂)]⁺: New Insights. *Inorg. Chem.* **2018**, *57*, 9316-9326.

- (33) Gindensperger, E.; Ko'ppel, H.; Daniel, C. Mechanism of Visible-Light Photoisomerization of a Rhenium(I) Carbonyl-Diimine Complex. *Chem. Commun.* **2010**, 46, 8225-8227.
- (34) Kayanuma, M.; Gindensperger, E.; Daniel, C. Inorganic Photoisomerization: The Case Study of Rhenium(I) Complexes. *Dalton Trans.* **2012**, 41, 13191-13203.
- (35) Costa, P. J.; Calhorda, M. J.; Bossert, J.; Daniel, C.; Romão, C. C. Photochemistry of Methyltrioxorhenium Revisited: A DFT/TD-DFT And CASSCF/MS-CASPT2 Theoretical Study, *Organometallics* **2006**, 25, 5235-5241.
- (36) Tseng, N. W.; Liu, J.; Ng, J. C. Y.; Lam, J. W. Y.; Sung, H. H. Y.; Williams, I. D.; Tang, B. Z. Deciphering Mechanism Of Aggregation-Induced Emission (AIE): Is E-Z Isomerisation Involved in an AIE Process? *Chem. Sci.* **2012**, 3, 493-497.
- (37) Kayanuma, M.; Daniel, C.; Gindensperger, E. Spectroscopic Trends in a Series of Re(I) A-Diimine Complexes as a Function of the Antenna/Photoisomerizable Ligands: A TD-DFT and MS-CASPT2 Study. *Can. J. Chem.* **2014**, 92, 979-986.
- (38) Santos, J. J.; Toma, S. H.; Lalli, P. M.; Riccio, M. F.; Eberlin, M. N.; Toma, H. E.; Araki, K. Exploring the Coordination Chemistry of Isomerizable Terpyridine Derivatives for Successful Analyses of Cis and Trans Isomers by Travelling Wave Ion Mobility Mass Spectrometry. *Analyst* **2012**, 137, 4045-4051.
- (39) Amaral, R. C.; Matos, L. S.; Zanoni, K. P. S.; Iha, N. Y. M. Photoreversible Molecular Motion of stpyCN Coordinated to Fac-[Re(Co)₃(Nn)]⁺ Complexes. *J. Phys. Chem. A.* **2018**, 122, 6071-6080.
- (40) Mandal, A.; Maity, A.; Bag, S.; Bhattacharya, P.; Das, A. K.; Basak, A. Design and Synthesis of Dual Probes for Detection of Metal Ions by LALDI MS and Fluorescence: Application in Zn(II) Imaging in Cells, *RSC Adv.* **2017**, 7, 7163-7169.
- (41) Sil, A.; Giri, D.; Patra, S. K. Arylene-vinylene Terpyridine Conjugates: Highly Sensitive, Reusable and Simple Fluorescent Probes for the Detection of Nitroaromatics. *J. Mater. Chem. C* **2017**, 5, 11100-11110.
- (42) Thompson, A. M. W. C. The Synthesis of 2,2':6',2''-Terpyridine Ligands-Versatile Building Blocks for Supramolecular Chemistry. *Cord. Chem. Rev.* **1997**, 160, 1-52.
- (43) Williams, J. A. G. The Coordination Chemistry of Dipyritylbenzene: N-Deficient Terpyridine or Panacea for Brightly Luminescent Metal Complexes. *Chem. Soc. Rev.* **2009**, 38, 1783-1801.

- (44) Hofmeier, E.; Schubert, H. U. S. Recent Developments in the Supramolecular Chemistry of Terpyridine-Metal Complexes. *Chem. Soc. Rev.* **2004**, *33*, 373-399.
- (45) Mukherjee, S.; Pal, P.; Maity, D.; Baitalik, S. Photophysics and Luminescence Switching Properties of a Series of Photochromic Styrylbenzene-Terpyridine Conjugate: Experimental and DFT/TD-DFT Investigation. *J. Photochem. Photobiol. A* **2019**, *378*, 94-104.
- (46) Pal, P.; Mukherjee, S.; Maity, D.; Baitalik, S. Synthesis, Structural Characterization, and Luminescence Switching of Diarylethene-Conjugated Ru(II)-Terpyridine Complexes by Trans–Cis Photoisomerization: Experimental and DFT/TD-DFT Investigation. *Inorg. Chem.* **2018**, *57*, 5743-5753.
- (47) Mukherjee, S.; Pal, P.; Sahoo, A.; Baitalik, S. Photo-switchable Iron-Terpyridine Complexes Functionalized with Styrylbenzene Unit. *J. Photochem. Photobiol. A*, **2021**, *407*, 113059.
- (48) Pal, P.; Ganguly, T.; Sahoo, A.; Baitalik, S. Emission Switching in the Near-Infrared by Reversible Trans-Cis Photoisomerization of Styrylbenzene-Conjugated Osmium Terpyridine Complexes. *Inorg. Chem.* **2021**, *60*, 4869-4882.
- (49) Pal, P.; Ganguly, T.; Maity, D.; Baitalik, S. Experimental And Theoretical Exploration of Photophysics and Trans-Cis Photoisomerization of Styrylbenzene Conjugated Terpyridine Complexes Of Ru(II): Strong Effect of Deprotonation from Second Coordination Sphere. *J. Photochem. Photobiol. A* **2020**, *392*, 112409.
- (50) Birks, J. B. Photophysics of Aromatic Molecules, Wiley, London, **1970**.
- (51) Turro, N. J. Modern Molecular Photochemistry. University Science Books, Mill Valley, **1991**.
- (52) Martinez, C. R.; Iverson, B. L. Rethinking the Term “pi-stacking”, *Chem. Sci.* **2012**, *3*, 2191-2201.
- (53) Thomas, S. W.; Joly, G. D.; Swager, T. M. Chemical Sensors Based on Amplifying Fluorescent Conjugated Polymers. *Chem. Rev.* **2007**, *107*, 1339-1386.
- (54) Leung, N. L. C.; Xie, N.; Yuan, W.; Liu, Y.; Wu, Q.; Peng, Q.; Miao, Q.; Lam, J. W. Y.; Tang, B. Z. Restriction of Intramolecular Motions: The General Mechanism Behind Aggregation-Induced Emission. *Chem. Eur. J.* **2014**, *20*, 15349-15353.
- (55) Ren, Y.; Lam, J. W. Y.; Dong, Y.; Tang, B. Z.; Wong, K. S. Enhanced Emission Efficiency and Excited State Lifetime Due to Restricted Intramolecular Motion in Silole Aggregates. *J. Phys. Chem. B* **2005**, *109*, 1135-1140.

- (56) Luo, J.; Xie, Z.; Lam, J. W. Y.; Cheng, L.; Tang, B. Z.; Chen, H.; Qiu, C.; Kwok, H. S.; Zhan, X.; Liu, Y. Aggregation-Induced Emission of 1-Methyl-1,2,3,4,5-Pentaphenylsilole. *Chem. Commun.* **2001**, 1740-1741.
- (57) Mei, J.; Leung, L. C. N.; Kwok, T. K. R.; Lam, W. Y. J.; Tang, B. Z. Aggregation-Induced Emission: Together We Shine, United We Soar! *Chem. Rev.* **2015**, *115*, 11718-11940.
- (58) Zhao, Z.; Lam, J. W. Y.; Tang, B. Z. Tetraphenylethene: A Versatile AIE Building Block For The Construction of Efficient Luminescent Materials for Organic Light-Emitting Diodes. *J. Mater. Chem.* **2012**, *22*, 23726-23740.
- (59) Wei, P.; Zhang, J. X.; Zhao, Z.; Chen, Y.; He, X.; Chen, M.; Gong, J.; Sung, H. Y. H.; Williams, I. D.; Lam, W. Y. J.; Tang, B. Z. Multiple Yet Controllable Photoswitching in a Single AIEgen System. *J. Am. Chem. Soc.* **2018**, *140*, 1966-1975.
- (60) Islam, M. M.; Hu, Z.; Wang, Q.; Feng, C. R. X. Pyrene-Based Aggregation-Induced Emission Luminogens And Their Applications. *Mater. Chem. Front.* **2019**, *3*, 762-781.
- (61) Kaur, M.; Kaur, H.; Kumar, M.; Bhalla, V. Light-up AIE-active Materials: Self Assembly, Molecular Recognition and Catalytic Applications. *Chem. Rev.* **2021**, *21*, 240-256.
- (62) An, B.-K.; Kwon, S.-K.; Jung, S.-D.; Park, S. Y. Enhanced Emission And Its Switching In Fluorescent Organic Nanoparticles. *J. Am. Chem. Soc.* **2002**, *124*, 14410-14415.
- (63) Du, X.; Wang, Z. Y. Donor-Acceptor Type Silole Compounds with Aggregation-Induced Deep-Red Emission Enhancement: Synthesis and Application for Significant Intensification Of Near-Infrared Photoluminescence. *Chem. Commun.* **2011**, *47*, 4276-4278.
- (64) Gao, B. R.; Wang, H. Y.; Hao, Y. W.; Fu, L. M.; Fang, H. H.; Jiang, Y.; Wang, L.; Chen, Q. D.; Xia, H.; Pan, L. Y.; Ma, Y. G. Time-Resolved Fluorescence Study of Aggregation-Induced Emission Enhancement by Restriction of Intramolecular Charge Transfer State. *J. Phys. Chem. B* **2009**, *114*, 128-134.
- (65) Mazumdar, P.; Das, D.; Sahoo, G. P.; Moran, G. S.; Misra, A. Aggregation Induced Emission Enhancement From Bathophenanthroline Microstructures and its Potential Use as Sensor of Mercury Ions in Water. *Phys. Chem. Chem. Phys.* **2014**, *16*, 6283-6293.
- (66) Mazumdar, P.; Das, D.; Sahoo, G. P.; Mora'n, G. S.; Misra, A. Aggregation Induced Emission Enhancement of 4,40-Bis(Diethylamino)Benzophenone with an

- Exceptionally Large Blue Shift and its Potential use as Glucose Sensor. *Phys. Chem. Chem. Phys.* **2015**, *17*, 3343-3354.
- (67) Zhu, L.; Yang, C.; Qin, J. An Aggregation-Induced Blue Shift Of Emission and the Self-Assembly of Nanoparticles From a Novel Amphiphilic Oligofluorene. *Chem. Commun.* **2008**, 6303-6305.
- (68) Wu, Q.; Zhang, T.; Peng, Q.; Wang, D.; Shuai, Z. Aggregation Induced Blue-Shifted Emission -The Molecular Picture From a QM/MM Study. *Phys. Chem. Chem. Phys.* **2014**, *16*, 5545-5552.
- (69) Banerjee, S.; Both, A. K.; Sarkar, M. Probing The Aggregation And Signaling Behavior Of Some Twisted 9,9'-Bianthryl Derivatives: Observation of Aggregation-Induced Blue-Shifted Emission. *ACS Omega* **2018**, *3*, 15709-15724.
- (70) (a) Gille, K.; Knoll, H.; Quitzsch, K.; Rate Constants of the Thermal Cis-Trans Isomerization of Azobenzene Dyes in Solvents, Acetone/Water Mixtures, and in Microheterogeneous Surfactant Solutions, *Int. J. Chem. Kinet.* **1999**, *31*, 337-350. (b) Yutaka, T.; Mori, I.; Kurihara, M.; Mizutani, J.; Kubo, K.; Furusho, S.; Matsumura, K.; Tamai, N.; Nishihara, H. Synthesis, Characterization, and Photochemical Properties of Azobenzene-Conjugated Ru(II) and Rh(III) Bis(Terpyridine) Complexes. *Inorg. Chem.* **2001**, *40*, 4986-4995.
- (71) Otsuki, J.; Suwa, K.; Narutaki, K.; Sinha, C.; Yoshikawa, I.; Araki, K. Photochromism of 2-(phenylazo)imidazoles. *J. Phys. Chem A* **2005**, *109*, 8064-8069.
- (72) Gauglitz, G.; Hubig, S.; Chemical Actinometry in the UV by Azobenzene in Concentrated-Solution - A Convenient Method. *J. Photochem.* **1985**, *30*, 121-125.
- (73) Ladanyi, V.; Dvorak, P.; Anshori, J. A.; Vetrakova, L.; Wirz, J.; Heger, D. Azobenzene Photoisomerization Quantum Yields in Methanol Redetermined. *Photochem. Photobiol. Sci.* **2017**, *16*, 1757-1761.
- (74) Frisch, M. J.; Trucks, G. W.; Schlegel, H. B.; Scuseria, G. E.; Robb, M. A.; Cheeseman, J. R.; Scalmani, G.; Barone, V.; Mennucci, B.; Petersson, G. A., *et al.* Gaussian 09, revision A.02; Gaussian Inc.: Wallingford, CT, **2009**.
- (75) Becke, A. D. Density Functional Thermochemistry. III. The role of exact exchange. *J. Chem. Phys.* **1993**, *98*, 5648-5652.
- (76) Lee, C. T.; Yang, W. T.; Parr, R. G. Development of the Colle-Salvetti Correlation-Energy Formula into a Functional of the Electron Density. *Phys. Rev. B*, **1988**, *37*, 785-789.

- (77) Casida, M. E.; Jamorski, C.; Casida, K. C.; Salahub, D. R. Molecular Excitation Energy to High- Lying Bound State From Time-Dependent Density Functional Response Theory: Charecterization and Correction of the Time Dependent Local Density Approximation Ionization Threshold. *J. Chem. Phys.* **1998**, *108*, 4439-4449.
- (78) Stratmann, R. E.; Scuseria, G. E.; Frisch, M. J. An Efficient Implementation Of Time-Dependent Density-Functional Theory for The Calculation of Excitation Energies of Large Molecules. *J. Chem. Phys.* **1998**, *109*, 8218-8224.
- (79) Walters, V. A.; Hadad, Y. C. M.; Thiel, S. D.; Colson, K. B.; WibergJohnson, P. M.; Foresman, J. B. Assignment of the A State in Bicyclobutane. The Multiphoton Ionization Spectrum and Calculations of Transition Energies. *J. Am. Chem. Soc.*, **1991**, *113*, 4782-4791.
- (80) (a) Tomasi, J.; Mennucci, B.; Cammi, R.; Quantum Mechanical Continuum Solvation Models. *Chem. Rev.* **2005**, *105*, 2999-3094. (b) Cossi, M.; Scalmani, G.; Rega, N.; Barone, V. New Developments in the Polarizable Continuum Model for Quantum Mechanical and Classical Calculations on Molecules in Solution. *J. Chem. Phys.* **2002**, *117*, 43-54.
- (81) Caricato, M.; Mennucci, B.; Tomasi, J.; Ingrosso, F.; Cammi, R.; Corni, S.; Scalmani, G. Formation and Relaxation of Excited States in Solution: A New Time Dependent Polarizable Continuum Model Based on Time Dependent Density Functional Theory. *J. Chem. Phys.* **2006**, *124*, 124520-124530.
- (82) Mennucci, B.; Cappelli, C.; Guido, C. A.; Cammi, R.; Tomasi, J. Structures and Properties of Electronically Excited Chromophores in Solution From the Polarizable Continuum Model Coupled to the Time-Dependent Density Functional Theory. *J. Phys. Chem. A* **2009**, *113*, 3009.
- (83) Dennington, R.; Keith, T.; Millam, J. *Gauss View 3*; Semichem, Inc.: Shawnee Mission, KS, 2007.
- (84) Boyle, N. M. O.; Tenderholt, A. L.; Langner, K. M. A Library for Package-independent Computational Chemistry Algorithms. *J. Comput. Chem.*, **2008**, *29*, 839.
- (85) Cai, K.; Xie, J.; Zhang, D.; Shi, W.; Yan, Q.; Zhao, D. Concurrent Cooperative J-Aggregates and Anticooperative H-Aggregates. *J. Am. Chem. Soc.* **2018**, *140*, 5764-5773.

- (86) Xie, N.-H.; Li, C.; Liu, J.-X.; Gong, W.-L.g.; Tang, B. Z.; Li, G.; Zhu, M.-Q. The Synthesis and Aggregation-Induced Near-Infrared Emission of Terrylenediimide-Tetraphenylethene Dyads. *Chem. Commun.* **2016**, 52, 5808-5811.
- (87) Wang, E.; Lam, J. W. Y.; Hu, R.; Zhang, C.; Zhaoc, Y. S.; Tang, B. Z. Twisted Intramolecular Charge Transfer, Aggregation-Induced Emission, Supramolecular Self-Assembly and the Optical Waveguide of Barbituric Acid-Functionalized Tetraphenylethene. *J. Mater. Chem. C* **2014**, 2, 1801-1807.
- (88) Bhattacharyya, S.; Chowdhury, A.; Saha, R.; Mukherjee, P. S. Multifunctional Self-Assembled Macrocycles with Enhanced Emission and Reversible Photochromic Behavior. *Inorg. Chem.* **2019**, 58, 3968-3981.
- (89) Sun, X.; Liao, M.-Y.; Yu, X.; Wu, Y.-S.; Zhong, C.; Chueh, C.-C.; Li, Z.; Li, Z. An Asymmetric 2,3-Fluoranthene Imide Building Block for Regioregular Semiconductors with Aggregation-Induced Emission Properties. *Chem. Sci.* **2022**, 13, 996-1002.



Chapter 3

**Synthesis, Characterization and Emission
Switching Behaviors of Styrylphenyl-
Conjugated Ru(II)-Terpyridine Complexes via
Aggregation and Trans-Cis Photoisomerization**

3.1 Introduction

Photo-switches are important components because of their diverse and potential applications in the fabrication of optical materials, memory devices and photomolecular machines¹⁻⁷ In the last few decades a plethora of research has been carried out at both laboratories and industrial level to construct such devices using organic, inorganic and hybrid counterparts.¹⁻⁹ Construction of a multi-addressable molecular switch often comprises of co-joining of one or more stimuli-responsive organic moiety with appropriate metal ion at the core and the resulting assembly could perform enhanced stimuli-responsive activity within broader spectral domain.¹⁰⁻¹³ Light, heat, voltage, and ionic species are frequently used to build up the stimuli-responsive molecular switches.¹⁴⁻¹⁸ Since light is the most convenient and environment benign external stimulus, numerous photo-responsive molecular building blocks are designed to harness the energy for constructing optical memory storage, smart surfaces, actuators to name but a few.¹⁷⁻²³ Most of these photo-responsive molecules are built on the skeletal framework of organic moieties such as azobenzene, stilbene, diarylethylene, spiropyrans etc. whose photoisomerization behaviors have been profusely studied.²⁴⁻³¹ Azobenzenes and stilbenes are typical class of compounds that undergo reversible *trans-cis* isomerization, which have potential applications in the field of optoelectronics.³²⁻³⁹ The photo-isomerization reports of their metal complexes are comparatively less explored,^{24-25,29-31,40-43} especially those of ruthenium metal complexes are rarely surveyed.⁴⁴⁻⁴⁶ On the other hand, coordination complexes based on ruthenium-terpyridine backbone provide unique photo-redox properties without compromising the isomeric purity as usually observed in their bipyridine analogues.^{10-13, 47-49} But, they are weakly emissive and short lived in nature due to the comparable energies of the radiative metal-to-ligand charge transfer (MLCT) states and non-radiative metal centre (MC) states arising out of the distorted octahedral geometries.⁵⁰ Improvement of their emission properties can be done by ligand modification.⁵¹⁻⁵⁷ Incorporation of stilbene unit(s) in the molecular skeleton of ruthenium-terpyridine complexes could help to improve the emission properties as well as to exhibit light responsive behaviors.

Most molecules which are typically non-emissive in their dilute solutions can be made emissive upon aggregation in different solvent mixtures.⁵⁸⁻⁶⁸ This process is called aggregation induced emission (AIE) and was first coined by Prof. Tang⁶⁹ and it occurs due to the restriction of intermolecular rotations (RIR).⁷⁰⁻⁷¹ Another phenomenon which was documented by Park et al explicated the aggregation induced emission enhancement (AIEE)

in which emissive compounds exhibit further emission enhancement upon aggregation.⁷² Ruthenium polypyridyl complexes usually have low emission quantum yields which can be improvised by AIE phenomenon using different solvents in varying ratios.⁷³⁻⁷⁸ It is expected that molecular systems comprising of polyarenes and polyheterocyclic moieties would show the AIE phenomenon.⁷⁹⁻⁸² Meanwhile, presence of a stilbene unit allows tunability through visible or UV light treatment.³⁰⁻³⁵ Multichannel emission switching can thus be obtained by light irradiation as well as upon inducing aggregation through the use of different solvent mixtures.

In our previously reported work, we have studied the photophysical tuning of polyarene-substituted and styrylphenyl conjugated terpyridine ligands by using light and via AIE.⁸² In this work, we have extended our studies by incorporating ruthenium (II) metal into our organic system (Chart 3.1). Previously, we also reported a series of styrylphenyl

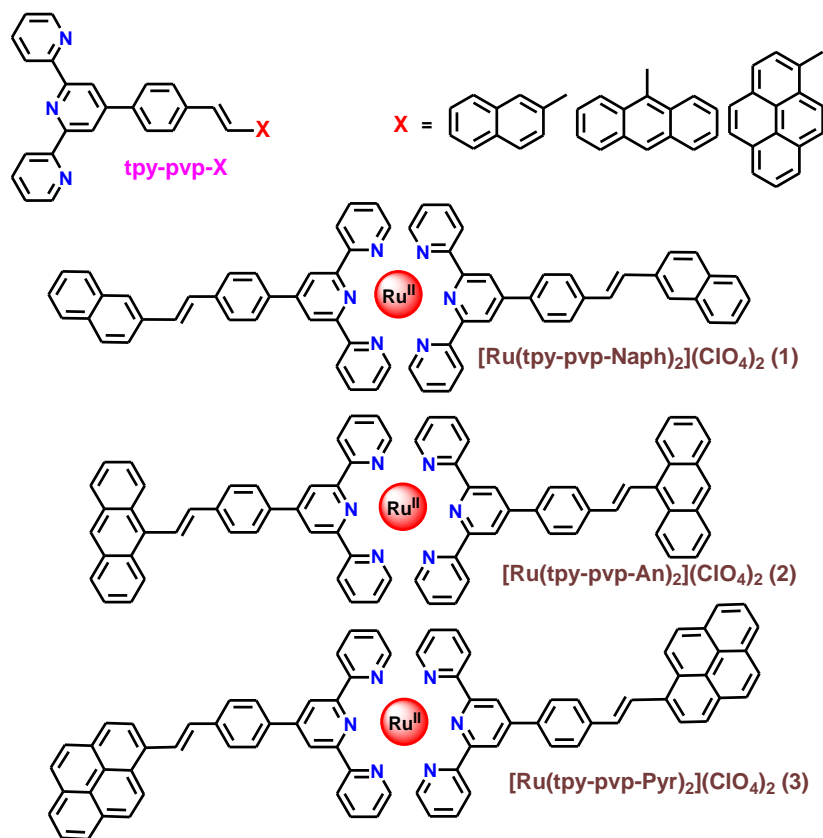


Chart 3.1 Chemdraw structures of the ligands and their Ru(II) complexes.

conjugated bis-terpyridine ruthenium(II) complexes having both electron-releasing and electron attracting substituents.⁴⁶ Herein, we designed three homoleptic ruthenium(II)-terpyridine complexes consisting of conjugated stilbene and polyarene unit at the 4' position of the terpyridine moieties. Incorporation of such stilbene unit in the molecular skeleton

would help to improve emission properties as well as to exhibit light induced *trans-cis* isomerization behaviors. Additionally, the presence of a polyarene unit would bring about the aggregation in the complexes. Among the polyarenes, we incorporated anthracene, naphthalene and pyrene moiety to fine tune the emission characteristics as well as the extent of aggregation and photo-isomerization in the resulting complexes. Hence, our target is to design strongly luminescent Ru(II)-terpyridine complexes followed by the investigation of their aggregation-induced emission modulation and light-induced isomerization behaviors. To the best of our knowledge, no reports are available in literature consisting simultaneous exhibition of aggregation and photo-isomerization of the metal complexes. We report in this work synthesis, characterization, photo-redox and aggregation induced physicochemical behaviours of the present systems along with *trans-cis* photoisomerization of both molecular and aggregated forms of the complexes. Additionally, DFT-TDDFT studies have also been performed to obtain the electronic properties of the molecular systems.

3.2 Experimental Section

3.2.1 Materials. Analytical grade chemicals and solvents were procured from Merck. The ligands, tpy-pvp-X (X=naphthalene, anthracene, and pyrene) were synthesized and thoroughly characterized by our recently reported procedure described in Chapter 2.⁸²

3.2.2 Synthesis of Metal Complexes. Complexes were synthesized by adopting a common procedure which is described below.

[Ru(tpy-pvp-An)₂](ClO₄)₂·2H₂O. Tpy-pvp-An (0.10 g, 0.20 mmol) and RuCl₃·3H₂O (0.03 g, 0.10 mmol) were taken in a round-bottomed flask 25 mL of ethylene glycol was added to it. This mixture was heated to 180°C with constant stirring for 6 h under argon atmosphere. Upon cooling, the solution was poured into NaClO₄·H₂O (1.5 g in 5mL of water) and stirred for few minutes until a red precipitate appeared. The compound was filtered and purified by silica gel column chromatography using MeCN as the eluent. Upon rotary evaporation of the eluent to a small volume (~10 mL), a microcrystalline complex was formed, which was filtered and recrystallized from the MeCN-MeOH (1:5, v/v) mixture. Yield: 0.17 g (65%). Anal. Calcd for C₇₄H₅₄N₆Cl₂O₁₀Ru: C, 65.39; H, 4.00; N, 6.18. Found: C, 65.32; H, 4.06; N, 6.21. ¹H NMR (400 MHz, DMSO-d₆): δ/ ppm 9.61 (s, 4H, 4H_{3'}), 9.19 (d, 4H, J = 8 Hz, 4H₆), 8.63(d, 4H, J = 8 Hz, 4H₇), 8.58 (t, 4H, J = 8 Hz, 4H₁₂), 8.31 (s, 2H, 2H₁₅), 8.22 (d, 4H, J = 8 Hz, 4H₁₄), 8.15-8.08 (m, 8H, 4H₄+4H₈), 7.98 (d, 2H, J = 16 Hz,

2H₉), 7.70-7.58(m, 8H, 4H₃+4H₁₁), 7.49 (d, 2H, J=16Hz, 2H₁₀), 7.33 (t, 8H, J = 8Hz, 4H₅+4H₁₃). Electrospray ionization mass spectrometry (ESI-MS) (positive, MeCN) m/z: 562.15 (100%) [Ru(tpy-pvp-An)]²⁺.

[Ru(tpy-pvp-Naph)₂](ClO₄)₂·2H₂O. Yield: 0.16g (64%). Anal. Calcd for C₆₆H₅₀N₆Cl₂O₁₀Ru: C, 61.01; H, 4.21; N, 7.03. Found: C, 60.97; H, 4.25; N, 7.06. ¹H NMR (400 MHz, DMSO-d₆): δ/ ppm 9.54 (s, 4H, 4H_{3'}), 9.15 (d, 4H, J = 8 Hz, 4H₆), 8.55(d, 4H, J = 8 Hz, 4H₇), 8.15 (s, 2H, 2H₁₇), 8.08 (t, 8H, J = 7 Hz, 4H₄+4H₈), 8.00-7.95 (m, 6H, 2H₁₁+2H₁₄+ 2H₁₆), 7.75 (d, 2H, J = 16 Hz, 2H₉), 7.64 (d, 2H, J = 16 Hz, 2H₁₀), 7.59-7.54(m, 10H, 4H₃+2H₁₂+2H₁₃+2H₁₅), 7.31 (t, 4H, J = 8 Hz, 4H₅). Electrospray ionization mass spectrometry (ESI-MS) (positive, MeCN) m/z: 512.09 (100%) [Ru(tpy-pvp-Naph)]²⁺.

[Ru(tpy-pvp-Pyr)₂](ClO₄)₂·3H₂O. Yield: 0.16g (62%). Anal. Calcd for C₇₈H₅₆N₆Cl₂O₁₁Ru: C, 65.73; H, 3.96; N, 5.89. Found: C, 65.70; H, 4.00; N, 5.92. ¹H NMR (400 MHz, DMSO-d₆): δ/ ppm 9.56 (s, 4H, 4H_{3'}), 9.17 (d, 4H, J = 8 Hz, 4H₆), 8.91(d, 2H, J = 8 Hz, 2H₁₄), 8.71-8.64 (m, 6H, 2H₁₁+2H₁₅+2H₁₇), 8.59 (d, 4H, J = 8 Hz, 4H₇), 8.41-8.35 (m, 8H, 2H₁₂+2H₁₃+2H₁₆+2H₁₈), 8.29 (d, 2H, J = 8 Hz, 2H₁₉), 8.15-8.09 (m, 8H, 4H₄+4H₈), 8.03(d, 2H, J = 16 Hz, 2H₉), 7.80 (d, 2H, J = 16 Hz, 2H₁₀), 7.61 (d, 4H, J = 4 Hz, 4H₃), 7.33 (t, 4H, J = 8 Hz, 4H₅). Electrospray ionization mass spectrometry (ESI-MS) (positive, MeCN) m/z: 586.16 (100%) [Ru(tpy-pvp-Pyr)]²⁺.

3.2.3 Instruments and Physical Methods. Description and detailed techniques of all the physico-chemical measurements along with the DFT/TD-DFT calculations are summarized in chapter 2. Details of the cyclic voltammetric experiment are provided below.

The electrochemical measurements were carried out with a BAS epsilon electrochemistry system. A three-electrode assembly comprising a Pt (for oxidation) or glassy carbon (for reduction) working electrode, Pt auxiliary electrode, and Ag/AgCl reference electrode was used. The cyclic voltammetric (CV) and square wave voltammetric (SWV) measurements were carried out at 25°C in MeCN solution of the complexes (*ca.* 10⁻³ M) and the concentration of the supporting electrolyte, tetraethylammonium perchlorate (TEAP) was maintained at 0.1 M. The scan rate is 100 mV/s for CV and 20 mV/s for SWV. The electrochemical measurements were carried in argon purged solutions. The potentials measured were compensated for the *iR* drop in the cell. All of the potentials reported in this study were referenced against the Ag/AgCl electrode, which under the given experimental conditions give a value of 0.36 V for the ferrocene/ferrocenium couple.

3.3 Results and Discussion

3.3.1 Synthesis and Characterization. Homoleptic bis-terpyridine Ru(II) complexes were synthesized by direct reaction of the ligands with $\text{RuCl}_3 \cdot 3\text{H}_2\text{O}$ in 2:1 proportion by refluxing in ethylene glycol under argon protection. The complexes were further purified by column chromatography and recrystallization techniques. Characterization of the complexes is performed by NMR and ESI mass spectrometric techniques as well as by elemental analysis.

The ESI mass spectra of complexes **1** and **3** together with their simulated isotopic distributions are shown in Figure 3.1. All the mononuclear complexes exhibit a single strong peak which corresponds to the $[\text{Ru}(\text{tpy-pvp-X})_2]^{2+}$ group. This is evident since the separation of the successive isotopic lines is 0.5 Da. Good correspondence is observed between the experimental and simulated patterns which confirms the presence of $[\text{Ru}(\text{tpy-pvp-X})_2]^{+2}$ species.

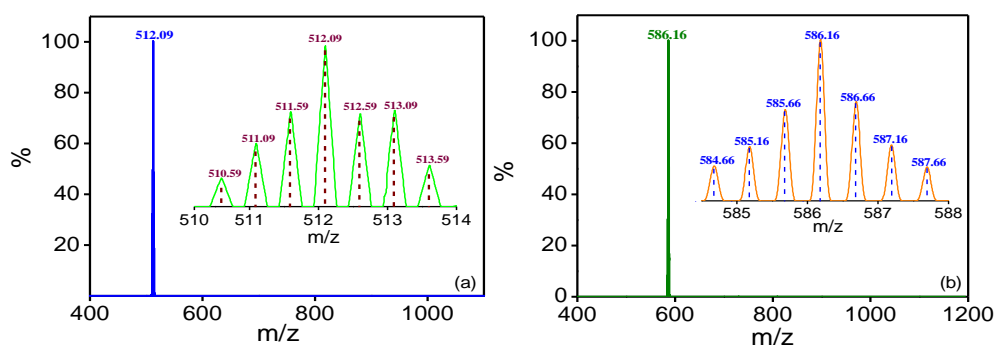


Figure 3.1. ESI (positive) mass spectrum for the complex cation of (a) $[(\text{Ru}(\text{tpy-pvp-Naph})_2)]^{2+}$ (**1**) ($m/z = 512.09$) and (b) $[(\text{Ru}(\text{tpy-pvp-Pyr})_2)]^{2+}$ (**3**) ($m/z = 586.16$) in MeCN showing both observed and simulated isotopic distribution patterns.

The ^1H NMR spectra of **1-3** obtained in $\text{DMSO-}d_6$ are presented in Figure 3.2. Tentative assignment of the protons was done with the help of both $\{^1\text{H-}^1\text{H}\}$ COSY NMR spectroscopy and by spectral assignments of the structurally related complexes (Figure 3.3). The comparatively simple nature of the NMR spectra indicates the presence of a symmetrical environment in the metal complexes. The singlet having the highest chemical shift is assigned to H_3 , while the neighbouring doublet corresponds to H_6 . The olefinic protons lie in the range of 7.49-8.03 ppm while the most up-field triplet peak is assigned to H_5 . A coupling value of $\sim 16\text{Hz}$ of the protons across the olefinic bond (H_9 and H_{10}) indicates the *trans-trans* conformation of the complexes.

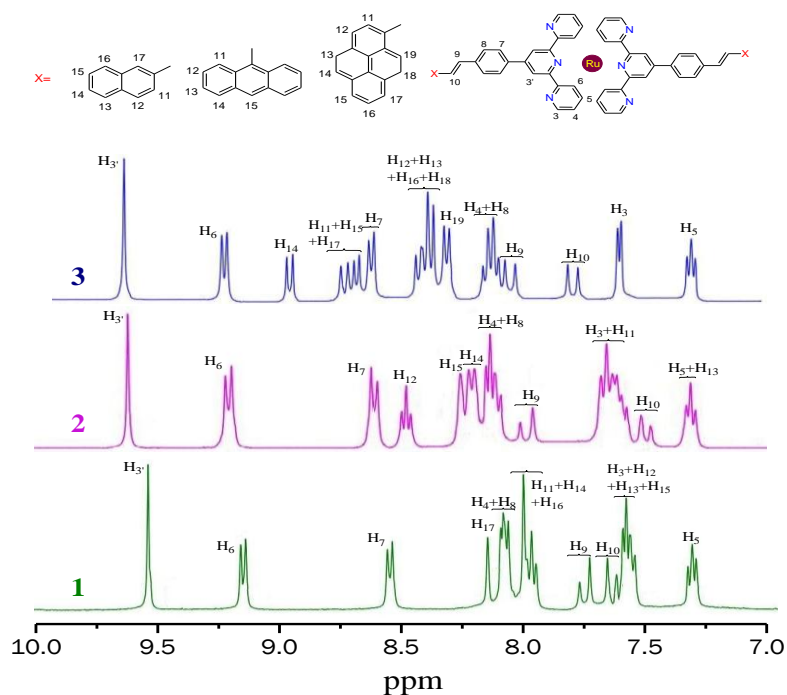


Figure 3.2. ^1H NMR spectra of **1-3** in $\text{DMSO-}d_6$.

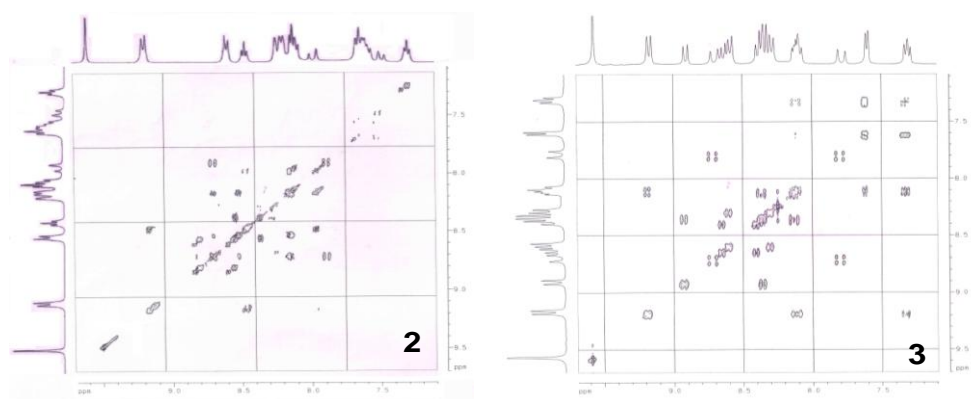


Figure 3.3. $\{^1\text{H-}^1\text{H}\}$ COSY NMR spectrum of **2** and **3** in $\text{DMSO-}d_6$.

3.3.2 Computational Investigations. The geometries of *trans-trans* and *trans-cis* forms of **1-3** are optimized with the DFT method by the aid of Gaussian 09 software in MeCN using B3LYP functional.⁸³⁻⁸⁶ The structures are optimized and stability of the wavefunction is also checked and corresponding frontier molecular orbitals of **1** along with their compositions are also provided in Figure 3.4 and 3.5. Calculations show that the

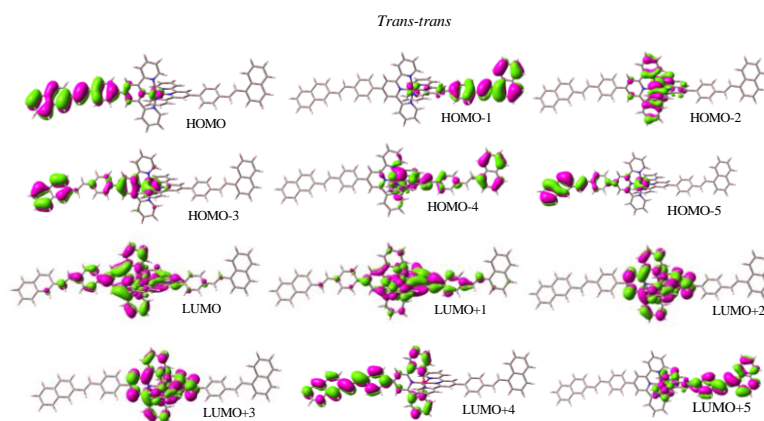


Figure 3.4. Schematic drawings of the selective frontier molecular orbitals of *trans-trans* form of **1** in MeCN.

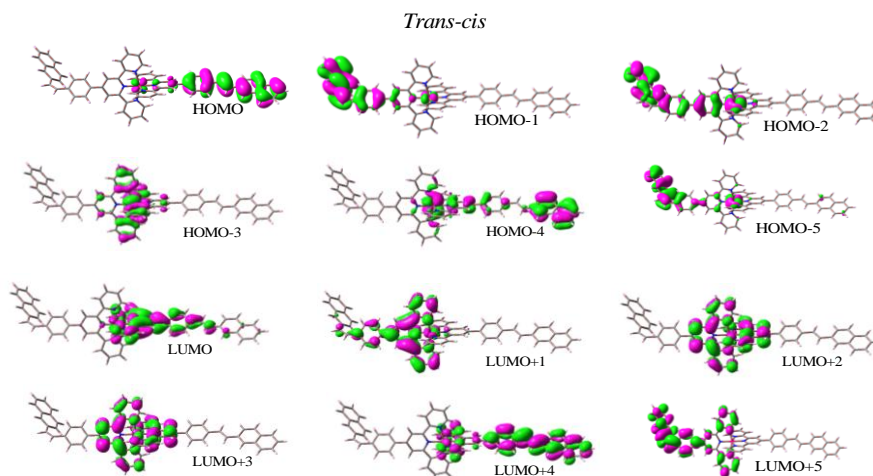


Figure 3.5. Schematic drawings of the selective frontier molecular orbitals of *trans-cis* form of **1** in MeCN.

HOMOs are localized mostly on the Ru(II) center and partially on the styrylphenyl and polyaromatic moiety. The LUMOs, on the other hand, are localized mostly on the terpyridine units. The HOMO-LUMO energy gap for **2** and **3** is similar while it is slightly higher for **1**. The electrostatic potential energy plots (ESP) are also calculated which shows the distribution of electron clouds in the entire molecule. ESP plots show that the electron density is mostly localized on the polyaromatic region while the terpyridine unit is quite electron deficient due to their coordination to the Ru(II) centre. This electron distribution is mostly similar in both forms of all three complexes.

The UV-vis absorption spectra of the *trans-trans* form of the compounds are obtained using TD-DFT calculation in acetonitrile medium. The corresponding spectral data along with proper band assignment are provided in Figure 3.6. A moderate correlation is observed between the experiment and calculations. The lowest energy band in *trans-trans* (495-505

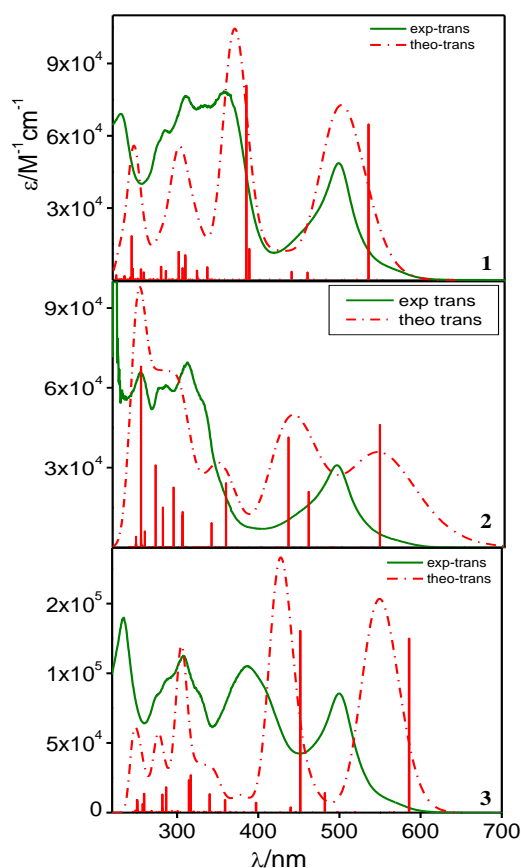


Figure 3.6. Theoretical (dashed red) and observed (green) absorption spectra of **1-3** in MeCN along with their oscillator strengths.

nm) and *trans-cis* (496-492 nm) forms arise due to dual contributions from the ruthenium to terpyridine and styrylbenzene to terpyridine CT transitions. The next higher energy band is mostly due to the ILCT transitions while the bands having highest molar extinction coefficient are assigned to mixed ILCT and π - π^* transitions in polyaromatic and heteroaromatic moieties of the ancillary tpy-pvp-X ligands in both forms of the complexes. There is a small blue shift of the MLCT band upon moving from *trans-trans* to *trans-cis* form in case of **1** and **3** derivatives. Further clarity for the band assignments is obtained from natural transition orbital (NTO) analysis (Figure 3.7) and electron density difference map (EDDM). Both NTO and EDM plots again confirm that the band at lowest energy is an admixture of MLCT as well as ILCT characters.

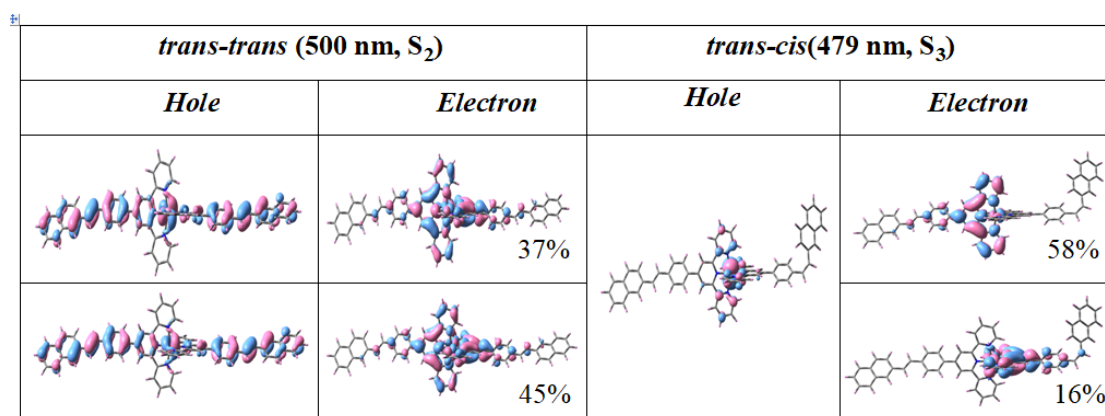


Figure 3.7. NTOs illustrating the nature of optically active singlet excited states in the absorption bands at 500 nm (S₂) for *trans-trans* and at 479 nm (S₃) for *trans-cis* forms of **1**. The occupied (holes) and unoccupied (electrons) NTO pairs that contribute more than 14% to each excited state are only represented. All transitions are mixed ¹MLCT/¹IL.

3.3.3 Absorption Spectra. The spectra and associated data for isomolar solutions of **1-3** in DMSO, MeCN and DCM are presented in Table 3.1, Figure 3.6. Each spectrum displays multiple peaks which span the entire UV-vis region. The lowest energy band centered at around 493-510 nm are typical of MLCT transition in ruthenium complexes. Assignment of band transitions are corroborated from theoretical calculations which reveal that the band around ~500 nm arises due to mixed ¹[Ru^{II}(d)⁶] → ¹[Ru^{II}(d)⁵ tpy-pvp-X(π*)¹] MLCT and some ILCT transitions wherein contribution of MLCT is greater. The next higher energy band in the region of 425-456 nm consist of equal contributions from both MLCT and ILCT transitions. These bands have the lowest molar absorption coefficient in comparison to the bands which lie mostly in the UV region and appear most probably due to ILCT as well as π- π* transitions in polyaromatic and heteroaromatic units. A moderate correlation is observed between the theoretical and experimental calculations. It is observed that the MLCT band varies with the nature of the polyaromatic moiety which is again reflected in our theoretical calculations. A small bathochromic shift of the MLCT band is observed upon increasing the polar character of the solvents.

3.3.4 Luminescence Spectra. The emission spectra as well as luminescence lifetime of **1-3** are recorded in DMSO, MeCN and DCM at RT (Table 3.1, Figure 3.8) and also in EtOH /MeOH (4:1, v/v) glass at 77K (Table 3.1, Figure 3.9). Excitation at their ¹MLCT bands at RT results in a short-lived weak emission having λ_{max} in the range of 634-752 nm (Table 3.1).

Table 3.1. Photophysical parameters for **1-3**.

Comps		Absorption $\lambda_{\text{max}}/\text{nm}$ ($\epsilon/\text{M}^{-1}\text{cm}^{-1}$)	Luminescence				
			$\lambda_{\text{max}}/\text{nm}$	τ/ns	Φ	k_r/s^{-1} ($\times 10^4$)	$k_{\text{nr}}/\text{s}^{-1}$ ($\times 10^8$)
1	DMSO (298K)	505(43700), 368(64700), 338(sh)(57500), 313(60000)	674	$\tau_1 = 26.0$ (22.6%) $\tau_2 = 45.0$ (77.4%)	2.1×10^{-3}	4.7	0.22
2		502(55900), 404(br)(23500), 334(sh)(86200), 316(99300)	663	$\tau_1 = 18.2$ (41.4%) $\tau_2 = 261.4$ (58.6%)	1.1×10^{-3}	0.42	0.04
3		510(62000), 395(69400), 336(sh)(55900), 312(72000), 292(sh)(64000)	752	$\tau_1 = 41.7$ (16.3%) $\tau_2 = 409.5$ (83.7%)	0.7×10^{-3}	0.17	0.02
1	MeCN (298K)	497(49200), 357(78000), 328(br)(73000), 310(76000), 284(sh)(62300), 230(69000)	666	$\tau_1 = 1.7$ (29.5%) $\tau_2 = 6.2$ (70.5%)	1.9×10^{-3}	3.1	1.6
2		493(46000), 447(br)(19300), 330(sh)(82900), 310(103700), 277(95400), 252(116200)	656	$\tau_1 = 1.3$ (5.4%) $\tau_2 = 6.7$ (94.6%)	1.1×10^{-3}	16.4	1.5
3		500(87500), 387(100000), 328(sh)(84700), 308(113000), 387(br)(95000), 235(140000)	747	$\tau_1 = 1.6$ (8.8%) $\tau_2 = 5.0$ (91.2%)	0.2×10^{-3}	4.0	2.0
1	DCM (298K)	500(83000), 348(br)(105000), 327(sh)(127800), 312(143000), 285(101000)	665	$\tau_1 = 2.8$ (10.1%) $\tau_2 = 12.0$ (89.9%)	1.3×10^{-3}	10.8	0.8
2		495(56000), 330(br)(107000), 311(130000), 287(113000), 286(sh)(85000)	634	$\tau_1 = 1.5$ (32.6%) $\tau_2 = 5.9$ (67.4%)	0.8×10^{-3}	13.6	1.7
3		505(70000), 378(71000), 328(br)(74000), 310(88000), 277(br)(66700)	742	$\tau_1 = 2.1$ (23.2%) $\tau_2 = 8.9$ (76.8%)	3.0×10^{-4}	3.2	1.1
1	77K	-	632	29.2 μs	0.56	-	-
2		-	634	15.0 μs	0.15	-	-
3		-	654	12.9 μs	0.13	-	-

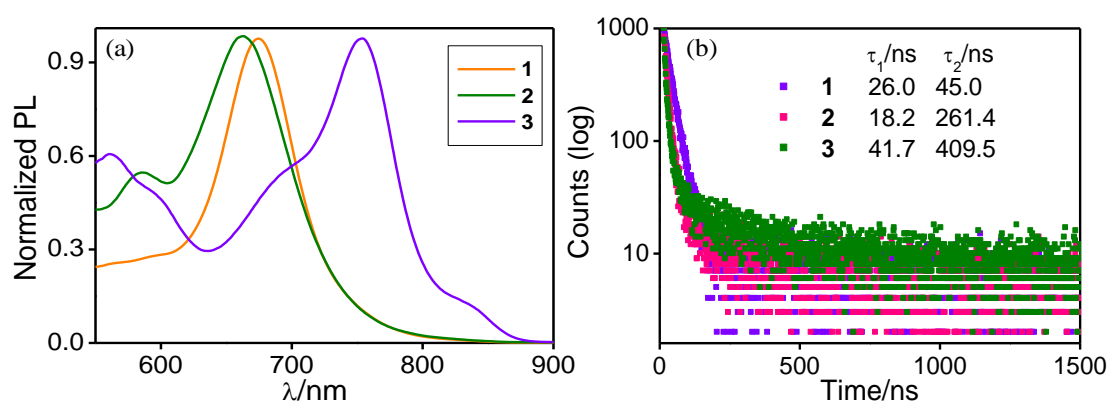


Figure 3.8. (a) Normalized emission spectra of isomolar solutions of **1-3** in DMSO. (b) Emission decay profiles upon excitation at 500 nm. Inset to Figure b gives the lifetime values of the complexes.

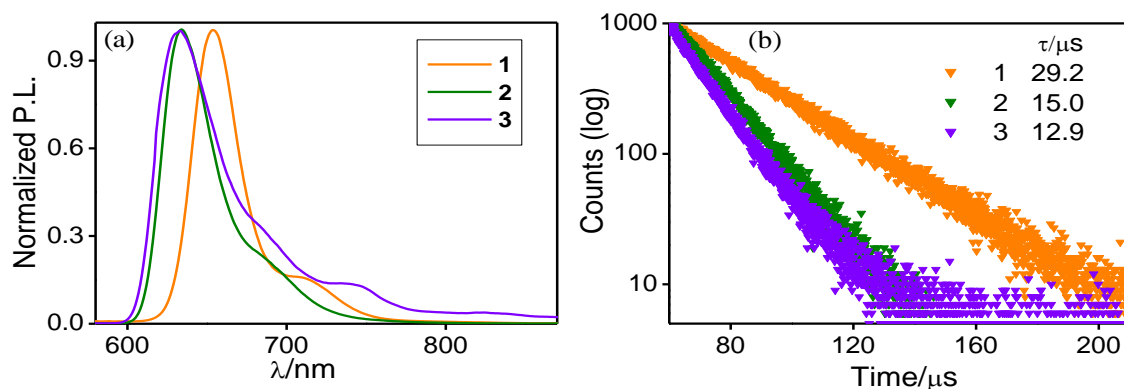


Figure 3.9. (a) Normalized emission spectra of **1-3** in EtOH-MeOH (4:1, v/v) glass at 77 K. (b) Emission decay profiles upon excitation at 500 nm. Inset to Figure b gives the lifetime values of the complexes at 77K.

On closer inspection, it is seen that the emission maximum of **3** is situated at ~750 nm while that of **1** and **2** lies in the range of 634 and 674 nm. In case of DMSO, a red shift of emission maxima along with an increase in emission quantum yield (QY) and lifetime is seen compared to that in MeCN and DCM. Luminescence lifetimes are found in the range of 5.0-12.0 ns in MeCN and DCM whereas between 45.0 and 409.5 ns in DMSO at RT. From previous literature reports of ruthenium-terpyridine complexes, we surmise that the emission in the present complexes occurs primarily from $^3\text{MLCT}$ state.⁸⁷⁻⁸⁹ On passing from RT to 77K, the emission maxima undergo a blue shift ($\lambda_{\text{max}}=632\text{-}654$ nm) with a drastic increase in emission intensity, quantum yield and lifetime (12.9-29.2 μs) which is also typical for $^3\text{MLCT}$ emitters (Table 3.1). Zero-zero spectroscopic energy (E_{00}) was estimated from their $^3\text{MLCT}$ emission maxima at 77 K (varying between 1.90 and 1.97 eV). The excited-state decays are found to be mostly bi-exponential in nature at RT while it is mono-exponential at 77K. The bi-exponential nature of the decay in both solvents can be explained as initial deactivation of the $^3\text{MLCT}$ state to give the short-lived component, while the longer-lived component arises from the equilibrated state of $^3\text{MLCT}$ and styrylbenzene units.

3.3.5 Electrochemistry. Cyclic voltammograms of complexes **1-3** are recorded in MeCN and related information is presented in Figure 3.10 and summarized in Table 3.2. The oxidation of the complexes corresponds to $\text{Ru}^{3+}/\text{Ru}^{2+}$ process. Interestingly, during anodic oxidation, while all the mononuclear complexes show a single metal centered ($\text{Ru}^{3+}/\text{Ru}^{2+}$) reversible oxidation peaks, pyrene additionally exhibits a ligand centered quasi-reversible

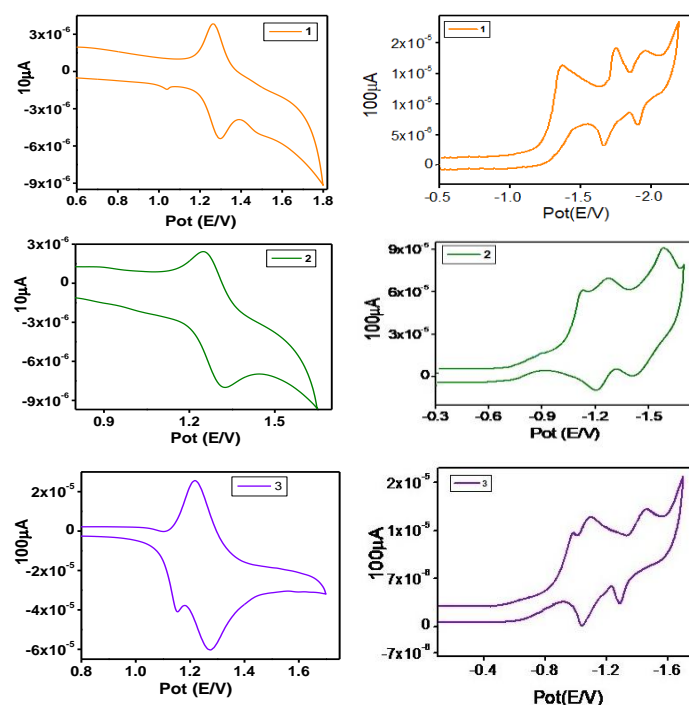


Figure 3.10. Cyclic voltammograms of **1-3** showing the oxidation (left panel) and reduction (right panel) in acetonitrile.

Table 3.2 Electrochemical data^a for **1-3** in MeCN.

Comps	Oxidation ^b	Reduction ^c
	$E_{1/2}/(\text{V})$	$E_{\text{red}}/(\text{V})$
1	1.28	-1.37, -1.74, -1.96
2	1.31	-1.13, -1.24, -1.52
3	1.25	-1.01, -1.09, -1.42

^aAll the potentials are referenced against Ag/AgCl electrode with $E_{1/2}=0.36$ V for Fc/Fc^+ couple. ^bReversible electron transfer process with a Pt working electrode. ^c $E_{1/2}$ values obtained using glassy carbon electrode.

peak at ~ 1.15 V.⁹⁰ This peak is due to the one-electron oxidation of the pyrene units. On the cathodic potential side, multiple quasi-reversible and irreversible reductions are observed in the range -1.01 to -1.96 V, which arise due to the reduction of the coordinated terpyridine units.

Spin densities of one-electron reduced and one-electron oxidized forms are shown in Figure 3.11. Theoretical calculation shows that the spin density for the one-electron oxidized form was found to be localized mainly on the ruthenium center and to some extent on the stilbene and polyaromatic moiety, while in one-electron reduced form they lay mainly on the terpyridine unit. Thus, spin density calculations support our assignment of the redox processes.

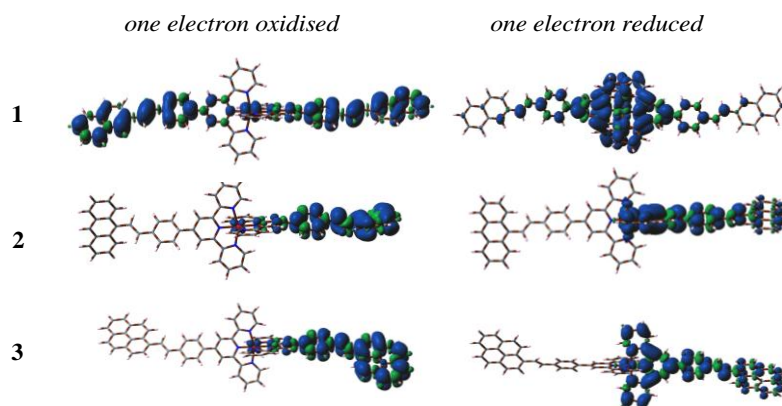


Figure 3.11. Spin density plots for one-electron oxidized (left panel) and one-electron reduced (right panel) forms of the complexes **1-3** in MeCN.

3.3.6 Aggregation-Induced Modulation of the Emission Spectral Characteristics.

We previously reported the aggregation behavior of the ancillary ligand which showed both AIEE and ACQ effects, depending on the type of solvent-mixtures.⁸² We already pointed out that terpyridine complexes of Ru(II) are either non-luminescent or weakly emissive at RT with very low excited-state lifetimes.⁵⁰ As one of the major foci of this work is to improve the luminescence characteristics of Ru(II)-terpyridine complexes, we are interested to impose aggregation phenomena upon employing several solvent/non-solvent systems. We used here three different systems; viz. DMSO/water, MeCN-water (where DMSO and MeCN acts as good solvent while water as the poor solvent) and DCM/hexane (where DCM is good solvent while hexane as the bad solvent). We actually used DCM/MeCN (50:1, v/v) due to the low solubility of the complexes in pure DCM.

With the increase in water fraction (f_w) in DMSO, the emission intensity as well as quantum yield (Φ) gradually decreases for all three complexes along with a small blue shift of λ_{\max} for **1** and **2**, whereas a red-shift of ~ 10 nm for **3** (Figure 3.12). By contrast, there is a systematic increase in emission intensity and quantum yield for all three complexes upon gradual addition of water fraction (f_w) in MeCN (Figure 3.13) as well as hexane fraction in DCM with the exception of complex **3** (Table 3.3 and Figure 3.14). It is to be noted that the extent of enhancement differs as the polyaromatic moiety changes in the complexes (highest for **1** and moderate for **2**). Notably, no significant enhancement takes place in case of pyrene substituent (**3**). The observed results indicate the probable formation of aggregates in the studied solvent systems. We have also calculated both the radiative (k_r) and non-radiative (k_{nr}) rate constants in the agglomerated (90%) forms of the complexes and the values are

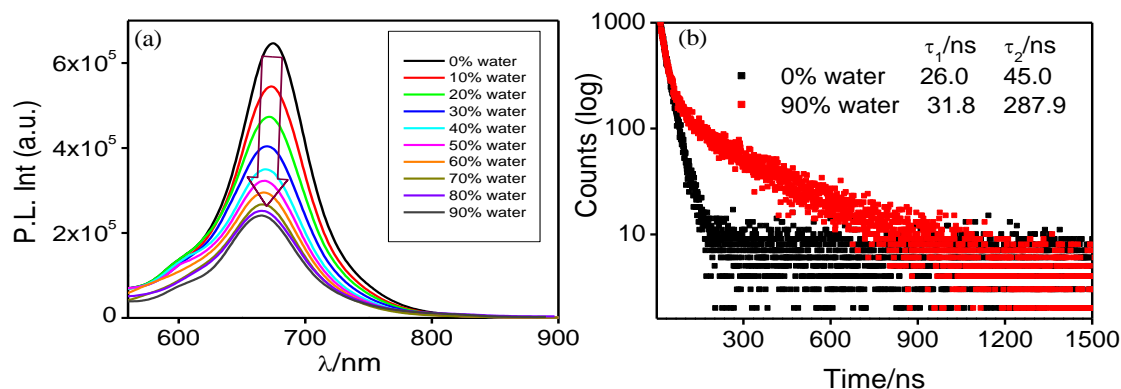


Figure 3.12. (a) Emission ($\lambda_{\text{ex}}=500$ nm) spectral change of **1** upon varying the relative ratio of DMSO and water. (b) Emission decay profile ($\lambda_{\text{ex}}=450$ nm NanoLED) along with their corresponding lifetime values for 0% and 90% f_w .

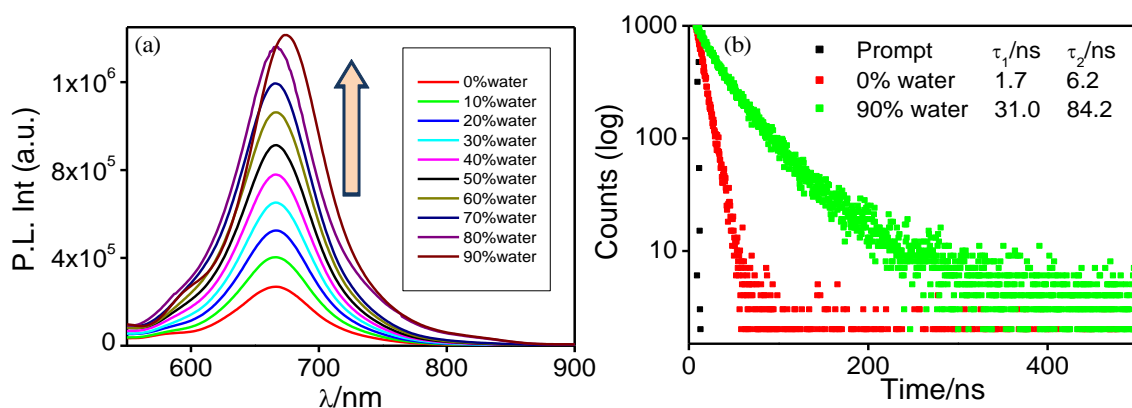


Figure 3.13. (a) Emission ($\lambda_{\text{ex}}=500$ nm) spectral change of **1** upon varying the relative ratio of MeCN and water. (b) Emission decay profiles ($\lambda_{\text{ex}}=450$ nm NanoLED) along with their lifetime values of 0% and 90% f_w .

presented in Table 3.3. For MeCN/water and DCM/hexane mixtures, where AIEE is observed, the values of k_r in the agglomerated (90%) forms increase, while the values of k_{nr} decrease compared to their free forms. By contrast, both k_r and k_{nr} decreases in DMSO/water mixture wherein ACQ occurs. With an aim to obtain direct evidence for the occurrence of aggregation, we performed the dynamic light scattering (DLS) experiment in selected solvent mixtures (DMSO/water, MeCN-water). It is clearly seen that with the increase in water fraction the size of the aggregate increases in both the solvent mixtures indicating the occurrence of aggregation (Figure 3.15). Excited state lifetimes of the complexes were also acquired in all three studied solvent mixtures. Lifetime is found to increase in all three media, albeit in different extent, with the exception of complex **3** in DCM-hexane.

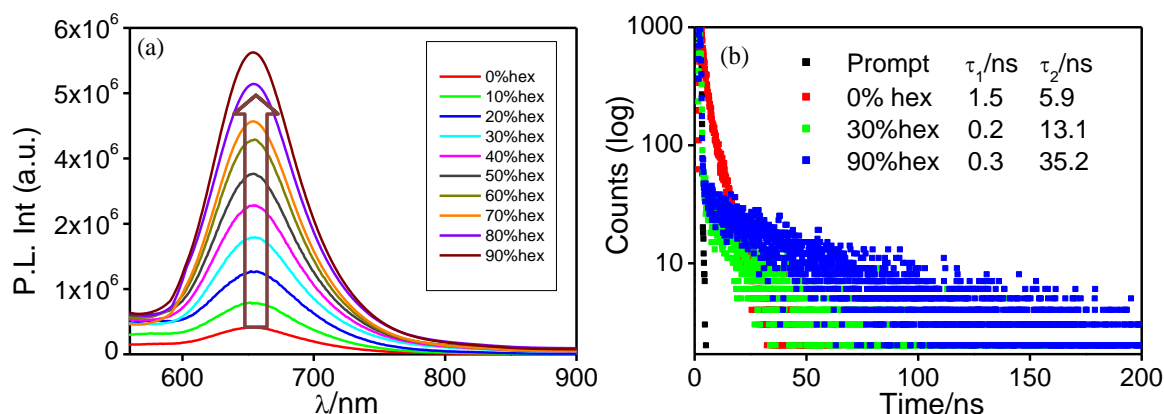


Figure 3.14. The emission ($\lambda_{\text{ex}}=500$ nm) (a) spectral change of **2** upon varying the relative ratio of DCM and hexane. Figure (b) shows the change in emission decay ($\lambda_{\text{ex}}=450$ nm NanoLED) along with the lifetime values of the initial and final form.

Table 3.3. Emission quantum yield in their free form ($\Phi_{0\%}$) and 90% aggregated form ($\Phi_{90\%}$).

solvent	comps	$\Phi_{0\%}$	$\Phi_{90\%}$	k_r / s^{-1}	k_{nr} / s^{-1} ($\times 10^7$)
DMSO/Water	1	2.1×10^{-3}	9.0×10^{-4}	3.1×10^3	0.35
	2	1.1×10^{-3}	5.4×10^{-4}	1.8×10^3	0.32
	3	0.7×10^{-3}	4.1×10^{-4}	7.0×10^2	0.17
MeCN/Water	1	1.9×10^{-3}	9.9×10^{-3}	1.2×10^5	1.2
	2	1.1×10^{-3}	2.5×10^{-3}	3.6×10^5	14.6
	3	0.2×10^{-3}	0.3×10^{-3}	0.4×10^5	13.8
DCM/Hexane	1	1.3×10^{-3}	1.8×10^{-2}	3.6×10^5	2.0
	2	0.8×10^{-3}	7.7×10^{-3}	2.2×10^5	2.8

Upon aggregation, the intermolecular rotations are freezed to some extent so that the excited state deactivation takes place mostly through the radiative pathway thereby increasing the lifetime of the complexes quite significantly.

We are now curious to elucidate plausible reason for the wide differences in the emission spectral characteristics of the complexes upon aggregation. Upon close inspection, it appears that complex **1** exhibits remarkable alteration in emission intensity upon aggregation, whereas complex **3** suffers a little change in emission. In case of complex **2**, the DCM-hexane mixture leads to maximum enhancement, whereas other solvent mixtures result in a very little alteration in emission upon aggregation. It is needless to mention that all the complexes consist of polycyclic aromatic hydrocarbons with extensive π -delocalization through substituted styrylphenyl unit. In case of **3**, we guess, two equally opposing effects are operative. The planar pyrene unit of **3** prefers close packing through π - π stacking interaction

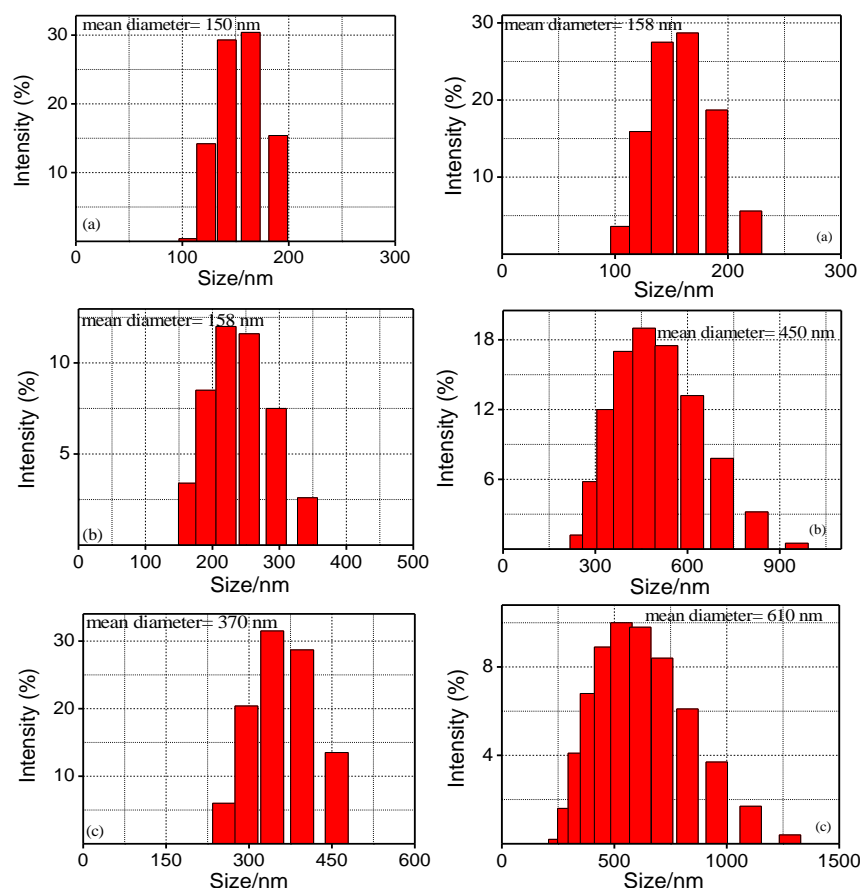


Figure 3.15. Left panel: Particle size distribution of **2** with different DMSO/water compositions: 0% (a) 40% (b) and 90% (c) water in DMSO. Right panel: Particle size distribution of **1** with different MeCN/water compositions: 0% (a) 40% (b) and 90% (c) water in MeCN.

in their aggregated form which leads to emission quenching.⁹¹⁻⁹⁴ On the other hand, the restricted intramolecular motion (RIM) imposed by styrylphenyl conjugated Ru-tpy unit could arrest the non-radiative decay pathway of the excited state(s) and induces enhancement of the emission characteristics.⁹¹⁻⁹⁴ These two opposing phenomena are probably responsible for a small change in emission intensity upon aggregation for **3**. As the naphthalene moiety renders relatively less π -electronic charge density compared to anthracene and pyrene, the effect of RIM is dominant over the π - π stacking interaction in less polar solvent mixtures (MeCN-water and DCM-hexane) and thereby induces greater aggregation-induced emission enhancement in **1** compared with both **2** (anthracene) and **3** (pyrene). The decrease in the non-radiative decay pathway due to RIM is evident from the decrease of the non-radiative rate constant (k_{nr}) in their 90% aggregated form with respect to its free form. Hence, the excited states are enabled to decay radiatively with consequent increase of the radiative rate

constant (k_r) and enhancement of emission intensity and quantum yield. In polar solvent mixture (DMSO-water), the formation of π -aggregate/excimer probably dominates over RIM in the aggregated state and leads to emission quenching. Complex **2**, on the other hand, displays intermediate behavior (more like **1** in DCM-hexane while close to **3** in other solvent mixtures). Thus, we are able to demonstrate different aggregation-induced emission spectral behavior in present Ru(II)-terpyridine complexes upon varying the polyaromatic substituent as well as on the type of the solvent mixtures.

3.3.7 Photoisomerization Behaviors. Presence of two $-C=C-$ units in the molecular structure indicates that the molecule will be sensitive to light irradiation. Hence, we carried out all the photoisomerization experiments using visible light. We carried out the experiments in a mixture of DCM/MeCN (50:1, v/v) since the rate of photo-isomerization was found to be extremely slow in other polar solvents like MeCN and DMSO.

The UV-vis absorption spectral profiles of **1-3** are presented in Figure 3.16. Upon shining light, we can see that the absorbance of MLCT (~ 500 nm) as well as ILCT (~ 300 - 400 nm) band undergoes a remarkable decrease along with simultaneous increase of

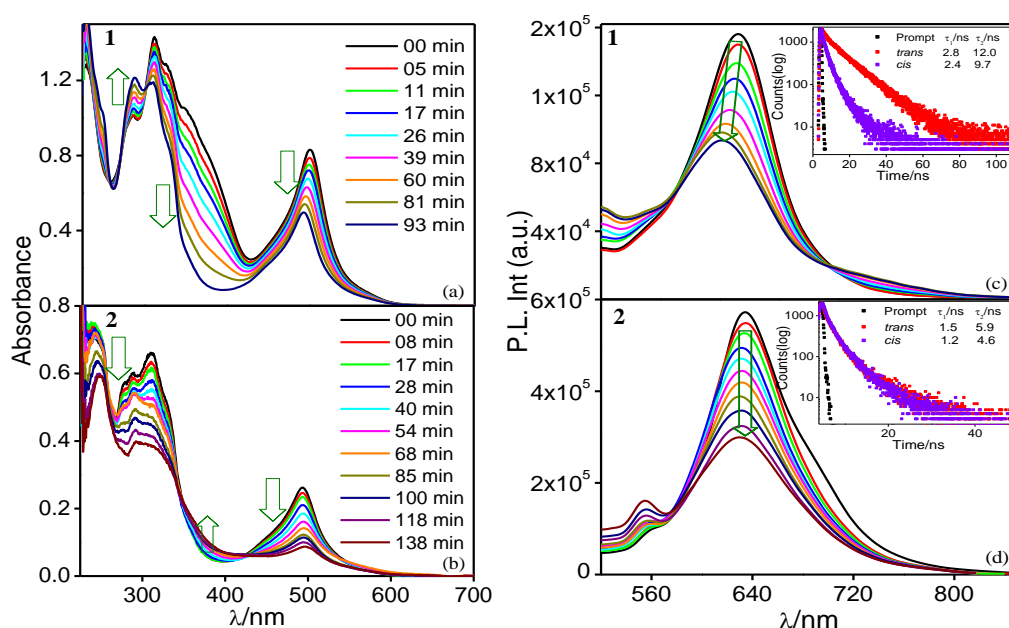


Figure 3.16. Absorption (left panel) and emission (right panel) ($\lambda_{\text{ex}} = 490$ nm) spectral change of **1** (a and c, respectively) and **2** (b and d, respectively), upon visible light irradiation in DCM. Isosbestic points appear at 304 nm for **1**, 427 and 345 nm for **2**. Inset to figure c and d shows the corresponding change in emission decay ($\lambda_{\text{ex}} = 450$ nm NanoLED) along with their lifetime values.

absorbance in the region 220-300 nm. Small blue shift of the MLCT band is observed only for **1** and **3**. A single step change and presence of clear isosbestic points suggest that two species are at equilibrium during the entire period of photo-irradiation leading to the isomerization of the *trans-trans* form of the complexes to either *trans-cis* or *cis-cis* form. The time taken to reach the photo-stationary state varies between 73 and 138 m. On the emission side, a gradual decrease in emission intensity is found for **1** and **2**. By contrast, in case of **3**, the emission intensity increases by small amount. Lifetime values of all the complexes are found to decrease upon photoisomerization (Figure 3.16).

In order to understand the mode of isomerization, we monitored the photoisomerization process through NMR spectroscopy (Figure 3.17). The photoisomerization of **1** was carried out in DMSO-*d*₆-CDCl₃ (1:5 v/v) mixture upon shining visible light for 15h. It is seen that the proton peaks across the double bond (H₉, H₁₀) as well as adjacent to the -C=C- unit (H₇, H₈, H₁₁, H₁₂ and H₁₇) undergo a decrease in intensity along with their concomitant evolution in the up-field region upon irradiation. The two olefinic protons (H₉ and H₁₀) within the range of 6.65-6.85 ppm in the coordinated *trans-trans* orientation undergo a remarkable up-field shift to the domain of 6.30-6.45 ppm along with simultaneous decrease

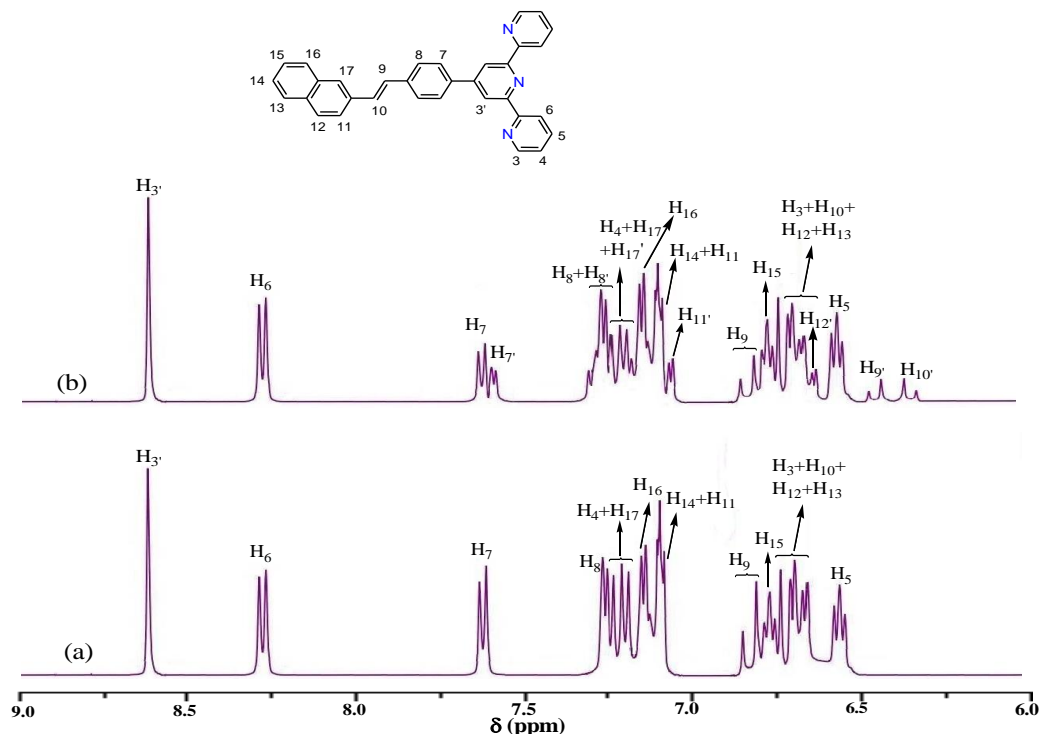


Figure 3.17. ¹H NMR spectrum of [Ru(tpy-pvp-Naph)₂]²⁺ (**1**) in DMSO-*d*₆-CDCl₃ (1:4, v/v) before (a) and after (b) photolysis with visible light for 15 h.

of coupling constant value ($J \approx 16 \text{ Hz} \rightarrow 12 \text{ Hz}$). These J values corroborate with the typically reported coordinated *trans* and *cis* stilbenes.^{34-35,40,44-45} Such NMR spectral change indicates the transformation of *trans-trans* \rightarrow *trans-cis* form.

DFT calculations also support the *trans-trans* \rightarrow *trans-cis* conversion. The overlay of the absorption spectra for both the forms is depicted in Figure 3.18. From DFT calculations also we find that there is a blue shift of the MLCT band on moving from *trans-trans* to *trans-cis* form for relevant complexes. A moderate correlation is observed between the experimental and calculated spectra.

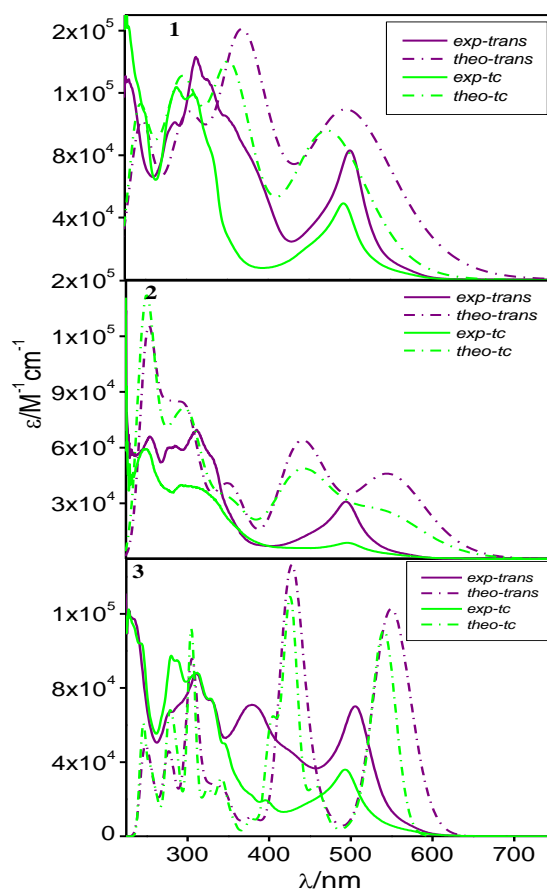


Figure 3.18. Overlay of the theoretical (green dotted line) and experimental (purple solid lines) absorption spectra of both *trans-trans* (purple) and *trans-cis* (green) forms of **1-3** in MeCN.

The *trans-trans* to *trans-cis* photo-isomerization rate constant (k_{iso}) and quantum yields ($\Phi_{\text{tt} \rightarrow \text{tc}}$) are evaluated from their absorption titration profiles and the relevant data is summarized in Table 3.4 and Figure 3.19. The reaction follows first order kinetics in the initial stage of photoisomerization and k_{iso} varies between 2.91 and 6.91×10^{-4} while $\Phi_{\text{tt} \rightarrow \text{tc}}$ varies within the domain of 0.012 - 0.026 . The *trans-cis* \rightarrow *trans-trans* backward isomerization

proceeds slowly in the dark but could be accelerated in the presence of UV light. Both the absorption and emission spectra almost revert back to their initial state upon UV light irradiation (Figure 3.19). This reverse photoisomerization was also monitored by ^1H NMR spectroscopy in $\text{DMSO-}d_6\text{-CDCl}_3$ (1:5 v/v) mixture. The previously obtained *trans-cis* form of **1** in $\text{DMSO-}d_6\text{-CDCl}_3$ was once again irradiated with

Table 3.4. Table for comparison of the values of rate constants (k_{iso}) and photoisomerization quantum yields ($\Phi_{t \rightarrow c}$) for *trans-trans* \rightarrow *trans-cis* process in both of their free and aggregated forms.

	1		2		3	
Free form	$k_{\text{iso}}/\text{s}^{-1}$ ($\times 10^{-4}$)	Φ ($\times 10^{-2}$)	$k_{\text{iso}}/\text{s}^{-1}$ ($\times 10^{-4}$)	Φ ($\times 10^{-2}$)	$k_{\text{iso}}/\text{s}^{-1}$ ($\times 10^{-4}$)	Φ ($\times 10^{-2}$)
	$tt\rightarrow tc$	$tt\rightarrow tc$	$tt\rightarrow tc$	$tt\rightarrow tc$	$tt\rightarrow tc$	$tt\rightarrow tc$
	3.38	1.19	2.91	2.09	6.91	2.63
Aggregated form	$k_{\text{iso}}/\text{s}^{-1}$ ($\times 10^{-4}$)	Φ ($\times 10^{-3}$)	$k_{\text{iso}}/\text{s}^{-1}$ ($\times 10^{-4}$)	Φ ($\times 10^{-3}$)	$k_{\text{iso}}/\text{s}^{-1}$ ($\times 10^{-4}$)	Φ ($\times 10^{-3}$)
	$tt\rightarrow tc$	$tt\rightarrow tc$	$tt\rightarrow tc$	$tt\rightarrow tc$	$tt\rightarrow tc$	$tt\rightarrow tc$
	30% f_{H}	1.62	9.89	2.28	6.61	-
90% f_{H}	1.32	7.09	1.59	5.57	-	-

UV light of 280 nm for prolonged time. It is seen that almost all of the protons nearly revert back to their initial *trans-trans* state after 32 hours, leaving some traces of the *trans-cis* form. We have also calculated the k_{iso} and $\Phi_{\text{tc} \rightarrow \text{tt}}$ for the backward process. k_{iso} varies between 0.78 and 1.49×10^{-4} while $\Phi_{\text{tc} \rightarrow \text{tt}}$ varies within the domain of $1.72\text{--}3.32 \times 10^{-3}$.

We do not have a very clear picture for the mechanism of emission quenching upon photo-isomerisation. From the bi-exponential nature of the decay profile we can infer that two excited state species ($^3\text{MLCT}$ and $^3\text{ILCT}$) are in equilibrium. Due to the strained nature of *trans-cis* form, the equilibrium between $^3\text{MLCT}$ and $^3\text{ILCT}$ is disrupted as a result of which the non-radiative ^3MC gets populated by thermal crossover, which is the probable reason for emission quenching.

3.3.8 Photoisomerization in the Aggregated Forms. During aggregation, the solvent separated molecules come closer and the agglomerates induce emission enhancement. Since the aggregated forms of the complexes also have the -C=C- units, hence it is expected that their aggregated form would also show *trans-trans* \rightarrow *trans-cis* isomerization upon light irradiation. Since the complexes in their molecular forms undergo photoisomerization in

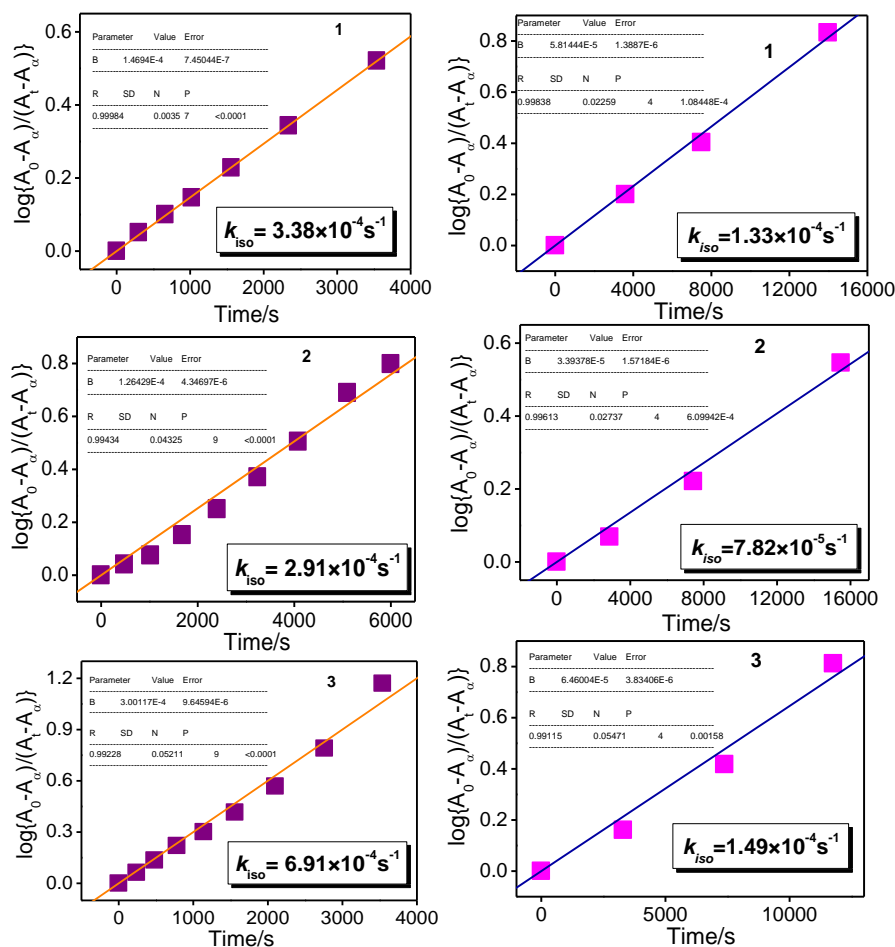


Figure 3.19. Linear plot of $\log(A_0 - A_t)/(A_t - A_e)$ vs. time (t) for the absorption spectral change due to $trans-trans \rightarrow trans-cis$ (left) and $trans-cis \rightarrow trans-trans$ (right) process of **1-3** upon irradiation with visible and UV light respectively in DCM/MeCN (50:1, v/v). Inset to these plots give the values of rate constant.

DCM only, we selected DCM/hexane mixture for monitoring the isomerization behavior of the aggregates. Herein, we used 30% and 90% f_H of DCM/hexane to observe the effect of aggregation on the isomerization behavior.

Upon shining visible light, we find a significant change in both absorption and emission spectral profiles for 30% and 90% f_H in **1** and **2** (Figure 3.20). A clear isosbestic point is also noticed in the absorption spectral profiles. A similarity in the spectral pattern with that of their molecular form signifies the incidence of $trans-trans \rightarrow trans-cis$ isomerization in all cases. For both the 30% and 90% f_H of a specific complex, we observe a similar spectral pattern barring the time of saturation. On taking a closer look, it is seen that

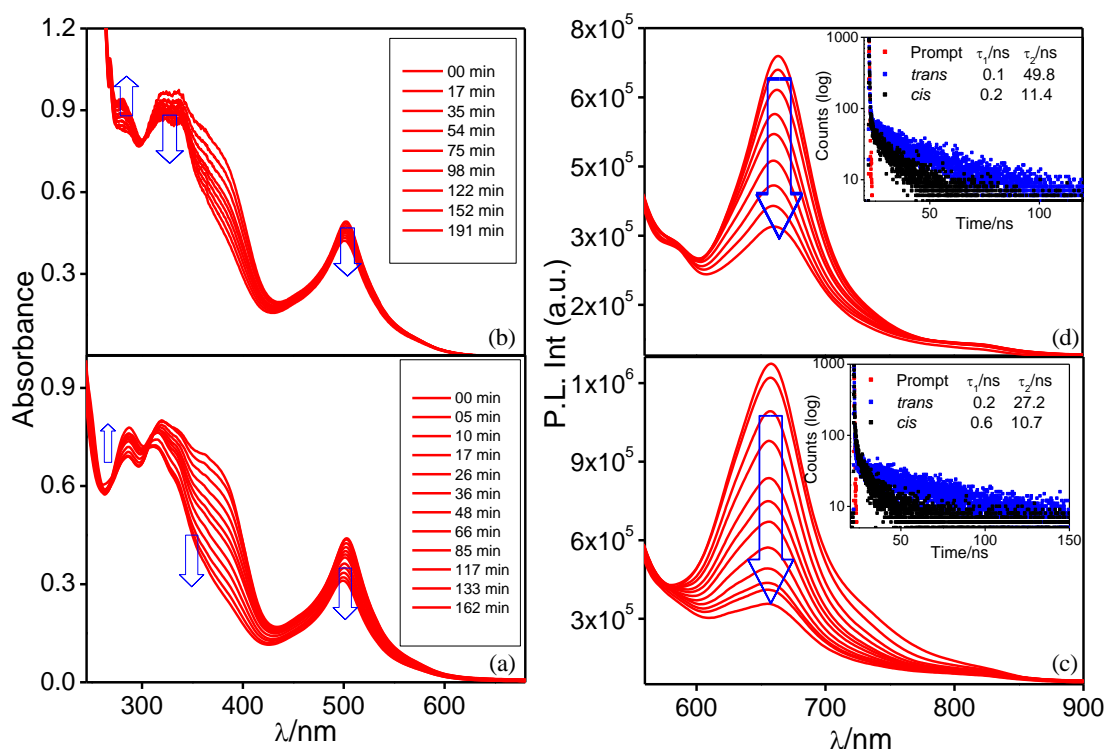


Figure 3.20. Absorption and emission ($\lambda_{\text{ex}}=490$ nm) spectral changes of 30% (a and c, respectively) and 90% (b and d, respectively) hexane fraction in DCM-hexane mixture of **1** upon irradiation with visible light. Isosbestic points appear at 306 nm for 30% aggregate and at 303 nm for 90% aggregate. Inset to the figure c and d shows the corresponding change in emission decay ($\lambda_{\text{ex}}=450$ nm NanoLED) along with their lifetime values.

the change in absorbance value for 90% f_H is lesser in comparison to that of 30% f_H . This suggests that the tendency to photoisomerize decreases along with the increase in the extent of aggregation. On the emission side, a gradual quenching upon visible light irradiation is seen in case of both 30 and 90% f_H (Figure 3.20c-d). We have also acquired the lifetimes of the aggregated forms upon photolysis. The values are found to decrease in both cases upon light irradiation. As DCM/hexane duo does not induce any change in the emission characteristics, we do not perform the aggregation induced isomerization experiment for **3**. The *trans-trans* to *trans-cis* photo-isomerization rate constant (k_{iso}) and quantum yields ($\Phi_{t \rightarrow c}$) are also estimated from their absorption spectral profiles as previously discussed and the relevant data are summarized in Table 3.3. It is affirmed that the rate of photoisomerization decreases upon aggregation as expected.

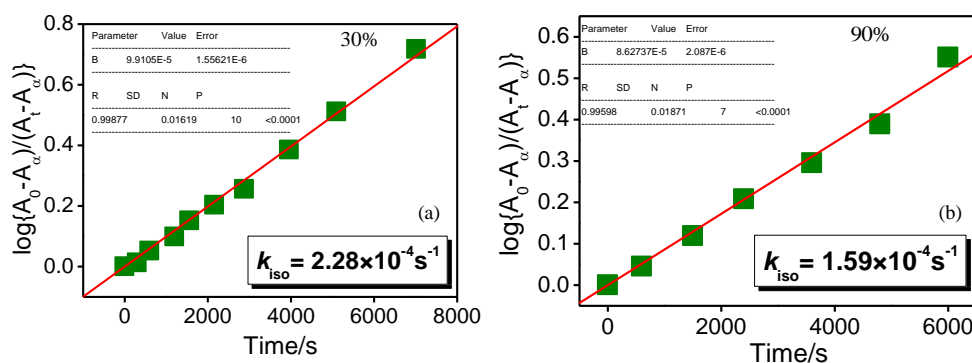


Figure 3.21. Linear plot of $\log(A_0 - A_\alpha)/(A_t - A_\alpha)$ vs. time (t) for the absorption spectral change due to *trans*→*cis* process of **1** upon irradiation with visible light of 30% (a) and 90% (b) hexane fraction in DCM-hexane mixture. Inset to these plots give the values of rate constant.

3.3.9 Accomplishment of the Metal Complexes over their Ligand Precursors. In our previous work, we designed a series of highly fluorescent styrylphenyl-conjugated terpyridine compounds incorporating polycyclic aromatic hydrocarbons (such as naphthalene, anthracene and pyrene) for their probable use as potential optoelectronic device. Taking advantage of the polycyclic aromatic hydrocarbons moiety, we explored the aggregation-induced emission switching behavior in different solvent-mixtures. Additionally, the compounds are utilized for the development of photo-switches based on alteration of their emission spectral characteristics through reversible *trans*-*cis* isomerization induced by light of appropriate wavelength. In this work, we have utilized these ligands to design a new array of homoleptic bis terpyridine complexes primarily to improve the room temperature emission characteristics of the resulting complexes so that they can act as suitable visible light sensitizers. Most of the Ru(II)-terpyridine complexes are either non-luminescent or very weakly luminescent⁵⁰ at RT with very low excited-state lifetime [$\tau=0.25$ ns for $\text{Ru}(\text{tpy})_2^{2+}$]. Notably, the resulting complexes exhibit intense absorption ($\epsilon=19300\text{-}87500 \text{ mol}^{-1} \text{ cm}^{-1}$ for the MLCT band) and moderately strong emission band ($\lambda_{\text{max}}= 656\text{-}752 \text{ nm}$) in the visible domain with reasonably long excited state lifetimes (5.0-409.5 ns). Thus, upon coordination, the absorption and emission spectral domain of ligands is shifted towards visible region with excited-state lifetime almost three-orders of magnitudes higher relative to the free ligands. Hence, the complexes can act as suitable visible light sensitizers. Taking advantage of the polyaromatic moiety, the complexes also exhibits both aggregation-induced emission quenching (ACQ) as well as emission enhancement (AIEE), depending upon nature of the solvent mixture employed. Moreover, the extent of AIEE is dramatically increased in the

complexes together with remarkable increase of excited-state lifetimes relative to their ligand precursors. The emission quantum yield is found to increase up to ~14 times for the metal complexes relative to only ~2 times for the ligands upon aggregation. Likewise, the enhancement of lifetimes occurs up to the extent of ~580 ns compared with only 4.38 ns for the ligands. With the aid of the stilbene motifs, the metal complexes also undergo reversible *trans-cis* photoisomerization in both of their free- and aggregated forms, although the rate and quantum yield of the photo-isomerization of the complexes are less compared with the ligands. Thus, the present systems are thought to be potential building blocks for the construction of smart molecular switches operating in the visible domain.

3.4 Conclusions

In this work, we introduced a new series of homoleptic bis-terpyridine complexes of Ru(II) by incorporating styrylphenyl unit coupled to anthracene, naphthalene and pyrene at the 4' position of terpyridine moiety. Detailed experimental and theoretical investigations on their photophysical, electrochemical, aggregation-induced emission and photo-isomerization behaviors are carried out in this work. Styrylphenyl unit promotes *trans-trans* to *trans-cis* isomerization in the complexes upon visible light irradiation, which is evident from their sequential absorption and emission spectral changes as well as by NMR spectroscopy. The reverse *trans-cis* to *trans-trans* isomerization was achieved upon UV light irradiation. Thus, “on-off” and “off-on” emission switching is viable upon shining alternatively with visible and UV light. Presence of polyaromatic as well as heteroaromatic moieties led us to explore the aggregation-induced properties of the complexes. The compounds show weak emission at RT but upon aggregation the emission intensity quantum yield, and excited-state lifetime increases substantially. Hence, aggregation phenomenon induced significant improvement of room temperature emission characteristics of the Ru(II)-terpyridine complexes. Interestingly, the aggregated form of the compounds also isomerizes upon visible light irradiation but at a much slower rate compared to their non-aggregated forms. In essence, we can efficiently control the mode of emission switching upon varying the solvent mixture as well as by treating with visible and UV light. Thus, the present systems are thought to be potential building blocks for the construction of smart molecular switches.

3.5 References

- (1) Feringa, B. L.; Van Delden, R. A.; Ter Wiel, M. K. J. In *Chiroptical Molecular Switches in Molecular Switches*. Ed.; Wiley-VCH: Weinheim, **2001**, 123-163.
- (2) Ko, C.-C.; Yam, V. W.-W. Coordination Compounds with Photochromic Ligands: Ready Tunability and Visible Light-Sensitized Photochromism. *Acc. Chem. Res.* **2018**, *51*, 149-159.
- (3) Saha, S.; Stoddart, J. F. Photo-Driven Molecular Devices. *Chem. Soc. Rev.* **2007**, *36*, 77-92.
- (4) Hofmeier, H.; Schubert, U. S. Recent Developments in the Supramolecular Chemistry of Terpyridine-Metal Complexes. *Chem. Soc. Rev.* **2004**, *33*, 373-399.
- (5) Kawata, S.; Kawata, Y. Three-dimensional Optical Data Storage Using Photochromic Materials. *Chem. Rev.* **2000**, *100*, 1777-1788.
- (6) Shum, J.; Leung, P. K.-K.; Lo, K. K.-W. Luminescent Ruthenium(II) Polypyridine Complexes for a Wide Variety of Biomolecular and Cellular Applications. *Inorg. Chem.* **2019**, *58*, 2231-2247.
- (7) Lee, L. C.-C.; Lo, K. K.-W. Strategic Design of Luminescent Rhenium(I), Ruthenium(II), and Iridium(III) Complexes as Activity-Based Probes for Bioimaging and Biosensing. *Chem Asian J.* **2022**, *17*, e202200840.
- (8) Ostroverkhova, O. Organic Optoelectronic Materials: Mechanisms and Applications. *Chem. Rev.* **2016**, *116*, 13279-13412.
- (9) Boelke, J.; Hecht, S. Designing Molecular Photoswitches for Soft Materials Applications, *Adv. Optical Mater.* **2019**, 1900404.
- (10) Mazza, E. L.; Puntoriero, F.; Nastasi, F. B.; Milette, L.; Hanan, G. S.; Campagna S. A Heptanuclear Light-Harvesting Metal-based Antenna Dendrimer with Six Ru(II)-Based Chromophores Directly Powering a Single Os(II)-Based Energy Trap. *Dalton Trans.* **2016**, *45*, 19238-19241.
- (11) Rupp, M. T.; Shevchenko, N.; Hanan, G. S.; Kurthb D. G. Enhancing the Photophysical Properties of Ru(II) Complexes by Specific Design of Tridentate Ligands. *Coord. Chem. Rev.* **2021**, *446*, 214127.
- (12) Medlycott E. A.; Hanan, G. S. Synthesis and Properties of Mono- and Oligo-nuclear Ru(II) Complexes of Tridentate Ligands: The Quest for Long-lived Excited States at Room Temperature. *Coord. Chem. Rev.* **2006**, *250*, 1763-1782.

- (13) Passalacqua, R.; Loiseau, F.; Campagna, S.; Fang, Y.-Q.; Hanan, G. S. In Search of Ruthenium(II) Complexes Based on Tridentate Polypyridine Ligands that Feature Long-lived Room-Temperature Luminescence: The Multichromophore Approach. *Angew. Chem. Int. Ed.* **2003**, *42*, 1608-1611.
- (14) Sahoo, A.; Ahmed, T.; Deb, S.; Baitalik, S. Neuro-Fuzzification Architecture for Modeling of Electrochemical Ion-Sensing Data of Imidazole-Dicarboxylate-Based Ru (II)-Bipyridine Complex. *Inorg. Chem.* **2022**, *61*, 10242-10254.
- (15) Daly, B.; Ling, J.; de Silva, A. P. Current Developments in Fluorescent PET (Photoinduced Electron Transfer) Sensors and Switches. *Chem. Soc. Rev.* **2015**, *44*, 4203-4211.
- (16) de Silva, A. P.; Fox, D. B.; Huxley, A. J. M.; Moody, T. S. Combining Luminescence, Coordination and Electron Transfer for Signalling Purposes. *Coord. Chem. Rev.* **2000**, *205*, 41-57.
- (17) Mukherjee, S.; Sahoo, A.; Deb, S.; Baitalik, S. Light and Cation-Driven Optical Switch Based on a Stilbene Appended Terpyridine System for the Design of Molecular-Scale Logic Devices. *J. Phys. Chem. A.* **2021**, *125*, 8261-8273.
- (18) Pal, P.; Sahoo, A.; Paul, A.; Baitalik, S. Anion and Light Responsive Molecular Switches Based on Stilbene Appended Ru(II) Terpyridyl Imidazole Complexes that Mimic Advanced Boolean and Fuzzy Logic Operations. *Euro. Jour. Inorg. Chem.* **2022**, *21*, e202200219.
- (19) de Jong, J. J. D.; Lucas, L. N.; Kellogg, R. M.; van Esch, J. H.; Feringa, B. L. Reversible Optical Transcription of Supramolecular Chirality into Molecular Chirality. *Science* **2004**, *304*, 278-281.
- (20) Eelkema, R.; Pollard, M. M.; Vicario, J.; Katsonis, N.; Ramon, B. S.; Bastiaansen, C. W. M.; Broer, D. J.; Feringa, B. L. Nanomotor Rotates Microscale Objects. *Nature* **2006**, *440*, 163-163.
- (21) Kobatake, S.; Takami, S.; Muto, H.; Ishikawa, T.; Irie, M. Rapid and Reversible Shape Changes of Molecular Crystals on Photoirradiation. *Nature* **2007**, *446*, 778-781.
- (22) Ichimura, K.; Oh, S. K.; Nakagawa, M. Light-Driven Motion of Liquids on a Photoresponsive Surface. *Science* **2000**, *288*, 1624-1626.
- (23) Feringa, B. L.; van Delden, R. A.; Koumura, N.; Geertsema, E. M. Chiroptical Molecular Switches. *Chem. Rev.* **2000**, *100*, 1789-1816.

- (24) Yutaka, T.; Mori, I.; Kurihara, M.; Mizutani, J.; Tamai, N.; Kawai, T.; Irie, M.; Nishihara, H. Photoluminescence Switching of Azobenzene-Conjugated Pt(II) Terpyridine Complexes by Trans-Cis Photoisomerization. *Inorg. Chem.* **2002**, *41*, 7143-7150.
- (25) Yam, V.W.W.; Lau, V. C. Y.; Wu, L. X. Synthesis, Photophysical, Photochemical and Electrochemical Properties of Rhenium(I) Diimine Complexes with Photoisomerizable Pyridyl-azo, -ethenyl or -ethyl Ligands. *J. Chem. Soc. Dalton Trans.* **1998**, 1461–1468.
- (26) Gindensperger, E.; Koppel, H.; Daniel, C. Mechanism of Visible-light Photoisomerization of a Rhenium(I) Carbonyl-Diimine Complex. *Chem. Commun.* **2010**, *46*, 8225-8227.
- (27) Waldeck, D. H. Photoisomerization Dynamics of Stilbenes. *Chem. Rev.* **1991**, *91*, 415-436.
- (28) Kayanuma, M.; Daniel, C.; Koppel, H.; Gindensperger, E. Photophysics of Isomerizable Re(I) Complexes: A Theoretical Analysis. *Coord. Chem. Rev.* **2011**, *255*, 2693-2703.
- (29) Kayanuma, M.; Gindensperger, E.; Daniel, C. Inorganic Photoisomerization: The Case Study of Rhenium(I) Complexes. *Dalton Trans.* **2012**, *41*, 13191-13203.
- (30) Bossert, J.; Daniel, C. Trans-Cis Photoisomerization of the Styrylpyridine Ligand in $[\text{Re}(\text{CO})_3(2,2'\text{-bipyridine})(t\text{-4-styrylpyridine})]^+$: Role of the Metal-to-Ligand Charge-Transfer Excited States. *Chem. Eur. J.* **2006**, *12*, 4835- 4843.
- (31) Yam, V. W. W.; Yang, Y.; Zhang, J.; Chu, B. W. K.; Zhu, N. Synthesis, Characterization, and Photoisomerization Studies of Azo- and Stilbene-Containing Surfactant Rhenium(I) Complexes. *Organometallics* **2001**, *20*, 4911-4918.
- (32) Kume, S.; Nishihara, H. Metal-based Photoswitches Derived from Photoisomerization. *Struct. Bonding* **2007**, *123*, 79–112.
- (33) Ko, C. C.; Yam, V. W. W. Transition Metal Complexes with Photochromic Ligands-Photosensitization and Photoswitchable Properties. *J. Mater. Chem.* **2010**, *20*, 2063-2070.
- (34) Ronaldo, C.; Amaral, A. B.; Iha N. Y. M. Molecular Engineered Rhenium(I) Carbonyl Complexes to Promote Photoisomerization of Coordinated Stilbene-like Ligands in the Visible Region. *Dalton Trans.* **2018**, *47*, 13081–13087.

- (35) Faustino, L. A.; Machado, A. E. H.; Patrocínio, A. O. T. Photochemistry of fac-[Re(CO)₃(dcbH₂)(trans-stpy)]⁺: New Insights on the Isomerization Mechanism of Coordinated Stilbene-like Ligands. *Inorg. Chem.* **2018**, *57*, 2933–2941.
- (36) Duan, G.; Yam, V. W. W. Syntheses and Photophysical Properties of N-Pyridylimidazol-2-ylidene Tetracyano ruthenates(II) and Photochromic Studies of Their Dithienylethene-Containing Derivatives. *Chem. Eur. J.* **2010**, *16*, 12642–12649.
- (37) Sun, S. S.; Lees, A. J. Synthesis, Photophysical Properties, and Photoinduced Luminescence Switching of Trinuclear Diimine Rhenium(I) Tricarbonyl Complexes Linked by an Isomerizable Stilbene-like Ligand. *Organometallics* **2002**, *2*, 39–49.
- (38) Irie, M. Diarylethenes for Memories and Switches. *Chem. Rev.* **2000**, *100*, 1685–1716.
- (39) Ikeda, T.; Tsutsumi, O. Optical Switching and Image Storage by Means of Azobenzene Liquid-Crystal Films. *Science* **1995**, *268*, 1873–1875.
- (40) Matos, L. S.; Amaral, R. C.; Iha, N. Y. M. Visible Photosensitization of trans-Styrylpyridine Coordinated to fac-[Re(CO)₃(dcbH₂)]⁺: New Insights. *Inorg. Chem.* **2018**, *57*, 9316–9326.
- (41) Polo, A. S.; Itokazu, M. K.; Frin, K. M.; Patrocínio, A. O. T.; Iha, N. Y. M. Light driven *Trans*-to-*Cis* Isomerization of Stilbene-like Ligands in fac-[Re(CO)₃(NN)(*trans*-L)]⁺ and Luminescence of their Photoproducts. *Coor. Chem. Rev.* **2006**, *250*, 1669–1680.
- (42) Tian, H.; Yang, S. Recent Progresses on Diarylethene Based Photochromic Switches. *Chem. Soc. Rev.* **2004**, *33*, 85–97.
- (43) Zanoni, K. P. S.; Iha, N. Y. M. Reversible *Trans* ⇌ *Cis* Photoisomerizations of [Re(CO)₃(ph₂phen)(stpyCN)]⁺ Towards Molecular Machines. *Dalton Trans.* **2017**, *46*, 9951–9958.
- (44) Pal, P.; Mukherjee, S.; Maity, D.; Baitalik, S. Synthesis, Structural Characterization, and Luminescence Switching of Diarylethene-Conjugated Ru(II)-Terpyridine Complexes by *Trans*-*Cis* Photoisomerization: Experimental and DFT/TD-DFT Investigation. *Inorg. Chem.* **2018**, *57*, 5743–5753.

- (45) Pal, P.; Ganguly, T.; Maity, D.; Baitalik, S. Experimental and Theoretical Exploration of Photophysics and *Trans-Cis* Photoisomerization of Styrylbenzene Conjugated Terpyridine Complexes of Ru(II): Strong Effect of Deprotonation from Second Coordination Sphere. *J. Photochem. Photobiol. A*. **2020**, 392, 112409.
- (46) Pal P.; Mukherjee, S.; Maity, D.; Baitalik, S. Synthesis, Photophysics, and Switchable Luminescence Properties of a New Class of Ruthenium(II)-Terpyridine Complexes Containing Photoisomerizable Styrylbenzene Units. *ACS Omega* **2018**, 3, 14526-14537.
- (47) Juris, A.; Balzani, V.; Barigelletti, F.; Campagna, S.; Belser, P.; von Zelewsky, A. Ru(II) Polypyridine Complexes: Photophysics, Photochemistry, Electrochemistry, and Chemiluminescence. *Coord. Chem. Rev.* **1988**, 84, 85–277.
- (48) Balzani, V.; Juris, A.; Venturi, M.; Campagna, S.; Serroni, S. Luminescent and Redox-active Polynuclear Transition Metal Complexes. *Chem. Rev.* **1996**, 96, 759-834.
- (49) Sauvage, J. P.; Collin, J. P. J.; Chambron, C.; Guillerez, S.; Coudret, C.; Balzani, V.; Barigelletti, F.; De Cola, L.; Flamigni, L. Ruthenium(II) and Osmium(II) bis(terpyridine) Complexes in Covalently-linked Multicomponent Systems: Synthesis, Electrochemical Behavior, Absorption Spectra, and Photochemical and Photophysical Properties. *Chem. Rev.* **1994**, 94, 993–1019.
- (50) Winkler, J. R.; Netzel, T.; Creutz, C.; Sutin, N. Direct Observation of Metal-to-Ligand Charge-Transfer (MLCT) Excited States of Pentaammineruthenium(II) Complex. *J. Am. Chem. Soc.* **1987**, 109, 2381-2392.
- (51) Mondal, D.; Bar, M.; Mukherjee, S.; Baitalik, S. Design of Ru(II) Complexes Based on Anthraimidazoledione Functionalized Terpyridine Ligand for Improvement of Room Temperature Luminescence Characteristics and Recognition of Selective Anions: Experimental and DFT/TD-DFT Study. *Inorg. Chem.* **2016**, 55, 9707-9724.
- (52) Karmakar, S.; Maity, D.; Mardanya, S.; Baitalik, S. Multichromophoric Bimetallic Ru(II) Terpyridine Complexes Based on Pyrenyl-bis-phenylimidazole Spacer: Synthesis, Photophysics, Spectroelectrochemistry, and TD-DFT Calculations. *Inorg. Chem.* **2014**, 53, 12036-12049.

- (53) Paul, A.; Bar, M.; Deb, S.; Baitalik, S. Long-Lived Trimetallic Complexes of Fe(II), Ru(II), and Os(II) Based on a Heteroditopic Bipyridine–Terpyridine Bridge: Synthesis, Photophysics, and Electronic Energy Transfer. *Inorg. Chem.* **2019**, *58*, 10065-10077.
- (54) Deb, S.; Sahoo, A.; Pal, P.; Baitalik, S. Exploitation of the Second Coordination Sphere to Promote Significant Increase of Room-Temperature Luminescence Lifetime and Anion Sensing in Ruthenium–Terpyridine Complexes. *Inorg. Chem.* **2021**, *60*, 6836-6851.
- (55) Duati, M.; Tasca, S.; Lynch, F. C.; Bohlen, H.; Vos, J. G. Enhancement of Luminescence Lifetimes of Mononuclear Ruthenium(II)–Terpyridine Complexes by Manipulation of the σ -Donor Strength of Ligands. *Inorg. Chem.* **2003**, *42*, 8377-8384.
- (56) Robson, K. C. D.; Koivisto, B.D.; Gordon, T. J.; Baumgartner, T.; Berlinguette, C. P. Triphenylamine-Modified Ruthenium(II) Terpyridine Complexes: Enhancement of Light Absorption by Conjugated Bridging Motifs. *Inorg. Chem.* **2010**, *49*, 5335-5337.
- (57) Brown, D. G.; Sanguantrakun, N.; Schulze, B.; Schubert, U. S.; Berlinguette, C. P. Bis(tridentate) Ruthenium–Terpyridine Complexes Featuring Microsecond Excited-State Lifetimes. *J. Am. Chem. Soc.* **2012**, *134*, 12354-12357.
- (58) Fan, W. J.; Sun, B.; Ma, J.; Li, X.; Tan, H.; Xu, L. Coordination-Driven Self-Assembly of Carbazole-Based Metallodendrimers with Generation-Dependent Aggregation Induced Emission Behavior. *Chem. Eur. J.* **2015**, *21*, 12947-12959.
- (59) Zhao, Z.; Zhang, H.; Lam, J. W. Y. Tang, B. Z. Aggregation-Induced Emission: New Vistas at the Aggregate Level. *Angew. Chem. Int. Ed.* **2020**, *59*, 9888-9907.
- (60) Prasad, P.; Gupta A.; Sasmal, P. K. Aggregation-Induced Emission Active Metal Complexes: A Promising Strategy to Tackle Bacterial Infections. *Chem. Commun.* **2021**, *57*, 174-186.
- (61) Goswami, N.; Yao, Q.; Luo, Z.; Li, J.; Chen, T.; Xie, J. Luminescent Metal Nanoclusters with Aggregation-Induced Emission. *J. Phys. Chem. Lett.* **2016**, *7*, 962-975.
- (62) Alama, P.; Climent, C.; Alemany, P.; Laskar, I. R. “Aggregation-Induced Emission” of Transition Metal Compounds: Design, Mechanistic Insights, and Applications. *J. Photochem. Photobiol. C: Photochem. Rev.* **2019**, *41*, 100317.

- (63) Yan, X.; Wang, H.; Hauke, C. E.; Cook, T. R.; Wang, M.; Saha, M. L.; Zhou, Z.; Zhang, M.; Li, X.; Huang, F.; Stang, P. J. A Suite of Tetraphenylethylene-Based Discrete Organoplatinum(II) Metallacycles: Controllable Structure and Stoichiometry, Aggregation-Induced Emission, and Nitroaromatics Sensing. *J. Am. Chem. Soc.* **2015**, *137*, 15276-15286.
- (64) Ravotto, L.; Ceroni, P. Aggregation Induced Phosphorescence of Metal Complexes: from Principles to Applications. *Coord. Chem. Rev.* **2017**, *346*, 62-76.
- (65) Yan, X.; Cook, T. R.; Wang, P.; Huang, F.; Stang, P. J. Highly Emissive Platinum(II) Metallacages. *Nat. Chem.* **2015**, *7*, 342-348.
- (66) Cheng, H. K.; Yeung, M. C. L.; Yam, V. W. W. Molecular Engineering of Platinum(II) Terpyridine Complexes with Tetraphenylethylene-Modified Alkynyl Ligands: Supramolecular Assembly via Pt···Pt and/or π - π Stacking Interactions and the Formation of Various Superstructures. *ACS Appl. Mater. Interfaces*, **2017**, *9*, 36220-36228.
- (67) Law, A. S. Y.; Lee, L. C. C.; Lo, K. K.-W.; Yam, V. W.W. Aggregation and Supramolecular Self-Assembly of Low-Energy Red Luminescent Alkynylplatinum(II) Complexes for RNA Detection, Nucleolus Imaging, and RNA Synthesis Inhibitor Screening. *J. Am. Chem. Soc.* **2021**, *143*, 5396-5405.
- (68) Yam, V. W. W. Chan, K. H. Y.; Wong, K. M.C.; Zhu, N. Luminescent Platinum(II) Terpyridyl Complexes: Effect of Counter Ions on Solvent-Induced Aggregation and Color Changes. *Chem. Eur. J.* **2005**, *11*, 4535-4543.
- (69) Luo, J.; Xie, Z.; Lam, J. W. Y.; Cheng, L.; Tang, B. Z.; Chen, H.; Qiu, C.; Kwok, H. S.; Zhan, X.; Liu, Y. Aggregation-Induced Emission of 1-Methyl-1,2,3,4,5-Pentaphenylsilole. *Chem. Commun.* **2001**, 1740-1741.
- (70) Ren, Y.; Lam, J. W. Y.; Dong, Y.; Tang, B. Z.; Wong, K. S. Enhanced Emission Efficiency and Excited State Lifetime Due to Restricted Intramolecular Motion in Silole Aggregates. *J. Phys. Chem. B* **2005**, *109*, 1135-1140.
- (71) Leung, N. L. C.; Xie, N.; Yuan, W.; Liu, Y.; Wu, Q.; Peng, Q.; Miao, Q.; Lam, J. W. Y.; Tang, B. Z. Restriction of Intramolecular Motions: The General Mechanism Behind Aggregation-Induced Emission. *Chem. Eur. J.* **2014**, *20*, 15349-15353.
- (72) An, B. K.; Kwon, S. K.; Jung, S. D.; Park, S. Y. Enhanced Emission and Its Switching in Fluorescent Organic Nanoparticles. *J. Am. Chem. Soc.* **2002**, *124*, 14410-14415.

- (73) Babua , E.; Mareeswaran, P. M.; Krishnan, M. M.; Sathish , V.; Thanasekarand, P.; Rajagopal , S. Unravelling the Aggregation Induced Emission Enhancement in Tris(4,7- diphenyl-1,10-phenanthroline)Ruthenium(II) complex. *Inorg. Chem. Commun.* **2018**, 98 , 7-10.
- (74) Patra , S. K.; Sen , B.; Rabha, M.; Khatua , S.; An aggregation-Induced Emission-Active bis-heteroleptic Ruthenium(II) Complex of Thiophenyl Substituted Phenanthroline for the Selective “Turn-Off” Detection of Picric acid. *New J. Chem.*, **2022**, 46, 169-177.
- (75) Chen, Y.; Xu, W. C.; Kou, J.-F.; Yu, B. L.; Wei, X.H.; Chao , H.; Ji , L.N. Aggregation-Induced Emission of Ruthenium(II) Polypyridyl Complex $[\text{Ru}(\text{bpy})_2(\text{pzta})]^{2+}$. *Inorg. Chem. Commun.*, **2010**, 13, 1140-1143.
- (76) Sheet, S. K.; Sen, B.; Patra, S. K.; Rabha, M.; Aguan, K.; Khatua, S. Aggregation-Induced Emission-Active Ruthenium(II) Complex of 4,7- Dichloro Phenanthroline for Selective Luminescent Detection and Ribosomal RNA Imaging. *ACS Appl. Mater. Interfaces* **2018**, 10, 14356-14366.
- (77) Lu, L.; Zhang, L.; Miao, W.; Wang, X.; Guo, G.; Aggregation-Induced Electrochemiluminescence of the Dichlorobis(1,10-phenanthroline)ruthenium(II) ($\text{Ru}(\text{phen})_2\text{Cl}_2$)/ Tri-n-propylamine (TPrA) System in H_2O -MeCN Mixtures for Identification of Nucleic Acids. *Anal. Chem.* **2020**, 92, 9613-9619.
- (78) Xu, H.; Zhang, X.; Lib, X.; Zhang, X.; Deng, J.; Zou, D.; Yang, J. Two Ru(II) Compounds with Aggregation Induced Emission as Promising Photosensitizers for Photodynamic Therapy. *J. Inorg. Biochem.* **2020**, 212 , 111233.
- (79) Yang, J.; Li,L.; Yu,Y.; Ren, Z.; Peng, Q.; Ye, S.; Lia, Q.; Li, Z.; Blue Pyrene-based AIEgens: Inhibited Intermolecular p–p Stacking through the Introduction of Substituents with Controllable Intramolecular Conjugation, and High External Quantum Efficiencies up to 3.46% in Non-doped OLEDs. *Mater. Chem. Front.* **2017**, 1, 91-99.
- (80) Wang , L. L.; Zhou , H.; Yang, T. L.; Ke, H.; Tu, Y. K.; Yao, H.; Jiang, W. Bis-Naphthalene Cleft with Aggregation-Induced Emission Properties through Lone-Pair $\cdots\pi$ Interactions. *Chem. Eur. J.* **2018**, 24, 16757 -16761.
- (81) Banerjee, S.; Both, A. K.; Sarkar, M.; Probing the Aggregation and Signaling Behavior of Some Twisted 9,9'-Bianthryl Derivatives: Observation of Aggregation-Induced Blue-Shifted Emission. *ACS Omega* **2018**, 3, 15709-15724.

- (82) Ganguly, T.; Pal, P.; Paul, A.; Baitalik, S. Synthesis and Manifold but Controllable Emission Switching of Stilbene Appended Terpyridine Derivatives Coupled with Anthracene, Naphthalene and Pyrene Units via Aggregation and Trans-Cis Isomerization. *J. of Photochem. & Photobiol. A: Chem.* **2022**, *430*, 113966.
- (83) Bossert, J.; Daniel, C.; Electronic Absorption Spectroscopy of $[\text{Ru}(\text{phen})_2(\text{bpy})]^{2+}$, $[\text{Ru}(\text{phen})_2(\text{dmbp})]^{2+}$, $[\text{Ru}(\text{tpy})(\text{phen})(\text{CH}_3\text{CN})]^{2+}$ and $[\text{Ru}(\text{tpy})(\text{dmp})(\text{CH}_3\text{CN})]^{2+}$ A Theoretical Study. *Coord. Chem. Rev.* **2008**, *252*, 2493-2503.
- (84) Sun, Y.; Turro, C. Highly Solvent Dependent Luminescence from $[\text{Ru}(\text{bpy})_n(\text{dppp}2)_{3-n}]^{2+}$ ($n = 0-2$). *Inorg. Chem.* **2010**, *49*, 5025-5032.
- (85) Reichardt, C.; Pinto, M.; Wachtler, M.; Stephenson, M.; Kupfer, S.; Sainuddin, T.; Guthmuller, J.; McFarland, S. A.; Dietzek, B. Photophysics of Ru(II) Dyads Derived from Pyrenyl-Substituted Imidazo[4,5-f][1,10]phenanthroline ligands. *J. Phys. Chem. A* **2015**, *119*, 3986-3994.
- (86) Yao, C. J.; Nie, H. J.; Yang, W. W.; Yao, J.; Zhong, Y.W. Combined Experimental and Computational Study of Pyren-2,7-Diyl Bridged Diruthenium Complexes with Various Terminal Ligands. *Inorg. Chem.* **2015**, *54*, 4688-4698.
- (87) Sauvage, J. P.; Collin, J. P. J.; Chambron, C.; Guillerez, S.; Coudret, C.; Balzani, V.; Barigelletti, F.; De Cola, L.; Flamigni, L. Ruthenium(II) and Osmium(II) bis(terpyridine) Complexes in Covalently-linked Multicomponent Systems: Synthesis, Electrochemical Behavior, Absorption Spectra, and Photochemical and Photophysical Properties. *Chem. Rev.* **1994**, *94*, 993-1019.
- (88) Browne, W. R.; O'Boyle, N. M.; McGarvey, J. J.; Vos, J. G. Elucidating Excited State Electronic Structure and Intercomponent Interactions in Multicomponent and Supramolecular Systems. *Chem. Soc. Rev.* **2005**, *34*, 641-663.
- (89) Pal, A. K.; Hanan, G. S. Design, Synthesis and Excited-State Properties of Mononuclear Ru(II) Complexes of Tridentate Heterocyclic Ligands. *Chem. Soc. Rev.* **2014**, *43*, 6184-6197.
- (90) Harriman, A.; Khatyr, A.; Ziessel, R.; Extending the Luminescence Lifetime of Ruthenium(II) Poly(pyridine) Complexes in Solution at Ambient Temperature. *Dalton Trans.* **2003**, 2061-2068.
- (91) Suzuki, S.; Sasaki, S.; Sairi, A. S.; Iwai, R.; Tang, B. Z.; Konishi, G. Principles Of Aggregation-Induced Emission: Design of Deactivation Pathways for Advanced AIEgens and Applications. *Angew. Chem. Int. Ed.* **2020**, *59*, 9856-9867.

- (92) Balasaravanan, R.; Siva, A. Synthesis, Characterization and Aggregation Induced Emission Properties of Anthracene Based Conjugated Molecules. *New J. Chem.* **2016**, *40*, 5099-5106.
- (93) Leung, N. L. C.; Xie, N.; Yuan, W.; Liu, Y.; Wu, Q.; Peng, Q.; Miao, Q.; Lam, J. W. Y.; Tang, B. Z. Restriction of Intramolecular Motions: The General Mechanism Behind Aggregation-Induced Emission. *Chem. Eur. J.* **2014**, *20*, 15349-15353.
- (94) Islam, M. M.; Hu, Z.; Wang, Q.; Redshaw, C.; Feng, X. Pyrene-Based Aggregation-Induced Emission Luminogens and their Applications. *Mater. Chem. Front.*, **2019**, *3*, 762-781.



Chapter 4

**Luminescent Ruthenium-Terpyridine
Complexes Coupled with Stilbene-Appended
Naphthalene, Anthracene and Pyrene Motifs
Demonstrate Fluoride Ion Sensing and
Reversible Trans-Cis Photoisomerization**

4.1 Introduction

Non-covalent interactions comprising of hydrogen bonding, π - π stacking, CH- π , cation- π and anion- π interactions have orchestrated immense attention in diverse fields of supramolecular chemistry and structural biology.¹⁻¹⁰ Although these forces are weak, their appearances are manifested in manifold interdisciplinary areas that encompass material science, catalysis, crystal engineering, and biology.¹¹⁻¹⁹ This sort of interaction is responsible for maintaining the basic structures of vital living organisms such as DNA, RNA, and protein.²⁰⁻²³ The occurrence of this type of weak interactions also introduces a new horizon in the field of supramolecular chemistry of anions such as anion-recognition and sensing, anion transport and many more.²⁴⁻²⁸

In this work, our aim is to recognize specific anions through the intermediacy of various non-covalent interactions, viz. hydrogen bonding, CH- π , anion- π and π - π stacking.²⁹⁻³¹ In order to achieve our objective, we employed herein Ru(II) complexes of polyheterocyclic ligands as they offer multiple optical channels to visualize the receptor-anion interplay.³²⁻⁴¹ Polypyridine-based Ru(II) complexes have been employed as the potential building blocks in numerous applications such as dye-sensitized solar cells, multi-channel sensors and switches as well as the active components in photochemical molecular devices and machines, by taking advantage of their robustness and favourable photophysical, photochemical, and electrochemical properties.⁴²⁻⁴⁸ Two categories of polypyridine ligands are usually employed to design the Ru(II) complexes, viz. bipyridine-type ($[\text{Ru}(\text{bpy})_3]^{2+}$, bpy = 2,2'-bipyridine) and terpyridine-type ($[\text{Ru}(\text{tpy})_2]^{2+}$, (tpy=2,2':6',2''-terpyridine). The photophysical and in particular the luminescence properties of $[\text{Ru}(\text{bpy})_3]$ -type derivatives are far superior because of suitable disposition of their lowest-lying emissive triplet metal-to-ligand charge transfer ($^3\text{MLCT}$) state that are well apart from the non-emitting triplet metal-centered (^3MC) state.⁴⁹⁻⁵⁰ But the bpy-type ligand always produces the octahedral complexes with mixtures of isomers (Δ and Λ), the separation of which is very tedious. On the other hand, the terpyridine-type ligand always yields rod-like octahedral complexes devoid of isomeric impurity, but the major shortcoming is their inferior RT emission characteristics due to smaller $^3\text{MLCT}$ - ^3MC energy barrier arising out of unfavorable bite angle of the terpyridines.⁵¹⁻⁵² Thereupon, the strategic design of ancillary ligand is indispensable since they play a decisive role in regulating the energetic aspects of the excited states that eventually dictates the emission properties.⁵³⁻⁵⁸

Herein, we have designed a new family of emissive stilbene-appended Ru(II)-terpyridine complexes of the type, $[(\text{tpy-PhCH}_3)\text{Ru}(\text{tpy-pvp-X})](\text{ClO}_4)_2$, consisting of a polyaromatic hydrocarbon unit (X) such as anthracene, naphthalene and pyrene at the 4' position of the terpyridines (Chart 4.1). The polyaromatic hydrocarbon along with stilbene moiety is expected to have their $^3\pi\text{-}\pi^*$ state which is quasi-isoelectronic to the $^3\text{MLCT}$ state in the complex entity. Upon photo-excitation, reversible intercomponent energy transfer is feasible between $^3\text{MLCT}$ and $^3\pi\text{-}\pi^*$ states so that the adjoining polyaromatic chromophores can act as an energy reservoir so as to repopulate the emissive $^3\text{MLCT}$ state, with an overall effect of ‘delaying’ the emission giving long-lived excited-state.⁵⁹⁻⁶¹ Thus, it is expected that the resulting metal-ligand complex assembly will be emissive at RT with reasonably long lifetime. In practice, the complexes feature moderately intense emission at RT having lifetime of 16.7 ns for naphthalene-, 11.4 ns for anthracene-, while substantially elevated lifetime of 8.3 μs for pyrene derivative.

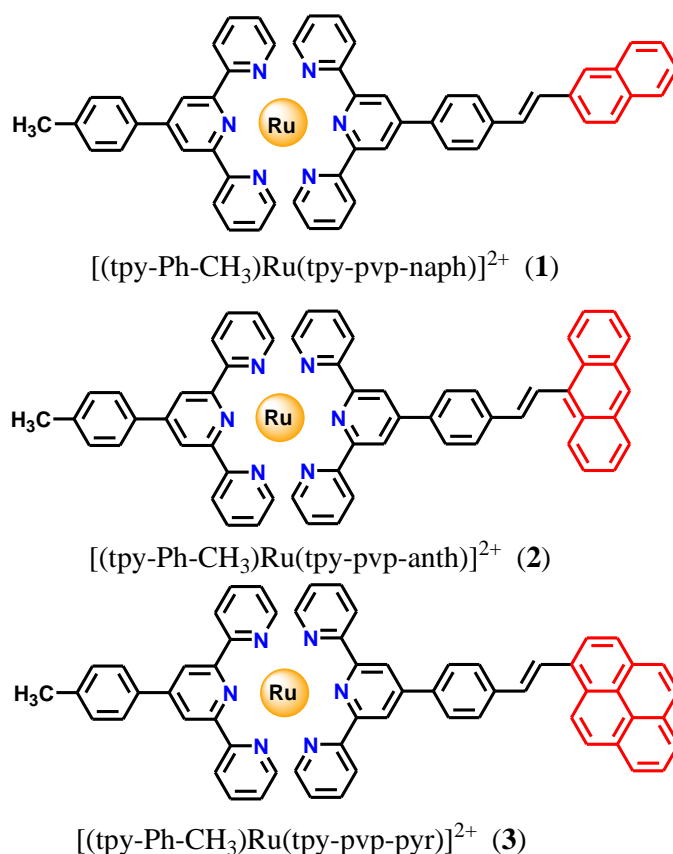


Chart 4.1. The molecular architectures of the complexes.

It is expected that upon complexation with Ru^{2+} ion, the terpyridine- as well as other aromatic protons (C-H groups) could be acidic and capable to take part in $\text{C-H}\cdots\text{A}^-$ (A^- =anion) type of hydrogen bonding interaction. Additionally, by virtue of the presence of delocalized π -acidic electron cloud, the complexes in principle could interact with selected anions via anion- π interactions. This sort of interaction is typically weak non-covalent forces that arise from the electrostatic attraction between the negatively charged anion and the electron-deficient π cloud of the aromatic ring.⁶²⁻⁶⁶ Taking advantage of favorable photophysical and electrochemical properties together with multiple acidic C-H protons and electron-rich π -electron delocalized polyaromatic motifs, the anion sensing characteristics of the complexes have been thoroughly studied in this work through multiple optical channels and spectroscopic techniques. Anion recognition and sensing is important due to their crucial roles in chemical and biological events. We are particularly interested to sense F^- because of its duplicitous nature and also due to its relevance in biology and environment. A wide range of receptor bearing hydrogen bond donor motifs such as $\text{NH}_{\text{Urea/Thiourea}}$, $\text{NH}_{\text{Imidazole/Pyrrole/Indole}}$, NH_{Amide} and $\text{OH}_{\text{Phenol/Catechol}}$ have already been utilized as the main binding motifs in designing receptors and the detail functioning of which are deliberated in many reviews.⁶⁷⁻⁷³

As already pointed out, in the design tactic of the complexes, we have included a stilbene motif onto the complex backbone. Apart from inducing π -electron delocalization in the complex backbone for augmenting their RT emission features, the stilbene motif could induce trans-cis isomerization upon treatment with light.⁷⁴⁻⁷⁸ To this end, we have investigated the reversible trans-cis isomerization of the complexes upon alternate treatment of visible and UV light so that the complexes can act as potential photo-molecular switches. As trans \rightarrow cis transformation leads to conformation change of the polyaromatic moieties in the complexes, it is expected that the extent of non-covalent interactions that are operative in the complexes would be substantially altered on going from trans to the cis-isomer. Hence, we also carried out the anion sensing characteristics of the cis-form of the complexes and compared with those with their trans-forms. In conjunction with experimental investigation, theoretical calculation employing density function theory (DFT) is also executed for a selective complex to elucidate the involvement of different non-covalent interactions that are operative during complex-fluoride interplay.

4.2 Experimental Section

4.2.1 Materials. $\text{RuCl}_3 \cdot x\text{H}_2\text{O}$ and sodium perchlorate are procured from Merck. Other chemicals and solvents used in the present investigation are purchased from local vendors. Tpy-pvp-X (X=naphthalene, anthracene, and pyrene) ligands are prepared and characterized and is described in Chapter 2.⁷⁹

4.2.2 Synthesis of Metal Complexes. The metal complexes are prepared by using a common method as described below.

[(tpy-PhCH₃)Ru(tpy-pvp-naph)](ClO₄)₂·2H₂O (1). $[\text{Ru}(\text{tpy-PhCH}_3)\text{Cl}_3]$ (0.11 g, 0.21 mmol) and AgBF_4 (0.13 g, 0.72 mmol) were added to 40 mL of acetone and stirred under refluxing condition for ~3 h. The white solid of AgCl was quickly filtered out, and the filtrate was treated with ~40 mL of EtOH, and the remaining acetone was rotary evaporated. Tpy-pvp-naph ligand (0.10 g, 0.21 mmol) was then added in its finely powdered form to the solution and refluxed for 6h with continuous stirring under argon protection. The red compound that deposited upon cooling was collected by filtration and thoroughly washed with chloroform and dried. It was then dissolved in a small amount of MeOH and then poured in into an aqueous solution of $\text{NaClO}_4 \cdot \text{H}_2\text{O}$ (1.5g in 5 mL of water) and stirred until a red precipitate was formed. The compound was filtered and purified by silica gel column chromatography upon eluting with MeCN-PhCH₃ (10:1, v/v) mixture. The desired compound was collected upon evaporation to a small volume. Recrystallization of the complex from MeCN-MeOH (1:1, v/v) mixture was done for further purification (0.15 g, yield: 63%). Anal. calcd. for $\text{C}_{55}\text{H}_{44}\text{N}_6\text{Cl}_2\text{O}_{10}\text{Ru}$: C, 58.93; H, 3.95; N, 7.49. Found: C, 58.89; H, 3.98; N, 7.52%. Electrospray ionization mass spectrometry (ESI-MS) (positive, MeCN) m/z : 443.11 (100%) $[(\text{tpy-PhCH}_3)\text{Ru}(\text{tpy-pvp-naph})]^{2+}$. ¹H NMR (300 MHz, DMSO-*d*₆): δ /ppm 9.49 (s, 2H, 2H_{3''}), 9.43 (s, 2H, 2H_{3'''}), 9.09 (t, 4H, $J=8.0$ Hz, 2H₆+2H_{6'}), 8.51 (d, 2H, $J=8.1$ Hz, 2H₇), 8.34 (d, 2H, $J=8.1$ Hz, 2H_{7'}), 8.12 (s, 1H, 2H₁₇), 8.05-8.03 (m, 8H, 4H₄+4H_{4'}+4H₈+4H_{8'}), 7.97-7.92 (m, 3H, H₁₁+H₁₄+H₁₆), 7.72 (d, 1H, $J=16.5$ Hz, H₉), 7.63-7.53 (m, 8H, H₃+H_{3'}+H₁₀+H₁₂+H₁₃+H₁₅), 7.26 (t, 4H, $J=6.6$ Hz, 4H₅+H_{5'}), 2.51 (s, 3H, CH₃).

[(tpy-PhCH₃)Ru(tpy-pvp-anth)](ClO₄)₂·2H₂O (2). Yield 0.17 g (66%). Anal. Calcd. for $\text{C}_{59}\text{H}_{46}\text{N}_6\text{Cl}_2\text{O}_{10}\text{Ru}$: C, 60.51; H, 3.95; N, 7.17. Found: C, 75.48; H, 3.99; N, 7.21%. ESI-MS) (positive, MeCN) m/z : 468.04 (100%) $[(\text{tpy-PhCH}_3)\text{Ru}(\text{tpy-pvp-anth})]^{2+}$. ¹H NMR (300 MHz, DMSO-*d*₆): δ /ppm 9.55 (s, 2H, 2H_{3''}), 9.45 (s, 2H, 2H_{3'''}), 9.16-9.08 (m, 4H, 2H₆+2H_{6'}), 8.63 (s, 1H, H₁₅), 8.58 (d, 2H, $J=8.4$ Hz, 2H₇), 8.47-8.45 (m, 2H, 2H₁₂), 8.42 (d, 2H, $J=7.3$ Hz, 2H₁₄), 8.36 (d, 2H, $J=8.2$ Hz, 2H_{7'}), 8.22-8.14 (m, 4H, 2H₈+2H_{8'}), 8.09-8.03 (m, 4H,

2H₄+2H_{4'}), 7.61-7.51 (m, 9H, H₃+H_{3'}+H₉+H₁₁+H₁₃), 7.28 (t, 4H, $J=6.5$ Hz, 2H₅+2H_{5'}), 7.19 (d, 1H, $J=16.5$ Hz, H₁₀), 2.55 (s, 3H, CH₃).

[(tpy-PhCH₃)Ru(tpy-pvp-pyr)](ClO₄)₂·3H₂O (**3**). Yield 0.17 g, (65%). Anal. Calcd. for C₆₁H₄₈N₆Cl₂O₁₁Ru: C, 60.39; H, 3.98; N, 6.92. Found: C, 60.35; H, 4.02; N, 6.96%. ESI-MS (positive, MeCN) m/z : 480.13 (100%) [(tpy-PhCH₃)Ru(tpy-pvp-pyr)]²⁺. ¹H NMR (300 MHz, DMSO-*d*₆): δ /ppm 9.54 (s, 2H, 2H_{3''}), 9.45 (s, 2H, 2H_{3'''}), 9.16-9.08 (m, 4H, 2H₆+2H_{6'}), 8.90 (d, 1H, $J=9.5$ Hz, H₁₄), 8.68 (d, 1H, $J=16.2$ Hz, H₉), 8.66-8.61 (m, 2H, H₁₁+H₁₅), 8.56 (d, 4H, $J=8.4$ Hz, 2H₇+2H_{7'}), 8.39-8.22 (m, 10H, 2H₈+2H_{8'}+H₁₂+H₁₃+H₁₆+H₁₇+H₁₈+2H₁₉), 8.15-8.03 (m, 4H, 2H₈+2H_{8'}), 7.77 (d, 1H, $J=16.1$ Hz, H₁₀), 7.56 (d, 4H, $J=5.6$ Hz, H₃+H_{3'}), 7.28 (t, 4H, $J=6.5$ Hz, 2H₅+2H_{5'}), 2.58 (s, 3H, CH₃).

Caution! Perchlorate salts of the metal complexes are potentially explosive and therefore should be handled in small quantities with care.

4.2.3 Instruments and Physical Methods. Details of instruments and physico-chemical measurements are provided in Chapter 2 and Chapter 3.

4.3 Results and Discussion

4.3.1 Synthesis and Characterization. The detailed synthesis of the terpyridine ligands are described in Chapter 2.⁷⁹ The metal complexes are prepared by straightforward reaction between the ligands and solvated Ru(II)-terpyridine precursor, [(tpy-PhCH₃)Ru(Me₂CO)₃]³⁺, obtained upon treating [(tpy-PhCH₃)RuCl₃] with AgBF₄, followed by their ion exchange using sodium perchlorate. Purification of the complexes is executed by column chromatography and recrystallization from appropriate solvent(s). The complexes are fully characterized via elemental analysis as well as by ESI mass and NMR spectrometry.

4.3.2 Mass Spectra. The ESI mass spectra are acquired in MeCN. The isotopic distribution patterns of both experimental and simulated spectra of **1** and **3** are displayed in Figure 4.1. The correlation among the experimental and simulated spectra is quite good. Each complex exhibits a single abundant peak corresponding to [(tpy-PhCH₃)Ru(tpy-pvp-X)]²⁺ species, as the separation between consecutive lines is 0.5 Da in their isotopic distribution.

4.3.3 NMR Spectroscopy. The complexes are unambiguously characterised by ¹H NMR spectroscopy that are acquired in DMSO-*d*₆ and presented Figure 4.2. The use of terpyridine moiety resulted in stereoisomerically pure complexes which is evident from their well-defined spectral pattern. Tentative assignment of the protons are carried out with the aid

of $\{^1\text{H}-^1\text{H}\}$ COSY NMR spectra and by comparing the spectra of structurally related complexes (Figures 4.3). The singlet at ~ 9.50 ppm is assigned as $\text{H}_{3'}$, whereas the adjacent singlet arises for $\text{H}_{3''}$ proton. The olefinic protons lie within 7.61-7.77 ppm whereas the most up-field triplet peak is assigned to H_5 and $\text{H}_{5'}$. A coupling constant value of ~ 16 Hz for the olefinic protons (H_9 and H_{10}) is the testimony of their *transoid* conformation.

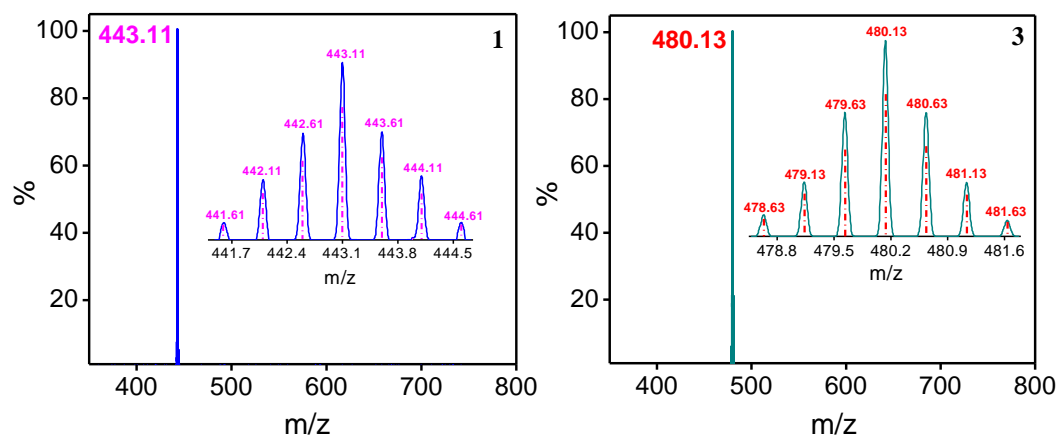


Figure 4.1. ESI (positive) mass spectrum for the complex cation of $[(\text{tpy}-\text{PhCH}_3)\text{Ru}(\text{tpy}-\text{pvp}-\text{naph})]^{2+}$ (**1**) ($m/z = 443.11$) and $[(\text{tpy}-\text{PhCH}_3)\text{Ru}(\text{tpy}-\text{pvp}-\text{pyr})]^{2+}$ (**3**) ($m/z = 480.13$) in MeCN.

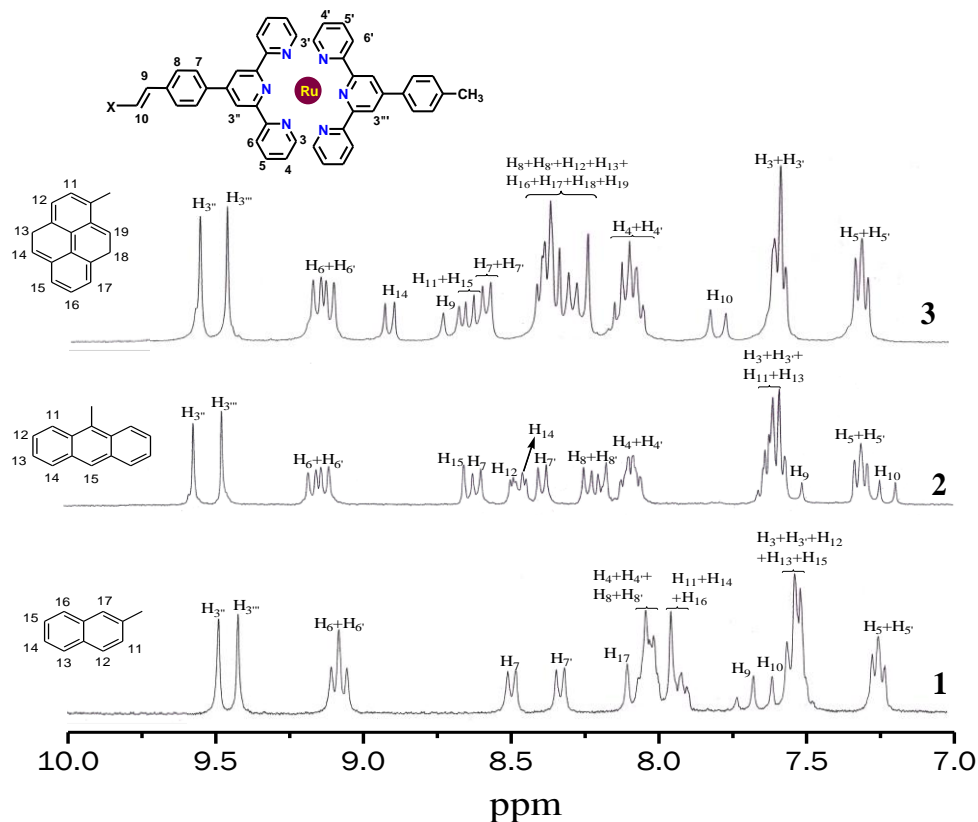


Figure 4.2. ^1H spectra of **1-3** in $\text{DMSO}-d_6$

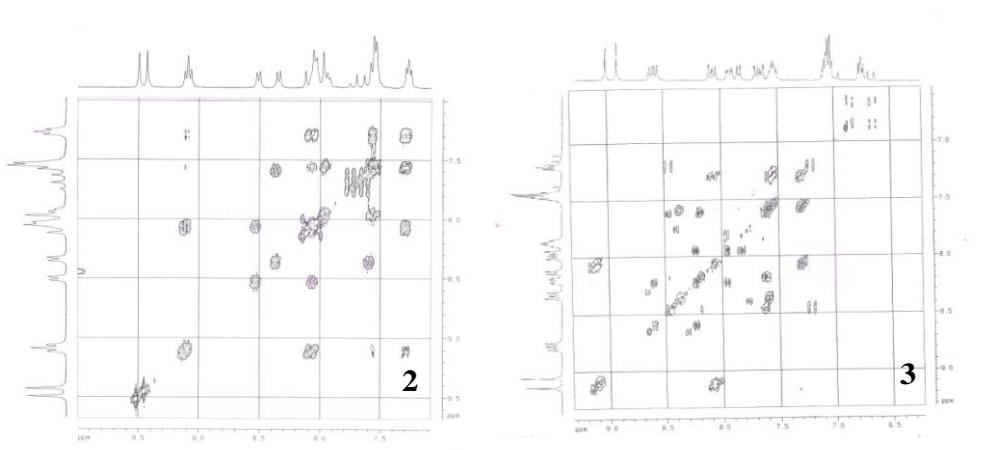


Figure 4.3. $\{^1\text{H}-^1\text{H}\}$ COSY NMR spectrum of **2** and **3** in $\text{DMSO}-d_6$.

4.3.4 Absorption Spectra. The spectra of isomolar solutions of **1-3** are acquired in MeCN and DMSO and relevant photophysical data are presented in Figure 4.4 and summarized in Table 4.1. The spectral pattern is mostly similar for all three complexes which comprise of very high intensity peaks in the UV and a moderately strong band in the visible domain Figure 4.4. Upon comparing the spectral pattern of structurally similar complexes of Ru(II), it appears that the lowest energy band located in the range of 490-494 nm (in MeCN) is primarily ruthenium→terpyridine charge transfer (MLCT) transitions. The next higher energy band in the range of 330-383 nm are mainly due to ILCT transitions, whereas very intense peaks below 330 nm are due to $\pi-\pi^*$ transitions in the polyaromatic and hetero-aromatic units.

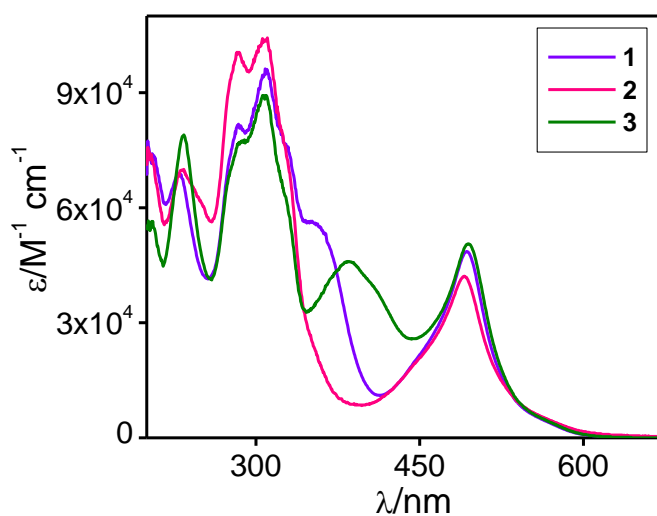


Figure 4.4. Absorption spectral profiles of **1-3** in MeCN.

Table 4.1. Photophysical data for **1-3**.

Comds		Absorption $\lambda_{\text{max}}/\text{nm}$ ($\epsilon/\text{M}^{-1}\text{cm}^{-1}$)	Luminescence				
			$\lambda_{\text{max}}/\text{nm}$	τ	Φ	k_r/s^{-1}	k_{nr}/s^{-1}
1	MeCN (298K)	493(48600), 355 (sh)(55700), 328(br)(76000), 309(95600), 283(sh)(81200), 230(69000)	662	$\tau_1 = 1.9 \text{ ns}$ $\tau_2 = 6.4 \text{ ns}$	3.3×10^{-3}	5.2×10^5	1.6×10^8
2		490(23400), 330(sh)(39000), 307(58100), 283(56500), 232(39200)	660	$\tau_1 = 1.4 \text{ ns}$ $\tau_2 = 4.8 \text{ ns}$	2.1×10^{-3}	4.3×10^5	2.1×10^8
3		494(35500), 383(br)(323000), 328(sh)(43400), 307(623000), 286(br)(545000), 233(55000)	745	$\tau_1 = 0.1 \mu\text{s}$ $\tau_2 = 3.4 \mu\text{s}$	0.4×10^{-3}	1.2×10^2	2.9×10^5
1	DMSO (298K)	500(52000), 370(br)(54000), 338(sh)(57500), 313(60000)	672	$\tau_1 = 3.4 \text{ ns}$ $\tau_2 = 16.7 \text{ ns}$	12.4×10^{-3}	7.4×10^5	5.9×10^7
2		499(45000), 333(br)(76000), 314(98000), 287(br) (81000)	658	$\tau_1 = 3.1 \text{ ns}$ $\tau_2 = 11.4 \text{ ns}$	6.3×10^{-3}	5.5×10^5	8.7×10^7
3		503(56000), 393(45000), 335(sh)(64000), 314(86000), 290(sh)(74000)	751	$\tau_1 = 1.2 \mu\text{s}$ $\tau_2 = 8.3 \mu\text{s}$	3.8×10^{-3}	4.6×10^2	1.2×10^5
1	77K	-	649	$29.0 \mu\text{s}$	0.5	1.6×10^4	1.8×10^4
2		-	629	$14.2 \mu\text{s}$	0.2	9.8×10^3	6.0×10^4
3		-	626	$12.6 \mu\text{s}$	0.1	4.7×10^3	7.4×10^4

4.3.5 Emission Spectra. The spectra of the complexes acquired in MeCN at RT and in MeOH/EtOH (1:4, v/v) glass at 77K are presented in Figure 4.5 and associated data are provided in Table 4.1. Upon excitation at the ¹MLCT band, **1** and **2** exhibit a broad and structureless emission band with peak maximum (λ_{max}) varying within the range of 660-672 nm at RT. By contrast, **3** exhibits very weak and broad emission band which is significantly red-shifted to the NIR region (~750 nm) in both solvents. Increase in solvent polarity from MeCN to DMSO results in bathochromic shift of λ_{max} value along with increase in quantum yields (Φ , Table 4.1). Upon purging thoroughly with nitrogen gas, substantial enhancement in emission intensity and Φ takes place in all cases (Figure 4.5 and Table 4.2). The change in the spectral pattern upon N₂ purging in case of pyrene derivative is quite different from the rest wherein the broad and weak band converged to a single gaussian type of peak together with red-shift as shown in Figure 4.5. Time-resolved emission decays for **1-3** measured under both aerated and deaerated conditions at RT are shown in Figure 4.6 and associated data are summarized in Table 4.1 and Table 4.2. Bi-exponential decay is observed in all cases at RT with the lifetime values being more or less similar for **1** and **2** ($\tau = 6.4 \text{ ns}$ for **1** and 4.9 ns for **2** in MeCN and $\tau = 16.7 \text{ ns}$ for **1** and 11.4 ns for **2** in DMSO). Complex **3**, on the other hand, displays an incredibly long lifetime value ($\tau = 3.4 \mu\text{s}$ in MeCN and $8.3 \mu\text{s}$ in DMSO). The

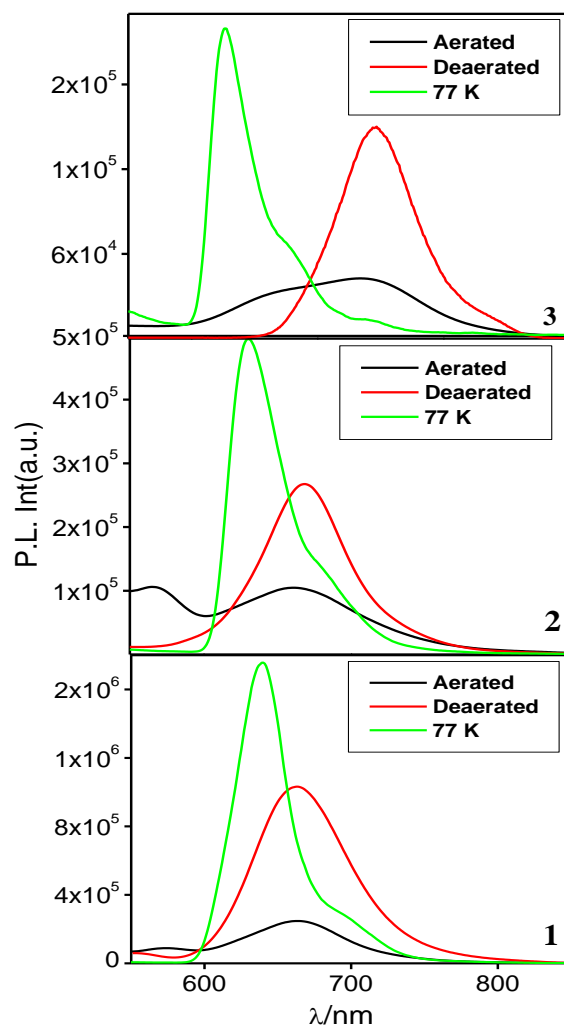


Figure 4.5. Luminescence spectral ($\lambda_{\text{ex}} = 500$ nm) profiles of **1-3** in MeCN at RT (aerated and deaerated) and in MeOH/EtOH (1:4, v/v) glass at 77K.

Table 4.2. Quantum yield and lifetime of **1-3** in MeCN.

compounds	$\Phi_{\text{deaerated}}$	$\tau_{\text{deaerated}}$
1	11.4×10^{-3}	$\tau_1 = 3.5$ ns, $\tau_2 = 15.7$ ns
2	2.8×10^{-3}	$\tau_1 = 0.3$ ns, $\tau_2 = 10.9$ ns
3	1.6×10^{-3}	$\tau_1 = 0.3$ μ s, $\tau_2 = 4.6$ μ s

polyaromatic hydrocarbons such as naphthalene, anthracene and pyrene possess a low-lying triplet state $\{^3(\pi-\pi^*)\}$ that is thought to be quasi-isoenergetic with the radiative $^3\text{MLCT}$ energy level of the Ru-tpy unit. Thus, a reversible inter-component excited-state energy transfer among the two equilibrated states ($^3\text{MLCT}$ and $^3\pi-\pi^*$) is a distinct possibility. Hence, the bi-exponential decay in both solvents is probably due to deactivation of the $^3\text{MLCT}$ state to give the short-lived component, while the relatively longer-lived component arises from the equilibrated state of $^3\text{MLCT}$ and $^3(\pi-\pi^*)$ state of stilbene-appended polyaromatic moiety.

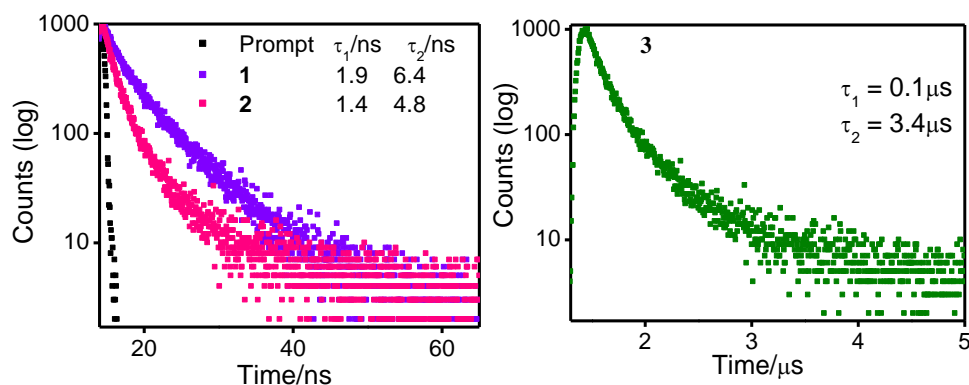
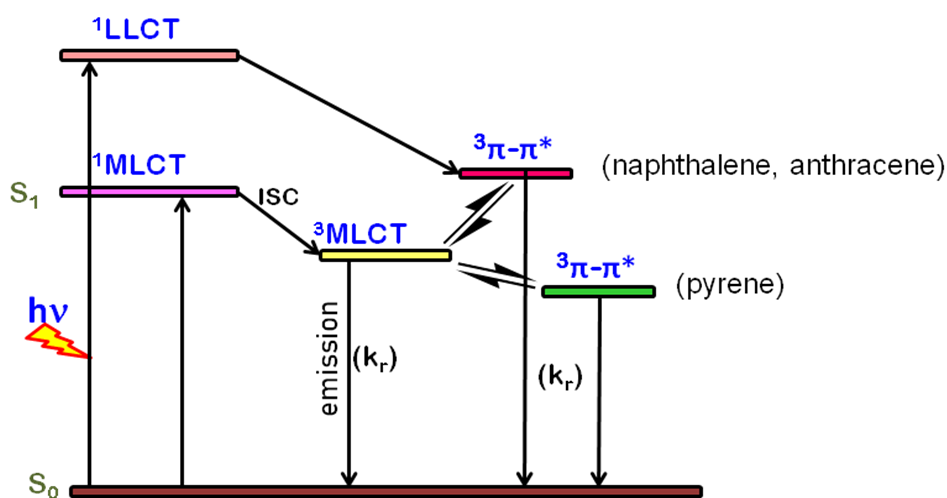


Figure 4.6. The emission decay ($\lambda_{\text{ex}} = 490$ nm) as well as lifetime values of **1-3** in MeCN.

We have also calculated the k_r and k_{nr} values and presented in Table 4.1. The RT luminescence property of **3** is consistent with deactivation of $^3(\pi-\pi^*)$ state of pyrene motif, as suggested by its k_r value. Hence, the aforementioned results indicate that the lowest emitting state in **3** is most probably $^3(\pi-\pi^*)$ while for **1** and **2** it is primarily $^3\text{MLCT}$. At 77K in frozen matrix, the λ_{max} experiences a hypsochromic shift ($\lambda_{\text{max}}=626\text{-}649$ nm) along with increase in luminescence intensity, Φ and τ . The decays also became mono-exponential in nature. The observed blue-shift along with marked increase in Φ and τ at 77K also bears the testimony of the quintessential $^3\text{MLCT}$ emitters. We have calculated the energy (E_{00}) of the emitting excited states from their 77K emission maxima and the estimated values are found to alter within 1.91-1.98 eV. A tentative state diagram describing the luminescence characteristics of complexes **1-3** is presented in Scheme 4.1.



Scheme 4.1. Simplified state diagram illustrating the emission characteristics of the complexes.

For most of the Ru-polypyridyl complexes, it is seen that the decay occurs mostly by competition between radiative and radiationless deactivations from the $^3\text{MLCT}$ state. This state is a weak emitter and hence non-radiative decay contributes majorly towards the lifetime values. This excited state decay can be expressed by equation 4.1³⁵

$$k_{\text{nr}} = k_{\text{nr}}^0 + k_{\text{nr}}' \quad (4.1)$$

where k_{nr} corresponds to radiationless decay constant, k_{nr}^0 is the direct decay from the excited $^3\text{MLCT}$ state to the ground state, and k_{nr}' is the surface crossing from the lowest $^3\text{MLCT}$ state to the ^3MC and is dependent on their energy level difference (ΔE). Due to the unfavourable bite angles of the terpyridines around Ru-center, this energy gap is substantially small thereby making the $\text{Ru}(\text{tpy})_2$ -type complexes as weak emitters at RT.

For proper assessment of the deactivation dynamics, we acquired the emission spectra and the excited state decays of the complexes (**1** and **2**) in acetonitrile upon varying temperature in the range of 263-343 K as portrayed in Figure 4.7. Both luminescence intensity as well as lifetime gradually decreases as the temperature is raised. We also fitted

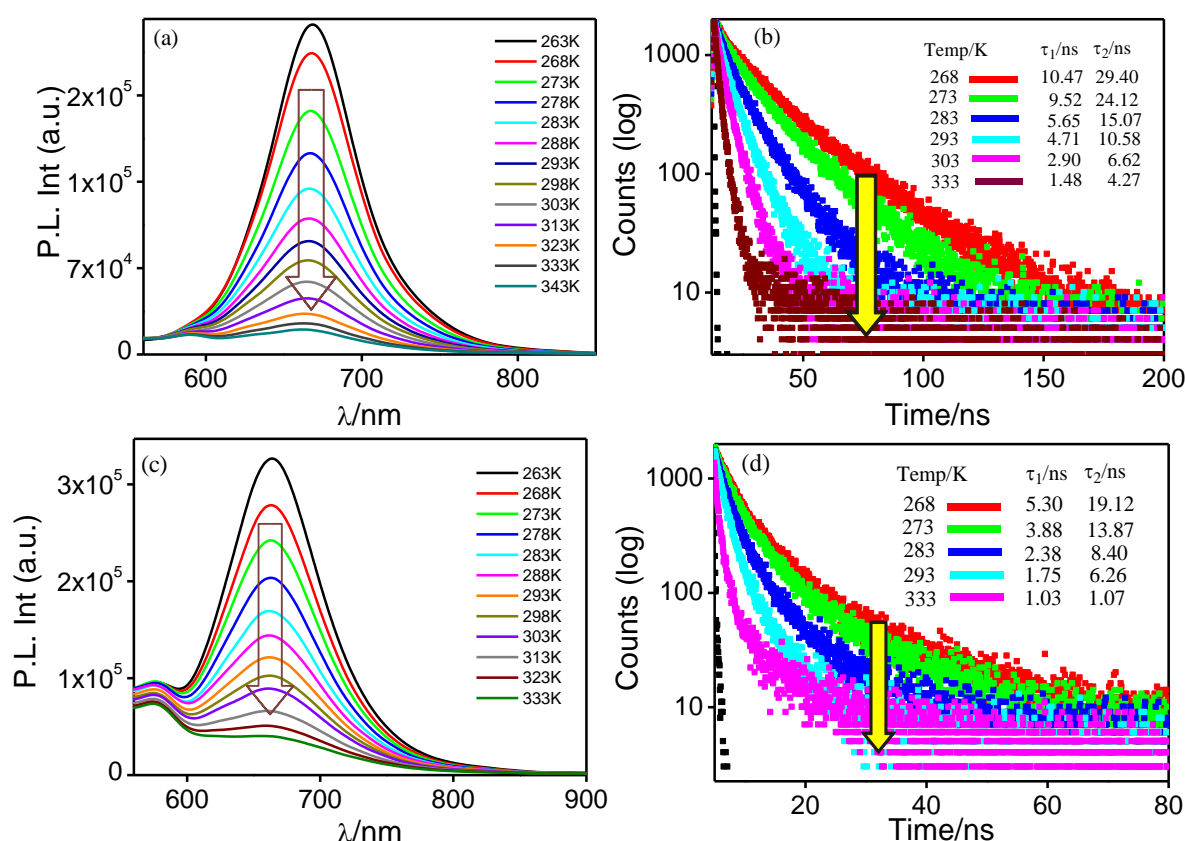


Figure 4.7. Change in the steady-state emission ($\lambda_{\text{ex}} = 490 \text{ nm}$) and decay profiles for complex **1** (a and b, respectively) and **2** (c and d, respectively) upon variation of temperature in MeCN in the range of 263-343 K.

the lifetime versus temperature data by nonlinear regression analysis technique using equation 4.2 (Figure 4.8).

$$(\tau(T))^{-1} = k_1 + k_2 (\exp [-\Delta E_2/RT]) / (1 + \exp [-\Delta E_2/RT]) \quad (4.2)$$

where k_1 represents temperature-independent rate constant which is sum of radiative (k_r) and non-radiative (k_{nr}) rate constants from $^3\text{MLCT}$ at 77 K, k_2 corresponds to temperature-dependent rate constant, and ΔE_2 is the activation energy for this surface-crossing process. Nonlinear regression analysis yields k_2 and ΔE_2 where k_2 lies in the range between 2.8×10^{12} and $1.1 \times 10^{13} \text{ s}^{-1}$ while ΔE_2 lies in the range of 3000-4000 cm^{-1} that are significantly greater than their parent analogue ($[\text{Ru}(\text{tpy})_2]^{2+}$, $\Delta E_2 = 1500 \text{ cm}^{-1}$) (Figure 4.8).⁴⁹⁻⁵⁰ This may be due to increased π -conjugation caused by incorporation of the styrylbenzene and polyaromatic unit in the $[\text{Ru}(\text{tpy})_2]^{2+}$ skeleton. When temperature is decreased, the energy gap between $^3\text{MLCT}$ and ^3MC state increases, thereby enhancing both emission intensity and lifetimes. But when temperature is increased, thermal equilibrium between the $^3\text{MLCT}$ and ^3MC states induces a decrease in ΔE_2 values leading to decreased emission intensity and lifetime.

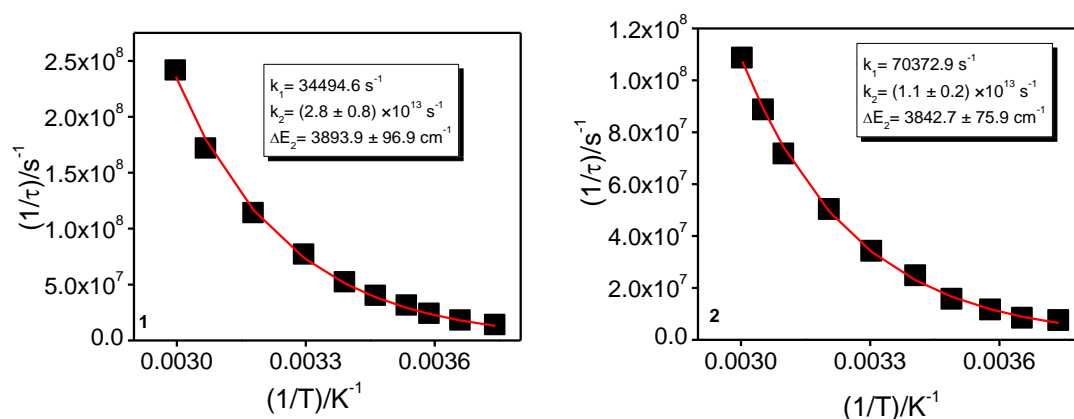


Figure 4.8. Nonlinear fitting of temperature-dependent lifetime data along with the values of different parameters for **1** and **2** in MeCN.

4.3.6 Redox Properties. Electrochemical measurements of **1-3** are conducted via cyclic voltammetry in deoxygenated MeCN and relevant voltammograms are presented in Figure 4.9, while relevant data are provided in Table 4.3. The single reversible oxidation peak at $\sim 1.3 \text{ V}$ signifies the $\text{Ru}^{3+}/\text{Ru}^{2+}$ process. Multiple quasi-reversible and irreversible waves are also observed between -1.15 and -1.40 V, which arise mostly due to reduction of the coordinated terpyridine units.

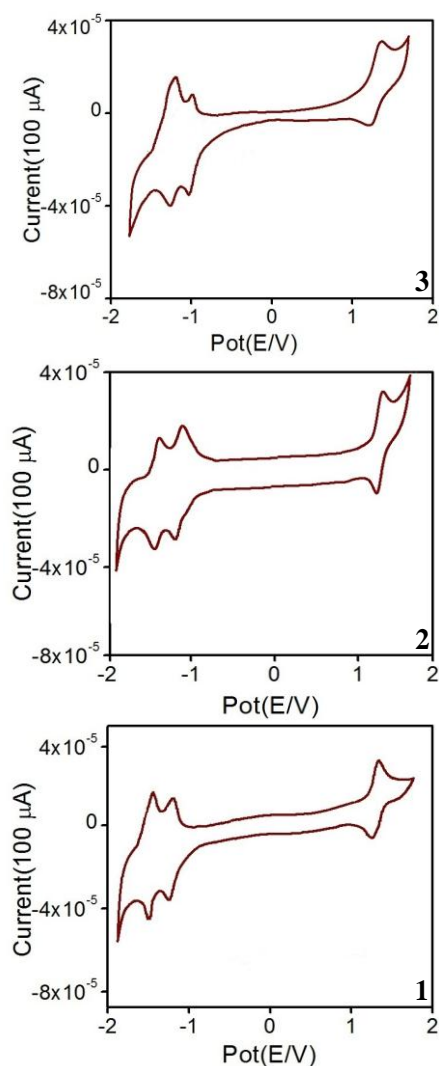


Figure 4.9. CVs of **1-3** showing both oxidation and reduction processes in MeCN.

Table 4.3. Electrochemical Data^a for **1-3** in MeCN.

Compds	Oxidation ^b	Reduction ^c
	$E_{1/2}$ /(V)	E_{red} /(V)
1	1.27	-1.18, -1.40
2	1.28	-1.17, -1.38
3	1.29	-1.14, -1.35

^aAll the potentials are referenced against Ag/AgCl electrode with $E_{1/2}=0.36$ V for Fc/Fc⁺ couple. ^bReversible electron transfer process with a Pt working electrode. ^c $E_{1/2}$ values obtained using glassy carbon electrode.

4.3.7 Anion Sensing Characteristics. The anion sensing characteristics are systematically investigated in MeCN via different optical channels and spectroscopic techniques. Tetrabutylammonium salts of F⁻, Cl⁻, Br⁻, I⁻, CN⁻, AcO⁻ and H₂PO₄⁻ are used here. The absorption and emission spectral response of **1** in presence of studied anions are depicted

in Figure 4.10. Only F^- , among the studied anions is able to induce remarkable change in their spectral profiles.

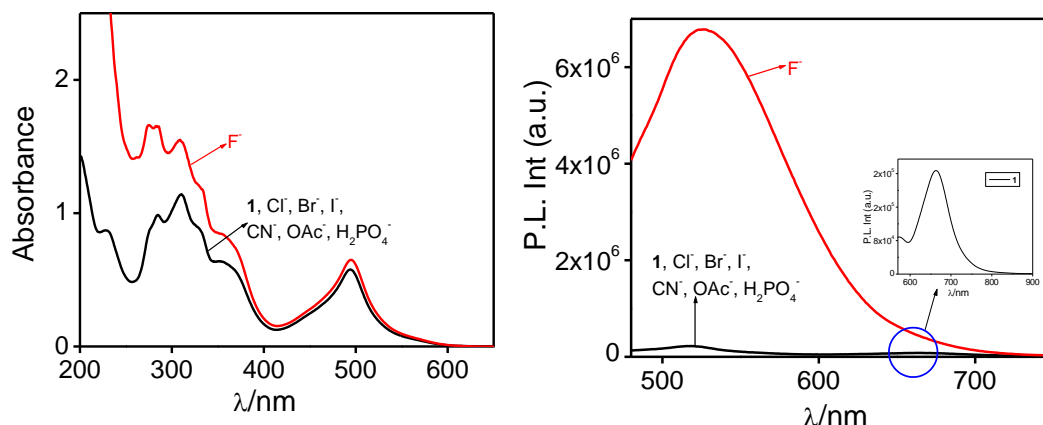


Figure 4.10. Absorption (left) and emission (right, $\lambda_{ex}=500$ nm) spectrum of **1** in MeCN (1.0×10^{-5} M) in absence and in presence of studied anions as their TBA salts.

In order to acquire quantitative insight about the receptor-anion interplay, we executed titration experiments upon gradual addition of F^- and monitor the changes via absorption and emission spectroscopy (Figure 4.11). It is seen that upon continuous addition of F^- , a significant increase in absorbance within the spectral domain of 200-400 nm occurs for all three complexes (Figure 4.11). This region mostly consists of mixed ILCT and $\pi-\pi^*$ transitions. On a closer inspection, it is evident that absorbance change mostly takes place in between 200 and 370 nm for **1**, while for **2**, the corresponding change occurs in the range of 200-465 nm. No detectable change in the MLCT band is observed either for **1** or **2**. By contrast, decrease in 1MLCT band intensity is noticed for **3** and successive spectral lines pass through clear isosbestic points (Figure 4.11). Saturation takes place upon addition of ~ 80 equiv of F^- . Additionally, the absorption peak at 284 nm for **1** is seen to split in two smaller peaks while for **2** the same peak (at 284 nm) undergoes a blue-shift to 272 nm. Thus, the change in the spectral pattern is similar for **1** and **2** while different for **3**.

In the emission side, we see a huge upsurge in emission intensity along with increase in Φ upon continuous addition of F^- in all cases. The peak at ~ 660 nm corresponding to 3MLCT state undergoes a small increase in emission intensity while the peak at ~ 520 nm due to the ligand-centered emission experiences dramatic increase in emission intensity and it seems to be the major emitting peak upon saturation. The extent of increase is maximum for **1** while it is the least for **3** (Table 4.4). On the contrary, free ligands display no noticeable

change in either absorption or emission spectral profile even in presence of excess F^- . We have also acquired the lifetimes of the complexes at the saturation point. Surprisingly, no significant change in their lifetime values is observed.

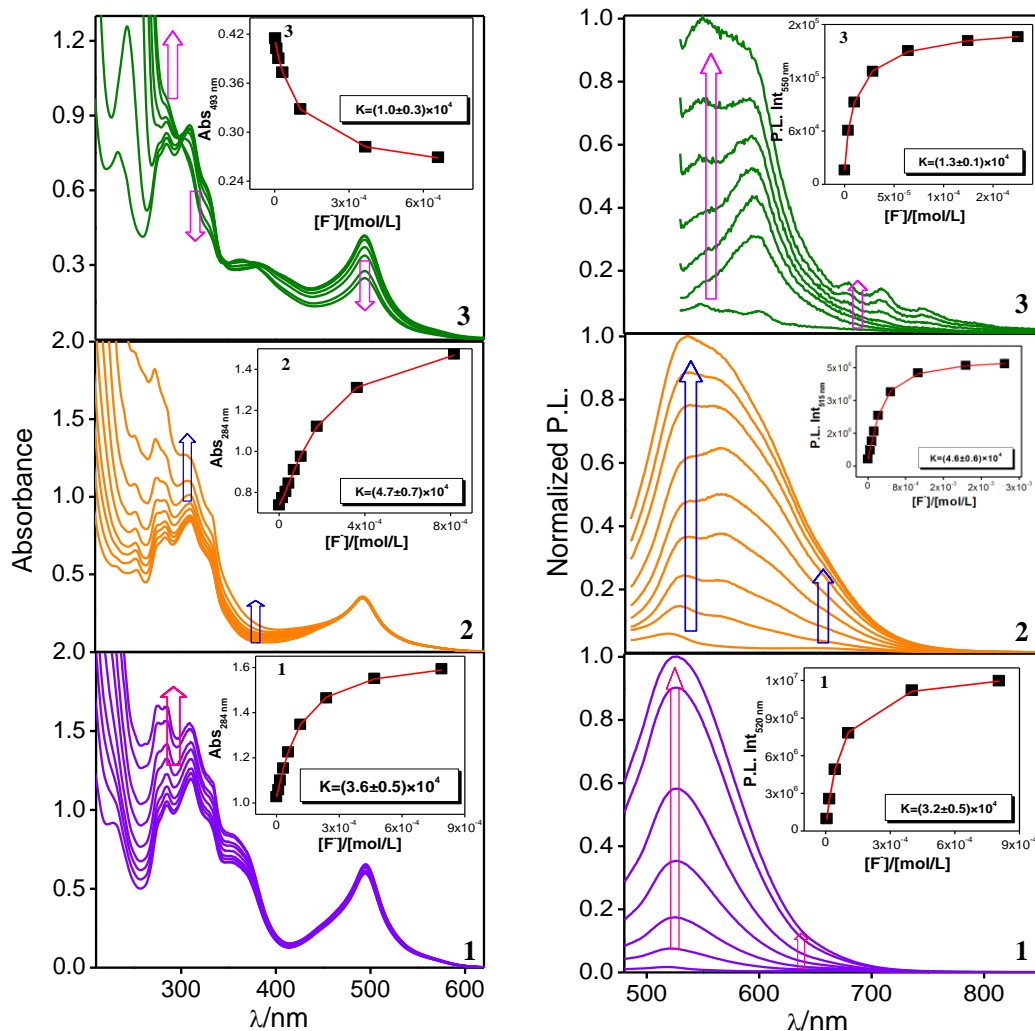


Figure 4.11. Absorption (left panel) and emission ($\lambda_{ex}=500$ nm) (right panel) titration profiles of the trans forms of **1-3** (1.0×10^{-5} M) in MeCN upon gradual addition of F^- . Insets to the figures in both left and right panels indicate the estimation of binding constants.

Table 4.4. Change in emission quantum yields (Φ) for both trans and cis forms of **1-3** upon interaction with F^- .

compounds	Φ_{Free}	$\Phi_{F^- \text{ saturated}}$
1-trans	3.3×10^{-3}	178.4×10^{-3}
2-trans	2.1×10^{-3}	98.3×10^{-3}
3-trans	0.4×10^{-3}	3.1×10^{-3}
1-cis	1.6×10^{-3}	132.4×10^{-3}
2-cis	1.1×10^{-3}	12.8×10^{-3}
3-cis	0.3×10^{-3}	3.0×10^{-3}

In order to acquire insight about the stoichiometry of complex-anion interaction, we performed Job's plot analysis by using emission titration data of the complexes as a function of the mole fraction of F^- (Figure 4.12). The point of intersection appears at ~ 0.5 mole fraction of F^- , suggesting the formation of 1:1 adduct between the complex and fluoride ion.

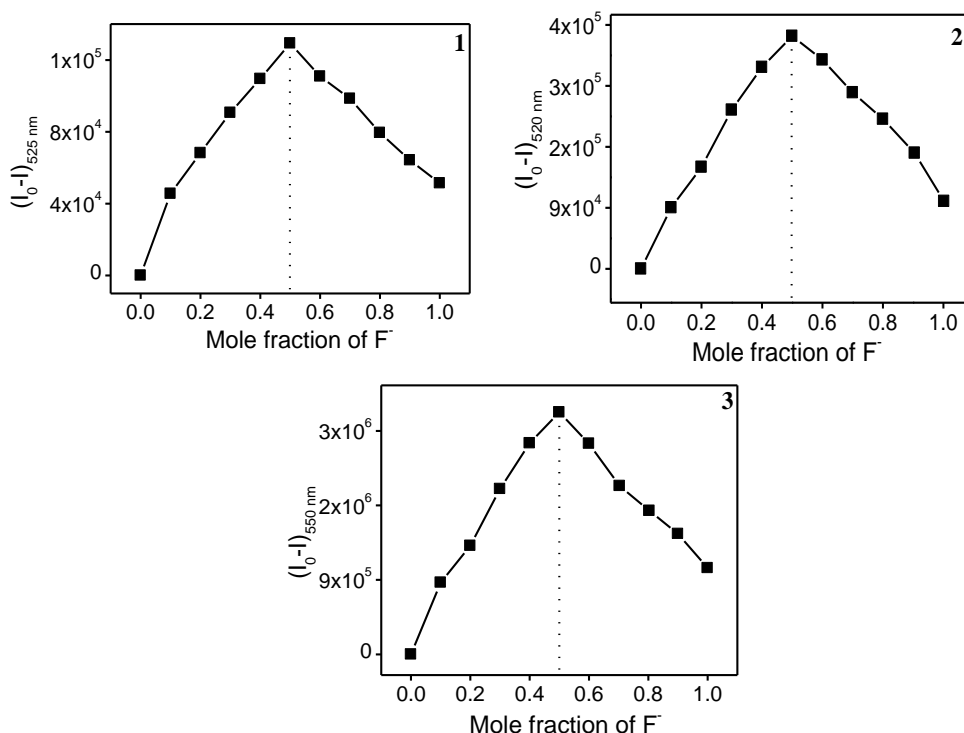


Figure 4.12. Job's plot referring to the 1:1 interaction between the complexes **1-3** and F^- in MeCN.

We have also acquired cyclic voltammograms of the complexes in MeCN upon incremental addition of F^- . We didn't notice any observable change in the potential of either Ru^{2+}/Ru^{3+} couple in the positive potential window or ligand-centered reductions in the negative potential domain.

We also estimated the binding constants (K) of the receptor-anion interplay by utilizing the absorption and emission titration data of the complexes by employing equation 4.3 for 1:1 stoichiometry (Figure 4.13, Table 4.5).

$$\Delta A = \frac{\Delta \epsilon b ([H] + [G] + (1/K)) \pm \sqrt{\Delta \epsilon^2 b^2 ([H] + [G] + (1/K))^2 - 4 \Delta \epsilon^2 b^2 [H][G]}}{2} \quad (4.3)$$

where ΔA is the change in absorbance, $[H]$ and $[G]$ is the concentration of metal complex and added anion, respectively. $\Delta \epsilon$ is the change in molar extinction coefficient, b is the absorption

path length, and K is the binding constant. The calculated K values are presented in Table 4.5. The values of K for naphthalene (**1**) and anthracene (**2**) derivatives are almost comparable ($\sim 10^4$) and are higher than that of pyrene derivative (**3**). We also calculated the detection limit of the complexes towards F^- that lie in the range of $1.2\text{--}9.3 \times 10^{-7}$ M (Table 4.5). Detection limit of a representative complex **1** is provided in Figure 4.13.

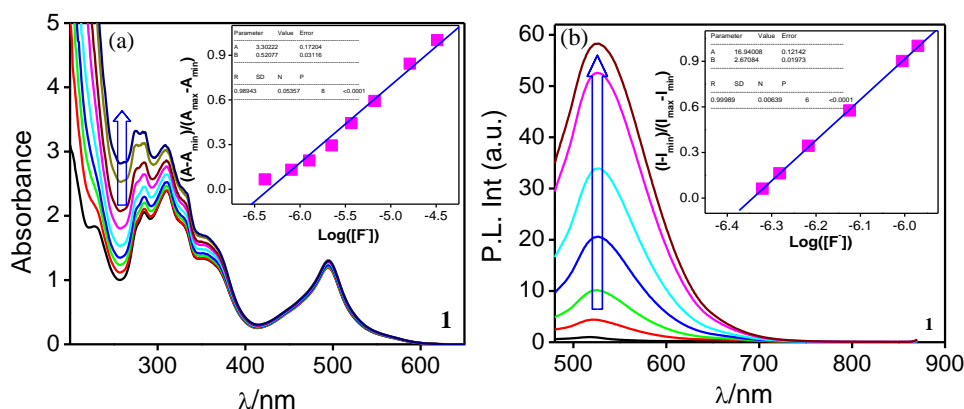


Figure 4.13. (a) Absorption and (b) emission spectral changes during the titration of the receptor **1-trans** (1.0×10^{-5} M) with F^- in MeCN, inset: (a) A plot of $(A - A_{\min}) / (A_{\max} - A_{\min})$ vs. $\text{Log}([F^-])$, the calculated detection limit of receptor is 3.0×10^{-7} M and (b) A plot of $(I - I_{\min}) / (I_{\max} - I_{\min})$ vs. $\text{Log}([F^-])$, the calculated detection limit of receptor is 4.2×10^{-7} M.

Table 4.5. Equilibrium constants (K) and detection limits for **1-3** towards F^- in MeCN.

Compounds	Binding Constant		Detection Limit/M	
	Absorption	Emission	Absorption	Emission
1-trans	3.6×10^4	3.2×10^4	3.0×10^{-7}	4.2×10^{-7}
2-trans	4.7×10^4	4.6×10^4	1.5×10^{-7}	1.2×10^{-7}
3-trans	1.0×10^4	1.3×10^4	9.3×10^{-7}	8.9×10^{-7}
1-cis	1.1×10^4	2.2×10^4	5.5×10^{-7}	6.0×10^{-7}
2-cis	1.8×10^4	2.1×10^4	6.8×10^{-7}	7.2×10^{-7}
3-cis	0.4×10^4	0.4×10^4	12.8×10^{-7}	27.5×10^{-7}

To elucidate the probable mode of interaction, ^1H NMR titration experiments are executed on both **1** and **2** upon systematic addition of F^- in CD_3CN . The titration profile for naphthalene derivative (**1**) is displayed in Figure 4.14, while that of the anthracene (**2**) is presented in Figure 4.15. In both cases, the signals due to $\text{H}_{3''}$ and $\text{H}_{3''}$ protons undergo downfield shift along with increased separation between them. Additionally, for the anthracene derivative, the $\text{H}_{3''}$ peak at 9.00 ppm splits further yielding a doublet and/or two closely situated singlets upon saturation (Figure 4.15). Similarly, the H_6 and H_6 protons

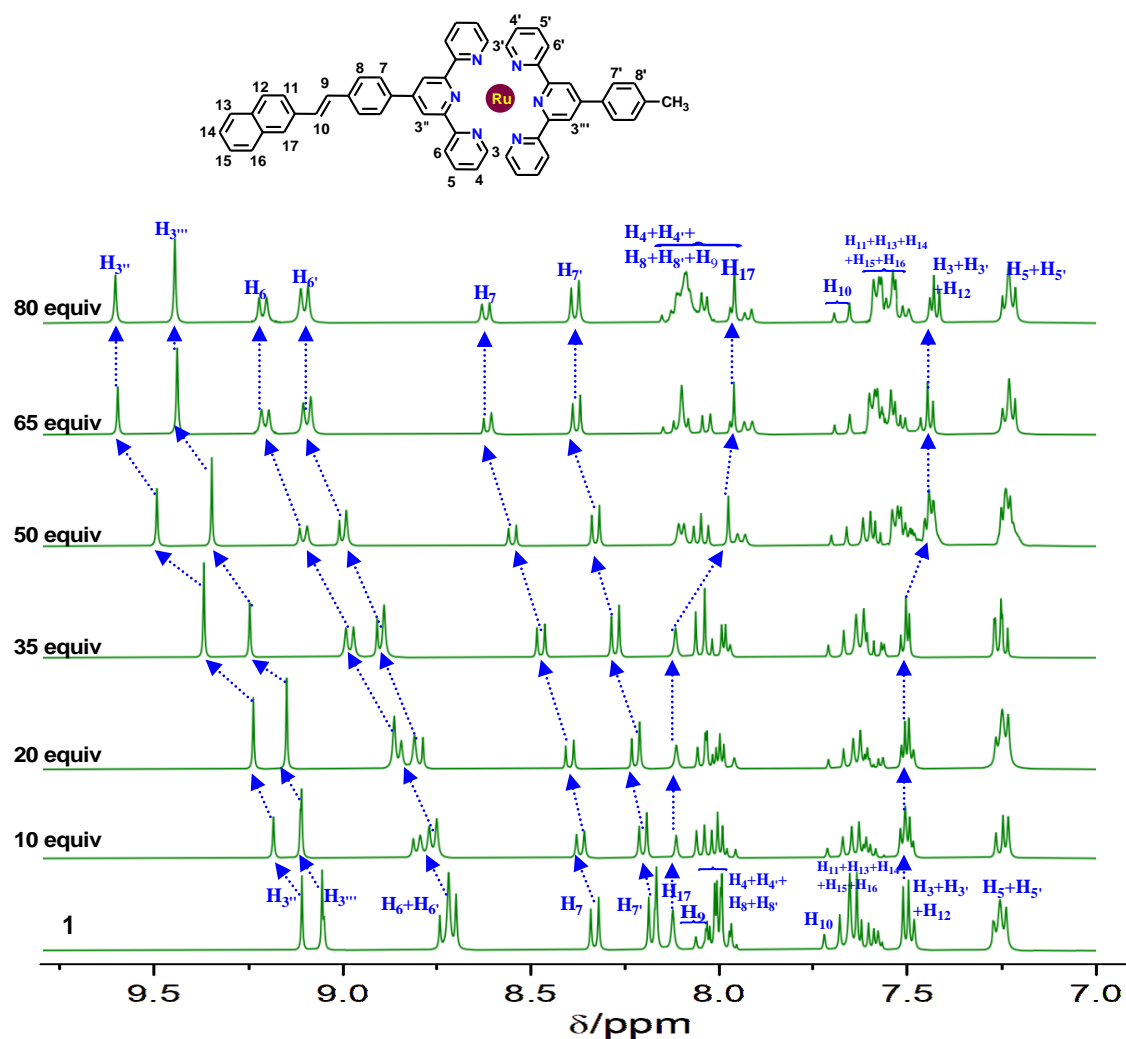


Figure 4.14. ^1H NMR spectral titration of **1** upon incremental addition of TBAF in CD_3CN .

that appear initially as multiplet, undergo further splitting to generate a well separated as well as clearly resolved doublet for both the derivatives. The said well-resolved doublets underwent further splitting in case of anthracene derivative. The doublets due to H_7 and H_7' protons attached to the phenyl group of tpy moiety in both cases also move towards the downfield region. Upon complexation with Ru^{2+} ion, the terpyridine as well as other aromatic protons (C-H groups) in the complexes became acidic and capable to take part in hydrogen bonding interaction with incoming F^- guest. The observed down-field shift of the above-mentioned protons is probably due to $\text{C-H}\cdots\text{F}$ hydrogen bonding interaction. The singlet owing to the polyaromatic moiety shifts towards the up-field region in both cases, albeit in different extent. The peaks due to H_3 - H_5 as well as H_3' - H_5' , associated with terpyridine moiety as well the polyaromatic protons undergo only a small change. Upon closer inspection, it is noticed that the ethylenic protons (H_9 and H_{10}) undergo a huge up-field shift (~ 1.00 ppm) for

anthracene derivative (**2**). By contrast, the corresponding shift in case of naphthalene (**1**) is small (Figure 4.14). It is of particular interest to note that the integration count of total number of protons became almost double in each case upon saturation, suggesting the formation of dimer-type species. The aforementioned shift of selected proton signals in presence of F^- is due to interplay of several non-classical interactions, viz. $CH\cdots F$ hydrogen bonding together with $CH-\pi$ and anion- π interactions. Additionally, we surmise that the combined influences of these non-covalent interactions induce two complex entities to come closer leading to the formation of dimer-type species.

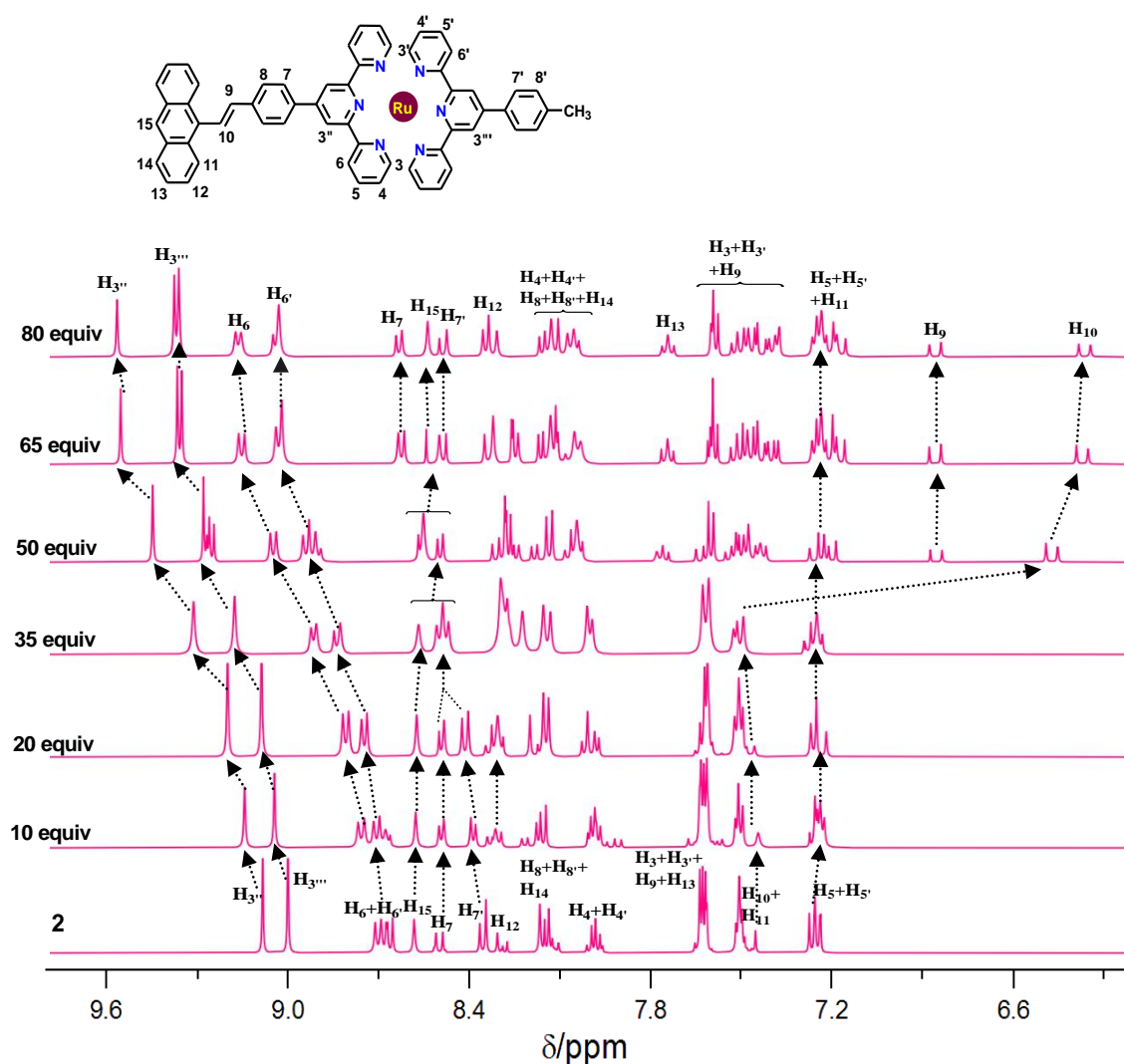


Figure 4.15. ¹H NMR spectral titration of **2** upon incremental addition of TBAF in CD₃CN.

In order to understand the mode of interaction in the complexes **1-3**, we also executed absorption, emission and ¹H NMR spectral titration experiment of the parent [Ru(tpy)₂]²⁺ complex upon incremental addition of F^- (Figure 4.16-4.17). Small but finite change takes

place in both absorption and emission spectral profiles, although the mode of change in absorption spectral profile differs from **1-3**. In the NMR titration profile, down-field shift of the peaks corresponding to H₃, H_{3'}, and H_{4'} protons also takes place in presence of F⁻. But in contrast to the studied complexes, no change in multiplicity of the peaks occurs. Additionally, no doubling of integration counts is observed upon saturation in case of [Ru(tpy)₂]²⁺. The down-field shift of the terpyridine proton resonances in [Ru(tpy)₂]²⁺ upon addition of F⁻ is most probably due to through-space electrostatic interaction with F⁻.⁸⁰ Of course, interaction between F⁻ and CH protons of the terpyridine motifs is a distinct possibility.

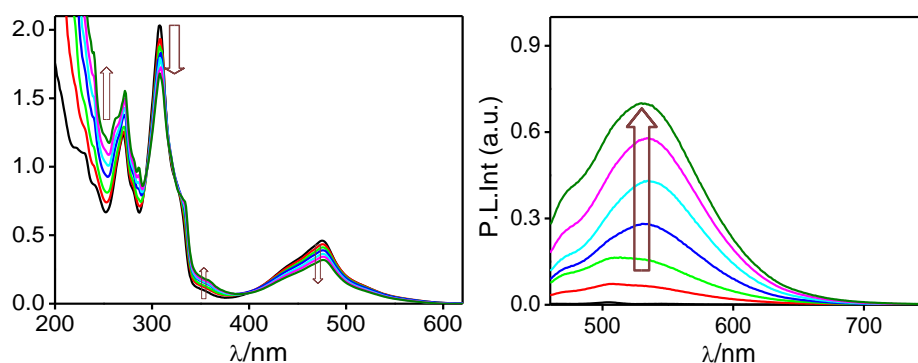


Figure 4.16. Absorption (left) and emission ($\lambda_{\text{ex}}=500$ nm) (right) titration profiles [Ru(tpy)₂]²⁺ (1.0 × 10⁻⁵ M) in MeCN upon gradual addition of F⁻.

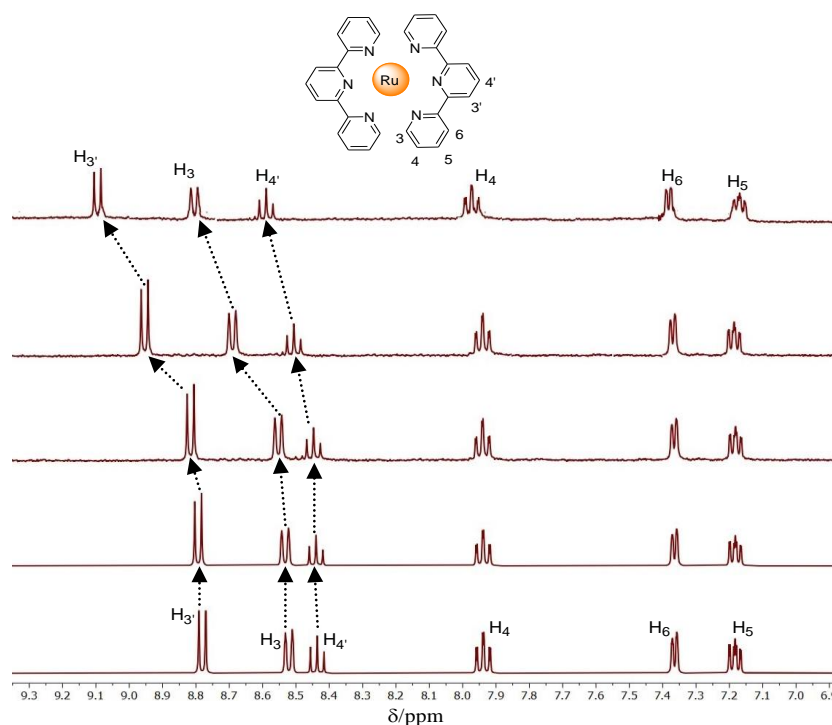


Figure 4.17. ¹H NMR spectral titration of [Ru(tpy)₂]²⁺ upon incremental addition of TBAF in CD₃CN.

To understand the mode of receptor-anion interaction, we also executed ^{19}F NMR titration experiments upon gradual addition of naphthalene (**1**) and anthracene (**2**) derivatives to the CD_3CN solution of TBAF and related spectral profiles are presented in Figure 4.18. Free TBAF shows a strong singlet at -127.84 ppm corresponding to F^- ion and a broad peak at -119.67 ppm for HF_2^- species. Addition of the complexes induces a small up-field shift of the singlet peak together with its gradual diminution, indicating shielding of F^- by the complex species due to formation of complex $\cdots\text{F}^-$ adduct. Upon saturation, although the peak intensity gradually diminishes in both cases, it is not completely removed for **1**, while for **2**, it gets completely removed. The intensity of the broad peak also decreases in both cases, albeit in different extent, but does not completely vanish. The observed difference in behaviour can be attributed to the differences in the extent of interactions among the complex and fluoride and it appears that anthracene derivative interacts strongly with fluoride ion compared with its naphthalene analogue. During the course of titration, no additional peak is evolved. Thus, ^{19}F NMR spectral investigations strongly indicate the occurrence of non-classical interactions among the complexes and F^- and ruled out the possibility of covalent attachment of fluorine in the complex backbone.

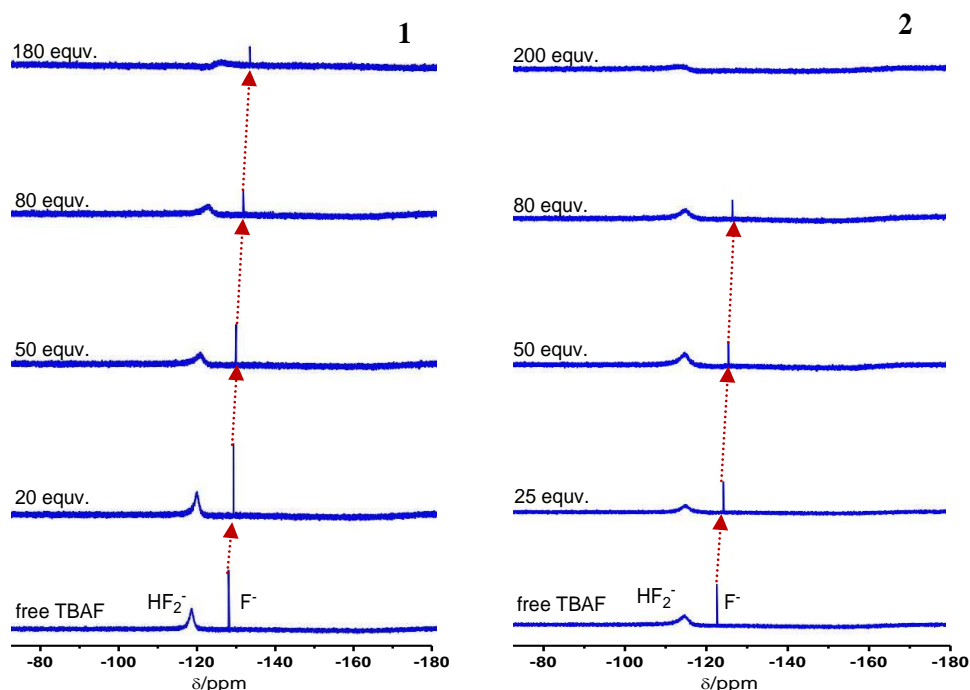


Figure 4.18. ^{19}F NMR titration of **1** (left panel) and **2** (right panel) with F^- showing complex $\cdots\text{F}^-$ interaction in CD_3CN at RT.

Doubling of the integration count of total number of protons in ^1H NMR spectra of complexes **1-2** motivates us to execute dynamic light scattering (DLS) experiments. The DLS experiments are performed in MeCN solutions of the complexes in their free forms as well as in presence of 80 equiv of F^- and the results are presented in Figure 4.19. Interestingly, the particle size is found to increase from initial 5-35 nm to 120-150 nm upon F^- addition. As no additional solvent is employed in the DLS experiment, the possibility of solvent-induced aggregation phenomenon could be ruled out. Thus, the outcome of both NMR and DLS experiments leads us to speculate the occurrence of some sort of aggregation through the intermediary of F^- ion.⁸¹

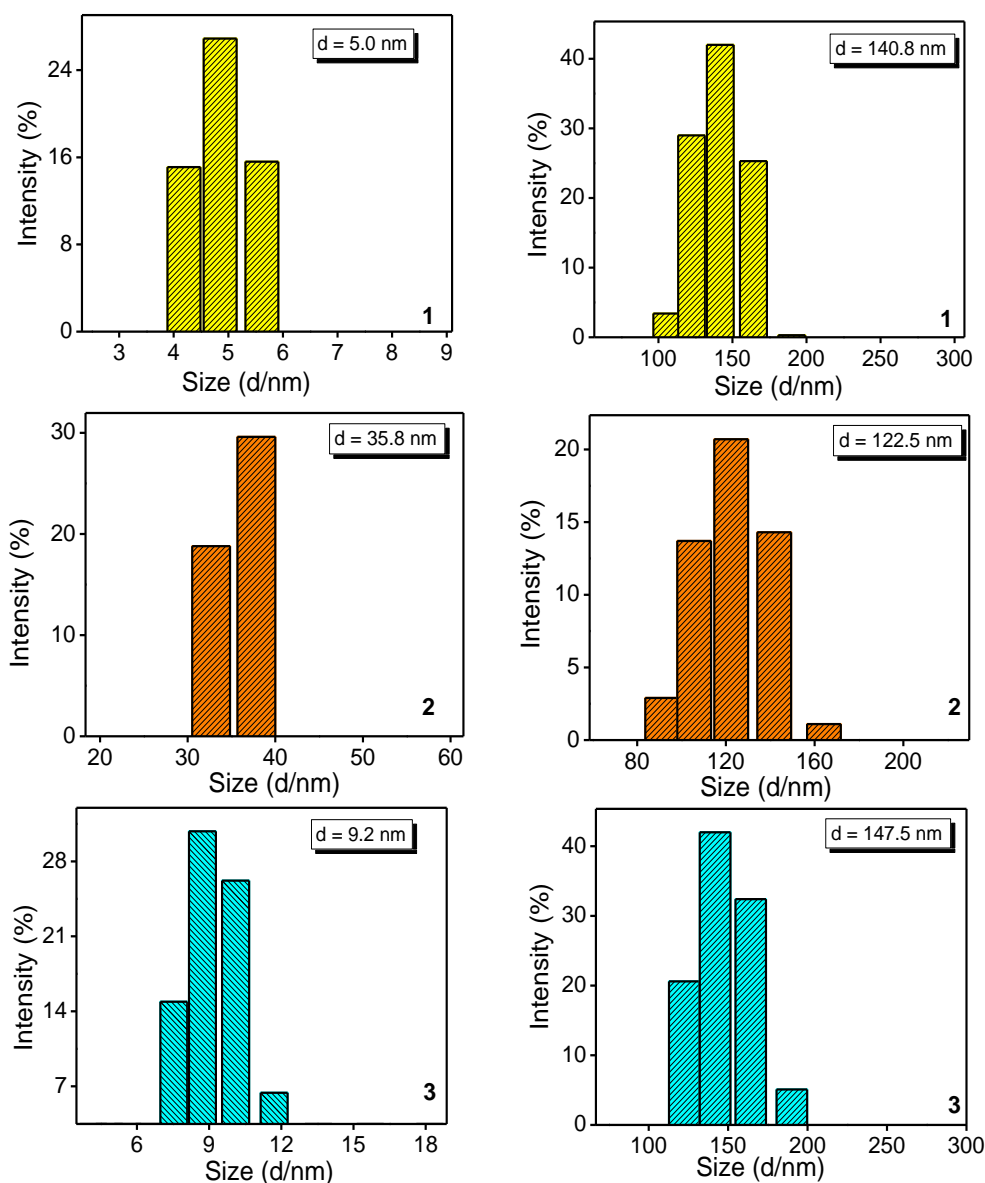


Figure 4.19. Particle size distribution of **1-3** with in MeCN in their free (left panel) and F^- saturated forms (right panel).

The outcomes of absorption, emission, ^1H and ^{19}F NMR spectroscopic measurements as well as DLS experiment unambiguously suggest that the complexes interact strongly with incoming F^- ion. The observed changes are probably due to combination of several non-classical interactions, viz. $\text{CH}\cdots\text{F}$ hydrogen bonding, $\text{CH}-\pi$, anion- π together with through-space electrostatic interaction between positively charged complex entity and F^- . These interactions, however weak they maybe, are able to bring the complex entities close to one another up to a certain extent. These non-covalent interactions help to hold the molecules together, thereby restricting the intramolecular motions (rotation and vibration) of the components. This restriction of intramolecular motions (RIM) inhibits non-radiative deactivation channels which in turn improves the emission characteristics of the complexes in presence of fluoride ion.

To substantiate our hypothesis on various types of non-covalent interactions that are operative among the complexes and fluoride ion, we have performed DFT calculations on a representative complex, **1** (Figure 4.20). We first optimized the ground state geometry of complex and calculated its energy (A). Next, we computed the change in energy due to interaction of F^- at some specified positions of the complex. We mainly considered two types of non-covalent interactions, viz. $\text{CH}\cdots\text{F}^-$ hydrogen bonding and anion- π . We initially optimized geometries involving only $\text{CH}\cdots\text{F}^-$ interactions pertaining to terpyridine and styrylbenzene moiety. We considered two as well as four numbers of feasible $\text{CH}\cdots\text{F}^-$ interactions (B and C). We then optimized the geometry of the complex by taking into consideration the fluoride-pi type interaction within a single entity (D) and subsequently optimized the geometry consisting of pi-fluoride-pi type interaction involving two adjacent naphthalene units (E). Systematic lowering of energy is observed upon increase in number of $\text{CH}\cdots\text{F}$ interactions (B and C). The energy in case of fluoride-pi type interaction within the single entity is also lowered, albeit in smaller extent (D). The energy of the optimized geometry involving the dimer-type species (E), on the other hand, gets remarkably lowered compared to those involving fluoride-pi interaction within the single entity as well as $\text{CH}\cdots\text{F}$ interactions (F). The combination of both fluoride-pi and $\text{CH}\cdots\text{F}$ interactions within the single entity does not significantly lower the energy, although the value is slightly lower than that of individual contribution. This observation is in-line with our ^1H NMR study wherein downfield shift of protons occurs upon F^- addition. We also observed the doubling of integration count in ^1H NMR as well as increase in size of the complex molecules in DLS study upon F^- addition which suggest the formation of some sort of dimer-type species. In this light, we calculated the energy of the complex molecule upon dimerization via pi-

fluoride-pi type interaction (E) and the results indicate a very drastic decrease in energy which is even lower than the forms involving both fluoride-pi and CH---F interaction within the single entity (F). Additionally, stabilization of the geometry involving simultaneous pi-

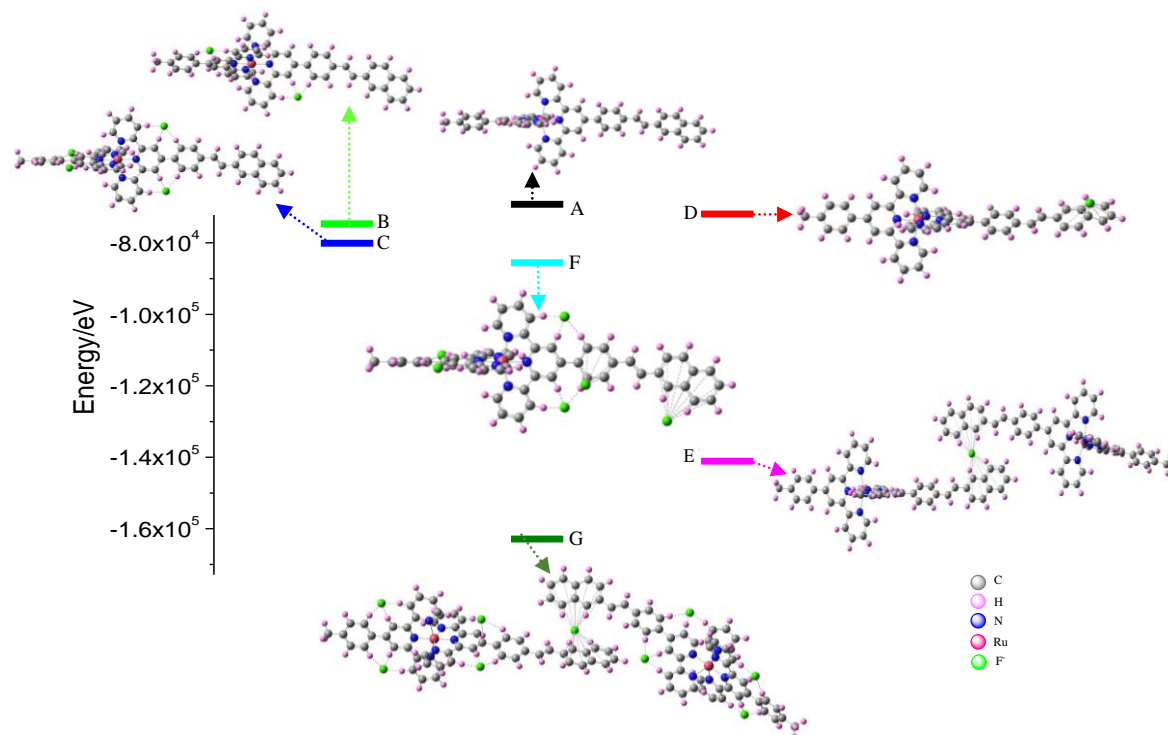


Figure 4.20. Calculated energy diagram showing decrease in energy of $1 \cdots F^-$ complex adduct due to CH---F and anion- π interactions.

fluoride-pi and CH---F interactions is the highest and has the lowest energy value than those of all the other forms mentioned above (G). Such remarkable stabilization is the manifestation for simultaneous occurrence of both anion-pi and CH---F interactions in the complex adduct. It is to be noted that the ground state energy of complex **1** is -6.9×10^4 eV which drastically decreases up to -1.4×10^5 eV when two complex moieties are associated via anion-pi interactions only. Further decrease in energy is observed when anion-pi and CH---F interactions occur simultaneously (-1.6×10^5 eV). Hence, DFT calculations indicate that anion-pi interaction is the major contributor towards the overall decrease in energy. We have also calculated the ESP plots of the ancillary ligand, free complex as well as the dimer-type adduct of the naphthalene derivative (**1**) (Figure 4.21). It is noticed that the free form of the complex is electron deficient in nature and in presence of F^- , the electron density is found to flow from F^- into the complex backbone leading to formation of dimer. Thus, although there is no solid experimental evidence (single crystal X-ray structure), the outcomes of DFT

calculations provide sufficient insight for the occurrence of substantial anion- π as well as finite CH \cdots F hydrogen bonding interactions among the complex entities through intermediary of F $^-$.

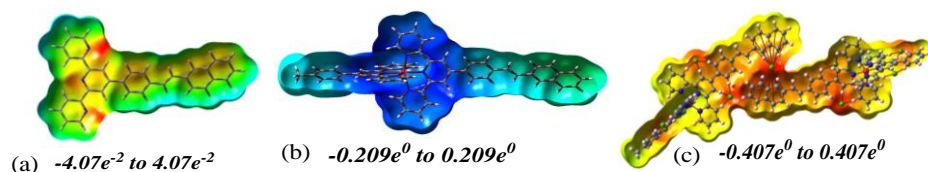


Figure 4.21. Electrostatic surface potential (ESP) plots of (a) ligand, (b) metal complex **1** and (c) dimer-type adduct of **1**---F $^-$ in MeCN.

We are interested to know whether the observed changes in the complexes in presence of fluoride ion are reversible or not. This is tested by the addition of a fluoride scavenger at the end of the titration experiments with fluoride. Herein, we used a Lewis acid (BF $_3$) as well as a protic acid (HClO $_4$) as the fluoride scavenger. BF $_3$ /HClO $_4$ is gradually added to the anion-treated solutions of **1** and **2** and the observed changes are monitored via absorption and emission spectroscopy (Figure 4.22). Interestingly, the initial state of the complexes almost gets restored at saturation. Moreover, the processes are reversible and could be repeated several times. Hence, the complexes under present investigation could function as on/off emission switches upon treating alternately with F $^-$ and either BF $_3$ or HClO $_4$, as shown in Scheme 4.2.

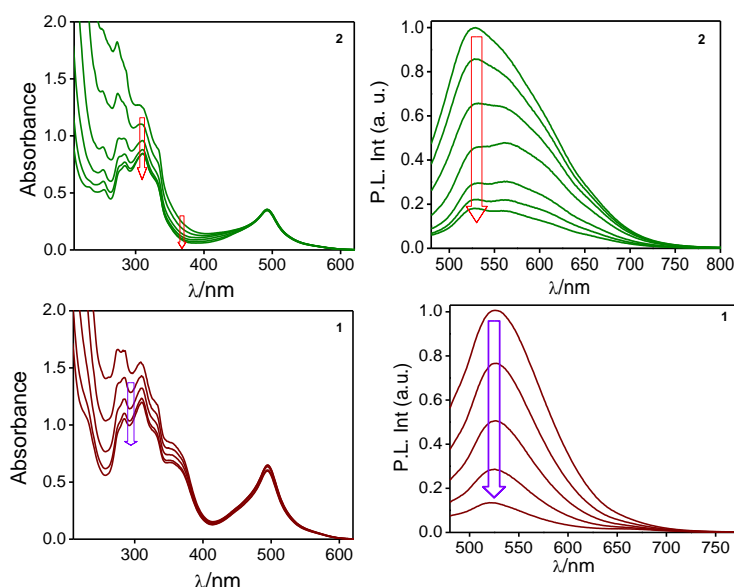
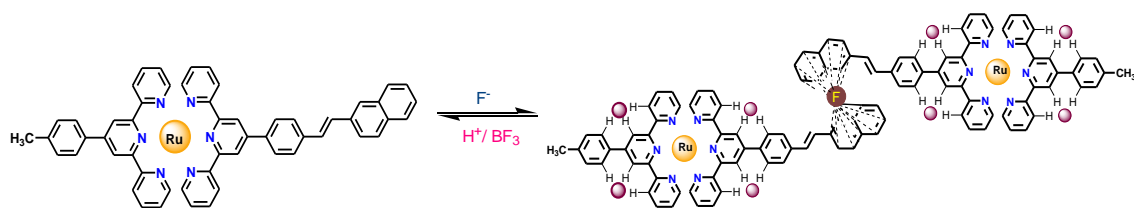


Figure 4.22. Change in absorption (left panel) and emission spectra (right panel) upon addition of H $^+$ to F $^-$ saturated solutions of **1** and **2**.



Scheme 4.2. Simplified scheme depicting the process of reversible F^-/H^+ addition.

4.3.8 Photo-Isomerization. As already mentioned, a stilbene motif is present in the complex backbone and transformation from trans→cis form upon interaction with light leads to conformation change in the polyaromatic as well as heteroaromatic moieties in the complexes. It is quite expected that the extent of different non-covalent interactions would also be substantially altered on going from trans to the cis-isomer. To this end, we carried out detailed photoisomerization behaviors of the present complexes. The influence of visible light irradiation ($\lambda_{\text{ex}} = 500$ nm) on the solutions of the complexes is followed via their absorption and emission spectra as a function of photolysis time (Figure 4.23). Similarity in the spectral

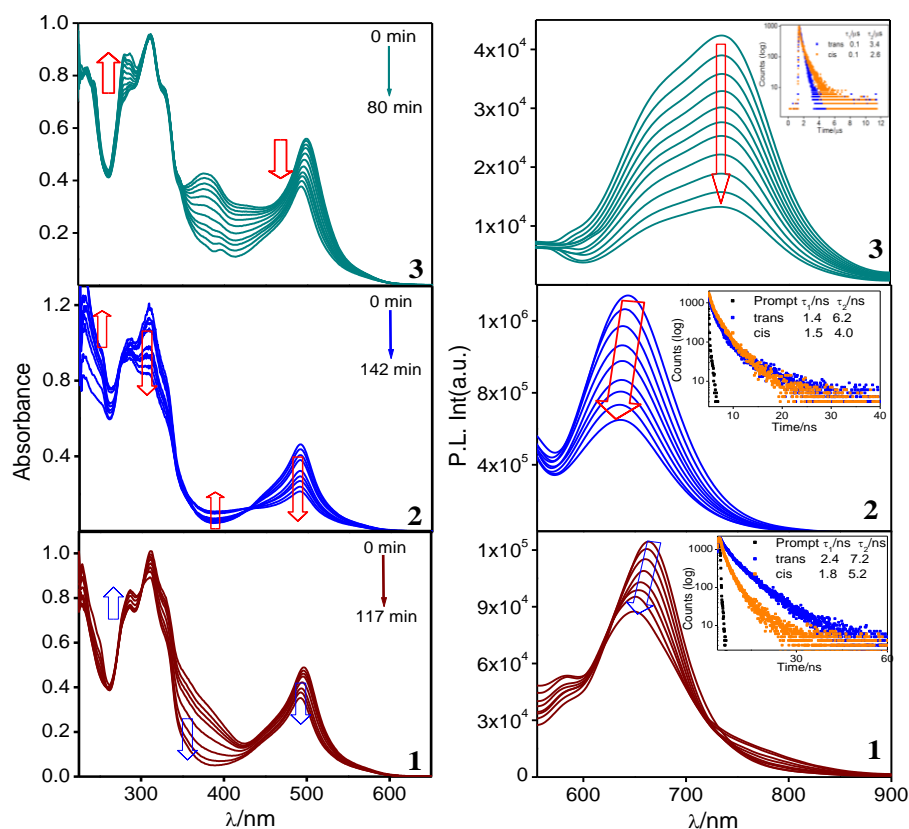


Figure 4.23. Absorption (left) and emission (right) ($\lambda_{\text{ex}} = 500$ nm) spectral change of **1**, **2** and **3** upon treatment with visible light. Insets to the right panel of figure represent emission decay ($\lambda_{\text{ex}} = 490$ nm NanoLED) along with their lifetime before and after photo-irradiation.

pattern is noticed for all three complexes. Systematic decrease in absorbance of both MLCT and mixed MLCT/ILCT bands occur with concomitant increase in the π - π^* bands in the UV region. Of course, the decrease in the absorbance is greater for ILCT bands in comparison to MLCT. Small but finite blue-shift of the MLCT band also takes place during the isomerization process. The process is accompanied with evolution of well-defined isosbestic points. The time required to reach the photo-stationary state varies within the range of 80-142 min, dependent on the type of polyaromatic motif in the complexes. The corresponding emission spectral changes upon irradiation are shown in Figure 4.23. Substantial reduction in emission intensity as well as quantum yield takes place accompanied with small blue-shift in their emission maxima. We have also measured the lifetimes of the complexes both in their initial and final forms. The results indicate only a small decrease in lifetime for all the complexes upon isomerization (Figure 4.23).

With regard to acquire a direct proof, the photoisomerization process is also monitored via ^1H NMR spectroscopy. For this purpose, we have performed the photoisomerization of a representative complex (**1**) in $\text{DMSO-}d_6\text{-CDCl}_3$ (1:5 v/v) solvent mixture for about 12 h (Figure 4.24). It is seen that the olefinic protons in the 6.62-6.52 ppm region gradually lose their intensity while a new peak is generated in the more up-field domain (~ 6.00 ppm). The extent of shift ($\Delta\delta$) is 0.60 ppm. Longer exposure to light leads to

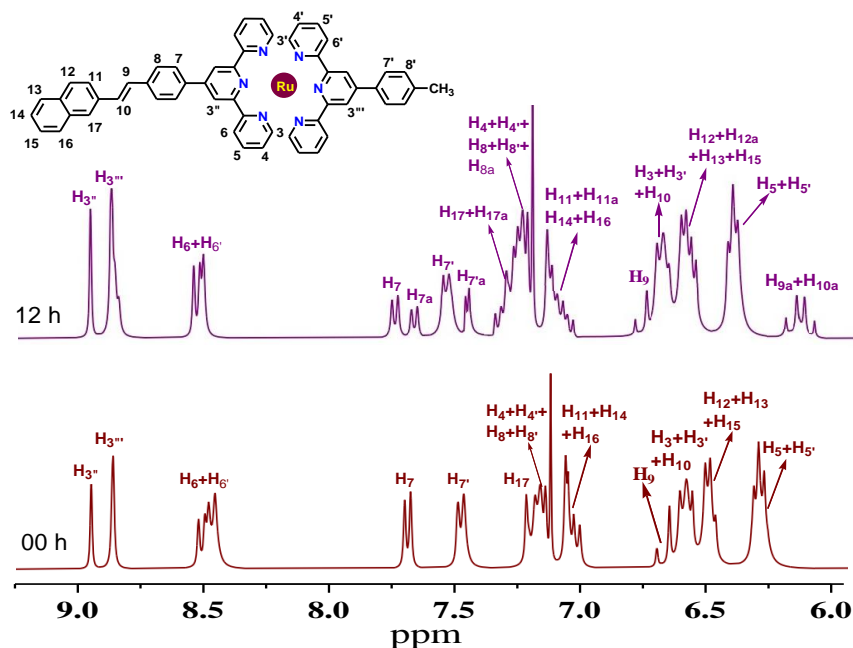


Figure 4.24. ^1H NMR spectrum of **1** in $\text{DMSO-}d_6\text{-CDCl}_3$ (1:5 v/v) before and after photolysis with visible light for 12h.

the generation of higher amount of cis form, although some trans isomer still remains even upon reaching saturation. Interestingly, the coupling constant (J) value of the olefinic protons also decreases from ~ 16 Hz to ~ 12 Hz upon isomerization. Chemical shift of the protons adjacent to the double bonds are also shifted to the more up-field region with a diminution in the intensity of the peaks. The observed changes corroborate the occurrence of trans \rightarrow cis photoisomerization upon visible light irradiation.

We also tried to carry out the backward cis \rightarrow trans photoisomerisation process by keeping the solution in dark for a long time. Since the process was extremely slow, we executed the backward process by irradiating with UV light of 280 nm (Figure 4.25). The initial state was almost reverted back after ~ 300 min of light irradiation.

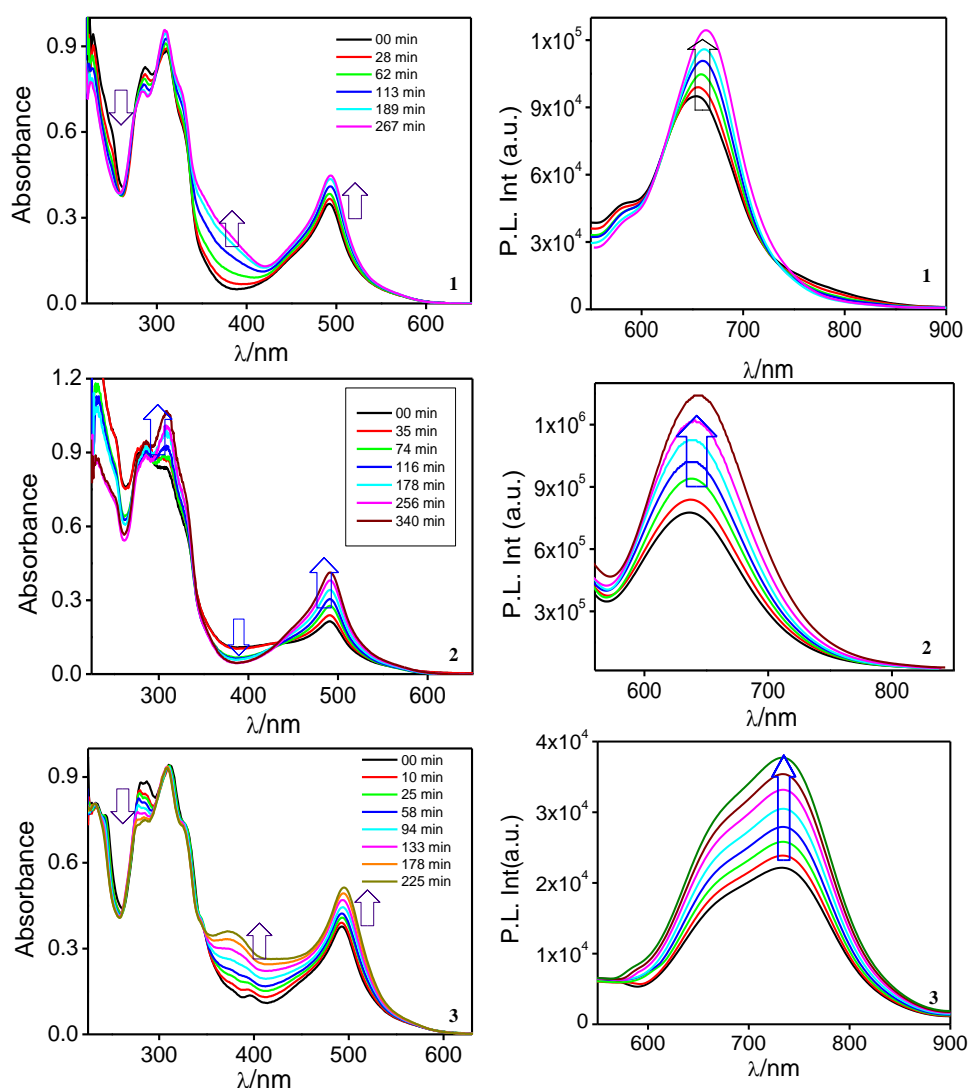


Figure 4.25. Absorption (left) and emission ($\lambda_{\text{ex}}=490$ nm, right) spectral changes in the cis forms of 1-3 upon UV light irradiation.

We have calculated rate constant (k_{iso}) as well as quantum yields (Φ) of both forward (trans \rightarrow cis, $\Phi_{\text{t}\rightarrow\text{c}}$) and backward (cis \rightarrow trans, $\Phi_{\text{c}\rightarrow\text{t}}$) photoisomerization process. The estimated values of k_{iso} and Φ are summarized in Table 4.6, while the related figures are presented in Figure 4.26. A first order kinetics is followed at the early stage of photoisomerization. For the forward process, the value of k_{iso} varies between 3.48 and 7.28

Table 4.6. Rate constant (k_{iso}) and quantum yield ($\Phi_{\text{t}\rightarrow\text{c}}$) for forward and backward photoisomerization process in the complexes.

	forward		backward	
	k_{iso} $\times 10^{-4}$	$\Phi_{\text{t}\rightarrow\text{c}}$ $\times 10^{-2}$	k_{iso} $\times 10^{-4}$	$\Phi_{\text{c}\rightarrow\text{t}}$ $\times 10^{-2}$
1	5.70	2.61	1.51	0.33
2	3.48	1.54	0.92	0.36
3	7.28	3.02	1.74	2.84

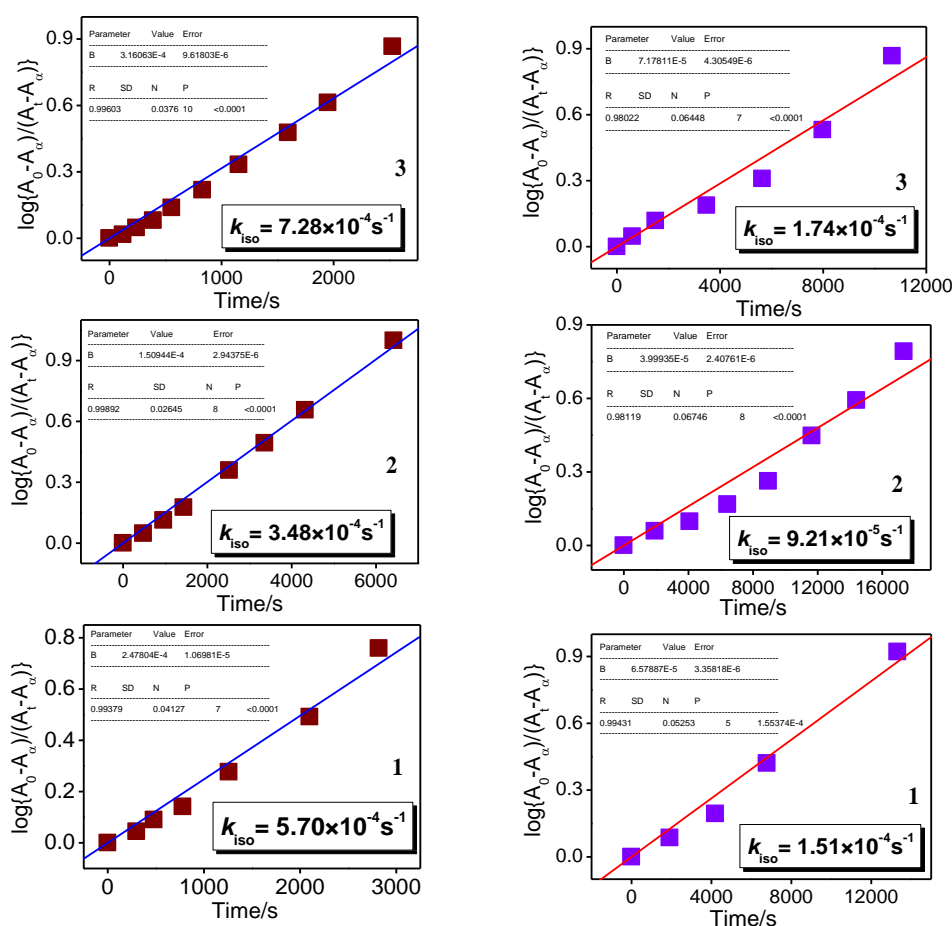
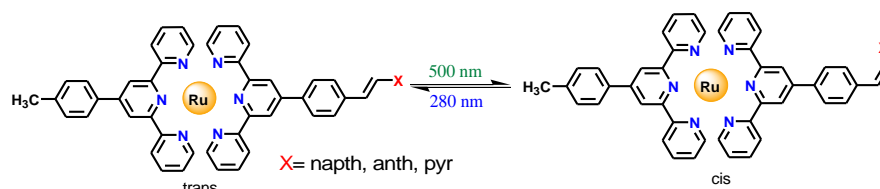


Figure 4.26. Linear plot of $\log(A_0 - A_f)/(A_t - A_f)$ vs. time (t) for the absorption spectral change due to trans \rightarrow cis (left) and cis \rightarrow trans (right) process of **1-3** upon irradiation with visible and UV light respectively. Inset to these plots give the values of rate constant of photoisomerization for the compounds.

$\times 10^{-4} \text{ s}^{-1}$ and $\Phi_{t \rightarrow c}$ alters within the range of $1.54\text{--}3.02 \times 10^{-2}$, while for the backward process, the corresponding values decreases by one-order of magnitude than that of the forward process. The reverse process is found to be much slower than that of the forward. Thus, the present complexes can behave as efficient photoswitches upon alternating treatment with 500 and 280 nm light as presented in Scheme 4.3.



Scheme 4.3. Simplified scheme depicting the process of reversible trans→cis photoisomerization.

4.3.9 Anion Sensing Characteristics of the Cis-form of the Complexes. As transformation from trans to the cis-form leads to conformation change in the polyaromatic moieties, it is expected that the extent of different non-classical interactions would be substantially altered on going from trans to the cis-isomer in the complexes. To this end, we also executed the anion sensing characteristics of the cis-form of the complexes and compared with their trans-forms. The absorption and emission spectral change in the cis-form of the complexes is monitored upon step-by-step inclusion of F^- (Figure 4.27). First of all, noticeable change in the spectral pattern is observed on passing from the trans to the cis form of the complexes, albeit the extent of change in the cis form is found to be less compared with their respective trans form. In particular, the absorption spectral pattern differs quite remarkably for all complexes wherein the change in the absorbance within the spectral domain of 200–300 nm is relatively smaller than their trans analogues. Additionally, the alteration in spectral profile in the visible region ($^1\text{MLCT}$ transition) is highest for the pyrene-derivative (**3**) in the trans form, while the corresponding change is maximum in the cis-form for the anthracene-derivative (**2**). In both cases, the spectral change is accompanied with visual color change. In line with trans isomers, considerable augmentation in emission intensity and Φ is also observed in respective cis-form, albeit to a small extent. The titration data of the cis- form of the complexes are also utilized for estimating both the binding constants and detection limits and the values are already presented in Table 4.5, Figure 4.27 and Figure 4.28 (for **2**). Upon comparing, it is evident that values of both binding constants and detection limits are less in cis- than that of the trans analogues. Considering the extent of

change in their spectral profiles as well as the values of binding constants for receptor-fluoride interactions, it appears that the trans-form is capable to take part in stronger non-covalent interactions relative to their cis-isomers. It is quite expected that the polyaromatic as well as the heteroaromatic motifs in the cis-forms are in strained conformations which in turn restrict them to take part in strong interaction with incoming anionic guest.

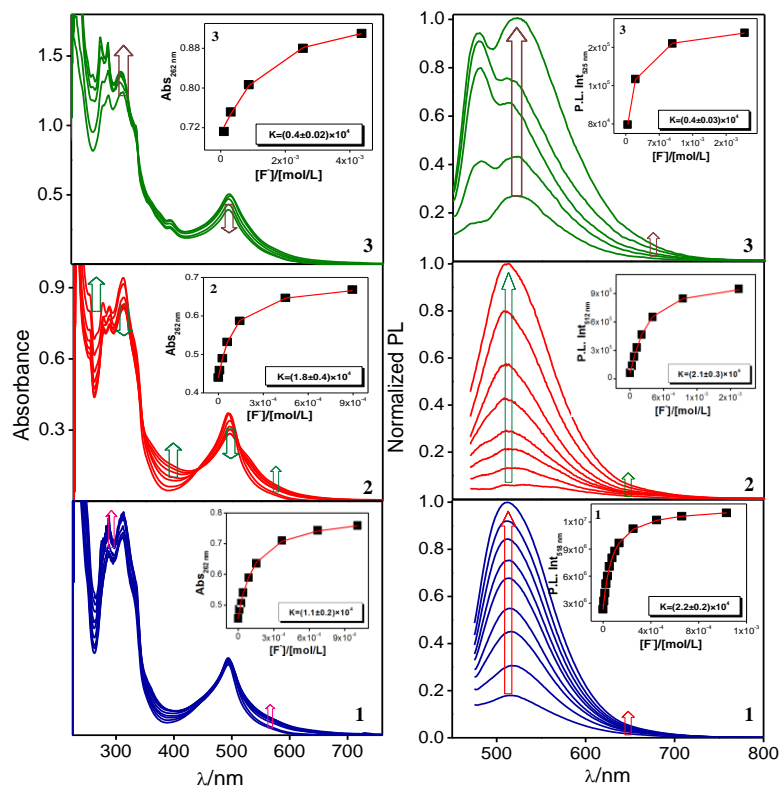


Figure 4.27. Absorption (left panel) and emission ($\lambda_{\text{ex}}=500$ nm) (right panel) spectral titrations with cis-forms of **1-3** (1.0×10^{-5} M) in MeCN upon gradual addition of F^- . Insets to the figures in both left and right panels indicate the estimation of binding constants.

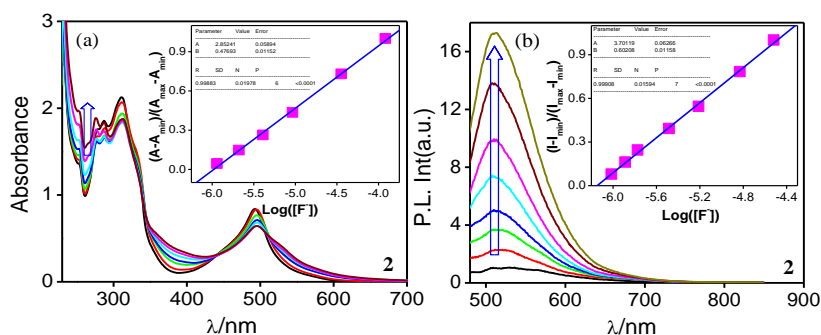


Figure 4.28. (a) Absorption and (b) emission spectral changes during the titration of the receptor **2-cis** (1.0×10^{-5} M) with F^- in MeCN, inset: (a) A plot of $(A-A_{\text{min}})/(A_{\text{max}}-A_{\text{min}})$ vs. $\text{Log}([F^-])$, the calculated detection limit of receptor is 6.8×10^{-7} M and (b) A plot of $(I-I_{\text{min}})/(I_{\text{max}}-I_{\text{min}})$ vs. $\text{Log}([F^-])$, the calculated detection limit of receptor is 7.2×10^{-7} M.

4.4 Conclusions

With regard to our sustained interest in designing prospective molecular sensors and switches, a new array of heteroleptic Ru(II)-terpyridine complexes coupled with stilbene-appended naphthalene, anthracene and pyrene motifs has been designed. The complexes display moderately intense emission at RT with elevated lifetimes (16.7 ns for naphthalene-, 11.4 ns for anthracene-, while 8.3 μ s for pyrene derivative). The most important aspect of the present study is the selective recognition of F^- among the studied anions. The outcomes of absorption, steady state and time-resolved emission, 1H and ^{19}F NMR spectroscopic measurements as well as DLS experiment unambiguously suggest that the complexes interact strongly with F^- via combination of several non-classical interactions, viz. $CH...F$ hydrogen bonding, $CH-\pi$, anion- π together with through space electrostatic interaction between positively charged complex entity and F^- . In conjunction with experimental investigations, theoretical calculation employing DFT is also executed for a selective complex to elucidate the mode of receptor-anion interaction.

Taking advantage of the stilbene motif, the complexes exhibit reversible trans-cis isomerization upon alternate treatment of visible and UV light so that the complexes can act as potential photo-molecular switches. The anion sensing characteristics of the cis-form of the complexes have also been executed and the extent of interaction is found to be substantially reduced than that of their trans-counterparts. Interestingly, the anion-treated solutions of the complexes get restored to their initial state upon treating with fluoride scavenger and the processes are reversible and could be repeated many times. Thus, in addition to their capability to act as potential photo-molecular switches, the complexes under present study also have the ability to function as on/off emission switches upon alternate treatment with F^- and $BF_3/HClO_4$.

4.5 References

- (1) Neel, A. J.; Hilton, M. J.; Sigman, M. S.; Toste, F. D. Exploiting Non-Covalent π Interactions for Catalyst Design. *Nature* **2017**, *543*, 637.
- (2) Biedermann, F.; Schneider, H.-J. Experimental Binding Energies in Supramolecular Complexes. *Chem. Rev.* **2016**, *116*, 5216.
- (3) Dougherty, D. A. The Cation- π Interaction. *Acc. Chem. Res.* **2013**, *46*, 4, 885-893.
- (4) Chifotides, H. T.; Dunbar, K. R. Anion- π Interactions in Supramolecular Architectures. *Acc. Chem. Res.* **2013**, *46*, 4, 894-906.
- (5) Platzer, G.; Mayer, M.; Beier, A.; Bräschweiler, S.; Fuchs, J. E.; Engelhardt, H.; Geist, L.; Bader, G.; Scherghuber, J.; Lichtenecker, R. *et al.* PI by NMR: Probing CH- π Interactions in Protein-Ligand Complexes by NMR Spectroscopy. *Angew. Chem. Int. Ed.* **2020**, *59*, 14861-14868.
- (6) Salonen, L. M.; Ellermann, M.; Diederich, F. Aromatic Rings in Chemical and Biological Recognition: Energetics and Structures. *Angew. Chem. Int. Ed.* **2011**, *50*, 4808-4842.
- (7) Zacharias, N.; Dougherty, D. A. Cation- π Interactions in Ligand Recognition and Catalysis. *Trends Pharmacol. Sci.* **2002**, *23*, 281-287.
- (8) Tam, A.Y.-Y.; Wong, K. M.-C.; Wang, G.; Yam, V. W.-W. Luminescent Metallogels of Platinum(II) Terpyridyl Complexes: Interplay of Metal...Metal, π - π and Hydrophobic-Hydrophobic Interactions on Gel Formation. *Chem. Commun.* **2007**, 2028-2030.
- (9) Wang, D.-X.; Wang, M.-X. Exploring Anion- π Interactions and their Applications in Supramolecular Chemistry. *Acc. Chem. Res.* **2020**, *53*, 7, 1364-1380.
- (10) Guha, S.; Saha, S.; Fluoride Ion Sensing by an Anion- π Interaction. *J. Am. Chem. Soc.* **2010**, *132*, 17674-17677.
- (11) Zhao, H.; Tang, L.; Fang, Y.; Liu, C.; Ding, W.; Zang, S.; Chen, Y.; Xu, W.; Yuan, Y.; Fang, D. *et al.* Manipulating Cation- π Interactions of Reader Proteins in Living Cells with Genetic Code Expansion. *J. Am. Chem. Soc.* **2023**, *145*, 30, 16406-16416.
- (12) Zhao, Y.; Beuchat, C.; Domoto, Y.; Gajewy, J.; Wilson, A.; Mareda, J.; Sakai, N.; Matile, S. Anion- π Catalysis. *J. Am. Chem. Soc.* **2014**, *136*, 2101-2111.
- (13) Haque, A.; Alenezi, K. M.; Khan, M. S.; Wong, W.Y.; Raithby, P. R. Non-Covalent Interactions (NCIs) in π -Conjugated Functional Materials: Advances and Perspectives. *Chem. Soc. Rev.* **2023**, *52*, 454-472.

- (14) Zhang, X.; Hao, X.; Liu, L.; Pham, A.-T.; Lopez-Andarias, J.; Frontera, A.; Sakai, N.; Matile, S. Primary Anion- π Catalysis and Autocatalysis. *J. Am. Chem. Soc.* **2018**, *140*, 17867-17871.
- (15) Tsuzuki, S. In *Structure and Bonding*. Wales, D., Ed.; Springer: Berlin, **2005**; Vol. 115.
- (16) Mascal, M.; Armstrong, A.; Bartberger, M. D. Anion-Aromatic Bonding: A Case for Anion Recognition by π -Acidic Rings. *J. Am. Chem. Soc.* **2002**, *124*, 6274-6276.
- (17) Alkorta, I.; Rozas, I.; Elguero, J. Interactions of Anions with Perfluoro Aromatic Compounds. *J. Am. Chem. Soc.* **2002**, *124*, 8593-8598.
- (18) Dawson, R. E.; Hennig, A.; Weimann, D. P.; Emery, D.; Ravikumar, V.; Montenegro, J.; Takeuchi, T.; Gabutti, S.; Mayor, M.; Mareda, J. *et al.* Experimental Evidence for the Functional Relevance of Anion- π Interactions. *Nat. Chem.* **2010**, *2*, 533-538.
- (19) Demeshko, S.; Dechert, S.; Meyer, F. Anion- π Interactions in a Carousel Copper(II)-Triazine Complex. *J. Am. Chem. Soc.* **2004**, *126*, 4508-4509.
- (20) Xiu, X.; Puskar, N. L.; Shanata, J. A. P.; Lester, H. A.; Dougherty, D. A. Nicotine Binding to Brain Receptors Requires a Strong Cation- π Interaction. *Nature* **2009**, *458*, 534.
- (21) Burley, S.; Petsko, G. Aromatic-Aromatic Interaction: A Mechanism of Protein Structure Stabilization. *Science* **1985**, *229*, 23-28.
- (22) Li, S.; Cooper, V. R.; Thonhauser, T.; Lundqvist, B. I.; Langreth, D. C. Stacking Interactions and DNA Intercalation. *J. Phys. Chem. B* **2009**, *113*, 11166-11172.
- (23) Steiner, T.; Koellner, G. Hydrogen Bonds with π -Acceptors in Proteins: Frequencies and Role in Stabilizing Local 3D Structures. *J. Mol. Biol.* **2001**, *305*, 535-557.
- (24) Gorteau, V.; Bollot, G.; Mareda, J.; Perez-Velasco, A.; Matile, S. Rigid Oligonaphthalenediimide Rods as Transmembrane Anion- π Slides. *J. Am. Chem. Soc.* **2006**, *128*, 14788-14789.
- (25) Zhao, Y.; Cotelle, Y.; Liu, L.; Lopez-Andarias, J.; Bornhof, A.-B.; Akamatsu, M.; Sakai, N.; Matile, S. The Emergence of Anion- π Catalysis. *Acc. Chem. Res.* **2018**, *51*, 2255-2263.
- (26) Jentsch, A.V.; Emery, D.; Mareda, J.; Metrangolo, P.; Resnati, G.; Matile, S. Ditopic Ion Transport Systems: Anion- π Interactions and Halogen Bonds at Work. *Angew. Chem., Int. Ed.* **2011**, *50*, 11675-11678.

- (27) Ramírez, G.-G.; Escudero-Adan, E. C.; Benet-Buchholz, J.; Ballester, P. Quantitative Evaluation of Anion- π Interactions in Solution. *Angew. Chem., Int. Ed.* **2008**, *47*, 4114-4118.
- (28) Tuo, D.-H.; Liu, W.; Wang, X.-Y.; Wang, X.-D.; Ao, Y.-F.; Wang, Q.-Q.; Li, Z.-Y.; Wang, D.-X. Toward Anion- π Interactions Directed Self-Assembly with Predesigned Dual Macrocyclic Receptors and Dianions. *J. Am. Chem. Soc.* **2019**, *141*, 1118-1125.
- (29) Amendola, V.; Bergamaschi, G.; Boiocchi, M.; Fabbrizzi, L.; Mosca, L. The Interaction of Fluoride with Fluorogenic Ureas: An ON¹-OFF-ON² Response. *J. Am. Chem. Soc.* **2013**, *135*, 6345-6355.
- (30) Amendola, V.; Gómez, D. E.; Fabbrizzi, L.; Licchelli, M. What Anions Do to N-H-Containing Receptors. *Acc. Chem. Res.* **2006**, *39*, 343-353.
- (31) Amendola, V.; Fabbrizzi, L.; Mosca, L. Anion recognition by hydrogen bonding: urea-based receptors. *Chem. Soc. Rev.* **2010**, *39*, 3889-3915.
- (32) Balzani, V.; Juris, A.; Venturi, M.; Campagna, S.; Serroni, S. Luminescent and Redox-Active Polynuclear Transition Metal Complexes. *Chem. Rev.* **1996**, *96*, 759-834.
- (33) Mo, H.-J.; Chao, H.-Y.; Ye, B.-H. A Ruthenium Biimidazole-Like Anion Receptor with Two Chelating N-H...O Intramolecular Hydrogen Bonds. *Inorg. Chem. Commun.* **2013**, *35*, 100-103.
- (34) Jr, P. A.; Tyson, D. S.; Kova', K. J.; Castellano, F. N. Luminescence Lifetime-Based Sensor for Cyanide and Related Anions. *J. Am. Chem. Soc.* **2002**, *124*, 6232-6233.
- (35) Deb, S.; Sahoo, A.; Pal, P.; Baitalik, S. Exploitation of the Second Coordination Sphere to Promote Significant Increase of Room-Temperature Luminescence Lifetime and Anion Sensing in Ruthenium-Terpyridine Complexes. *Inorg. Chem.* **2021**, *60*, 6836-6851.
- (36) Paul, A.; Sahoo, A.; Bhattacharya, S.; Baitalik, S. Anion and Temperature Responsive Molecular Switches Based on Trimetallic Complexes of Ru(II) and Os(II) That Demonstrate Advanced Boolean and Fuzzy Logic Functions. *Inorg. Chem.* **2022**, *61*, 3186-3201.
- (37) Dietrich, J.; Thorenz, U.; Forster, C.; Heinze, K. Effects of Sequence, Connectivity, and Counter Ions in New Amide-Linked Ru(tpy)₂-Re(bpy) Chromophores on Redox Chemistry and Photophysics. *Inorg. Chem.* **2013**, *52*, 1248-1264.

- (38) Bar, M.; Deb, S.; Paul, A.; Baitalik, S. Stimuli-Responsive Luminescent Bis-Tridentate Ru(II) Complexes toward the Design of Functional Materials. *Inorg. Chem.* **2018**, *57*, 12010-12024.
- (39) Bar, M.; Maity, D.; Das, K.; Baitalik, S. Asymmetric Bimetallic Ruthenium(II) Complexes Selectively Sense Cyanide in Water Through Significant Modulation of Their Ground and Excited State Properties. *Sensors and Actuators B* **2017**, *251*, 208-223.
- (40) Zhang, Y. M.; Wu, S. H.; Yao, C. J.; Nie, H. J.; Zhong Y. W. A Bis(terpyridine) Ruthenium Complex with Three Redox-active Amine Sites: Electrochemical, Optical, and Computational Studies. *Inorg. Chem.* **2012**, *51*, 11387-11395.
- (41) Shao J. Y.; Zhong Y. W. pH Value-Dependent Electronic Absorption and Ru(III/II) Potential of Bis-Tridentate Pincer Ruthenium Complexes. *J. Organomet. Chem.* **2017**, *845*, 144-150.
- (42) Badjic, J. D.; Balzani, V.; Credi, A.; Silvi, S.; Stoddart, J. F. A Molecular Elevator. *Science* **2004**, *303*, 1845-1849.
- (43) Harriman, A.; Ziessel, R. Making Photoactive Molecular-Scale Wires. *Chem. Commun.* **1996**, 1707-1716.
- (44) Breivogel, A.; Förster, C.; Heinze, K.; A Heteroleptic Bis (Tridentate) Ruthenium (II) Polypyridine Complex with Improved Photophysical Properties and Integrated Functionalizability. *Inorg. Chem.* **2010**, *49*, 7052-7056.
- (45) Kreitner, C.; Erdmann, E.; Seidel, W. W. Heinze, K. Understanding the Excited State Behavior of Cyclometalated Bis (Tridentate) Ruthenium (II) Complexes: A Combined Experimental and Theoretical Study. *Inorg. Chem.* **2015**, *54*, 11088.
- (46) Cui, B. B.; Zhong Y. W.; Yao, J. Three-State Near-Infrared Electrochromism at the Molecular Scale. *J. Am. Chem. Soc.* **2015**, *137*, 4058-4061.
- (47) Yang, W. W.; Zhong, Y. W.; Yoshikawa, S.; Shao, J. Y.; Masaoka, K. S.; Yao, J.; Haga, M. Tuning of Redox Potentials by Introducing a Cyclometalated Bond to Bis-Tridentate Ruthenium(II) Complexes Bearing Bis(N-methylbenzimidazolyl)benzene or -Pyridine Ligands. *Inorg. Chem.* **2012**, *51*, 890-899.
- (48) Kalyanasundaram, K.; Grätzel, M. Applications of Functionalized Transition Metal Complexes in Photonic and Optoelectronic Devices. *Coord. Chem. Rev.* **1998**, *177*, 347-414.

- (49) Campagna, S.; Puntoriero, F.; Nastasi, F.; Bergamini, G.; Balzani, V. Photochemistry and Photophysics of Coordination Compounds: Ruthenium. *Top. Curr. Chem.* **2007**, *280*, 117-214.
- (50) Juris, A.; Balzani, V.; Barigelletti, F.; Campagna, S.; Belser, P.; Von Zelewsky, A. Ru(II) Polypyridine Complexes: Photophysics, Photochemistry, Electrochemistry, and Chemiluminescence. *Coord. Chem. Rev.* **1988**, *84*, 85-277.
- (51) Brown, D. G.; Sanguantrakun, N.; Schulze, B.; Schubert, U. S.; Berlinguette, C. P. Bis(tridentate) Ruthenium-Terpyridine Complexes Featuring Microsecond Excited-State Lifetimes. *J. Am. Chem. Soc.* **2012**, *134*, 12354-12357.
- (52) Hofmeier, H.; Schubert, U. S. Recent Developments in the Supramolecular Chemistry of Terpyridine-Metal Complexes. *Chem. Soc. Rev.* **2004**, *33*, 373-399.
- (53) Baranoff, E.; Collin, J.-P.; Flamigni, L.; Sauvage, J.-P. From Ruthenium(II) to Iridium(III): 15 Years of Triads Based on Bis-Terpyridine Complexes. *Chem. Soc. Rev.* **2004**, *33*, 147-155.
- (54) Paul, A.; Bar, M.; Deb, S.; Baitalik, S. Long-Lived Trimetallic Complexes of Fe(II), Ru(II), and Os(II) Based on a Heteroditopic Bipyridine-Terpyridine Bridge: Synthesis, Photophysics, and Electronic Energy Transfer. *Inorg. Chem.* **2019**, *58*, 10065-10077.
- (55) Mondal, D.; Bar, M.; Mukherjee, S.; Baitalik, S. Design of Ru(II) Complexes Based on Anthraimidazoledione-Functionalized Terpyridine Ligand for Improvement of Room-Temperature Luminescence Characteristics and Recognition of Selective Anions: Experimental and DFT/TD-DFT Study. *Inorg. Chem.* **2016**, *55*, 9707-9724.
- (56) Mondal, D.; Biswas, S.; Paul, A.; Baitalik, S. Luminescent Dinuclear Ruthenium Terpyridine Complexes with a Bis-Phenylbenzimidazole Spacer. *Inorg. Chem.* **2017**, *56*, 7624-7641.
- (57) Ganguly, T.; Pal, P.; Maity, D.; Baitalik, S. Synthesis, Characterization and Emission Switching Behaviors of Styrylphenyl-Conjugated Ru(II)-Terpyridine Complexes via Aggregation and Trans-Cis Photoisomerization. *J. Photochem. Photobiol. A* **2023**, *440*, 114662.
- (58) Karmakar, S.; Maity, D.; Mardanya, S.; Baitalik, S. Multichromophoric Bimetallic Ru(II) Terpyridine Complexes Based on Pyrenyl-bis-phenylimidazole Spacer: Synthesis, Photophysics, Spectroelectrochemistry, and TD-DFT Calculations. *Inorg. Chem.* **2014**, *53*, 12036-12049.

- (59) Goze, C.; Sabatini, C.; Barbieri, A.; Barigelletti, F.; Ziessel, R. Rhenium-Terpyridine Complexes with Multiple Ethynylpyrenyl or Ethynyltoluyl Subunits: X-ray Structure, Redox, and Spectroscopic Properties. *Inorg. Chem.* **2007**, *46*, 7341-7350.
- (60) Pal, A. K.; Hanan, G. S. Design, Synthesis and Excited-State Properties of Mononuclear Ru(II) Complexes of Tridentate Heterocyclic Ligands. *Chem. Soc. Rev.* **2014**, *43*, 6184-6197.
- (61) Prieto, J. P.; Pe´rez, L. P.; Gonza´lez-Be´jar, M.; Miranda, M. A. Stiriba, S.-E. Pyrene-Benzoylthiophene Bichromophores as Selective Triplet Photosensitizers. *Chem. Commun.* **2005**, 5569.
- (62) Schottel, B. L.; Chifotides, H. T.; Shatruk, M.; Chouai, A.; Pe´rez, L. M.; Bacsá, J.; Dunbar, K. R. Anion- π Interactions as Controlling Elements in Self-Assembly Reactions of Ag(I) Complexes with π -Acidic Aromatic Rings. *J. Am. Chem. Soc.* **2006**, *128*, 5895-5912.
- (63) Capo´, M.; Buchholz, J. B.; Ballester, P. Anion- π - π Interactions in a Dinuclear M_2L_2 Metallocycle. *Inorg. Chem.* **2008**, *47*, 10190-10192.
- (64) Benito, C. M.; Bauzá, A.; Lago, A. B.; Ruiz-Pérez, C.; Jiménez, C. A.; Torres, M. E.; Frontera, A.; Pasán, J. Anion- π Interactions in Hollow Crystals of a Copper(II)-Cyamelurate Coordination Complex. *Cryst. Growth Des.* **2018**, *18*, 4, 2636-2644.
- (65) Kuzniak, E.; Pinkowicz, D.; Hooper, J.; Srebro-Hooper, M.; Hetman´czyk, Ł.; Podgajny, R. Molecular Deformation, Charge Flow, and Spongelike Behavior in Anion- π $\{[M(CN)_4]^{2-}; [HAT(CN)_6]\}_\infty$ (M=Ni, Pd, Pt) Supramolecular Stacks. *Chem. Eur. J.* **2018**, *24*, 16302-16314.
- (66) Zeng, H.; Liu, P.; Feng, G.; Huang, F. π -Metalated [1₅]Paracyclophanes: Synthesis and Binding to Oxo Anions via Anion- π Interactions. *J. Am. Chem. Soc.* **2019**, *141*, 16501-16511.
- (67) Zhou, Y.; Zhang, J. F.; Yoon, J. Fluorescence and Colorimetric Chemosensors for Fluoride-Ion Detection. *Chem. Rev.* **2014**, *114*, 5511-5571.
- (68) Busschaert, N.; Caltagirone, C.; Rossom, W. V.; Gale, P. A. Applications of Supramolecular Anion Recognition. *Chem. Rev.* **2015**, *115*, 8038-8155.
- (69) Singh, H.; Tiwari, K.; Tiwari, R.; Pramanik, S. K.; Das, A. Small Molecule as Fluorescent Probes for Monitoring Intracellular Enzymatic Transformations. *Chem. Rev.* **2019**, *119*, 11718-11760.

- (70) Ghosh, A.; Verma, S.; Ganguly, B.; Ghosh, H. N.; Das, A. Influence of Urea N-H Acidity on Receptor-Anionic and Neutral Analyte Binding in a Ruthenium(II)-Polypyridyl-Based Colorimetric Sensor. *Eur. J. Inorg. Chem.* **2009**, 2496-2507.
- (71) Jose, D. A.; Kar, P.; Koley, D.; Ganguly, B.; Thiel, W.; Ghosh, H. N.; Das, A. Phenol- and Catechol-Based Ruthenium(II) Polypyridyl Complexes as Colorimetric Sensors for Fluoride Ions. *Inorg. Chem.* **2007**, 46, 14.
- (72) Das, P.; Mahato, P.; Ghosh, A.; Mandal, A. K.; Banerjee, T.; Saha, S.; Das, A. Urea/Thiourea Derivatives and Zn(II)-DPA Complex as Receptors for Anionic Recognition-A Brief Account. *J. Chem. Sci.* **2011**, 123, 2, 175-186.
- (73) Jose, D. A.; Kumar, D. K.; Ganguly, B.; Das, A. Efficient and Simple Colorimetric Fluoride Ion Sensor Based on Receptors Having Urea and Thiourea Binding Sites. *Org. Lett.* **2004**, 6, 20, 3445-3448.
- (74) Kume, S.; Nishihara, H. Metal-based Photoswitches Derived from Photoisomerization. *Struct. Bonding* **2007**, 123, 79-112.
- (75) Ko, C.-C.; Yam, V. W. W. Transition Metal Complexes with Photochromic Ligands Photosensitization and Photoswitchable Properties. *J. Mater. Chem.* **2010**, 20, 2063-2070.
- (76) Ko, C.-C.; Yam, V. W.-W. Coordination Compounds with Photochromic Ligands: Ready Tunability and Visible Light-Sensitized Photochromism. *Acc. Chem. Res.* **2018**, 51, 149-159.
- (77) Duan, G.; Yam, V. W.-W. Syntheses and Photophysical Properties of N Pyridylimidazol-2-ylidene Tetracyano Ruthenates(II) and Photochromic Studies of Their Dithienylethene-Containing Derivatives. *Chem. Eur. J.* **2010**, 16, 12642-12649.
- (78) Pal, P.; Mukherjee, S.; Maity, D.; Baitalik, S. Synthesis, Structural Characterization, and Luminescence Switching of Diarylethene-Conjugated Ru(II)-Terpyridine Complexes by Trans-Cis Photoisomerization: Experimental and DFT/TD-DFT Investigation. *Inorg. Chem.* **2018**, 57, 5743-5753.
- (79) Ganguly, T.; Pal, P.; Paul, A.; Baitalik, S. Synthesis and Manifold but Controllable Emission Switching of Stilbene-Appended Polyaromatic Terpyridine Derivatives via Aggregation and Trans-Cis Isomerization. *Photochem. Photobiol. A* **2022**, 430, 113966.
- (80) Baggi, G.; Boiocchi, M.; Ciarrocchi, C.; Fabbrizzi L. Enhancing the Anion Affinity of Urea-Based Receptors with a Ru(terpy)₂²⁺ Chromophore. *Inorg. Chem.* **2013**, 52, 5273-5283.

- (81) Tuo, D-H.; Liu, W.; Wang, X.-Y.; Wang, X.-D.; Ao, Y.-F.; Wang, Q-Q.; Li, Z.-Y.; Wang D-X. Toward Anion- π Interactions Directed Self-Assembly with Predesigned Dual Macrocyclic Receptors and Dianions. *J. Am. Chem. Soc.* **2019**, *141*, 1118-1125.



Chapter 5

**Modulation of Room Temperature Emission
Characteristics of Heteroleptic Ruthenium-
Terpyridine Complexes via Aggregation**

5.1 Introduction

Ruthenium(II) complexes derived from polypyridine ligands can act as potential building blocks for the fabrication of photochemical molecular devices and machines by taking advantage of their remarkable amalgamation of photophysical and redox behaviours.¹⁻⁸ The polypyridines typically comprise of either bidentate chelating units, viz. 2,2'-bipyridine (bpy) and 1,10-phenanthroline (phen) or tridentate sites such as 2,2':6',2''-terpyridine (tpy) motif connected with different types of spacers to control the topology and electronic nature of the resulting metal-ligand assembly.⁹⁻¹⁵ The incredible progress made in the chemistry of bipyridine and oligopyridines was originated by the discovery of the remarkably effectual photosensitizing behaviour of $[\text{Ru}(\text{bpy})_3]^{2+}$ and thereafter flourished by the design of several other tris-bidentate Ru(II) complexes.¹⁴⁻¹⁹ But the synthesis of tris(bpy)-type complexes is always associated with formation of diastereomeric mixtures and separation of which is very tedious. Bis-terpyridine type complexes, on the other hand, produces achiral rod-like structures when substituted at the 4'-position of the tpy ligands.²⁰⁻²⁵ However, the major shortcomings is their non-luminescence characteristics together with very short excited-state lifetimes ($\tau = 0.25$ ns for of $[\text{Ru}(\text{tpy})_2]^{2+}$) which is the main constraint for their potential use as efficient photosensitizers.^{21,26-27} Several synthetic strategies have been adopted by various research groups to design luminescent terpyridine-type complexes of Ru(II) with elevated excited-state lifetimes at RT. In most of approaches, the emphasis was given to enlarge the energy barrier among the radiative triplet metal-to-ligand charge transfer ($^3\text{MLCT}$) and non-luminescent triplet metal-centered (^3MC) states. Lowering the energy of $^3\text{MLCT}$ state could be accomplished by incorporating electron-withdrawing group-,²⁸⁻³² coplanar heteroaromatic motif,³³⁻³⁵ organic chromophores,³⁶ etc. Certainly, execution of such protocols leads to augmentation of RT emission characteristics of the designed complexes in comparison to $[\text{Ru}(\text{tpy})_2]^{2+}$.³⁷ An alternative strategy is to destabilize the ^3MC state by employing cyclometalated ligands.³⁸⁻⁴² Modification of the terpyridine motif could be done by replacing the pyridines with other heterocyclic rings to enlarge the bite angle of the tridentate ligand.⁴³

With regard to our continued interest to design luminescent Ru(II)-terpyridine complexes, we have recently reported a new family of emissive stilbene-appended Ru(II)-terpyridine complexes of the type, $[(\text{tpy}-\text{PhCH}_3)\text{Ru}(\text{tpy}-\text{pvp}-\text{X})](\text{ClO}_4)_2$, consisting of a polyaromatic hydrocarbon unit such as anthracene, naphthalene and pyrene at the 4' position of the terpyridines (Chart 5.1).⁴⁴ The incorporation of polyaromatic hydrocarbon along with stilbene moiety is expected to have their $^3\pi-\pi^*$ state which is quasi-isoelectronic to the

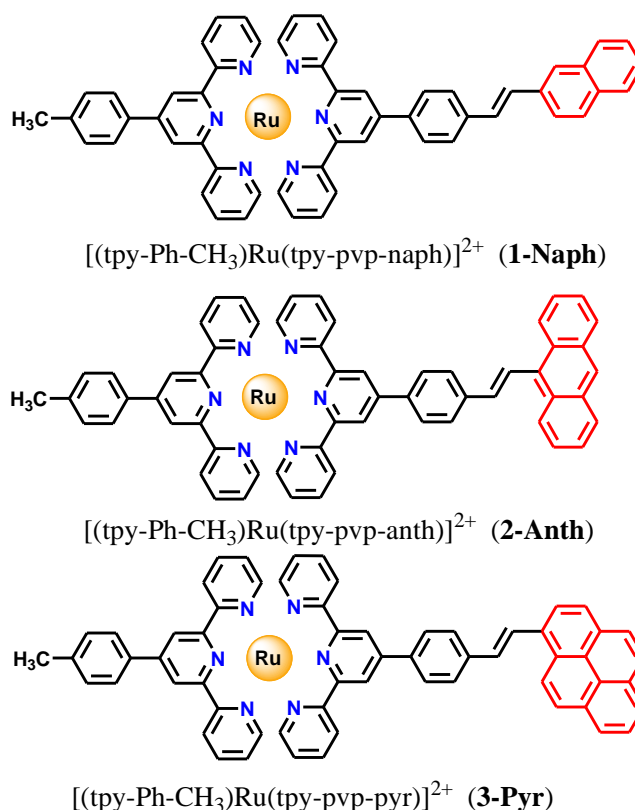


Chart 5.1. Chemdraw structures of the complexes.

$^3\text{MLCT}$ state in the complex entity. Upon photo-excitation, reversible intercomponent energy transfer is feasible between $^3\text{MLCT}$ and $^3\pi\text{-}\pi^*$ states so that the adjoining polyaromatic chromophores can act as an energy reservoir so as to repopulate the emissive $^3\text{MLCT}$ state, with an overall effect of ‘delaying’ the emission yielding long-lived excited-state.⁴⁵⁻⁴⁷ In practice, the complexes display moderately strong emission at RT having lifetime of 16.7 ns for naphthalene-, 11.4 ns for anthracene-, while substantially elevated lifetime of 8.3 μs for pyrene derivative. Additionally, by taking advantage of polyaromatic and heteroaromatic motifs, the anion recognition characteristics of the complexes have been investigated via the intermediary of different non-covalent interactions.

In this work our target is to modulate the photophysical properties in general and RT emission features in particular of the said complexes via aggregation through the usage of dissimilar solvents.⁴⁸⁻⁵² Molecules that are typically non-emissive in their dilute solutions could be made emissive upon inducing aggregation via suitable solvent mixtures.⁵³⁻⁶¹ This protocol is termed as aggregation induced emission (AIE) and was first developed by Tang.⁶² Another protocol, pioneered by Park and co-workers,⁶³ demonstrated aggregation induced emission enhancement (AIEE), wherein the emissive molecules display further augmentation

in the emission characteristics upon aggregation.⁶⁴⁻⁶⁵ Restrictions of intermolecular rotations (RIR) are the probable cause of both AIE and AIEE.⁶⁶⁻⁶⁷ Ru(II) complexes based on terpyridine-type ligands usually either non-luminescent or weakly emissive at RT with low quantum yield and short excited state lifetime. In the design protocol, we introduced different polyaromatic hydrocarbon along with stilbene moiety in the complexes. It is expected that the present complexes, by virtue of their delocalized pi-electron cloud, will take part in the aggregation process through the judicious choice of solvent mixtures.⁶⁸⁻⁷⁵ Herein, our objective is to modulate the RT emission behaviours of the present Ru(II)-terpyridine complexes upon inducing aggregation through the use of different solvent mixtures. To fulfil our objective, we have thoroughly investigated the modulation of luminescence characteristics of the present stilbene-appended heteroleptic Ru(II)-terpyridine complexes of the type, [(tpy-PhCH₃)Ru(tpy-pvp-X)](ClO₄)₂, wherein X = naphthalene, anthracene, and pyrene moiety via aggregation through the use of appropriate solvent mixtures. Interestingly, the complexes display both aggregation-induced emission quenching as well as emission augmentation, depending upon nature of the solvent mixtures. Additionally, in opposing to majority of the reported systems that display bathochromic-shift of emission peak upon aggregation, the present complexes show emission augmentation and/or quenching, keeping either the emission maximum unchanged or slightly-blue shifted, depending upon the solvent mixtures. The augmentation of emission maximum accompanied with blue-shift is called Aggregation-Induced Blue-Shifted Emission (AIBSE) and extensive investigations are being executed in recent time to fabricate quantum efficient systems.⁷⁶⁻⁸⁰

In the design protocol, we have incorporated a styrylbenzene moiety onto the complex architecture that could lead to trans-cis isomerization upon treatment with light.⁸¹⁻⁹² We have already investigated the reversible trans-cis isomerization of the free form of the complexes upon alternative treatment of visible and UV light.⁴⁴ In this work, we also executed trans-cis photoisomerization of the aggregated form of the complexes. As will be demonstrated, substantial alteration of both rate and quantum yield of photoisomerization takes place on passing from free-form to the respective aggregated form of the complexes.⁹¹

5.2 Experimental Section

5.2.1 Materials. RuCl₃·xH₂O and sodium perchlorate are purchased from Merck. Other chemicals and solvents are procured from local vendors. The terpyridine ligands, tpy-pvp-X (X=naphthalene, anthracene, and pyrene) ligands as well as their heteroleptic Ru(II)

complexes of the type, $[(\text{tpy-PhCH}_3)\text{Ru}(\text{tpy-pvp-X})](\text{ClO}_4)_2$ have been prepared and thoroughly characterized, the details of which are provided in Chapter 2 and Chapter 4.

Caution! *Perchlorate salts of the metal complexes are potentially explosive and therefore should be handled in small quantities with care.*

5.2.2. Instruments and Physical Methods. Details of instruments and physico-chemical measurements are previously discussed in Chapter 2.

5.3 Results and Discussions

5.3.1 Synthesis and Characterization. The details of synthesis and characterization of the heteroleptic complexes have already been provided in chapter 4.⁴⁴

5.3.2 Computational Investigation. The DFT optimized geometry together with the frontier molecular orbitals of **1-Naph** are presented in Figure 5.1. The compositions of respective HOMOs and LUMOs are presented in Table 5.1. The HOMOs are localized mostly on the Ru(II) centre and partially on the styrylphenyl and polyaromatic moiety. The LUMOs, on the other hand, are localized primarily on the terpyridine units.

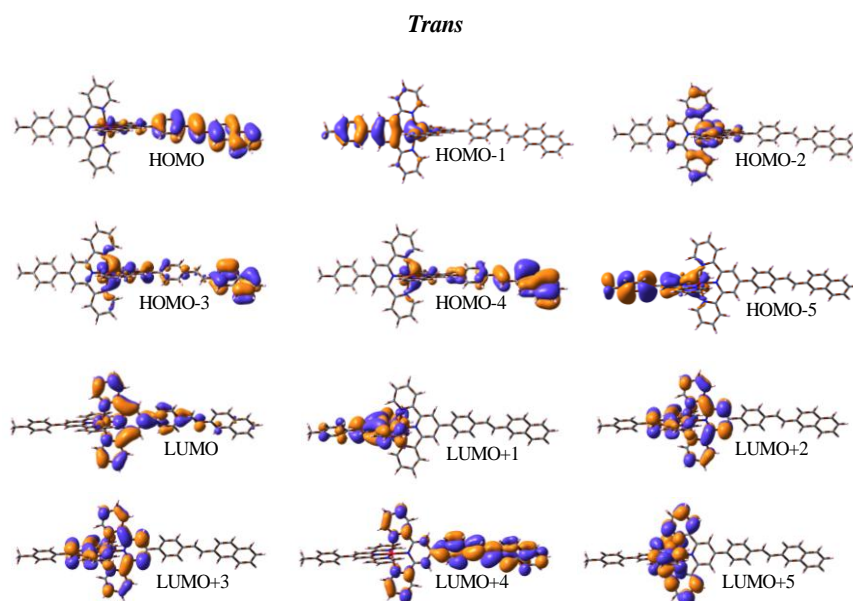


Figure. 5.1. Schematic drawings of the selective frontier molecular orbitals of trans form of **1-Naph** in MeCN.

5.3.3 Aggregation-induced Modulation of the Emission Characteristics of the Complexes. The molecular architecture of the complexes consists of extensive hetero-aromatic as well as polyaromatic moieties which endow the complexes to exhibit typical aggregation induced behaviours. Herein, we have investigated the aggregation phenomena by

Table 5.1. Selected MOs along with their energies and compositions in the ground state for $[(\text{tpy}-\text{PhCH}_3)\text{Ru}(\text{tpy}-\text{pvp}-\text{naph})]^{2+}$ in MeCN.

MO	$[(\text{tpy}-\text{PhCH}_3)\text{Ru}(\text{tpy}-\text{pvp}-\text{naph})]^{2+}$					
	Energy/eV	% compositions				
		<i>trans</i>	<i>trans</i>			
			Ru	naptha	Pvp	Mpt cap tpy
LUMO+5	-1.58		0.00	0.00	0.00	49.89 50.09
LUMO+4	-1.91		0.35	25.98	43.75	0.07 29.84
LUMO+3	-2.41		3.11	0.00	0.31	51.05 45.51
LUMO+2	-2.49		0.00	0.00	0.33	47.39 52.27
LUMO+1	-2.65		7.88	0.01	0.08	90.05 1.96
LUMO	-2.70		7.66	2.32	10.73	2.01 77.25
HOMO	-5.63		5.97	46.49	42.62	0.67 4.24
HOMO-1	-6.08		60.56	0.00	0.00	32.68 6.74
HOMO-2	-6.13		69.83	0.13	0.03	15.04 14.94
HOMO-3	-6.15		46.10	31.18	4.38	5.15 13.17
HOMO-4	-6.37		16.67	62.04	14.28	1.87 5.12
HOMO-5	-6.91		12.25	0.00	0.00	86.21 15.28

employing different solvent mixtures. As the emission spectral characteristics of the complex chromophores are critically dependent on the microenvironment, we investigated their emission spectral characteristics in a mixed environment of binary solvent mixtures. Herein, we employed five different types of solvent mixtures, viz. DMSO-H₂O, DMSO-CHCl₃, DMF-H₂O, MeCN-H₂O (where DMSO, DMF and MeCN act as good solvent whereas H₂O as the poor solvent) as well as DCM/hexane (where DCM is good solvent while hexane as the bad solvent). The emission spectra of all three complexes, acquired upon varying the ratio of DMSO/H₂O mixture is shown in Figure 5.2. It is to be noted that all three complexes display a broad emission band within the spectral domain of 600-900 nm together with a sharp peak in the range of 513-520 nm, upon excitation at 450 nm. The longer wavelength bands are mostly due to deactivation from the ³MLCT state, while the sharp peak within the narrow range of 513-520 nm corresponds to the ligand-centred emission, arising out of the deactivation of ³ILCT and/or ³ π - π^* state. We have also recorded the excitation spectra of all three complexes within the spectral range of 200-630 nm, keeping the emission maximum fixed at ~670 nm. The relevant excitation spectra are provided in Figure 5.3. The excitation spectral profiles clearly indicate that the tail of the excitation spectrum extend below 550 nm in all cases. Since no detectable change in the ligand centred emission takes place upon aggregation, we displayed the emission spectral profiles of the complexes within the spectral domain of 600-900 nm for clarity. It is seen that upon increasing the water fraction (f_w), the emission intensity gradually decreases in all three cases which is also evident from their

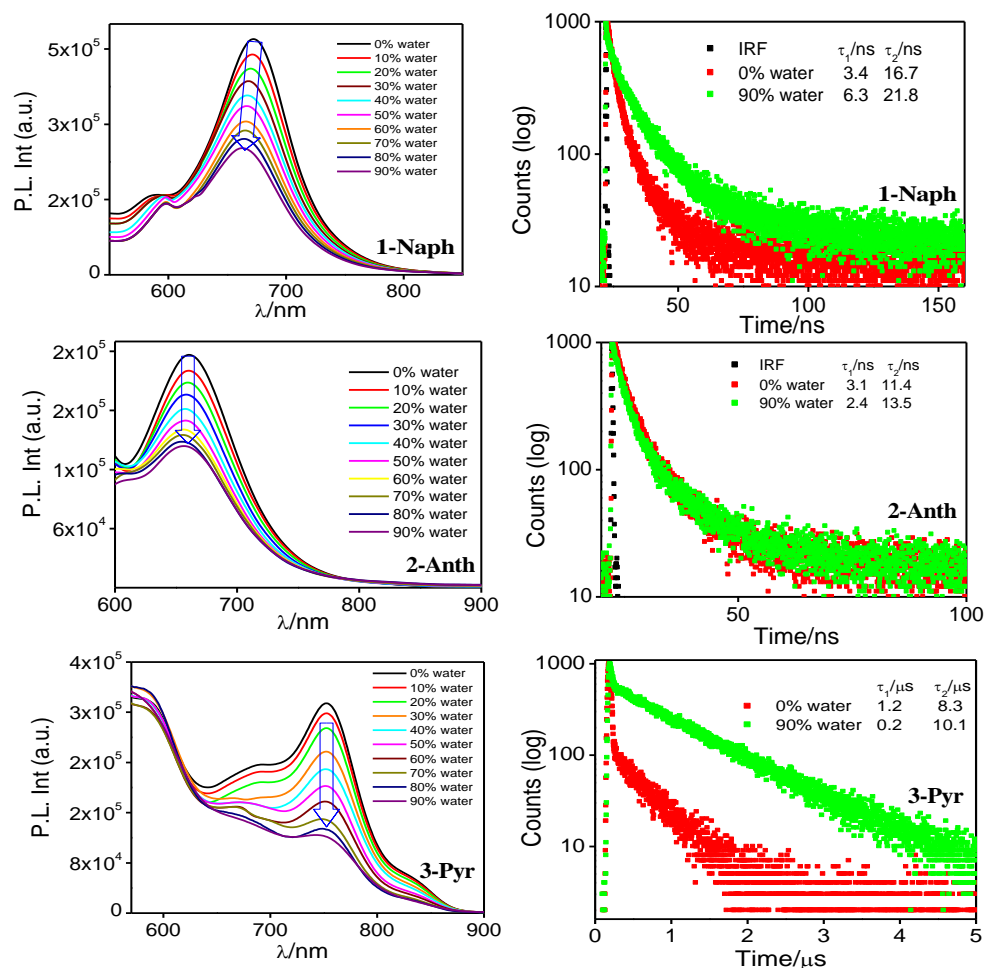


Figure 5.2. The emission ($\lambda_{ex}=500$ nm, left panel) spectral changes of the complexes upon varying the relative ratio of DMSO and H₂O. Right panel shows the corresponding change in emission decay ($\lambda_{ex}=450$ nm NanoLED) along with the lifetime values of the initial and final form of the complexes.

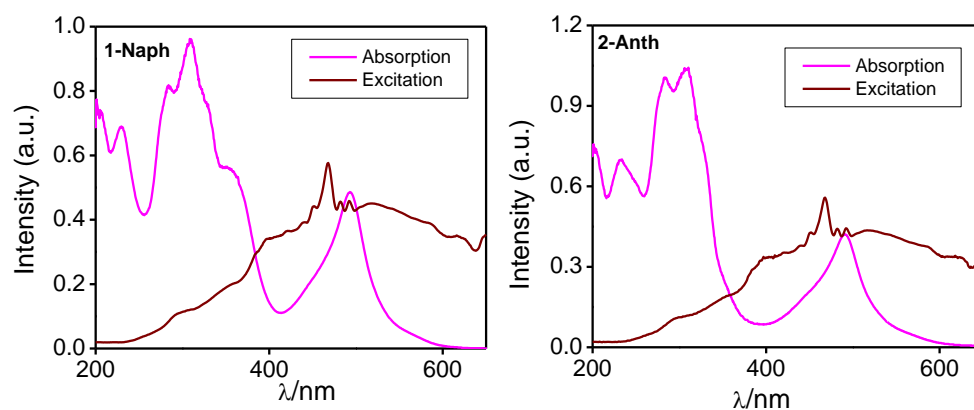


Figure 5.3. Overlay of the absorption and excitation ($\lambda_{em}=670$ nm) spectrum of **1-Naph** and **2-Anth** in MeCN.

quantum yield values (Table 5.2). A small blue-shift is noticed only in case of naphthalene derivative. We have also measured the lifetimes of the free as well as 90% f_w forms of all three complexes by time-correlated single photon counting (TCSPC) technique upon exciting with 450 nm NanoLED and the measured average lifetime (τ_{avg})⁹³ of the complexes in different solvent mixtures are provided in Table 5.3. The lifetime value is seen to increase in almost all cases, albeit in different extent upon saturation ($f_w=90\%$, Table 5.3). We have also studied the aggregation behaviours of the complexes in DMSO upon increasing the $CHCl_3$ fraction, wherein we observed gradual quenching of emission together with increase in lifetime, similar to that of DMSO/ H_2O mixture.

Table 5.2. Emission quantum yield of the complexes in their free form ($\phi_{0\%}$) and 90% aggregated form ($\phi_{90\%}$).

solvent	Compounds	$\phi_{0\%}$ ($\times 10^{-3}$)	$\phi_{90\%}$ ($\times 10^{-3}$)
DMSO/ H_2O	1-Naph	12.4	5.7
DMSO/ H_2O	2-Anth	6.3	3.8
DMSO/ H_2O	3-Pyr	3.8	0.08
MeCN/ H_2O	1-Naph	3.3	4.5
MeCN/ H_2O	2-Anth	2.1	4.8
MeCN/ H_2O	3-Pyr	0.4	1.7
DCM/Hexane	1-Naph	6.8	25.1
DCM/Hexane	2-Anth	2.1	11.7

Table 5.3. Average lifetime (τ_{avg}) values of the trans and cis isomers of complexes in their free and aggregated forms.

Compound	Average Lifetime (τ_{avg})										
	DMSO/H ₂ O		DMSO/CHCl ₃		MeCN/H ₂ O		DCM/Hexane			Photoisomerized	
	free	90% H ₂ O	free	90% CHCl ₃	free	90% H ₂ O	free	50% hexane	90% hexane	50% cis hexane	90% cis hexane
1-Naph	14.3 ns	17.5 ns	14.3 ns	11.1 ns	5.0 ns	11.5 ns	5.4 ns	58.3 ns	124.3 ns	11.6 ns	5.7 ns
2-Anth	7.7 ns	8.3 ns	7.7 ns	6.5 ns	3.7 ns	7.81 ns	4.7 ns	9.6 ns	16.1 ns	9.2 ns	4.2 ns
3-Pvr	4.9 μ s	6.6 μ s	4.9 μ s	6.3 μ s	1.9 μ s	2.4 μ s	-	-	-	-	-

Figure 5.4 demonstrates the change in the emission spectral profiles of the complexes upon variation of MeCN/ H_2O ratio. In contrast to the observed behaviour in DMSO/ H_2O and DMSO- $CHCl_3$, the luminescence intensity steadily enhances here upon increase in water fraction, indicating the occurrence of aggregation induced emission enhancement. Small variation in the extent of enhancement, depending upon the nature of polyaromatic moiety, is also noticed (Table 5.2). Lifetimes are also measured and we see that the 90% f_w show an increased values of lifetimes in all cases compared to their non-aggregated form (Table 5.3).

We also studied the AIEE phenomenon in non-aqueous solvent systems upon employing DCM/hexane mixture (Figure 5.5). Upon gradual increase in hexane volume (f_H),

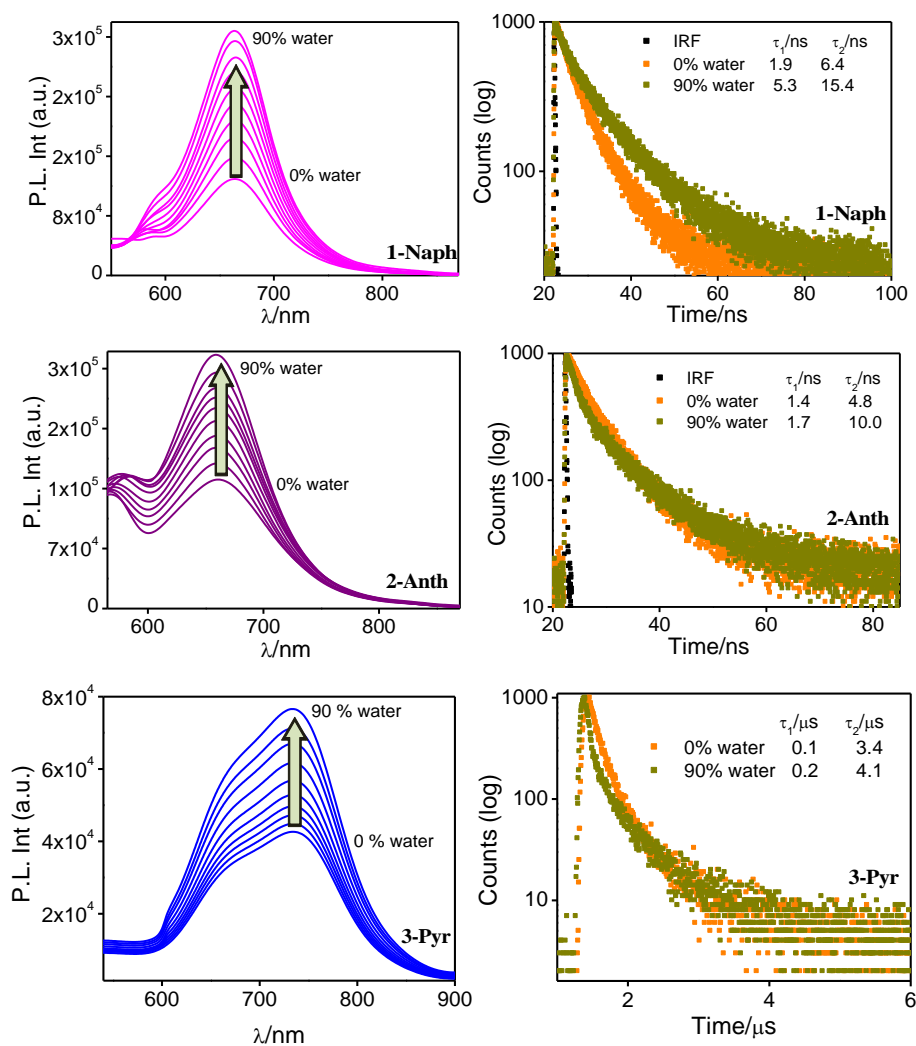


Figure 5.4. The emission ($\lambda_{\text{ex}}=500$ nm) (left panel) spectral changes of the complexes upon varying the relative ratio of MeCN and H₂O. Right panel shows the corresponding changes in emission decay ($\lambda_{\text{ex}}=450$ nm NanoLED) along with the lifetime values of the initial and final form of the complexes.

the luminescence intensity drastically increases up to 90% f_H for both **1-Naph** and **2-Anth** but no change is observed for **3-Pyr** (Table 5.2). Lifetime values of the complexes in their 50% and 90% aggregated form are also measured and shown in Figure 5.5 and Table 5.3. In contrast to previous three set of binary solvent mixtures, drastic increase in lifetime takes place for both **1-Naph** and **2-Anth** upon increase in hexane fraction. In line with steady state spectra, almost no change in lifetime is observed in case of complex **3-Pyr**. It is of interest to note the extent of emission enhancement is much higher for DCM/hexane mixture than that of MeCN/ H₂O system. It is well known that the intramolecular motions (rotation and vibration) often induce non-radiative deactivation of the excited-states. Upon aggregation, the

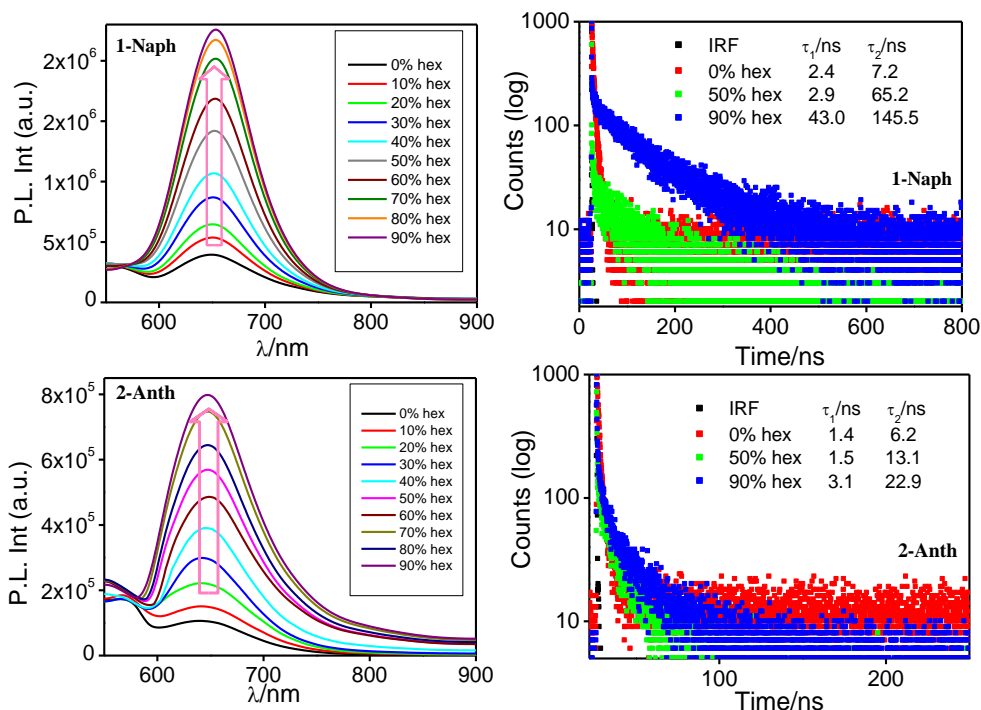


Figure 5.5. The emission ($\lambda_{\text{ex}}=500$ nm) (left panel) spectral changes of **1-Naph** and **2-Anth** upon varying the relative ratio of DCM and hexane. Right panel shows the corresponding change in emission decay ($\lambda_{\text{ex}}=450$ nm NanoLED) along with the lifetime values of the 0%, 50% and 90% hexane fraction.

molecules come in close proximity due to which the intramolecular motions (rotation and vibration) freeze leading to decrease in non-radiative decays. The quantum yield as well as lifetime in their free- ($\Phi_{0\%}$) and 90% aggregated form ($\Phi_{90\%}$) of the complexes is provided in Table 5.2 and Table 5.3.

An aggregation phenomenon is also conducted in DMF/H₂O mixture, wherein no detectable change in emission spectral characteristics of the complexes is noticed. Thus, water induces different mode of self-assembly depending upon the nature of the good solvents (DMF, DMSO and MeCN) employed.

The outcomes of the above experiments clearly indicate that aggregation-induced quenching as well as enhancement of emission takes place in all the three studied complexes, critically dependent on the type of solvent mixtures. We are now interested to elucidate the mode of emission alteration upon variation of the solvent mixtures. In case of DMSO, it is anticipated that addition of non-solvents induces close packing through π - π stacking interaction in all three complexes, albeit in different extent, in their aggregated forms which leads to emission quenching. On the other hand, the effect of restricted intramolecular

motions (RIM) is probably dominant over the π - π stacking interaction in MeCN-H₂O and DCM-hexane mixtures and thereby induces aggregation-induced emission enhancement. It is of interest to note that the extent of emission quenching and/or enhancement is higher for **3-Pyr** than that of **1-Naph** and **2-Anth**, probably because of its larger π -delocalization. Hence, we are successful in demonstrating different aggregation-induced emission spectral behavior in present Ru(II)-terpyridine complexes upon varying the polyaromatic substituent as well as the type of the solvent mixtures.

In order to obtain direct proof for the occurrence of aggregation phenomena, we carried out dynamic light scattering (DLS) experiments in DMSO/ H₂O and MeCN/ H₂O mixtures. In both cases, the experiments are performed on varying the composition of water (0%, 50% and 90%) and the result for **1-Naph** is presented in Figure 5.6. Interestingly, the size of the aggregate is found to increase in all three complexes, albeit in different extent,

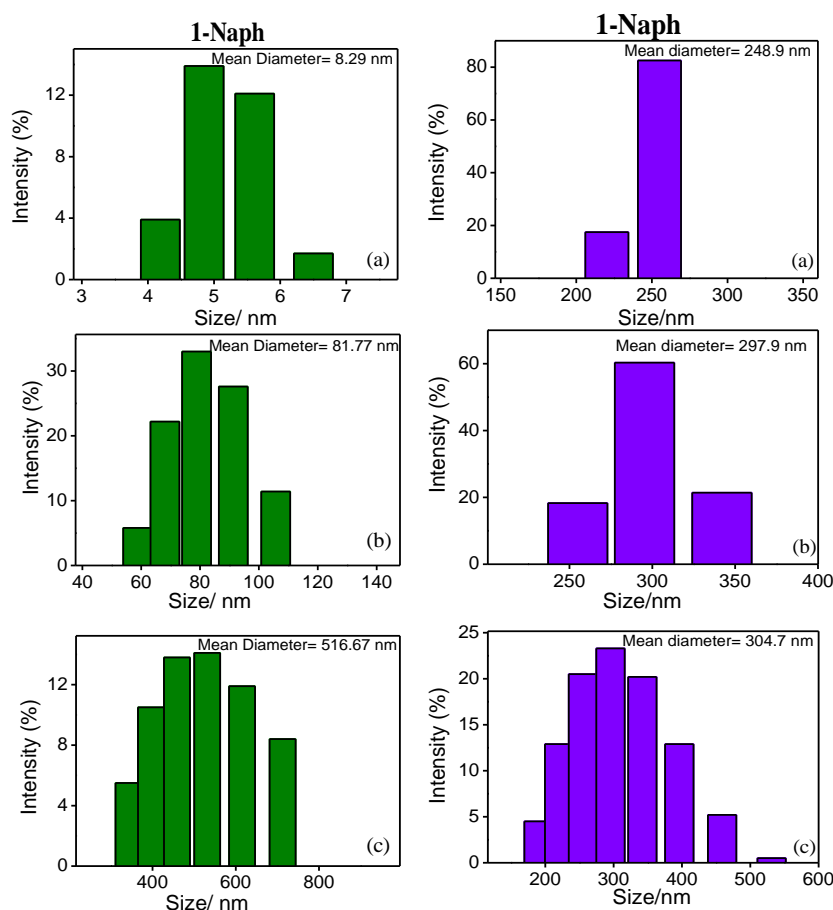


Figure 5.6. Left Panel: Particle size distribution of **1-Naph** with different MeCN/water compositions: 0% (a) 50% (b) and 90% (c) water in MeCN. Right Panel: Particle size distribution of **1-Naph** with different DMSO/water compositions: 0% (a) 50% (b) and 90% (c) water in DMSO.

with the increase in the water fraction of the binary mixtures. Increase in the size of the aggregates supports the occurrence of aggregation. For acquiring further support in favour of aggregation, we recorded the ^1H -NMR spectrum of a representative complex (**1-Naph**) upon step-by-step addition of D_2O to its $\text{DMSO-}d_6$ solution (Figure 5.7). Upon incremental incorporation of D_2O , systematic change in the spectral pattern together with chemical shifts of selected protons is observed. Most of the proton resonances experience up-field shift upon sequential addition of D_2O . Slight alteration of proton multiplicities also takes place for selected proton resonances. Thus, both DLS and ^1H NMR spectral measurements suggest the occurrence of aggregation.

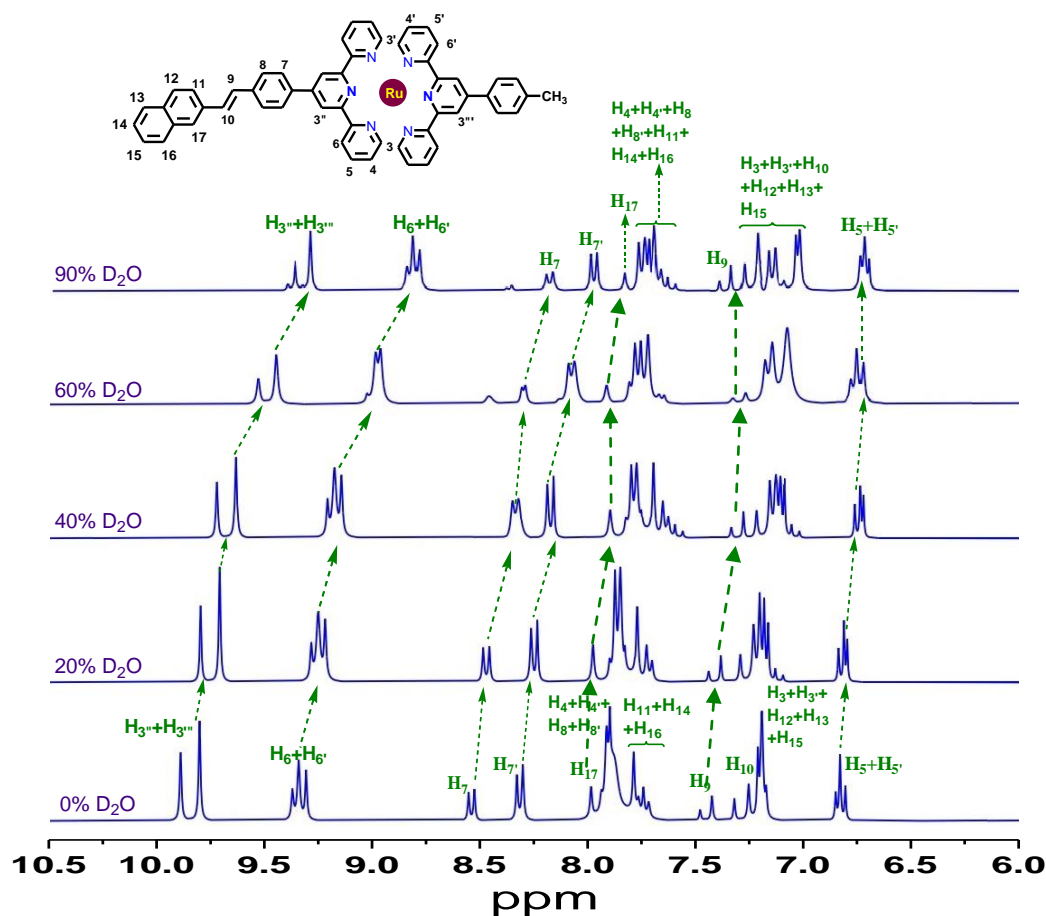


Figure 5.7. ^1H NMR spectral profile of **1-Naph** upon incremental addition of D_2O in $\text{DMSO-}d_6$.

We have also conducted DFT calculations on the free-form as well as the aggregated form of a representative complex (**1-Naph**) by bringing two molecules in close proximity in an anti-parallel arrangement and estimated their energies (Figure 5.8). Calculations reveal a

significant decrease in energy of the aggregated form, promoting system stability and facilitating spontaneous aggregation.

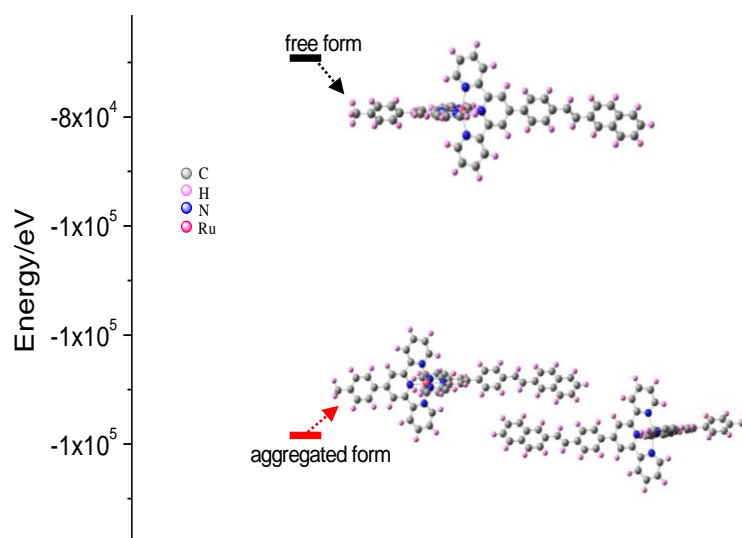


Figure 5.8. The calculated energy diagram of the free- and aggregated form of **1-Naph** in MeCN and water, respectively.

5.3.4 Photoisomerization in the Aggregated Forms of the Complexes. By virtue of the presence of stilbene moiety, the aggregated form of the complexes is also expected to undergo trans to cis isomerization upon light irradiation. We used the DCM/hexane solvent system for this purpose as the rate of isomerisation is appreciably faster in non-polar solvents as seen in our previous study. In the event of investigating the effect of light irradiation on the aggregated forms of the complexes, we take DCM/hexane mixture in two different ratios with different “extent of aggregation”, viz. 50% and 90% f_H .

A significant change in both the absorption and emission spectral profile takes place for both 50% and 90% f_H of **1-Naph** upon light irradiation as shown in Figure 5.9. Presence of isosbestic points in the absorption spectra as well as the similarity in the spectral pattern of photoisomerization with non-aggregated form indicates the occurrence of trans to cis isomerization. Time taken to reach the photostationary state is highest in case of 90% f_H which is suggestive of the fact that the tendency to isomerize decreases as the “extent of aggregation” increases. In the emission side, steady quenching of luminescence intensity is observed upon continuous light irradiation in both the hexane fractions. The successive emission spectrum passes through well-defined iso-emissive point in both the aggregated forms of the complexes. We have also measured the lifetime of the complexes in their

photostationary state. It is seen that the lifetime value decreases as we move from the trans form of the aggregated complexes to their respective cis form (Table 5.3). Scheme 5.1 illustrates the conformational change in the aggregated form of the complexes on passing from trans to cis isomer.

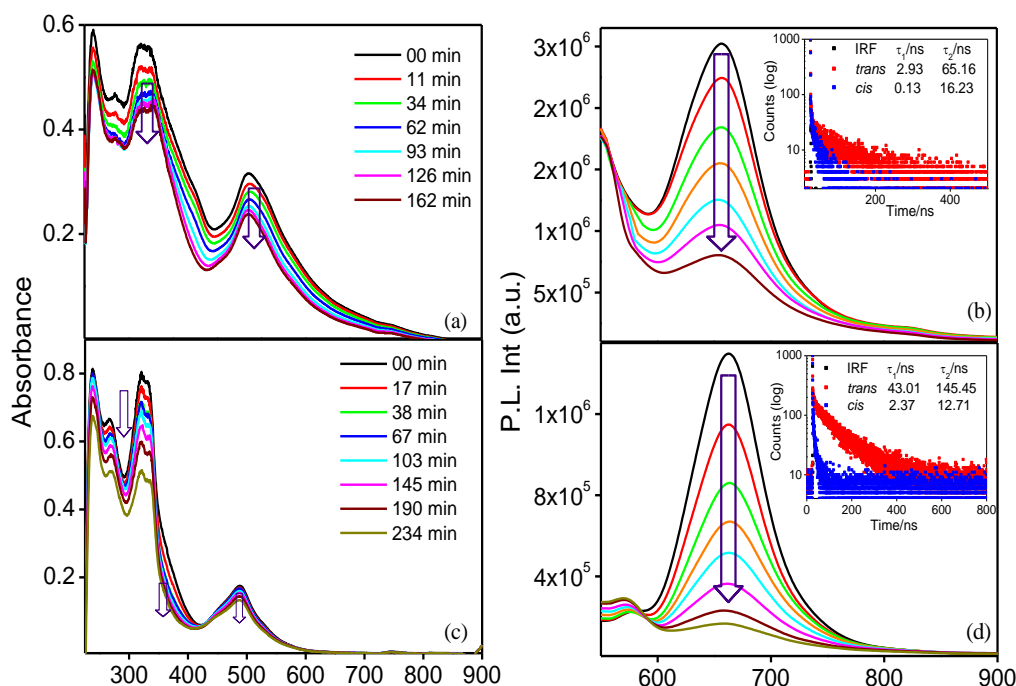
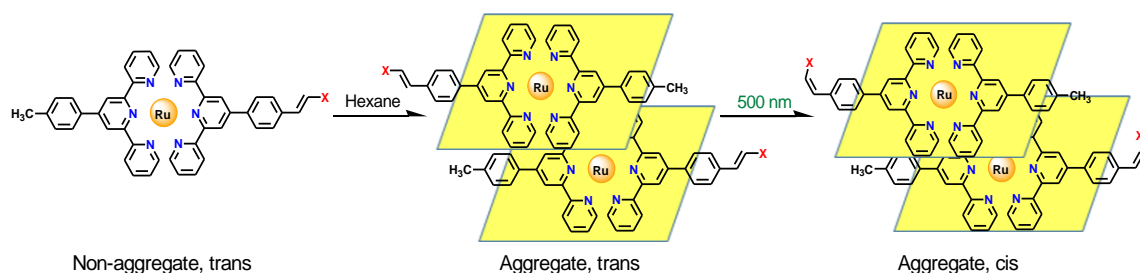


Figure 5.9. Absorption (left) and emission (right, $\lambda_{\text{ex}}=490$ nm) spectral changes of 50% (a and b, respectively) and 90% (c and d, respectively) hexane fraction in DCM-hexane mixture of **1-Naph** upon irradiation with visible light. Inset to the figure b and d shows the corresponding change in emission decay ($\lambda_{\text{ex}}=450$ nm NanoLED) along with lifetime upon photo-irradiation.



Scheme 5.1. Conformational change in the aggregated form of the complexes on passing from trans to cis isomer.

Additionally, we have estimated the rate constant (k_{iso}) and quantum yields ($\Phi_{\text{t} \rightarrow \text{c}}$) of the photo-isomerization process in their aggregated forms (50% to 90% f_{H}) by using

absorption titration profiles and compared with their non-aggregated counterparts (Figure 5.10, Table 5.4). It is observed that the k_{iso} value decreases as we move from 50% to 90% f_H . Thus, the rate of photoisomerization decreases as we move from the non-aggregated to their aggregated states. This is quite expected since aggregation results in the increase in the rotor volume of the molecule due to which C=C bond rotation becomes extremely difficult.

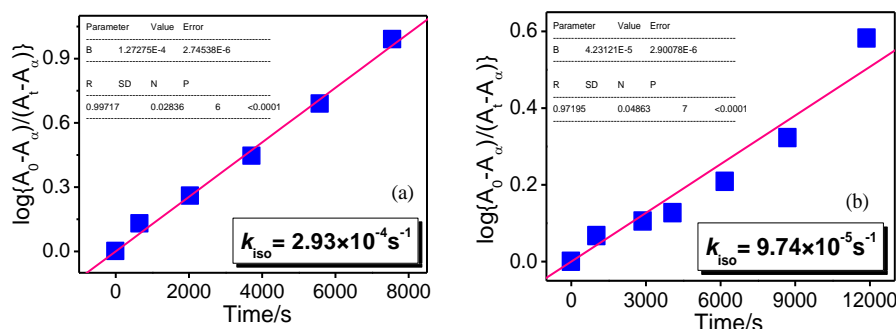


Figure 5.10. Linear plot of $\log(A_0 - A_f)/(A_t - A_f)$ vs. time (t) for the absorption spectral change due to trans→cis process of **1-Naph** upon irradiation with visible light of 50% (a) and 90% (b) hexane fraction in DCM-hexane mixture. Inset to these plots give the values of rate constant of photo-isomerization.

Table 5.4. Table for comparison of the values of rate constants (k_{iso}) and photoisomerization quantum yields ($\Phi_{t \rightarrow c}$) for trans→cis process in both of their free and aggregated forms.

	1-Naph		2-Anth		3-Pyr	
Free form	k_{iso}/s^{-1} ($\times 10^{-4}$)	$\Phi_{t \rightarrow c}$ ($\times 10^{-2}$)	k_{iso}/s^{-1} ($\times 10^{-4}$)	$\Phi_{t \rightarrow c}$ ($\times 10^{-2}$)	k_{iso}/s^{-1} ($\times 10^{-4}$)	$\Phi_{t \rightarrow c}$ ($\times 10^{-2}$)
Free form	5.70	2.61	3.48	1.54	7.28	3.02
Aggregated form	k_{iso}/s^{-1} ($\times 10^{-4}$)	$\Phi_{t \rightarrow c}$ ($\times 10^{-2}$)	k_{iso}/s^{-1} ($\times 10^{-4}$)	$\Phi_{t \rightarrow c}$ ($\times 10^{-3}$)	k_{iso}/s^{-1}	$\Phi_{t \rightarrow c}$
50% f_H	2.93	1.7×10^{-2}	1.60	6.65×10^{-3}	-	-
90% f_H	0.97	8.8×10^{-2}	0.96	6.58×10^{-3}	-	-

5.4 Conclusions

Aggregation-induced modulation of the room temperature luminescence characteristics of heteroleptic Ru(II)-terpyridine complexes have been undertaken in this work via appropriate combination of solvents. The complexes exhibit both aggregation-induced emission enhancement (AIEE) and aggregation-caused emission quenching (ACQ) phenomena, critically dependent on the type of solvent mixtures. Interestingly, the room temperature lifetime of the complexes increases quite significantly upon aggregation. Taking advantage of stilbene motif, trans→cis photoisomerization of the aggregated forms of the complexes are also executed. Interestingly, the aggregated form of the compounds also isomerizes upon

visible light irradiation but at a much slower rate compared to their non-aggregated forms as expected. In essence, the room temperature emission characteristics of the present heteroleptic Ru(II)-terpyridine complexes have been modulated to a significant extent upon aggregation. Moreover, the mode of emission switching was efficiently controlled upon varying the solvent mixture as well as by treating with light of appropriate wavelength. Thus, the present systems are thought to be potential building blocks for the construction of smart molecular switches.

5.5 References

- (1) Gratzel, M. Photoelectrochemical cells. *Nature* **2001**, *414*, 338- 344.
- (2) Lee, C. Y.; Farha, O. K.; Hong, B. J.; Sarjeant, A. A.; Nguyen, S. B. T.; Hupp, J. T. Light-Harvesting Metal-Organic Frameworks (MOFs): Efficient Strut-to-Strut Energy Transfer in Bodipy and Porphyrin-Based MOFs. *J. Am. Chem. Soc.* **2011**, *133*, 15858-15861.
- (3) Barigelletti, F.; Flamigni, L. Photoactive Molecular Wires Based on Metal Complexes. *Chem. Soc. Rev.* **2000**, *29*, 1-12.
- (4) Bignozzi, C. A.; Argazzi, R.; Kleverlaan, C. Molecular and Supramolecular Sensitization of Nanocrystalline Wide Band-Gap Semiconductors with Mononuclear and Polynuclear Metal Complexes. *J. Chem. Soc. Rev.* **2000**, *29*, 87-96.
- (5) Sun, L. C.; Hammarstrom, L.; Akermark, B.; Styring, S. Towards Artificial Photosynthesis: Ruthenium-Manganese Chemistry for Energy Production. *Chem. Soc. Rev.* **2001**, *30*, 36-49.
- (6) Balzani, V.; Ceroni, P.; Juris, A.; Venturi, M.; Campagna, S.; Puntoriero, F.; Serroni, S. Dendrimers Based on photoactive Metal Complexes. Recent Advances. *Coord. Chem. Rev.* **2001**, *219*, 545-572.
- (7) Benniston, A. C.; Grosshenny, V.; Harriman, A.; Ziessel, R. Electron Delocalization in Ethynyl Bridged Binuclear Ruthenium(II) Polypyridine Complexes. *Angew. Chem. Int. Ed. Engl.* **1994**, *33*, 1884-1886.
- (8) Tyson, D. S.; Luman, C. R.; Castellano, F. N. Photodriven Electron and Energy Transfer from a Light-Harvesting Metallodendrimer. *Inorg. Chem.* **2002**, *41*, 3578-3586.
- (9) Juris, A.; Balzani, V.; Barigelletti, F.; Campagna, S.; Belser, P.; Von Zelewsky, A. Ru(II) Polypyridine Complexes: Photophysics, Photochemistry, Eletrochemistry, and Chemiluminescence. *Coord. Chem. Rev.* **1988**, *84*, 85-277.
- (10) Balzani, V.; Juris, A.; Venturi, M.; Campagna, S.; Serroni, S. Luminescent and Redox-Active Polynuclear Transition Metal Complexes. *Chem. Rev.* **1996**, *96*, 759-833.
- (11) Medlycott, E. A.; Hanan, G. S. Designing Tridentate Ligands for Ruthenium(II) Complexes with Prolonged Room Temperature Luminescence Lifetimes. *Chem. Soc. Rev.* **2005**, *34*, 133-142.

- (12) Medlycott, E. A.; Hanan, G. S. Synthesis and Properties of Mono- and Oligo-Nuclear Ru(II) Complexes of Tridentate Ligands: The Quest for Long-Lived Excited States at Room Temperature. *Coord. Chem. Rev.* **2006**, *250*, 1763-1782.
- (13) Schubert, U. S.; Eschbaumer, C. Macromolecules Containing Bipyridine and Terpyridine Metal Complexes: Towards Metal Iosupramolecular Polymers. *Angew. Chem., Int. Ed.* **2002**, *41*, 2892-2896.
- (14) Whittle, B.; Everest, N. S.; Howard, C.; Ward, M. D. Synthesis and Electrochemical and Spectroscopic Properties of a Series of Binuclear and Trinuclear Ruthenium and Palladium Complexes Based on a New Bridging Ligand Containing Terpyridyl and Catechol Binding Sites. *Inorg. Chem.* **1995**, *34*, 2025-2032.
- (15) Haga, M. A.; Ali, M. M.; Koseki, S.; Fujimoto, K.; Yoshimura, A.; Nozaki, K.; Ohno, T.; Nakajima, K.; Stufkens, D.J. Proton-Induced Tuning of Electrochemical and Photophysical Properties in Mononuclear and Dinuclear Ruthenium Complexes Containing 2,2'-Bis (benzimidazol-2-yl)-4,4'-bipyridine: Synthesis, Molecular Structure, and Mixed-Valence State and Excited-State Properties. *Inorg. Chem.* **1996**, *35*, 3335-3347.
- (16) Saha, D.; Das, S.; Bhaumik, C.; Dutta, S.; Baitalik, S. Monometallic and Bimetallic Ruthenium(II) Complexes Derived from 4,5-Bis(benzimidazol-2-yl)imidazole (H₃Imbzim) and 2,2'-Bipyridine as Colorimetric Sensors for Anions: Synthesis, Characterization, and Binding Studies. *Inorg. Chem.* **2010**, *49*, 5, 2334-2348.
- (17) Baitalik, S.; Flörke, U.; Nag, K. Mononuclear and Binuclear Ruthenium(II) Complexes Containing 2,2'-Bipyridine or 1,10-Phenanthroline and Pyrazole-3,5-Bis(benzimidazole). Synthesis, Structure, Isomerism, Spectroscopy, and Proton-Coupled Redox Activity. *Inorg. Chem.* **1999**, *38*, 3296-3308.
- (18) Schubert, U.S.; Hofmeier, H.; Newkome, G.R. *Modern terpyridine chemistry*. John Wiley & Sons 2006.
- (19) Hofmeier, H.; Schubert, U. S. Recent Developments in the Supramolecular Chemistry of Terpyridine-Metal Complexes. *Chem. Soc. Rev.* **2004**, *33*, 373-399.
- (20) Mondal, D.; Biswas, S.; Paul, A.; Baitalik, S. Luminescent Dinuclear Ruthenium Terpyridine Complexes with a Bis-Phenylbenzimidazole Spacer. *Inorg. Chem.* **2017**, *56*, 7624-7641.
- (21) Deb, S.; Sahoo, A.; Pal, P.; Baitalik, S. Exploitation of the Second Coordination Sphere to Promote Significant Increase of Room-Temperature Luminescence Lifetime

- and Anion Sensing in Ruthenium–Terpyridine Complexes. *Inorg. Chem.* **2021**, *60*, 6836-6851
- (22) Paul, A.; Bar, M.; Deb, S.; Baitalik, S. Long-Lived Trimetallic Complexes of Fe(II), Ru(II), and Os(II) Based on a Heteroditopic Bipyridine–Terpyridine Bridge: Synthesis, Photophysics, and Electronic Energy Transfer. *Inorg. Chem.* **2019**, *58*, 10065-10077.
- (23) Karmakar, S.; Maity, D.; Mardanya, S.; Baitalik, S. Multichromophoric Bimetallic Ru(II) Terpyridine Complexes Based on Pyrenyl-bis-phenylimidazole Spacer: Synthesis, Photophysics, Spectroelectrochemistry, and TD-DFT Calculations. *Inorg. Chem.* **2014**, *53*, 12036-12049.
- (24) Brown, D. G.; Sanguantrakun, N.; Schulze, B.; Schubert, U. S.; Berlinguette, C. P. Bis(tridentate) Ruthenium–Terpyridine Complexes Featuring Microsecond Excited State Lifetimes. *J. Am. Chem. Soc.* **2012**, *134*, 12354-12357.
- (25) Baranoff, E.; Collin, J.-P.; Flamigni, L.; Sauvage, J.-P. From Ruthenium(II) to Iridium(III): 15 Years of Triads Based on Bis Terpyridine Complexes. *Chem. Soc. Rev.* **2004**, *33*, 147-155.
- (26) Pal, P.; Mukherjee, S.; Maity, D.; Baitalik, S. Synthesis, Structural Characterization, and Luminescence Switching of Diarylethene-Conjugated Ru(II)–Terpyridine Complexes by Trans–Cis Photoisomerization: Experimental and DFT/TD-DFT Investigation. *Inorg. Chem.* **2018**, *57*, 5743-5753.
- (27) Pal, P.; Ganguly, T.; Maity, D.; Baitalik, S. Experimental and Theoretical Exploration of Photophysics and Trans–Cis Photoisomerization of Styrylbenzene Conjugated Terpyridine Complexes of Ru(II): Strong Effect of Deprotonation from Second Coordination Sphere. *J. Photochem. Photobiol. A.* **2020**, *392*, 112409.
- (28) Wang, J.; Fang, Y. Q.; Hanan, G. S.; Loiseau, F.; Campagna, S. Synthesis and Properties of the Elusive Ruthenium(II) Complexes of 4'-cyano-2,2':6',2''-terpyridine. *Inorg. Chem.* **2005**, *44*, 5-7.
- (29) Indelli, M. T.; Bignozzi, C. A.; Scandola, F.; Collin, J.-P. Design of Long-Lived Ru(II) Terpyridine MLCT States Tricyano Terpyridine Complexes. *Inorg. Chem.* **1998**, *37*, 6084-6089.
- (30) Kubel, J.; Schroot, R.; Wachtler, M.; Schubert, U. S.; Dietzek, B.; Jager, M. Photoredox-Active Dyads Based on a Ru(II) Photosensitizer Equipped with Electron Donor or Acceptor Polymer Chains: A Spectroscopic Study of Light-Induced

- Processes Toward Efficient Charge Separation. *J. Phys. Chem. C* **2015**, *119*, 4742-4751.
- (31) Maestri, M.; Armaroli, N.; Balzani, V.; Constable, E. C.; Thompson, A. M. W. C. Complexes of the Ruthenium(II)-2,2':6',2'' Terpyridine Family. Effect of Electron-Accepting and-Donating Substituents on the Photophysical and Electrochemical Properties. *Inorg. Chem.* **1995**, *34*, 2759-2767.
- (32) Maity, D.; Das, S.; Mardanya, S.; Baitalik, S. Synthesis, Structural Characterization, and Photophysical, Spectroelectrochemical, and Anion-Sensing Studies of Heteroleptic Ruthenium(II) Complexes Derived from 4'-Polyaromatic-Substituted Terpyridine Derivatives and 2,6-Bis(benzimidazol-2-yl)pyridine. *Inorg. Chem.* **2013**, *52*, 6820-6838.
- (33) Encinas, S.; Flamigni, L.; Barigelletti, F.; Constable, E. C.; Housecroft, C. E.; Schofield, E. R.; Figgemeier, E.; Fenske, D.; Neuburger, M.; *et al.* Electronic Energy Transfer and Collection in Luminescent Molecular Rods Containing Ruthenium(II) and Osmium(II) 2,2':6',2''-Terpyridine Complexes Linked by Thiophene-2,5-diyl Spacers. *Chem. Eur. J.* **2002**, *8*, 137-150.
- (34) Dietrich, J.; Thorenz, U.; Förster, C.; Heinze, K. Effects of Sequence, Connectivity, and Counter Ions in New Amide-Linked Ru(tpy)₂-Re(bpy) Chromophores on Redox Chemistry and Photophysics. *Inorg. Chem.* **2013**, *52*, 1248-1264.
- (35) Duati, M.; Tasca, S.; Lynch, F. C.; Bohlen, H.; Vos, J. G.; Stagni, S.; Ward, M. D. Enhancement of Luminescence Lifetimes of Mononuclear Ruthenium(II)-Terpyridine Complexes by Manipulation of the Sigma-Donor Strength of Ligands. *Inorg. Chem.* **2003**, *42*, 8377-8384.
- (36) Maestri, M.; Armaroli, N.; Balzani, V.; Constable, E. C.; Thompson, A. M. W. C. Complexes of the Ruthenium(II)-2,2':6',2''-Terpyridine Family. Effect of Electron-accepting and -donating Substituents on the Photophysical and Electrochemical Properties. *Inorg. Chem.* **1995**, *34*, 2759-2767.
- (37) Coe, B. J.; Thompson, D. W.; Culbertson, C. T.; Schoonover, J. R. and Meyer, T. J. Synthesis and Photophysical Properties of Mono(2,2',2''-terpyridine) Complexes of Ruthenium(II). *Inorg. Chem.* **1995**, *34*, 3385-3395.
- (38) Wadman, S. H.; Lutz, M.; Tooke, D. M.; Spek, A. L.; Hartl, F.; Havenith, R. W. A.; van Klink, G. P. M.; van Koten, G. Consequences of N,C,N- and C,N,N-Coordination Modes on Electronic and Photophysical Properties of Cyclometalated Aryl Ruthenium(II) Complexes. *Inorg. Chem.* **2009**, *48*, 1887-1900.

- (39) Kreitner, C.; Erdmann, E.; Seidel, W. W.; Heinze, K. Understanding the Excited State Behavior of Cyclometalated Bis(tridentate)ruthenium(II) Complexes: A Combined Experimental and Theoretical Study. *Inorg. Chem.* **2015**, *54*, 11088-11104.
- (40) Beley, M.; Collin, J.-P.; Louis, R.; Metz, B.; Sauvage, J.-P. 3,3',5,5'-Tetrapyridylbiphenyl: A Biscyclometalating Bridging Ligand with a High Coupling Ability in Ru III, Ru II Mixed Valence System. *J. Am. Chem. Soc.* **1991**, *113*, 8522-8524.
- (41) Duati, M.; Fanni, S.; Vos, J. G. A New Luminescent Ru(terpy) Complex Incorporating a 1,2,4-Triazole Based σ -Donor Ligand. *Inorg. Chem. Commun.* **2000**, *3*, 68-70.
- (42) Constable, E. C.; Dunne, S. J.; Rees, D. G. F.; Schmitt, C. X. Reversible Cyclometallation at a Ruthenium(II) Centre. *Chem. Commun.* **1996**, 1169.
- (43) Jäger, M.; Kumar, R. J.; Görls, H.; Bergquist, J.; Johansson, O. Facile Synthesis of Bistridentate RuII Complexes Based on 2,6-Di(quinolin-8-yl)pyridyl Ligands: Sensitizers with Microsecond ³MLCT Excited State Lifetimes. *Inorg. Chem.* **2009**, *48*, 3228-3238.
- (44) Ganguly, T.; Das, S.; Maity, D.; Baitalik, S. Luminescent Ruthenium-Terpyridine Complexes Coupled with Stilbene-Appended Naphthalene, Anthracene, and Pyrene Motifs Demonstrate Fluoride Ion Sensing and Reversible Trans-Cis Photoisomerization. *Inorg. Chem.* **2024**, *63*, 6883-6897.
- (45) Goze, C.; Sabatini, C.; Barbieri, A.; Barigelletti, F.; Ziessel, R. Ruthenium-Terpyridine Complexes with Multiple Ethynylpyrenyl or Ethynyltoluyl Subunits: X-ray Structure, Redox, and Spectroscopic Properties. *Inorg. Chem.* **2007**, *46*, 7341-7350.
- (46) Pal, A. K.; Hanan, G. S. Design, Synthesis and Excited-State Properties of Mononuclear Ru(II) Complexes of Tridentate Heterocyclic Ligands. *Chem. Soc. Rev.* **2014**, *43*, 6184-6197.
- (47) Prieto, J. P.; Pérez, L. P.; González-Bejar, M.; Miranda, M. A. Stiriba, S.-E. Pyrene-Benzoylthiophene Bichromophores as Selective Triplet Photosensitizers. *Chem. Commun.* **2005**, 5569.
- (48) Chen, Z.; Qin, H.; Yin, Y.; Deng, D.D.; Qin, S.Y.; Li, N.; Wang, K.; Sun, Y. Full-Color Emissive D-D-A Carbazole Luminophores: Red-To-NIR Mechano-Fluorochromism, Aggregation-Induced Near-Infrared Emission and Application in Photodynamic Therapy. *Chem. Eur. J.* **2023**, *29*, e202203797.

- (49) Yin, Y.; Chen, Z.; Li, R.H.; Yi, F.; Liang, X.C.; Cheng, S.Q.; Wang, K.; Sun, Y.; Liu, Y. Highly Emissive Multipurpose Organoplatinum (II) Metallacycles with Contrasting Mechanoresponsive Features. *Inorg. Chem.* **2022**, *61*, 2883-2891.
- (50) Wang, M.G.; Lan, J.J.; Li, S.D.; Hao, Y.Z.; Chen, S.M.; Wang, F. A Room-Temperature Phosphorescent Metal-Organic Framework Based on Proline-Tetrazole Ligand. *Adv. Optical Mater.* **2024**, *12*, 2301843.
- (51) Zhang, M.; Saha, M.L.; Wang, M.; Zhou, Z.; Song, B.; Lu, C.; Yan, X.; Li, X.; Huang, F.; Yin, S.; Stang, P.J. Multicomponent Platinum (II) Cages with Tunable Emission and Amino Acid Sensing. *J. Am. Chem. Soc.* **2017**, *139*, 5067-5074.
- (52) Zhang, M.; Yin, S.; Zhang, J.; Zhou, Z.; Saha, M.L.; Lu, C.; Stang, P.J. Metallacycle-Cored Supramolecular Assemblies With Tunable Fluorescence Including White-Light Emission. *PNAS*, **2017**, *114*, 3044-3049.
- (53) Zhao, Z.; Zhang, H.; Lam, J.W.Y. Tang, B. Z. Aggregation-Induced Emission: New Vistas at the Aggregate Level. *Angew. Chem. Int. Ed.* **2020**, *59*, 9888-9907.
- (54) Goswami, N.; Yao, Q.; Luo, Z.; Li, J.; Chen, T.; Xie, J. Luminescent Metal Nanoclusters with Aggregation-Induced Emission. *J. Phys. Chem. Lett.* **2016**, *7*, 962-975.
- (55) Alama, P.; Climent, C.; Alemany, P.; Laskar, I. R. "Aggregation-Induced Emission" of Transition Metal Compounds: Design, Mechanistic Insights, and Applications. *Jour. of Photochem. Photobiol. C: Photochem. Rev.* **2019**, *41*, 100317.
- (56) Yan, X.; Wang, H.; Hauke, C. E.; Cook, T. R.; Wang, M.; Saha, M. L.; Zhou, Z.; Zhang, M.; Li, X.; Huang, F.; Stang, P.J. A Suite of Tetraphenylethylene-Based Discrete Organoplatinum(II) Metallacycles: Controllable Structure and Stoichiometry, Aggregation-Induced Emission, and Nitroaromatics Sensing. *J. Am. Chem. Soc.* **2015**, *137*, 15276-15286.
- (57) Ravotto, L.; Ceroni, P. Aggregation Induced Phosphorescence of Metal Complexes: From Principles to Applications. *Coord. Chem. Rev.* **2017**, *346*, 62-76.
- (58) Yan, X.; Cook, T. R.; Wang, P.; Huang, F.; Stang, P. J. Highly emissive Platinum(II) Metallacages. *Nat. Chem.* **2015**, *7*, 342-348.
- (59) Cheng, H.-K.; Yeung, M. C.-L.; Yam, V. W.-W. Molecular Engineering of Platinum(II) Terpyridine Complexes with Tetraphenylethylene-Modified Alkynyl Ligands: Supramolecular Assembly via Pt···Pt and/or π - π Stacking Interactions and the Formation of Various Superstructures. *ACS Appl. Mater. Interfaces*, **2017**, *9*, 36220-36228.

- (60) Law, A. S.Y.; Lee, L. C.-C.; Lo, K. K.-W.; Yam, V. W.W. Aggregation and Supramolecular Self-Assembly of Low-Energy Red Luminescent Alkynylplatinum(II) Complexes for RNA Detection, Nucleolus Imaging, and RNA Synthesis Inhibitor Screening. *J. Am. Chem. Soc.* **2021**, *143*, 5396-5405.
- (61) Yam, V. W.-W. Chan, K. H. Y.; Wong, K. M.C.; Zhu, N. Luminescent Platinum(II) Terpyridyl Complexes: Effect of Counter Ions on Solvent-Induced Aggregation and Color Changes. *Chem. Eur. J.* **2005**, *11*, 4535-4543.
- (62) Luo, J.; Xie, Z.; Lam, J. W. Y.; Cheng, L.; Tang, B. Z.; Chen, H.; Qiu, C.; Kwok, H. S.; Zhan, X.; Liu, Y. Aggregation-Induced Emission of 1-Methyl-1,2,3,4,5-Pentaphenylsilole. *Chem. Commun.* **2001**, 1740-1741.
- (63) An, B.-K.; Kwon, S.-K.; Jung, S.-D.; Park, S. Y. Enhanced Emission and its Switching in Fluorescent Organic Nanoparticles. *J. Am. Chem. Soc.* **2002**, *124*, 14410-14415.
- (64) Mudi, N.; Shyamal, M.; Giri, P. K.; Samanta, S. S.; Tagle, R. R.; Misra, A. Anthracene Scaffold as Highly Selective Chemosensor for Al³⁺ and its AIEE Activity. *Photochem. Photobiol. Sci.* **2023**, *22*, 1491-150.
- (65) Maity, S.; Shyamal, M.; Das, D.; Mazumdar, P.; Sahoo, G.P.; Misra, A. Aggregation Induced Emission Enhancement From Antipyrine-Based Schiff Base And Its Selective Sensing Towards Picric Acid. *Sens. Actuators B*: **2017**, *248*, 223-233.
- (66) Ren, Y.; Lam, J. W. Y.; Dong, Y.; Tang, B. Z.; Wong, K. S. Enhanced Emission Efficiency and Excited State Lifetime Due to Restricted Intramolecular Motion in Silole Aggregates. *J. Phys. Chem. B* **2005**, *109*, 1135-1140.
- (67) Leung, N. L. C.; Xie, N.; Yuan, W.; Liu, Y.; Wu, Q.; Peng, Q.; Miao, Q.; Lam, J. W. Y.; Tang, B. Z. Restriction of Intramolecular Motions: The General Mechanism behind Aggregation-Induced Emission. *Chem. Eur. J.* **2014**, *20*, 15349-15353.
- (68) Babua, E.; Mareeswaran, P. M.; Krishnan, M. M.; Sathish, V.; Thanasekarand, P.; Rajagopal, S. Unravelling the Aggregation Induced Emission Enhancement in Tris(4,7-diphenyl-1,10-phenanthroline)Ruthenium(II) Complex. *Inorg. Chem. Commun.* **2018**, *98*, 7-10.
- (69) Sheet, S. K.; Sen, B.; Patra, S. K.; Rabha, M.; Aguan, K.; Khatua, S. Aggregation Induced Emission-Active Ruthenium(II) Complex of 4,7- Dichloro Phenanthroline for Selective Luminescent Detection and Ribosomal RNA Imaging. *ACS Appl. Mater. Interfaces* **2018**, *10*, 14356-14366.

- (70) Lu, L.; Zhang, L.; Miao, W.; Wang, X.; Guo, G.; Aggregation-Induced Electrochemiluminescence of the Dichlorobis(1,10-phenanthroline)ruthenium(II) ($\text{Ru}(\text{phen})_2\text{Cl}_2$) Tri-*n*-propylamine (TPrA) System in H_2O -MeCN Mixtures for Identification of Nucleic Acids. *Anal. Chem.* **2020**, 92, 9613-9619.
- (71) Xu, H.; Zhang, X.; Lib, X.; Zhang, X.; Deng, J.; Zou, D.; Yang, J. Two Ru(II) Compounds with Aggregation Induced Emission as Promising Photosensitizers for Photodynamic Therapy. *J. Inorg. Biochem.* **2020**, 212, 111233.
- (72) Wang, C.; Liu, Y.; Feng, X.; Zhou, C.; Liu, Y.; Yu, X.; Zhao, G. Phase Regulation Strategy of Perovskite Nanocrystals from 1D Orthomorphous NH_4PbI_3 to 3D Cubic $(\text{NH}_4)_{0.5}\text{Cs}_{0.5}\text{Pb}(\text{I}_{0.5}\text{Br}_{0.5})_3$ Phase Enhances Photoluminescence. *Angew. Chem.* **2019**, 131, 11768-11772.
- (73) Wang, C.; Zhao, G. Codoping of Lead-Free Double Perovskites Promotes Near-Infrared Photoluminescence. *Angew. Chem. Int. Ed.* **2021** 133, 548-550.
- (74) Zhao, G.-J.; Han, K.-L.; Hydrogen Bonding in the Electronic Excited State. *Acc. Chem. Res.* **2012**, 45, 404-413.
- (75) Lu, C.; Zhang, M.; Tang, D.; Yan, X.; Zhang, Z. Y.; Zhou, Z.; Song, B.; Wang, H.; Li, X.; Yin, S.; Sepehrpour, H.; Stang, P. J. Fluorescent Metallacage-Core Supramolecular Polymer Gel Formed by Orthogonal Metal Coordination and Host-Guest Interactions. *J. Am. Chem. Soc.* **2018**, 140, 7674-7680.
- (76) Yang, J.; Li, L.; Yu, Y.; Ren, Z.; Peng, Q.; Ye, S.; Lia, Q.; Li, Z.; Blue Pyrene-based AIEgens: Inhibited Intermolecular π - π Stacking through the Introduction of Substituents with Controllable Intramolecular Conjugation, and High External Quantum Efficiencies up to 3.46% in Non-doped OLEDs. *Mater. Chem. Front.* **2017**, 1, 91-99.
- (77) Mazumdar, P.; Das, D.; Sahoo, G.P.; Salgado-Morán, G.; Misra, A. Aggregation Induced Emission Enhancement of 4, 4'-Bis (Diethylamino) Benzophenone with an Exceptionally Large Blue Shift and its Potential use as Glucose Sensor. *Phys. Chem. Chem. Phys.* **2015**, 17, 3343-3354.
- (78) Wang, L.L.; Zhou, H.; Yang, T.L.; Ke, H.; Tu, Y.K.; Yao, H.; Jiang, W. Bis-Naphthalene Cleft with Aggregation-Induced Emission Properties through Lone-Pair... π Interactions. *Chem. Eur. J.* **2018**, 24, 16757-16761.
- (79) Banerjee, S.; Both, A.K.; Sarkar, M. Probing the Aggregation and Signaling Behavior of some Twisted 9, 9'-Bianthryl Derivatives: Observation of Aggregation-Induced Blue-Shifted Emission. *ACS Omega* **2018**, 3, 15709-15724.

- (80) Yin, Y.; Guan, Q.; Chen, Z.; Deng, D.D.; Liu, S.; Sun, Y.; Liu, S.H. Force-Triggered Hypso-And Bathochromic Bidirectional Fluorescence Switching Beyond 120 nm and its Anticounterfeiting Applications. *Sci. Adv.* **2024**, *10*, eadk5444.
- (81) Kume, S.; Nishihara, H. Metal-based Photoswitches Derived from Photoisomerization. *Struct. Bonding* **2007**, *123*, 79-112.
- (82) Ko, C.-C.; Yam, V. W. W. Transition Metal Complexes with Photochromic Ligands Photosensitization and Photoswitchable Properties. *J. Mater. Chem.* **2010**, *20*, 2063-2070.
- (83) Ronaldo, C.; Amaral, A. B.; Iha N. Y. M. Molecular Engineered Rhenium(I) Carbonyl Complexes to Promote Photoisomerization of Coordinated Stilbene-like Ligands in the Visible Region. *Dalton Trans.* **2018**, *47*, 13081-13087.
- (84) Duan, G.; Yam, V. W.-W. Syntheses and Photophysical Properties of N Pyridylimidazol-2-ylidene Tetracyano ruthenates(II) and Photochromic Studies of Their Dithienylethene-Containing Derivatives. *Chem. Eur. J.* **2010**, *16*, 12642- 12649.
- (85) Sun, S.-S.; Lees, A. J. Synthesis, Photophysical Properties, and Photoinduced Luminescence Switching of Trinuclear Diimine Rhenium(I) Tricarbonyl Complexes Linked by an Isomerizable Stilbene-like Ligand. *Organometallics* **2002**, *21*, 39-49.
- (86) Irie, M. Diarylethenes for Memories and Switches. *Chem. Rev.* **2000**, *100*, 1685-1716.
- (87) Ikeda, T.; Tsutsumi, O. Optical Switching and Image Storage by Means of Azobenzene Liquid-Crystal Films. *Science*. **1995**, *268*, 1873-1875.
- (88) Matos, L.S.; Amaral, R. C.; Iha, N. Y. M. Visible Photosensitization of trans Styrylpyridine Coordinated to fac-[Re(CO)₃(dcbH₂)]⁺: New Insights. *Inorg. Chem.* **2018**, *57*, 9316-9326.
- (89) Polo, A. S.; Itokazu, M. K.; Frin, K. M.; Patrocínio, A. O. T.; Iha N. Y. M. Light driven Trans-to-Cis Isomerization of Stilbene-like Ligands in fac [Re(CO)₃(NN)(trans-L)]⁺ and Luminescence of their Photoproducts. *Coord. Chem. Rev.* **2006**, *250*, 1669-1680.
- (90) Zanoni, K. P. S.; Iha, N. Y. M. Reversible Trans⇌Cis Photoisomerizations of [Re(CO)₃(ph₂phen)(stpyCN)]⁺ Towards Molecular Machines. *Dalton Trans.* **2017**, *46*, 9951-9958.
- (91) Ganguly, T.; Pal, P.; Paul, A.; Baitalik, S. Synthesis and Manifold but Controllable Emission Switching of Stilbene-Appended Polyaromatic Terpyridine Derivatives via

Aggregation and Trans-Cis Isomerization. *Photochem. Photobiol. A* **2022**, 430, 113966.

- (92) Li, Z.; Zeng, X.; Gao, C.; Song, J.; He, F.; He, T.; Guo, H.; Yin, J. Photoswitchable Diarylethenes: From Molecular Structures to Biological Applications. *Coord. Chem. Rev.* **2023**, 497, 215451.
- (93) Kishore, V.V.N.R.; Narasimhan, K.L.; Periasamy, N. On the Radiative Lifetime, Quantum Yield and Fluorescence Decay of Alq in Thin Films. *Phys. Chem. Chem. Phys.* **2003**, 5, 1386-1391.



Chapter 6

Remarkable Increase in the Rate of Trans-Cis Photoisomerization of Os(II)-Terpyridine Complexes via Oxidation and Reduction

6.1 Introduction

Tailored design of phosphorescent molecules that are capable to emit in the near-infrared (NIR) as well as in the infrared (IR) domain are now receiving huge attention due to their diverse applicability in chemistry and biology.¹⁻¹¹ It would be borne in mind that ~50% of the solar radiation that comes to the Earth is composed of NIR radiation. The implication of NIR light is particularly useful in biological recognition and sensing due to their invisibility to the human eye and minimal interference with biological tissues.¹¹⁻¹⁵ Apart from immense biological implications, the NIR light have shown their promise in the field of fibre optic communication, NIR OLEDs, and night vision-readable displays, to name a few.¹⁶⁻¹⁹ Hence, fabrication of efficient NIR luminescent materials possessing elevated quantum yield and lifetime is now an important task for the chemists and material scientists.²⁰⁻²⁴ Quite a few synthetic strategies, viz. extending the π -conjugation in the organic framework,²⁵⁻²⁸ enhancing spin-orbit interactions²⁹⁻³⁶ or by fusing proper functional groups,³⁷⁻⁴⁰ have been adopted to enlarge the spectral domain of the dyes towards the NIR domain. The spin-orbit coupling interaction is found to be very efficient to induce mixing of the singlet and triplet states and thus could trigger the generation of longer wavelength absorption and emission.

Molecular or supramolecular assemblies that are able to reversibly change their physicochemical behaviors on treatment with suitable external stimuli are found to be useful for the fabrication of potential photomolecular switches and memory devices.⁴¹⁻⁵⁹ Among the diverse stimuli, light is believed to be the most convenient source for operation of the devices as it is environmentally benign, could be straightforwardly applied to any state of the material and desired wavelength of light could easily be utilized for exciting a particular molecular component. A wide range of organic compounds have been employed for the fabrication of diverse NIR emissive materials.²⁵⁻²⁸ In spite of their several favorable characteristics and advantage of tunable structures, most of the organic chromophores suffers from susceptibility to photo-bleaching and of limited Stokes shifts.⁶⁰ To get-rid of the shortcomings, transition metal complexes have come out as a potential alternative for the fabrication of NIR emissive materials.²⁰⁻²⁴ The efficacy of the metal complexes over their organic counterparts is because of better tunability in the optoelectronic and photo-redox properties of the former, which could be systematically modulated in a desired fashion upon judicious choice of metal and organic ligands.⁶¹⁻⁷¹ The photo-redox properties of the metal complexes could be modulated further under the action of suitable external stimuli.⁷²⁻⁷⁸

In this work, our primary objective is to design NIR emissive metal complexes and

systematic modulation of their photo-redox properties upon treating the complexes with light of appropriate wavelengths. We are interested in the polypyridine complexes of Os(II) due to their amazing absorption- and emission spectral characteristics in the NIR domain as well as reversible electrochemical behaviors that could be employed for designing of photochemical molecular devices, sensors and switches.^{29-36,69-71,79-85} In order to fulfil our objective, we designed herein a new array of linear stilbene-appended homoleptic-Os(II)-terpyridine complexes of composition, $[\text{Os}(\text{tpy-pvp-X})_2](\text{ClO}_4)_2$, possessing a polyaromatic unit (anthracene, naphthalene and pyrene) in the complex architecture (Chart 6.1). The reason of choosing terpyridine chelating units over their bipyridine counterpart is to synthesize linear rod-like structure devoiding of any isomeric mixtures.⁸⁶ Two stilbene units in the complex framework are also able to induce reversible trans-trans (*t-t*) to trans-cis (*t-c*) and/or cis-cis (*c-c*) isomerization upon irradiating with specific light source. Different polyaromatic hydrocarbon motifs have been integrated into the complex architecture for fine tuning of their emission spectral features along with modulation of the photo-isomerization rate.

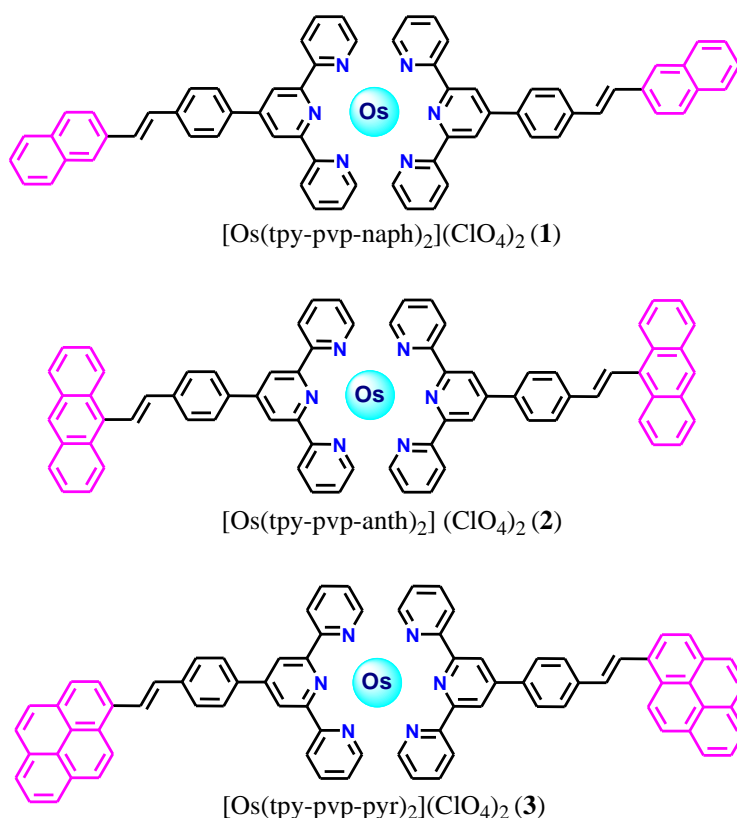


Chart 6.1. Molecular structures of the complexes.

The efficacy of these photo-switches critically depends on their rate of isomerization. Slow photoisomerization is unsuitable for meeting the need for a quick response. Therefore,

inducing fast photoswitching is one of the major prerequisites for majority of applications such as optical switches, drug delivery, information storage, to ensure a rapid response to the light signal.⁸⁷⁻⁹² One of the most interesting aspects of the present study is remarkable improvement of rate and quantum yield of photo-isomerization via chemical oxidation as well as reduction of the complexes. Although, NIR emitting Os(II)-polypyridyl complexes are reported in our laboratory^{23-24,71,79-82} and also by other research groups,^{68-70,83-85, 93-97} but as per our literature survey, we found no such work that display multi-step photo-switching properties. In conjunction with experiment, computational studies have also been made on all the three conformations (*t-t*, *t-c*, and *c-c*) of the complexes to gain insight into their electronic structures and for accurate assignment of their absorption and emission spectral bands.

6.2 Experimental Section

6.2.1 Materials. OsO₄ and NaClO₄ are procured from Merck. Reagent grade chemicals and solvents used in the present investigation are purchased from local vendors.

6.2.2 Synthesis of the Ligands. Tpy-pvp-X (X=naphthalene, anthracene, and pyrene) ligands are prepared and characterized by our reported method and is already described in Chapter 2.

6.2.3 Synthesis of the Metal Complexes. All the Os(II) complexes were synthesized by practicing a common synthetic protocol outlined below.

[Os(tpy-pvp-naph)₂](ClO₄)₂·2H₂O (1). Tpy-pvp-naph (0.100 g, 0.22 mmol) was dispersed in 15 mL of ethylene glycol and to it K₂OsCl₆ (0.052 g, 0.11 mmol) was added and refluxed for 12h under argon protection and thereafter allowed the solution to come down at room temperature. The solution was filtered and the filtrate was discharged into an aqueous solution of NaClO₄ (1.5 g NaClO₄ in 5 mL of water) when a dark chocolate colored compound deposited. The compound was collected by filtration and purified by silica gel column chromatography upon eluting with MeCN-PhCH₃ (10:1, v/v) mixture. Rotary evaporation of the eluted solvent mixture gives rise to microcrystalline solid which on further recrystallization from MeCN-MeOH (1:2, v/v) mixture generates desired complex. Yield: 0.20g (68%). Anal. Calcd. for C₆₆H₅₀N₆OsCl₂O₁₀: C, 56.73; H, 3.79; N, 6.17. Found: C, 56.80; H, 3.74; N, 6.23. HRMS (positive, MeCN) Calculated: m/z=557.1763 and m/z=1213.2880; Found: m/z=557.1413 (100%) [Os(tpy-pvp-naph)₂]²⁺ and m/z=1213.0559 (20%) {[Os(tpy-pvp-naph)₂](ClO₄)₂·2H₂O}⁺. ¹H NMR (400 MHz, DMSO-*d*₆, δ/ppm): 9.57 (s, 4H, 4H₃), 9.14 (d, *J* = 8.2 Hz, 4H, 4H₆), 8.51 (d, *J* = 7.9 Hz, 4H, 4H₇), 8.13 (s, 2H, 2H₁₇), 8.07 (d, *J* = 8.0

Hz, 4H, 4H₈), 8.04-7.91 (m, 10H, 4H₄+2H₁₁+2H₁₄+2H₁₆), 7.68 (q, $J = 16.4$ Hz, 4H, 2H₉+2H₁₀), 7.56 (p, $J = 7.0$ Hz, 6H, 2H₁₂+2H₁₃+2H₁₅), 7.47 (d, $J = 5.8$ Hz, 4H, 4H₃), 7.24 (t, $J = 6.6$ Hz, 4H, 4H₅). ¹³C NMR (400 MHz, DMSO-*d*₆, δ /ppm): 160.27, 155.15, 152.71, 145.97, 139.76, 138.28, 134.94, 134.68, 133.74, 133.29, 130.82, 128.84, 128.78, 128.47, 128.39, 128.15, 127.66, 127.11, 126.82, 125.46, 124.13, 119.78.

[Os(tpy-pvp-anth)₂](ClO₄)₂·3H₂O (2). Yield: 0.19g (66%). Anal. Calcd. for C₇₄H₅₆N₆OsCl₂O₁₁: C, 60.55; H, 3.92; N, 5.67. Found: C, 60.61; H, 3.85; N, 5.73. HRMS (positive, MeCN) Calculated: $m/z = 608.1933$; Found: $m/z = 608.2035$ (100%), [Os(tpy-pvp-anth)₂]²⁺. ¹H NMR (400 MHz, DMSO-*d*₆, δ /ppm): 9.60 (s, 4H, 4H₃), 9.16 (d, $J = 8.3$ Hz, 4H, 4H₆), 8.65 (s, 2H, 2H₁₅), 8.58 (d, $J = 8.1$ Hz, 4H, 4H₇), 8.51-8.38 (m, 6H, 4H₄+2H₉), 8.28-8.13 (m, 8H, 4H₈+4H₁₁), 8.01-7.88 (m, 4H, 4H₁₃), 7.68-7.55 (m, 8H, 4H₁₂+4H₁₄), 7.50 (d, $J = 5.7$ Hz, 4H, 4H₃), 7.31-7.16 (m, 6H, 4H₅+2H₁₀). ¹³C NMR (400 MHz, DMSO-*d*₆, δ /ppm): 160.28, 155.21, 152.79, 139.49, 138.30, 136.60, 135.08, 132.61, 131.60, 129.65, 129.30, 128.78, 128.49, 127.95, 127.25, 127.14, 126.99, 126.54, 126.17, 125.99, 125.51, 119.84.

[Os(tpy-pvp-pyr)₂](ClO₄)₂·3H₂O (3). Yield: 0.18g (65%). Anal. Calcd. for C₇₈H₅₆N₆OsCl₂O₁₁: C, 62.07; H, 3.39; N, 5.52. Found: C, 62.11; H, 3.34; N, 5.57. HRMS (positive, MeCN) Calculated: $m/z = 631.1920$; Found: $m/z = 631.1428$ (100%) [Os(tpy-pvp-pyr)₂]²⁺. ¹H NMR (400 MHz, DMSO-*d*₆, δ /ppm): 9.60 (s, 4H, 4H₃), 9.17 (d, $J = 8.3$ Hz, 4H, 4H₆), 8.92 (d, $J = 9.5$ Hz, 2H, 2H₁₄), 8.73-8.61 (m, 6H, 2H₉+2H₁₁+2H₁₅), 8.56 (d, $J = 8.1$ Hz, 4H, 4H₇), 8.41-8.34 (m, 6H, 2H₁₆+2H₁₇+2H₁₈), 8.30 (d, $J = 8.1$ Hz, 6H, 4H₈+2H₁₂), 8.17-8.08 (m, 4H, 2H₁₃+2H₁₉), 7.96 (t, $J = 8.0$ Hz, 4H, 4H₄), 7.82 (d, $J = 16.0$ Hz, 2H, 2H₁₀), 7.49 (d, $J = 8.0$ Hz, 4H, 4H₃), 7.25 (t, $J = 8.0$ Hz, 4H, 4H₅). ¹³C NMR (400 MHz, DMSO-*d*₆, δ /ppm): 160.31, 155.19, 140.07, 138.30, 131.75, 131.56, 131.20, 130.97, 128.79, 128.62, 128.48, 128.18, 127.9, 126.97, 125.90, 125.77, 124.83, 124.60, 124.14, 119.85.

Caution! *Perchlorate salts of the metal complexes are potentially explosive and therefore should be handled in small quantities with care.*

6.2.4 Instruments and Physical Methods. The details of instruments and physico-chemical measurements are provided in Chapter 2 and Chapter 3.

6.3 Results and Discussion

6.3.1 Synthesis and Characterization. The desired Os(II) complexes are prepared upon refluxing K₂OsCl₆ and respective terpyridine ligand (tpy-pvp-X) in a 1:2 ratio under argon atmosphere in ethylene glycol medium followed by their ion exchange with NaClO₄.

Purification of the complexes is accomplished by column chromatography and recrystallization from appropriate solvent(s). The complexes are fully characterized via elemental analysis as well as by NMR and ESI mass spectrometry, the details of which are dispensed in the experimental section.

6.3.2 Mass Spectra. The high resolution mass spectra (HRMS) of complexes **1-3** are acquired in MeCN. Experimental and simulated isotopic distribution pattern of **1** is provided in Figure 6.1, whereas for **2** and **3** in Figure 6.2. A moderately good correlation among the experimental and simulated spectral pattern is noticed in almost all cases. The mass separation of 0.5 Da among the consecutive spectral lines indicate the existence of $[\text{Os}(\text{tpy-pvp-X})_2]^{2+}$ species in each of the three complexes. The most abundant peak at 557.1413 for **1**, 608.2035 for **2**, and 631.1428 for **3** corresponds to the respective bi-positive cationic species. A less abundant peak at $m/z=1213.0559$ is also noticed in case of **1**, suggesting the presence of mono-positive species of the type $\{[\text{Os}(\text{tpy-pvp-naph})_2]\text{ClO}_4\}^+$.

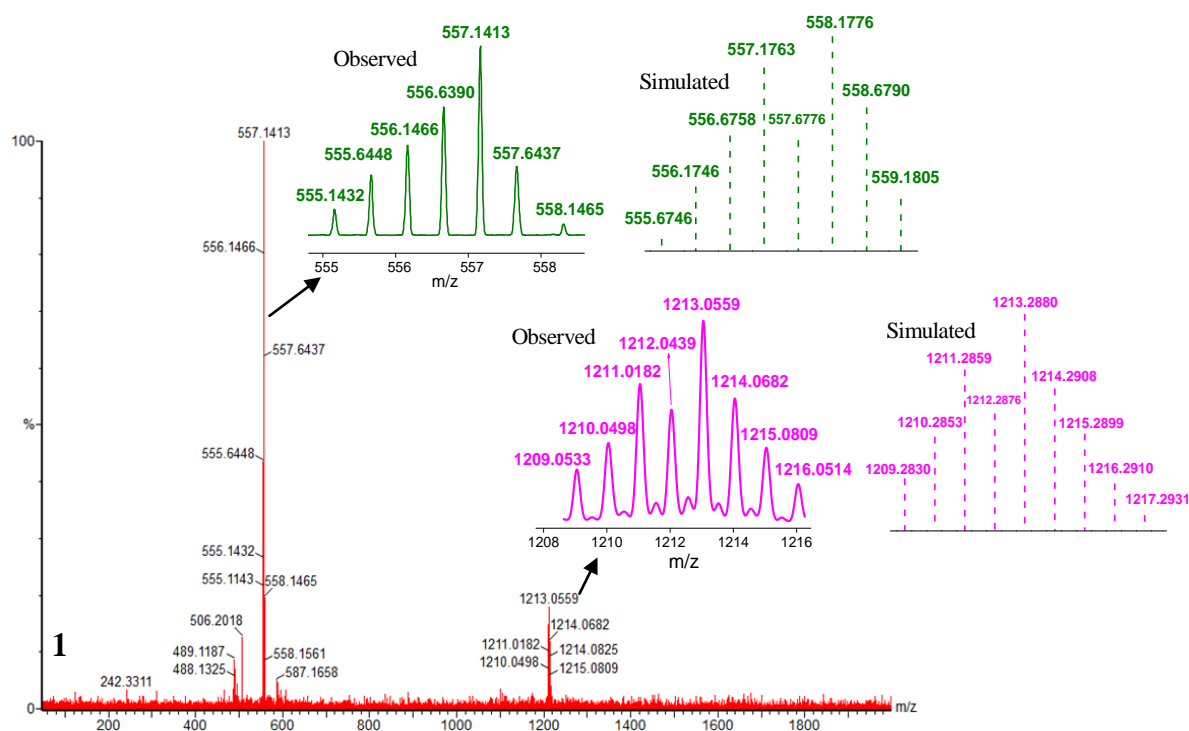


Figure 6.1. Experimental and simulated HRMS spectrum (positive) of **1** in MeCN. The abundant peak at $m/z=557.1413$ corresponds to $[\text{Os}(\text{tpy-pvp-naph})_2]^{2+}$ ion, while the relatively less abundant peak at $m/z=1213.0559$ correlates with $\{[\text{Os}(\text{tpy-pvp-naph})_2]\text{ClO}_4\}^+$ species.

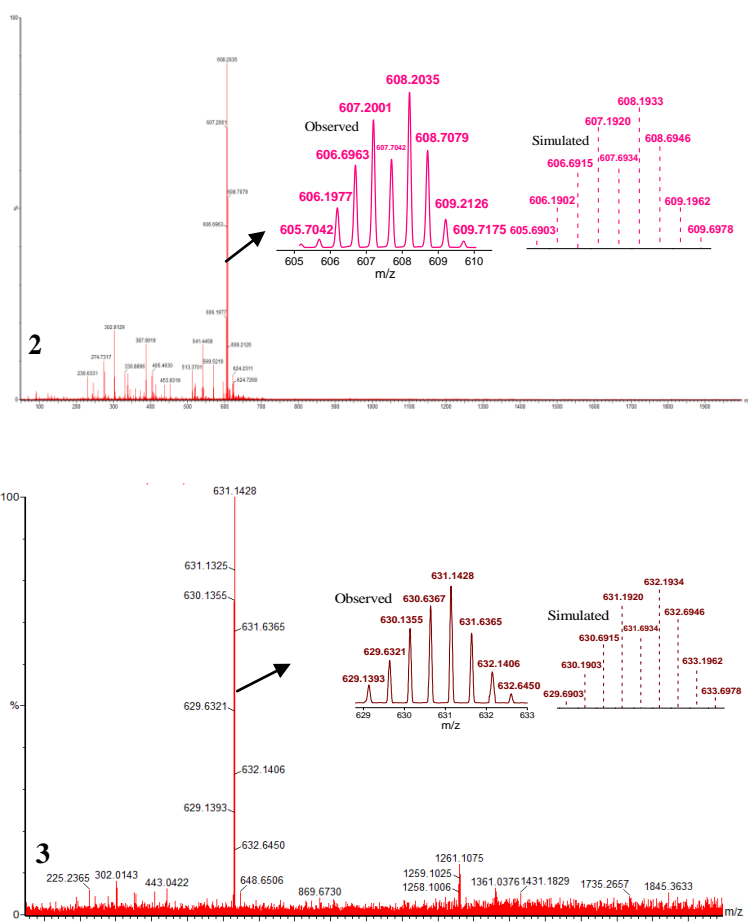


Figure 6.2. Experimental and simulated HRMS (positive) spectrum of **2** and **3** in MeCN. The abundant peak at $m/z=608.2035$ corresponds to $[\text{Os}(\text{tpy-pvp-anth})_2]^{2+}$ and at $m/z=631.1428$ corresponds to $[\text{Os}(\text{tpy-pvp-pyr})_2]^{2+}$ species.

6.3.3 NMR Spectra. ^1H and ^{13}C NMR spectra of the complexes are acquired in $\text{DMSO-}d_6$ and are shown in Figure 6.3 and Figure 6.4. Tentative assignment of all the proton resonances in the complexes is made with the help of their $\{^1\text{H-}^1\text{H}\}$ COSY NMR spectra, relative areas of peaks, usual chemical shift and coupling constant values of different protons associated with aromatic and hetero-aromatic moieties in the complexes as well as by comparing the ^1H NMR spectra of structurally similar compound. The COSY NMR spectra of the complexes **2** and **3** are provided in Figure 6.5. A sharp and most downfield singlet within the chemical shift region of 9.60-9.57 ppm is observed for all three complexes which corresponds to H_3 proton as it does not possess any cross peak in the respective $\{^1\text{H-}^1\text{H}\}$ COSY NMR spectrum. The most up-field peak in the range of 7.31-7.16 ppm, on the other hand, corresponds to H_5 which in turn is coupled with H_3 . A doublet within 8.58-8.51 ppm is assigned as H_7 , while its cross-peak in the domain of 8.30-8.09 ppm is due to H_8 . For the

anthracene (**2**) derivative, the multiplet in the range of 8.51-8.38 ppm corresponds to both H₄ and H₉ protons which again have a cross peak within 7.31-7.16 ppm, due to H₅ and H₁₀ protons. In a similar manner, the peak at 8.92 ppm corresponds to H₁₄, has a cross peak at ~8.38 ppm, assignable as H₁₆, H₁₇ and H₁₈ protons in complex **3**. Following similar approach, the rest of the peaks in the NMR spectra of the complexes are also assigned with the help of {¹H-¹H} COSY NMR spectra. The olefinic protons (H₉ and H₁₀) in the complexes appear within 8.73-7.16 ppm range. The *J* value of ~16Hz of the said protons across the double bond confirms their *transoid* orientation.

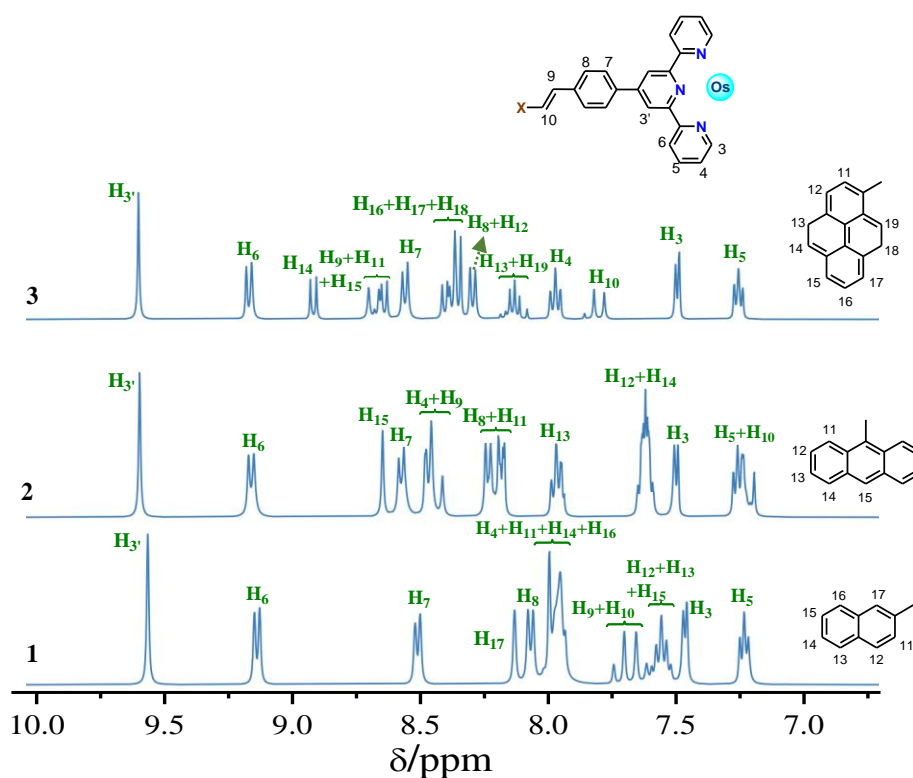


Figure 6.3. ¹H NMR spectra of **1-3** in DMSO-*d*₆.

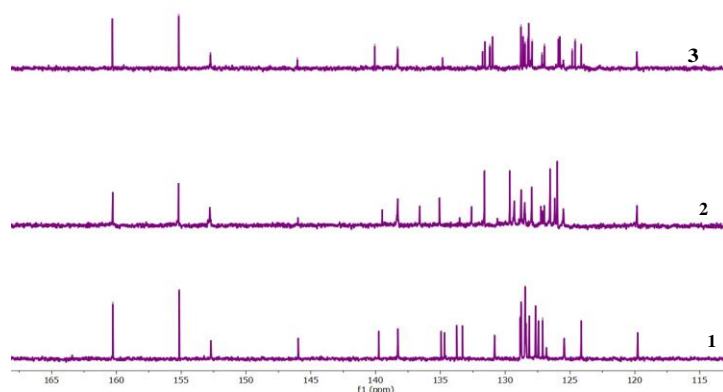


Figure 6.4. ¹³C NMR spectra of **1-3** in DMSO-*d*₆.

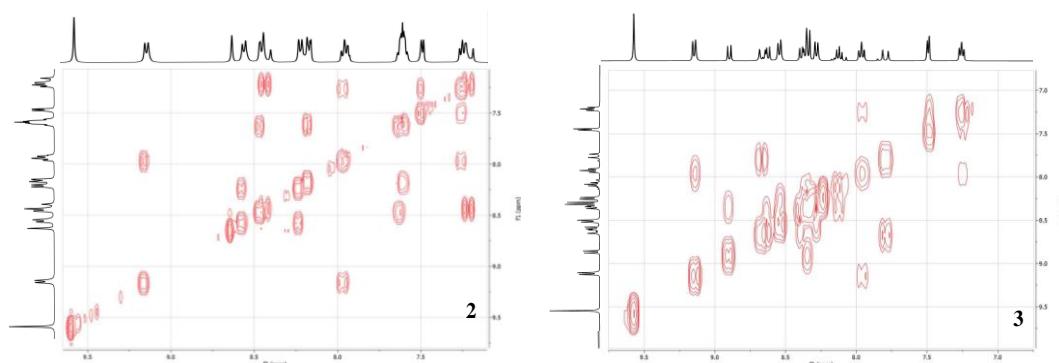


Figure 6.5. $\{^1\text{H}-^1\text{H}\}$ COSY NMR spectra of **2** and **3** in $\text{DMSO}-d_6$.

6.3.4 Geometry Optimization of the Complexes via DFT. The geometries of the complexes are optimized at the B3LYP level of theory using 6-31g(d) and SDD as basis sets. The optimized structure of the complexes together with their highest occupied molecular orbital (HOMO) and lowest unoccupied molecular orbital (LUMO) for complex **1** are provided in Figure 6.6- 6.7 and Table 6.1. The HOMOs are mostly Os d-orbital character with some additional contribution from the π -cloud of the polyaromatic unit. By contrast, the LUMOs are predominantly located on the terpyridine unit in the molecular backbone.

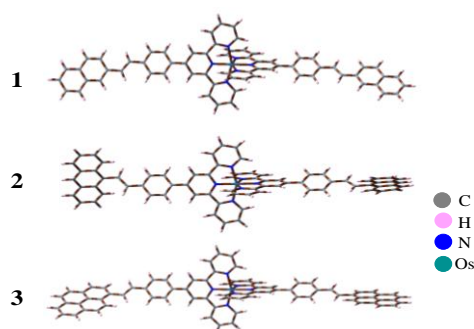


Figure 6.6. Optimized structures of *t-t* form of **1-3** in MeCN.

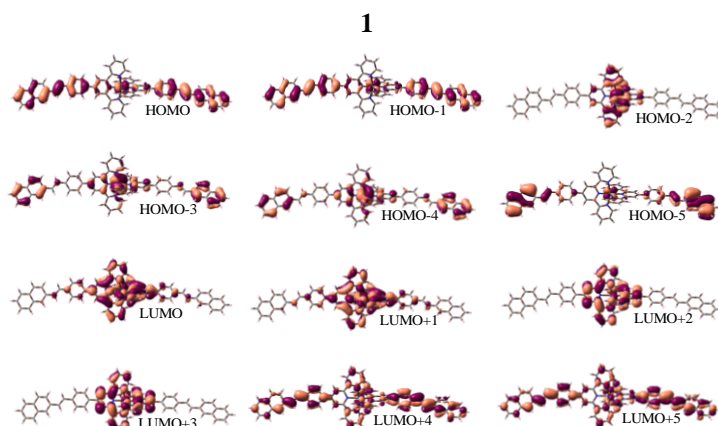


Figure 6.7. Schematic drawings of the selective frontier molecular orbitals of *t-t* forms of **1** in MeCN.

Table 6.1. Selected MOs along with their energies and compositions in the ground state of $[\text{Os}(\text{tpy-pvp-naph})_2]^{2+}$ (**1**) in their *t-t*, *t-c* and *c-c* forms in MeCN.

MO	[Os(tpy-pvp-naph) ₂] ²⁺														
	Energy/ev			% Compositions											
	t-t	t-c	c-c	t-t				t-c				c-c			
				naph	tpy	pvp	Os	naph	tpy	pvp	Os	naph	tpy	pvp	Os
LUMO+5	-1.93	-1.83	-1.83	23.97	32.81	42.78	0.43	19.83	40.22	39.53	0.41	19.83	39.92	39.82	0.41
LUMO+4	-1.93	-1.93	-1.83	23.87	32.95	42.75	0.41	24.10	32.56	42.91	0.41	19.78	39.93	39.86	0.40
LUMO+3	-2.41	-2.41	-2.41	0.00	95.22	0.68	4.09	0.00	95.24	0.66	4.09	0.00	95.24	0.65	4.09
LUMO+2	-2.53	-2.54	-2.54	0.00	99.37	0.62	0.00	0.00	99.38	0.60	0.00	0.00	99.37	0.61	0.00
LUMO+1	-2.7	-2.70	-2.7	2.05	77.74	9.46	10.07	1.18	79.71	8.23	10.86	0.98	80.08	8.04	10.88
LUMO	-2.71	-2.71	-2.71	2.03	77.87	9.56	10.53	1.75	78.63	9.03	10.57	0.98	80.16	8.15	10.69
HOMO	-5.58	-5.58	-5.70	40.06	7.61	40.77	11.55	40.47	7.35	40.87	11.29	39.60	9.27	35.18	15.94
HOMO-1	-5.58	-5.70	-5.70	40.12	7.39	40.88	11.60	39.52	9.28	34.88	16.29	39.68	9.04	35.24	16.01
HOMO-2	-5.94	-5.94	-5.94	0.00	34.57	0.04	65.38	0.012	34.62	0.036	65.32	0.05	34.59	0.04	65.31
HOMO-3	-6.02	-6.0	-6.00	26.99	22.16	4.61	46.23	38.09	18.56	4.78	38.56	37.74	18.61	4.72	38.90
HOMO-4	-6.02	-6.02	-6.01	27.24	22.25	4.63	45.85	26.90	22.30	4.51	46.28	38.20	18.62	4.69	38.47
HOMO-5	-6.34	-6.33	-6.33	72.61	4.33	16.04	7.01	62.85	5.60	22.21	9.319	62.69	5.69	22.22	9.38

6.3.5 Absorption and Emission Spectral Characteristics. The UV-vis absorption spectra of the complexes are acquired in MeCN and pertinent data are provided in Table 6.2 and associated spectra are presented in Figure 6.8. The complexes have similar spectral

Table 6.2. Absorption and emission spectral data of **1-3**.

Comp ds		Absorption $\lambda_{\text{max}}/\text{nm}$ ($\epsilon/\text{M}^{-1}\text{cm}^{-1}$)	Luminescence				
			$\lambda_{\text{max}}/\text{nm}$	τ/ns	Φ^a	$k_r/\text{s}^{-1} \times 10^5$	$k_{nr}/\text{s}^{-1} \times 10^6$
1	MeCN (298K)	673(7000), 497(32000), 364(58900), 316(61000), 286(sh)(47000), 232(55000)	740	112.5	13.4×10^{-3}	1.2	8.8
2		672(7500), 496(32400), 396(br)(29000), 314(68700), 254(sh)(137200)	736	103.2	1.6×10^{-3}	0.2	9.7
3		673(10000), 500(52400), 390(br)(77000), 311(78200), 288(sh)(65600), 235(107400)	744	84.5	7.5×10^{-3}	0.9	11.7
1	77K	-	729	2.3 μs	0.3	1.3	0.3
2		-	724	3.0 μs	0.13	0.4	0.2
3		-	745	2.1 μs	0.02	0.1	0.5

^aLuminescence quantum yields are determined by a relative method via the equation $\Phi_r = \Phi_{\text{std}}(A_{\text{std}}/A_r)(I_r/A_r)/(\eta_r^2/(\eta_{\text{std}}^2))$, using $[\text{Ru}(\text{bpy})_3]^{2+}$ as the standard. Φ_r and Φ_{std} are the quantum yields of unknown and standard samples ($\Phi_{\text{std}}=0.032$ (at 298K) in MeCN at $\lambda_{\text{ex}}=450\text{ nm}$), A_r and A_{std} (<0.1) are the solution absorbance at the excitation wavelength (λ_{ex}), I_r and I_{std} are the integrated emission intensities, and η_r and η_{std} are the refractive indices of the solvent. Experimental errors in the reported luminescence quantum yields are $\sim 20\%$.

behavior and only a small variation in spectral pattern is observed upon variation of the polyaromatic hydrocarbon unit. Tentative assignments of all the absorption bands in the complexes have been made upon comparing the spectra of structurally related complexes as well as by taking into consideration the results of TD-DFT calculations (Table 6.3, for complex **1**). The computed absorption spectra are also overlaid in Figure 6.8 and are found to be well correlated. Thus, the intense band at $\sim 500\text{ nm}$ mostly corresponds to metal-to-ligand $\{\text{Os}(\text{II}) \rightarrow \text{tpy-pvp-X}\}$ charge transfer transition of singlet character ($^1\text{MLCT}$). A relatively broad and weak band is noted beyond 500 nm , which extend into the red region before tailing off at 730 nm . This band arises due to the spin- forbidden direct population to the $^3\text{MLCT}$ states $\{^1[\text{Os}^{\text{II}}(\text{d}\pi)^6] \rightarrow ^3[\text{Os}^{\text{II}}(\text{d}\pi)^5\text{tpy}(\pi^*)^1]\}$ as a consequence of the high spin-orbit coupling constant of the Os centre. Since the calculations are all performed for singlet-singlet transitions, we did not come by any spin-forbidden bands in the computed spectra. The intense bands within $311\text{-}364\text{ nm}$ arise because of combined MLCT and ILCT transitions while the highly intense bands beyond 300 nm is attributed to the $\pi\text{-}\pi^*$ transitions.

The emission spectra of the complexes acquired in MeCN at room temperature and in EtOH-MeOH (4:1, v/v) glass at 77K, are presented in Figure 6.9. The relevant spectral

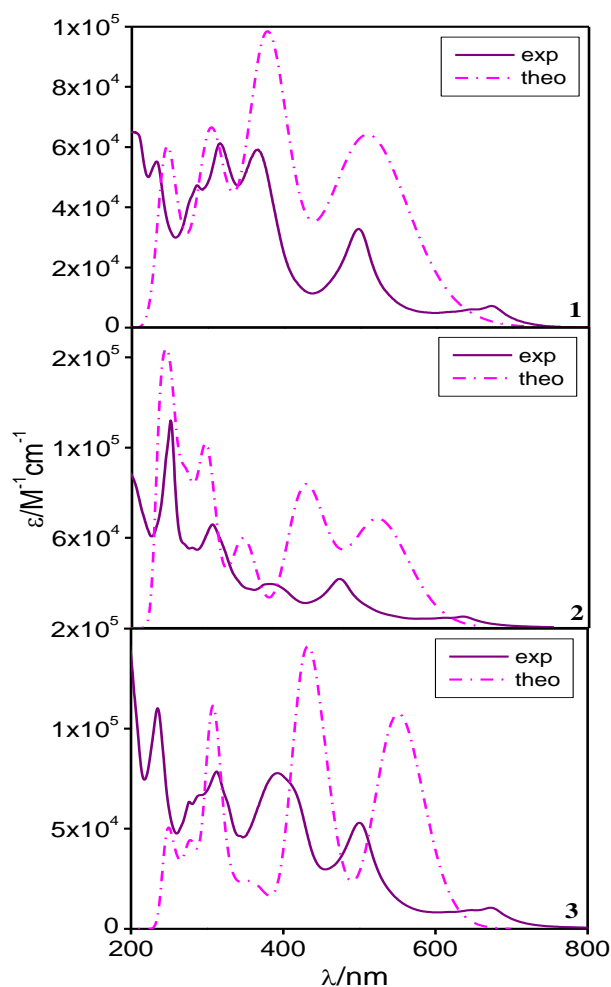


Figure 6.8. Overlay of the experimental (purple solid line) and calculated (magenta dotted line) absorption spectra of **1-3** in MeCN.

parameters are already provided in Table 6.2. On excitation at the $^1\text{MLCT}$ region, all the complexes exhibit a broad and structureless phosphorescent band lying within the NIR domain of 736-744 nm, dependent on the substituent. This band arises primarily due to radiative deactivation of the $^3\text{MLCT}$ state of the complexes. The estimated quantum yields (Φ) are found to be in the range of $1.6\text{-}13.4 \times 10^{-3}$. The radiative (k_r) as well as non-radiative (k_{nr}) rate constants are also calculated and provided in Table 6.2. At 77K, the complexes **1** and **2** display blue-shifted emission band while for complex **3**, the band maximum remains almost unchanged. Substantial augmentation in Φ is noticed for all three cases, which is indicative of typical $^3\text{MLCT}$ emitter. The E_{00} values of the emitting excited state ($^3\text{MLCT}$) of the complexes are determined by using their λ_{max} values at 77K and are found to lie in the range of 1.65-1.71 eV. All the complexes exhibit mono-exponential decay at RT as well as in EtOH-

Table 6.3. Selected UV-vis energy transitions at the TD-DFT/B3LYP level of [Os(tpy-pvp-naph)₂]²⁺ (**1**) in their *t-t*, *t-c* and *c-c* forms in MeCN.

λ_{exp} /nm	Excited State	λ_{cal} /nm	Oscillator strength	Key transitions	Character
<i>t-t</i> [Os(tpy-pvp-naph) ₂] ²⁺					
497	S5	518	1.45	H-3→L+1 (10%), H-1→L+1 (41%), H→L (38%)	MLCT
364	S21	380	2.35	H-1→L+4 (45%), H→L+5 (44%)	MLCT, ILCT
315	S55	310	0.21	H-9→L+1 (80%)	MLCT, ILCT
285	S61	306	0.24	H-12→L (65%), H-11→L+1 (19%)	ILCT, π - π^*
	S60	305	0.30	H-12→L+1 (68%), H-11→L (13%)	ILCT, π - π^*
230	S142	247	0.59	H-16→L (10%), H-15→L+1 (10%), H-4→L+12 (12%), H-3→L+13 (11%)	π - π^*
<i>t-c</i> [Os(tpy-pvp-naph) ₂] ²⁺					
497	S5	512	1.11	H-1→L+1 (18%), H→L (41%)	MLCT
359	S25	362	0.48	H-1→L+5 (83%)	MLCT, ILCT
	S21	378	1.25	H→L+4 (86%)	MLCT, ILCT
317	S54	311	0.13	H-9→L (52%), H-7→L+1 (13%)	ILCT, π - π^*
	S61	305	0.27	H-12→L (30%), H-12→L+1 (35%)	ILCT, π - π^*
286	S68	299	0.25	H-6→L+4 (33%), H→L+11 (53%)	π - π^*
232	S175	235	0.12	H-19→L+1 (11%), H-9→L+8 (52%)	π - π^*
<i>c-c</i> [Os(tpy-pvp-naph) ₂] ²⁺					
497	S5	505	0.82	H-4→L (10%), H-3→L+1 (12%), H- 1→L+1 (36%), H→L (34%)	MLCT
359	S21	378	0.17	H-6→L (50%), H-5→L+1 (40%)	MLCT, ILCT
	S25	364	1.07	H-1→L+4 (43%), H→L+5 (42%)	MLCT, ILCT
317	S55	310	0.17	H-9→L+1 (42%), H-8→L (17%), H- 7→L+1 (19%)	ILCT, π - π^*
	S59	306	0.30	H-12→L (54%), H-10→L (23%), H- 2→L+7 (10%)	ILCT, π - π^*
286	S69	297	0.12	H-6→L+5 (15%), H-5→L+4 (16%), H-1→L+11 (23%), H→L+10 (23%)	π - π^*

MeOH (4:1, v/v) glass at 77K (inset to Figure 6.9). The lifetimes of the complexes lie in the range of 84.5-112.5 ns at RT, while substantially elevated to the domain of 2.1-3.0 μ s at 77K in EtOH-MeOH glass, again indicating the characteristics of the ³MLCT emitter.

The photophysical properties of terpyridine-type complexes of Os(II) have been previously investigated by various research groups, viz. Sauvage, Balzani, Harriman,

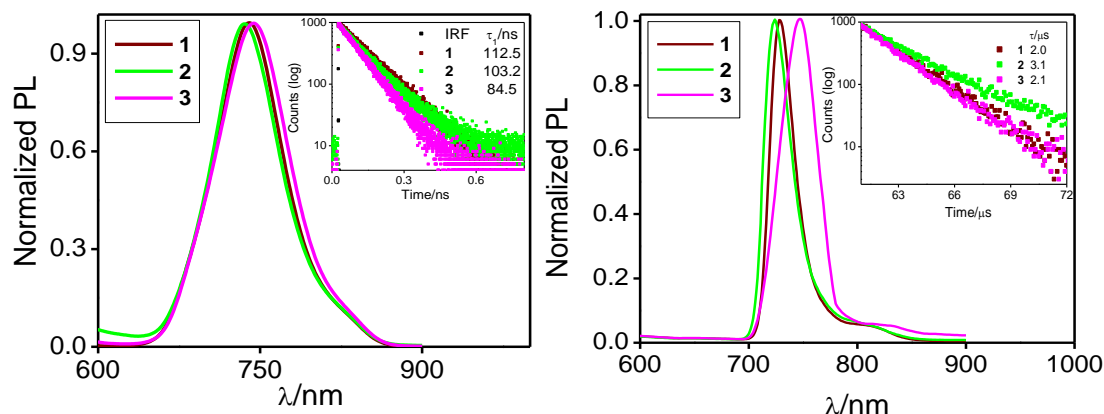
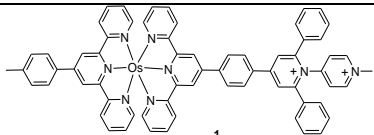
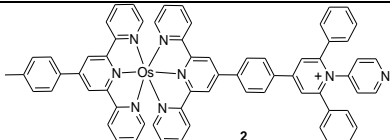
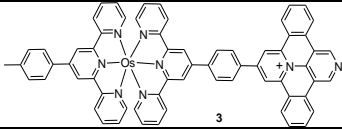
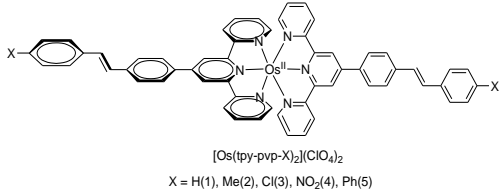
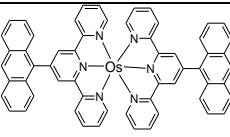
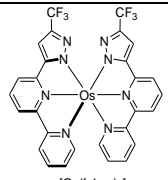
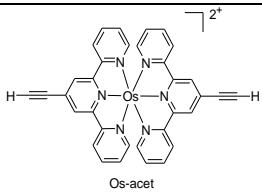
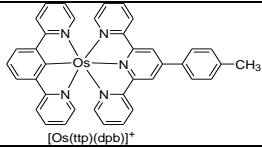
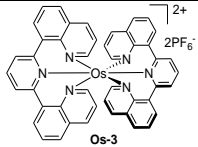
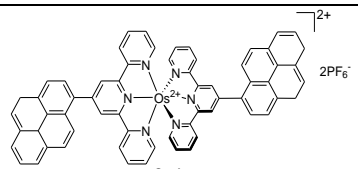
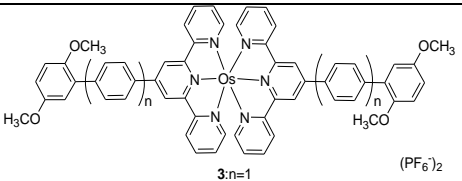
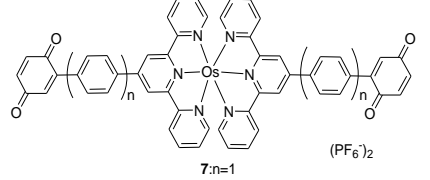
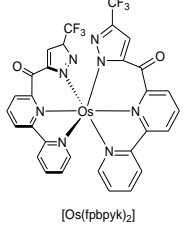
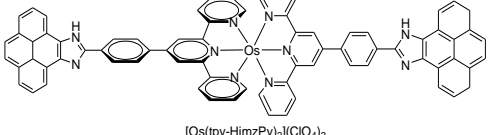
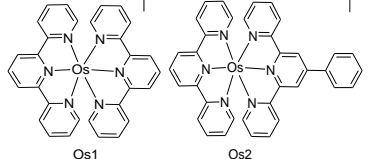
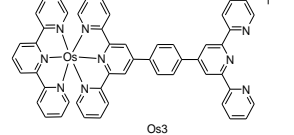
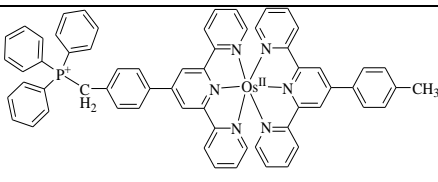
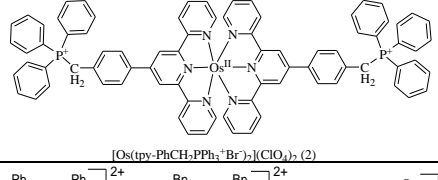
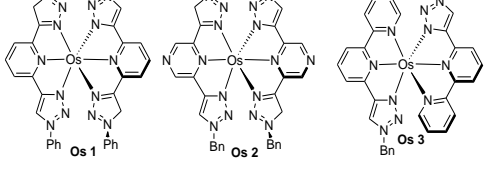


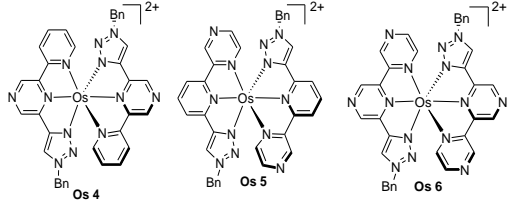
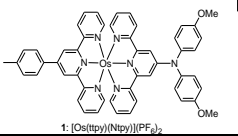
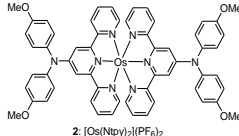
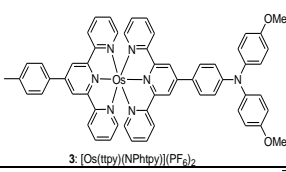
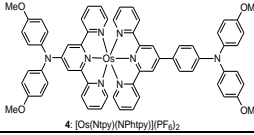
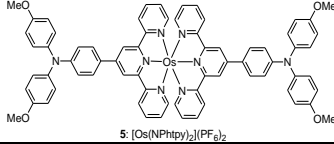
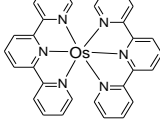
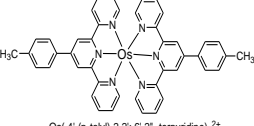
Figure 6.9. Luminescence spectral ($\lambda_{\text{ex}} = 500$ nm) profiles of **1-3** in MeCN at RT (left) and in MeOH/EtOH (1:4, v/v) glass at 77K (right). Inset to the figures depict the emission decay profiles ($\lambda_{\text{ex}} = 490$ nm) as well as lifetimes of the complexes.

Campagna, Hanan, Barigelletti, Zhong, Elliott to name but a few.^{29-32,34-36,96,100-111} Table 6.4 provides absorption and emission spectral characteristics of representative Os(II)-terpyridine-type complexes. Although the photophysical properties of terpyridine-type Os(II) complexes closely resemble their Ru(II) counterparts, incorporating Os²⁺ ion in a similar chemical environment results in a bathochromic shift of both absorption and emission maxima, mainly due to larger size of 5d orbitals compared to 4d orbitals as well as stronger spin-orbit coupling effect of the later. With few exceptions, most of the terpyridine complexes are found to be weakly emissive (Table 6.4). Several strategies, viz. incorporation of electron donating and electron accepting groups, polyaromatic as well as hetero-aromatic moieties at the 4'-position of the terpyridine motif, along with use of cyclometalating coordination motifs, have been adopted to enhance the emission quantum yield and excited state lifetime of the resulting complexes.¹⁰⁰⁻¹¹¹ Herein, we designed three homoleptic Os(II)-terpyridine complexes upon incorporating stilbene units together with polyaromatic hydrocarbon (naphthalene, anthracene and pyrene) moieties at the 4' position of the terpyridine to improve emission characteristics of the resulting complexes as well as to induce reversible *t-c* isomerization triggered by light. Fortunately, the complexes in the present study features intense luminescence in the 736-744 nm spectral range having lifetimes between 84.5 and 112.5 ns and emission quantum yields within the range of 0.0016-0.0134 at RT. It will be demonstrated in the later section that by virtue of the presence of stilbene units, the complexes are able to display reversible *t-t* to *c-c* photo-isomerization.

Table 6.4. Absorption and emission spectral characteristics of representative Os(II) complexes.

Compounds	Absorption $^1\text{MLCT}$, $\lambda_{\text{max}}/\text{nm}$ ($\epsilon, \text{M}^{-1}\text{cm}^{-1}$)	Luminescence			Ref.
		$\lambda_{\text{max}}/\text{nm}$	τ/ns	Φ	
	673(9000), 499(34000)	No emission	-	-	100
	673(10000), 498(36000)	760	2.1	4.0×10^{-4}	
	673(9000), 499(32000)	760	1.1	1.6×10^{-5}	
 [Os(tpy-pvp-X) ₂](ClO ₄) ₂ X = H(1), Me(2), Cl(3), NO ₂ (4), Ph(5)	1: 680(8100), 506(35100) 2: 680(7200), 505(32300) 3: 680(9200), 505(41300) 4: 680(6600), 503(29200) 5: 680(8500), 504(37200)	750 752 751 747 749	159 157 165 127 160	8.0×10^{-3} 7.0×10^{-3} 1.0×10^{-2} 7.0×10^{-3} 9.0×10^{-3}	56
 Os(An-tpy) ₂ ²⁺	-	728	86	2.0×10^{-4}	101
 [Os(tpbp) ₂]	715(2900), 650(2800), 465(9900)	935	597	1.4×10^{-1}	102
 Os-acet	-	737	195	4.6×10^{-3}	103
 [Os(tp)(dpb)] ⁺	765(2000), 537(13000), 503(13650)	824	-	5.4×10^{-6}	104
 Os-3	602(2900), 465(5100)	812	59	1.2×10^{-4}	105
 Os-4	667(4600), 490(20000)	740	246	6.0×10^{-2}	105

 <p>3:n=1 4:n=2 (PF₆⁻)₂</p>	3:676(8200), 497(30900) 4:678(8900), 499(31700)	742 739	219 215	2.09×10 ⁻² 1.74×10 ⁻²	106
 <p>7:n=1 8:n=2 (PF₆⁻)₂</p>	7:677(7900),501(32100) 8:677(7700),499(34000)	744 742	- -	1.79×10 ⁻⁴ 2.56×10 ⁻⁴	
 <p>[Os(tpbpyk)₂]</p>	775(270), 508(830)	994		7.0×10 ⁻³	107
 <p>[Os(tpy-HimzPy)₂](ClO₄)₂</p>	674(br)(5200), 499(25070)	750	112.5	3.3×10 ⁻¹	80
 <p>Os1 Os2 2+</p>	Os1: 476(-) Os2: 481	Os1: 583/702 Os2: 588/709	Os1: 177.32 Os2: 98.92	Os1: 0.137 Os2: 0.174	96
 <p>Os3 2+</p>	492	583/719	92.19	0.240	
 <p>[(tpy-PhCH₂)Os(tpy-PhCH₂PPh₃⁺Br⁻)](ClO₄)₂ (1)</p>	670(6000),490(24170)	732	101	5.28×10 ⁻³	108
 <p>[Os(tpy-PhCH₂PPh₃⁺Br⁻)](ClO₄)₂ (2)</p>	670 (7800), 490 (31700)	732	109	6.45×10 ⁻³	
 <p>Os 1 Os 2 Os 3 2+</p>	Os 1: 530(2960),436(5570) Os 2: 570(2400),452(3900) Os 3: 631(2830),581(3320)	Os 1:595 Os 2:650 Os 3:702	Os 1:63 Os 2:269 Os 3:88	Os 1:0.008 Os 2:0.011 Os 3:0.01	109

 <p>Os 4 Os 5 Os 6</p>	<p>Os 4:633(2480),587(2620) Os 5:656(2910),596(3320) Os 6: 641(2230),590(2620)</p>	<p>Os 4:702 Os 5:733 Os 6:710</p>	<p>Os 4:155 Os 5:135 Os 6:186</p>	<p>Os 4:0.012 Os 5:0.011 Os 6:0.017</p>	109
 <p>1: [Os(tpy)(Ntpy)](PF₆)₂</p>	678 (6600), 502 (28000)	No emission	-	-	110
 <p>2: [Os(Ntpy)₂](PF₆)₂</p>	692(75000),518 (23000)	No emission	-	-	
 <p>3: [Os(tpy)(NPhtpy)](PF₆)₂</p>	672 (7800), 502 (31000)	720		(3.0-5.0) × 10 ⁻³	
 <p>4: [Os(Ntpy)(NPhtpy)](PF₆)₂</p>	584 (8500), 516 (36000)	No emission	-	-	
 <p>5: [Os(NPhtpy)₂](PF₆)₂</p>	676(12000),515 (45000)	720	-	(3.0-5.0) × 10 ⁻³	
 <p>Os(2,2':6',2''-terpyridine)₂²⁺</p>	657(3650), 477(13750)	718	269	4.1 × 10 ⁻³	111
 <p>Os(4'-(p-tolyl)-2,2':6,2''-terpyridine)₂²⁺</p>	668(7700), 490(29750)	736	236	1.2 × 10 ⁻²	

6.3.6 Electrochemical Behaviors. Electrochemical properties of the complexes are investigated by using cyclic voltammetry (CV) as well as square wave voltammetry (SWV) in MeCN at 25°C. The voltammograms are acquired in the argon purged solution of the complexes and the concentration of the solution is maintained at ~10⁻³ M, while that of the supporting electrolyte, tetraethylammonium perchlorate (TEAP) at 0.1M. The voltammograms are displayed in Figure 6.10, while the related redox data are tabulated in Table 6.5. All complexes display a single reversible oxidation and three quasi-reversible reduction peaks. The oxidation peak, with $E_{1/2}$ value ranging from +0.93 to +0.96 V, corresponds to Os^{II}/Os^{III} process, while the peaks in the negative potential region (from -1.10

to -1.85 V) correspond to the reductions of the coordinated tpy moieties in the ancillary ligand. Spin densities of $1e^-$ oxidized and $1e^-$ reduced state of the complexes are calculated and displayed in Figure 6.11. The spin density is primarily located on Os-center for $1e^-$ oxidized, while on terpyridine motif in the $1e^-$ reduced state of the complexes. Hence, spin density computation corroborates our assignment of the redox processes.

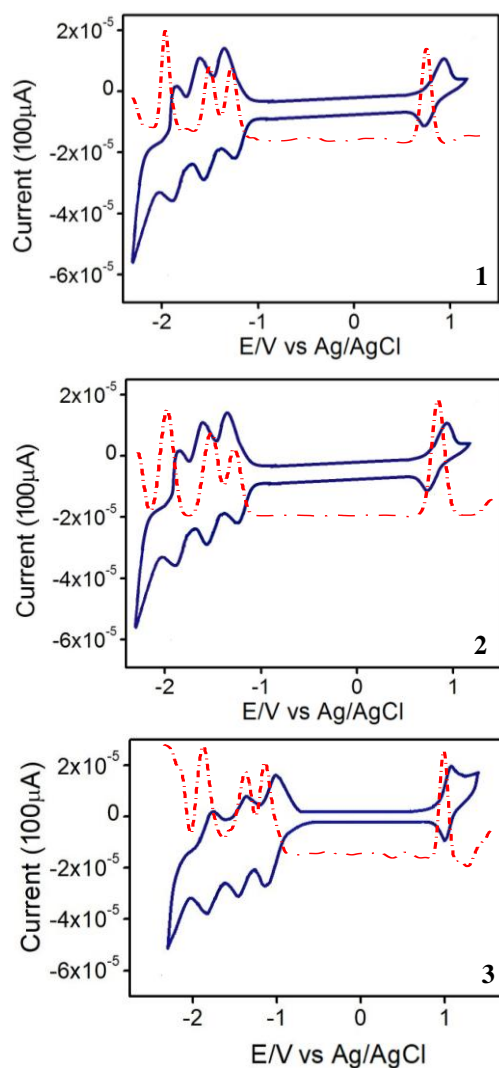


Figure 6.10. CVs (solid blue lines) and SWVs (dotted red lines) of the MeCN solutions of **1-3** ($ca \sim 10^{-3}$ M) showing both oxidation and reduction processes.

Table 6.5. Redox data^a for **1-3** in MeCN.

Compds	Oxidation ^b	Reduction ^c
	$E_{1/2}/(V)$	$E_{red}/(V)$
1	0.93	-1.14, -1.37, -1.84
2	0.95	-1.12, -1.35, -1.80
3	0.96	-1.10, -1.36, -1.85

^aAll the potentials are referenced against Ag/AgCl electrode with $E_{1/2} = 0.36$ V for Fc/Fc⁺ couple.

^bReversible oxidative electron transfer process with a Pt working electrode. ^c E_{red} values obtained by using glassy carbon electrode.

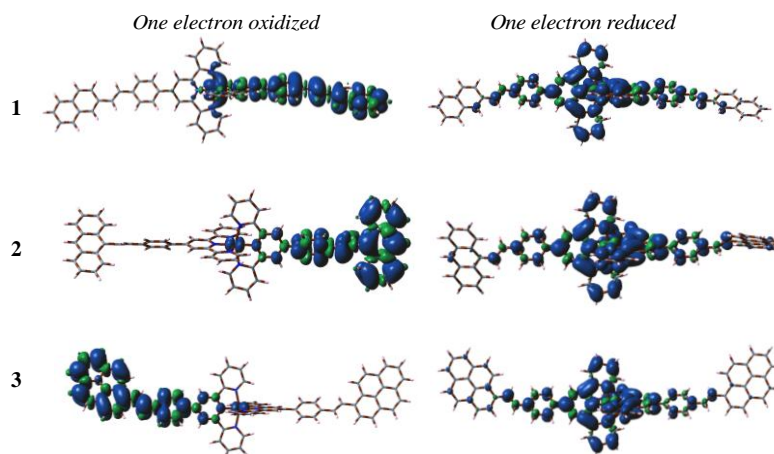


Figure 6.11. Spin density plots for one-electron oxidized (left panel) and one-electron reduced (right panel) *t-t* forms of **1-3** in MeCN.

6.3.7 Photoisomerization Behaviors. Since the present molecular backbone consists of two styrylbenzene units, it is anticipated that light irradiation will bring about changes in their molecular structures. Herein, we irradiated the MeCN solution of the complexes with visible light (500 nm) and followed the changes via absorption and emission spectroscopy as shown in Figure 6.12. A single step change takes place for all three complexes. Light irradiation leads to a decrease in the absorbance of the MLCT and ILCT bands accompanied with a minor blue-shift of the former. Small but finite increase in π - π^* band intensity is also noticed in some case. Upon close inspection, it is observed that all the spectral lines pass through distinct isosbestic point(s), indicating that two or more species are in equilibrium with one another. Time required to attain the photo-stationary state is found to vary between 20 min and 542 min, dependent on the polyaromatic moiety. It is of particular interest to note that the time taken to isomerize is very less (only ~20 min) for anthracene derivative in comparison to the others. In the emission side, all the three complexes undergo a single step change wherein the intensity of the emission peak gradually decreases for **1** and **3** while it increases for **2**, accompanied with a minor blue-shift in case of **3**. In line with the steady state spectra, change in lifetime is also noticed wherein the value decreases slightly for **1**, while increases for both **2** and **3** (inset to Figure 6.12). Thus, the observed change in the spectral profiles may be attributed to transformation of either one or both stilbene units from the *t-t* to either their *t-c* or *c-c* forms. It is to be noted that the emission intensity gradually decreases in naphthalene (**1**) and pyrene (**3**) complexes, while increases for anthracene (**2**) derivative upon photo-isomerization. Additionally, the extent of change is more marked in case of **2** than that

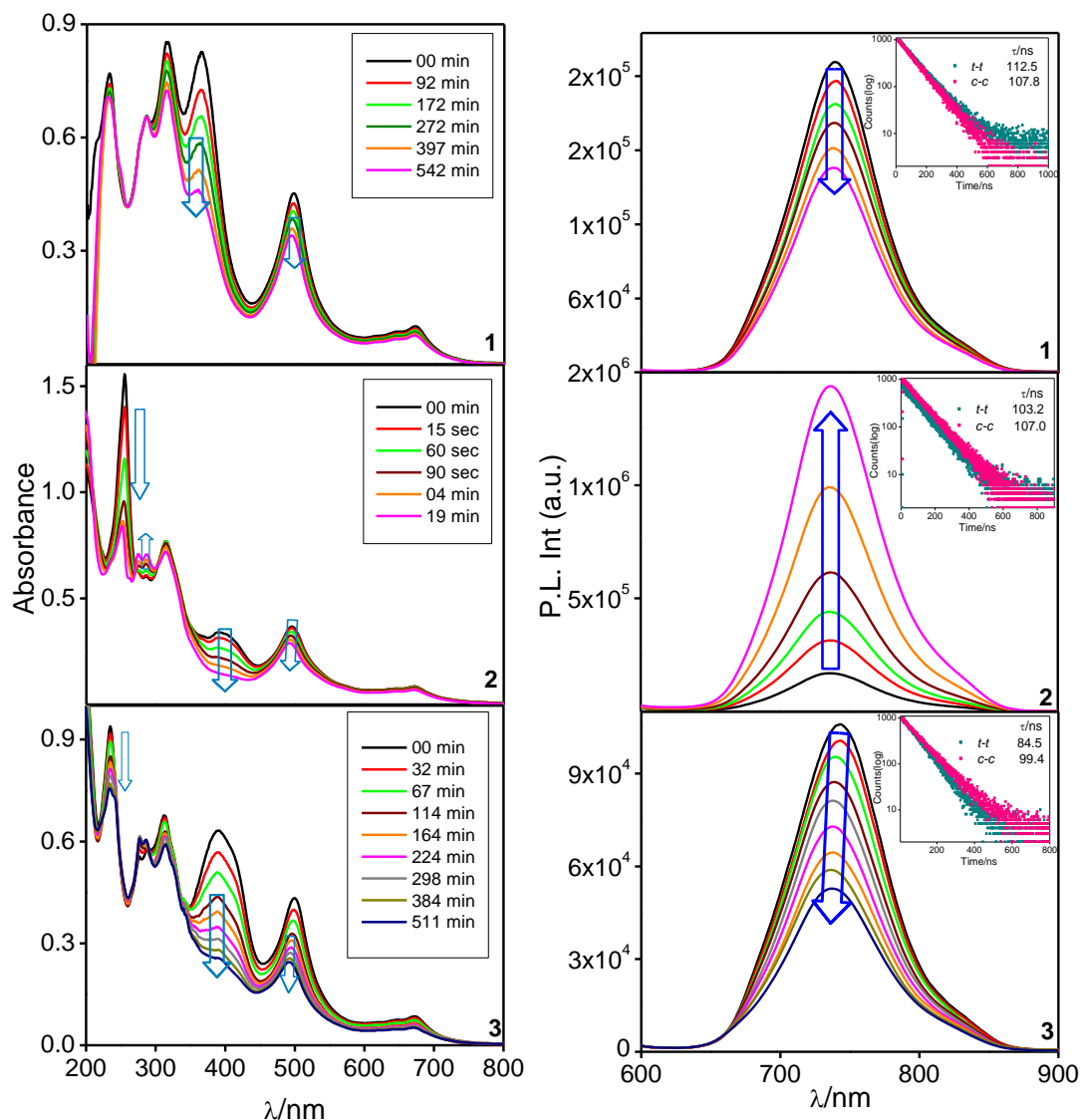


Figure 6.12. Absorption (left panel) and emission ($\lambda_{\text{ex}} = 490$ nm, right panel) spectral change of **1-3** in MeCN upon treatment with light of $\lambda = 500$ nm. Inset to figure in right panel shows the decay profiles of $t-t$ and $c-c$ forms along with their lifetime values.

of the rest two complexes. The observed difference in emission spectral behavior is not very clear to us. To gain some insight on the anomaly of the anthracene derivative, we have optimized the geometries of the $c-c$ form of all three complexes and the corresponding profiles are demonstrated in Figure 6.13. It is noticed that the optimized geometry of the naphthalene and pyrene derivatives is more or less similar and the polyaromatic moieties in both cases, adopt a *syn* orientation. On the other hand, in case of **2**, the anthracene moieties

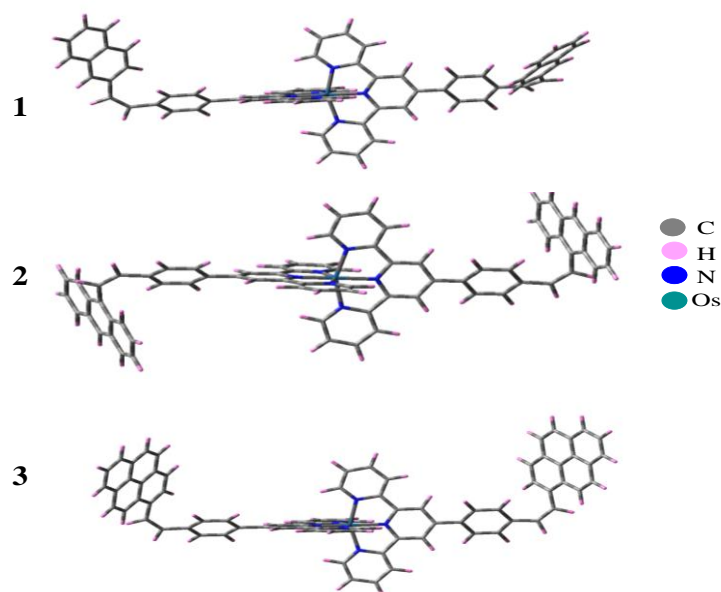


Figure 6.13. Optimized structures of *c-c* form of **1-3** in MeCN.

adopt an *anti*-orientation across the complex backbone. We surmise that deactivation of the excited state in the *c-c* form of complexes **1** and **3** occurs primarily due to deactivation of $^3\text{MLCT}$ state. By contrast, excited state deactivation probably takes place from the equilibrated $^3\text{MLCT}$ and $^3\pi\text{-}\pi^*$ states, which in turn is responsible for emission enhancement on passing from *t-t* to *c-c* form in the anthracene complex (**2**).

Isomerization process is also monitored via ^1H NMR spectroscopy to elucidate the mode of isomerization (Figure 6.14). The spectral pattern indicates that nearly all the protons within the molecular backbone experience some changes in their chemical environment. Overall up-field shift of the proton resonances is observed upon light irradiation for ~3 h. Notably, the protons associated to $\text{C}=\text{C}$ (H_9 and H_{10}) moiety undergoes a significant up-field shift. During the course of light irradiation, the H_9 and H_{10} proton appearing at $\delta = \sim 8.50$ and ~ 7.20 ppm respectively, show a decrease in their peak intensity along with simultaneous generation of two new doublets at 6.85 and 6.63 ppm, corroborating to H_9 and H_{10} , respectively. Coupling constant (J) of these protons (~ 16 Hz) gets significantly decreased to ~ 12 Hz. The singlet at H_3 converts to a multiplet along with generation of a new peak at 9.51 ppm (H_3^{m}). A new doublet also arises for H_3 , H_4 , H_6 , and H_7 protons, upon prolonged irradiation. The singlet associated with H_{15} proton exhibits significant reduction in intensity, concurrently with the emergence of a distinct singlet at 8.13 ppm. Likewise, the other protons also undergo an up-field shift along with change in multiplicity as shown in Figure 6.14. Even after prolonged irradiation for up to 10 h, complete conversion from the *t-t* to *c-c* forms

does not take place leading to the coexistence of both *t-t* and *c-c* forms in the photo-stationary state.

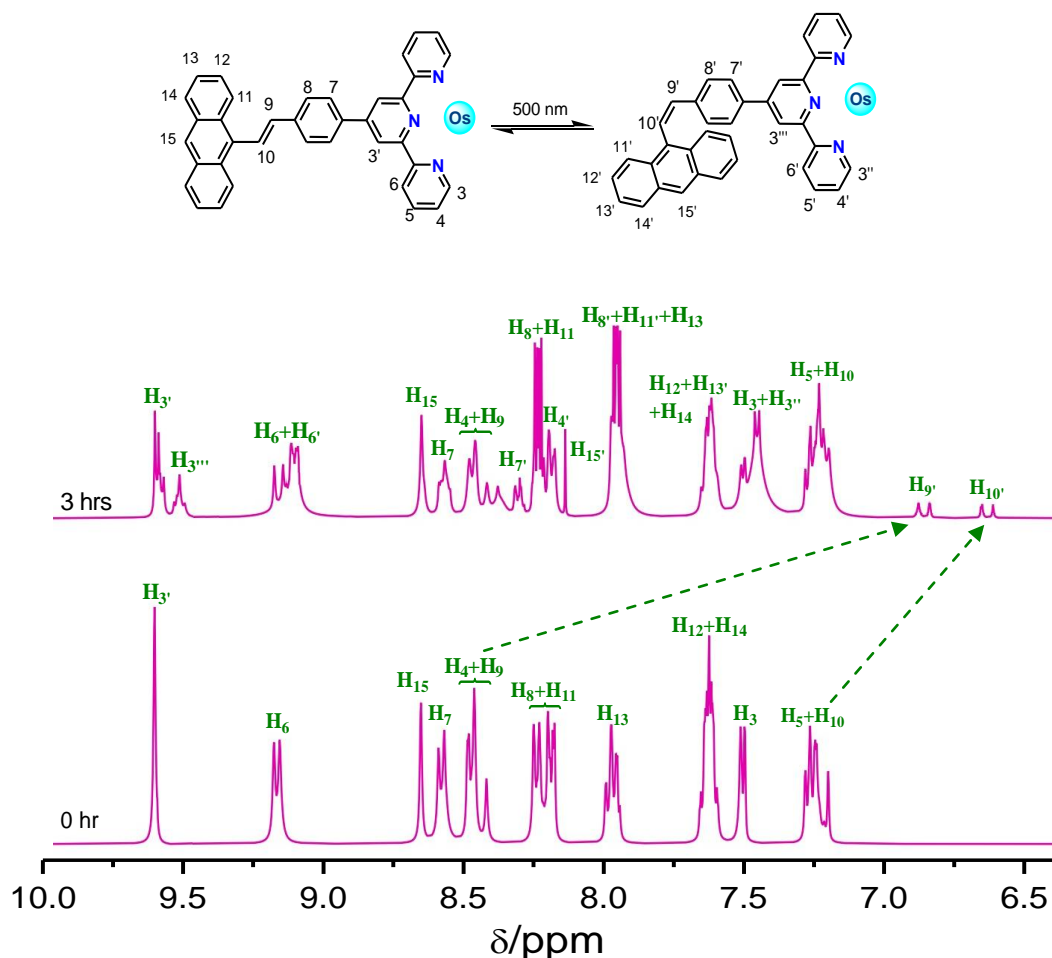


Figure 6.14. ^1H NMR spectrum of **2** in $\text{DMSO}-d_6$ before (a) and after (b) photolysis with visible light for 3 h.

To further validate our hypotheses, we conducted DFT and TD-DFT computations on both *t-c* and *c-c* forms of the complexes (Figure 6.15). The optimized structure of **1** together with their HOMO and LUMO orbitals is presented in Figure 6.16, while their structural compositions are showed in Table 6.1. The corresponding spectral parameters and band assignment are depicted in Table 6.3. From the DFT calculations, we see that a small hypsochromic shift in the MLCT band upon conversion from *t-t* to *c-c* form occurs which is in-line with our experimental spectra. Fascinatingly, the experimental absorption spectra obtained upon saturation, corroborates well with the *c-c* form obtained theoretically (Figure 6.15).

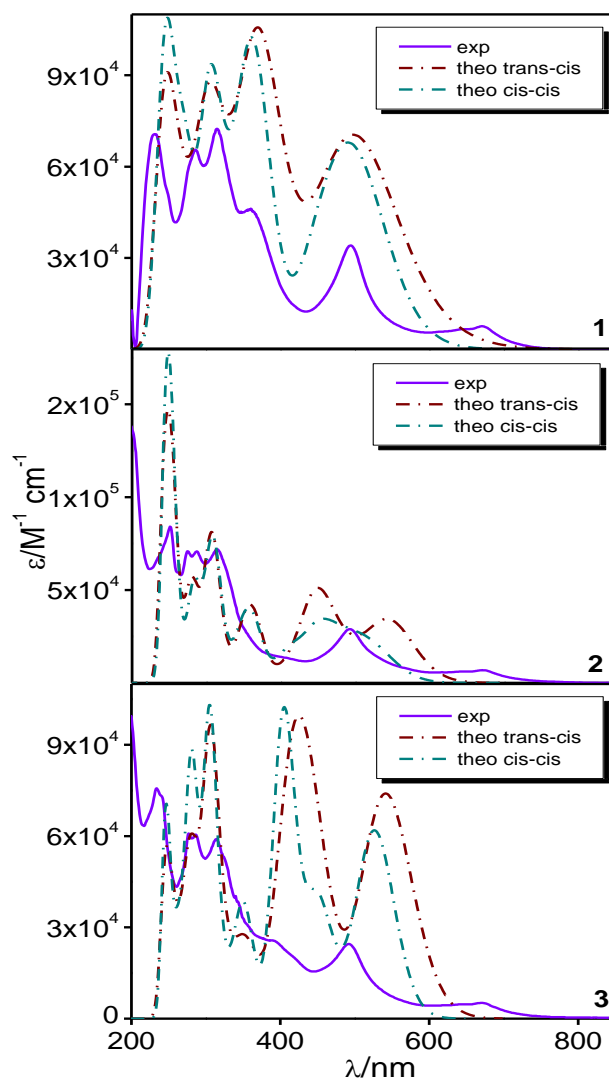


Figure 6.15. Overlay of the experimental *c-c* form (violet solid lines) with theoretical *t-c* (wine dotted line) and *c-c* (dark cyan dotted line) forms of **1-3** in MeCN.

The rate constants (k_{iso}) and quantum yields ($\Phi_{t \rightarrow cc}$) associated with the photoisomerization process are also determined using their absorption titration profiles. The corresponding data have been summarized in Table 6.6 and are graphically presented in Figure 6.17. The k_{iso} alters between 7.3×10^{-5} and $2.6 \times 10^{-3} \text{ s}^{-1}$, while $\Phi_{t \rightarrow cc}$ varies between 3.4×10^{-3} and 0.14. It is noteworthy that the rate constants vary in the order **2**>**3**>**1**, probably because of the difference in the electronic and steric environment induced by polyaromatic moiety across the stilbene bond in the complexes.

To check for the reversibility of the isomerization process, we irradiated the photolyzed solutions of the complexes with UV light of 270 nm and the progress of the

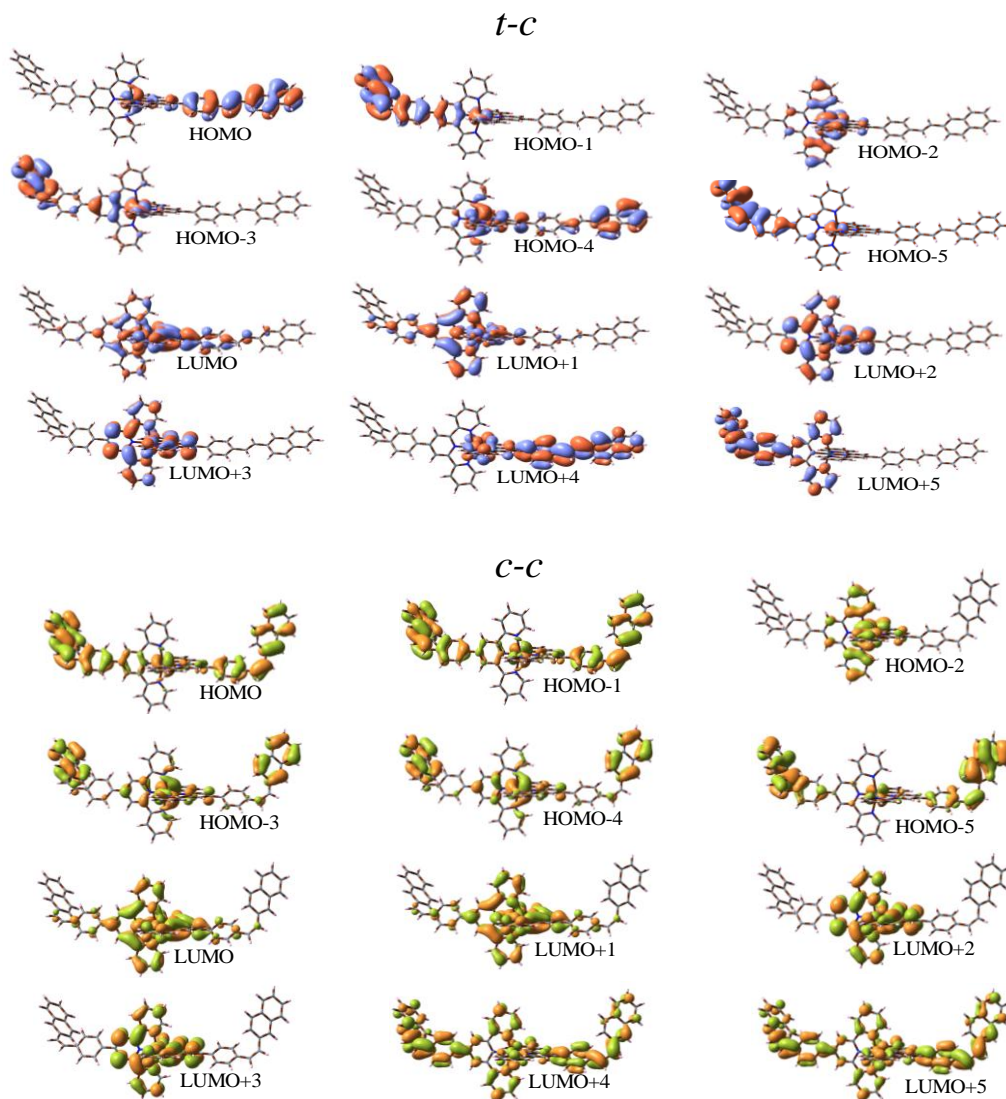


Figure 6.16. Schematic drawings of the selective frontier molecular orbitals of *t-c* and *c-c* forms of **1** in MeCN.

reaction is monitored through absorption and emission spectroscopy. It is evident that the spectra obtained upon prolonged UV irradiation almost revert back to their initial *t-t* forms. We also calculated the rate constant (k_{iso}) and quantum yield ($\Phi_{cc \rightarrow tt}$) of the reverse process and the corresponding data have been compiled in Table 6.6. The reverse *c-c* to *t-t* process is much slower as evident by their k_{iso} and $\Phi_{cc \rightarrow tt}$ values (k_{iso} varies in the domain of 3.6×10^{-5} - $1.2 \times 10^{-4} \text{ s}^{-1}$, while $\Phi_{cc \rightarrow tt}$ alters within the range of 2.3×10^{-5} - 9.1×10^{-3}).

Previously, we noticed emission quenching upon *t-t* \rightarrow *c-c* isomerization, the reason of which is not well understood. It is probable that upon going from *t-t* to *t-c* or *c-c* forms, a significant amount of strain is gradually imposed on the molecular backbone, which in turn may be

responsible for observed diminution in emission intensity. We also tried to visualize the probable mechanism of isomerization. It is known that for the Os-tpy complexes the lowest emitting excited state is $^3\text{MLCT}$ in nature. We surmise that photoisomerization occurs through the intermediary of closely lying $^3\text{LLCT}/^3\pi\text{-}\pi^*$ state, situated on the stilbene moiety, which in turn is in equilibrium with $^3\text{MLCT}$ state (Scheme 6.1).

Table 6.6. Quantum Yield and Rate Constants of Photoisomerization in **1-3**.

Method	Time (Minutes)			Rate constant ($k_{\text{iso}}/\text{s}^{-1}$)			Quantum yield (Φ)		
	1	2	3	1	2	3	1	2	3
Free form $t\text{-}t \rightarrow c\text{-}c$	542	19	511	7.3×10^{-5}	2.6×10^{-3}	1.1×10^{-4}	3.4×10^{-3}	0.14	4.3×10^{-3}
Reverse $c\text{-}c \rightarrow t\text{-}t$	790	210	970	6.2×10^{-5}	1.2×10^{-4}	3.6×10^{-5}	3.6×10^{-5}	9.1×10^{-3}	2.3×10^{-5}
CAN+hv	05	02	03	9.3×10^{-3}	4.5×10^{-2}	3.3×10^{-2}	0.43	0.62	0.57
Na+hv	25	14	20	2.7×10^{-3}	6.2×10^{-3}	4.6×10^{-3}	16.6×10^{-3}	15.6×10^{-2}	14.8×10^{-3}

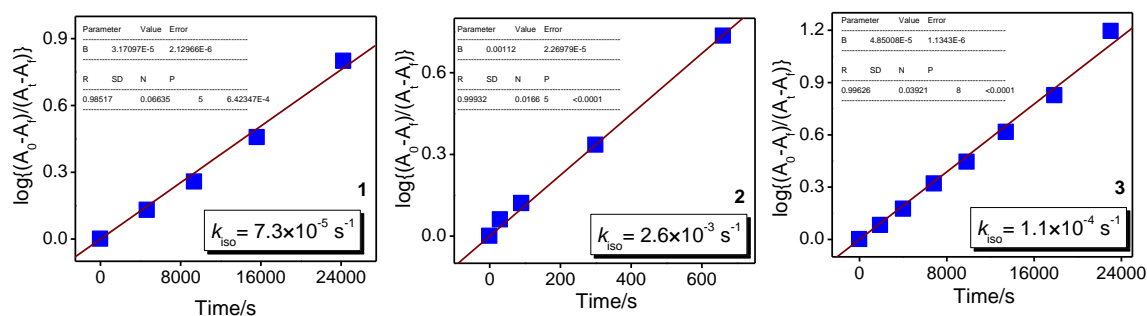
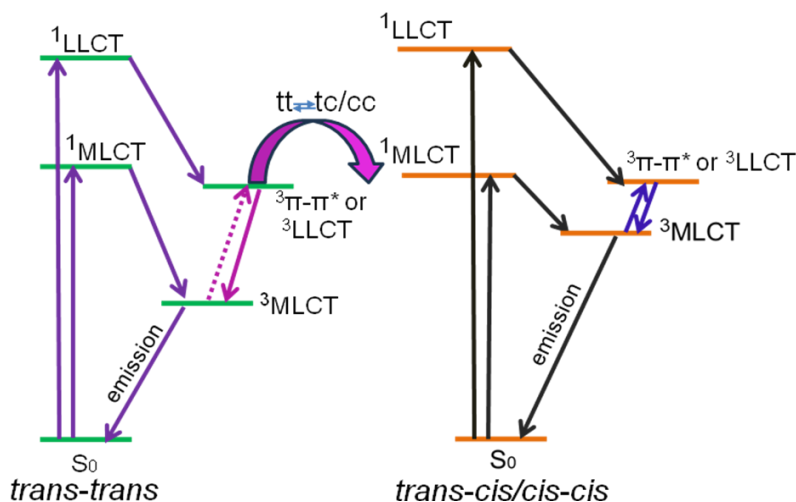


Figure 6.17. Linear plot of $\log(A_0 - A_f)/(A_t - A_f)$ vs. time (t) for the absorption spectral change due to $t\text{-}t \rightarrow c\text{-}c$ process of **1-3** MeCN upon irradiation with visible light of 500 nm. Inset to these plots give the values of rate constant of the forward photo-isomerization.



Scheme 6.1. Simplified Jablonski diagram depicting photoisomerization together with competing photophysical processes in **1-3**.

The photoisomerization behaviors of various 4d and 5d transition metal complexes, incorporating stilbene- and azo-appended polyheterocyclic complexes, are previously reported by different research groups, viz. Yam, Nishihara, Lees, and Iha, to name a few.^{41-52,113-120} Although extensive study has been conducted on the stilbene- and azo-appended bipyridine systems, especially in combination with Re and Ir carbonyl complexes, analogous reports based on stilbene-appended terpyridine systems are relatively sparse in the literature. Representative examples of the complexes exhibiting photo-induced *trans-cis* isomerization are already listed in Chapter 1. We previously reported photoisomerization behaviors of a new array of homo- and heteroleptic Ru(II) complexes based on stilbene-appended terpyridine ligands coupled with both electron donating and electron-withdrawing substituents (H, CH₃, Ph, Cl and NO₂)^{54,112} as well as polyaromatic (naphthalene, anthracene and pyrene) hydrocarbon^{53,55} unit at the 4'-position of the tpy moiety to modulate their optical behaviors as well as the rate of isomerization. Thereafter, we reported isomerization properties of analogous Os(II) complexes based on the said electron releasing and electron-withdrawing groups⁵⁶ to extend the optical and emission spectral window to the NIR domain. In the present work, we designed a new array of Os(II)-terpyridine complexes comprising of stilbene-appended naphthalene, anthracene, and pyrene motifs to enhance their emission spectral characteristics in the NIR domain as well as to induce fast and efficient multi-state photo-switching through reversible *trans-cis* photoisomerization under the influence of chemical oxidant (CAN) and reductant (Na).

6.3.8 Enhancement of Photoisomerization Rate via Chemical Oxidation and Reduction. Since the rate of isomerization of the complexes is extremely slow, we are now interested to tune their rate and quantum yield to make the complexes useful for practical applications. Following our previously adopted protocol,⁹⁹ we executed herein the photoisomerization studies of the complexes in their oxidized as well as reduced forms. We have employed ceric ammonium nitrate (CAN) for oxidation, while metallic sodium for the reduction of the complexes. Both the oxidation and reduction of the complexes are monitored through absorption and emission spectroscopy.

The oxidation of the complexes in MeCN via CAN is presented in Figure 6.18. Upon gradual addition of CAN, the ¹MLCT band at ~500 nm gradually diminishes in intensity along with a small increase in absorbance of the π - π^* band. The decrease in 500 nm band is also accompanied with evolution of a broad band in the longer wavelength region of ~750-1100 nm for all three complexes. This longer wavelength band is found to be most prominent for **1** and least for **3** and could be assigned as terpyridine to Os³⁺ charge transfer (LMCT)

transition. All the absorption spectral lines pass through clean isosbestic points, indicating that two species are in equilibrium with one another. Almost complete quenching of luminescence take place for all three complexes upon oxidation, which can be attributed to the electron transfer from the terpyridine-type motif(s) to the excited luminophore. Thus, by the use of CAN, the *t-t* form of the complexes in their Os^{II} oxidation states converted to the respective *t-t* forms in Os^{III} states.

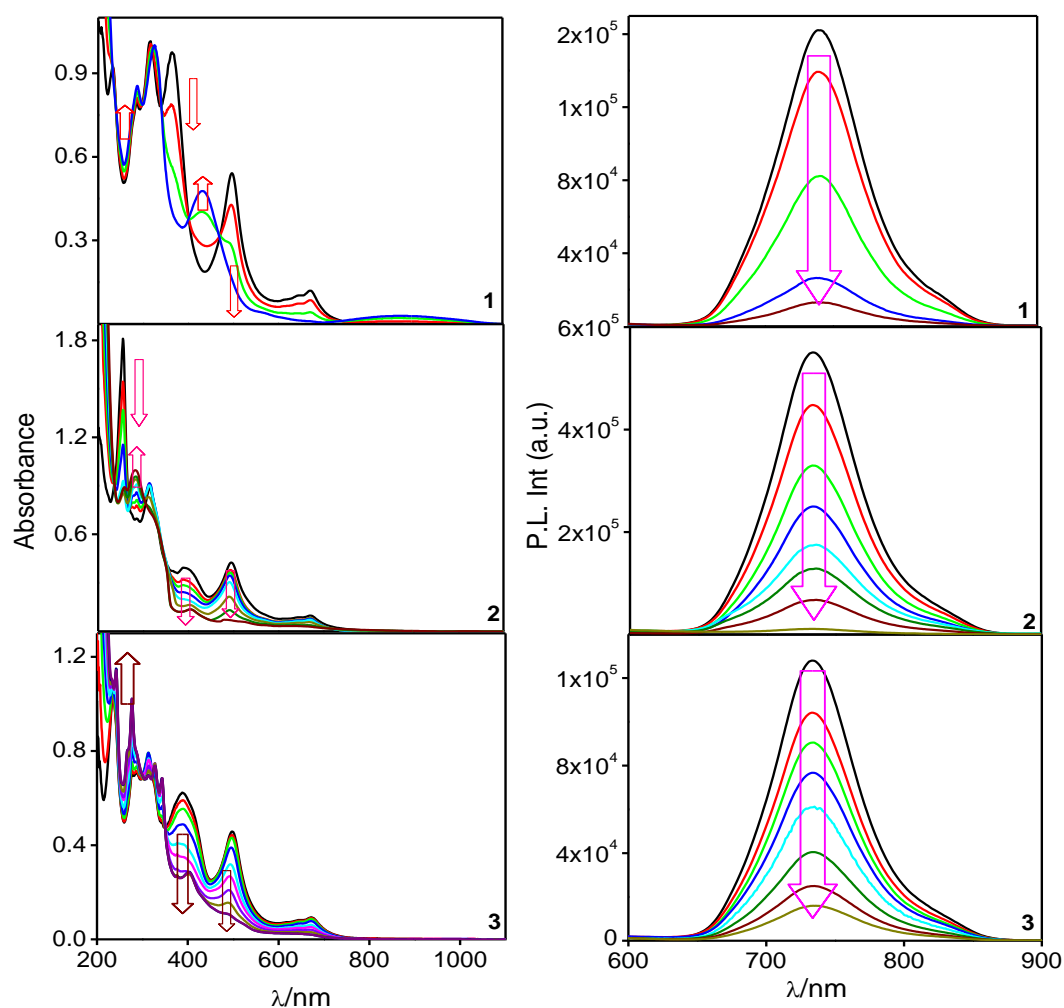


Figure 6.18. Absorption (left) and emission (right, $\lambda_{\text{ex}}=490$ nm) spectral changes of **1-3** in MeCN upon treating with CAN.

We are now interested to examine the photo-isomerization behaviors of the oxidized form of the complexes. To this end, the CAN saturated solutions are irradiated with visible light (500 nm) and the changes are again monitored via absorption and emission spectroscopy. Associated spectral changes are displayed in Figure 6.19. A single step change

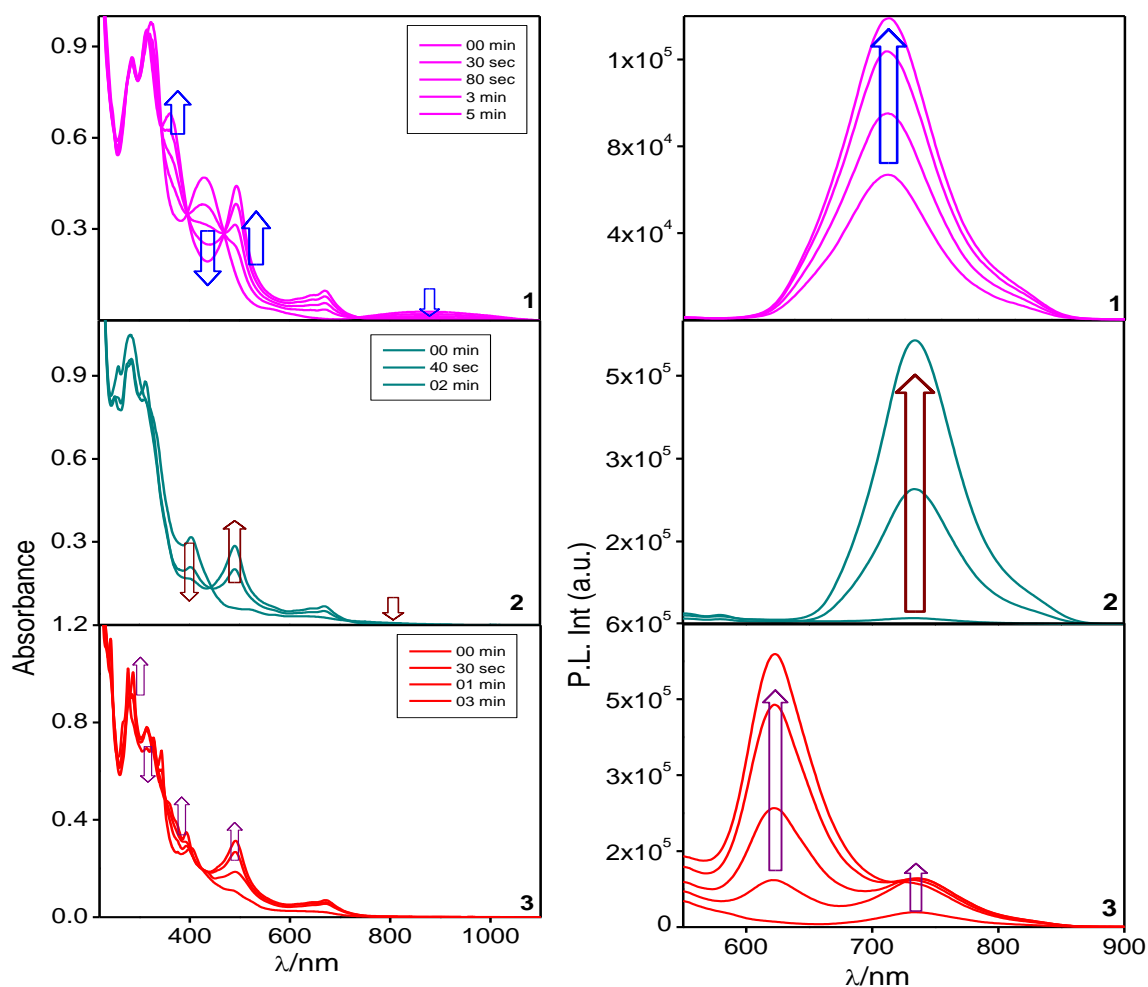


Figure 6.19. Change in absorption (left) and emission (right, $\lambda_{\text{ex}} = 490$ nm) spectra of CAN-treated MeCN solutions of **1**, **2** and **3** upon irradiating with visible light (500 nm).

is noticed in all three cases. Upon shining light on the oxidized form of the complexes, it is observed that the MLCT band regains its intensity together with a decrease in the absorbance of ILCT band (Figure 6.19). All the spectral lines pass through multiple clean isosbestic points, indicating that the species are in equilibrium. Upon saturation, the final spectrum closely resembles the spectrum obtained upon photolysis of the respective complex in absence of CAN and also aligns well with the calculated spectrum of the *c-c* form of the complexes. It is quite remarkable to note that saturation takes place at 2 min for **2**, 3 min for **3**, and 5 min for **1**, which are far less compared to the time required for conversion from *t-t* to the respective *c-c* state of the complexes in absence of CAN (19 min for **2**, 511 min for **3**, and 542 min for **1**). Steady increase in emission intensity takes place upon irradiation on the oxidized solutions of the complexes and eventually gets saturated. In case of **3**, an additional

new band at 622 nm is found to be generated upon light irradiation and ultimately saturates after ~ 3 min. The rate constant (k_{iso}) and quantum yields ($\Phi_{t \rightarrow cc}$) of isomerization for the oxidized form of the complexes are calculated (Figure 6.20) and tabulated in Table 6.6. k_{iso} varies in the domain of $0.93\text{--}4.5 \times 10^{-2} \text{ s}^{-1}$ and $\Phi_{t \rightarrow cc}$ ranges within 0.43–0.62 under visible light.

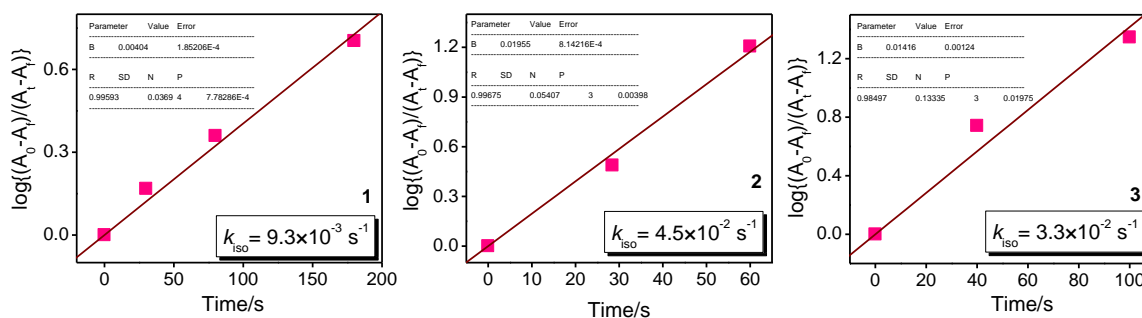


Figure 6.20. Linear plot of $\log(A_0 - A_f)/(A_t - A_f)$ vs. time (t) for the absorption spectral change due to $t \rightarrow c$ process of **1–3** upon irradiation of the CAN treated solutions with visible light of 500 nm. Inset to these plots give the values of rate constant.

From the above changes in the absorption and emission spectral profiles, it seems that light irradiation onto the oxidized form of the complexes leads to photo-excitation of Ce(III) to Ce(III)*, which in-turn leads to facile reduction of Os(III) to Os(II) together with isomerization from $t \rightarrow c$ forms and itself being oxidized to initial Ce(IV) state. The above observations along with their k_{iso} values make it evident that the oxidized forms of the complexes undergo remarkably faster photoisomerization. Moreover, no signature of re-oxidation of the Os(II) center is observed even after being left for several hours. Following oxidation, the Os center become electron deficient which in turn drag the electron density across the C=C bond and impart more single-bond character. As a result, light irradiation facilitates easy and fast rotation across the phenylene-vinylene motif in the oxidized forms of the complexes, which in turn is also reflected in the profoundly accelerated rate of the $t \rightarrow c$ isomerization process (Table 6.6). Essentially, the photoisomerization of the complexes from their $t \rightarrow c$ forms proceeds through a three-state switching process as depicted in Scheme 6.2.

The significant acceleration in the rate of photoisomerization, achieved through chemical oxidation, motivates us to investigate the isomerization behavior of the complexes in their reduced states. For this purpose, we used metallic Na dissolved in MeCN as the reducing agent and the reduction process of the complexes are monitored through absorption

and emission spectroscopy (Figure 6.21). Gradual addition of the said Na source to the complex solutions results in remarkable enhancement in the absorbance of π - π^* band within the spectral domain of ~ 200 - 300 nm, while the MLCT or ILCT band intensity remains almost unaltered. This suggests that the electron donated by Na primarily occupies the ligand-based π^* orbitals situated in the higher-energy region. In the emission side, within the spectral range of 430 - 650 nm, an increase in emission intensity is observed for **1** and **2** (probably due to radiative deactivation of $^3\text{ILCT}$ and/or $^3\pi$ - π^* state) while it decreases for **3**, keeping the band intensity at 740 nm almost unaltered, although the exact reason is not very clear to us.

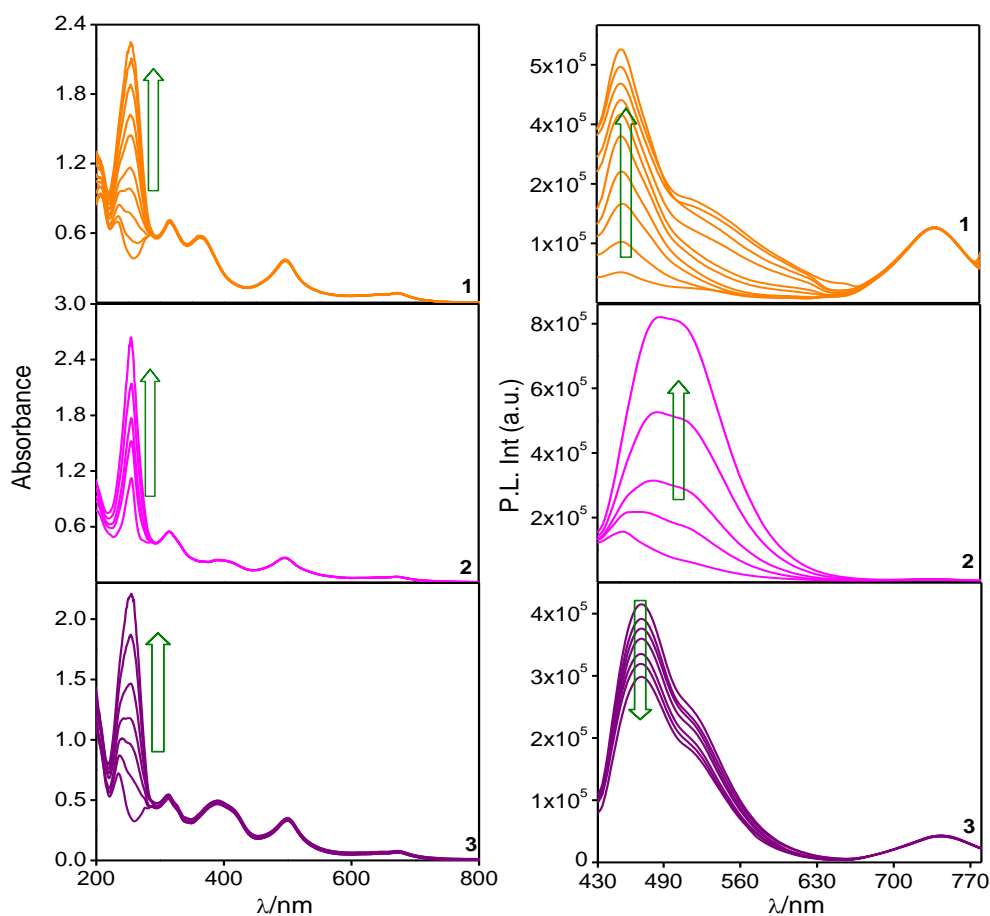


Figure 6.21. Absorption (left) and emission ($\lambda_{\text{ex}} = 400$ nm, right) spectral changes of **1-3** upon gradual addition of Na in MeCN.

Now, the reduced form of the complexes is again irradiated with light (500 nm), and the resulting changes are monitored spectroscopically (Figure 6.22). Significant diminution in the intensity of π - π^* absorptions takes place in all three cases. Additionally, for **2** and **3**, the intensities of both the MLCT and ILCT bands diminish simultaneously together with a small

blue shift in the MLCT band. The time required to reach the photostationary state lies within 14-25 min, which is again remarkably less than the time required for isomerization in their free forms, but comparatively greater than that of the oxidized forms. A similar one-step change is also noticed in case of emission spectra for complexes **1-3**. In this case, the intense emission band within the spectral domain of 430-650 nm gradually decreases for **1** and **2** while it increases for **3**. In addition to decrease in band intensity at ~ 495 nm, complex **2** exhibits a small increase in emission at ~ 740 nm, probably originated from $^3\text{MLCT}$ state.

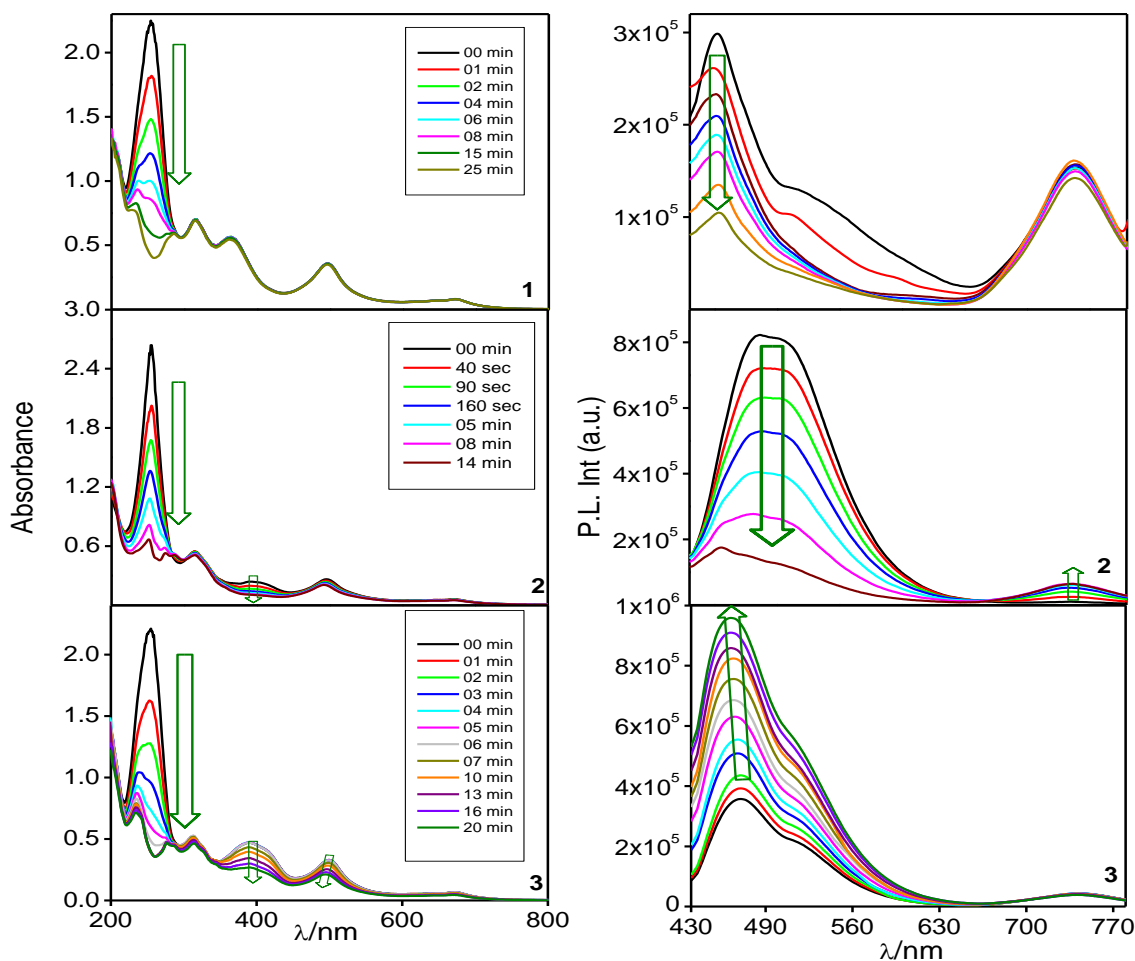


Figure 6.22. Absorption (left) and emission ($\lambda_{\text{ex}} = 400$ nm, right) spectral changes upon irradiation of Na saturated solution of **1-3** in MeCN.

Detailed analysis reveals that the spectrum obtained after photolysis of the sodium-treated solution of the complex also closely resembles the *c-c* form of the Os(II) monomers, particularly in the absorption spectral profile. This suggests that, upon irradiation, the reduced form likely reverts to its original state together with isomerization from *t-t* to the *c-c* configuration. The rate constants (k_{iso}) and quantum yields ($\Phi_{t \rightarrow c}$) are also calculated,

revealing that the isomerization process occurs significantly faster in the reduced state of the complexes compared to their non-reduced forms (Figure 6.23). Reduction lowers the overall charge in the complexes which ultimately reduces their solvation in polar solvent like MeCN. This in turn shrinks the effective rotor volume of the complexes, thereby facilitating the movement of groups across the double bond and increasing the rate of isomerization. Upon comparison of the rate of photoisomerization in three forms viz. free-, oxidized- and reduced state, it is observed that the k_{iso} value is highest for the oxidized form and lowest for their free forms. Thus, substantial alteration in the kinetics of photoisomerization process is achieved through oxidation and reduction of the complexes. Out of the three complexes, the anthracene derivative is seen to undergo comparatively faster photo-induced isomerization than the

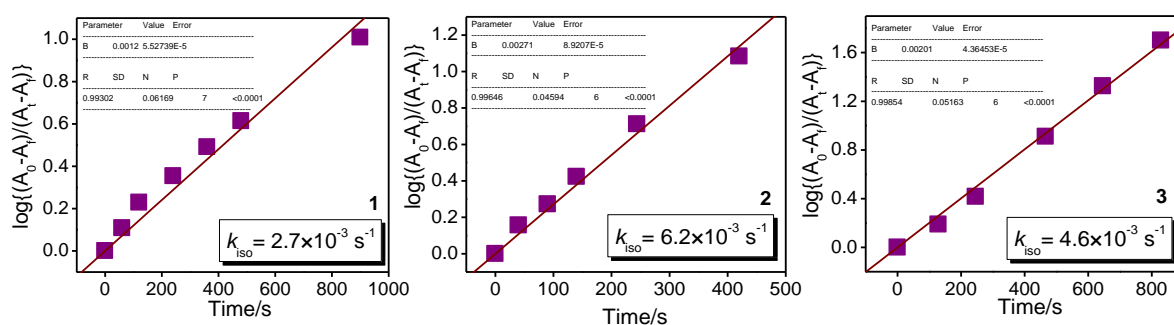
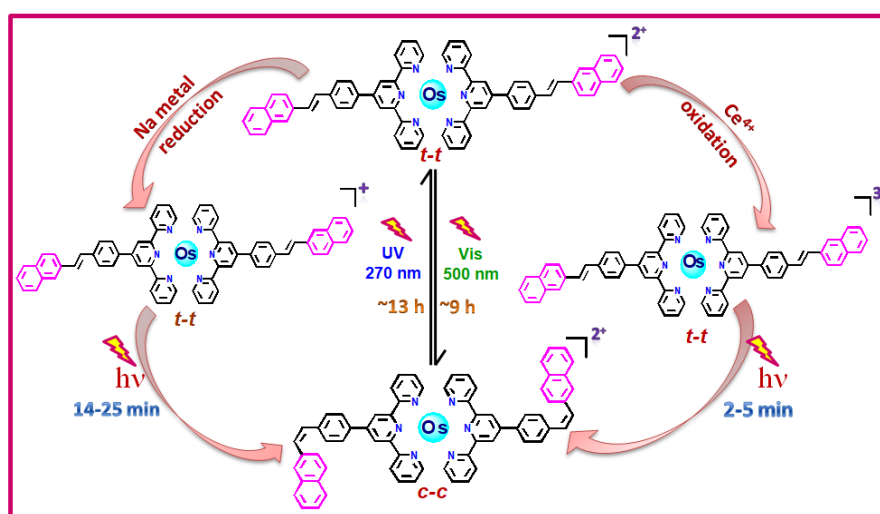


Figure 6.23. Linear plot of $\log(A_0 - A_f)/(A_t - A_f)$ vs. time (t) for the absorption spectral change due to $t \rightarrow c$ process of **1-3** upon irradiation of the Na treated solutions with visible light of 500 nm. Inset to these plots give the values of rate constant.



Scheme 6.2. Multistep switching via oxidation-reduction and reversible $t \rightleftharpoons c$ isomerization.

naphthalene and pyrene derivatives. Most interestingly, the photoisomerization of the complexes from their *t-t* to *c-c* forms proceeds through a three-state switching involving an oxidized or reduced form of the complex, which notably accelerates the entire process (Scheme 6.2). Thus, the present complexes can act as ultrafast and efficient ‘on-off’ multi-state emission switches that function in the NIR domain in presence of a chemical oxidant/reductant and light.

6.4 Conclusions

A new family of luminescent homoleptic Os(II)-terpyridine complexes comprising of stilbene-appended naphthalene, anthracene, and pyrene motifs are designed, thoroughly characterized and detailed experimental and theoretical investigation on their photophysical, electrochemical, and photoisomerization behaviors have been made. All complexes are moderately emissive in the NIR region with elevated lifetimes at RT. The stilbene motifs facilitate reversible trans-trans to cis-cis photoisomerization under alternative treatment with visible and UV light, enabling the complexes to function as photo-molecular switches in the near-infrared domain. Interestingly, remarkable increase in the rate of photo-isomerization has been achieved via oxidation of the complexes by ceric ammonium nitrate (CAN) as well as upon reduction with metallic Na. Notably, the rate constant becomes ~2 orders of magnitude higher relative to their free form. In essence, prompt and efficient multi-state ‘on-off’ photo-switching can be achieved in the NIR domain upon utilization of both chemical oxidant and reductant under the influence of light. Thus, the complexes could be promising building blocks for the fabrication of potential photochemical molecular devices.

6.5 References

- (1) Valeur, B. *Molecular Fluorescence: Principles and Applications*; Wiley, **2002**.
- (2) Michalet, X.; Pinaud, F. F.; Bentolila, L. A.; Tsay, J. M.; Doose, S.; Li, J. J.; Sundaresan, G.; Wu, A. M.; Gambhir, S. S.; Weiss, S. Quantum Dots for Live Cells, in Vivo Imaging, and Diagnostics. *Science*. **2005**, *307*, 538-44.
- (3) Mullen, K.; Scherf, U. *Organic Light Emitting Devices-Synthesis, Properties and Applications*; Wiley, **2006**.
- (4) Liu, H. Y.; Wu, P. J.; Kuo, S. Y.; Chen, C. P.; Chang, E. H.; Wu, C. Y.; Chan, Y. H. Quinoxaline-Based Polymer Dots with Ultrabright Red to Near-Infrared Fluorescence for In Vivo Biological Imaging. *J. Am. Chem. Soc.* **2015**, *137*, 10420-10429.
- (5) Yao, C.-J.; Zhong, Y.-W.; Nie, H.-J.; Abruña, H. D.; Yao, J. Near-IR Electrochromism in Electropolymerized Films of a Biscyclometalated Ruthenium Complex Bridged by 1,2,4,5-Tetra(2-pyridyl)benzene. *J. Am. Chem. Soc.* **2011**, *133*, 20720-20723.
- (6) Wang, H.; Shao, J.-Y.; Duan, R.; Wang, K.-Z. Zhong, Y.-W. Synthesis and Electronic Coupling Studies of Cyclometalated Diruthenium Complexes Bridged by 3,3',5,5'-Tetrakis(benzimidazol-2-yl)-Biphenyl. *Dalton Trans.* **2021**, *50*, 4219-4230.
- (7) Shao, J.-Y.; Yang, W.-W.; Yao, J.; Zhong, Y.-W. Biscyclometalated Ruthenium Complexes Bridged by 3,3',5,5'-Tetrakis(N-methylbenzimidazol-2-yl)biphenyl: Synthesis and Spectroscopic and Electronic Coupling Studies. *Inorg. Chem.* **2012**, *51*, 4343-4351.
- (8) Amiot, C. L.; Xu, S. P.; Liang, S.; Pan, L. Y.; Zhao, J. X. J. Fluorescent Analogs of Biomolecular Building Blocks: Design and Applications. *Sensors*. **2008**, *8*, 3082-3105.
- (9) Sargent, E. H. Infrared Photovoltaics Made by Solution Processing. *Nat. Photonics*. **2009**, *3*, 325-331.
- (10) Luo, S. L.; Zhang, E. L.; Su, Y. Q.; Cheng, T. M.; Shi, C. M. A Review of NIR Dyes in Cancer Targeting and Imaging. *Biomater. Res.* **2011**, *32*, 7127-7138.
- (11) Bulach, V.; Sguerra, F.; Hosseini, M. W. Porphyrin Lanthanide Complexes for NIR Emission. *Coord. Chem. Rev.* **2012**, *256*, 1468-1478.
- (12) Müller, B. J.; Borisov, S. M.; Klimant, I. Red- to NIR-Emitting, BODIPY-Based, K⁺-Selective Fluoroionophores and Sensing Materials. *Adv. Funct. Mater.* **2016**, *26*, 7697-7707.

- (13) Luo, S. L.; Zhang, E. L.; Su, Y. Q.; Cheng, T. M.; Shi, C. M. A Review of NIR Dyes in Cancer Targeting and Imaging. *Biomaterials*. **2011**, *32*, 7127-7138.
- (14) Kiyose, K.; Kojima, H.; Nagano, T. Functional Near-Infrared Fluorescent Probes. *Chem. Asian J.* **2008**, *3*, 506-515.
- (15) Hilderbrand, S. A.; Weissleder, R. Near-Infrared Fluorescence: Application to In Vivo Molecular Imaging. *Curr. Opin. Chem. Biol.* **2010**, *14*, 71-79.
- (16) Qian, G.; Wang, Z. Y. Near-Infrared Organic Compounds and Emerging Applications. *Chem. Asian J.* **2010**, *5*, 1006-1029.
- (17) Zhuo, M. P.; Wang, X. D.; Liao, L. S. Recent Progress of Novel Organic Near-Infrared-Emitting Materials. *Small Sci.* **2022**, *2*, 2200029.
- (18) Zampetti, A.; Minotto, A.; Cacialli, F. Near-Infrared (NIR) Organic Light-Emitting Diodes (OLEDs): Challenges and Opportunities. *Adv. Funct. Mater.* **2019**, *29*, 1807623.
- (19) Li, H.; Kim, Y.; Jung, H.; Hyun, J. Y.; Shin, I. Near-Infrared (NIR) Fluorescence-Emitting Small Organic Molecules for Cancer Imaging and Therapy. *Chem. Soc. Rev.* **2022**, *51*, 8957-9008.
- (20) Otto, S.; Grabolle, M.; Forster, C.; Kreitner, C.; Resch-Genger, U.; Heinze, K. $[\text{Cr}(\text{ddpd})_2]^{3+}$: A Molecular, Water-Soluble, Highly NIR-Emissive Ruby Analogue. *Angew. Chem., Int. Ed.* **2015**, *54*, 11572-11576.
- (21) Sinha, N.; Jiménez, J.; Pfund, B.; Prescimone, A.; Piguet, C.; Wenger, O. S. A Near-Infrared-II Emissive Chromium(III) Complex. *Angew. Chem., Int. Ed.* **2021**, *133*, 23722-23728.
- (22) Hua, L.; Zhang, K. Y.; Liu, H.-W.; Chan, K.-S.; Lo, K. K.-W. Luminescent Iridium(III) Porphyrin Complexes as Near-Infrared-Emissive Biological Probes. *Dalton Trans.* **2023**, *52*, 12444-12453.
- (23) Bar, M.; Maity, D.; Deb, S.; Das, S.; Baitalik, S. Ru-Os Dyads Based on a Mixed Bipyridine-Terpyridine Bridging Ligand: Modulation of the Rate of Energy Transfer and pH-Induced Luminescence Switching in the Infrared Domain. *Dalton Trans.* **2017**, *46*, 12950-12963.
- (24) Mardanya, S.; Karmakar, S.; Mondal, D.; Baitalik, S. Homo- and Heterobimetallic Ruthenium(II) and Osmium(II) Complexes Based on a Pyrene-Biimidazolate Spacer as Efficient DNA-Binding Probes in the Near-Infrared Domain. *Inorg. Chem.* **2016**, *55*, 3475-3489.

- (25) Chen, C. Y.; Wu, S. J.; Wu, C. G.; Chen, J. G.; Ho, K. C. A Ruthenium Complex with Superhigh Light-Harvesting Capacity for Dye Sensitized Solar Cells. *Angew. Chem. Int. Ed.* **2006**, *118*, 5954-5957.
- (26) Li, J. Y.; Lee, C.; Chen, C. Y.; Lee, W. L.; Ma, R.; Wu, C. G. Diastereoisomers of Ruthenium Dyes with Unsymmetric Ligands for DSC: Fundamental Chemistry and Photovoltaic Performance. *Inorg. Chem.* **2015**, *54*, 10483-10489.
- (27) Chen, C. Y.; Chen, J. G.; Wu, S. J.; Li, J. Y.; Wu, C. G.; Ho, K. C. Multifunctionalized Ruthenium-Based Supersensitizers for Highly Efficient Dye-Sensitized Solar Cells. *Angew. Chem. Int. Ed.* **2008**, *47*, 7342-7345.
- (28) Chen, C. Y.; Wang, M.; Li, J. Y.; Pootrakulchote, N.; Alibabaei, L.; Ngoc-le, C. H.; Decoppet, J. D.; Tsai, J. H.; Grätzel, C.; Wu, C. G. Highly Efficient Light-Harvesting Ruthenium Sensitizer for Thin-Film Dye-Sensitized Solar Cells. *ACS Nano*. **2009**, *3*, 3103-3109.
- (29) Argazzi, R.; Larramona, G.; Contado, C.; Bignozzi, C. A. Preparation and Photoelectrochemical Characterization of a Red Sensitive Osmium Complex Containing 4,4',4''-Tricarboxy-2,2':6',2'' Terpyridine and Cyanide Ligands. *J. Photochem. Photobiol. A*. **2004**, *164*, 15-21.
- (30) Altobello, S.; Argazzi, R.; Caramori, S.; Contado, C.; Fre, S.; Rubino, P.; Chone, C.; Larramona, G.; Bignozzi, C. A. Sensitization of Nanocrystalline TiO with Black Absorbers Based on Os and Ru Polypyridine Complexes. *J. Am. Chem. Soc.* **2005**, *127*, 15342-15343.
- (31) Wu, K. L.; Ho, S. T.; Chou, C. C.; Chang, Y. C.; Pan, H. A.; Chi, Y.; Chou, P. T. Engineering of Osmium(II)-Based Light Absorbers for Dye-Sensitized Solar Cells. *Angew. Chem. Int. Ed.* **2012**, *23*, 5642-5646.
- (32) Ronca, E.; Angelis, F.; Fantacci, S. Time-Dependent Density Functional Theory Modeling of Spin-Orbit Coupling in Ruthenium and Osmium Solar Cell Sensitizers. *J. Phys. Chem. C*. **2014**, *118*, 17067-17078.
- (33) Fantacci, S.; Ronca, E.; Angelis, F. Impact of Spin-Orbit Coupling on Photocurrent Generation in Ruthenium Dye-Sensitized Solar Cells. *J. Phys. Chem. Lett.* **2014**, *5*, 375-380.
- (34) Juwita, R.; Liao, J. M.; Chen, C. Y.; Tsai, H. H. G. Enhancing Near-Infrared Absorption in Terpyridyl Ru/Os Complexes with Ancillary Ligands to Activate Spin-Forbidden Transitions in Dye-Sensitized Solar Cells: A TDDFT Investigation. *J. Phys. Chem. A*. **2024**, *128*, 880-894.

- (35) Kinoshita, T.; Fujisawa, J.; Nakazaki, J.; Uchida, S.; Kubo, T.; Segawa, H. Enhancement of Near-IR Photoelectric Conversion in Dye Sensitized Solar Cells Using an Osmium Sensitizer with Strong Spin Forbidden Transition. *J. Phys. Chem. Lett.* **2012**, *3*, 394-398.
- (36) Zhang, X.; Canton, S. E.; Smolentsev, G.; Wallentin, C. J.; Liu, Y.; Kong, Q.; Attenkofer, K.; Stickrath, A. B.; Mara, M. W.; Chen, L. X. Highly Accurate Excited-State Structure of $[\text{Os}(\text{bpy})_2\text{dcbpy}]^{2+}$ Determined by X-Ray Transient Absorption Spectroscopy. *J. Am. Chem. Soc.* **2014**, *136*, 8804-8809.
- (37) Li, J. Y.; Chen, C. Y.; Lee, C. P.; Chen, S. C.; Lin, T. H.; Tsai, H. H.; Ho, K. C.; Wu, C. G. Unsymmetrical Squaraines Incorporating the Thiophene Unit for Panchromatic Dye-Sensitized Solar Cells. *Org. Lett.* **2010**, *12*, 5454-5457.
- (38) Li, J. Y.; Chen, C. Y.; Ho, W. C.; Chen, S. H.; Wu, C.-G. Unsymmetrical Squaraines Incorporating Quinoline for Near Infrared Responsive Dye-Sensitized Solar Cells. *Org. Lett.* **2012**, *14*, 5420-5423.
- (39) Qin, C.; Numata, Y.; Zhang, S.; Yang, X.; Islam, A.; Zhang, K.; Chen, H.; Han, L. Novel Near-Infrared Squaraine Sensitizers for Stable and Efficient Dye-Sensitized Solar Cells. *Adv. Funct. Mater.* **2014**, *24*, 3059-3066.
- (40) Tsai, H. H. G.; Tan, C. J.; Tseng, W. H. Electron Transfer of Squaraine-Derived Dyes Adsorbed on TiO_2 Clusters in Dye-Sensitized Solar Cells: A Density Functional Theory Investigation. *J. Phys. Chem. C* **2015**, *119*, 4431-4443.
- (41) Polo, A. S.; Itokazu, M. K.; Frin, K. M.; Patrocínio, A. O. T.; Iha, N. Y. M. Light Driven Trans-to-Cis Isomerization of Stilbene-Like Ligands in $\text{fac-}[\text{Re}(\text{CO})_3(\text{NN}) (\text{Trans-L})]^+$ and Luminescence of their Photoproducts. *Coord. Chem. Rev.* **2006**, *250* (13- 14), 1669-1680.
- (42) Zanoni, K. P. S.; Iha, N. Y. M. Reversible $\text{Trans} \rightleftharpoons \text{Cis}$ Photoisomerizations of $[\text{Re}(\text{CO})_3(\text{Ph}_2\text{phen})(\text{StpyCN})]^+$ Towards Molecular Machines. *Dalton Trans.* **2017**, *46* (30), 9951-9958.
- (43) Matos, S.; Amaral, R. C.; Iha, N. Y. M. Visible Photosensitization of Trans-Styrylpyridine Coordinated to $\text{fac-}[\text{Re}(\text{CO})_3(\text{Dcbh}_2)]^+$: New Insights. *Inorg. Chem.* **2018**, *57* (15), 9316-9326.
- (44) Ko, C.-C.; Kwok, W.-M.; Yam, V. W.-W.; Phillips, D. L. Triplet MLCT Photosensitization of the Ring-Closing Reaction of Diarylethenes by Design and Synthesis of a Photochromic Rhenium(I) Complex of a Diarylethene-Containing 1,10-Phenanthroline Ligand. *Chem.-Eur. J.* **2006**, *12*, 5840-5848.

-
- (45) Li, Q., *Intelligent Stimuli-Responsive Materials*; Ed.; John Wiley & Sons, Inc.: Hoboken, NJ, **2013**.
- (46) Kobatake, S.; Takami, S.; Muto, H.; Ishikawa, T.; Irie, M. Rapid and Reversible Shape Changes of Molecular Crystals on Photoirradiation. *Nature*. **2007**, *446*, 778-781.
- (47) Irie, M.; Yokoyama, Y. Diarylethenes for Memories and Switches. *Chem. Rev.* **2000**, *100* (5), 1685-1716.
- (48) Irie, M.; Fukaminato, T.; Matsuda, K.; Kobatake, S. Photochromism of Diarylethene Molecules and Crystals: Memories, Switches, and Actuators. *Chem. Rev.* **2014**, *114*, 12174-12277.
- (49) Waldeck, G. H. Photoisomerization Dynamics of Stilbenes. *Chem. Rev.* **1991**, *91*, 415-436.
- (50) Cui, B. B.; Zhong, Y. W.; Yao, J. Three-State Near-Infrared Electrochromism at the Molecular Scale. *J. Am. Chem. Soc.* **2015**, *137*, 4058-4061.
- (51) Kume, S.; Nishihara, H. Photochrome-coupled Metal Complexes: Molecular Processing of Photon Stimuli. *Dalton Trans.* **2008**, 3260-3271.
- (52) Yutaka, T.; Mori, I.; Kurihara, M.; Mizutani, J.; Kubo, K.; Furusho, S.; Matsumura, K.; Tamai, N.; Nishihara, H. Synthesis, Characterization, and Photochemical Properties of Azobenzene-Conjugated Ru(II) and Rh(III) Bis(terpyridine) Complexes. *Inorg. Chem.* **2001**, *40*, 4986-4995.
- (53) Ganguly, T.; Pal, P.; Maity, D.; Baitalik, S. Synthesis, Characterization and Emission Switching Behaviors of Styrylphenyl-Conjugated Ru(II)-Terpyridine Complexes via Aggregation and Trans-Cis Photoisomerization. *J. Photochem. Photobiol. A.* **2023**, *440*, 114662.
- (54) Pal, P.; Mukherjee, S.; Maity, D.; Baitalik, S. Synthesis, Structural Characterization, and Luminescence Switching of Diarylethene-Conjugated Ru(II)-Terpyridine Complexes by Trans-Cis Photoisomerization: Experimental and DFT/TD-DFT Investigation. *Inorg. Chem.* **2018**, *57*, 5743-5753.
- (55) Ganguly, T.; Das, S.; Maity, D.; Baitalik, S. Luminescent Ruthenium–Terpyridine Complexes Coupled with Stilbene-Appended Naphthalene, Anthracene, and Pyrene Motifs Demonstrate Fluoride Ion Sensing and Reversible Trans-Cis Photoisomerization. *Inorg. Chem.* **2024**, *63*, 6883-6897.

- (56) Pal, P.; Ganguly, T.; Sahoo, A.; Baitalik, S. Emission Switching in the Near-Infrared by Reversible Trans-Cis Photoisomerization of Styrylbenzene-Conjugated Osmium Terpyridine Complexes. *Inorg. Chem.* **2021**, *60*, 4869-4882.
- (57) Yao, L.-Y.; Yam, V. W.-W. Photoinduced Isomerization-Driven Structural Transformation between Decanuclear and Octadecanuclear Gold(I) Sulfido Clusters. *J. Am. Chem. Soc.* **2015**, *137*, 3506-3509.
- (58) Kayanuma, M.; Gindensperger, E.; Daniel, C. Inorganic Photoisomerization: The Case Study of Rhenium(I) Complexes. *Dalton Trans.* **2012**, *41*, 13191-13203.
- (59) Costa, P. J.; Calhorda, M. J.; Bossert, J.; Daniel, C.; Romão, C. C. Photochemistry of Methyltrioxorhenium Revisited: A DFT/TD-DFT and CASSCF/MS-CASPT2 Theoretical Study. *Organometallics* **2006**, *25*, 5235-5241.
- (60) Martinic, I.; Eliseeva, S. V.; Nguyen, T. N.; Pecoraro, V. L.; Petoud, S. Near-Infrared Optical Imaging of Necrotic Cells by Photostable Lanthanide-Based Metallacrowns. *J. Am. Chem. Soc.* **2017**, *139*, 8388-8391.
- (61) Juris, A.; Balzani, V.; Barigelletti, F.; Campagna, S.; Belser, P.; von Zelewsky, A. Ru(II) Polypyridine Complexes: Photophysics, Photochemistry, Electrochemistry, and Chemiluminescence. *Coord. Chem. Rev.* **1988**, *84*, 85-277.
- (62) Balzani, V.; Juris, A.; Venturi, M.; Campagna, S.; Serroni, S. Luminescent and Redox-Active Polynuclear Transition Metal Complexes. *Chem. Rev.* **1996**, *96*, 759-834.
- (63) Passalacqua, R.; Loiseau, F.; Campagna, S.; Fang, Y.-Q.; Hanan, G. S. In Search of Ruthenium(II) Complexes Based on Tridentate Polypyridine Ligands that Feature Long-Lived Room-Temperature Luminescence: The Multichromophore Approach. *Angew. Chem. Int. Ed.* **2003**, *42*, 1608-1611.
- (64) Medlycott, E. A.; Hanan, G. S. Synthesis and Properties of Mono- and Oligo-Nuclear Ru(II) Complexes of Tridentate Ligands: The Quest for Long-Lived Excited States at Room Temperature. *Coord. Chem. Rev.* **2006**, *250*, 1763-1782.
- (65) Rupp, M. T.; Shevchenko, N.; Hanan, G. S.; Kurth, D. G. Enhancing the Photophysical Properties of Ru(II) Complexes by Specific Design of Tridentate Ligands. *Coord. Chem. Rev.* **2021**, *446*, 214127.
- (66) Dietrich, J.; Thorenz, U.; Förster, C.; Heinze, K. Effects of Sequence, Connectivity, and Counter Ions in New Amide-Linked Ru(tpy)₂-Re(bpy) Chromophores on Redox Chemistry and Photophysics. *Inorg. Chem.* **2013**, *52*, 1248-1264.

- (67) Kreitner, C.; Erdmann, E.; Seidel, W. W.; Heinze, K. Understanding the Excited State Behavior of Cyclometalated Bis(tridentate)ruthenium(II) Complexes: A Combined Experimental and Theoretical Study. *Inorg. Chem.* **2015**, *54*, 11088-11104.
- (68) Baitalik, S.; Wang, X.-Y.; Schmehl, R. H. A Trimetallic Mixed Ru(II)/Fe(II) Terpyridyl Complex with a Long-Lived Excited State in Solution at Room Temperature. *J. Am. Chem. Soc.* **2004**, *126*, 16304-16305.
- (69) Sauvage, J. P.; Collin, J. P.; Chambron, J. C.; Guillerez, S.; Coudret, C.; Balzani, V.; Barigelli, F.; De Cola, L.; Flamigni, L. Ruthenium(II) and Osmium(II) Bis(terpyridine) Complexes in Covalently-Linked Multicomponent Systems: Synthesis, Electrochemical Behavior, Absorption Spectra, and Photochemical and Photophysical Properties. *Chem. Rev.* **1994**, *94*, 993-1019.
- (70) Browne, W. R.; O'Boyle, N. M.; McGarvey, J. J.; Vos, J. G. Elucidating Excited State Electronic Structure and Intercomponent Interactions in Multicomponent and Supramolecular Systems. *Chem. Soc. Rev.* **2005**, *34*, 641-663.
- (71) Paul, A.; Ganguly, T.; Bar, M.; Baitalik, S.; Controlling the Direction of Intercomponent Energy Transfer by Appropriate Placement of Metals in Long-Lived Trinuclear Complexes of Fe(II), Ru(II), and Os(II). *Inorg. Chem.* **2021**, *60*, 412-422.
- (72) Deb, S.; Sahoo, A.; Pal, P.; Baitalik, S. Exploitation of the Second Coordination Sphere to Promote Significant Increase of Room-Temperature Luminescence Lifetime and Anion Sensing in Ruthenium-Terpyridine Complexes. *Inorg. Chem.* **2021**, *60*, 6836-6851.
- (73) Mondal, D.; Biswas, S.; Paul, A.; Baitalik, S. Luminescent Dinuclear Ruthenium Terpyridine Complexes with a Bis-Phenylbenzimidazole Spacer. *Inorg. Chem.* **2017**, *56*, 7624-7641.
- (74) McConnell, A. J.; Wood, C. S.; Neelakandan, P. P.; Nitschke, J. R. Nitschke, J. R. Stimuli-Responsive Metal-Ligand Assemblies. *Chem. Rev.* **2015**, *115*, 7729-7793.
- (75) Flamigni, L.; Barigelli, F.; Armaroli, N.; Ventura, B.; Collin, J.-P.; Sauvage, J.-P.; Williams, J. A. G. Triplet-Triplet Energy Transfer between Porphyrins Linked via a Ruthenium(II) Bisterpyridine Complex. *Inorg. Chem.* **1999**, *38*, 661-667.
- (76) Dikova, Y. M.; Yufit, D. S.; Williams, J. A. G. Platinum(IV) Complexes with Tridentate, NNC-Coordinating Ligands: Synthesis, Structures, and Luminescence. *Inorg. Chem.* **2023**, *62*, 1306-1322.
- (77) Develay, S.; Blackburn, O.; Thompson, A. L.; Williams, J. A. G. Cyclometalated Platinum(II) Complexes of Pyrazole-Based, N⁴C⁴N-Coordinating, Terdentate

- Ligands: The Contrasting Influence of Pyrazolyl and Pyridyl Rings on Luminescence. *Inorg. Chem.* **2008**, *47*, 11129-11142.
- (78) Wilkinson, A. J.; Goeta, A. E.; Foster, C. E.; Williams, J. A. G. Synthesis and Luminescence of a Charge-Neutral, Cyclometalated Iridium(III) Complex Containing N⁺C⁻N⁻ and C⁺N⁺C⁻-Coordinating Terdentate Ligands. *Inorg. Chem.* **2004**, *43*, 6513-6515.
- (79) Paul, A.; Das, S.; Bar, M.; and Baitalik, S. Tuning of Photo-Redox Behaviours and Thermodynamic and Kinetic Aspects of Intercomponent Energy Transfer in Trimetallic Complexes of Ru (II) and Os (II) by Exploiting Their Second Coordination Sphere. *Dalton Trans.* **2021**, *50*, 14872-14883.
- (80) Maity, D.; Bhaumik, C.; Mondal, D.; Baitalik, S. Ru(II) and Os(II) Complexes Based on Terpyridyl-Imidazole Ligand Rigidly Linked to Pyrene: Synthesis, Structure, Photophysics, Electrochemistry, and Anion-Sensing Studies. *Inorg. Chem.* **2013**, *52*, 13941-13955.
- (81) Maity, D.; Bhaumik, C.; Mondal, D.; Baitalik, S. Photoinduced Intramolecular Energy Transfer and Anion Sensing Studies of Isomeric Ru(II) Os(II) Complexes Derived From an Asymmetric Phenanthroline-Terpyridine Bridge. *Dalton Trans.* **2014**, *43*, 1829-1845.
- (82) Bar, M.; Pal, P.; Maity, D.; Baitalik, S. Heterobimetallic Ru-Os Complexes Function as Multichannel Sensors for Selected Anions by Taking Profit of Metal-Ligand Interaction. *Sens. Actuators B: Chem.* **2018**, *266*, 493-505.
- (83) Belser, P.; Dux, R.; Baak, M.; De Cola, L.; Balzani, V. Electronic Energy Transfer in a Supramolecular Species Containing the [Ru(bpy)₃]²⁺, [Os(bpy)₃]²⁺, and Anthracene Chromophoric Units. *Angew. Chem. Int. Ed.* **1995**, *34*, 595-598.
- (84) De Cola, L.; Barigelletti, F.; Balzani, V.; Belser, P.; Von Zelewsky, A.; Seel, C.; Frank, M.; Voegtle, F. Polynuclear Complexes of Tris(Bipyridine) Bridging Ligands. Energy Transfer From Ru Based to Os-Based Components. *Coord. Chem. Rev.* **1991**, *111*, 255-260.
- (85) Li, G.; Zhu, D.; Wang, X.; Su, Z.; Bryce, M. R. Dinuclear Metal Complexes: Multifunctional Properties and Applications. *Chem. Soc. Rev.* **2020**, *49*, 765-838.
- (86) Hofmeier, H.; Schubert, U. S. Recent Developments in the Supramolecular Chemistry of Terpyridine-Metal Complexes. *Chem. Soc. Rev.* **2004**, *33*, 373-399.

- (87) Szymanski, W.; Beierle, J. M.; Kistemaker, H. A. V.; Velema W. A.; Feringa, B. L.; Reversible Photocontrol of Biological Systems by the Incorporation of Molecular Photoswitches. *Chem. Rev.* **2013**, *113*, 6114-6178.
- (88) Fedele, C.; Ruoko, T. P.; Kuntze, K.; Virkki, M.; Priimagi, A. New Tricks and Emerging Applications From Contemporary Azobenzene Research. *Photochem. Photobiol. Sci.* **2022**, *21*, 1719-1734.
- (89) Ihrig, S. P.; Eisenreich, F.; Hecht, S. Photoswitchable Polymerization Catalysis: State of the Art, Challenges, and Perspectives, *Chem Comm.* **2019**, *55*, 4290-4298.
- (90) Wang, Z.; Erhart, P.; Li, T.; Zhang, Z. Y.; Sampredo, D.; Hu, Z.; Wegner, H. A.; Brummel, O.; Libuda, J.; Nielsen, M. B.; Moth-Poulsen, K.; Storing Energy With Molecular Photoisomers. *Joule.* **2021**, *5*, 3116-3136.
- (91) Huang, X.; Li, T.; Recent Progress in the Development of Molecular-Scale Electronics Based on Photoswitchable Molecules. *J. Mater. Chem. C.* **2020**, *8*, 821-848.
- (92) Oscurato, S. L.; Reda, F.; Salvatore, M.; Borbone, F.; Maddalena, P.; Ambrosio, A. Shapeshifting Diffractive Optical Devices. *Laser Photonics Rev.* **2022**, *16*, 2100514.
- (93) Juris, A.; Balzani, V.; Campagna, S.; Denti, G.; Serroni, S.; Frei, G.; Güdel, H. U. Near-Infrared Luminescence of Supramolecular Species Consisting of Osmium(II)-and/or Ruthenium(II)-Polypyridine Components. *Inorg. Chem.* **1994**, *33*, 1491-1496.
- (94) Mateyise, N. G. S.; Conradie, M. M.; Conradie, J. Synthesis, Electrochemistry and Density Functional Theory of Osmium(II) Containing Different 2,2':6',2''-Terpyridines. *Molecules.* **2024**, *29*, 5078.
- (95) Serroni, S.; Campagna, S.; Puntoriero, F.; Pietro, C. D.; McClenaghan, N. D.; Loiseau, F. Dendrimers Based On Ruthenium(II) And Osmium(II) Polypyridine Complexes and the Approach Of Using Complexes as Ligands and Complexes as Metals. *Chem. Soc. Rev.* **2001**, *30*, 367-375.
- (96) Ge, C.; Zhu, J.; Ouyang, A.; Lu, N.; Wang, Y.; Zhang, Q.; Zhang, P. Near-Infrared Phosphorescent Terpyridine Osmium (II) Photosensitizer Complexes for Photodynamic and Photooxidation Therapy. *Inorg. Chem. Front.* **2020**, *7*, 4020-4027.
- (97) Sasaki, Y.; Yanai, N.; Kimizuka, N. Osmium Complex-Chromophore Conjugates with Both Singlet-to-Triplet Absorption and Long Triplet Lifetime through Tuning of the Heavy-Atom Effect. *Inorg. Chem.* **2022**, *61*, 5982-5990.
- (98) Ganguly, T.; Pal, P.; Paul, A.; Baitalik, S. Synthesis and Manifold but Controllable Emission Switching of Stilbene-Appended Polyaromatic Terpyridine Derivatives via

- Aggregation and Trans-Cis Isomerization. *Photochem. Photobiol. A* **2022**, 430, 113966.
- (99) Das, S.; Bar, M.; Ganguly, T.; Baitalik, S. Control of Photoisomerization Kinetics via Multistage Switching in Bimetallic Ru (II)-Terpyridine Complexes. *Inorg. Chem.* **2024**, 63, 6600-6615.
- (100) Fortage, J.; Dupeyre, G.; Tuyères, F.; Marvaud, V.; Ochsenbein, P.; Ciofini, I.; Hromadová, M.; Pospíšil, L.; Arrigo, A.; Trovato, E.; Puntoriero, F.; Laine, P. P.; Campagna, S. Molecular Dyads of Ruthenium (II)-or Osmium (II)-Bis (terpyridine) Chromophores and Expanded Pyridinium Acceptors: Equilibration between MLCT and Charge-Separated Excited States. *Inorg. Chem.* **2013**, 52, 11944-11955.
- (101) Albano, G.; Balzani, V.; Constable, E.C.; Maestri, M.; Smith, D.R.. Photoinduced Processes In 4'-(9-Anthryl)-2, 2': 6', 2 ''-Terpyridine, its Protonated Forms and Zn (II), Ru (II) and Os (II) Complexes. *Inorg. Chim. Acta*, **1998**, 277, 225-231.
- (102) Chen, K.; Cheng, Y. M.; Chi, Y.; Ho, M. L.; Lai, C. H.; Chou, P. T.; Peng, S. M.; Lee, G. H.; Osmium Complexes with Tridentate 6-Pyrazol-3-yl 2, 2'-Bipyridine Ligands: Coarse Tuning of Phosphorescence from the Red to the Near-Infrared Region. *Chem. Asian J.* **2007**, 2, 155-163.
- (103) Benniston, A. C.; Harriman, A.; Li, P.; Sams, C. A. Comparison of the Photophysical Properties of Osmium (II) Bis (2,2':6',2''-Terpyridine) and the Corresponding Ethynylated Derivative. *J. Phys. Chem. A* **2005**, 109, 2302-2309.
- (104) Beley, M.; Chodorowski, S.; Collin, J. P.; Sauvage, J. P.; Flamigni, L.; Barigelletti, F. Luminescent Dinuclear Complexes Containing Ruthenium (II)-and Osmium (II)-Terpyridine-Type Chromophores Bridged by A Rigid Biscyclometalating Ligand. *Inorg. Chem.* **1994**, 33, 2543-2547.
- (105) Yuan, Z.; He, J.; Mahmood, Z.; Xing, L.; Ji, S.; Huo, Y.; Zhang, H. L. Deciphering The Ligand's Geometric Effect On The Photophysical Properties Of Osmium Complex And Its Application In Triplet-Triplet Annihilation Upconversion. *Dyes Pigm.* **2022**, 199, 110049.
- (106) Alemán, E. A.; Shreiner, C. D.; Rajesh, C. S.; Smith, T.; Garrison, S. A.; Modarelli, D. A. Photoinduced Electron-Transfer Within Osmium (II) And Ruthenium (II) Bis-Terpyridine Donor Acceptor Dyads. *Dalton Trans.* **2009**, 33, 6562-6577.
- (107) Chen, J. L.; Chi, Y.; Chen, K.; Cheng, Y. M.; Chung, M. W.; Yu, Y. C.; Lee, G. H.; Chou, P. T. Shu, C. F. New Series Of Ruthenium (II) And Osmium (II) Complexes

- Showing Solid-State Phosphorescence In Far-Visible And Near-Infrared. *Inorg. Chem.* **2010**, *49*, 823-832.
- (108) Bhattacharya, S.; Pal, P.; Gorain, S.; Baitalik, S. Enhancing Near-Infrared Absorption in Osmium (II) Complexes Under the Cumulative Influence of Terpyridine Ligand and Anions: Combined Experimental and DFT/TD-DFT Investigation. *EurJIC*. **2024**, 202400758.
- (109) Scattergood, P. A.; Roberts, J.; Omar, S. A.; Elliott, P. I. Observation Of An Inversion In Photophysical Tuning In A Systematic Study Of Luminescent Triazole-Based Osmium (II) Complexes. *Inorg. Chem.* **2019**, *58*, 8607-8621.
- (110) Sun, M. J.; Shao, J. Y.; Yao, C. J.; Zhong, Y. W.; Yao, J. Osmium Bisterpyridine Complexes With Redox-Active Amine Substituents: A Comparison Study With Ruthenium Analogues. *Inorg. Chem.* **2015**, *54*, 8136-8147.
- (111) Beley, M.; Collin, J. P.; Sauvage, J. P.; Sugihara, H.; Heisel, F.; Miehé, A. Photophysical and photochemical properties of ruthenium and osmium complexes with substituted terpyridines. *J. Chem. Soc., Dalton Trans.* **1991**, *11*, 3157-3159.
- (112) Pal, P.; Mukherjee, S.; Maity, D.; Baitalik, S. Synthesis, Photophysics, and Switchable Luminescence Properties of a New Class of Ruthenium (II)-Terpyridine Complexes Containing Photoisomerizable Styrylbenzene Units. *ACS Omega* **2018**, *3*, 14526-14537.
- (113) Wrighton, M. S.; Morse, D. L.; Pdungsap, L. Intraligand Lowest Excited States In Tricarbonylhalobis(Styrylpyridine) Rhenium(I) Complexes. *J. Am. Chem. Soc.* **1975**, *97*, 2073-2079.
- (114) Yutaka, T.; Mori, I.; Kurihara, M.; Mizutani, J.; Tamai, N.; Kawai, Tsuyoshi.; Irie, M.; Nishihara, H. Photoluminescence Switching Of Azobenzene-Conjugated Pt(II) Terpyridine Complexes By Trans-Cis Photoisomerization. *Inorg. Chem.* **2002**, *41*, 7143-7150.
- (115) Wenger, O. S.; Henling, L. M.; Day, Winkler, M. W. Jay R.; Gray H. B. Photoswitchable Luminescence of Rhenium(I) Tricarbonyl Diimines. *Inorg. Chem.* **2004**, *43*, 2043-2048.
- (116) Yam V. W. W.; Lau, V. C. Y.; Wu, L. X. Synthesis, Photophysical, Photochemical And Electrochemical Properties Of Rhenium(I) Diimine Complexes With Photoisomerizable Pyridyl-Azo, -Ethenyl Or -Ethyl Ligands. *J. Chem. Soc., Dalton Trans.* **1998**, 1461-1468.

- (117) Lin, J. L.; Chen, C. W.; Sun, S. S.; Lees, A. J. Photoswitching Tetranuclear Rhenium(I) Tricarbonyl Diimine Complexes With A Stilbene-Like Bridging Ligand. *Chem. Comm.* **2011**, 47, 6030-6032.
- (118) Patrocinio A. O. T.; Iha N. Y. M. Photoswitches and Luminescent Rigidity Sensors Based on fac-[Re(CO)₃(Me₄phen)(L)]⁺. *Inorg. Chem.* **2008**, 47, 10851-10857.
- (119) Yam, V. W.W.; Yang, Y.; Zhang, J.; Chu, B. W.-K., Zhu, N. Synthesis, Characterization, And Photoisomerization Studies Of Azo- And Stilbene-Containing Surfactant Rhenium(I) Complexes. *Organometallics*. **2001**, 20, 4911-4918.
- (120) Faustino, L. A.; Machado A. E. H.; Patrocinio A. O. T. Photochemistry of fac-[Re(CO)₃(dcbH₂)(trans-stpy)]⁺: New Insights on the Isomerization Mechanism of Coordinated Stilbene-like Ligands. *Inorg. Chem.* **2018**, 57, 2933-2941.



Chapter 7

Osmium-Terpyridine Complexes Linked with Stilbene-Coupled Naphthalene, Anthracene, and Pyrene Moieties Act as Multichannel Sensors for F^- and Hg^{2+} via Non-Classical Interactions

7.1 Introduction

Supramolecular interaction has garnered considerable attention in numerous areas at the forefront of chemistry and biology.¹⁻⁶ Non-covalent interactions, viz. van der Waals forces, hydrogen bonding, electrostatic, cation- π , CH- π , anion- π and π - π stacking, to name a few, govern the assembly and functionality of such supramolecular architectures.²⁻⁸ Although weak, these interactions play a fundamental role in preserving the essential structures of vital biological molecules like DNA, RNA, and proteins.⁹⁻¹² The significance of these weak interactions has also opened up new frontiers in the field of supramolecular chemistry of ions encompassing both anion and cation recognition, sensing, and transport.¹³⁻²⁰

Designing of phosphorescent materials emitting in the near-infrared (NIR) as well as IR region are now gaining great attention for their potential applications in biology, chemistry, and technology.²¹⁻²⁵ NIR light, by virtue of its low interference and invisibility, could be safely used for sensing of specific anion and cations in biological systems.²¹⁻³¹ The chemosensors, often constructed through covalent or non-covalent coupling of binding sites and signaling subunits, operate as meticulously designed molecular systems. When suitably designed, these systems are capable of transforming guest binding interactions into recognizable signal accompanied with considerable change in the absorption, emission and redox behaviors.²¹⁻³¹ Among the various output signals, those stemming from modifications in emission spectral characteristics are particularly compelling, and quite a large number of chromogenic and fluorogenic chemosensors has already been documented for sensing of selected anions and cations.³²⁻³⁵

In this work, our main objective is to utilize NIR-emissive receptors that are capable of multi-channel recognition of selected anions and cations through the intermediacy of various non-covalent interactions. In order to accomplish our objective, we employed herein a new class of our recently reported $\text{Os}(\text{tpy-pvp-X})_2(\text{ClO}_4)_2$ complexes consisting of a polyaromatic unit such as anthracene, naphthalene and pyrene at the 4' position of the terpyridine moiety having absorption and emission spectral window in the visible and stretching into the NIR domain (Chart 7.1). By virtue of the presence of extended π -conjugation via stilbene units together with polyaromatic hydrocarbons, the present complexes are expected to recognize specific anions and cations through the intermediacy of multiple non-covalent interactions, viz. hydrogen bonding, cation- π , CH- π , anion- π and π - π stacking.

Upon complexation with Os^{2+} ion, the terpyridine and other aromatic protons within

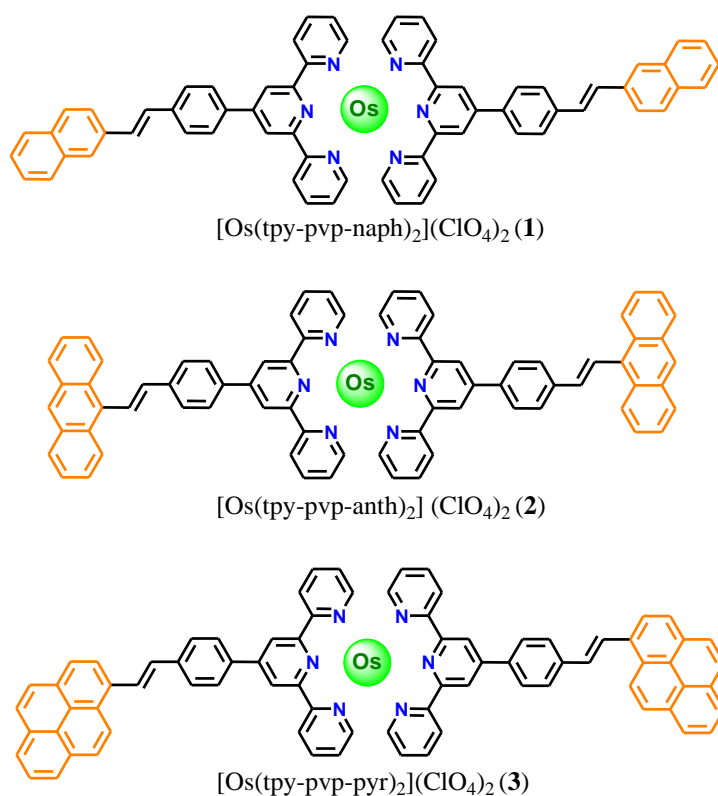


Chart 7.1. The chemdraw structures of the Os(II) complexes.

the complex backbone are expected to become acidic to some extent, enabling them to participate in C-H---A⁻-type (A=anion) hydrogen bonding interactions with anions.³⁶⁻⁴¹ Anion recognition and sensing are paramount due to their pivotal roles in chemical and biological processes. Due to the duplicitous nature of fluoride ion and its relevance to both biological and environmental contexts, we have focused on developing chemosensors specifically designed to detect F⁻. A diverse array of receptor motifs incorporating hydrogen bond donors, such as NH_{Urea/Thiourea}, NH_{Imidazole/Pyrrrole/Indole}, NH_{Amide} and OH_{Phenol/Catechol}, have been extensively utilized as the primary binding motifs in the design of chemosensors, with their mechanisms and functions thoroughly explored in numerous reviews.⁴²⁻⁴⁷ Now, by virtue of having a delocalized π -acidic electron cloud, the present complexes are expected to interact with selected anions through anion- π interactions.⁴⁷⁻⁵⁰ Relative to ubiquitous cation- π , the anion- π interactions are less explored due to its ostensibly counterintuitive nature. Since these interactions are mostly dependent on the distance, hence anion- π interactions are comparatively weaker than the cation- π interactions because the van der Waals radii of anions are larger than cations.⁵¹⁻⁵² Leveraging the favourable photophysical and electrochemical properties, coupled with the presence of multiple acidic C-H protons and electron-rich π -electron delocalized polyaromatic motifs, the anion-sensing characteristics of

the complexes are comprehensively investigated in this work through multiple optical channels and spectroscopic techniques.

Among the heavy metals, mercury (Hg) poses significant health and environmental risks due to its toxic, persistent, and non-biodegradable nature.⁵³⁻⁵⁵ Once released into the environment, mercury can accumulate into the ecosystems and contaminates soil, water, and food chains. This bioaccumulation of Hg can lead to severe health issues in humans, including neurological damage, kidney failure, Minamata disease, and developmental disorders, particularly when exposure occurs through contaminated water or seafood.⁵⁶⁻⁵⁷ Due to these dangers, regulatory agencies such as the World Health Organization (WHO) and the Environmental Protection Agency (EPA) enforce strict limits on mercury levels to minimize its harmful effects on both human health and the environment.⁵⁸⁻⁵⁹ Optical detection methods, such as fluorescence and colorimetric changes, are highly convenient due to their simplicity and sensitivity, with fluorescent probes offering the key advantage of intracellular detection.⁶⁰⁻⁶² The presence of various aromatic and heteroaromatic moieties within their architecture renders the present complexes rich in π -electron density. Consequently, interaction with cationic moieties is likely to be energetically favourable. Additionally, cation- π interaction should also be operative, governed by electrostatic forces and cation-induced polarization.⁶³ Cation- π interactions are crucial in fields like chemistry, biology, and materials science, playing significant roles in processes such as steroid biosynthesis, acetylcholine receptor binding and ion selectivity in potassium channels.⁶⁴⁻⁶⁷ Initially thought to be purely electrostatic, these interactions also involve induction, dispersion, and covalent contributions, particularly in transition metal cation- π systems.^{64,68-71} While studies predominantly focus on main group cations like Li, Na, and K, transition metal based cation- π interactions, especially with M^{2+} --- π systems, are less explored due to the complexity of their open-shell electronic structures.⁷²⁻⁷⁷ Despite some research on transition metal-polyaromatic hydrocarbon complexes,⁷⁸⁻⁸⁰ their untapped potential in the field of toxic metal sensing offers a promising avenue for advancing detection technologies. Due to the toxic nature of Hg^{2+} ion, we have concentrated on developing chemosensors specifically tailored for its detection. Although there are documentation of cation- π and very few instances of anion- π interactions in metal complexes,^{72-80,81-85} to the best of our knowledge, there are no reports of such interactions based on Os(II)-terpyridine type complexes. This is the first report wherein the present Os-terpyridine complexes display simultaneous anion- π and cation- π interactions with F^- and Hg^{2+} , respectively.

Incorporation of a stilbene unit makes room for the *trans-cis* photoisomerization upon shining light which in turn will re-orient the conformation of the polyaromatic moieties within the complex backbone.⁸⁶⁻⁹⁰ Thus, it is quite expected that the extent of both anion- π as well as cation- π interactions will change among the two isomeric forms of the complexes. To this end, we will also thoroughly investigate the anion and cation sensing experiments with the *cis*-form of the complexes. In conjunction with experimental demonstration, computation analysis using density functional theory as well as time-dependent DFT has been executed to obtain the electronic properties of the molecular systems as well as the mode of ion-receptor interactions.

7.2 Experimental Section

7.2.1 Materials. Synthesis and characterization of Tpy-pvp-X (X=naphthalene, anthracene, and pyrene) ligands have been described in Chapter 2.

7.2.2 Synthesis of the Metal Complexes. The homoleptic Os(II)-terpyridine complexes are synthesized upon refluxing K_2OsCl_6 and the respective ligand (tpy-pvp-X) in a 1:2 ratio under an argon atmosphere in an ethylene glycol medium followed by their ion exchange with using sodium perchlorate ($NaClO_4$). Purification of the complexes is accomplished by column chromatography and recrystallization from appropriate solvent(s). The detailed synthesis and characterization of the complexes have been meticulously discussed in Chapter 6.

7.2.3 Instruments and Physical Methods. Details of instruments and physico-chemical measurements are provided in Chapter 2.

7.3 Results and Discussion

7.3.1 Anion Sensing Behaviors of the Complexes. The anion sensing characteristics of **1-3** are systematically investigated in MeCN via different optical channels and spectroscopic techniques. Tetrabutylammonium salts of F^- , Cl^- , Br^- , I^- , CN^- , AcO^- and $H_2PO_4^-$ are utilized for this purpose. The absorption and emission spectral response of the complex **2** in presence of studied anions are depicted in Figure 7.1. Amongst the anions, F^- induces the maximum change while the remaining anions are unable to induce any detectable change in their spectral profile.

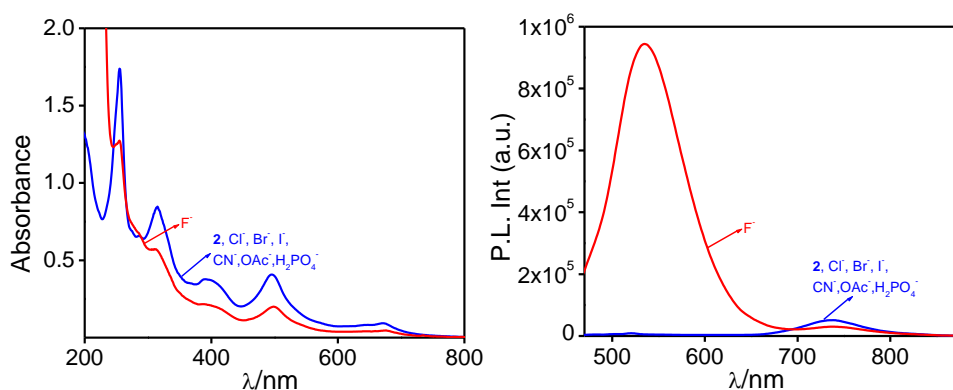


Figure 7.1. Absorption (left) and emission (right, $\lambda_{\text{ex}}=450$ nm) spectrum of **2** in MeCN (1.0×10^{-5} M) in absence and in presence of studied anions as their TBA salts.

To acquire quantitative insight about the receptor-anion interplay, we performed titration experiments upon gradual addition of F^- and monitor the changes via absorption and emission spectroscopy (Figure 7.2). In the absorption spectra, decrease in absorbance of the MLCT and ILCT bands occur with concomitant increase in the $\pi-\pi^*$ band intensities for both **2** and **3**. For **1**, simultaneous increase in the absorbance of both ILCT and $\pi-\pi^*$ bands take place together with a small decrease in absorbance of the MLCT bands. The decrease in the absorbance of the MLCT band is the maximum for **2**, while minimum for **1**. All the spectral lines pass through one or more isosbestic points indicating the presence of two or more species in equilibrium with one another. Complete saturation occurs upon addition of 92 equivalents of F^- . On the emission side, upon excitation at 450 nm, the emission intensity of the peak at ~ 740 nm slightly decreases with concomitant rise of a new peak at ~ 530 nm for all three complexes. The peak in shorter wavelength region is generally due to the ligand-centred emission arising out of the deactivation of $^3\text{ILCT}$ state, while the lower energy band at longer wavelength (~ 740 nm) emerges due to deactivation from the $^3\text{MLCT}$ state. Continued addition of F^- results in enormous intensification of the shorter wavelength peak and ultimately saturates at 92 equiv. An increase in the Φ value is also noticed for the F^- saturated solutions. Thus, a dual emission is observed for the complexes upon F^- addition. We have also measured the lifetime values of the complexes upon F^- addition and the corresponding decays are illustrated in Figure 7.3. The lifetime values are seen to decrease in case of **1** and **2**, while it increases for **3**.

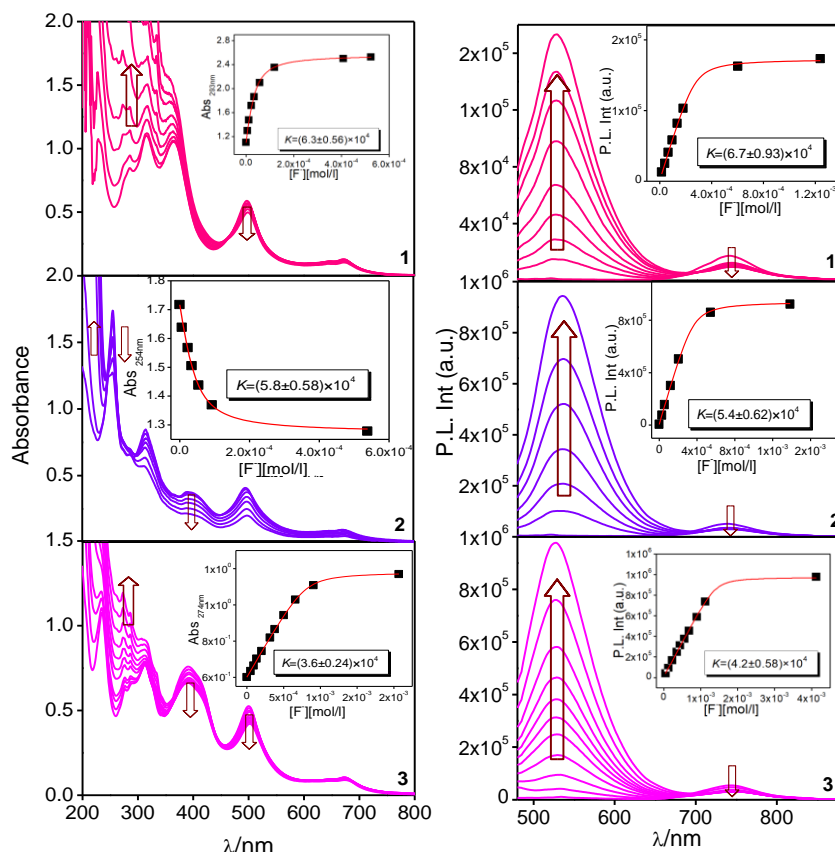


Figure 7.2. Absorption (left panel) and emission ($\lambda_{\text{ex}}=450$ nm) (right panel) titration profiles of the *t-t* forms of **1-3** in MeCN upon gradual addition of F^- . Insets to the figures in both left and right panels indicate the estimation of binding constants.

To elucidate the probable mode of interaction, ^1H NMR titration experiment is executed upon systematic addition of F^- to the $\text{DMSO}-d_6$ solution of **1** and the corresponding profile is displayed in Figure 7.4. It is observed that the signals due to H_3 , H_6 and H_7 undergo

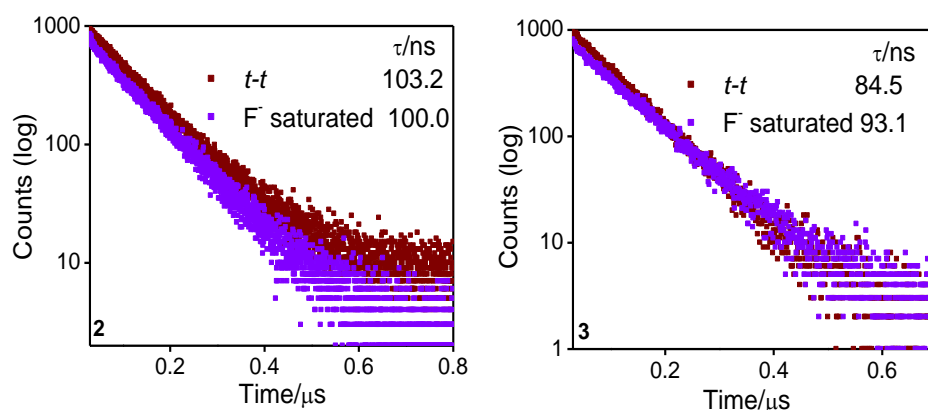


Figure 7.3. The emission decay profiles ($\lambda_{\text{ex}} = 490\text{nm}$) as well as lifetime values of *t-t* forms of **2** and **3** in their free and F^- -saturated state in MeCN.

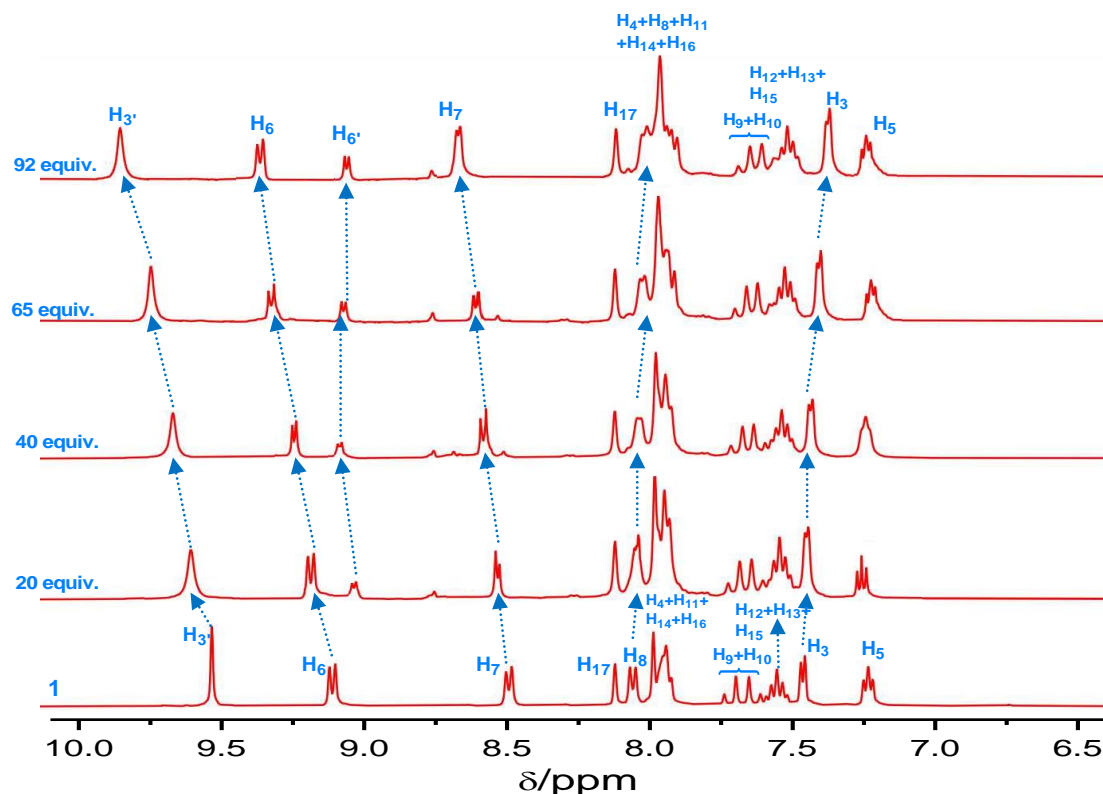


Figure 7.4. ^1H NMR spectral titration of t-t form of **1** upon incremental addition of TBAF in $\text{DMSO}-d_6$.

significant downfield shift and the extent of shift varies between 0.1 and 0.3 ppm. The well-resolved doublets for H_6 proton, initially observed at 9.13 ppm, splits into two new doublets at 9.21 and 9.09 ppm. As F^- is gradually added, one of the doublets shift towards the up-field region while the other one towards the downfield region as shown in Figure 7.4. Change in multiplicity is also observed for H_8 , H_4 , H_{11} , H_{14} and H_{16} protons, which undergo an up-field shift, resulting in the formation of a multiplet. The ethylenic protons, H_9 and H_{10} , also exhibit a slight up-field shift. The H_3 proton experiences a small up-field shift, while the H_5 proton undergoes a small downfield shift. Upon complexation with Os^{2+} , the terpyridine and other aromatic protons within the complexes acquired acidic properties, facilitating their involvement in hydrogen bonding interactions with incoming F^- guests. The observed chemical shifts in selected proton signals in presence of F^- ions could be due to occurrence of a combination of non-covalent interactions, including $\text{CH}\cdots\text{F}$ hydrogen bonding, $\text{CH}-\pi$, and anion- π interactions. It is to be noted that the integration count of total number of protons in the F^- saturated spectrum increases relative to its initial form which is indicative of some sort of association among the complex molecules.

To investigate the mode of receptor-anion interaction, we also conducted ^{19}F NMR titration experiments by gradually adding anthracene (**2**) derivative to a $\text{DMSO-}d_6$ solution of TBAF. The corresponding spectral profiles are shown in Figure 7.5. Free TBAF exhibits a strong singlet at -106.9 ppm, corresponding to the F^- ion. Upon addition of the complex, the singlet peak undergoes a slight upfield shift and gradually diminishes, indicating shielding of F^- ions due to the formation of complex--- F^- adduct. Notably, no additional peaks appear during the titration, confirming the absence of covalent attachment of fluorine to the complex backbone. Thus, the ^{19}F NMR spectral analysis strongly supports the occurrence of non-classical interactions between the complexes and F^- ions.

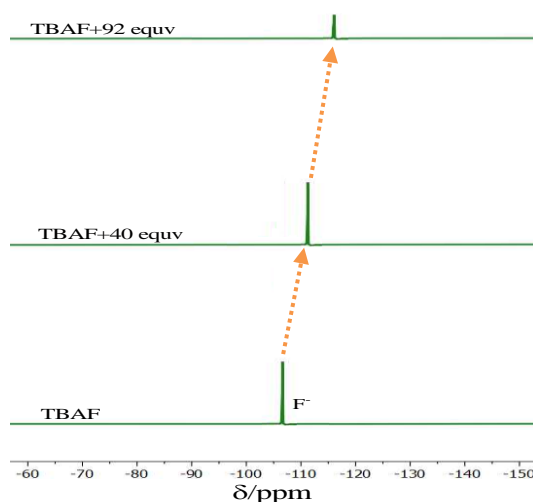


Figure 7.5. ^{19}F NMR titration of **2** with F^- showing complex--- F^- interaction in $\text{DMSO-}d_6$ at RT.

To determine the stoichiometry of the complex-anion interaction, Job's plot analysis is conducted using emission titration data of the complexes upon varying the mole fraction of F^- . The point of intersection at approximately 0.5 mole fraction of F^- in the Job's plot indicates a 1:1 adduct formation between the complex and the fluoride ion (Figure 7.6).

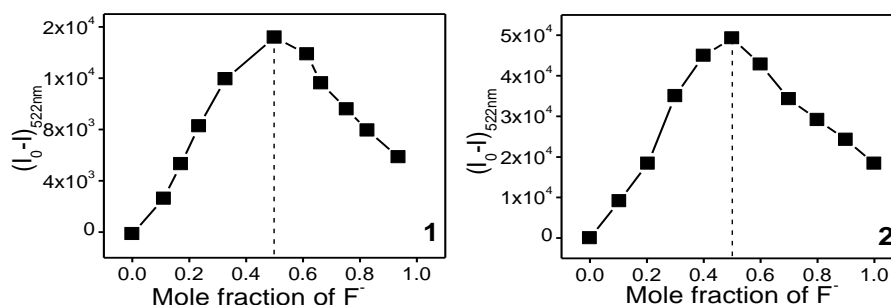


Figure 7.6. Job's plot referring to the 1:1 interaction between the complexes **1** and **3** and F^- in MeCN.

We further determined the binding constants (K) for the receptor-anion interactions by analyzing the absorption and emission titration data of the complexes, using equation 7.1 for 1:1 stoichiometry (inset to Figure 7.2). The resulting K values are summarized in Table 7.1.

$$\Delta A = \frac{\Delta \epsilon b ([H] + [G] + (1/K)) \pm \sqrt{\Delta \epsilon^2 b^2 ([H] + [G] + (1/K))^2 - 4 \Delta \epsilon^2 b^2 [H][G]}}{2} \quad (7.1)$$

where ΔA is the change in absorbance, $[H]$ and $[G]$ is the concentration of metal complex and added anion, respectively. $\Delta \epsilon$ is the change in molar extinction coefficient, b is the absorption path length, and K is the binding constant. Non-linear regression analysis of absorption/emission spectral data as a function of anion concentration leads to the value of binding constants. The binding constants for the naphthalene (**1**) derivative is found to be the highest followed by anthracene (**2**), both of which are notably higher than that of the pyrene derivative (**3**). Additionally, the detection limits of the complexes for F^- are calculated that range between 8.5×10^{-8} and 7.4×10^{-5} M (Table 7.1).

Table 7.1. Equilibrium constants (K) and detection limits for **1-3** towards F^- and Hg^{2+} in MeCN.

Compound	Binding Constant (K)				Detection Limit /M			
	F^-		Hg^{2+}		F^-		Hg^{2+}	
	Absorption	Emission	Absorption	Emission	Absorption	Emission	Absorption	Emission
1 (<i>t-t</i>)	6.3×10^4	6.7×10^4	9.3×10^4	9.3×10^4	1.2×10^{-7}	8.5×10^{-8}	1.6×10^{-7}	3.1×10^{-8}
2 (<i>t-t</i>)	5.8×10^4	5.4×10^4	5.9×10^4	5.6×10^4	1.6×10^{-7}	2.0×10^{-7}	7.9×10^{-7}	6.3×10^{-7}
3 (<i>t-t</i>)	3.6×10^4	4.2×10^4	7.3×10^4	7.2×10^4	7.4×10^{-7}	4.9×10^{-7}	4.0×10^{-7}	2.9×10^{-7}
1 (<i>c-c</i>)	5.4×10^4	5.6×10^4	5.6×10^4	4.2×10^4	4.1×10^{-7}	2.4×10^{-7}	5.6×10^{-7}	3.9×10^{-7}
2 (<i>c-c</i>)	3.3×10^4	4.6×10^4	6.2×10^4	5.3×10^4	7.1×10^{-7}	6.0×10^{-7}	2.8×10^{-7}	1.6×10^{-7}
3 (<i>c-c</i>)	2.9×10^4	3.4×10^4	3.3×10^4	3.4×10^4	9.5×10^{-7}	9.5×10^{-7}	1.1×10^{-6}	1.0×10^{-6}

Increase in the integration count of total number of protons in the 1H NMR spectrum of **1** prompted us to conduct the dynamic light scattering (DLS) experiments {Figure 7.7}. The DLS spectra are acquired in MeCN for the free as well as its F^- saturated forms of the complexes. It is seen that the size of the particle increases from 3.2-84.0 to 23.0-460.5 nm domain on addition of F^- . Taking into consideration that no additional solvent was used in the DLS experiment, the possibility of solvent-induced aggregation is eliminated. Therefore, the

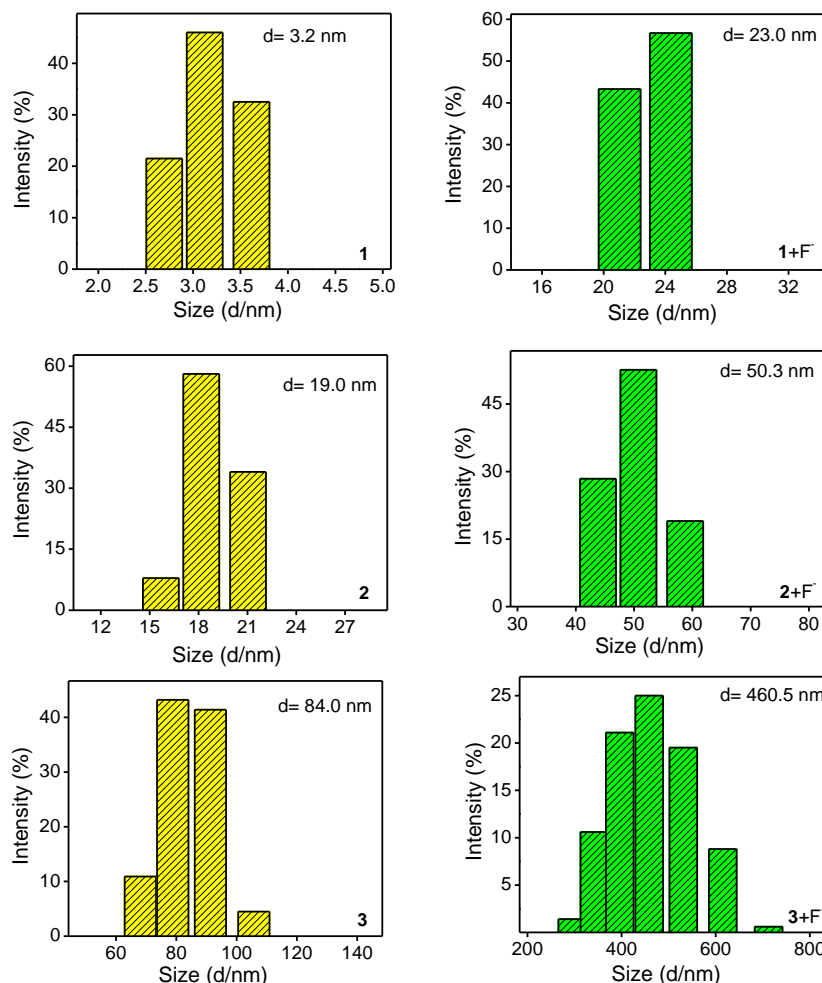


Figure 7.7. DLS plot to determine the particle size distribution of **1-3** in their free (left) and F^- (right) saturated forms in MeCN.

aggregation primarily occurs due to non-covalent interactions drawing the molecules closer together, effectively increasing their size. As aggregation is known to enhance emission through the restriction of intramolecular motions (RIM), the observed increase in emission intensity upon F^- addition can be attributed to this phenomenon. Despite an increase in the total integration count of the protons, no evidence for the formation of a dimer-type adduct was observed. Consequently, the results of both NMR and DLS experiments clearly suggest the aggregate formation mediated by F^- ions.

Since the conformation of the molecules significantly alter on going from the *t-t* to *c-c* form, it is expected that the extent of different non-classical interactions would also be substantially modified. To this end, we also investigated the anion sensing characteristics of the *c-c* form of the complexes and compared with their *t-t* counterpart. The absorption and

emission spectral change in the *c-c* form of the complexes is monitored upon stepwise inclusion of F^- (Figure 7.8). A closer inspection reveals that there is a marked difference in the spectral pattern of the *c-c* form relative to the *t-t* isomer of the respective complex. In the absorption spectra, F^- addition leads to increase in absorbance of the MLCT and ILCT bands along with a small decrease in the $\pi-\pi^*$ band intensity. Interestingly, the spectral window stretches up to ~ 1000 nm in case of **1** and **3** in presence of F^- . Again, all the spectral lines pass through clear isosbestic points indicating that two or more species are in equilibrium with each other. Spectral saturation takes place upon addition of 84 equiv of F^- for the *c-c* form of the complexes. Interestingly, the amount required to reach saturation is little less in comparison to their *t-t* analogues (92 equiv). In the emission spectra, the *c-c* forms of the complexes display two bands at ~ 500 and 740 nm. The former peak is attributed to the ligand

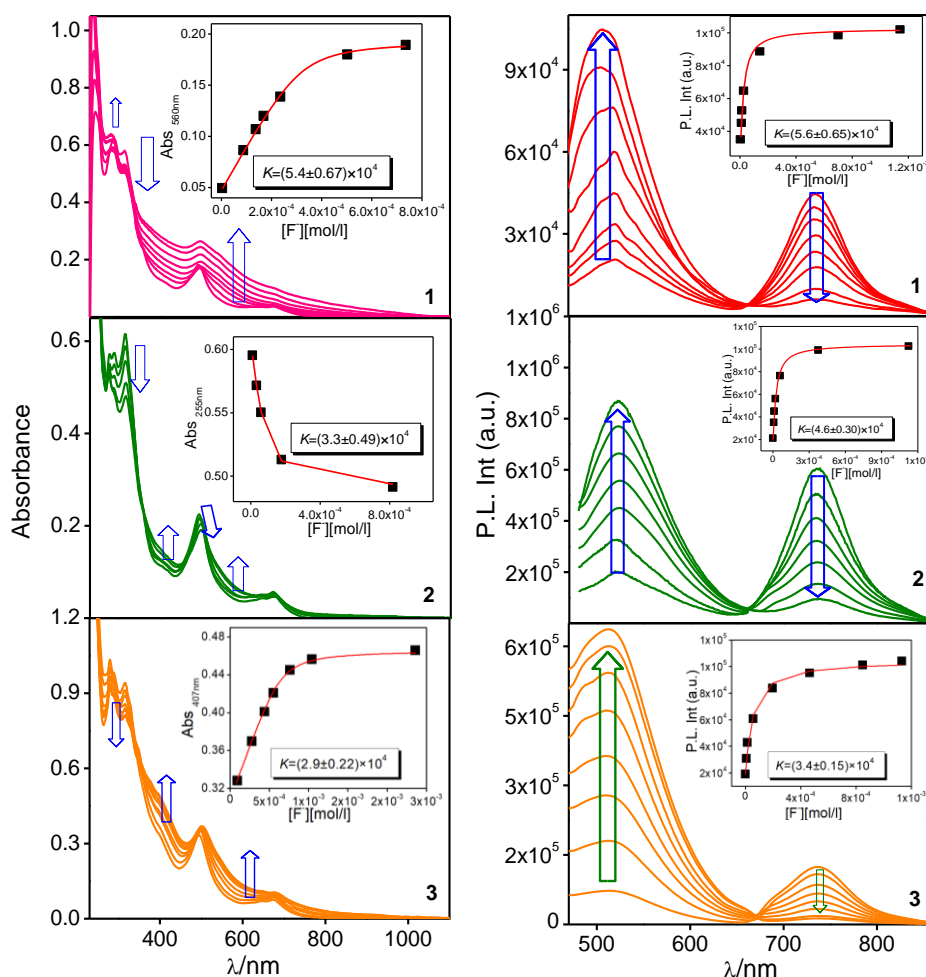


Figure 7.8. Absorption (left panel) and emission ($\lambda_{\text{ex}}=450$ nm) (right panel) titration profiles of the *c-c* forms of **1-3** in MeCN upon gradual addition of F^- . Insets to the figures in both left and right panels indicate the estimation of binding constants.

centered, while the peak at 740 nm corresponds to the MLCT emission. Upon F^- addition, the MLCT peak intensity gradually decreases while the ligand-centered band increases. We have also measured the lifetimes of the F^- -saturated $c-c$ forms of complexes, wherein small decrease in lifetime is noticed for **1** and **2** (Figure 7.9). By contrast, F^- saturated solution of **3** exhibits a bi-exponential decay together with slight increase in lifetime.

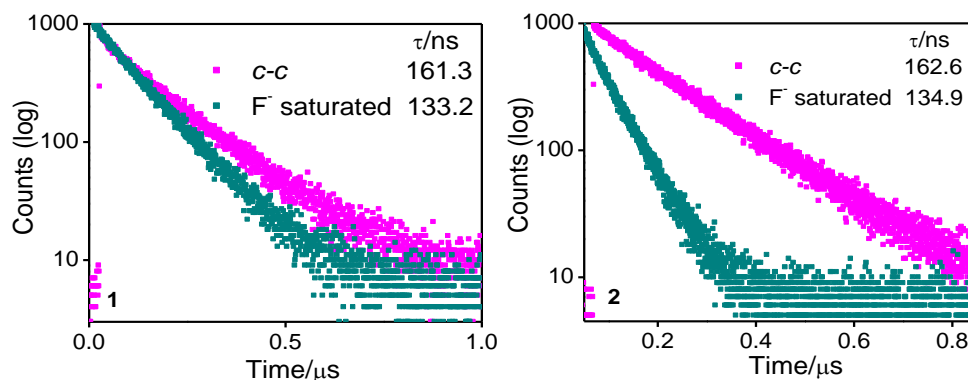


Figure 7.9. The emission decay profiles ($\lambda_{ex} = 490\text{nm}$) as well as lifetime values of $c-c$ forms of **1** and **2** in their free and F^- -saturated state in MeCN.

To elucidate the probable mode of interaction, 1H NMR titration experiment is also executed on the $c-c$ form of **2** upon systematic addition of F^- in $DMSO-d_6$ and the corresponding profile is displayed in Figure 7.10. We have already provided the 1H NMR spectra of the anthracene derivative (**2**) due to photoisomerization in our previous chapter. It is observed that two set of proton peaks exist: the residual proton signals of the complex moiety due to their $t-t$ form and the proton peaks due to their isomerised $c-c$ forms. Fluoride addition affects both types of protons in the NMR spectrum. The protons associated with $H_{3'}$ at 9.60 ppm and $H_{3''}$ at 9.47 ppm experience a downfield shift to 9.90 and 9.67 ppm, respectively. The multiplet corresponding to H_6 and H_6' , having their chemical shift position within 9.17-9.08 ppm, also shifts towards downfield, resulting in two doublets at 9.44 and 9.31 ppm. The $H_{7'}$ proton at 8.56 ppm experiences a slight downfield shift, forming a multiplet within 8.88-8.76 ppm range. A significant downfield shift from 8.13 to 8.51 ppm also takes place for the $H_{15'}$ proton (singlet linked with $c-c$ form of the anthracene moiety). Interestingly, apart from the $H_{15'}$, most of the protons associated with the anthracene moiety undergo an up-field shift accompanied by changes in their multiplicities. Upon addition of up to 25 equiv of F^- , the $H_{9'}$ and $H_{10'}$ protons associated to the ethylenic bond exhibit a slight up-field shift from their initial positions of 6.87 and 6.65 ppm to 6.75 and 6.48 ppm,

respectively. However, upon the addition of 84 equiv of F^- , they undergo a pronounced downfield shift to 7.16 and 6.75 ppm, respectively. The observed down-field shift of the above-mentioned protons is probably due to $C-H\cdots F^-$ hydrogen bonding interaction. The

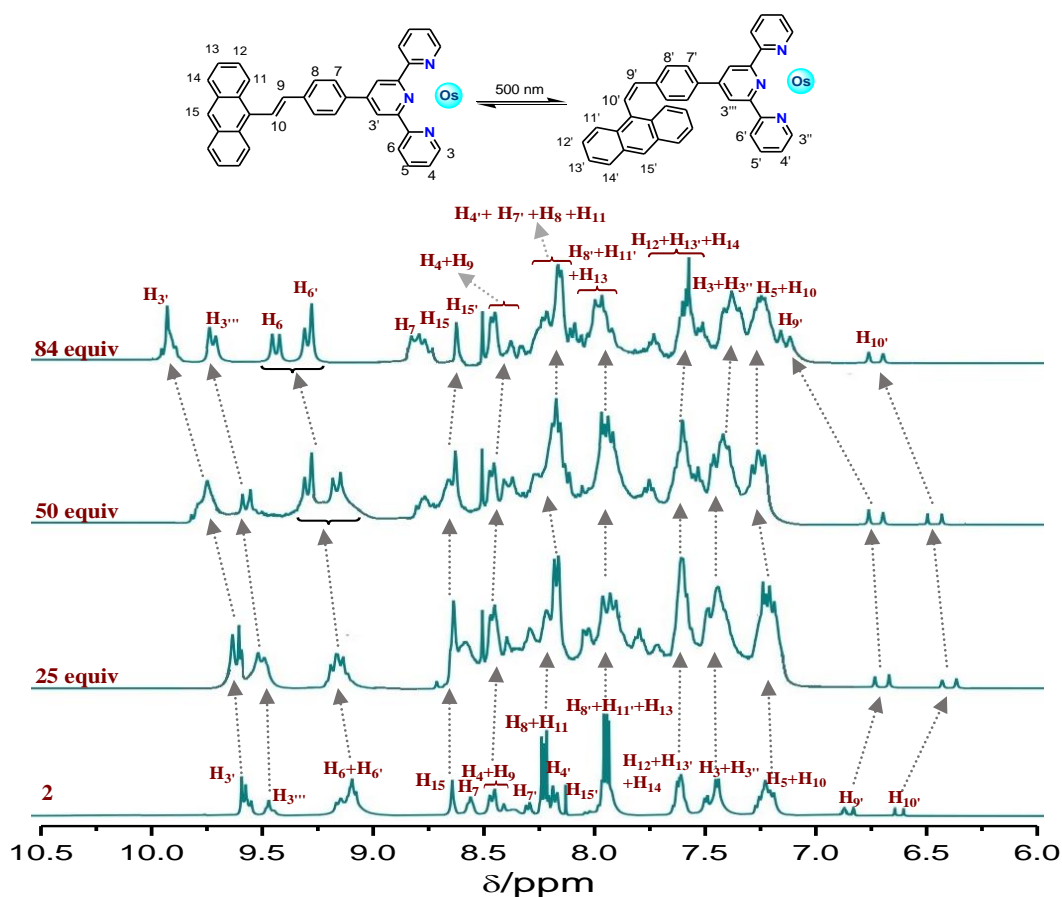


Figure 7.10. 1H NMR spectral titration of the c-c form of **2** upon incremental addition of TBAF in $DMSO-d_6$.

peaks due to terpyridine protons (H_3 - H_6) undergo both up-field and downfield shift together with change in their multiplicities, indicating the occurrence of some sort of interactions among the complex moiety and the incoming F^- . The observed shifts in selected proton signals in the presence of F^- can be attributed to the interplay of various non-classical interactions, including $CH\cdots F$ hydrogen bonding, as well as $CH-\pi$ and anion- π interactions. A significant increase in strain is induced across the complex backbone on going from their *t-t* to *c-c* forms. Consequently, the extent of $C-H\cdots F^-$ interaction between the different protons with incoming F^- will alter on passing from *t-t* to *c-c* analogues.

We also determined the binding constants (K) for the receptor-anion interactions in the *c-c* form of the complexes by analyzing their absorption and emission titration data and

upon employing equation 7.1 for 1:1 stoichiometry (presented in the inset of Figure 7.8). It is observed that the values of K in the c - c forms are lower compared to their analogous t - t isomers and the observed value for the c - c forms lie in the order **1>2>3**. The enhanced sensitivity of the t - t forms of the complexes over their c - c isomers towards F^- is also reflected in the extent of change in their absorption and emission spectral profiles. This lowering of the binding value most probably arises due to the increased strain generated in the c - c form of the complexes. The limit of detection towards F^- in the c - c forms of the complexes are also calculated and found to range between 1.6×10^{-7} and 1.1×10^{-6} M, which are lower than that of their analogous t - t isomers (Table 7.1).

To obtain direct proof for the occurrence of non-covalent interactions, we conducted DFT calculations on t - t as well as on the c - c form of the complexes and calculated the energy values associated with each mode of interaction (Figure 7.11). We first optimized the ground state geometry of **1** in both of its t - t and c - c states and calculated their energy values (A and D respectively). Next, we computed the energy due to interaction with F^- at some specified positions of the complex. We mainly considered two types of non-covalent interactions, viz. $CH \cdots F^-$ hydrogen bonding and anion- π . Initially geometries involving only $CH \cdots F^-$ interactions within the terpyridine and styrylbenzene moieties are optimized. Four feasible $CH \cdots F^-$ interactions (B and E) are identified, and their energy values are found to decrease relative to their free forms. This is followed by optimization of geometries including both F^- -

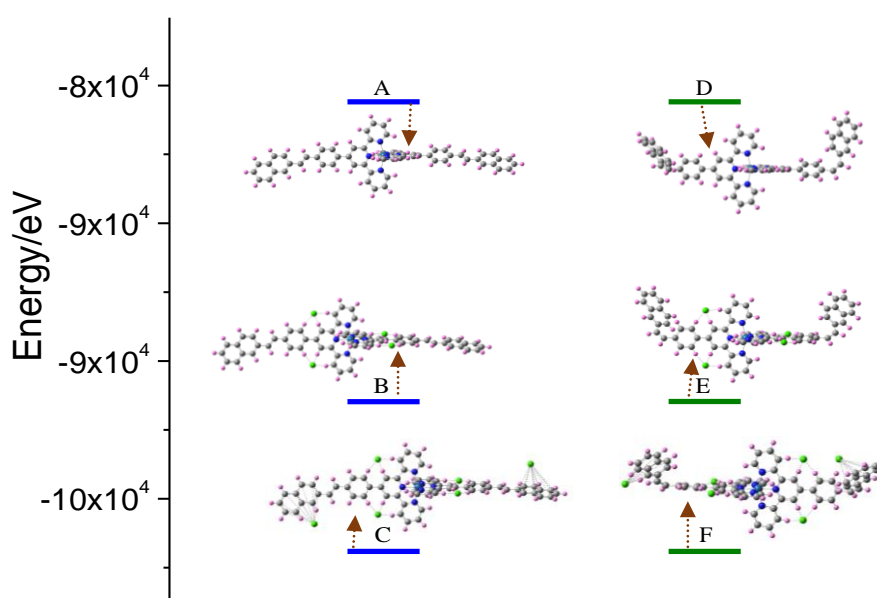


Figure 7.11. Calculated energy diagram showing decrease in energy of **1**... F^- complex adduct due to $CH \cdots F$ and anion- π interactions in different forms of the complex.

π and CH---F interactions within the single entity (C and F). The energy is seen to be lower than the rest of the optimized structures indicating that the increase in non-covalent interactions stabilizes the complex...F⁻ adduct. Although the energy of the complex decreases upon F⁻ addition, there is not much energy difference between the different isomerized states of the complex.

7.3.2 Cation Sensing Behaviors of the Complexes. Since the complexes possess a delocalized π -electron cloud throughout the entire complex backbone, we are also interested to investigate the cation sensing characteristics of the complexes. The cation sensing behaviors of **1-3** are systematically investigated in MeCN via different optical channels and spectroscopic techniques. We tested for a wide variety of cations, viz. Li⁺, Na⁺, K⁺, Be⁺², Mg⁺², Ca⁺², Zn⁺², Cd⁺² and Hg⁺² wherein significant change in their absorption and emission spectra is exhibited by Hg⁺² only (Figure 7.12).

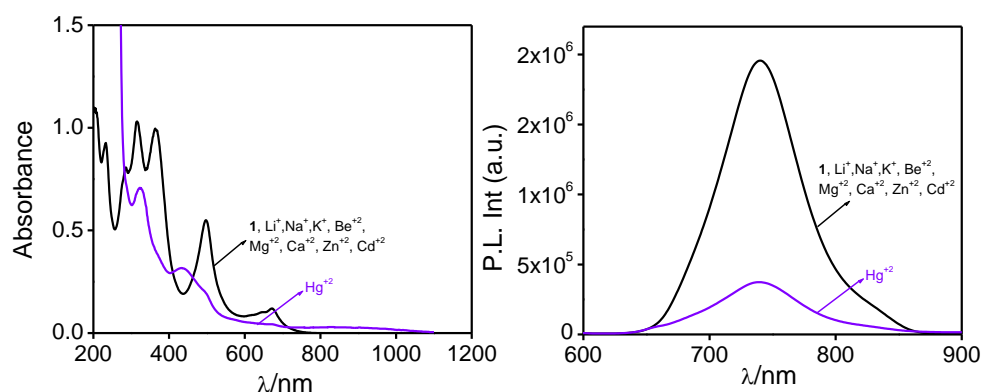


Figure 7.12. Absorption (left) and emission (right, $\lambda_{\text{ex}}=500$ nm) spectrum of **1** in MeCN (1.0×10^{-5} M) in absence and in presence of studied cations.

Figure 7.13 shows the change in the absorption and emission spectra of the acetonitrile solution of the complexes upon addition of HgCl₂. In the absorption spectra, a gradual decrease in absorbance of the MLCT band is unanimously observed in all three complexes while small increase in absorbance of the mixed ILCT and π - π^* band takes place in case of **1** and **3** only. All the spectral lines pass through one or more isosbestic points indicating that two species are in equilibrium with each other. Interestingly, a broad band arises in the NIR region of ~700-1100 nm for **1**. Regarding their emission properties, **1** and **3** demonstrates a gradual decrease in emission intensity, while **2** exhibits an increase in emission intensity. Notably, the emission maximum (λ_{max}) remains unchanged for all three complexes. We have also measured the lifetime of the complexes upon reaching saturation

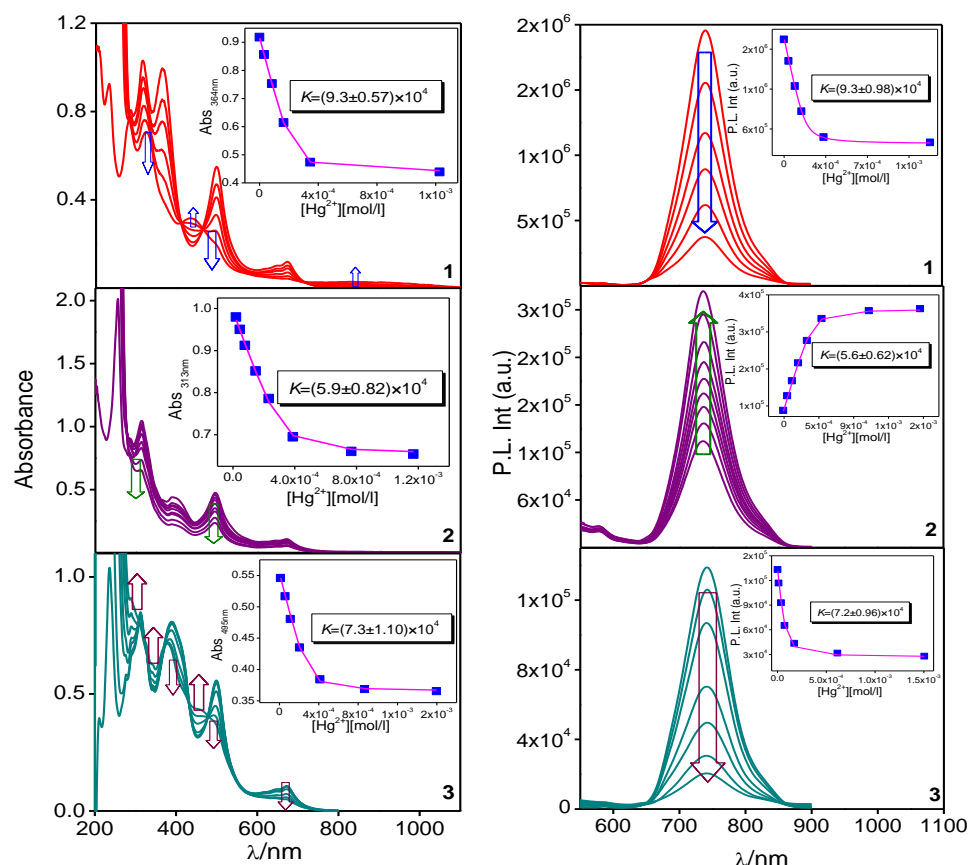


Figure 7.13. Absorption (left) and emission (right, $\lambda_{\text{ex}} = 500$ nm) spectral changes upon incremental addition of Hg^{+2} to the *t-t* form of **1-3** (1.0×10^{-5} M) in MeCN solution. Insets to the figures in both left and right panels indicate the estimation of binding constants.

with Hg^{+2} . Hg^{+2} induces significant decrease in lifetime values of **1** and **3**, while a minor increase is noticed for **2** with respect to their *t-t* analogues (Figure 7.14). The observed change in spectral properties could be due to non-classical interaction among the π -electron cloud of the complex backbone and Hg^{2+} ion.

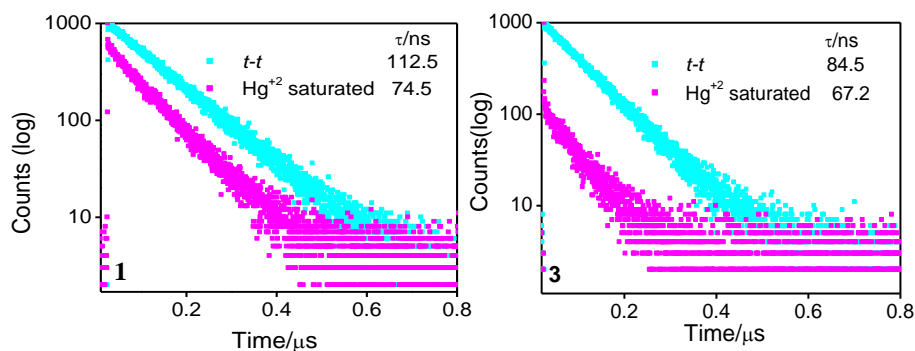


Figure 7.14. The emission decay profiles ($\lambda_{\text{ex}} = 490\text{nm}$) as well as lifetime values of *t-t* forms of **1** and **3** in their free and Hg^{+2} saturated state in MeCN.

To obtain a direct proof for the cation- π interactions, we also record the ^{13}C NMR spectrum of the *t-t* form of **1** in $\text{DMSO}-d_6$ upon addition of 95 equiv of Hg^{+2} (Figure 7.15). It is noticed that most of the ^{13}C NMR peaks of Hg^{+2} -saturated solution is shifted towards the downfield region by ~ 0.20 - 2.71 ppm, with the most substantial downfield shift of 2.71 ppm occurring for the signal at 145.91 ppm. This observation is probably due to dragging of electron density from the $\text{C}^{\delta-}$ units in the complex framework by the Hg^{+2} ions. This change in ^{13}C NMR peak position clearly indicates the occurrence of some sort of non-covalent interactions between the complex cation and Hg^{+2} , thereby leading to the formation of a $\mathbf{1}\dots\text{Hg}^{+2}$ adduct.

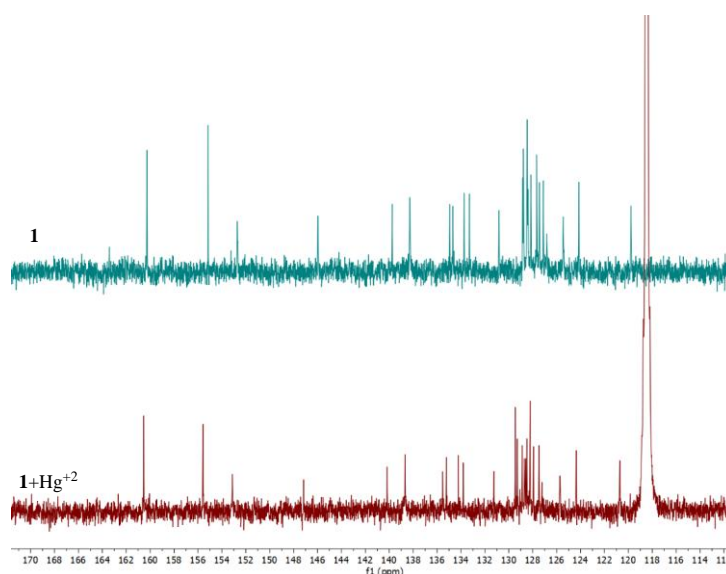


Figure 7.15. ^{13}C NMR spectra of **1** (*t-t*) in their free and Hg^{+2} saturated forms in $\text{DMSO}-d_6$.

To elucidate the stoichiometry of the complex-anion interaction, Job's plot analysis is again performed using emission titration data, wherein the mole fraction of mercury ion (Hg^{+2}) was systematically varied (Figure 7.16). The analysis revealed that the point of maximum emission change occurs at ~ 0.5 mole fraction of Hg^{+2} , indicating the formation of a 1:1 adduct between the metal complex and Hg^{+2} . This 1:1 stoichiometry suggests that each metal center within the complex coordinates with a single Hg^{+2} , most likely through non-covalent interactions such as cation- π as well as electrostatic interactions.

We also carried out the DLS study of the complexes in their Hg^{+2} -saturated forms to speculate any change in the particle size upon addition of the cation (Figure 7.17). Surprisingly, the particle size increases from 3.2 - 84.0 to 102.8 - 146.2 nm, indicating the occurrence of some sort of association upon addition of the Hg^{+2} ion. As previously

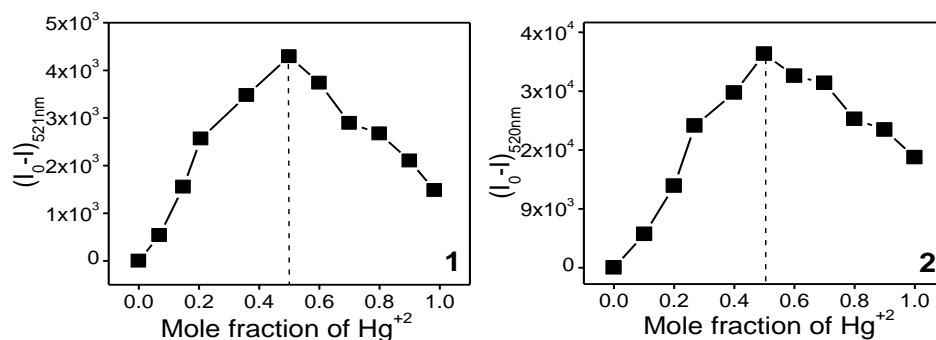


Figure 7.16. Job's plot referring to the 1:1 interaction between the complexes **1** and **2** and Hg^{2+} in MeCN.

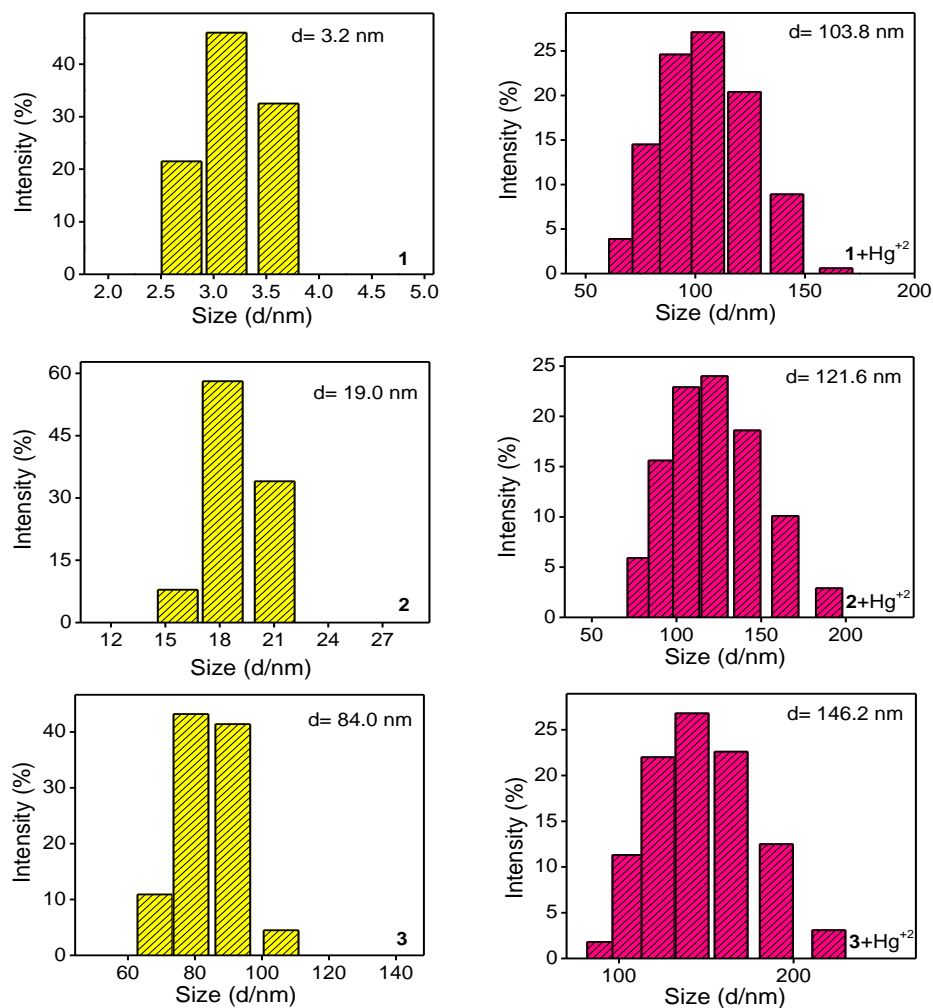


Figure 7.17. DLS plot to determine the particle size distribution of **1-3** in their free (left) and Hg^{2+} (right) saturated forms in MeCN.

discussed, since no other solvent is involved, the observed increase in particle size is solely due to the addition of Hg^{+2} , which in turn induces some sort of association. This aggregation arises from non-covalent interactions that bring the molecules closer, increasing their size.

Since the structural orientations of the complexes are significantly altered on going from the *t-t* to the *c-c* form, we are also interested to investigate the efficacy of *c-c* form of the complexes to interact with the Hg^{+2} ions. The changes are monitored by absorption and emission spectroscopy (Figure 7.18). It is of interest to see that the nature of change in the absorption spectra is substantially altered wherein the MLCT and ILCT band lose their intensity together with a small increase in the $\pi-\pi^*$ band intensity. All the spectral lines pass through an isosbestic point indicating that two or more species are in equilibrium with one another. In the emission spectra, when excited at 450 nm, **1** and **2** exhibit a decrease in the emission intensity of the MLCT band, while the ligand-centered band remains unaffected. By

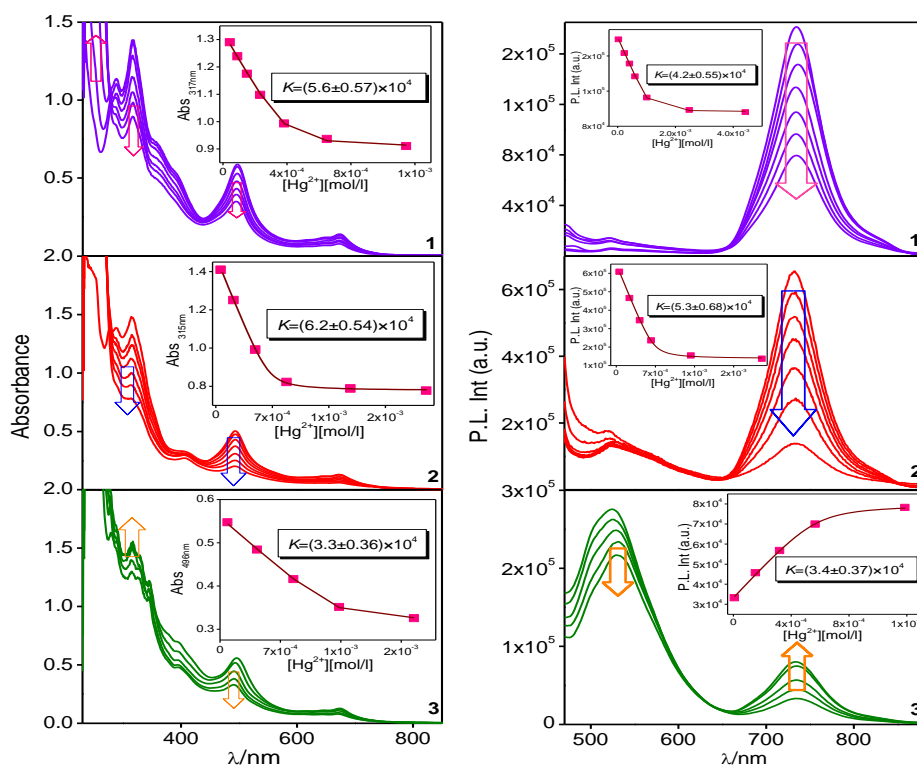


Figure 7.18. Absorption (left) and emission (right, $\lambda_{\text{ex}} = 450$ nm) spectral changes upon incremental addition of Hg^{+2} to the cis-cis form of **1-3** (1.0×10^{-5} M) in MeCN solution. Insets to the figures in both left and right panels indicate the estimation of binding constants.

contrast, for **3**, an increase in intensity of the MLCT band takes place with concomitant decrease in the ligand-centred band. The lifetime of the complexes is found to decrease upon addition of Hg^{+2} to their *c-c* forms (Figure 7.19).

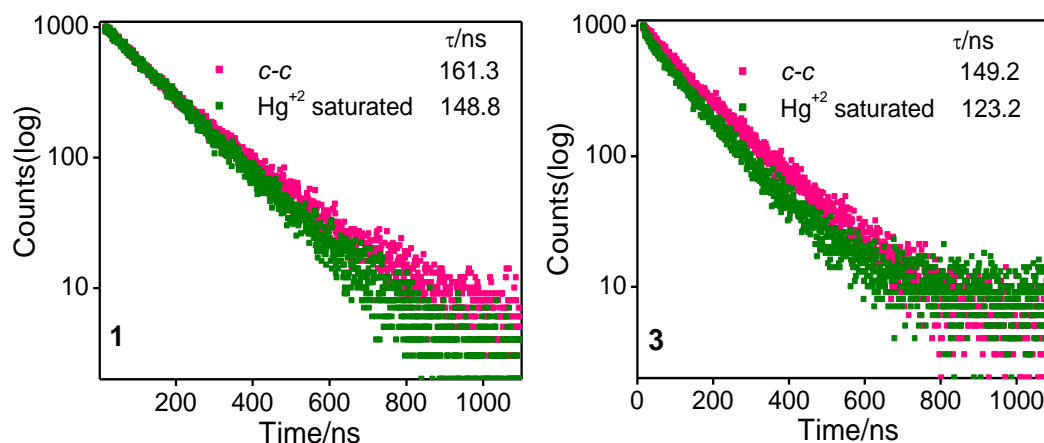


Figure 7.19. The emission decay profiles ($\lambda_{\text{ex}} = 490\text{nm}$) as well as lifetime values of *c-c* forms of **1** and **3** in their free and Hg^{+2} saturated state in MeCN.

To quantitatively evaluate the receptor-cation interactions, binding constants (K) are determined by analyzing the absorption and emission titration data of the complexes (Figure 7.13 and 7.18 inset, Table 7.1), utilizing the 1:1 binding model as described by equation 7.1. While for the *t-t* forms, the binding constants lie in the range $5.6\text{--}9.3 \times 10^4$, for the respective *c-c* forms, they lie in the range $3.3\text{--}6.2 \times 10^4$. The data clearly indicate that the K values for receptor-mercury (Hg^{+2}) interactions in their *c-c* forms are consistently lower relative to corresponding *t-t* isomers. This decrease in binding affinity can be attributed to the structural changes induced during *c-c* isomerization, which likely alters the spatial arrangement and electronic environment of the binding site, reducing its ability to interact strongly with ions. The order of the binding constants is **1**>**3**>**2** for the *t-t* form, while for the *c-c* form the order is **2**>**1**>**3**. This reflects the influence of polyaromatic hydrocarbon substituents on the receptor's binding efficiency, suggesting that both steric and electronic effects play critical role in modulating the receptor's cation recognition capabilities. The detection limits of the complexes towards Hg^{2+} were also found to substantially higher in their *t-t* form (3.1×10^{-8} to 7.9×10^{-7} M) compared with the *c-c* isomers (1.6×10^{-7} to 1.1×10^{-6} M).

7.4 Conclusions

With regard to our sustained interest in designing prospective molecular sensors and switches that function in the near-infrared (NIR) domain, we employed herein a new array of homoleptic Os(II)-terpyridine complexes coupled with stilbene-appended naphthalene,

anthracene and pyrene motifs for simultaneous recognition of selective anion and cation. The complexes are found to selectively sense F^- among a wide range of anions as well as Hg^{2+} amongst the cations via multiple optical channels and spectroscopic techniques. The results of absorption, steady-state and time-resolved emission experiments together with 1H , ^{13}C , ^{19}F NMR spectroscopic analyses and dynamic light scattering (DLS) experiments unequivocally demonstrate strong association among the complexes and F^- as well as Hg^{2+} ions. These interactions arise from a sophisticated interplay of non-classical forces, including $CH\cdots F$ hydrogen bonding, $CH-\pi$, anion- π , cation- π interactions, and through-space electrostatic attraction between the complex and the F^- and Hg^{2+} ions.

The stilbene units enable $t-t \rightarrow c-c$ photoisomerization upon exposure to light, which subsequently reorient the conformation of the stilbene-coupled polyaromatic moieties within the complex backbone. The anion and cation sensing investigations are also conducted on the $c-c$ form of the complexes to examine the effect of orientation of polyaromatic moieties on their sensing efficacy. Substantial alteration of sensing efficacy is indeed observed on passing from $t-t$ to $c-c$ form of the complexes. In conjunction with experimental demonstration, computation analysis using density functional theory as well as time-dependent DFT has been executed to obtain the mode of ion-receptor interactions. Thus, the present complexes can be used as efficient sensors in the NIR region.

7.5 References

- (1) Neel, A. J.; Hilton, M. J.; Sigman, M. S.; Toste, F. D. Exploiting Non-Covalent π Interactions for Catalyst Design. *Nature* **2017**, *543*, 637.
- (2) Wang, D.-X.; Wang, M.-X.; Exploring Anion- π Interactions and Their Applications in Supramolecular Chemistry. *Acc. Chem. Res.* **2020**, *53*, 1364-1380.
- (3) Chifotides, H. T.; Dunbar, K. R. Anion- π Interactions in Supramolecular Architectures. *Acc. Chem. Res.* **2013**, *46*, 4, 894-906.
- (4) Biedermann, F.; Schneider, H.-J. Experimental Binding Energies in Supramolecular Complexes. *Chem. Rev.* **2016**, *116*, 5216.
- (5) Haque, A.; Alenezi, K. M.; Khan, M. S.; Wong, W.Y.; Raithby, P. R. Non-Covalent Interactions (NCIs) in π -Conjugated Functional Materials: Advances and Perspectives. *Chem. Soc. Rev.* **2023**, *52*, 454-472.
- (6) Wang, D.-X.; Wang, M.-X. Exploring Anion- π Interactions and their Applications in Supramolecular Chemistry. *Acc. Chem. Res.* **2020**, *53*, 7, 1364-1380.
- (7) Salonen, L. M.; Ellermann, M.; Diederich, F. Aromatic Rings in Chemical and Biological Recognition: Energetics and Structures. *Angew. Chem. Int. Ed.* **2011**, *50*, 4808-4842.
- (8) Tam, A.Y.-Y.; Wong, K. M.-C.; Wang, G.; Yam, V. W.-W. Luminescent Metallogels of Platinum(II) Terpyridyl Complexes: Interplay of Metal...Metal, π - π and Hydrophobic-Hydrophobic Interactions on Gel Formation. *Chem. Commun.* **2007**, 2028-2030.
- (9) Burley, S.; Petsko, G. Aromatic-Aromatic Interaction: A Mechanism of Protein Structure Stabilization. *Science* **1985**, *229*, 23-28.
- (10) Li, S.; Cooper, V. R.; Thonhauser, T.; Lundqvist, B. I.; Langreth, D. C. Stacking Interactions and DNA Intercalation. *J. Phys. Chem. B* **2009**, *113*, 11166-11172.
- (11) Xiu, X.; Puskar, N. L.; Shanata, J. A. P.; Lester, H. A.; Dougherty, D. A. Nicotine Binding to Brain Receptors Requires a Strong Cation- π Interaction. *Nature* **2009**, *458*, 534.
- (12) Steiner, T.; Koellner, G. Hydrogen Bonds with π -Acceptors in Proteins: Frequencies and Role in Stabilizing Local 3D Structures. *J. Mol. Biol.* **2001**, *305*, 535-557.
- (13) Gorteau, V.; Bollot, G.; Mareda, J.; Perez-Velasco, A.; Matile, S. Rigid Oligonaphthalenediimide Rods as Transmembrane Anion- π Slides. *J. Am. Chem. Soc.* **2006**, *128*, 14788-14789.

- (14) Tuo, D.-H.; Liu, W.; Wang, X.-Y.; Wang, X.-D.; Ao, Y.-F.; Wang, Q.-Q.; Li, Z.-Y.; Wang, D.-X. Toward Anion- π Interactions Directed Self-Assembly with Predesigned Dual Macrocyclic Receptors and Dianions. *J. Am. Chem. Soc.* **2019**, *141*, 1118-1125.
- (15) Zhao, Y.; Cotellet, Y.; Liu, L.; Lopez-Andarias, J.; Bornhof, A.-B.; Akamatsu, M.; Sakai, N.; Matile, S. The Emergence of Anion- π Catalysis. *Acc. Chem. Res.* **2018**, *51*, 2255-2263.
- (16) Ramírez, G.-G.; Escudero-Adan, E. C.; Benet-Buchholz, J.; Ballester, P. Quantitative Evaluation of Anion- π Interactions in Solution. *Angew. Chem., Int. Ed.* **2008**, *47*, 4114-4118.
- (17) Zhao, H.; Tang, L.; Fang, Y.; Liu, C.; Ding, W.; Zang, S.; Chen, Y.; Xu, W.; Yuan, Y.; Fang, D. *et al.* Manipulating Cation- π Interactions of Reader Proteins in Living Cells with Genetic Code Expansion. *J. Am. Chem. Soc.* **2023**, *145*, 30, 16406-16416.
- (18) Zacharias, N.; Dougherty, D. A. Cation- π Interactions in Ligand Recognition and Catalysis. *Trends Pharmacol. Sci.* **2002**, *23*, 281-287.
- (19) Tsuzuki, S. In Structure and Bonding. Wales, D., Ed.; Springer: Berlin, **2005**; Vol. 115.
- (20) Zhang, X.; Hao, X.; Liu, L.; Pham, A.-T.; Lopez-Andarias, J.; Frontera, A.; Sakai, N.; Matile, S. Primary Anion- π Catalysis and Autocatalysis. *J. Am. Chem. Soc.* **2018**, *140*, 17867-17871.
- (21) Michalet, X.; Pinaud, F. F.; Bentolila, L. A.; Tsay, J. M.; Doose, S.; Li, J. J.; Sundaresan, G.; Wu, A. M.; Gambhir, S. S.; Weiss, S. Quantum Dots for Live Cells, in Vivo Imaging, and Diagnostics. *Science* **2005**, *307*, 538-44.
- (22) Yao, C.-J.; Zhong, Y.-W.; Nie, H.-J.; Abruña, H. D.; Yao, J. Near-IR Electrochromism in Electropolymerized Films of a Biscyclometalated Ruthenium Complex Bridged by 1,2,4,5-Tetra(2-pyridyl)benzene. *J. Am. Chem. Soc.* **2011**, *133*, 20720-20723.
- (23) Bar, M.; Maity, D.; Deb, S.; Das, S.; Baitalik, S. Ru-Os Dyads Based on a Mixed Bipyridine-Terpyridine Bridging Ligand: Modulation of the Rate of Energy Transfer and pH-Induced Luminescence Switching in the Infrared Domain. *Dalton Trans.* **2017**, *46*, 12950-12963.
- (24) Paul, A.; Ganguly, T.; Bar, M.; Baitalik, S.; Controlling the Direction of Intercomponent Energy Transfer by Appropriate Placement of Metals in Long-Lived Trinuclear Complexes of Fe(II), Ru(II), and Os(II). *Inorg. Chem.* **2021**, *60*, 412-422.
- (25) Bulach, V.; Sguerra, F.; Hosseini, M. W. Porphyrin Lanthanide Complexes for NIR Emission. *Coord. Chem. Rev.* **2012**, *256*, 1468-1478.

- (26) Wang, H.; Shao, J.-Y.; Duan, R.; Wang, K.-Z. Zhong, Y.-W. Synthesis and Electronic Coupling Studies of Cyclometalated Diruthenium Complexes Bridged by 3,3',5,5'-Tetrakis(benzimidazol-2-yl)-Biphenyl. *Dalton Trans.* **2021**, 50, 4219-4230.
- (27) Shao, J.-Y.; Yang, W.-W.; Yao, J.; Zhong, Y.-W. Biscyclometalated Ruthenium Complexes Bridged by 3,3',5,5'-Tetrakis(N-methylbenzimidazol-2-yl)biphenyl: Synthesis and Spectroscopic and Electronic Coupling Studies. *Inorg. Chem.* **2012**, 51, 4343-4351.
- (28) Busschaert, N.; Caltagirone, C.; Rossom, W. V.; Gale, P. A. Applications of Supramolecular Anion Recognition. *Chem. Rev.* **2015**, 115, 8038-8155.
- (29) Mardanya, S.; Karmakar, S.; Mondal, D.; Baitalik, S. Homo- and Heterobimetallic Ruthenium(II) and Osmium(II) Complexes Based on a Pyrene-Biimidazolate Spacer as Efficient DNA-Binding Probes in the Near-Infrared Domain. *Inorg. Chem.* **2016**, 55, 3475-3489.
- (30) Mondal, D.; Biswas, S.; Paul, A.; Baitalik, S. Luminescent Dinuclear Ruthenium Terpyridine Complexes with a Bis-Phenylbenzimidazole Spacer. *Inorg. Chem.* **2017**, 56, 7624-7641.
- (31) Maity, D.; Bhaumik, C.; Mondal, D.; Baitalik, S. Photoinduced Intramolecular Energy Transfer and Anion Sensing Studies of Isomeric Ru(II) Os(II) Complexes Derived From an Asymmetric Phenanthroline-Terpyridine Bridge. *Dalton Trans.* **2014**, 43, 1829-1845.
- (32) Máñez, R. M.; Sancenón, F. Fluorogenic and Chromogenic Chemosensors and Reagents for Anions. *Chem. Rev.* **2003**, 103, 4419-4476
- (33) David, C. I., Lee, H. I. Cutting-Edge Advances in Colorimetric and Fluorescent Chemosensors for Detecting Lethal Cyanide Ion: A Comprehensive Review. *Microchem. Jour.* **2024**, 110359.
- (34) Ilakiyalakshmi, M.; Dhanasekaran K.; Napoleon, A. A. A Review on Recent Development of Phenothiazine-Based Chromogenic and Fluorogenic Sensors for the Detection of Cations, Anions, and Neutral Analytes. *Top. Curr. Chem.* **2024**, 382, 29.
- (35) Dutta, S.; Sahana, A. Ratiometric Fluorescence Based and Chromogenic Sensors for Detection of Fluoride Ion and their Application in Real Samples. *Anal. Methods* **2024**, 16, 344-370.
- (36) Flamigni, L.; Barigelletti, F.; Armaroli, N.; Ventura, B.; Collin, J.-P.; Sauvage, J.-P.; Williams, J. A. G. Triplet-Triplet Energy Transfer between Porphyrins Linked via a Ruthenium(II) Bisterpyridine Complex. *Inorg. Chem.* **1999**, 38, 661-667.

- (37) Develay, S.; Blackburn, O.; Thompson, A. L.; Williams, J. A. G. Cyclometalated Platinum(II) Complexes of Pyrazole-Based, N^CN-Coordinating, Tridentate Ligands: The Contrasting Influence of Pyrazolyl and Pyridyl Rings on Luminescence. *Inorg. Chem.* **2008**, *47*, 11129-11142.
- (38) Dikova, Y. M.; Yufit, D. S.; Williams, J. A. G. Platinum(IV) Complexes with Tridentate, NNC-Coordinating Ligands: Synthesis, Structures, and Luminescence. *Inorg. Chem.* **2023**, *62*, 1306-1322.
- (39) Maity, D.; Bhaumik, C.; Mondal, D.; Baitalik, S. Ru(II) and Os(II) Complexes Based on Terpyridyl-Imidazole Ligand Rigidly Linked to Pyrene: Synthesis, Structure, Photophysics, Electrochemistry, and Anion-Sensing Studies. *Inorg. Chem.* **2013**, *52*, 13941-13955.
- (40) Maity, D.; Bhaumik, C.; Mondal, D.; Baitalik, S. Photoinduced Intramolecular Energy Transfer and Anion Sensing Studies of Isomeric Ru(II) Os(II) Complexes Derived from an Asymmetric Phenanthroline-Terpyridine Bridge. *Dalton Trans.* **2014**, *43*, 1829-1845.
- (41) Bar, M.; Pal, P.; Maity, D.; Baitalik, S. Heterobimetallic Ru-Os Complexes Function as Multichannel Sensors for Selected Anions by Taking Profit of Metal-Ligand Interaction. *Sens. Actuators B: Chem.* **2018**, *266*, 493-505.
- (42) Zhou, Y.; Zhang, J. F.; Yoon, J. Fluorescence and Colorimetric Chemosensors for Fluoride-Ion Detection. *Chem. Rev.* **2014**, *114*, 5511-5571.
- (43) Jose, D. A.; Kar, P.; Koley, D.; Ganguly, B.; Thiel, W.; Ghosh, H. N.; Das, A. Phenol- and Catechol-Based Ruthenium(II) Polypyridyl Complexes as Colorimetric Sensors for Fluoride Ions. *Inorg. Chem.* **2007**, *46*, 14.
- (44) Das, P.; Mahato, P.; Ghosh, A.; Mandal, A. K.; Banerjee, T.; Saha, S.; Das, A. Urea/Thiourea Derivatives and Zn(II)-DPA Complex as Receptors for Anionic Recognition-A Brief Account. *J. Chem. Sci.* **2011**, *123*, 2, 175-186.
- (45) Ghosh, A.; Verma, S.; Ganguly, B.; Ghosh, H. N.; Das, A. Influence of Urea N-H Acidity on Receptor-Anionic and Neutral Analyte Binding in a Ruthenium(II)-Polypyridyl-Based Colorimetric Sensor. *Eur. J. Inorg. Chem.* **2009**, 2496-2507.
- (46) Singh, H.; Tiwari, K.; Tiwari, R.; Pramanik, S. K.; Das, A. Small Molecule as Fluorescent Probes for Monitoring Intracellular Enzymatic Transformations. *Chem. Rev.* **2019**, *119*, 11718-11760.
- (47) Guha, S.; Saha, S.; Fluoride Ion Sensing by an Anion- π Interaction. *J. Am. Chem. Soc.* **2010**, *132*, 17674-17677.

- (48) Zhang, X.; Hao, X.; Liu, L.; Pham, A.-T.; Lopez-Andarias, J.; Frontera, A.; Sakai, N.; Matile, S. Primary Anion- π Catalysis and Autocatalysis. *J. Am. Chem. Soc.* **2018**, *140*, 17867-17871.
- (49) Mascal, M.; Armstrong, A.; Bartberger, M. D. Anion-Aromatic Bonding: A Case for Anion Recognition by π -Acidic Rings. *J. Am. Chem. Soc.* **2002**, *124*, 6274-6276.
- (50) Alkorta, I.; Rozas, I.; Elguero, J. Interactions of Anions with Perfluoro Aromatic Compounds. *J. Am. Chem. Soc.* **2002**, *124*, 8593-8598.
- (51) Marshall, M. S.; Steele, R. P.; Thanthiriwatte, K. S.; Sherrill, C. D. Potential Energy Curves for Cation- π Interactions: Off-Axis Configurations are also Attractive. *J. Phys. Chem. A* **2009**, *113*, 13628-13632.
- (52) Quinonero, D.; Garau, C.; Frontera, A.; Ballester, P.; Costa, A.; Deya, P. Structure and Binding Energy of Anion- π and Cation- π Complexes: A Comparison of MP2, RI-MP2, DFT, and DF-DFT Methods. *J. Phys. Chem. A* **2005**, *109*, 4632-4637.
- (53) Kim, H. N.; Ren, W. X.; Kim, J. S.; Yoon, J. Fluorescent and Colorimetric Sensors for Detection of Lead, Cadmium, and Mercury Ions. *Chem. Soc. Rev.* **2012**, *41*, 3210-3244.
- (54) Chen, N.; Zhang, Y.; Liu, H.; Wu, X.; Li, Y.; Miao, L.; Shen, Z.; Wu, A. High-Performance Colorimetric Detection of Hg^{2+} Based on Triangular Silver Nanoprisms. *Sensors* **2016**, *1*, 521-527.
- (55) Ramesh, G.V.; Radhakrishnan, T.P. A Universal Sensor for Mercury (Hg , Hg^{I} , Hg^{II}) Based on Silver Nanoparticle-Embedded Polymer Thin Film. *ACS Appl. Mater. Interfaces* **2011**, *3*, 988-994.
- (56) Carvalho, C.M.; Chew, E.H.; Hashemy, S.I.; Lu, J.; Holmgren, A. Inhibition of the Human Thioredoxin System: A Molecular Mechanism of Mercury Toxicity. *J. Biol. Chem.* **2008**, *283*, 11913.
- (57) Clarkson, T.W.; Magos, L.; Myers, G.J. The Toxicology of Mercury-Current Exposures and Clinical Manifestations. *NEJM* **2003**, *349*, 1731-1737.
- (58) U.S. EPA. Draft Guidance for Implementing the January 2001, *Methylmercury Water Quality Criterion* [S]; EPA-823-R-01-001; Office of Science and Technology: Washington, DC, 2006, 1-20.
- (59) WHO. *Guideline Levels for Methylmercury in Fish* [S], CAC/GL7-1991; WHO: Geneva, Switzerland, 1991, 1.
- (60) Sigaeva, A.; Ong, Y.; Damle, V.G.; Morita, A.; van der Laan, K.J.; Schirhagl, R. Optical Detection of Intracellular Quantities Using Nanoscale Technologies. *Acc. Chem. Res.* **2019**, *52*, 1739-1749.

- (61) Broz, P., Inflammasomes: Intracellular Detection of Extracellular Bacteria. *Cell Res.* **2016**, *26*, 859-860.
- (62) Liu, J.; Fraire, J.C.; De Smedt, S.C.; Xiong, R.; Braeckmans, K. Intracellular Labeling with Extrinsic Probes: Delivery Strategies and Applications. *Small* **2020**, *16*, 2000146.
- (63) Dougherty, D. A. The Cation- π Interaction. *Acc. Chem. Res.* **2013**, *46*, 4, 885-893.
- (64) Dougherty, D. A. Cation- π Interactions in Chemistry and Biology: A New View of Benzene, Phe, Tyr, and Trp. *Science* **1996**, *271*, 163-168.
- (65) Meadows, E. S.; De Wall, S. L. D.; Barbour, L. J.; Gokel, G. W. Alkali Metal Cation- π Interactions Observed by Using a Lariat Ether Model System. *J. Am. Chem. Soc.* **2001**, *123*, 3092-3107.
- (66) Mahadevi, A. S.; Sastry, G. N. Cation- π Interaction: Its Role and Relevance in Chemistry, Biology, and Material Science. *Chem. Rev.* **2013**, *113*, 2100-2138.
- (67) Minoux, H.; Chipot, C. Cation- π Interactions in Proteins: Can Simple Models Provide an Accurate Description. *J. Am. Chem. Soc.* **1999**, *121*, 10366-10372.
- (68) Reddy, A. S.; Sastry, G. N. Cation [$M = H^+, Li^+, Na^+, K^+, Ca^{2+}, Mg^{2+}, NH_4^+, NMe_4^+$] Interactions with the Aromatic Motifs Of Naturally Occurring Amino Acids: A Theoretical Study. *J. Phys. Chem. A* **2005**, *109*, 8893-8903.
- (69) Gokel, G. W.; Barbour, L. J.; De Wall, S. L. D.; Meadows, E. S. Macrocyclic Polyethers as Probes to Assess and Understand Alkali Metal Cation- π Interactions. *Coord. Chem. Rev.* **2001**, *222*, 127-154.
- (70) Soteras, I.; Orozco, M.; Luque, F. J. Induction Effects in Metal Cation-Benzene Complexes. *Phys. Chem. Chem. Phys.* **2008**, *10*, 2616-2624.
- (71) Tsuzuki, S.; Mikami, M.; Yamada, S. Origin of Attraction, Magnitude, and Directionality of Interactions in Benzene Complexes with Pyridinium Cations. *J. Am. Chem. Soc.* **2007**, *129*, 8656-8662.
- (72) Kolakkandy, S.; Pratihari, S.; Aquino, A. J. A.; Wang, H.; Hase, W. L. Properties of Complexes Formed by Na^+ , Mg^{2+} , and Fe^{2+} Binding with Benzene Molecules. *J. Phys. Chem. A* **2014**, *118*, 9500-9511.
- (73) Meyer, F.; Khan, F. A.; Armentrout, P. B. Thermochemistry of Transition Metal Benzene Complexes: Binding Energies of $M(C_6H_6)_x^+$ ($x = 1, 2$) for $M = Ti$ to Cu . *J. Am. Chem. Soc.* **1995**, *117*, 9740-9748.
- (74) Duncan, M. A. Structures, Energetics and Spectroscopy of Gas Phase Transition Metal Ion-Benzene Complexes. *Int. J. Mass Spectrom.* **2008**, *272*, 99-118.

- (75) Wedderburn, K. M.; Bililign, S.; Levy, M.; Gdanitz, R. Geometries and Stabilities of 3d-Transition Metal-Cation Benzene Complexes, $M^+ Bz_n$ ($M = Sc-Cu$, $n = 1, 2$). *Chem. Phys.* **2006**, 326, 600-604.
- (76) Maner, J. A.; Mauney, D. T.; Duncan, M. A. Imaging Charge Transfer in a Cation- π System: Velocity-Map Imaging of $Ag^+(\text{benzene})$ Photodissociation. *J. Phys. Chem. Lett.* **2015**, 6, 4493- 4498.
- (77) Armentrout, P.B.; Yang, B.; Rodgers, M.T. Metal Cation Dependence of Interactions with Amino Acids: Bond Energies of Rb^+ and Cs^+ to Met, Phe, Tyr, and Trp. *J. Phys. Chem. B* **2013**, 117, 3771-3781.
- (78) Jaeger, T. D.; van Heijnsbergen, D.; Klippenstein, S. J.; von Helden, G.; Meijer, G.; Duncan, M. A. Vibrational Spectroscopy and Density Functional Theory of Transition-Metal Ion-Benzene and Dibenzene Complexes in the Gas Phase. *J. Am. Chem. Soc.* **2004**, 126, 10981-10991.
- (79) Scott, A. C.; Buchanan, J. W.; Flynn, N. D.; Duncan, M. A. Photodissociation of Iron-Pyrene and Iron-Perylene Cation Complexes. *Int. J. Mass Spectrom.* **2007**, 266, 149-155.
- (80) Buchanan, J. W.; Reddic, J. E.; Grieves, G. A.; Duncan, M. A. Metal and Multimetal Complexes with Polyaromatic Hydrocarbons: Formation and Photodissociation of Fex-(Coronene)y Cations. *J. Phys. Chem. A* **1998**, 102, 6390-6394.
- (81) Song, W.; Gao, J.; Gao, Y.; Shan, G.-G.; Geng, Y.; Shaoa, K.; Su, Z.-M. Constructing Anion- π Interactions in Cationic Iridium(III) Complexes to Achieve Aggregation Induced Emission Properties. *Inorg. Chem. Front.* **2024**, 11, 1198.
- (82) Demeshko, S.; Dechert, S.; Meyer, F. Anion- π Interactions in a Carousel Copper(II)-Triazine Complex. *J. Am. Chem. Soc.* **2004**, 126, 4508-4509.
- (83) Schottel, B. L.; Chifotides, H. T.; Shatruk, M.; Chouai, A.; Pe´rez, L. M.; Bacsá, J.; Dunbar, K. R. Anion- π Interactions as Controlling Elements in Self-Assembly Reactions of $Ag(I)$ Complexes with π -Acidic Aromatic Rings. *J. Am. Chem. Soc.* **2006**, 128, 5895-5912.
- (84) Capo´, M.; Buchholz, J. B.; Ballester, P. Anion- π - π Interactions in a Dinuclear M_2L_2 Metallocycle. *Inorg. Chem.* **2008**, 47, 10190-10192.
- (85) Kuzniak, E.; Pinkowicz, D.; Hooper, J.; Srebro-Hooper, M.; Hetman´czyk, L.; Podgajny, R. Molecular Deformation, Charge Flow, and Spongelike Behavior in Anion- π $\{[M(CN)_4]^{2-}; [HAT(CN)_6]\}_\infty$ ($M=Ni, Pd, Pt$) Supramolecular Stacks. *Chem. Eur. J.* **2018**, 24, 16302-16314.

- (86) Ganguly, T.; Pal, P.; Maity, D.; Baitalik, S. Synthesis, Characterization and Emission Switching Behaviors of Styrylphenyl-Conjugated Ru(II)-Terpyridine Complexes via Aggregation and Trans-Cis Photoisomerization. *J. Photochem. Photobiol. A* **2023**, *440*, 114662.
- (87) Pal, P.; Mukherjee, S.; Maity, D.; Baitalik, S. Synthesis, Structural Characterization, and Luminescence Switching of Diarylethene-Conjugated Ru(II)-Terpyridine Complexes by Trans-Cis Photoisomerization: Experimental and DFT/TD-DFT Investigation. *Inorg. Chem.* **2018**, *57*, 5743-5753.
- (88) Ganguly, T.; Pal, P.; Paul, A.; Baitalik, S. Synthesis and Manifold but Controllable Emission Switching of Stilbene-Appended Polyaromatic Terpyridine Derivatives via Aggregation and Trans-Cis Isomerization. *Photochem. Photobiol. A* **2022**, *430*, 113966.
- (89) Yam, V. W.W.; Lau, V.C.Y.; Cheung, K.K. Synthesis, Photophysics and Photochemistry of Novel Luminescent Rhenium(I) Photoswitchable Materials. *J. Chem. Soc., Chem. Commun.* **1995**, 259-261.
- (90) Ko, C.-C.; Yam, V. W. W. Transition Metal Complexes with Photochromic Ligands Photosensitization and Photoswitchable Properties. *J. Mater. Chem.* **2010**, *20*, 2063-2070.



List of Publications

- (1) **Ganguly, T.**; Baitalik, S. Osmium-Terpyridine Complexes Linked with Stilbene-Coupled Naphthalene, Anthracene, and Pyrene Moieties Act as Multichannel Sensors for F^- and Hg^{2+} via Non-Classical Interactions. (*Submitted to Inorg. Chem.* **2025**)
- (2) **Ganguly, T.**; Abedin, T.; Maity, D.; Baitalik, S. Remarkable Increase in the Rate of Trans-Cis Photoisomerization of Os (II)-Terpyridine Complexes via Oxidation and Reduction. *Inorg. Chem.* **2025**, *64*, 4415-4430.
- (3) **Ganguly, T.**; Baitalik, S. Modulation of Room Temperature Emission Characteristics of Heteroleptic Ruthenium-Terpyridine Complexes via Aggregation. *Inorg. Chim. Acta* **2024**, *572*, 122278.
- (4) **Ganguly, T.**; Das, S.; Maity, D.; Baitalik, S. Luminescent Ruthenium-Terpyridine Complexes Coupled with Stilbene-Appended Naphthalene, Anthracene and Pyrene Motifs Demonstrate Fluoride Ion Sensing and Reversible Trans-Cis Photoisomerization. *Inorg. Chem.* **2024**, *63*, 6883-6897.
- (5) **Ganguly, T.**; Pal, P.; Maity, D.; Baitalik, S. Synthesis, Characterization and Emission Switching Behaviors of Styrylphenyl-Conjugated Ru(II)-Terpyridine Complexes via Aggregation and Trans-Cis Photoisomerization. *J. Photochem. Photobiol. A: Chem.* **2023**, *440*, 114662.
- (6) **Ganguly, T.**; Pal, P.; Paul, A.; Baitalik, S. Synthesis and Manifold but Controllable Emission Switching of Stilbene-appended Polyaromatic Terpyridine Derivatives via Aggregation and Trans-Cis isomerization. *J. Photochem. Photobiol. A: Chem.* **2022**, *430*, 113966.
- (7) Das, S.; Bar, M.; **Ganguly, T.**; Baitalik, S. Control of Photoisomerization Kinetics via Multistage Switching in Bimetallic Ru (II)-Terpyridine Complexes. *Inorg. Chem.* **2024**, *63*, 6600-6615.
- (8) Das, S.; Pal, P.; **Ganguly, T.**; Baitalik, S. Influences of both N,N,N- and N,N,C-Coordination Modes of Tollyl-Terpyridine on the Photophysical Properties of Cyclometalated Ru(II) Complexes: Combined Experimental and Theoretical Investigations on Acid/Base Dependent Reversible Cyclometalation. *Inorg. Chem.* **2023**, *62*, 12872-12885.

- (9) Manna, K.; **Ganguly, T.**; Baitalik, S. Jana, R. Visible-Light-and PPh₃-Mediated Direct C-N Coupling of Nitroarenes and Boronic Acids at Ambient Temperature. *Org. Lett.* **2021**, 23, 8634-8639.
- (10) Pal, P.; **Ganguly, T.**; Sahoo, A.; Baitalik, S. Emission Switching in the Near-Infrared by Reversible Trans-Cis Photoisomerization of Styrylbenzene-Conjugated Osmium Terpyridine Complexes. *Inorg. Chem.* **2021**, 60, 4869-4882.
- (11) Pal, P.; **Ganguly, T.**; Das, S.; Baitalik, S. pH-Responsive Colorimetric, Emission and Redox Switches Based on Ru(II)-Terpyridine Complexes. *Dalton Trans.* **2021**, 50, 186-196.
- (12) Paul, A.; **Ganguly, T.**; Bar, M.; Baitalik, S. Controlling the Direction of Intercomponent Energy Transfer by Appropriate Placement of Metals in Long-Lived Trinuclear Complexes of Fe(II), Ru(II), and Os(II). *Inorg. Chem.* **2021**, 60, 412-422.
- (13) Pal, P.; **Ganguly, T.**; Maity, D; Baitalik, S. Experimental and Theoretical Exploration of Photophysics and Trans-Cis Photoisomerization of Styrylbenzene Conjugated Terpyridine Complexes of Ru(II): Strong Effect of Deprotonation From Second Coordination Sphere. *J. Photochem. Photobiol. A.* **2020**, 392, 112409.
- (14) Pal, P.; **Ganguly, T.**; Karmakar, S; Baitalik, S. Anion- and Solvent Induced Modulation of Photophysical Properties of a Luminescent Bimetallic Ru(II) Complex: Experimental and TD-DFT Study. *Inorg. Chim. Acta.* **2020**, 502, 119337.

Publications 1-6 are included in the thesis
